

Surface Modification and Functionalization of Colloidal Nanoparticles

Dissertation

zur Erlangung des Doktorgrades

der Naturwissenschaften

(Dr. rer. nat.)

dem

Fachbereich Physik

der Philipps-Universität Marburg

vorgelegt von

Ralph Alexander Sperling

aus

Wiesbaden

Marburg/Lahn, 2008

Vom Fachbereich Physik der Philipps-Universität

als Dissertation angenommen am:

Erstgutachter: Prof. Dr. W. Parak

Zweitgutachter: Prof. Dr. W. Heimbrod

Tag der mündlichen Prüfung: 16.12.2008

Zusammenfassung

Thema dieser kumulativen Dissertation ist die Oberflächenmodifikation, Funktionalisierung und Biokonjugation anorganischer kolloidaler Nanopartikel. Solche Partikel besitzen einen Durchmesser zwischen ca. 1 und 100 nm und bestehen aus einem anorganischen, kristallinen Kern, der üblicherweise durch eine Schicht organischer Ligandenmoleküle bedeckt ist. Diese Ligandenmoleküle kontrollieren einerseits das Wachstum der Nanokristalle bei der Synthese und stabilisieren andererseits die Partikel in Lösung gegen Aggregation. Neben dem Kernmaterial bestimmt die Oberfläche maßgeblich die Eigenschaften der Nanopartikel, in Hinsicht auf das Verhalten im umgebenden Medium sowie die chemische und biologische Funktionalität, die durch chemische Gruppen und Biomoleküle modifiziert werden kann.

Ziel dieser Arbeit war es, die Oberfläche von kolloidalen Nanopartikeln kontrolliert zu funktionalisieren und mit Molekülen zu versehen, die die Partikel in biologisch relevanter, wässriger Umgebung stabil halten und ggf. eine spezifische Wechselwirkung mit biologischen Systemen ermöglichen.

Zunächst wurden hydrophobe Nanopartikel aus z.B. Gold oder CdSe/ZnS mit Hilfe eines amphiphilen Polymers von der organischen in die wässrige Phase überführt. Das Polymer besitzt Carboxylgruppen, die die Partikel durch elektrostatische Abstoßung stabilisieren und als Ankergruppen für die weitere chemische Funktionalisierung dienen. Neben der direkten Funktionalisierung des amphiphilen Polymers in organischer Lösung konnten verschiedene Moleküle an die Nanopartikel mit Polymerhülle in wässriger Lösung angebunden werden, unabhängig vom Kernmaterial der Partikel. Mit Hilfe von Polyethylenglycol (PEG), einem inerten linearen Polymer, konnten die Partikel zusätzlich sterisch stabilisiert werden. Ein bifunktionales PEG mit verschiedenen funktionellen Endgruppen erlaubte es, die Partikel mit neuen chemischen Funktionen zu versehen. Bei hinreichend großen PEG Molekülen konnte durch Gelelektrophorese eine Trennung von Partikeln mit genau einer oder zwei reaktiven funktionellen Gruppen erreicht werden. Für die Größencharakterisierung von Nanopartikeln wurden verschiedene komplementäre Methoden miteinander verglichen. Das System wurde auf verschiedene Kernmaterialien und funktionale Moleküle erweitert.

Komplementär dazu wurden citrat-stabilisierte Goldpartikel mit thiol-modifizierter DNA versehen und durch Gel-Elektrophorese charakterisiert, was über den Partikeldurchmesser Rückschlüsse auf die DNA Konformation ermöglichte. Zusätzlich wurde im Rahmen einer Kollaboration gezeigt, dass solche DNA-modifizierte Partikel dazu verwendet werden können, DNA-Oligomere durch Laser-induziertes Aufschmelzen von Partikelaggregaten nachzuweisen.

Abstract

Subject of this cumulative dissertation is the surface modification, functionalization and bioconjugation of inorganic colloidal nanoparticles. Such particles have a diameter of about 1 – 100 nm and consist of an inorganic, crystalline core that is commonly covered by a shell of organic ligand molecules. These ligand molecules control the growth of the particles during synthesis and also stabilize the particles in solution against aggregation. Besides the core material, the particle surface determines the properties of the particles, as to their interaction with the surrounding medium and to chemical and biological functionality that can be modified by reactive groups and biomolecules.

This work aimed to functionalize the surface of colloidal nanoparticles in a controlled fashion and to modify the particles with molecules that provide stability in biological relevant, aqueous environment and that possibly also provide specific interaction with biological systems.

First hydrophobic nanoparticles, e.g. made of gold or CdSe/ZnS, were transferred from organic to the aqueous phase by means of an amphiphilic polymer. The polymer consists of carboxylic groups that stabilize the particles by electrostatic repulsion and provide anchor groups for further chemical functionalization. Besides the direct functionalization of the amphiphilic polymer in organic solution, different molecules could be bound to the polymer shell in aqueous solution, regardless to the core material. By means of poly(ethylene glycol), PEG, an inert linear polymer, the particles could be sterically stabilized. Bifunctional PEG with different functional groups allows for modification of the particles with new chemical functions. By means of sufficiently large PEG molecules, a separation of particles with exactly one or two reactive functional groups could be achieved by gel electrophoresis. For the size characterization of nanoparticles, different complementary methods were compared. The system was applied to particles of different core materials and different functional molecules.

Complementary to this, citrate-stabilized gold nanoparticles were modified by thiol-modified DNA and characterized by gel electrophoresis which provided information about the DNA conformation. In a collaborative work it was demonstrated that such DNA-modified particles can be used for the detection of DNA oligomers by laser-induced melting of nanoparticle aggregates.

Table of Contents

Table of Contents	1
Preface.....	3
1 Introduction.....	3
1.1 Particle synthesis	4
1.2 Stabilization against aggregation	7
1.3 Ligand exchange	9
2 Phase transfer	11
2.1 Ligand exchange	11
2.2 Ligand modification	13
2.3 Additional coating layers	13
2.4 Polymer coatings	14
2.5 Silanization	17
2.6 Comparison and remarks	17
3 Particle Functionalization	18
3.1 Chemical functional groups.....	18
3.2 Poly(ethylene glycol)	21
3.3 Biomolecules	23
3.3.1 Biotin, Avidin and Derivatives	25
3.3.2 DNA.....	26
3.3.3 Peptides, Proteins, Enzymes and Antibodies	28
3.4 Fluorescent dyes and other functions, multifunctional particles	30
4 Characterization techniques	32
4.1 Size characterization	32
4.2 Stability, surface and conjugates.....	37

5	Applications, Outlook	39
5.1	Biological applications	39
5.2	Technical applications	43
5.3	Concerns about toxicity.....	44
5.4	Conclusion and Outlook	45
6	Publications	46
6.1	Nanoparticle modification and functionalization.....	46
6.2	Nanoparticle characterization	47
6.3	Collaborative work	48
6.3.1	Materials science.....	48
6.3.2	Biological systems.....	50
7	Bibliography.....	52
8	Appendix [A1] – [A12]	74

Acknowledgement

Wissenschaftlicher Werdegang

Preface

This cumulative work consists of two parts, a general introduction and the collected publications. The introduction is a review about the surface modification of colloidal nanoparticles, with a focus on inorganic core materials, in particular gold and semiconductor quantum dots. After particle synthesis, different strategies like ligand exchange or additional coating layers for phase transfer are discussed, as well as the modification of nanoparticles with chemical functional groups. Bioconjugation of nanoparticles with peptides, proteins or DNA yields to hybrid materials with combined functionality and a number of applications for biolabeling and sensing.

In section 6, the author's publications^[1-14] contributing to the field are briefly summarized and the personal contribution is outlined. As appendix [A1] – [A12], the corresponding papers are attached.

1 Introduction

Colloidal nanoparticles, e.g. inorganic nanocrystals, are very small, nano-scale objects dispersed in a solvent. Already synthesized of gold at the times of Faraday, they generated ever-increasing interest since with the development of high resolution transmission electron microscopy, the ability to synthesize those particles of desired size in a controlled fashion and finally the advent of a broad range of different material systems that have come up in the last few decades. Depending on the material they consist of, nanoparticles can possess a number of different properties such as high electron density and strong optical absorption (e.g. metal particles, in particular Au), photoluminescence in form of fluorescence (semiconductor quantum dots, e.g. CdSe or CdTe) or phosphorescence (doped oxide materials, e.g. Y_2O_3), or magnetic moment (e.g. iron oxide or cobalt nanoparticles).

Nanoparticles with those properties originating from the core material are then used as building blocks for larger, more complex structures, or for hybrid materials e.g. in polymer blends. Besides this, so-called biological applications have gained in importance because they combine the unique properties of inorganic, synthetic nanoparticles with complex biomolecules or biological systems such as cells or even organisms; the most prominent application being labeling for microscopy. Prerequisite for every possible application is the proper surface functionalization of such nanoparticles which determines their interaction with the environment. These interactions ultimately affect the colloidal stability of the particles, and may yield to a controlled assembly or to the delivery of nanoparticles to a target, e.g. by appropriate functional molecules on the particle surface.

This work aims to review different strategies of surface modification and functionalization of colloidal nanoparticles with a special focus on inorganic nanocrystals, in particular the material systems gold and semiconductor nanoparticles, such as CdSe/ZnS. However, throughout the article the discussion also includes other materials as many of the analyzed principles and strategies are often of general nature and apply in the same way to other nanoparticles. Naturally, surface modification starts with an existing surface and yields a new surface with possibly new properties, the area of surface modification taking place between the particle synthesis and final possible applications.

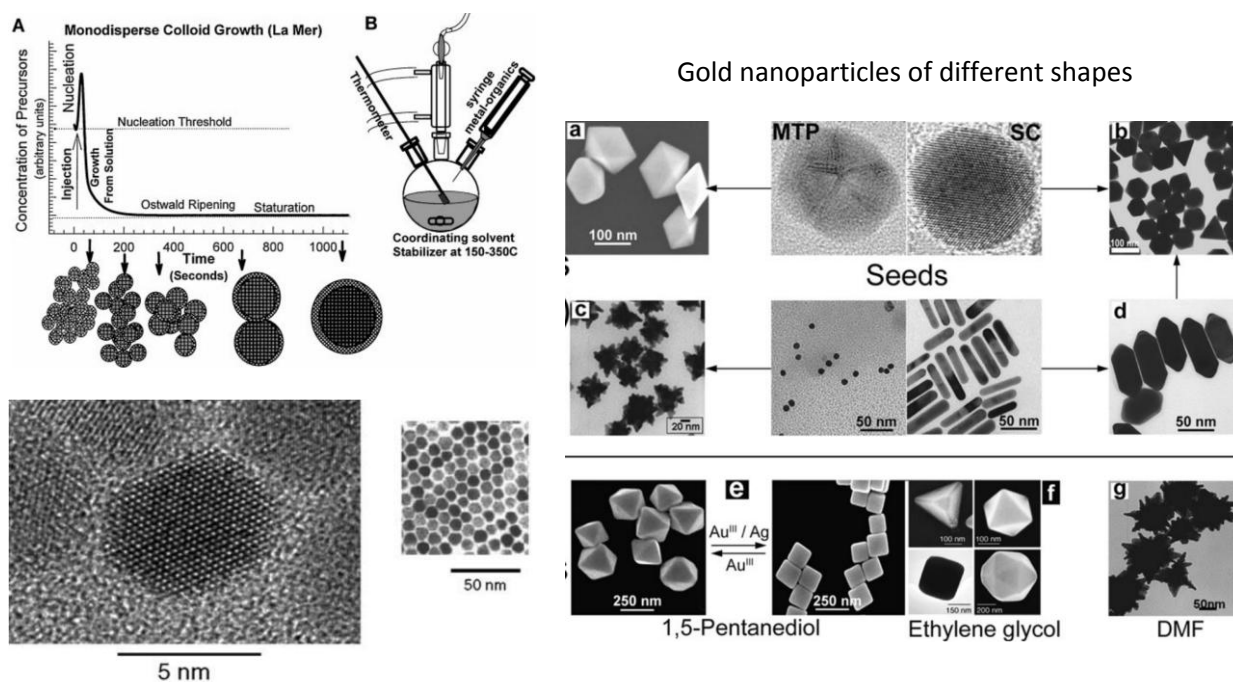


Figure 1: Top left: Scheme of crystal growth over time and typical setup for synthesis in a three-neck flask (taken from reference^[15]). Bottom left: CdSe nanoparticles under high resolution transmission electron microscopy (TEM). On the left image, the crystal structure of a single nanoparticle is seen, the smaller image shows a 2D assembly of particles on the TEM grid (taken from reference^[16]). Images on the right: Gold nanoparticles of different shapes, grown under different synthetic conditions (TEM and SEM pictures, taken from reference^[17], details about the syntheses are found therein).

1.1 Particle synthesis

Nowadays nanoparticles of a large variety of different materials, differing in their elemental composition, size, shape, and physical or chemical properties, can be synthesized.^[15, 18] Colloidal nanoparticles are dispersed in a solvent which can be either water-based or an organic solvent for hydrophilic or hydrophobic particles, respectively, while amphiphilic nanoparticles can be dispersed in both kinds of solvents. The term nanoparticles usually applies to particles between 1 – 100 nm, small particles consisting of only a few to some hundred atoms are often called clusters, and due to their small size which is similar to molecules, the terms dispersion and solution are often equally used.

Gold nanoparticles,^[19] maybe the most common class of such nanoparticles, are generally synthesized by the reduction of gold salts, resulting in nucleation and growth of metallic particles in solution. Aqueous synthesis is nowadays commonly carried out by the citrate-reduction route^[20] that yields gold nanoparticles with a narrow and monomodal size distribution, the average particle diameter can be controlled between about 2 – 200 nm by the stoichiometry of the reagents, i.e. precursor salt and reduction agent. The particles are stabilized by citrate ions bound to the surface of the nanoparticles, resulting in negatively charged particles that repel each other by electrostatic repulsion.

Alternatively, gold nanoparticles can be synthesized by reduction of Au salts in presence of other molecules that bind to the particle surface, control particle growth and provide stability against aggregation. Examples include dimethylaminopyridine – DMAP,^[21] mercaptosuccinic acid,^[22] methoxy-PEG-thiol,^[23] peptides^[24] or dendrimers,^[25] just to name a few. Common to all these

approaches is that the additive molecules have a chemical moiety which is able to bind to the nanoparticle surface, slow down particle growth and eventually yield to a preferred size of the particles induced by the geometry of the micelle-like arrangement of ligand molecules around the inorganic nanoparticle core. In contrast to the citrate method, in these systems particle size can be controlled only in a rather narrow range, depending on the ligand molecules used.

The same principle applies for the synthesis of gold nanoparticles in organic solvents, as pioneered by Brust et al.,^[26] where the Au-containing precursor salt is first transferred to the organic phase by a quaternary ammonium salt. The reduction step takes place in a two-phase system, in which the nanoparticles nucleate in the organic phase inside inverse micelles of the phase transfer agent only^[27] or additional ligand molecules such as dodecanethiol.^[26] The particles usually obtained are monodisperse with a size of typically between 3 – 6 nm, controlled by stoichiometry or reaction conditions, and hydrophobic due to the hydrocarbon chains of the stabilizing ligand molecules. Variations include other thiol-containing ligand molecules,^[28, 29] peptides,^[30] amines^[31] or different solvent systems.^[32-34]

Other syntheses for Au nanoparticles in a single-phase organic solvent employ alkylamines^[35-37] that also can bind to the gold surface of the particles, though not as strong as thiols.^[31] Also other ligand molecules like cetyltrimethylammonium bromide – CTAB,^[38] block copolymer micelles,^[39, 40] thioethers,^[41, 42] poly(ethylene glycol)^[43] or other polymers^[44-46] have been demonstrated. A special system are clusters of gold^[47, 48] or other metals,^[49] very small particles often consisting of a defined number of gold atoms and ligand molecules,^[50-52] the most prominent species probably being Au₅₅.^[53] Recently, also photoluminescent properties have been reported for certain, mostly very small gold nanoparticles.^[9, 54-57]

The next major class of nanoparticles is semiconductor nanocrystal quantum dots, exhibiting unique fluorescent properties. The energy bandgap and thus emission maximum not only depends on the semiconductor material but also on the particle size, the so-called quantum confinement shifts the energy levels further apart when the particles size is decreased,^[58, 59] as already qualitatively described by a simple electron-in-a-box model with the dimensions of the particle core, hence the term “quantum dot”.^[60] By this, fluorescent probes that span a certain range of the optical spectrum^[61] can be generated by particles of the same material, only differing in size. Figure 2 shows typical absorption and emission spectra of a series of CdSe/ZnS quantum dots, and the bandgap energy spanned by a number of different materials. Synthesis is usually carried out by thermal decomposition of organometallic precursors in a coordinating solvent which provides a micelle-like ligand shell that controls the growth of the particles. A common setup is shown in Figure 1 on the top left, a common material system is CdSe in trioctylphosphine/oxide – TOP/TOPO serving as the solvent and surfactant. Alternatively, there are other cadmium-based^[62-64] or different material systems such as ZnS,^[65] InP,^[66, 67] HgTe^[68] or ternary alloys^[69, 70] and synthesis routes taking place in aqueous solution, e.g. for CdS^[71, 72] or CdTe^[73] nanoparticles. In order to increase the fluorescence quantum yield commonly an additional shell of a material with a larger band gap is grown around the nanoparticles which better confines the exciton wave functions and avoids recombination via surface defect states or other non-radiative mechanisms. Beside the popular CdSe/ZnS core/shell quantum dots^[74, 75] also other materials,^[76, 77] multi-shell systems^[78-81] and doped nanocrystals have been

reported,^[82, 83] a more detailed discussion about the synthesis and properties of quantum dots can be found in dedicated reviews.^[18, 84]

For completeness, other material systems should be mentioned such as different metal nanoparticles (e.g. Ni^[85] Ag/Pd,^[86] Fe/Au,^[87]), various alloys,^[88] silicon,^[89] silica^[90, 91] or phosphorescent nanoparticles based on rare-earth-doped materials^[92] such as NaYF₄^[93, 94] or related oxides.^[95] Another class are magnetic materials, including iron oxide (Fe₂O₃ or Fe₃O₄),^[96-103] cobalt^[104-106] or others.^[107-109] Such small nanoparticles consist only of a single magnetic domain and exhibit superparamagnetic behavior, further details can be found in review articles.^[110, 111]

Besides the most commonly found spherical nanoparticles, also other shapes like rods,^[112, 113] tetrapods^[114, 115] or other branched particles,^[116, 117] hollow shells^[118, 119] or other shapes^[120-122] can be synthesized. Usually these are only found for certain core materials and ligand systems that allow the preferred anisotropic growth along certain crystal axes, e.g. by stronger binding of the ligand to certain crystal facets, as discussed in greater detail and with more examples in a number of reviews.^[16, 17, 123-129] On the right-hand side of Figure 1, differently shaped Au nanoparticles are shown.

Recently, also composite particles with domains of different materials have been demonstrated,^[130-135] e.g. heterodimers of CdS and FePt,^[136] Co/CdSe^[137] and others,^[138-140] that can possess e.g. both fluorescent and magnetic properties.

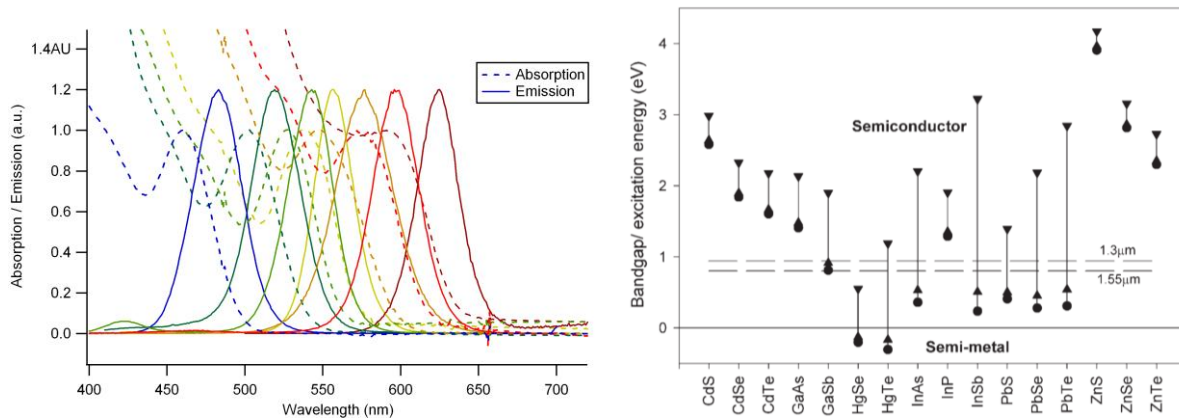


Figure 2: Left: Optical absorption (broken lines) and emission spectra (continuous lines) of different CdSe/ZnS quantum dots samples. Normalized data, same samples drawn in same color. Right: Size-dependent band gap energy of semiconductor quantum dots for different material systems, ranging from 3 nm (triangles on top) via 10 nm particles (lower triangles) to the bulk bandgap (spherical markers, graph taken from literature^[61]).

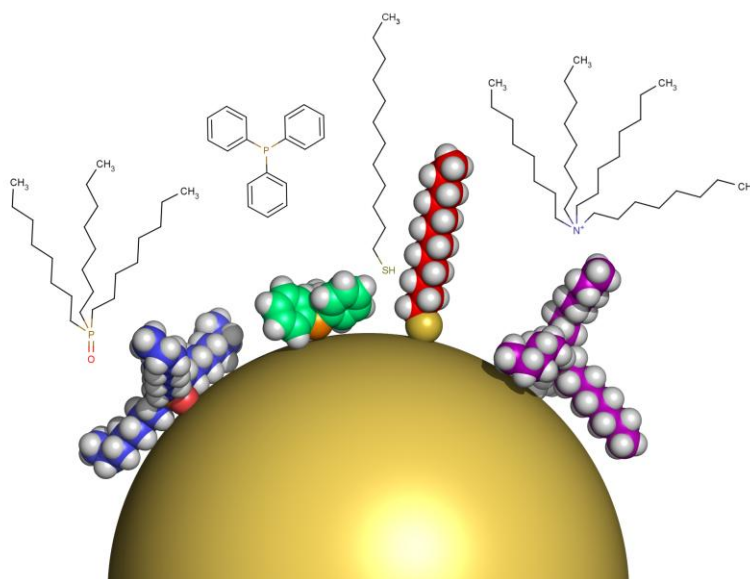


Figure 3: Nanoparticle of 5 nm core diameter with different hydrophobic ligand molecules both drawn to scale. The particle is idealized as smooth sphere, the schematic molecule structures above are not drawn to scale. Left to right: TOPO (trioctylphosphine oxide), TPP (triphenylphosphine), DDT (dodecanethiol), TOAB (tetraoctylammonium bromide). The spatial conformation of the molecules is only shown schematically as derived from their chemical structure and space-filling models.

1.2 Stabilization against aggregation

The ligand molecules bound to the nanoparticle surface not only control the growth of the particles during synthesis, but also prevent aggregation of the nanoparticles. The repulsive force between particles can in principle be due to electrostatic repulsion, steric exclusion or a hydration layer on the surface. Depending on the particle system, i.e. the core material, and the solvent in which the particles are dispersed, the choice of the right ligand might yield to stable particles. First the ligand molecules have to be bound to the particle surface by some attractive interaction, either chemisorption, electrostatic attraction or hydrophobic interaction, most commonly provided by a head group of the ligand molecule. Various chemical functional groups possess a certain affinity to inorganic surfaces, the most famous example being thiol to gold. In many cases, this principle is already exploited during synthesis, as briefly pointed out before. As to the interaction of the ligand molecule with the solvent, polar or charged ligand molecules provide solubility in polar or aqueous solvents while nanoparticles with apolar ligand molecules such as hydrocarbon chains are only soluble in apolar organic solvents, e.g. in hexane, toluene or chloroform. Certain amphiphilic ligand molecules, e.g. poly(ethylene glycol), possess amphiphilic properties, and nanoparticles with those or other ligand molecules can be soluble in a number of solvents with intermediate polarity.

In organic solvents, the nanoparticle surface is covered by hydrophobic ligand molecules that prevent aggregation of the particle cores. However, the bonds between the inorganic nanoparticles surface and e.g. an electron-donating end group of a ligand molecule, such as thiol,^[141-143] amine or phosphine,^[31] undergo dynamic binding and unbinding processes.^[144, 145] This yield to the important consequence that the ligand molecules can get off, e.g. by excessive washing or mass action by another incoming ligand, which might compromise the stability of the nanoparticles that ultimately aggregate and precipitate. In particular, in case of fluorescent quantum dots, irradiation with light can enhance oxidation of the inorganic particle surface^[146] and photo-oxidation may eventually result

in aggregation caused by desorption of the stabilizing ligands.^[146-148] Figure 3 displays some commonly used hydrophobic ligand molecules drawn to scale with a 5 nm particle.

In aqueous solution, the ligand-nanoparticle interaction is basically the same but a number of different effects important for stability arise. Most commonly, hydrophilic nanoparticles are stabilized by electrostatic repulsion by the equally charged ligand molecules on the particle surface. However, in presence of high salt concentration the electric field is shielded and the nanoparticles can come close to each other until eventually attractive forces cause the particles to agglomerate, as e.g. induced dipole interaction, i.e. van-der-Waals force, or hydrogen bonds.^[149] Depending on the isoelectric point (pI) and the pH of the solution, nanoparticles can also lose or change the sign of their charge. While this is in principle well understood and described by theory, nanoparticles are often quite complex objects with properties different to simple model systems: The particles are not spherical hard objects but covered with a soft organic ligand shell of which the charge distribution is in most of the cases not known.^[150] Heterogeneity in the surface coverage can result e.g. in hydrophobic patches on the nanoparticle surface, or the ligand shell can undergo conformational changes dependent on external factors. Furthermore, bi- or multivalent, oppositely charged ions or polyelectrolytes can bridge the particles by electrostatic attraction, again causing aggregation.

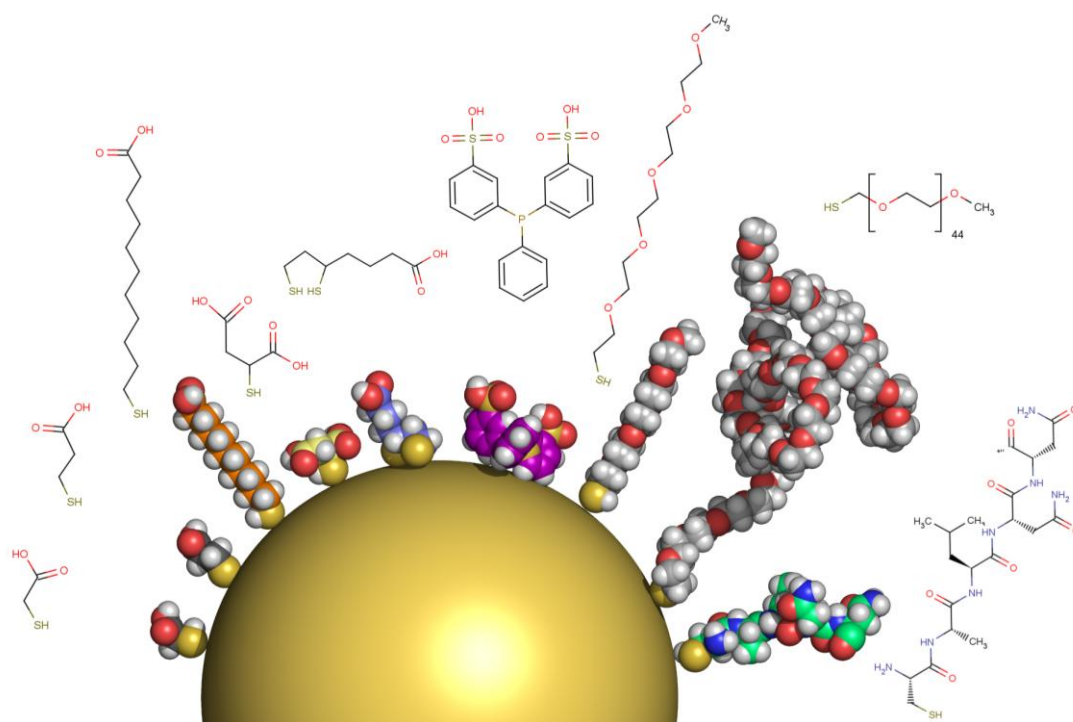


Figure 4: Nanoparticle of 5 nm core diameter with different hydrophilic ligand molecules drawn to scale. The particle is idealized as smooth sphere, the schematic structures of the molecules above are not drawn to scale. Left to right: MAA (mercaptoacetic acid), MPA (mercaptpropionic acid), MUA (mercaptoundecanoic acid), MSA (mercaptosuccinic acid), DHLA (dihydrolipoid acid), bis-sulfonated triphenylphosphine, mPEG₅-SH, mPEG₄₅-SH (2000 g/mol), short peptide (CALNN).

As already pointed out, the possible choice of ligand molecules can depend on the material of the nanoparticle core, the particle size and the solvent. Generally, it is found that strongly binding molecules forming a dense layer stabilize particles better than weakly binding ones, in particular in further processing and purification steps after the particle synthesis. In aqueous solution, strongly charged ligand molecules, containing e.g. carboxylic or sulfonic acid groups, are found to stabilize the

particles for longer time and also at more elevated salt concentrations. Finally, ligand molecules providing steric stabilization are found to be much more resistant to high salt concentrations than electrostatically stabilized nanoparticles,^[23] provided they are strongly bound to the nanoparticle surface, while in the few cases of nanoparticles that are not stabilized by ligand molecules, often poor stability to external factors is observed. Also a combination of electrostatic and steric stabilization is found, e.g. in case of certain polymers^[151, 152] or dendrimers.^[25, 153]

1.3 Ligand exchange

In order to improve the stability of given nanoparticles, the ligand molecules on the surface can be exchanged by others that can possibly provide new properties or functionality to the particles. In most cases, the incoming ligand molecule is binding more strongly to the inorganic nanoparticles surface.

A common example is Au nanoparticles in aqueous solution synthesized by citrate reduction. The resulting nanoparticles have negatively charged citrate ions adsorbed on their surface and are thus stabilized by electrostatic repulsion. While such colloids may be stable for years in the as-synthesized solution, they can not be concentrated well and aggregate irreversibly e.g. in the presence of salts. The citrate layer can be replaced by ligands binding stronger to the particle surface, popular examples include sulfonated phosphines or mercaptocarboxylic acids, common examples being mercetoacetic acid (MAA), mercaptopropionic acid (MPA) or mercaptoundecanoic acid (MUA).^[142] Modifying the nanoparticles with phosphines already allows for achieving highly concentrated particle solutions, the particles can be precipitated by salt-induced aggregation and redissolved again as single particles in low-salt buffers. Then, thiol-containing ligand molecules can be added to again replace the phosphine, a strategy that is commonly employed for the attachment of thiol-modified DNA to nanoparticles. If the particles are not completely saturated with the new ligand molecule, the remaining phosphine molecules covering the surface help to stabilize the nanoparticle.

In organic solution, Au nanoparticles are commonly synthesized by the Brust two-phase method employing tetraoctylammonium bromide and dodecanethiol as stabilizing ligands that also control the size of the resulting nanoparticles. Alternatively, the nanoparticles can also be synthesized in the absence of the thiol ligand, solely with the organic quaternary ammonium ion. In this way, synthesis and final capping of the nanoparticles become independent steps in the synthesis process and the commonly used dodecanethiol can be substituted by a variety of other molecules^[154] in order to vary the surface properties and functionalization of the nanoparticles generated by this synthetic route.

Thiol groups are considered to show the highest affinity to noble metal surfaces, in particular to gold (~ 50 kcal/mol).^[143] While this binding is often termed “chemisorption”, sometimes also noted as covalent bond, the exact processes and the microscopic nature are still subject to research and discussion. Contrary to the case of SAMs on a well-defined planar crystal face, the surface of a nanoparticle consists not only of a number of different crystal facets but also to a large part of edges, terraces and vertices,^[155] resulting in binding sites with different affinities for the ligand molecules. This complicates the characterization of the ligand shell compared to “classical” self-assembled monolayers (SAM), like the well-studied Au-thiol system.^[143] In addition, bound ligands appear to be mobile on the surface, i.e. able to diffuse to some extent on the particle surface after having bound.^[155] In aqueous phase, the replacement of ligand molecules may be facilitated by additional detergents,^[156] and the incoming, stronger binding ligand may render the particles more stable in

regard to possible aggregation at high salt concentrations or acidic pH.^[141, 157] Ligands with two thiol moieties also have been reported.^[158]

The same principles hold for semiconductor quantum dots,^[159] CdSe and CdSe/ZnS among others, that are often stabilized by trioctylphosphine – TOP, or its oxide – TOPO, binding preferentially to the Cd or Zn atoms of the nanocrystals. Also in these systems, binding dynamics and surface diffusion is found,^[160] the surface coverage may depend on the particle size and the geometric shape of the involved ligand molecules.^[161] Besides TOP and/or TOPO, also hexadecylamine or other amines are commonly used ligands for CdSe quantum dots,^[145] which can also be replaced by stronger binding molecules, e.g. with one or more thiol groups.^[144, 162] In case of quantum dots, the ligand shell may influence the fluorescence properties of the particles,^[145, 163-165] in particular the quantum yield, especially in aqueous phase as discussed in the following section.

Furthermore, ligand exchange has also been demonstrated with dendrimers^[153, 166] and thiol-containing peptides in case of gold nanoparticles,^[167] and as well with proteins binding to quantum dots by replacing mercaptoacetic acid on the surface.^[168] The same principles also apply to Au rods, where the replacement of the CTAB double layer by thiol-containing PEG has been reported.^[169, 170]

These considerations imply that for ligand exchange, the new ligand molecules should have an affinity as strong as possible to the inorganic core in order to quickly and effectively replace the original surfactant molecules. In addition, the molecular geometry of the ligands in relation of the particle diameter is a factor that influences how densely the molecules are packed around the particles, which in turn influences ultimately the colloidal stability of the particles.

However, ligand-coated nanoparticles differ from simple micelles consisting of the ligand molecules alone which are only held together by intramolecular forces, in that on nanoparticles, ligand molecules are additionally attached to the nanoparticles surface, in most cases of a chemical functional group. This bond can be electrostatic, e.g. for gold nanoparticles capped with tetraoctylammonium bromide or covalent-like as for instance the gold-thiol bond. Naturally, ligand molecules that are strongly bound to the nanoparticle surface or more tightly to each other will be less subject to get off the particles' surface.^[30, 171] In analogy to the concept of critical micelle concentration (CMC), such ligand molecules bind dynamically to the particle surface and are thus subject to mass action and may be washed off by continued purification of the nanoparticles.^[142]

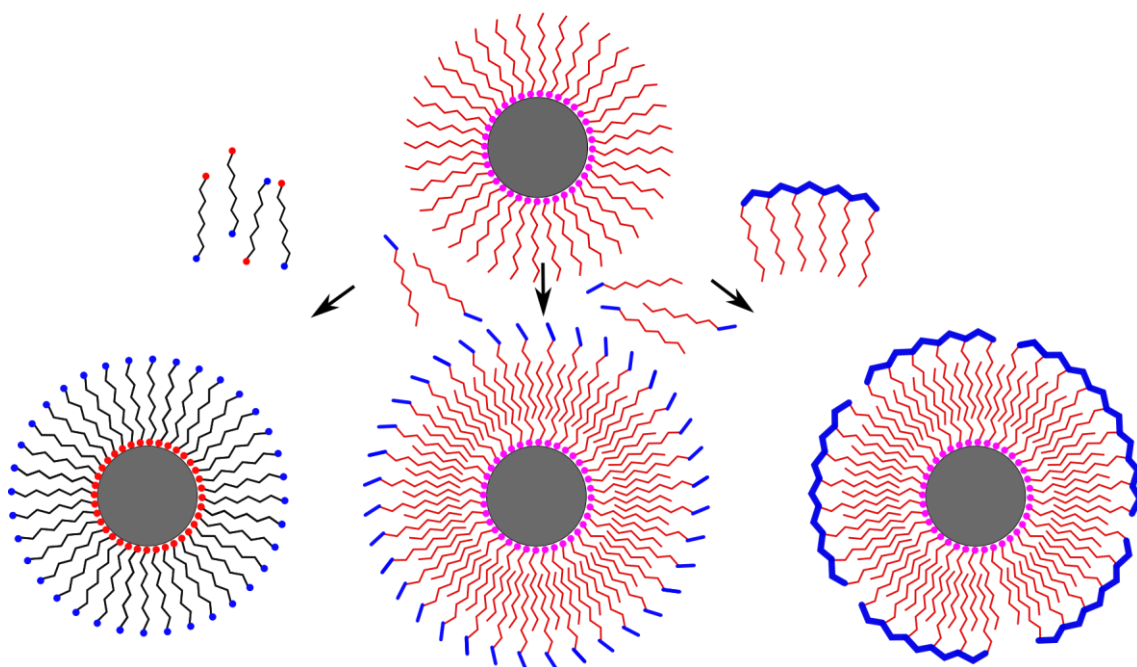


Figure 5: Different strategies for phase transfer of nanoparticles. Left: Ligand exchange, the incoming ligand has one head group binding to the nanoparticles surface (red), the other end (blue) is e.g. hydrophilic. Center: Additional layer of ligand molecules adsorbing e.g. by hydrophobic interaction. Right: Amphiphilic polymer with hydrophobic side chains (red) and a hydrophilic backbone (blue).

2 Phase transfer

Nanoparticles dispersed in a given solvent *A* can be transferred to a different, non-miscible solvent *B*, either from apolar organic solvents to the aqueous phase or vice versa.^[172] This process is termed phase transfer.

Since many types of colloidal nanoparticles are synthesized in organic solvents, for certain possible applications they have to be transferred to aqueous solution, e.g. to be compatible with biological systems. For other applications hydrophobic nanoparticles are required to be compatible with a given solvent/or material system, e.g. for polymers blends,^[5, 173] even though the particles might have been synthesized in aqueous solution. In these cases, phase transfer becomes necessary if the desired particle type can not be synthesized with the corresponding ligand on the surface.

In general, for phase transfer in both directions there exist three strategies: Ligand exchange, ligand modification and additional layers of molecules that stabilize the particles in the desired phase. In addition to these approaches, silanization is also used for surface modification and phase transfer, representing a case in between this classification.

2.1 Ligand exchange

In the ligand exchange strategy, the molecules stabilizing the particles in one phase are replaced by other ligands that allow the transfer to the second phase and provide colloidal stability there. Generally, the ligand molecules compatible with phase *A* are not compatible with phase *B*, and the ligand molecules required to solubilize the nanoparticles in phase *B* are not soluble in phase *A*. So a prerequisite for the exchange to occur is a higher affinity of the new ligand molecule to the surface of the nanoparticle. In this case, the ligand molecules of phase *B* bind to nanoparticles present on the

phase boundary, replacing the original ligand molecules of phase A. Due to the higher binding affinity, finally the ligand molecules are quantitatively replaced and the particle is eventually transferred from phase A to phase B, because the new ligand molecules only solubilize the particle in the desired phase B, but not in A. On the left side of Figure 5 the ligand exchange strategy is sketched.

Commonly used ligand molecules include thiol groups that bind strongly to inorganic surfaces of nanoparticles, e.g. Au and Ag^[174] or CdSe, replacing the weaker bound ligands the nanoparticles usually have from synthesis.

Examples include the transfer of TOP/TOPO-coated CdSe/ZnS quantum dots to aqueous solution by replacing the phosphine-based hydrophobic ligands with a hydrophilic thiol-based molecule, often mercaptocarboxylic acids (e.g. mercaptopropionic acid, mercaptoundecanoic acid, etc.). Variations include derivatives with multiple moieties, e.g. mercaptosuccinic acid (two carboxylic groups),^[146] lipoic acid (or dihydrolipoic acid, resp., with two sulfhydryl groups).^[175, 176] Optionally, the free end of the ligands can also be modified with different residues,^[162] e.g. with poly(ethylene glycol) as demonstrated for Au nanoparticles^[33] or quantum dots,^[177] and often a mixture of different ligand molecules is employed, e.g. to introduce additional functional groups to the particle surface.^[178]

For the transfer of hydrophilic particles to the organic phase the same concept applies, this time one chemical group has to bind strongly to the nanoparticle surface in order to replace the original ligand molecules, the other end has to be of hydrophobic character. Examples include the phase transfer by linear hydrocarbon molecules with e.g. a single thiol or amino group^[179] or molecules with more than one hydrocarbon chain and as well possibly multiple anchor groups,^[158] like dihydrolipoic acid^[175] or other ligands.^[180, 181] Other examples include Au nanoparticles with resorcinarene,^[181] platinum nanoparticles have been transferred to the organic phase by dodecylamine,^[182] as well as CdS particles with octadecanethiol.^[183]

Molecules like mercaptocarboxylic acids that are used to stabilize nanoparticles in the aqueous phase are often readily soluble in organic solvents, e.g. toluene or THF.^[184] Thus transfer from organic to the aqueous phase often occurs spontaneously,^[33, 176] while the transfer of nanoparticles from the aqueous to the organic phase is often more difficult because ligands for the organic phase are often very poorly soluble in the aqueous phase.

In order to facilitate the contact of the nanoparticles with the phase boundary, additional components can be added, e.g. acetone that decreases the surface tension at the interface^[185] or a strong acid^[186-188] or base^[182] that protonates the negatively charged groups (or deprotonates positively charged amino groups), rendering the particle less charged and thus less oleophobic. For a few weakly binding ligands also spontaneous transfer without the help of additional agents has been reported.^[21]

In addition, ligand exchange protocols with amphiphilic molecules have been reported which allow to dissolve the same particles in both polar and apolar solvents. Examples include small molecules that can change their orientation depending on the surrounding solvent^[189] or polymers that can be either nonionic^[190] or ionic like poly(ethylene imine) (PEI)^[191] and poly(acrylic acid),^[192] in which the positively or negatively charged moieties can bind to the inorganic particle surface *and* render the surface of the whole particle polar. In those approaches the ligand exchange takes place in the same

phase in which the nanoparticles are already present but the new ligand molecules are then able to disperse the particles in other solvents.

An important issue in regard to ligand exchange and phase transfer is the stability of the optical properties in case of fluorescent quantum dots. Especially when brought to the aqueous phase, both the particle surface and possibly the thiol group of the ligands are prone to oxidation. Often the fluorescence quantum yield is reduced and desorption of the ligand molecules can eventually yield to aggregation. This effect can be further enhanced by irradiation of the particles with light.^[147, 148]

Hydrophobic nanoparticles of different core materials have been transferred to the organic phase by different polyelectrolytes adsorbing to the inorganic particle surface,^[193] stabilizing the particles by electrostatic repulsion, or by ligand exchange with a PEI-PEG copolymer.^[194]

2.2 Ligand modification

An alternative approach to phase transfer is ligand modification: The ligand molecule stabilizing the nanoparticles in phase *A* is rendered hydrophilic or hydrophobic to transfer and stabilize the particles in phase *B*. Hydrophilic nanoparticles stabilized by a mercaptocarboxylic acid can be modified for instance by a hydrophobic molecule that is chemically bound to its carboxylic terminal groups (e.g. dicyclohexylamine to mercaptoacetic acid^[195]), or by modification with a compound that can change its polarity e.g. by stripping off a capping agent (cyclodextrin rings complexing octadecanethiol,^[196] or by formation of a complex of cyclodextrin with oleic acid present on the nanoparticle surface^[197]), or by covalent attachment an amphiphilic, V-shaped ligand.^[198] The concept of ligand modification might provide efficient phase transfer because the particles are modified with a new ligand in the same phase they are already in. However, it is restricted to certain systems that are compatible with each other and where the colloidal stability of the nanoparticles is maintained during the reaction.

2.3 Additional coating layers

The third strategy for phase transfer is an additional molecular layer on the particles that adsorbs on the original ligand molecules and changes the surface properties accordingly. In this way, a ligand bilayer is formed that allows to transfer hydrophilic particles from the aqueous phase to organic solvents^[199, 200] and as well hydrophobic nanoparticles to water.^[201-203] The molecules acting as phase transfer agents have to be amphiphilic, comprise a hydrophobic and a hydrophilic part, commonly one or more aliphatic chains and a polar, often charged, end group. This approach is sketched in Figure 5 (center) for small molecules and on the right for oligomeric or polymeric molecules.

One common class of such surfactants for the transfer from aqueous to organic phase are quaternary ammonium salts in which four hydrocarbon chains are bound to a nitrogen atom that is thus positively charged, the counter-ions usually being chloride or bromide. Those molecules are known as classical phase transfer agents and are also used in colloidal science not only for the phase transfer of ionic precursors, e.g. AuCl_4^- , to the organic phase (two-phase synthesis, see section 1.1) but for the transfer of hydrophilic nanoparticles to the organic phase as well. The ammonium salt is dissolved in the organic phase and can adsorb electrostatically onto the negatively charged surface of nanoparticles. The actual kind of hydrophilic ligand molecule is not important, the phase transfer can work well with nanoparticles coated with e.g. citrate, sulfonated phosphines or mercaptocarboxylic acids. The quaternary ammonium salts employed for phase transfer include tetraoctylammonium bromide,^[204] cetyltrimethylammonium chloride^[205] and others. After phase transfer, the ligand shell

can again be replaced by strongly binding ligands, like dodecanethiol in the case of Au nanoparticles. In another example, octadecyl-p-vinyl-benzyltrimethylammonium chloride has been used of which the vinyl moiety can be employed for the covalent embedding of particles in a polymer matrix.^[206]

A similar procedure can be applied for transfer of hydrophobic particles to the aqueous phase, for example with cetyltrimethylammonium bromide (CTAB) and dodecylamine-capped Au,^[207] in which the now the hydrocarbon chains of the CTAB adsorb on the octadecylamine layer by hydrophobic interaction while the positively charged ammonium moiety points outwards into solution.

The same approach utilizing an additional ligand layer for phase transfer applies also to lipids that have been used for the coating of hydrophobic nanoparticles.^[89, 208-211] The additional layer conserves the native environment of the inorganic nanoparticles because the original ligand molecules are not replaced. This might be beneficial e.g. to prevent sensitive core materials from oxidation. Due to the additional layer bound by hydrophobic interactions, this coating strategy can be applied regardless of the material of the inorganic particle core. Variations include the embedding of hydrophobic quantum dots into the lipid bilayer of vesicles and liposomes^[212] and paramagnetic lipids that yield fluorescent nanoparticles with additional magnetic properties.^[213, 214]

Naturally, by any additional layer the nanoparticle size is increased, and due to the nature of organic molecules these organic shells appear to be rather soft. In the following, the coating of nanoparticles with amphiphilic and other polymers will be pointed out in more detail.

2.4 Polymer coatings

Although there are a number of well-established variations of phase transfer by ligand exchange, in particular mercaptocarboxylic acid-based ligands for the transfer of nanoparticles from the organic to the aqueous phase, this approach suffers from several drawbacks: i) Small ligands with one head group binding to the nanoparticle surface can easily desorb and impair the stabilization of the particles, especially in solutions free of excess unbound ligands. ii) Although thiol-containing ligands bind relatively strong to various metal particles and quantum dots, in general the ligand molecule has to be carefully chosen to the given core material which is reflected in the large variety of reported protocols.

In contrast, an additional amphiphilic coating layer that adsorbs by hydrophobic interaction to the hydrophobic ligand molecules of the nanoparticles has the advantage that it does not depend on the inorganic core material (and possibly not even on the exact type of ligand molecules) since the adsorption is solely based on hydrophobic interaction of hydrocarbon chains and van-der-Waals forces between the molecules. In case of amphiphilic polymers, many contact points between the ligand molecules and the polymer prevent facile desorption of the polymer molecule from the particle, e.g. by thermal fluctuations. Finally, the coated particles have the same physical and chemical surface properties independent of their core material. On the right side of Figure 5 the approach of an additional shell of polymer molecules is sketched.

One common example includes a poly(acrylic acid)-based polymer with hydrophobic side-chains. Poly(acrylic acid) is a highly charged linear polyelectrolyte, its carboxylic groups can be modified with aliphatic amines via an amide bond.^[215] For the phase transfer of nanoparticles, poly(acrylic acid) with a molecular weight of 2000 g/mol modified with 40 % octylamine (in respect to the number of

carboxylic groups) has been used by Bruchez and coworkers^[216] and is probably also used for commercial water-soluble quantum dots. The comb-like polymer is soluble in organic solvent and can be added to hydrophobic nanoparticles, e.g. quantum dots with TOP/TOPO ligands. After evaporation of the solvent, the solid can be dissolved in an aqueous buffer, yielding stable, single nanoparticles. In order to increase the stability, the polymer shell has been further cross-linked with lysine by EDC chemistry.^[216] The same kind of polymer has been used to disperse quantum dots in ethanol.^[217] A longer poly(acrylic acid) backbone has been modified with a mixture of octylamine and isopropylamine.^[218] Recently the grafting density and length of the hydrophobic side-chains has been studied in great detail,^[219] as well as the modification with aminopentanol^[220] or crosslinking of the shell with diamino propanol,^[221] which resulted in a large number of hydroxyl groups on the particle surface.

Interestingly, also the synthesis of CdTe/CdSe quantum dots has been carried out in presence of poly(acrylic acid) with 40 % modification with dodecylamine,^[222] yielding amphiphilic nanoparticles which were soluble in a number of organic solvents as well as in water, where the polymer is assumed to form a double layer around the particles.

Another closely related class of amphiphilic polymers is based on poly(maleic anhydride) copolymers that are synthesized by copolymerization of maleic anhydride with olefins, resulting in alternating copolymers. When coming into contact with water, the maleic anhydride rings hydrolyze and open, forming two carboxylic groups each. Compared to modified poly(acrylic acid), the hydrophobic side chains are not randomly grafted and the density of carboxylic groups is higher. The phase transfer of hydrophobic nanoparticles of a variety of different core materials has been demonstrated by Pellegrino et al.,^[223] using commercial poly(maleic anhydride alt-1-tetradecene) which is no longer available. The still available analogue poly(maleic anhydride alt-1-octadecene) can be used with an adopted procedure.^[224] A similar commercial derivative with tertiary amino groups has also been used for nanoparticle coating and phase transfer^[225] saving the step of postmodification with dimethylethylenediamine and EDC.^[226]

An extremely useful property of the maleic anhydride moieties is their spontaneous reactivity towards primary amines (and to alcohols under acidic conditions) which can be exploited for a pre-modification of the polymer before it is used for particle coating.^[2] Each maleic anhydride ring yields a free carboxylic group after reaction with the amine. This has been demonstrated for poly(ethylene glycol)^[227] resulting in nanoparticles with increased stability, e.g. in biological environment.^[228]

Recently, another design for amphiphilic polymer has been presented combining the advantage of maleic anhydride moieties for pre-modification and custom modification with side-chains.^[2] Hydrophobic side-chains consisting of dodecylamine are grafted to a poly(maleic anhydride)-based backbone, leaving a part of the anhydride rings intact. If desired, additional functional molecules like fluorescent dyes, sugars, biotin or PEG can be covalently grafted to the polymer if they exhibit an amine function. This again saves the additional steps and purification of postmodification with additional crosslinkers.

The discussed comb-like amphiphilic polymers used for nanoparticle are made up of either an alternating or random sequence of building blocks that consist commonly of aliphatic chains as hydrophobic elements and charged groups as hydrophilic parts. The hydrophobic side chains cover or

intercalate the hydrophobic ligand molecules of the nanoparticles while the hydrophilic backbone is exposed to the outside aqueous environment. Even though the attraction between polymer and the particle is due to rather weak van-der-Waals forces between the aliphatic chains, the hydrophobic interaction and the large number of contact points by the several side-chains of the polymer result in a very stable coating. By this, the thickness of the shell is increased by only one additional monolayer of polymer and, due to the nature of the interaction, this coating approach works in principle for any hydrophobic nanoparticles regardless of the inorganic core material.^[2, 7, 223]

Nanoparticles can also be directly synthesized in presence of such polymers,^[222] or other weakly adsorbing species like poly(vinyl pyrrolidone), PVP.^[229] Furthermore the particle modification by adsorption of polyelectrolytes has been reported, either as additional layer^[230] or replacing the original surfactant^[192, 193] of different core materials. As shown by Nann, quantum dots coated with branched poly(ethylene imine), PEI, could be dispersed in both aqueous and organic solution,^[191] the primary amino groups either binding to particle surface or pointing outwards to solution.

A variety of other multi-dentate polymer has been demonstrated to coat nanoparticles by direct binding to the inorganic particle surface: Hydrophilic and hydrophobic oligomers with phosphine anchor groups^[173] and a PEG-modified polymeric variant with phosphine oxide that can be used for phase transfer of different core materials to aqueous solution.^[231]

Other comb-like polymers contain a mixture of simple aliphatic side-chains and others with primary amines at their ends. The polymer can bind to the nanoparticle surface via the amino groups, additionally, it was modified by fluorescent dye molecules.^[232] A similar polymer was used to transfer negatively charged quantum dots to organic solution, after electrostatic adsorption of the polymer by its amino groups.^[233] Also a polymer with tertiary amines and pyrene as fluorescence marker^[234] has been shown to stabilize quantum dots in organic solution. In addition, poly(acrylic acid) modified with free thiol and amino groups at the ends of the side chains has been demonstrated as coating for quantum dots, resulting in a relatively thin shell with apparently little effect on the quantum yield of the particles after transfer to the aqueous phase.^[235]

Alternatively to coating particles with amphiphilic or other polymers, nanoparticles with a polymer shell can be obtained by lateral crosslinking or polymerization of the small molecules forming the ligand shell,^[29, 236-238] or in an alternative approach by growing a polymer off the particle surface from the attached ligands.^[239]

Yet another class of again amphiphilic polymers used for the coating of nanoparticles is block-copolymers, consisting in general of a hydrophobic and a hydrophilic part, the latter potentially a polyelectrolyte. These polymers form micellar structures with their hydrophilic or hydrophobic part inside, in contrast to the respective solvent in which they are dispersed. Such structures can be used for the synthesis of nanoparticles,^[240-242] coating^[243] and for phase transfer; certain copolymers were also laterally cross-linked.^[244, 245] The thickness of the polymer shell can be adjusted by the choice of polymers with appropriate block lengths.^[246] In a number of cases, the coating by block-copolymer micelles does not yield individual particles but a few to many particles inside the same micelle,^[247] which in turn can be exploited for the generation of multifunctional objects in case of nanoparticles of different materials.^[248] Besides of the few examples given here, a much more detailed discussion

of block-copolymers, the grafting-from approach and other polymers used for nanoparticle coatings and composite materials can be found in a recent review.^[249]

Finally, dextran-coated nanoparticles, in particular iron oxide, are readily obtained by the synthesis carried out in presence of the polymer, as already mentioned in a previous section, as well as nanoparticles with dendrimer shells. Nanoparticles coated with poly(ethylene glycol) will be discussed in Section 3.2 about chemical surface modification, if not already mentioned previously in the case of PEG-containing small ligands.

2.5 Silanization

Nanoparticles of different core materials can also be modified with a silica shell, which can be considered as an inorganic polymer. The method comprises first a ligand exchange procedure in which a first layer of silanes is bound to the nanoparticle surface. Then, using this first layer, a polymeric, cross-linked inorganic silica shell is deposited on the particles which can be further derivatized. Nanoparticles of different materials,^[250-252] in particular noble metals^[253] (Au,^[254, 255] Ag^[256]), fluorescent quantum dots (CdSe/ZnS^[257-259]), phosphorescent^[92] and magnetic nanoparticles (e.g. Fe,^[260] Co,^[261] CoFe₂O₄^[108]) and particles of different shapes have been coated with silica shells.

This technique is outside the focus of this work, however, in the following sections many concepts and techniques equally apply to silica-coated nanoparticles as well, since the inner material composition is in principle not important for further conjugation steps. More detailed descriptions of successfully applied silanization techniques can be found in the work of the different groups cited above.

2.6 Comparison and remarks

The described methods for phase transfer reflect general strategies which, however, may not be applicable to any particular or given particle system. The critical issue of the phase transfer of colloidal nanoparticles is their colloidal stability. Nanoparticles are stabilized in one phase *A* and shall be transferred to another, non-miscible phase *B*, where the particles are at first not able to disperse. In the process of the phase transfer, e.g. by ligand exchange, modification or additional coating, the particles might partially lose their surface properties to be stably dispersed in phase *A*, while not yet being 'compatible' with phase *B*. This is the moment in which aggregation and precipitation of particles can occur, possibly in an irreversible manner.

These considerations imply that for phase transfer, as well as for ligand exchange in 1.3, the binding affinity of the ligand molecules and their geometric shape in relation of the particle diameter has a strong influence on how rapidly the particle surface is changed and how densely the ligand molecules are packed on the particle surface, respectively. Both factors ultimately determine how efficient the phase transfer works and how stable the nanoparticles will be in the new phase.

3 Particle Functionalization

3.1 Chemical functional groups

Ligand particles stabilizing the nanoparticles against aggregation can simply consist of an inert molecular chain (hydrocarbon chain or PEG) or have functional groups which are in most cases terminating linear molecules (see above). In the case of water-soluble nanoparticles these functional groups are often carboxylic acids stabilizing the nanoparticles by electrostatic repulsion, and can be exploited for the conjugation of other molecules to the particles. Common examples include Au nanoparticles or quantum dots stabilized with mercaptocarboxylic acids.

In the same way, other functional groups can be introduced to the nanoparticle by their ligand molecules or a mixture of different ligands. Already in the organic phase, for instance the dodecanethiol monolayer of Au nanoparticles can be modified with bifunctional ligands by place-exchange reactions to introduce e.g. bromide, ferrocene, hydroxyl, carboxyl functional groups.^[48, 51]

This strategy can also be applied for phase transfer by ligand exchange, when the incoming ligand already contains the desired functional group, as demonstrated for hydrophobic CdSe/ZnS quantum dots and ligands comprising e.g. $-\text{COOH}$, $-\text{OH}$, $-\text{NH}_2$,^[262-264] or CdTe and for instance a mixture of MPA and aminoethylthiol.^[265]

Quantum dots in aqueous solution stabilized with mercaptoacetic acid have been modified by co-adsorption of thiol-containing PEG and short peptides.^[266] In the case of lipid-coated quantum dots a part of the lipids can carry e.g. amino groups or PEG^[208] in order to add additional functionality and steric stabilization.

Iron oxide nanoparticles with (di)mercaptosuccinic acid have been shown to exhibit both carboxylic and thiol functional groups.^[267, 268]

Another interesting case are quantum dots stabilized with mercaptoacetic acid to which a protein (BSA) was adsorbed. The amino groups of the protein could then be exploited for further conjugation chemistry.^[168]

Alternatively, functional groups present on the nanoparticle surface can be converted to other functional groups by bifunctional molecules. Especially in case of nanoparticles dispersed in aqueous solution the reaction conditions may harm the stability of the nanoparticles, so often rather mild reactions have to be chosen like they are applied for the chemical modification of biomolecules (bioconjugation chemistry), a large number of bifunctional molecules are commercially available.^[269] The commonly found carboxylic groups can be reacted with primary amines by means of a condensation reaction to yield amide bonds. For this, a water-soluble carbodiimide (e.g. EDC) is commonly used, cf. Figure 6. After forming an intermediate compound with the carboxylic moiety, the activated group is reactive towards primary amines. In case of primary amines present on the particle surface, active ester compounds (N-hydroxy-succinimide, NHS) can be used to equally form amide bonds, one example is SMCC containing a NHS group reacting with primary amines, converting them to maleimides that are reactive towards thiols,^[270] as sketched on the right of Figure 6. There are a number of other crosslinker molecules and different derivatives available, for instance with

sulfo-NHS functionality and/or hydrophilic spacer arms of different length to improve water-solubility.

The majority of ligands molecules or additional amphiphilic coatings stabilize the nanoparticles by negatively charged carboxylic groups. These can be converted e.g. to hydroxyl groups^[221] or tertiary amines.^[226] Primary amines are commonly introduced by partial conversion of functional groups, for instance carboxylic acids, by (partial) ligand exchange or adsorption of polyelectrolytes.^[178, 193, 230, 262, 263, 265, 271, 272] At pH values below the pK value of the amines, the particles are positively charged and can be prone to aggregation during the modification steps, e.g. by ligand exchange. Silica coating, however, seems to yield very robust nanoparticles functionalized with primary amines.^[255, 273]

In the last few years, click-chemistry attracted much attention^[274, 275] and has also been applied to nanoparticle derivatization in both organic^[276, 277] and aqueous solution,^[278-280] as well as to e.g. polymer nanoparticles^[281] and carbon nanotubes.^[282] The concept of click-chemistry consists of “spring-load”-like chemical reactions that occur spontaneously and with high yield and selectivity between stable functional groups under mild conditions,^[283] the perhaps most common example between alkyne and azide moieties in presence of a catalyst.^[284]

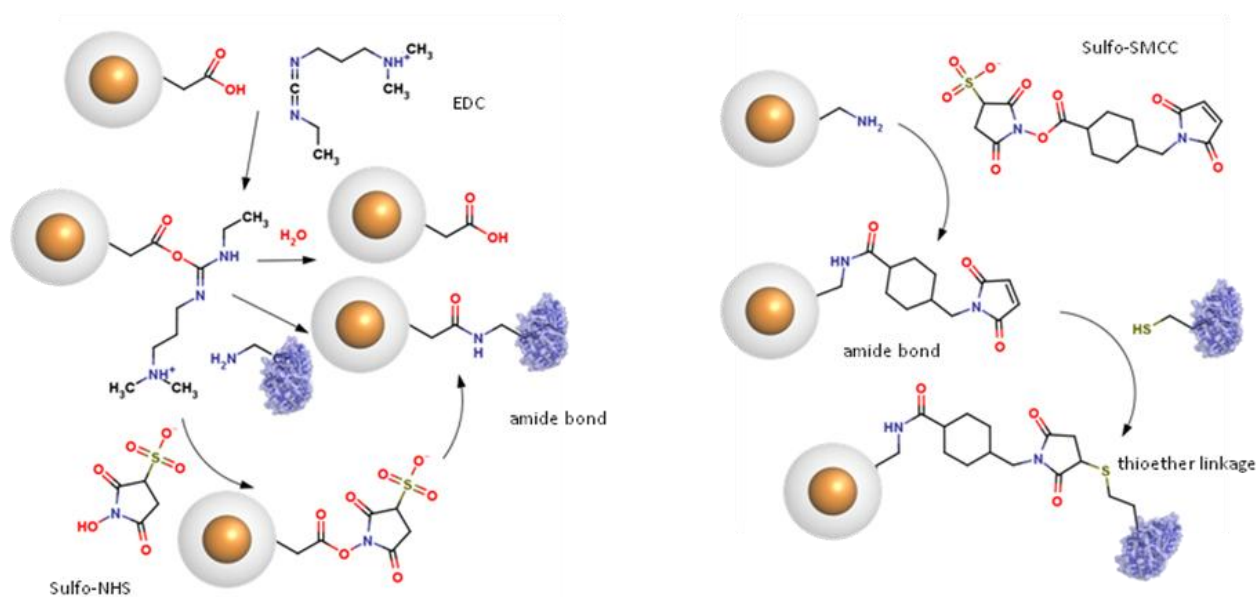


Figure 6: Left: Common conjugation reaction for particles with carboxylic acid function: The water-soluble carbodiimide EDC forms an unstable intermediate, a so-called “activated” carboxylic group. This can either hydrolyze or react with a primary amino group under formation of a stable amide bond. Optionally, the it can be reacted with NHS or sulfo-NHS, the active ester has an extended half-life and reacts also with primary amines. Right: Particles with primary amino groups can be reacted with active ester compounds to form amide bonds. Sulfo-SMCC is a heterobifunctional crosslinker with an sulfo-NHS group and a maleimide function on the other end that is reactive towards thiol groups.

Common to all chemical surface modification schemes involving functional groups that are present on the nanoparticle surface is that they solely depend on the ligand shell or surface coating, not on the actual inorganic core material. Therefore, provided that the nanoparticles are stable under the reaction condition and subsequent purification, the same chemical routes for functionalization apply for Au nanoparticles, quantum dots or magnetic particles,^[270-272] as well as for silica nanoparticles.^[285]

Since the surface of nanoparticles is covered by a large number of ligand molecules ranging from some tens for small clusters to hundreds or thousands, the number of functional groups per particle generally exceeds a few, is given by a statistic distribution and not always easily accessible by analytic methods. Due to the multivalency of nanoparticles, only rather simple structures like particles surrounded by molecules or other particles can be easily generated, or inter-particle crosslinking can occur in experiments with other multivalent objects.

For a number of applications, monovalent particles or particles with a defined number of functional groups are desirable, and several strategies to prepare such particles have been found in the last years. The principle difficulty is that nanoparticles consist of many identical atoms and a number of equal surface facets, so in the first instance all particle modification will be subject to statistics involving competing equivalent binding sites. One obvious approach is therefore dilution or stoichiometric control, i.e. to adjust the experimental conditions in a way that only a minor fraction of nanoparticles reacts at all to a certain molecule with the desired function, leaving the other particles unmodified and eventually only a negligible fraction that has two or more modifications. One way is then to separate the modified particles from the unmodified majority, as shown e.g. by Levy et al.,^[171] where Au nanoparticles modified with a polypeptide could be immobilized on an affinity column by a oligohistidine domain present in the peptide. After washing out all unbound particles, the immobilized particles could be eluted by addition of imidazole yielding particles modified with a single peptide with a single amino group at its terminal end.

Another way uses methods from solid-phase peptide synthesis where the solid phase (a resin-packed column) is modified with a cleavable, thiol-terminated molecule at very low grafting density.^[286-288] When the distance between two thiol-terminated molecules is (in average) orders of magnitudes larger than the particle diameter, every gold nanoparticle binding to the resin via a thiol-gold linkage is only bound by one single molecule. After washing out all unbound particles, the linker arm is cleaved and the nanoparticles are eluted from the column, each particle carrying one single fragment of the linker arm exhibiting a single free functional group. A variation of this concept includes ligand molecules electrostatically adsorbed on the solid phase.^[289, 290]

Alternatively, there are a number of systems and separation methods that allow the statistical binding of a few ligand molecules to the nanoparticles and the subsequent separation according to the number of attached molecules. For this, each attached molecule has to change at least one property of the particle sufficiently in order to allow separation, e.g. by size or electric charge. This concept probably has been first developed for small gold clusters of which fractions with a different number of e.g. amine-containing ligands could be separated by ion exchange chromatography.^[291] Monofunctional gold clusters prepared by this method have already been commercially available for several years.

As shown for larger gold nanoparticles modified by single-stranded DNA oligomers with a thiol function, particles with exactly 0, 1, 2, 3... attached DNA molecules could be separated by gel electrophoresis.^[292] The attachment of each additional DNA molecule renders the Au nanoparticle significantly larger, so that the fractions appear as discrete bands on the gel. Depending on the nanoparticle size, this effect appears above a certain molecular weight or number of base pairs of the DNA, resp. Dependent on the agarose concentration, separation is observed for instance with 43 bases in case of 10 nm but not of 20 nm nanoparticles,^[4] or by means of a long extension strand

hybridized to the short first one.^[293] The fractions of particles can be extracted from the gel and the defined number of functional groups (here: DNA molecules) has been probed by the controlled assembly of particle groupings.^[293-295] The restriction to DNA molecules of a certain size that allow the complete separation of the different fractions has recently been elegantly overcome by ion exchange chromatography,^[296] demonstrating the separation of 20 nm Au nanoparticles with a defined number of short DNA molecules (15 bases).

Separation by gel electrophoresis has been applied to polymer-coated nanoparticles which have been modified with poly(ethylene glycol).^[1] When the PEG had a molecular weight ≥ 5000 g/mol, discrete bands could be separated by gel electrophoresis, and by employing bifunctional PEG nanoparticles with a defined number of chemical reactive groups could be prepared (cf. Figure 7). Based on the same principle, quantum dots with a defined number of maltose binding protein^[297] and a single monovalent streptavidin molecule have been demonstrated recently,^[264] which allowed the preparation of quantum dots conjugated with single antibodies.

Finally, it is worth to mention two other concepts have recently developed, one exploiting a general topological feature for the attachment of two functional groups by exchanging two ligands at singular positions of the nanoparticle surface^[298, 299] the other by polymerizing the vinyl-thiophenol ligand molecules attached to the nanoparticle surface, resulting in nanoparticles with only one single carboxylic group left, and only smaller fractions or particles with two or more groups.^[300]

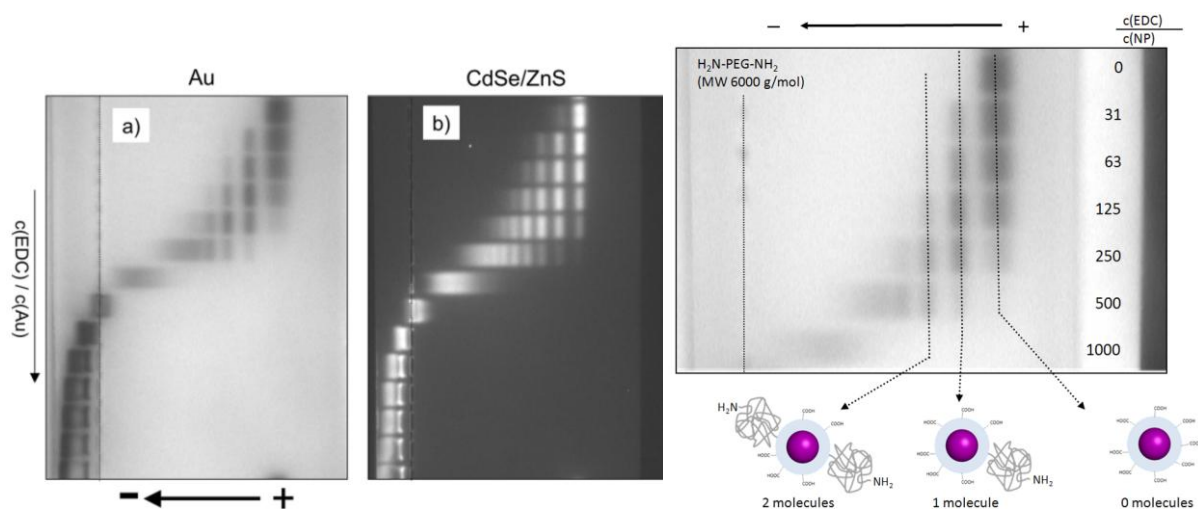


Figure 7: Left: Gel electrophoresis of polymer-coated, PEG-modified Au and CdSe/ZnS conjugates. Stoichiometric ratio of EDC/NP was increased from top to bottom, yielding to nanoparticles with an increased number of covalently bound PEG molecules. With a molecular weight of ≥ 5000 g/mol, discrete bands of particles with exactly 0, 1, 2, 3 ... PEG molecules are resolved. At very high EDC concentrations, the nanoparticles are saturated with PEG and migrate towards the negative electrode. Right figure: With bifunctional PEG molecules, this allows for preparation of nanoparticles with controlled valency, i.e. a defined number of functional groups. Nanoparticles modified with $\text{H}_2\text{N-PEG-NH}_2$ yield nanoparticles with exactly one or two amino groups, separated by gel electrophoresis.^[1]

3.2 Poly(ethylene glycol)

Poly(ethylene glycol), PEG, is a linear polymer consisting of repeated units of $\text{CH}_2\text{-CH}_2\text{-O}$, depending on the molecular weight the same molecular structure is also termed poly(ethylene oxide) or polyoxyethylene, PEO or POE, respectively. The polymer is well soluble in a number of organic polar and apolar solvents, as well as in water where it is heavily hydrated, forming random coils with diameters much larger than proteins of comparable molecular weight. Due to its simple structure

and chemical stability, it is a prototype of an inert, biocompatible polymer. The inertness and non-toxic properties of PEG give rise to a number of applications in medicine, chemistry or biotechnology: PEG is used for nonionic surfactants and as additive in cosmetics, pharmaceuticals and food. When bound to surfaces,^[301] PEG repels other molecules by steric effects, the incoming molecule is not attracted by e.g. electrostatic force and can not penetrate the hydrated PEG layer. This results in inert hydrophilic surfaces with less “stickyness”. The same applies for molecules or particles: PEG-modified proteins^[302] or drugs show increased water solubility and decreased immunogenicity in organisms, antibodies bind much less to the drug or protein, resulting e.g. in an increased half-life in the blood stream. PEG-modified nanoparticles are more stable at high salt concentrations and in biological environments, they show less nonspecific binding to proteins and cells.^[178, 303-306]

The modification of other molecules with PEG is often called “PEGylation”, for proteins, PEG with functional groups is coupled to certain amino acids, most commonly lysine and cysteine, exhibiting amino and cysteine groups, respectively. An increasing variety of mono-, homo- and heterobifunctional PEG reagents is commercially available, with different functional groups, molecular weights and multiple arms.^[307] Those reagents can be used for the PEGylation of synthetic nanoparticles in the same way as for proteins and coupled to available functional groups on the nanoparticle surface, provided by the ligands or additional shells.^[304, 308]

While monofunctional PEG molecules, e.g. with a methoxy group at the free end, yield basically more stable and inert particles,^[169, 309] bifunctional PEG molecules can be used to introduce new functional groups on the surface, like with bifunctional crosslinkers in conjugation chemistry.^[310] In particular mixed PEG layers of mono- and bifunctional molecules are useful because they stabilize the particles by sterically by PEG molecules without free functional end and provide a number of new functional groups by the bifunctional PEG molecules.^[1, 170, 178] Again, the conjugation chemistry used for PEGylation and the further modification does not depend any more on the material of the particle cores and applies in the same way for other particle species.^[311, 312]

Apart from the post-modification approach by covalent chemistry, PEG-modified nanoparticles can be also obtained by ligand molecules that contain a block of PEG^[177, 263, 264] or entirely consist of PEG with a functional group that can bind to the nanoparticle surface.^[305, 313] Again, particle synthesis can already be carried out in presence of these ligands,^[23, 43] new PEG-containing ligands can be introduced by place-exchange reactions or added as additional molecules like lipids^[208, 211] or polymers^[194] that have been modified with PEG before used for the coating process.^[2] As already discussed, such PEG-containing ligands can be used for phase transfer of nanoparticles,^[33, 314] and due to the solubility of PEG itself also PEG-coated nanoparticles can be dispersed in polar organic solvents like chloroform, methanol, DMSO and DMF.^[166]

As for any additional shell, the overall particle diameter is increased by PEG modification. Increasing grafting density and molecular weight of the employed PEG molecules yields to thicker shells that can be found in order of a few to tens of nanometers,^[3] the thickness of about the order of the hydrodynamic diameter of a free PEG molecule that forms a random coil.^[315, 316] In Figure 8 (left), PEG with a MW of 2000 and 5000 g/mol is drawn to scale with a 10 nm nanoparticle (core: 5 nm).

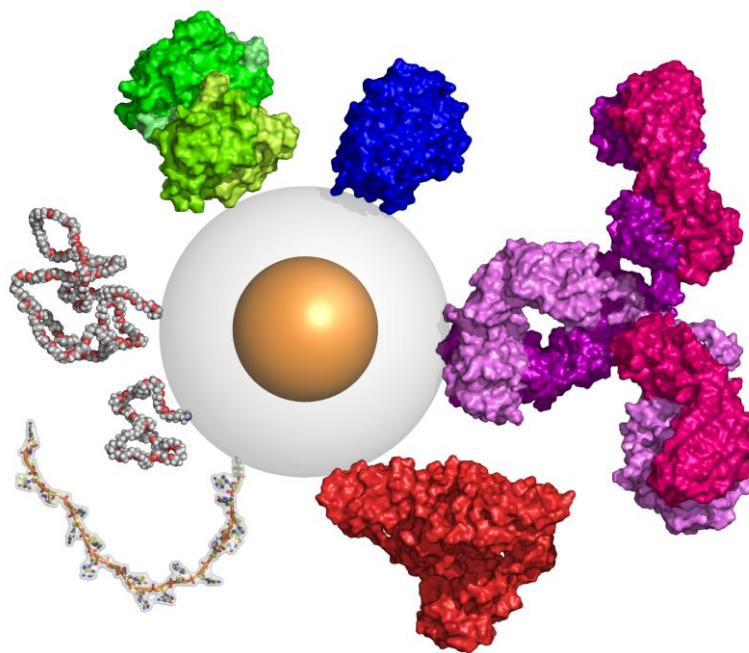


Figure 8: Relative size of nanoparticles and biomolecules, drawn to scale. Schematic representation of a nanoparticle with 5 nm core diameter, 10 nm shell diameter, with PEG molecules of 2000 g/mol and 5000 g/mol (on the left, light grey), streptavidin (green), transferrin (blue), antibody (IgG, purple), albumin (red), single-stranded DNA (20mer, cartoon and space-filling). Proteins are crystal structures taken from Protein Data Bank (<http://www.rcsb.org>), PEG and DNA have been modeled from their chemical structure and space filling.

3.3 Biomolecules

Bioconjugation of colloidal nanoparticles is the “natural” extension of the described concepts of ligand exchange and chemical functionalization to biomolecules. Nature offers a large variety of organic molecules of different composition, size and complexity that serve to provide structure and function to biological process and organisms. Examples include on the one hand small molecules like lipids, vitamins, peptides, sugars and larger ones such as natural polymers including proteins, enzymes, DNA and RNA.

Conjugation of inorganic nanoparticles to biomolecules generates hybrid materials that can be used to let the nanoparticles interact specifically with biological systems. On the other hand, biomolecules can be seen as ordinary, though sometimes complex, molecules or polymers that can be exploited for the functionalization or spatial assembly of nanoparticles. Nanoparticle-biomolecule conjugates bring together the unique properties and functionality of both materials, e.g. fluorescence or magnetic moment of the inorganic particles and e.g. the ability of biomolecules for highly specific binding by molecular recognition.

The strategy for the conjugation of biomolecules to nanoparticles generally falls into four classes:

- Ligand-like binding to the surface of the inorganic particle core, commonly by chemisorption of e.g. thiol groups
- Electrostatic adsorption of positively charged biomolecules to negatively charged nanoparticles or vice versa

- Covalent binding by conjugation chemistry, exploiting functional groups on both particle and biomolecules and
- Non-covalent, affinity-based receptor-ligand systems, as discussed in the following.

Besides the first three approaches, affinity-based systems found in nature have attracted increasing attention during the last years. Maybe the most well-known example in the last several decades is the avidin-biotin system.^[317-320] Based on molecular recognition, the system consists of a ligand, the small molecule biotin (vitamin H), and a receptor, the protein avidin that is present e.g. in egg white. The globular protein avidin is made up by four identical subunits, yielding four binding pockets that specifically recognize and bind to biotin (Figure 9, left). The dissociation constant is of the order of 10^{-15} M and the bond, though not covalent, is found to be extremely stable, resisting harsh chemical conditions and elevated temperature. Besides the natural glycoprotein avidin (pI ~ 10), analogue proteins expressed in bacteria or recombinant proteins without carbohydrates and a near-neutral pI are available, the most common streptavidin and neutravidin. Also monomeric streptavidin with however reduced affinity to biotin has been reported^[321] and by genetic modification resulting in deactivated binding pockets, a tetrameric but monovalent streptavidin derivative with only one single binding site for biotin has also recently been demonstrated.^[322]

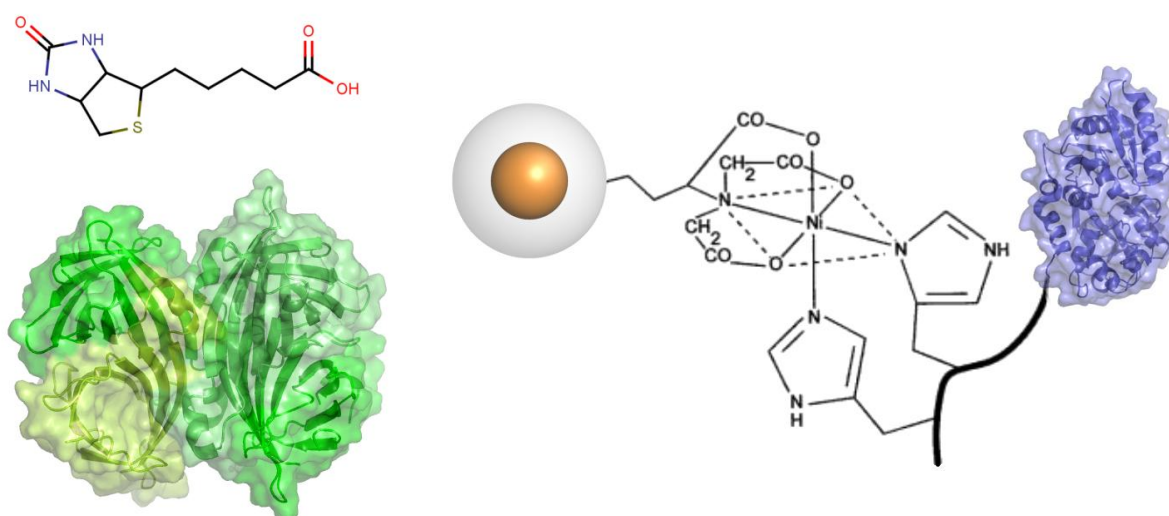


Figure 9: Left: Structure of biotin (top) and streptavidin (bottom). Streptavidin is a ~ 53 kDa protein of four identical barrel-like subunits, each tetrameric protein has four binding sites for biotin. Right: Schematic drawing of NTA- Ni^{2+} attached to a nanoparticles forming a complex with a protein with two terminal histidine residues (image of NTA-histidine complex adopted from literature^[323]). All objects are not drawn to scale in respect to each other.

The strong bond and specificity of the biotin-avidin system has allowed to employ it for a large number of applications in bio(nano)technology, and a large variety of biotinylation reagents and biomolecules like DNA oligomers, peptides, antibodies and fluorescent dyes readily modified with biotin or avidin (or one of its derivatives) are commercially available. Nanoparticles modified with biotin or avidin enable these materials to be used within the technologically already well-established conjugation platform.

So-called protein tags are another class of such affinity-based systems and commonly used for protein purification: Proteins can be expressed with additional fusion proteins or short amino acid sequences by genetic engineering in order to manipulate the desired protein by this handle-like tag. One example is the protein hAGT that binds specifically and eventually by a covalent bond to benzylguanine.^[324] Another well-known system is polyhistidine, commonly introduced by six or more histidine residues to one of the terminal ends of a protein. Polyhistidine is found to bind strongly and specifically to nitrilotriacetic acid (NTA) via a chelating complex with Ni²⁺ or other bivalent metal ions, as sketched in Figure 9 (right). This system is widely used for affinity purification of proteins that have been expressed with this polyhistidine tag: These proteins are specifically immobilized on a column with Ni-NTA. After washing out other unmodified molecules, the desired protein is eluted with an excess of imidazole that competes with polyhistidine in binding to the Ni-NTA complex. Systematic studies with two, three or more NTA groups^[325] revealed that three NTA moieties can bind to a strand of six histidines, resulting in a stable bond of higher binding energy compared to other stoichiometries.

A more detailed review about the NTA-polyhistidine system can be found in the seminal work of Hainfeld et. al. who modified small Au clusters with NTA-terminated ligands^[323] which were then used to label proteins by their polyhistidine tag for electron microscopy. In the following, also larger Au nanoparticles^[326] and quantum dots^[327, 328] have been modified with NTA-containing ligands, as well as silanized iron oxide nanoparticles^[273] by conjugation of amine-containing NTA to carboxylic groups on the particle surface. After loading the NTA groups with bivalent ions, the modified particles could be used for conjugation to proteins with polyhistidine residues. It remains to be noted that in many of the systems mentioned here in fact several single NTA moieties were present that could bind together to the same oligohistidine residues of the proteins.

Mattoussi et al. reported the specific and strong binding of polyhistidine-containing proteins to CdSe/ZnS nanoparticles with a DHLA ligand layer^[175] without NTA or bivalent ions present. Recently it was shown that the polyhistidine moiety can directly bind to the inorganic particle, apparently to Zn atoms present in the ZnS shell^[329] as demonstrated by control experiments with different target molecules and ligands without NTA or free carboxylic groups. In this seemingly robust self-assembly approach, no conjugation chemistry and only few purification steps are necessary which led to the conjugation of quantum dots with a number of different proteins for a variety of applications.^[178, 330]

3.3.1 Biotin, Avidin and Derivatives

The biotin-avidin system consists of a small molecule (biotin) and a protein either with (avidin) or without carbohydrates (streptavidin, neutravidin and other derivatives). Here, in order to avoid later redundancy, both species serve as examples for the discussion of different conjugation strategies of small and large biomolecules to nanoparticles, which apply accordingly to a number of different biomolecules such as DNA, antibodies, peptides or generic proteins. Afterwards, the linking of those different classes of biomolecules to nanoparticles by the same strategies, including the biotin-avidin system itself in addition to NTA-polyhistidine, will be reviewed.

Biotin as a small molecule with one free carboxylic group, also readily available with a number of modifications such as -NH₂ or -NHS, is covalently bound to nanoparticle by conjugation chemistry^[314, 331] or directly to the inorganic particle surface by accordingly modified ligand molecules,^[332] as discussed previously. For the conjugation, only physicochemical properties such as solubility, charge,

or functional groups of the biotin molecule are of importance, not necessarily the biological functionality or related consequences.

Avidin, streptavidin and other variants are regular proteins, characterized by their molecular weight, isoelectric point, hydrophobicity and available functional amino acid residues commonly consisting of carboxylic acids, amino groups and thiols.

As zwitterionic molecules, proteins are positively charged at pH values below their isoelectric point and negatively above. This offers the possibility to adsorb avidin electrostatically to negatively charged nanoparticles, while streptavidin and neutravidin having a lower pI were reported to bind significantly less.^[333, 334] To improve the stability of the nanoparticle-protein complex, an additional covalent crosslinking has been performed on a similar system.^[335]

By exploiting the functional groups on the protein surface, streptavidin has been covalently linked to quantum dots with carboxylic groups^[173, 216, 336] or primary amines,^[178] commonly by EDC/NHS. Alternatively streptavidin has been bound by direct adsorption to the inorganic quantum dot surface via a polyhistidine tag,^[178] also in the case of monovalent streptavidin.^[264]

Naturally, biotin-modified nanoparticles can be decorated with an additional shell of streptavidin^[314, 332] when added in excess. As demonstrated by the authors, nanoparticles modified with larger number of biotin molecules can form large aggregates with streptavidin by inter-particle crosslinking, due to the multivalency of both the nanoparticles and streptavidin. This effect is not only found for nanoparticles with biotin-avidin but presents a general problem in case of two or more all multivalent binding partners, as well as for covalent conjugation where often both nanoparticles and target molecules have a larger number of reactive functional group, e.g. carboxylic acids and amines, as also in the case of proteins.

3.3.2 DNA

Deoxyribonucleic acid – DNA, is a linear polymer containing the genetic information of organisms in form of the sequence of the four oligonucleotides being the monomeric building blocks, as analogously for RNA. Besides its biological function, DNA and RNA can be employed as generic polymeric molecules of which the most prominent feature, duplex formation with a strand of complementary sequence, presents a very specific mechanism of molecular recognition. As this mechanism depends on the simple linear sequence of nucleotides, DNA can be used as “programmable” object with a very large number of possible sequences and conformations, and exploited e.g. as building block and structural element for the assembly of artificial structures, as it will be discussed later.

Synthetic DNA oligomers of arbitrary sequences and with a large variety of functional end groups, which are commercially available, can be conveniently attached in aqueous solution to gold nanoparticles by a thiol-gold bond, in the same way as a place-exchange reaction already discussed for other ligand molecules.^[337-340] DNA oligomers are usually added in quite large excess to the gold particles and spontaneously bind to the nanocrystal surface. Variations include DNA oligomers modified by a cyclic steroid derivative with two thiols groups^[341] or by up to three mercaptohexyl linkers.^[342]

The same strategy of ligand exchange has also been applied to Au rods,^[343] silver nanoparticles,^[344] mercaptopropionic acid-stabilized CdSe/ZnS quantum dots,^[345, 346] and Pt nanoparticles have decorated with amino-modified DNA.^[182]

Even under optimized conditions,^[347] the binding of DNA to nanoparticles does not occur quantitatively, however the DNA density can be influenced by adjusting the excess ratio or by dilution with other ligands, e.g. short “spacer” oligomers.^[348] In the case of rather long DNA strands, attachment of a single DNA molecule increases the size of the Au-DNA conjugate sufficiently to separate discrete bands by gel electrophoresis, consisting of nanoparticles with exactly 0, 1, 2, 3... DNA molecules per particle.^[293] Recently the separation of such conjugates has been demonstrated by ion exchange chromatography, enabling the separation of nanoparticles with a defined number of shorter DNA oligomers.

While double-stranded DNA forms its characteristic double helix structure by Watson-Cricks basepairing, single-stranded DNA is more flexible^[349] and can take a curved or coiled conformation. In Figure 8 (bottom left), a 20mer ssDNA strand is displayed in scale with a 5 or 10 nm nanoparticle, respectively. Single stranded DNA attached to nanoparticles is found to undergo a stretching when an increased surface coverage induces steric pressure, or when it is hybridized with a complementary strand, which results in a stiffer double helix.^[4, 348, 350]

Due to the large numbers of different possible sequences for a DNA or RNA strand of given length, there also exists an even larger variety of possible conformations (in terms of secondary and tertiary structure) of these linear molecules. It has been found that certain sequences can strongly bind to a target molecule by molecular recognition, determined by geometric matching of the surfaces of the two molecules and which is mediated by electrostatic, hydrophobic van-der-Waals forces or hydrogen bonds. This can be exploited to generate so-called aptamer sequences to a given target molecule by molecular evolution, technically realized by multiple randomization, selection and amplification of strongly binding sequences, resulting in an optimized strand of DNA, RNA or peptide for the target molecule with affinities comparable to antibodies.^[351-353] Aptamers have been attached to gold nanoparticles via a thiol function,^[354, 355] to quantum dots or silica-coated Au particles by covalent conjugation chemistry,^[356, 357] to avidin-modified magnetic nanoparticles,^[335] as well as biotinylated DNA aptamers to quantum dots with streptavidin.^[358]

Due to its phosphate backbone, DNA is negatively charged and effectively a polyelectrolyte molecule. Naturally, this results in electrostatic adsorption of DNA to positively charged surfaces, such as nanoparticles with quaternary amines,^[359-361] as of RNA to nanoparticles with tertiary amines.^[225, 226] However, also nonspecific, i.e. generally unwanted, adsorption of DNA to nanoparticles has been found, especially when incubated at high stoichiometric excess,^[4, 350] also in case of single nucleotides.^[362]

Besides the ligand-like direct binding of DNA to the nanoparticle surface, also conjugation chemistry can be employed to covalently bind the DNA to functional groups available on the nanoparticle surface. This has been carried out with EDC chemistry to bind amino-functionalized DNA to nanoparticles with carboxylic groups, and thiol-modified DNA to maleimide groups.^[211, 363] Alternatively, nanoparticle derivatization can be carried out in organic solution^[364] prior to the coupling to amino-modified DNA oligomers, or the 5' end phosphate group of DNA can react with

EDC and imidazole to primary amino groups^[269] present on the particle surface.^[314] Apart from covalent conjugation chemistry, the non-covalent receptor-ligand system avidin-biotin has also been used for the binding of DNA to nanoparticles, both with biotin-modified DNA^[358] and biotin-modified nanoparticles.^[365] In Figure 8, a strand of 20mer ssDNA is drawn to scale a 5 or 10 nm nanoparticle, respectively.

3.3.3 Peptides, Proteins, Enzymes and Antibodies

Peptides and proteins are polymeric compounds of amino acids, linked to linear sequences by amide bonds. Short sequences, peptides consisting usually of up to 50 – 100 amino acids, are commercially available by custom synthesis, while proteins are usually found in form of larger poly-amino acids. However, there are also rather small proteins and there is no general and well-defined differentiation between those terms. Special classes of proteins comprise enzymes and antibodies, enzymes being highly specialized molecules with reactive centers that catalyze biochemical reactions and are responsible for metabolism. Antibodies, also known as immunoglobulins, are large Y-shaped proteins with important functions in the immune system. They have the ability to specifically bind with their active region to an antigen, in principle an arbitrary target molecule, mediated by molecular recognition. Other proteins are used by the cell e.g. for signaling or structure formation.

Proteins are made up by a sequence of generally 20 different standard amino acids (in addition to other naturally occurring or synthetic amino acids) which are linked together by amide bonds and which possess different side chains residues. Naturally, each peptide or protein has one carboxylic and one primary amino group at its ends, while the amino acid side chains introduce additional functional groups or other properties depending on their molecular structure. The amino acid sequence determines the unique properties of each of a large number of possible structures, i.e. 20^n for a sequence of n amino acids, in terms of charge, polarity and hydrophobicity. These in turn determine the secondary and tertiary structure that a protein is folding into and that ultimately results in the functional biomolecule. In many cases, the specific function of a protein (enzyme, antibody) is determined by its geometric and physicochemical properties of the outer surface, given by the almost arbitrary motifs of the folded amino acid sequence. Often the inside of a protein is hydrophobic while hydrophilic amino acid side chains tend to point outwards into solution, while e.g. membrane proteins generally have a partially hydrophobic surface. Cysteine residues, even if far apart in the sequence, can come spatially close to each other in folded proteins and form stabilizing disulfide bonds. The thiol group of a terminal cysteine residue can also be exploited as anchor group for the attachment of a peptide to the surface of nanoparticles.

The above said clearly makes peptides and proteins interesting objects to be combined with inorganic nanoparticles, both for basic research and applications that make use of the specific functions of these biomolecules.

Peptides as rather small molecules with a “programmable” sequence of amino acids allow the rational design of ligand molecules that are optimized to stabilize nanoparticles,^[366] introduce various functional groups,^[367-369] besides examples for particle synthesis^[24] and phase transfer^[247] with the help of peptides. Making use of the biological functionality of certain peptides, the specific uptake of nanoparticles by cells can be optimized by conjugation of nanoparticles with the corresponding peptide, as reported for Au nanoparticles^[167, 305, 370] or quantum dots^[332] by ligand exchange with cysteine-containing peptides. Also coating of quantum dots with lipids pre-modified with e.g. TAT

peptide has been reported.^[210] Peptide modification can also be carried by covalent conjugation chemistry, as demonstrated for quantum dots with amino groups^[371] or magnetic iron oxide nanoparticles.^[272, 372, 373] In addition, quantum dots modified with streptavidin (that is also commercially available) have been conjugated to different biotinylated peptides.^[374-377] Small monofunctional Au cluster have been modified by conjugation chemistry with a peptide containing a polyhistidine tag that bound to the inorganic surface of CdSe/ZnS quantum dots,^[329, 378] or alternatively to quantum dots modified with NTA.^[273] Figure 4 illustrates the relative size of a short peptide (five amino acids) in respect to a 5 nm nanoparticle, Figure 8 shows a number of different proteins in comparison with a 5 or 10 nm nanoparticle.

There are several strategies for conjugation of proteins to nanoparticles available, including enzymes or antibodies. First, “nonspecific” adsorption can be employed: The nanoparticles are incubated with the protein which adsorbs to the particles, either by electrostatic attraction if both partners are oppositely charged, by van-der-Waals forces, hydrogen bridges, gold-thiol bonds (from cysteine residues) or by hydrophobic interaction, e.g. when the pH is close to the pI of the protein or the nanoparticle so that the electrostatic repulsion is reduced. After adsorption, the protein can be irreversibly immobilized by those forces or a combination of them.^[379] Potentially, the protein can get into intimate contact with the particle surface by partial or complete denaturation,^[168] giving rise e.g. to hydrophobic interaction of the inner part of the protein and/or an increased contact area between the binding partners. Electrostatic binding has been demonstrated e.g. for protease to MPA-modified quantum dots,^[380] and desorption of proteins can be triggered by increasing the electrolyte concentration that effectively shields the attractive electrostatic interaction.^[381] Traditionally, these effects have been exploited for the preparation of so-called immunogold, small Au nanoparticles conjugated with antibodies that have been used as labels for immunostaining in electron microscopy^[56, 382-386] and that have already been commercially available for many years. A related issue is surface passivation or “blocking”, carried out with inert proteins or with such that do not interfere with the assay aimed-at, which bind to “sticky” surface spots and prevent thus undesired binding of functional proteins. Common examples are serum albumins (bovine or from other sources^[387]), which have also been used to functionalize nanoparticles with amino groups originating from their lysine residues.^[168]

Examples of modification of nanoparticles with proteins by covalent conjugation chemistry include transferrin on quantum dots^[237, 388, 389] or rods,^[390] bungarotoxin,^[391] also magnetic nanoparticles possessing amino groups have been modified by enzymes.^[270] By click-chemistry, lipase has been conjugated to Au NP,^[279] as well as peptides to gold rods.^[392]

Streptavidin-functionalized nanoparticles have been used to label the biotinylated motor protein kinesin with quantum dots,^[393] or biotinylated epidermal growth factor.^[394]

Proteins with a polyhistidine modification have been bound to nanoparticles modified by NTA, e.g. adenovirus knob protein to small Au clusters,^[323] the enzyme glutathione S-transferase^[328] to quantum dots or by direct binding of the polyhistidine tag to the Zn-containing inorganic surface of CdSe/ZnS quantum dots as discussed before, e.g. for maltose binding protein^[175, 330] or fluorescent proteins.^[395]

Antibodies, besides adsorbed to gold nanoparticles as mentioned above, have been conjugated to quantum dots covalently by EDC,^[216, 396] as well to magnetic-fluorescent composites^[397] and by bifunctional crosslinkers to thiol-containing, silanized CdTe quantum dots.^[398] Antibody fragments possessing free thiol groups have been bound to free amino groups of quantum dots by means of a heterobifunctional crosslinker,^[310] and biotinylated antibodies to streptavidin-modified quantum dots.^[399] More protocols and a comparison of the different approaches are also available.^[400]

Silica-coated nanoparticles of different core materials with amino groups have been modified with antibodies by bis-NHS reagents.^[252] As shown by Weissleder et al.,^[401] dextran-coated magnetic iron oxide nanoparticles can be covalently conjugated with peptides,^[372] oligonucleotides,^[402] proteins and antibodies.^[403]

Gold nanorods have been modified first with methoxy-PEG-thiol and thiolated antibodies,^[404] or PEG with free biotin or thiol groups to which then streptavidin or other gold spheres could be bound.^[170]

Small biomolecules include quantum dots modified with dopamine via EDC chemistry,^[146, 405] with serotonin via a PEG spacer^[406] or gold nanoparticles decorated with sugar molecules.^[407]

Further examples can be found in a number of reviews about bioconjugation of gold nanoparticles,^[408] quantum dots,^[409] or nanoparticle-enzyme conjugates,^[410] and in the other works mentioned in section 5.1 about biological applications. In Figure 8, different proteins and an IgG antibody are drawn to scale with a 5 or 10 nm nanoparticle, respectively.

3.4 Fluorescent dyes and other functions, multifunctional particles

Apart from chemical functional groups or biomolecules, nanoparticles have also been modified with a number of other functionalities. Common examples include fluorescent dyes^[6, 346, 411, 412] or fluorescent proteins^[395] that can be used for fluorescence labeling of non-fluorescent particles,^[272, 369] or to generate systems exhibiting energy transfer. Common examples include fluorescent dyes which are quenched by gold nanoparticles, or which can be excited by fluorescence resonant energy transfer via a quantum dot serving as donor.^[178, 413] Such systems will be discussed further in section 5.1 about sensors. Other functions include paramagnetic ligand molecules^[213] or chelator molecules for radionuclides.^[414, 415]

In summary, nanoparticle synthesis, phase transfer, functionalization and bioconjugation all have some common aspects and overlap, e.g. in regard to the binding of organic ligand molecules to the inorganic particle surface, and often there is no clear distinction possible since those ligands often introduce chemical functionality, as finally do complex molecules that again may change the physico-chemical properties of the particles as well.

The motivation for particle modification is the control over the interaction of the particles with their environment, which is naturally taking place at the particle surface. By appropriate modification, phase transfer, specific and non-specific binding to target molecules or surfaces, biomolecules or cells can be tuned, e.g. for the controlled targeting or assembly of nanoparticles. Furthermore, more functionality can be added to the properties the particle inherently has from its core material, e.g. for biological impact (for drug delivery or therapy) or fluorescence emission for non-luminescent materials. For multifunctional particles, three approaches can be identified: i) composite materials generated in-situ during synthesis, e.g. by growing nanocrystals with domains of different functional

materials^[136, 137, 140] ii) post-modification of particles with functional molecules, e.g. fluorescent quantum dots with paramagnetic organic molecules^[213, 416] or non-fluorescent nanoparticles with fluorescent dyes^[356, 417-419] or bio-functional molecules^[272, 335, 369] or iii) assembly of composite materials e.g. by combination of different nanoparticles with different functionality,^[397] or e.g. microbeads or capsules loaded with a mixture of different classes of nanoparticles or functional molecules.^[420, 421]

While in the first approach certain material properties, e.g. differences in lattice parameters, might be limiting for the crystal growth, the second offers great flexibility for the price of finding robust systems and the appropriate conditions for the nanoparticle modification, the third usually results in objects rather large compared to single nanoparticles.

4 Characterization techniques

Nanoparticles as objects on a length scale between macroscopic (μm) objects and small molecules are not resolved by standard imaging microscopy, nor are they strictly monodisperse like a bulk of identical small molecules. There are, however, a number of techniques “borrowed” from the classical disciplines physics or (bio)chemistry that allow for accessing certain properties of the nanoparticles. Here the focus is put on single nanoparticles of about 2 – 50 nm diameter and a narrow size distribution, in contrast to “technical” particles found in form of clay, concrete, ceramics etc.

Classically, nanoparticles are characterized by transmission electron microscopy (TEM) down to atomic resolution, or scanning electron microscopy for particles larger than 15 nm. The de-Broglie wavelength of electron beams depends on the acceleration voltage and is much shorter than the wavelength of light, allowing much higher resolution down to single atoms. Though electron optics is relatively demanding in terms of apparatus design, electron microscopy is an imaging technique that allows to directly “see” the particles and their morphology. However, contrast is only good for materials with high electron density, in fact gold nanoparticles were the first objects studied with this technique, limiting TEM to inorganic materials, preferably heavy elements. Organic material is not directly visible, but can be negatively stained by addition of heavy metal salts to the sample on the grid.^[208] TEM images can be evaluated statistically to get average size and size distribution, generally of the inorganic particle core. As to ligands, the situation is complicated by the organic nature of those molecules that are not directly visible and soft. Theoretically, the overall particle diameter is the core diameter plus two times the thickness of the ligands shell, however, it is found that the inter-particle distance is not a good measure for the thickness of the ligand shell because the ligand molecules can interdigitate with those of adjacent particles.^[27] In addition, due to the dry preparation of the sample on the grid, all solvent is evaporated causing shrinking of the organic shell compared to the native state in a solvent. Besides many available techniques that are however often limited to the characterization of the material composition or size of the core and first ligand layer (XRD, XPS,^[161] NMR,^[422] NIR,^[423] SERS,^[424] ICP-MS^[425, 426] and others), in the following a number of other techniques will be discussed that have been applied for the size characterization of more complex (bio-)conjugated nanoparticles, i.e. particles with rather thick organic shells.

4.1 Size characterization

Maybe the most basic property of a nanoparticle, besides its material composition, is its size. When dispersed in a solvent, this size is not only the diameter of the hard inorganic particle core but includes its organic ligand shell, possibly other, more complex molecules on the particle surface, and solvent molecules. This yields to an effective, hydrodynamic diameter that is characterized by the diffusion of the particle in its solvent, by a number of different techniques, the diffusion constant can be determined from which then the hydrodynamic diameter is calculated via the Stokes-Einstein relation.

In dynamic light scattering (DLS), the thermal diffusion of particles causes intensity fluctuations of the light scattered by the particles. From the auto- or cross-correlated signal the diffusion constant can be derived, and with appropriate models the particle size distribution. This well-established method is fast and convenient to perform, it has been applied extensively to nanoparticles.^[228, 262, 264, 297, 305, 313] However, the scattering cross-section strongly depends on the particle diameter, so large

particles contribute with a strong weight to statistics, and the transition from an intensity distribution to a volume or number distribution should to be performed with care. Furthermore, the organic ligand layer is often neglected, as are thicker organic coating shells or biomolecules, yielding to a composite system with different optical properties and their size relation, e.g. in case of small inorganic nanoparticles of given size with possibly several organic layers of varying thickness.

Fluorescence correlation spectroscopy (FCS) is based on the diffusion of fluorescent particles or molecules into and out of the focal volume of a confocal optical microscope. By the confocal setup, only fluorescent light from particles in the focal volume is detected, at high dilution single particles cause intensity fluctuations, of which the dynamics is characterized by the autocorrelation, from which the diffusion constant can be derived. By principle, this method is limited to fluorescent nanoparticles but has been applied with great success to quantum dots of different materials.^[427-429]

Thermophoresis is the effect that small particles move along a temperature gradient, commonly towards to cooler regions as it has been explained by solvation energy.^[430] For particle sizing, a laser can be used to heat a small spot in a flat cuvette, resulting in a static radial temperature gradient in which the particles are depleted. While recording the spatial distribution of the fluorescent particles, the heat gradient is switched off and the nanoparticles diffuse back resulting in an isotropic distribution. The diffusion constant can be derived from the dynamics of the spatial particle distribution, in a way very similar to the technique of fluorescence recovery after photobleaching (FRAP) that has been used to study the lateral diffusion in cell membranes.^[3]

Another related technique is based on single particle tracking, where the diffusion movement of nanoparticles is directly observed under an optical microscope.^[431-433] Analysis of the particle tracks and statistic evaluation allows for calculation of the diffusion coefficient and hence the particle size.

All these techniques are based on free diffusion of the nanoparticles, interacting only with their solvent. A number of other techniques rely on a force field applied to the nanoparticles, or a solid matrix that interacts with the particles in solution.

Analytical ultracentrifugation exploits particle sedimentation for the size characterization. Sedimentation velocity depends on the different mass densities of particles and medium, and on the particle size. While this method works well for homogenous particles of known density, the density of more complex core/shell nanoparticles strongly depends on the thickness of organic shell, which has to be taken into account for the model applied to derive the particle size.^[434, 435] Alternatively, magnetic sedimentation has been applied.^[436]

Size exclusion chromatography (SEC), also known as gel filtration or gel permeation chromatography (GPC), is a technique commonly used for the characterization of polymers and proteins. The separation by particle size takes place in a column packed with a porous gel as matrix, termed stationary phase. The sample is applied under a flow of a solvent, termed mobile phase. While passing the column, small particles can diffuse into the pores of the stationary phase while larger particles are sterically excluded. This results in the retention of small particles that spend more time in diffusing into the pores and out again, while large particles come out first. The stationary phase is characterized by its pore size which allows separation of particles of a certain size range, and size characterization after calibration with standards of known size, e.g. polymers or globular proteins, which allows for an universal calibration based on the particle volume, in contrast to molecular

weight.^[437, 438] Size exclusion chromatography has been applied to a number of nanoparticles of different materials in both organic solvents^[234, 439-442] and aqueous phase,^[3, 209, 228, 235, 264, 332, 443, 444] in some cases also in preparative scale. In addition, the separation of nanoparticles of different shapes by SEC has been reported.^[445] Often, this method is limited by the colloidal stability of the particles which can irreversibly aggregate or adsorb to the stationary phase by loss of ligand molecules or reduced electrostatic repulsion in presence of salt. Therefore, additional free ligand molecules or other surfactants are commonly added to the mobile phase.^[442, 446]

Electrophoresis is the movement of particles in presence of an electric field, also termed electrokinetic phenomena.^[447] Charged particles are attracted by the oppositely charged electrode, the electric field is mediated by an electrolyte as conductive medium that also causes a hydrodynamic drag on the particles, resulting in a constant velocity in a constant electric field. Qualitatively, small negatively charged particles migrate faster to the positive electrode than large ones, as do stronger charged particles, while positively charged particles will move towards the negative electrode. Quantitatively, electrophoresis is under certain restrictions described by Henry's equation, relating electrophoretic mobility to particle size, charge (zeta potential) and ionic strength of the surrounding medium. However, real systems are often found in the intermediate regime where simple approximations such as the Hückel and the Helmholtz-Smoluchowsky limits for low and high ionic strength, respectively, may not be valid, or the shell of ligand molecules is found to strongly influence the mobility.^[150, 448]

Free electrophoresis is used for separation of nanoparticles by capillary electrophoresis,^[449-453] where small amounts of samples can be analyzed with high resolution. Gel electrophoresis employs usually poly(acryl amide) or agarose,^[454] a polysaccharide extracted from algae, to form a gel with the conductive medium. The gel avoids flow in the medium, e.g. by convection, and secondly serves as separation matrix by a sieving effect due to the pores.^[455] Agarose gel electrophoresis is commonly used for water-soluble nanoparticles because it allows analysis of a large number of samples in parallel and direct comparison to each other by convenient optical detection, i.e. a camera. In addition, the separation is sometimes superior to other methods (e.g. SEC) allowing for the separation of nanoparticles with a discrete number of attached molecules, as discussed previously. So far, quantitative analysis of particle size and possibly the conformation of molecules to the nanoparticles has been addressed in different systems, however, the validity of the applied models and approximations should be confirmed carefully.^[456] Colloidal nanoparticles, in particular if decorated with large, soft and complex molecules, are not ideal rigid spheres with a certain homogenous surface charge as commonly assumed, only recently also soft shells have been described theoretically.^[457, 458] In real systems, the charge distribution around the particles is not known, and little is known about dynamic effects in presence of an electric field or gel matrix (which might by itself be hard to characterize),^[455] in particular for complex nanoparticle-biomolecule conjugates.^[295] While it is clear that separation is based on both size and charge of the particles, the experimental data can often not be fully interpreted quantitatively^[150, 453] or even qualitatively, as in the case for nanoparticles modified with poly(ethylene glycol), a neutral polymer, in which the particles migrate towards the negative electrode, implying a positive net charge (cf. Figure 7, left). While this effect has been observed by several groups even for methoxy-terminated PEG,^[1, 305, 456] no well-supported explanation seems available so far. While gel electrophoresis is mostly applied to nanoparticles for analytical purposes,^[4, 350, 448, 459, 460] nanoparticles can be also extracted from the gel

for further experiments^[1, 293, 294] and also column electrophoresis with continuous elution has been reported.^[461]

Depending on the nanoparticle material, the particle size often directly affects other physical properties that can be used for size characterization. Maybe the most prominent example is optical spectroscopy: The characteristic plasmon peak of gold nanoparticles depends on the nanoparticle size, by its position in the absorption spectrum in terms of energy or wavelength, the particle size can be calculated according to Mie scattering theory.^[462] While the experimental spectra fit well to model calculations for large nanoparticles, the size-dependence of the spectral position of the plasmon absorption decreases for nanoparticles around or smaller than 10 nm in diameter,^[463] which is attributed to increasing surface effects, besides the influence of the refractive index of the surrounding medium.^[464] In Figure 10, absorption spectra of spherical gold nanoparticles with different diameters are displayed. Plasmon resonance is also found for other metal particles like silver, and for rod-shaped particles that exhibit two peaks resulting from a longitudinal and transversal mode. Recently, the absorption of rods and other shapes has been modeled theoretically with excellent agreement to experimental data.^[465] In fluorescent semiconductor nanoparticles, spatial confinement of the wave functions of electron and hole of an exciton results in a size-dependent quantization of the energy levels, and thus size-dependent absorption and emission spectra. Being one of the key features of colloidal quantum dots, this effect can also be used to estimate the size of such particles from their optical spectra by means of empirically found calibration curves.^[466] However, for core/shell particles such as CdSe/ZnS there is no such data available, thus commonly the e.g. ZnS shell is neglected which, in fact, is equal to the assumption of a larger, homogenous CdSe particle.

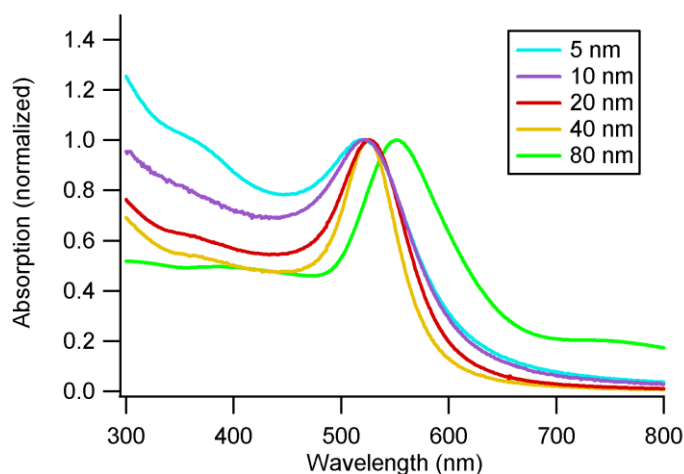


Figure 10: Optical absorption spectra of gold nanoparticles of different size. The spectral position of the plasmon peak changes very little for small particle diameters. The peak width is influenced by the size distribution of the sample in the cuvette, single-particle spectroscopy yields to more narrow peaks. All spectra shown have been normalized.

Together with gravimetric methods, i.e. drying and weighting the mass of a sample after recording the absorption spectrum, and with the particle diameter from TEM, optical absorption spectroscopy is commonly used for concentration measurements, by applying the empirical extinction coefficient to Beer's law. While this approach works reasonably well, is convenient in application and yields

reproducible results, often additional organic shells are neglected (despite in thermogravimetry) which can result in deviations of a few to several ten percent in regard to absolute numbers for concentrations.

In addition, scanning probe microscopy including AFM (atomic force microscopy) have been used for the characterization of nanoparticles immobilized to flat surfaces.^[264, 467-469] In combination with fluorescence microscopy, single quantum dots exhibiting differences in quantum yield and the presence of dark quantum dots could be accessed.^[470]

Small-angle x-ray and neutron scattering (SAXS^[471-473] and SANS^[474]) have as well been employed for colloidal nanoparticles, the size and possibly also the core/shell architecture of nanoparticles can be derived by means of a layer model with known parameters.

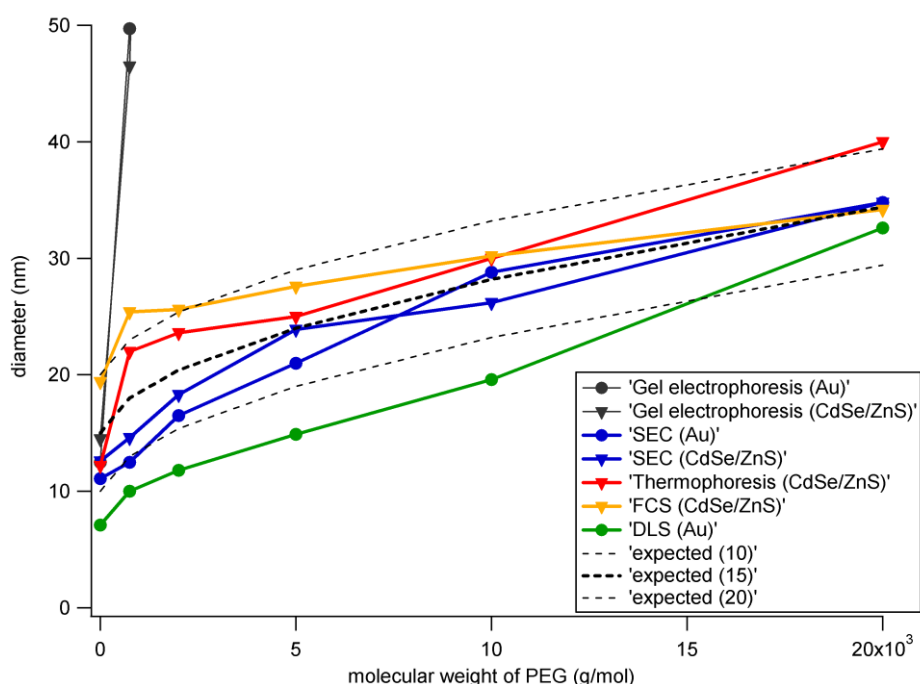


Figure 11: Nanoparticles saturated with PEG of different molecular weight, "0 g/mol" are plain polymer-coated nanoparticles, hydrodynamic diameter determined by different techniques. Dotted lines are theoretical values consisting of a hypothetical core diameter (10, 15 or 20 nm) plus two times the thickness of the PEG layer that depends on the molecular weight (hydrodynamic diameters for PEG from literature, determined by SEC, data for particles plotted from reference^[3]).

To summarize, there are a number of different techniques with different measurement strategies available that have been successfully applied to the size determination of nanoparticles and to the characterization of particle modification based on the change in size e.g. due to additional molecules or coating layers. However, when absolute values of different methods are compared, often deviations are found that are larger than expected. In Figure 11, diameters of nanoparticles with PEG of different molecular weight is shown, determined by different methods. The observed deviations may be due to the fact that "size" is measured by means of different physical effects, involving possibly different physical properties of the particles, e.g. by interaction of a matrix, or when dry particles vs. particles in solution are compared. Secondly, depending on the method, deviations contribute differently to statistics, as data is collected in completely different ways, i.e. in ensemble or single-particle measurements. Naturally, reliably results are obtained by application and comparison of several complementary methods.^[3, 178, 297]

Finally, a number of techniques are limited to certain classes of particles, i.e. inorganic particles (TEM) or fluorescent particles (FCS, thermophoresis), while others offer the additional benefit of optional preparative or semi-preparative separation, as found for gel electrophoresis, SEC and ultracentrifugation, in contrast to purely analytical methods.

4.2 Stability, surface and conjugates

Apart from nanoparticle size, also other physicochemical properties as colloidal stability under influence of increased salt concentration or different pH values, the optical stability of fluorescence emission, or the number of functional groups or attached molecules are of special interest for characterization.

In case of fluorescent nanoparticles, quantum yield is one of the important parameters which determines, in combination with the extinction coefficient at the excitation wavelength, the brightness of a fluorescent probe. Quantum yield is influenced by the quality of the inorganic core or core/shell system and the local environment of the nanoparticle, in particular the organic ligand shell. Ligand exchange can lead to a decrease and for some systems also to an increase in fluorescence quantum yield, depending on how the organic ligand molecules influence the electron density in the outer regions of the nanocrystal, i.e. how they change the possibly present trap states that can yield to non-fluorescent recombination of excitons.

For fluorescent ligand molecules attached to the nanoparticles, energy transfer can occur, yielding to a distance-sensitive change in emission of the donor in respect to the acceptor molecule. This can be exploited to gain information about e.g. the distance between particle and fluorescent ligand molecule, or binding/unbinding events commonly used for sensor systems.

Gold and other metal nanoparticles show a plasmon resonance in the absorption spectrum. If nanoparticles aggregate, the plasmons of different adjacent particles can couple, yielding to an effective larger particle size and therefore to a remarkable red shift of the plasmon resonance.^[475] While solutions of single small Au nanoparticles have a ruby-red color, aggregated particles show a blue to grey color. This color shift can be used to probe the colloidal stability of nanoparticles under variation of the environmental conditions, e.g. pH, salt concentration, ligand binding,^[141, 157] or exploited for sensor systems where the assembly or disassembly of particle aggregates is triggered by the presence of analyte molecules.

Characterization of the nanoparticle surface in regard to bound ligand molecules provides information about basic physicochemical properties of the nanoparticles, such as size and electric charge, and possibly about the conjugation with new ligand molecules or biomolecules. Beside the particle size, electric charge can be measured in terms of the particle zeta potential, which is the electric potential at the slipping plane of the electric double layer of ions around the particle, commonly realized by a combined setup of DLS and electrophoresis.^[238, 448] It should be noted that, despite of an explicit theoretic description for idealized cases, real systems might be more complex e.g. in regard to the charge distribution in multiple soft ligand shells, resulting in deviations between different methods, e.g. DLS and gel electrophoresis. The resulting absolute numbers should be taken with care and if possible always compared to control samples acquired with the same setup.

As to chemical functional groups, there are a number of colorimetric assays reported that allow for the quantification of amine groups, thiols, and others.^[304, 310] Possibly, a chromophore released by the reaction with the target analyte^[373] has to be separated from the nanoparticles because of overlapping absorption spectra. Furthermore, the binding of ligand molecules to metal nanoparticles can be probed by surface-enhanced Raman scattering (SERS).^[392]

Other functional molecules, in particular biomolecules, present on the particle surface can be assayed by their specific function, e.g. binding capability to a substrate, as demonstrated for target molecules immobilized on flat surfaces or microbeads in solution. Again, the attachment of larger biomolecules can be observed by the increase of the total particle size as discussed before. In combination with organic fluorophores conjugated to the molecule of interest, the presence of those molecules on the particle surface can be accessed by the absorption or fluorescence emission,^[336, 338, 347, 476] or by stepwise photobleaching of the organic dye.^[391]

5 Applications, Outlook

Applications of colloidal nanoparticles, in particular of those discussed in the present work, fall three classes:

- Labeling, tracing, imaging
- Sensing and detection
- Active elements, e.g. for heat mediation, optical sensitizing or delivery vehicles

Naturally, the material of the particles often plays the key role in applications by providing unique inherent properties like strong optical absorption or scattering, fluorescence emission or magnetic moment. Secondly, the particle surface and its modification determine particle stability, interaction with the particle environment, and possibly controlled assembly or targeting.

5.1 Biological applications

Biological applications of gold nanoparticles go back several decades when antibody-conjugated Au nanoparticles were used to specifically stain tissue sections for electron microscopy.^[382] Further examples include immunoassays in which the strong scattering of Au nanoparticles binding to antibodies was used for detection,^[477, 478] instead of absorbing products of enzymatic reactions as in classical ELISA formats. Variations include post-reaction silver enhancement^[479] or electrochemical read-out.^[480] The light-scattering properties of gold nanoparticles can be exploited in dark-field microscopy;^[392, 481] in photothermal imaging light is absorbed by gold nanoparticles which then dissipate the energy to their local environment, causing a change of temperature which induces a change in the refractive index of the surrounding medium, which can consequently be seen in phase contrast.^[482] In photoacoustic imaging contrast is produced by sound waves generated by the absorption of light by Au nanoparticles, by the local expansion of the surrounding medium again by dissipated heat, this technique has been applied for imaging in animals.^[483] In surface-enhanced Raman scattering (SERS) spectroscopy,^[484] inelastic scattering of light on molecules can be greatly enhanced in close proximity to a curved metal surface, i.e. a metal nanoparticle, by plasmon resonance resulting in a locally enhanced electric field. This effect can be used for the detection of biomolecules^[485] or other trace analytes^[485] and also for bioimaging.^[486, 487] Besides, Au nanoparticles have been used as X-ray^[488] contrast agent, and neutron-activated Au nanoparticles can be used as radioactive tracers.^[13, 489]

Similarly, fluorescent quantum dots have been widely used as light-emitting labels in biological systems.^[490] Their size-dependant narrow emission spectrum paired with a broad absorption allows for multiplexed detection with a single excitation light source, rendering quantum dots an attractive system for simultaneous labeling of different target molecules or cellular structures in biology.^[56, 178, 216, 310, 491-493] In particular for applications in biological environment, i.e. under physiological conditions, appropriate surface modification and functionalization is crucial for particle stability and targeting. Besides staining for fluorescence microscopy in regard to imaging, also single-particle tracking has been employed to study dynamic processes inside living cells.^[393, 399] Especially here, the unique spectral characteristics and long-term stability of fluorescence make the advantage of inorganic semiconductor quantum dots compared to “classic” organic dyes, a more detailed

discussion can be found in a recent review article.^[494] In the same way, also phosphorescent nanoparticles of different materials can be used as light-emitting labels, as well as fluorescent gold nanoparticles have been reported.^[9, 55, 56] The same applies for other, intrinsically non-fluorescent nanoparticle materials such as organic polymers or silica which can be doped with fluorescent organic dyes for labeling applications.^[495] While for cells or thin tissue samples nanoparticles emitting in the whole visible spectrum can be employed, for imaging applications in animals^[208, 266, 304, 308, 371, 496] the near infrared (NIR) spectrum is more appropriate^[497, 498] because of the reduced optical attenuation in tissue, allowing for imaging of deeper layers below the skin. Two-photon excitation has also been demonstrated for this purpose.^[390, 499] A more detailed discussion and more examples are found in several dedicated reviews.^[500-503] Furthermore, quantum dots have been used as fluorescent labels in flow cytometry,^[504] see also below about microbeads and multiplexing.

Magnetic nanoparticles are mainly used in magnetic resonance imaging (MRI) where they are introduced as contrast-providing agents,^[505] or in fluorescence microscopy when conjugated with organic fluorophores.^[272, 419] Here again, surface functionalization is crucial if specific targeting is part of the desired application. Both surface modification and applications of magnetic iron oxide nanoparticles have been reviewed recently.^[506-509]

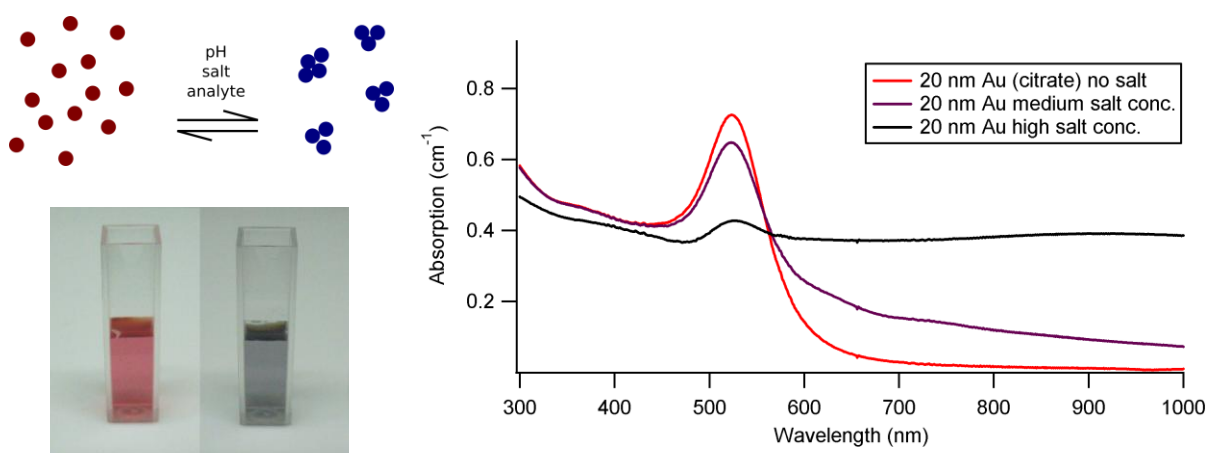


Figure 12: A solution of single gold nanoparticles exhibits red color. When the particles agglomerate due to increased salt concentration or change in pH, the inter-particle distance is decreased, the plasmon oscillations can couple between adjacent particles, resulting in red-shifted optical absorption and thus blue-to-grey color when observed from outside. Depending on the surface coating of the particles, this effect can be reversible and/or specific to analyte molecules.

As to sensors, the general principle is detection by a change of some physical property of the particle or particle system triggered by the presence of an analyte. Perhaps the most common example is gold nanoparticles that change their optical properties upon aggregation^[475] (cf. Figure 12), as pioneered by Mirkin and coworkers,^[337, 510, 511] Au nanoparticles can be modified with single-stranded DNA, and the nanoparticles can be cross-linked by an additional strand of complementary linker DNA. The resulting particle aggregates show a strong red-shift of the plasmon absorption; this effect can be exploited in a variety of different detection schemes.^[512-517] Aggregation only occurs in presence of the linker DNA, so the system can be used for detection of a certain DNA sequence by modifying the nanoparticles with the complementary partial sequences. By raising temperature, the double strands linking the nanoparticles together will melt, while the melting transition, i.e. the melting temperature is sensitive to base-pair mismatches.^[340] With laser-induced optical heating, a single base mismatch can be identified in a linker strand of 30 bases.^[10] Similar systems include

enzyme detection, e.g. for nucleases that digest the DNA strands linking the nanoparticle aggregates together. Alternatively, silver particles can be employed for such systems,^[344] and also DNA-mediated aggregates of magnetic particles have been demonstrated for detection DNA cleavage by NMR.^[518] The assembly and disassembly of such DNA-mediated nanoparticle aggregates can also be controlled to some extent by enzymes, which cut or extend the DNA,^[410, 519, 520] or proteases which cut e.g. peptides or proteins linking the particles.^[521] Besides such systems based on aggregation, also a change of the refractive index in proximity of the nanoparticle can be detected by the spectral shift of the plasmon resonance. This has been demonstrated for single gold particles in dark-field microscopy where the binding of proteins to the particles could be monitored.^[522]

The strong optical absorption of gold nanoparticles is also exploited in lateral flow assays which are used e.g. for the detection of hormones in already well-established commercial applications.^[523]

A second class of nanoparticle-based sensor systems makes use of fluorescence resonant energy transfer (FRET) consisting of a donor and an acceptor, commonly fluorescent nanoparticles of which the fluorescence energy is transferred to an organic dye with red-shifted emission, or dye molecules on the surface of gold nanoparticles which quench the emission of the dye. In this way, the emission of the FRET system is shifted from the wavelength of the donor to that of the acceptor, or for quenching, the emission intensity is reduced (cf. Figure 13).

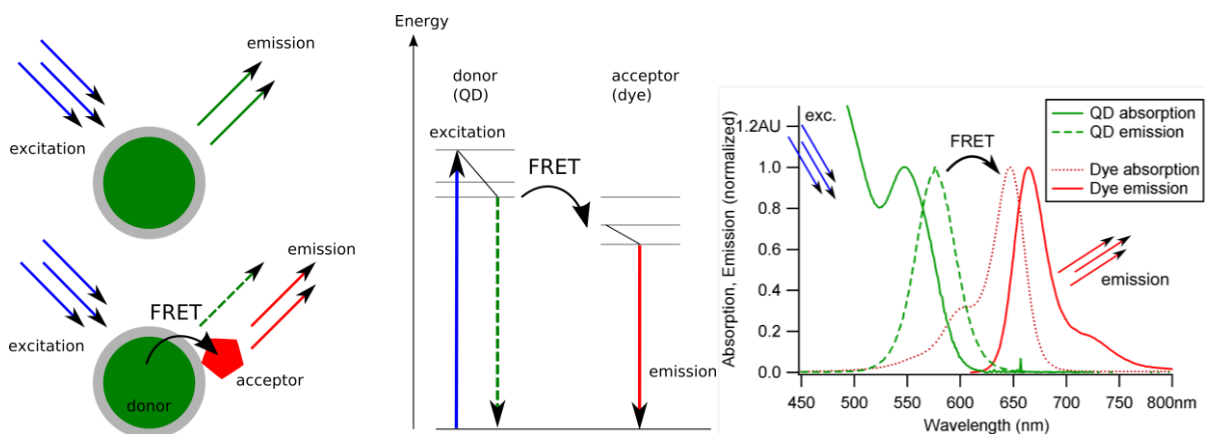


Figure 13: When a quantum dot (green) is conjugated to a fluorescent dye (red), the emitted light at its native wavelength (top left) is decreased in intensity due to fluorescence resonance energy transfer (FRET) to the dye (bottom left). The spectral overlap of donor emission with absorption of the acceptor (right image, dotted lines), the spatial distance and the stoichiometry between donor and acceptor determines the efficiency for energy transfer. Ideally, the FRET acceptor shows no absorption at the excitation wavelength used for the donor.

In a FRET process, energy transfer is described by Förster theory, the strong distance-dependency of the transfer rate ($\propto r^{-6}$) offers a number of possible sensor configurations: The presence of an analyte can change the distance of the acceptor in respect to the donor, e.g. by conformational changes or by release of e.g. the dye molecule from the particle, e.g. by enzymatic reactions or competitive binding. In the latter cases, energy transfer will be reduced or not occur any more and the donor will emit fluorescent light at its native wavelength, or not quenched, respectively.^[6, 356, 358, 368, 377, 524, 525] In Figure 14, the basic principle of a FRET-based sensor system is sketched.

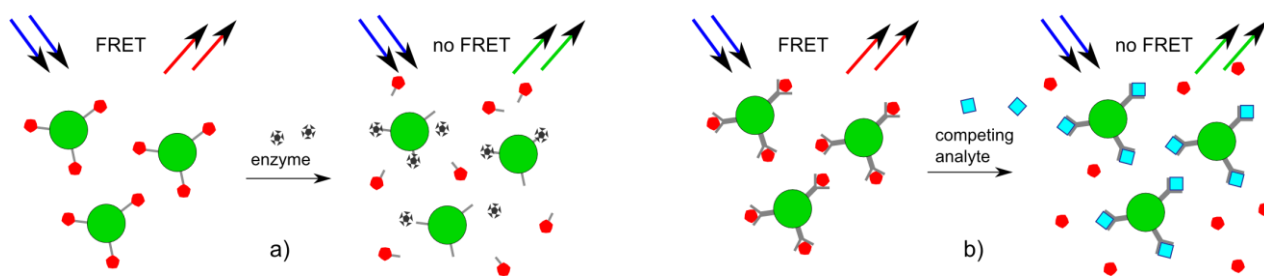


Figure 14: FRET system consisting of a quantum dot (donor, green) and organic dye (acceptor, red). a) The analyte (e.g. enzyme) breaks the linker molecule (e.g. peptide or DNA), the dye is released. Hence, FRET does no longer occur, the quantum dots emit at their native wavelength. b) The non-covalently bound acceptor dye is released by competitive binding of the analyte. This process depends on the binding energies between the partners and mass action, and allows for quantification in the range between no and complete replacement of the acceptor dye. Other configurations can consist of a conformational change of the linker molecule, or the analyte itself acts as FRET acceptor or quencher.

The key issue for these kinds of applications is the functionalization of nanoparticles with receptor molecules that allow the interaction with the analyte molecules and a matching FRET partner. Further examples of such sensor systems for the detection of analyte molecules can be found in review articles.^[11, 526, 527]

For the third class of applications, nanoparticles act as active elements, e.g. as heat-mediating elements. Gold nanoparticles, spherical or rod-shaped, strongly absorb light of equal or higher energy than their plasmon resonance. After excitation, the energy is dissipated into the environment, yielding to an elevated temperature around the particle. Beside optical excitation, gold nanoparticles can be excited to oscillations by electromagnetic fields, also yielding to heat dissipation in their surrounding, as it is carried out with magnetic nanoparticles.^[528-530] This heating effect can be exploited for hyperthermia as cancer therapy, in which nanoparticles are localized in tumor tissue which is then destroyed by slightly elevated temperatures mediated by the nanoparticles,^[531, 532] or for laser ablation.^[309] The key issue for this application is the specific targeting of tumor cells, yielding to an accumulation of nanoparticles in the malignant cells or tissue, the condition for selective therapy that does not harm benign cells or tissue. In principle, tumor targeting can be achieved “macroscopically” by external forces, e.g. a magnetic field directing magnetic particles to a tumor close to the magnet, or by biochemical targeting of nanoparticles functionalized with appropriate molecules allowing for molecular recognition of malignant cells and ligand-receptor-based binding of nanoparticles to the desired target. Here again, this only can be achieved by proper surface functionalization also taking into account the colloidal stability of nanoparticles in a biological environment. Recent reviews about magnetic nanoparticles can be found elsewhere.^[533-535]

Uptake by cells can occur either unspecifically, i.e. by electrostatic adsorption of the particles to the outer cell membrane, or by specific binding to receptor molecules on the membrane.^[536] In both cases, the particles are internalized by the cell in vesicles. From there, they can enter into the cytoplasm by disruption of the vesicle, or the particles can be forced into the cell from outside by electroporation or other techniques.^[537] For specific uptake, the nanoparticles have to be functionalized with appropriate biomolecules that provide the desired interaction, and assure the colloidal stability under physiological conditions. Nanoparticles can be used as carriers for drug or gene delivery,^[538] in which drugs, DNA or RNA molecules are immobilized on the particle that facilitates the uptake by cells. Once in the cell, the drug or genes are taken off the particles by the cell itself or the release can be triggered from outside, e.g. as demonstrated for the light-induced

melting of microcapsules loaded with gold nanoparticles.^[539] Quantum dots have also been demonstrated to act as pH sensor inside cells.^[540]

Finally, oxide^[541] and silver nanoparticles^[542] were found to have anti-microbial properties, allowing for possible application as a modifier for adhesive plasters or textiles.^[543]

General reviews about the application of nanoparticles in biological systems can be found in a number of articles,^[544, 545] focusing on analytics,^[517, 523] gold particles,^[12, 546] quantum dots^[503, 547-550] or magnetic nanoparticles.^[508]

5.2 Technical applications

As in biological systems, nanoparticles can also be used for imaging and sensing also in technical applications, as fluorescent markers or e.g. by the color change of aggregated Au nanoparticles or quenching of fluorescence emission, as demonstrated for the detection of mercury ions.^[551, 552] CdSe quantum dots have been used as sensors for the detection of cyanide^[553] and copper ions.^[554] Antibody-conjugated quantum dots have been used for the detection of non-biological molecules, like TNT in a competitive FRET-based system.^[555]

As simple fluorescent markers, quantum dots have been utilized as tracers for flow velocimetry in microfluidic devices,^[556] the temperature-dependent emission allowed for sensing the temperature of the environment^[557] as well as for pH sensors^[220, 558] or gas sensors.^[559] A combined system of Au nanoparticles and quantum dots has been reported in which the fluorescence emission varied with the distance of the particles as a function of temperature.^[560]

Semiconductor nanoparticles have been used for electric devices such as single-electron transistors,^[561] photodiodes, solar cells^[562-565] or light-emitting diodes,^[566-569] also stimulated emission of quantum dots has been investigated.^[570] TiO₂ nanoparticles serve as the matrix of dye-based solar cells.^[571, 572]

Another broad field are nanoparticle-based composite materials, e.g. organic polymer blends^[567] or inorganic oxide matrices^[217, 570] that have been used in some of the above applications or for electrospinning.^[5] SiO₂ nanoparticles are employed as additive in polymer composites,^[573, 574] i.e. in order to provide scratch resistance to thin polymer films.

Quantum dots with different emission wavelengths can be embedded into polymeric microbeads, the relative intensities allow a barcode-like library of microsized objects that can be used for high-throughput applications. Due to the unique optical properties, nanoparticles of all emission wavelengths can be excited by a single light source and their narrow emission spectra allow for a large number of different species and hence possible combinations of relative intensity.^[168, 500, 575-577] Polymer beads with incorporated magnetic nanoparticles can be used for magnetoseparation.^[397]

As to basic research, the self-assembly of nanoparticles to more complex structures is studied, aiming for possible applications e.g. in electronics. Regular 3D assemblies of nanoparticles have been demonstrated,^[578] also 2D lattices of nanoparticles on surface, e.g. by the Langmuir-Blodgett or other layer-by-layer techniques,^[205, 579-581] and the linear arrangement of nanoparticles^[582] along template molecules. Assembly of particle groupings with a well-controlled number of constituents and/or geometry has been achieved with DNA-modified nanoparticles^[293, 295, 363, 519, 583] or chemical

derivatization.^[170, 287, 299, 378, 584] Particles of different materials yield to multifunctional structures^[397] with e.g. magnetic moment and fluorescent properties. More examples of the assembly of nanoparticles are found in a number of reviews.^[408, 585-587]

Finally, due to the extremely high surface-to-volume ratio of nanoparticles, they are ideally suited for catalytic purposes as recently summarized in a review.^[588]

5.3 Concerns about toxicity

For completeness, concerns about possible toxic effects of nanoparticles^[589-592] should be mentioned. In principle, this toxicity can be either due to the material itself in terms of toxic chemical elements, the most prominent example being cadmium-based nanoparticles such as CdSe or CdTe. Or, toxicity can be caused by size and shape of nanoparticles, i.e. by their physical presence, as known for fibrous materials such as asbestos. Indeed, the release of Cd²⁺ ions and related toxic effects are reported for CdSe quantum dots in cell culture, decreased effects for CdSe/ZnS core/shell particles and silica-coated CdSe particles, respectively. This suggests that leaching of toxic materials can be reduced by additional coating layers,^[591] beside the fact that for many applications the actual concentrations are very low, assumingly not causing acute toxicity. The same holds true for inherently inert, biocompatible materials like gold nanoparticles. However, there are reports in which cell viability depends on the surface coating of gold nanoparticles, and recently also the binding of small gold clusters to the major groove of DNA causing toxic effects has been reported.^[592]

As for cells, the same principles also apply to tissue^[593, 594] and higher organisms, to which nanoparticles can be applied e.g. for labeling/imaging^[595-597] or therapy.^[598, 599] Here an additional aspect is the distribution of nanoparticles after e.g. oral or intravenous application and their fate in regard to degradation or excretion.^[600, 601] First studies suggest that nanoparticles are mostly accumulated in liver and spleen, as e.g. probed with radiolabeled nanoparticles.^[414] Common surface modification consists of PEGylation of the nanoparticles in order to increase their inertness and thus half-life in the blood circulation,^[208, 304] and possibly other molecules for specific targeting.^[266, 308] Eventually, also the toxicity of the ligand molecules has to be taken into account, as e.g. for CTAB, the commonly used ligand for the synthesis of gold rods.^[169] In contrast, certain oxide materials or organic polymers are found to degrade completely in the body, suggesting these systems as really biocompatible.^[602, 603]

Taking into account the foreseen large-scale production of nanomaterials in the near future, their impact on the environment, i.e. whole eco systems, needs to be studied to a great extent in order to gain knowledge about the long-term effects in air, water and soil.^[604] There, big differences are expected between the effects of single dispersed particles and those of aggregates.

5.4 Conclusion and Outlook

Today, nanoparticles of a large number of different core materials and sizes can be synthesized, and their surface can be modified by a number of different techniques in order to increase the stability of the particles in solution, or to tailor the surface chemistry, e.g. in regard to specific interactions with biological molecules. Compared to existing systems, the unique properties of the different particles including strong fluorescence, magnetic moment or optical absorption are expected to bring a real advantage for a number of applications.

As to the uptake of nanoparticles by cells, cytotoxicity, or the fate of nanoparticles in the environment, still very little is known, and a major task for the future will be to draw a general picture of the effects of particles of different size, shape and material composition. One prerequisite for that is standardization that would allow a comparison of the results acquired in different studies for different particles and possibly different systems they are interacting with.

More standardization is also needed in particle characterization, e.g. for the size measurement. Many methods are limited to certain particle species, e.g. fluorescent particles, and different techniques often probe different physical properties of the particles in order to derive the particle size.

Finally, the systems used for many proof-of-principle experiments have to be transferred to larger scale and robustness which both are, besides standardization and safety, important issues in regard to real applications or possible products. However, for analytical in vitro assays the routine use of nanoparticles in real applications seems already possible in close future.

6 Publications

For the cumulative thesis presented here, the publications contributing to the field of research are attached and shortly summarized, and the author's contributions to each publication are outlined below. The published papers or submitted manuscripts are attached as Appendix A1 – A12. The in some cases extensive Supporting Information has been omitted, it can be found on the web.

6.1 Nanoparticle modification and functionalization

Hydrophobic nanoparticles can be transferred to the aqueous phase by means of an amphiphilic polymer, regardless of the core material. The comb-like polymer consists of hydrophobic side chains (hydrocarbon chains) and an amphiphilic backbone (maleic anhydride) that forms carboxylic groups in aqueous solution. In this work, the covalent attachment of molecules to the polymer was developed. Poly(ethylene glycol), an inert polymer, was used as prototype for large, hydrophilic molecules. By agarose gel electrophoresis, nanoparticles with exactly 0, 1, 2... attached molecules could be separated. In this way, employing bifunctional PEG molecules, monofunctional nanoparticles can be prepared. The terminal functional group retains its reactivity, as shown by the attachment of a second PEG molecule. This approach allows for the generation of monofunctional nanoparticles that are expected to serve as molecule-like building blocks for larger constructs, preventing inter-particle crosslinking due to a larger number of reactive sites.

- **[A1]**^[1] R. A. Sperling, T. Pellegrino, J. K. Li, W. H. Chang, W. J. Parak: "Electrophoretic separation of nanoparticles with a discrete number of functional groups", *Advanced Functional Materials* **2006**, *16*, 943-948.
- *Patent*: W. H. Chang, J. K. Li, R. A. Sperling, T. Pellegrino, W. J. Parak, US020070134679 A1, 2007, "Method for separating nanoparticles with a controlled number of anchor points".
 - All experiments, development of protocols, data evaluation

A custom design of a comb-like amphiphilic polymer was developed. Starting with a commercially available poly(maleic anhydride butylene) as backbone, hydrophobic side chains like dodecylamine can be statistically grafted to the backbone. The amine group reacts spontaneously with the maleic anhydride moieties, and by appropriately chosen stoichiometry a part of the maleic anhydride can be left unreacted and intact. To these reactive groups, other functional molecules can be coupled in an additional step, as demonstrated for fluorescent dyes, galactose, biotin and PEG. Alternatively, the particles can be modified in aqueous solution after phase transfer, as with other particle surface coatings.

- **[A2]**^[2] C.-A. J. Lin*, R. A. Sperling*, J. K. Li, T.-Y. Yang, P.-Y. Li, M. Zanella, W. H. Chang, W. J. Parak: "Design of an amphiphilic polymer for nanoparticle coating and functionalization", *SMALL* **2008**, *4*, 334-341.
- *Patent*: W. H. Chang, C.-A. J. Lin, J. K. Li, M. Oheim, A. Yakovlev, A. Feltz, C. Luccardini, M. T. Fernández-Argüelles, R. A. Sperling, W. J. Parak, "Amphiphilic polymer, method for forming the same and application thereof", Taiwanese and US patent submitted.
 - Polymer design, part of characterization (*both authors contributed equally)

6.2 Nanoparticle characterization

Polymer-coated nanoparticles (Au and CdSe/ZnS) were modified with poly(ethylene glycol) of different molecular weight. The particle size was characterized by different methods including transmission electron microscopy (TEM), agarose gel electrophoresis, size exclusion chromatography (SEC), thermophoresis and fluorescence correlation spectroscopy (FCS). While each method yielded consistent results, e.g. increasing particle diameter with increasing molecular weight of the PEG, the absolute numbers showed differences when compared to each other. The different methods are either based on free diffusion or include an interaction with a matrix (gel electrophoresis, SEC), or are sometimes limited to fluorescent particles. Furthermore, particles modified with PEG have a soft shell with a thickness of several nanometers that complicates exact quantitative analysis, which implies that absolute numbers for the size of nanoparticles should be taken with care.

- **[A3]**^[3] R. A. Sperling, T. Liedl, S. Duhr, S. Kudera, M. Zanella, C.-A. J. Lin, W. Chang, D. Braun, W. J. Parak: "Size determination of (bio-) conjugated water-soluble colloidal nanoparticles - a comparison of different techniques", *Journal of Physical Chemistry C* **2007**, *111*, 11552 - 11559.
 - Preparation of samples, main part of characterization and data evaluation

Citrate-stabilized gold nanoparticles were conjugated with thiol-modified single-stranded DNA of different length. The electrophoretic mobility in agarose gel electrophoresis was evaluated in dependence of agarose concentration, DNA length, particle diameter and number of attached DNA molecules per particle. Data evaluation was performed by Ferguson analysis for different gel concentrations and alternatively by calibration of the gels with nanoparticles of known size. Both methods yielded similar diameters of the conjugates, the second method with reduced experimental effort. The scattering of the resulting data was partially attributed to the thick soft shell of DNA molecules interacting with the gel matrix. However, quantitative analysis allowed for deducing conformational changes of the DNA molecules from a stretched conformation at high grafting density and short molecules, to a more coiled form for longer DNA and lower grafting densities, respectively.

- **[A4]**^[4] T. Pellegrino*, R. A. Sperling*, A. P. Alivisatos, W. J. Parak: "Gelelectrophoresis of Gold-DNA Nanoconjugates", *Journal of Biomedicine and Biotechnology* **2007**, *2007*, article ID 26796.
 - Data evaluation (*both authors contributed equally)

6.3 Collaborative work

6.3.1 Materials science

Hydrophobic gold nanoparticles were modified with dodecanethiol by ligand exchange, resulting in stable particles that could be dispersed in a polymer matrix. In the lab of our collaboration partner Dr. Gyeong-Man Kim (Halle), a PMMA solution containing the nanoparticles of about 4 nm diameter was used for electrospinning. Depending on the process parameters, the resulting polymer fibers had a diameter of 20-100 nm, by means of TEM it was found that the nanoparticles were arranged in chain-like structures that were formed during the spinning process.

- **[A5]**^[5] G.-M. Kim, A. Wutzler, H.-J. Radosch, G. H. Michler, P. Simon, R. A. Sperling, W. J. Parak: "One-Dimensional Arrangement of Gold Nanoparticles by Electrospinning", *Chemistry of Materials* **2005**, *17*, 4949-4957.
 - Preparation of gold nanoparticles, surface modification by ligand exchange with dodecanethiol that is compatible with desired polymer for electrospinning.

Quantum dots were transferred to aqueous solution by means of an amphiphilic polymer that had been modified with a fluorescent dye. Due to the spectral overlap of the emission of the quantum dots and the absorption of the organic dye in the polymer shell, fluorescence energy transfer was observed, resulting in reduced QD emission and increased emission of the dye. The fluorescent dye served as a model for a calcium-sensitive dye that is intended for a future FRET-based sensor system for application inside cells.

- **[A6]**^[6] M. T. Fernández-Argüelles, A. Yakovlev, R. A. Sperling, C. Luccardini, S. Gaillard, A. S. Medel, J.-M. Mallet, J.-C. Brochon, A. Feltz, M. Oheim, W. J. Parak: "Synthesis and characterization of polymer-coated quantum dots with integrated acceptor dyes as FRET-based nanoprobes", *NanoLetters* **2007**, *7*, 2613-2617.
 - Part of sample characterization

The amphiphilic polymer coating approach was extended for the transfer of hydrophobic manganese ferrite nanoparticles to aqueous solution. The polymer-coated nanoparticles were compared to other coating strategies and the influence of the surface coating on the magnetic relaxation in regard to magnetic resonance imaging was studied.

- **[A7]**^[7] U. I. Tromsdorf, N. C. Bigall, M. Kaul, O. T. Bruns, M. S. Nikolic, B. Mollwitz, R. A. Sperling, R. Reimer, H. Hohenberg, W. J. Parak, S. Förster, U. Beisiegel, G. Adam, H. Weller: "Size and Surface Effects on the MRI Relaxivity of Manganese Ferrite Nanoparticle Contrast Agents ", *Nanoletters* **2007**, *7*, 2422-2427.
 - Preparation and characterization of part of the samples

Yttrium oxide nanoparticles were prepared by a sol-gel method and doped with Eu^{3+} and Tb^{3+} . The nanoparticles were found to be partially aggregated due to the high-temperature doping process. The particles could be partially dispersed in organic solution by means of addition of TOPO or other surfactants and sonication, or in aqueous solution by means of dichloroacetic acid and sonication. TEM revealed that the particles consisted mostly of small clusters and primary particles.

- **[A8]**^[8] A. Pandey, M. K. Roy, A. Pandey, M. Zanella, R. C. Sperling, W. J. Parak, H. C. Verma: "Chloroform- and water-soluble sol-gel derived $\text{Eu}^{+++}/\text{Y}_2\text{O}_3$ (red) and $\text{Tb}^{+++}/\text{Y}_2\text{O}_3$ (green) nanophosphors: synthesis, characterisation and surface modification ", *Nanotechnology* **2007**, *submitted*.
 - Surface modification and characterization (in part)

Small gold nanoclusters were prepared by synthesis in organic solution and an additional etching step. The particles were transferred to the aqueous phase by dihydrolipoic acid (DHLLA), the resulting diameter was smaller than 2 nm and nanoparticles exhibited red fluorescence emission. Though the quantum yield was considerably less than for typical semiconductor quantum dots, these very compact and cadmium-free probes are an interesting alternative in regard to biolabeling applications. The DHLLA-modified nanoparticles were conjugated with single biotin moieties and used for fluorescence labeling of cells.

- **[A9]**^[9] C.-A. Lin, R. A. Sperling, M. Zanella, W. Chang, J. Li, T.-Y. Yang, J.-L. Shen, H.-I. Yeh, W. Parak: "Synthesis, Characterization and Bio-conjugation of Fluorescent Gold Nanoclusters toward Biological Labeling Applications", *ACS Nano* **2008**, *submitted*.
 - Part of sample characterization

6.3.2 Biological systems

Citrate-stabilized gold nanoparticles with a diameter of 10 nm were conjugated with thiol-modified single-stranded DNA. Particles modified with strand A and particles with strand B were mixed, by addition of a linker strand with one end complementary to A and the other end to B, the nanoparticles could be cross-linked. The nanoparticle aggregates exhibited a blue-shifted optical absorption that could be used to generate DNA melting curves of which the melting temperature is decreased in case of a DNA mismatch. By employing a pulsed laser for optical heating, the melting transition could be observed in microseconds, resulting in a significant reduction of analysis time compared to temperature ramps of minutes to hours as in conventional experiments.

- **[A10]**^[10] J. Stehr, C. Hrelescu, R. A. Sperling, G. Raschke, M. Wunderlich, A. Nichtl, D. Heindl, K. Kürzinger, W. J. Parak, T. A. Klar, J. Feldmann: "Gold Nano-Stoves for Microsecond DNA Melting Analysis", *Nanoletters* **2008**, *8*, 619-623.
- *Patent*: J. Stehr, T. Klar, J. Feldmann, C. Hrelescu, W. Parak, G. Raschke, R. Sperling, M. Wunderlich, K. Kürzinger, D. Heindl, A. Nichtl, "Genotypisierung mittels optisch geheizter Nanopartikel-Aggregate", German patent submitted.
 - Preparation of DNA-modified nanoparticles, purification and characterization.

In a short review article, the application of quantum dots for biolabeling and bioanalytics was discussed.

- **[A11]**^[11] C.-A. J. Lin, T. Liedl, R. A. Sperling, M. T. Fernández-Argüelles, J. M. Costa-Fernández, R. Pereiro, A. Sanz-Medel, W. H. Chang, W. J. Parak: "Bioanalytics and Biolabeling with Semiconductor Nanoparticles (Quantum Dots)", *Journal of Materials Chemistry* **2007**, *17*, 1343-1346.

In a review article, biological applications of gold nanoparticles were summarized, including biolabeling, imaging, sensing, drug or gene delivery or hyperthermal therapy.

- **[A12]**^[12] R. A. Sperling, P. R. Gil, F. Zhang, M. Zanella, W. J. Parak: "Biological Applications of Gold Nanoparticles", *Chemical Society Reviews* **2008**, *37*(9), 1896 - 1908.

In regard to the biodistribution of nanoparticles in organisms, a series of experiments in rats was carried out. Gold nanoparticles with a core diameter of 5 nm were administered via the lungs, guts or by intravenous injection. Prior to application, the nanoparticles were rendered radioactive in a neutron reactor and after incubation of 1 to 24 h, the animals were sacrificed and the organs were dissected. The analysis of radioactivity enabled the sensitive and quantitative detection of the relative particle concentration in the different organs. In this study, gold nanoparticles with sulfonated phosphine, polymer-coating and different length of poly(ethylene glycol) were compared.

- ^[13] W. G. Kreyling, J. Lipka, S. Takenaka, A. Wenk, R. A. Sperling, W. J. Parak, M. Semmler-Behnke: "Quantitative biokinetics of PEGylated and phosphine-coated 5 nm gold nanoparticles administered either to the lungs, circulation or gut of rats", **2008**, *in preparation*.
 - Preparation of gold nanoparticles with different surfaces, purification and characterization.

Certain leukemia cells or cells infected by a leukemia-inducing virus have been found to be affected by an antioxidant mixture consisting of vitamins, amino acids and trace elements. The proliferation and invasiveness of the cancer cells is reduced by this nutrition mixture. The effect of gold nanoparticles on this mechanism has been studied, comparing the impact of polymer-coated and PEGylated nanoparticles on different cell types.

- ^[14] E. Baydoun, S. Sharakeh, R. A. Sperling, P. R. Gil, A. Meinhardt, W. J. Parak: "Gold nanoparticles affect the antiproliferative effect of SNS on HTLV-1 infected cells", **2008**, *in preparation*.
 - Synthesis and modification of gold nanoparticles with different surface coatings, purification and characterization of the particles.

7 Bibliography

- [1] R. A. Sperling, T. Pellegrino, J. K. Li, W. H. Chang, W. J. Parak: "Electrophoretic separation of nanoparticles with a discrete number of functional groups", *Advanced Functional Materials* **2006**, *16*(7), 943-948.
- [2] C.-A. J. Lin, R. A. Sperling, J. K. Li, T.-Y. Yang, P.-Y. Li, M. Zanella, W. H. Chang, W. J. Parak: "Design of an amphiphilic polymer for nanoparticle coating and functionalization", *Small* **2008**, *4*(3), 334-341.
- [3] R. A. Sperling, T. Liedl, S. Duhr, S. Kudara, M. Zanella, C.-A. J. Lin, W. Chang, D. Braun, W. J. Parak: "Size determination of (bio-) conjugated water-soluble colloidal nanoparticles - a comparison of different techniques", *Journal of Physical Chemistry C* **2007**, *111*(31), 11552 -11559.
- [4] T. P., R. A. Sperling, A. P. Alivisatos, W. J. Parak: "Gelelectrophoresis of Gold-DNA Nanoconjugates", *Journal of Biomedicine and Biotechnology* **2007**, *2007*, article ID 26796.
- [5] G.-M. Kim, A. Wutzler, H.-J. Radosch, G. H. Michler, P. Simon, R. A. Sperling, W. J. Parak: "One-Dimensional Arrangement of Gold Nanoparticles by Electrospinning", *Chemistry of Materials* **2005**, *17*, 4949-4957.
- [6] M. T. Fernández-Argüelles, A. Yakovlev, R. A. Sperling, C. Luccardini, S. Gaillard, A. S. Medel, J.-M. Mallet, J.-C. Brochon, A. Feltz, M. Oheim, W. J. Parak: "Synthesis and characterization of polymer-coated quantum dots with integrated acceptor dyes as FRET-based nanoprobe", *NanoLetters* **2007**, *7*(9), 2613-2617.
- [7] U. I. Tromsdorf, N. C. Bigall, M. Kaul, O. T. Bruns, M. S. Nikolic, B. Mollwitz, R. A. Sperling, R. Reimer, H. Hohenberg, W. J. Parak, S. Förster, U. Beisiegel, G. Adam, H. Weller: "Size and Surface Effects on the MRI Relaxivity of Manganese Ferrite Nanoparticle Contrast Agents", *Nanoletters* **2007**, *7*(8), 2422-2427.
- [8] A. Pandey, M. K. Roy, A. Pandey, M. Zanella, R. A. Sperling, W. J. Parak, H. C. Verma: "Chloroform- and water-soluble sol-gel derived $\text{Eu}^{3+}/\text{Y}_2\text{O}_3$ (red) and $\text{Tb}^{3+}/\text{Y}_2\text{O}_3$ (green) nanophosphors: synthesis, characterisation and surface modification", *Nanotechnology* **2008**, *submitted*.
- [9] C.-A. Lin, R. Sperling, M. Zanella, W. Chang, J. Li, T.-Y. Yang, J.-L. Shen, H.-I. Yeh, W. Parak: "Synthesis, Characterization and Bio-conjugation of Fluorescent Gold Nanoclusters toward Biological Labeling Applications", *ACS Nano* **2008**, *submitted*.
- [10] J. Stehr, C. Hrelescu, R. A. Sperling, G. Raschke, M. Wunderlich, A. Nichtl, D. Heindl, K. Kürzinger, W. J. Parak, T. A. Klar, J. Feldmann: "Gold Nano-Stoves for Microsecond DNA Melting Analysis", *Nanoletters* **2008**, *8*, 619-623.
- [11] C.-A. J. Lin, T. Liedl, R. A. Sperling, M. T. Fernández-Argüelles, J. M. Costa-Fernández, R. Pereiro, A. Sanz-Medel, W. H. Chang, W. J. Parak: "Bioanalytics and Biolabeling with Semiconductor Nanoparticles (Quantum Dots)", *Journal of Materials Chemistry* **2007**, *17*(14), 1343-1346.
- [12] R. A. Sperling, P. R. Gil, F. Zhang, M. Zanella, W. J. Parak: "Biological Applications of Gold Nanoparticles", *Chemical Society Reviews* **2008**, *37*(9), 1896 - 1908.
- [13] W. G. Kreyling, J. Lipka, S. Takenaka, A. Wenk, R. A. Sperling, W. J. Parak, M. Semmler-Behnke: "Quantitative biokinetics of PEGylated and phosphine-coated 5 nm gold nanoparticles administered either to the lungs, circulation or gut of rats", *in preparation* **2008**.
- [14] E. Baydoun, S. Sharakeh, R. A. Sperling, P. R. Gil, A. Meinhardt, W. J. Parak: "Gold nanoparticles affect the antiproliferative effect of SNS on HTLV-1 infected cells", **2008**, *in preparation*.
- [15] C. B. Murray, C. R. Kagan, M. G. Bawendi: "Synthesis and Characterization of Monodisperse Nanocrystals and Close-Packed Nanocrystals Assemblies", *Annu. Rev. Mater. Sci.* **2000**, *30*, 545-610.
- [16] L. Manna, E. C. Scher, A. P. Alivisatos: "Shape control of colloidal semiconductor nanocrystals", *J. Clust. Sci.* **2002**, *13*(4), 521-532.
- [17] M. Grzelczak, J. Perez-Juste, P. Mulvaney, L. M. Liz-Marzan: "Shape control in gold nanoparticle synthesis", *Chemical Society Reviews* **2008**, *37*(9), 1783-1791.
- [18] O. Masala, R. Seshadri: "Synthesis routes for large volumes of nanoparticles", *Annual Review of Materials Research* **2004**, *34*, 41-81.
- [19] M. C. Daniel, D. Astruc: "Gold Nanoparticles: Assembly, Supramolecular Chemistry, Quantum-Size-Related Properties, and Applications toward Biology, Catalysis, and Nanotechnology", *Chemical Reviews* **2004**, *104*(1), 293-346.
- [20] J. Turkevich, P. C. Stevenson, J. Hillier: "A study of the nucleation and growth processes in the synthesis of colloidal gold", *J. Discuss. Faraday Soc.* **1951**, 55-75.
- [21] F. Griffin, D. Fitzmaurice: "Preparation and thermally promoted ripening of water-soluble gold nanoparticles stabilized by weakly physisorbed ligands", *Langmuir* **2007**, *23*(20), 10262-10271.
- [22] S. Chen, K. Kimura: "Synthesis and Characterization of Carboxylate-Modified Gold Nanoparticle Powders Dispersible in Water", *Langmuir* **1999**, *15*, 1075-1082.
- [23] T. Sakura, T. Takahashi, K. Kataoka, Y. Nagasaki: "One-pot preparation of mono-dispersed and physiologically stabilized gold colloid", *Colloid & Polymer Science* **2005**, *284*(1), 97.

- [24] J. M. Slocik, M. O. Stone, R. R. Naik: "Synthesis of gold nanoparticles using multifunctional peptides", *Small* **2005**, *1*(11), 1048-1052.
- [25] J. Zheng, M. S. Stevenson, R. S. Hikida, P. G. V. Patten: "Influence of pH on Dendrimer-Protected Nanoparticles", *Journal of Physical Chemistry B* **2002**, *106*(6), 1252-1255.
- [26] M. Brust, M. Walker, D. Bethell, D. J. Schiffrin, R. Whyman: "Synthesis of thiol-derivatised gold nanoparticles in a two-phase liquid-liquid system", *J. Chem. Soc., Chem. Commun.* **1994**, *1994*, 801-802.
- [27] J. Fink, C. J. Kiely, D. Bethell, D. J. Schiffrin: "Self-Organization of Nanosized Gold Particles", *Chemistry of Materials* **1998**, *10*(3), 922-926.
- [28] L. A. Porter, D. Ji, S. L. Westcott, M. Graupe, R. S. Czernuszewicz, N. J. Halas, T. R. Lee: "Gold and Silver Nanoparticles Functionalized by the Adsorption of Dialkyl Disulfides", *Langmuir* **1998**, *14*(26), 7378-7386.
- [29] M. Alloisio, A. Demartini, C. Cuniberti, M. Muniz-Miranda, E. Giorgetti, A. Giusti, G. Dellepiane: "Photopolymerization of diacetylene-capped gold nanoparticles", *Physical Chemistry Chemical Physics* **2008**, *10*(16), 2214-2220.
- [30] L. Fabris, S. Antonello, L. Armelao, R. L. Donkers, F. Polo, C. Toniolo, F. Maran: "Gold Nanoclusters Protected by Conformationally Constrained Peptides", *J. Am. Chem. Soc.* **2006**, *128*(1), 326-336.
- [31] D. V. Leff, L. Brandt, J. R. Heath: "Synthesis and Characterization of Hydrophobic, Organically-Soluble Gold Nanocrystals Functionalized with Primary Amines", *Langmuir* **1996**, *12*(20), 4723-4730.
- [32] M. Brust, J. Fink, D. Bethell, D. J. Schiffrin, C. Kienly: "Synthesis and Reactions of Functionalised Gold Nanoparticles", *J. Chem. Soc., Chem. Commun.* **1995**, *1995*, 1655-1656.
- [33] A. G. Kanaras, F. S. Kamounah, K. Schaumburg, C. J. Kiely, M. Brust: "Thioalkylated tetraethylene glycol: a new ligand for water soluble monolayer protected gold clusters", *Chem. Comm.* **2002**, *2002*, 2294-2295.
- [34] S. Stoeva, K. J. Klabunde, C. M. Sorensen, I. Dragieva: "Gram-Scale Synthesis of Monodisperse Gold Colloids by the Solvated Metal Atom Dispersion Method and Digestive Ripening and Their Organization into Two- and Three-Dimensional Structures", *Journal of the American Chemical Society* **2002**, *124*(10), 2305-2311.
- [35] X. Y. Chen, J. R. Li, L. Jiang, X. Y. Chen, J. R. Li: "Two-dimensional arrangement of octadecylamine-functionalized gold nanoparticles using the LB technique", *Nanotechnology* **2000**, *11*, 108-111.
- [36] N. R. Jana, X. Peng: "Single-phase and gram-scale routes toward nearly monodisperse Au and other noble metal nanocrystals", *Journal of the American Chemical Society* **2003**, *125*(47), 14280-14281.
- [37] X. Lu, H.-Y. Tuan, B. A. Korgel, Y. Xia: "Facile Synthesis of Gold Nanoparticles with Narrow Size Distribution by Using AuCl or AuBr as the Precursor", *Chemistry - A European Journal* **2008**, *14*(5), 1584-1591.
- [38] C. Fan, L. Jiang: "Preparation of Hydrophobic Nanometer Gold Particles and Their Optical Absorption in Chloroform", *Langmuir* **1997**, *13*(11), 3059-3062.
- [39] J. H. Youk, M.-K. Park, J. Locklin, R. Advincula, J. Yang, J. Mays: "Preparation of Aggregation Stable Gold Nanoparticles Using Star-Block Copolymers", *Langmuir* **2002**, *18*(7), 2455-2458.
- [40] P. Zheng, X. Jiang, X. Zhang, W. Zhang, L. Shi: "Formation of Gold@Polymer Core-Shell Particles and Gold Particle Clusters on a Template of Thermoresponsive and pH-Responsive Coordination Triblock Copolymer", *Langmuir* **2006**, *22*(22), 9393-9396.
- [41] X.-M. Li, M. R. d. Jong, K. Inoue, S. Shinkai, J. Huskens, D. N. Reinhoudt: "Formation of gold colloids using thioether derivatives as stabilizing ligands", *J. Mater. Chem.* **2001**, *11*, 1919-1923.
- [42] T. Peterle, A. Leifert, J. Timper, A. Sologubenko, U. Simon, M. Mayor: "Multidentate thioether ligands coating gold nanoparticles", *Chemical Communications* **2008**(29), 3438-3440.
- [43] W. P. Wuelfing, S. M. Gross, D. T. Miles, R. W. Murray: "Nanometer Gold Clusters Protected by Surface-Bound Monolayers of Thiolated Poly(ethylene glycol) Polymer Electrolyte", *Journal of the American Chemical Society* **1998**, *120*(48), 12696-12697.
- [44] I. Hussain, S. Graham, Z. X. Wang, B. Tan, D. C. Sherrington, S. P. Rannard, A. I. Cooper, M. Brust: "Size-controlled synthesis of near-monodisperse gold nanoparticles in the 1-4 nm range using polymeric stabilizers", *Journal of the American Chemical Society* **2005**, *127*(47), 16398-16399.
- [45] Z. X. Wang, B. E. Tan, I. Hussain, N. Schaeffer, M. F. Wyatt, M. Brust, A. I. Cooper: "Design of polymeric stabilizers for size-controlled synthesis of monodisperse gold nanoparticles in water", *Langmuir* **2007**, *23*(2), 885-895.
- [46] S. K. Bajpai, Y. M. Mohan, M. Bajpai, R. Tankhiwale, V. Thomas: "Synthesis of polymer stabilized silver and gold nanostructures", *Journal Of Nanoscience And Nanotechnology* **2007**, *7*(9), 2994-3010.
- [47] G. Schmid: "Large clusters and colloids. Metals in the embryonic state", *Chem. Rev.* **1992**, *92*(8), 1709-1727.
- [48] A. C. Templeton, W. P. Wuelfing, R. W. Murray: "Monolayer-Protected Cluster Molecules", *Accounts of Chemical Research* **2000**, *33*(1), 27-36.
- [49] J. P. Wilcoxon, B. L. Abrams: "Synthesis, structure and properties of metal nanoclusters", *Chemical Society Reviews* **2006**, *35*, 1162-1194.
- [50] P. D. Jadzinsky, G. Calero, C. J. Ackerson, D. A. Bushnell, R. D. Kornberg: "Structure of a thiol monolayer-protected gold nanoparticle at 1.1 Å resolution", *Science* **2007**, *318*(5849), 430-433.
- [51] R. S. Ingram, M. J. Hostetler, R. W. Murray: "Poly-hetero- ω -functionalized Alkanethiolate-Stabilized Gold Cluster Compounds", *Journal of the American Chemical Society* **1997**, *119*(39), 9175-9178.
- [52] M. W. Heaven, A. Dass, P. S. White, K. M. Holt, R. W. Murray: "Crystal Structure of the Gold Nanoparticle [N(C₈H₁₇)₄][Au₂₅(SCH₂CH₂Ph)₁₈]", *J. Am. Chem. Soc.* **2008**, *130*(12), 3754-3755.

- [53] G. Schmid: "The relevance of shape and size of Au55 clusters", *Chem. Soc. Rev.* **2008**, 37(9), 1909-1930.
- [54] T. Huang, R. W. Murray: "Visible luminescence of water-soluble monolayer-protected gold clusters", *Journal Of Physical Chemistry B* **2001**, 105(50), 12498-12502.
- [55] H. W. Duan, S. M. Nie: "Etching colloidal gold nanocrystals with hyperbranched and multivalent polymers: A new route to fluorescent and water-soluble atomic clusters", *Journal Of The American Chemical Society* **2007**, 129(9), 2412-2413.
- [56] H. He, C. Xie, J. Ren: "Nonbleaching Fluorescence of Gold Nanoparticles and Its Applications in Cancer Cell Imaging", *Anal. Chem.* **2008**, 80(15), 5951-5957.
- [57] N. Schaeffer, B. Tan, C. Dickinson, M. J. Rosseinsky, A. Laromaine, D. W. McComb, M. M. Stevens, Y. Wang, L. Petit, C. Barentin, D. G. Spiller, A. I. Cooper, R. Levy: "Fluorescent or not? Size-dependent fluorescence switching for polymer-stabilized gold clusters in the 1.1-1.7 nm size range", *Chemical Communications* **2008**, DOI: 10.1039/b809876j(38), 3986-3988.
- [58] P. E. Lippens, M. Lannoo: "Calculation of the band gap for small CdS and ZnS crystallites", *Phys. Rev. B.* **1989**, 39, 10935-10942.
- [59] M. G. Bawendi, M. L. Steigerwald, L. E. Brus: "The quantum mechanics of large semiconductor clusters ("quantum dots")", *Annu. Rev. Phys. Chem.* **1990**, 41, 477-496.
- [60] W. J. Parak, L. Manna, T. Nann, in *Nanotechnology, Vol. Volume 1: Principles and Fundamentals* (Ed.: G. Schmid), WILEY-VCH, **2008**, pp. 73-96.
- [61] A. L. Rogach, A. Eychmüller, S. G. Hickey, S. V. Kershaw: "Infrared-Emitting Colloidal Nanocrystals: Synthesis, Assembly, Spectroscopy, and Applications", *Small* **2007**, 3(4), 536-557.
- [62] C. B. Murray, D. J. Norris, M. G. Bawendi: "Synthesis and Characterization of Nearly Monodisperse CdE (E = S, Se, Te) Semiconductor Nanocrystallites", *Journal of the American Chemical Society* **1993**, 115, 8706-8715.
- [63] A. L. Rogach, L. Katsikas, A. Kornowski, D. Su, A. Eychmüller, H. Weller: "Synthesis and Characterization of Thiol-Stabilized CdTe Nanocrystals", *Ber. Bunsenges. Phys. Chem.* **1996**, 100(11), 1772-1778.
- [64] Z. A. Peng, X. Peng: "Formation of High-Quality CdTe, CdSe, and CdS Nanocrystals Using CdO as Precursor", *Journal of the American Chemical Society* **2001**, 123(1), 183-184.
- [65] Y. W. Jun, J. E. Koo, J. Cheon: "One-step synthesis of size tuned zinc selenide quantum dots via a temperature controlled molecular precursor approach", *Chemical Communications* **2000**, 2000/14, 1243-1244.
- [66] A. A. Guzelian, J. E. B. Katari, A. V. Kadavanich, U. Banin, K. Hamad, E. Juban, A. P. Alivisatos, R. H. Wolters, C. C. Arnold, J. R. Heath: "Synthesis of Size-Selected, Surface-Passivated InP Nanocrystals", *Journal of Physical Chemistry B* **1996**, 100(17), 7212-7219.
- [67] M. Green, P. O'Brien: "A novel metalorganic route for the direct and rapid synthesis of monodispersed quantum dots of indium phosphide", *Chem. Commun.* **1998**, 1998, 2459-2460.
- [68] A. L. Rogach, M. T. Harrison, S. V. Kershaw, A. Kornowski, M. G. Burt, A. Eychmüller, H. Weller: "Colloidally Prepared CdHgTe and HgTe Quantum Dots with Strong Near-Infrared Luminescence", *Physica Status Solidi B* **2001**, 224(1), 153-158.
- [69] N. Al-Salim, A. G. Young, R. D. Tilley, A. J. McQuillan, J. Xia: "Synthesis of CdSeS Nanocrystals in Coordinating and Noncoordinating Solvents: Solvent's Role in Evolution of the Optical and Structural Properties", *Chem. Mater.* **2007**, 19(21), 5185-5193.
- [70] X. Zhong, M. Han, Z. Dong, T. J. White, W. Knoll: "Composition-Tunable ZnxCd1-xSe Nanocrystals with High Luminescence and Stability", *J. Am. Chem. Soc.* **2003**, 125(28), 8589-8594.
- [71] L. Spanhel, M. Haase, H. Weller, A. Henglein: "Photochemistry of Colloidal Semiconductors. 20. Surface Modification and Stability of Strong Luminescing CdS Particles", *Journal of the American Chemical Society* **1987**, 109, 5649-5655.
- [72] R. D. Stramel, T. Nakamura, J. K. Thomas: "Photophysical and Photochemical Properties of CdS with Limited Dimensions", *J. Chem. Soc., Faraday Trans. I* **1988**, 84(5), 1287-1300.
- [73] A. L. Rogach, L. Katsikas, A. Kornowski, D. Su, A. Eychmüller, H. Weller: "Synthesis, Morphology and Optical Properties of Thiol-Stabilized CdTe Nanoclusters in aqueous Solution", *Ber. Bunsen. Phys. Chem.* **1997**, 101(11), 1668-1670.
- [74] B. O. Dabbousi, J. Rodriguez-Viejo, F. V. Mikulec, J. R. Heine, H. Mattoussi, R. Ober, K. F. Jensen, M. G. Bawendi: "(CdSe)ZnS Core-Shell Quantum Dots: Synthesis and Characterization of a Size Series of Highly Luminescent Nanocrystallites", *Journal of Physical Chemistry B* **1997**, 101(46), 9463-9475.
- [75] T. Mokari, U. Banin: "Synthesis and Properties of CdSe/ZnS Core/Shell Nanorods", *Chemistry of Materials* **2003**, 15(20), 3955-3960.
- [76] Y.-W. Cao, U. Banin: "Synthesis and Characterization of InAs/InP and InAs/CdSe Core/Shell Nanocrystals", *Angewandte Chemie, International Edition* **1999**, 38(24), 3692-3694.
- [77] S. Kim, B. Fisher, H.-J. Eisler, M. Bawendi: "Type-II Quantum Dots: CdTe/CdSe(Core/Shell) and CdSe/ZnTe(Core/Shell) Heterostructures", *Journal of the American Chemical Society* **2003**, 125(38), 11466-11467.
- [78] P. Reiss, S. Carayon, J. Bleuse, A. Pron: "Low polydispersity core/shell nanocrystals of CdSe/ZnSe and CdSe/ZnSe/ZnS type: preparation and optical studies", *Synth. Met.* **2003**, 139, 649-652.
- [79] D. V. Talapin, I. Mekis, S. Götzinger, A. Kornowski, O. Benson, H. Weller: "CdSe/CdS/ZnS and CdSe/ZnSe/ZnS Core-Shell-Shell Nanocrystals", *Journal of Physical Chemistry B* **2004**, 108(49), 18826-18831.

- [80] R. Xie, U. Kolb, J. Li, T. Basche, A. Mews: "Synthesis and Characterization of Highly Luminescent CdSe-Core CdS/ZnO.5Cd0.5S/ZnS Multishell Nanocrystals", *J. Am. Chem. Soc.* **2005**, *127*(20), 7480-7488.
- [81] A. Aharoni, T. Mokari, I. Popov, U. Banin: "Synthesis of InAs/CdSe/ZnSe Core/Shell1/Shell2 Structures with Bright and Stable Near-Infrared Fluorescence", *Journal of the American Chemical Society* **2006**, *128*, 257-264.
- [82] F. V. Mikulec, M. Kuno, M. Bennati, A. D. Hall, R. G. Griffin, M. G. Bawendi: "Organometallic Synthesis and Spectroscopic Characterization of Manganese-Doped CdSe Nanocrystals", *Journal of the American Chemical Society* **2000**, *122*(11), 2532-2540.
- [83] W. C. Kwak, Y. M. Sung, T. G. Kim, W. S. Chae: "Synthesis of Mn-doped zinc blende CdSe nanocrystals", *Applied Physics Letters* **2007**, *90*(17), 173111.
- [84] J. v. Embden, J. Jasieniak, D. E. Gómez, P. Mulvaney, M. Giersig: "Review of the Synthetic Chemistry Involved in the Production of Core/Shell Semiconductor Nanocrystals", *Australian Journal of Chemistry* **2007**, *60*(7), 457-471.
- [85] D. H. Chen, S. H. Wu: "Synthesis of nickel nanoparticles in water-in-oil microemulsions", *Chemistry of Materials* **2000**, *12*(5), 1354-1360.
- [86] C. Damle, A. Kumar, M. Sastry: "Synthesis of Ag/Pd Nanoparticles and Their Low-Temperature Alloying within Thermally Evaporated Fatty Acid Films", *Journal of Physical Chemistry B* **2002**, *106*(2), 297-302.
- [87] B. Ravel, E. E. Carpenter, V. G. Harris: "Oxidation of iron in iron/gold core/shell nanoparticles", *Journal of Applied Physics* **2002**, *91*(10), 8195-8197.
- [88] R. Ferrando, J. Jellinek, R. L. Johnston: "Nanoalloys: From Theory to Applications of Alloy Clusters and Nanoparticles", *Chem. Rev.* **2008**, *108*(3), 845-910.
- [89] F. Erogbogbo, K.-T. Yong, I. Roy, G. Xu, P. N. Prasad, M. T. Swihart: "Biocompatible Luminescent Silicon Quantum Dots for Imaging of Cancer Cells", *ACS Nano* **2008**, *2*(5), 873-878.
- [90] W. Stöber, A. Fink, E. Bohn: "Controlled growth of monodisperse silica spheres in the micron size range", *Journal of Colloid and Interface Science* **1968**, *26*(1), 62.
- [91] W. Tan, K. Wang, X. He, X. J. Zhao, T. Drake, L. Wang, R. P. Bagwe: "Bionanotechnology based on silica nanoparticles", *Medicinal Research Reviews* **2004**, *24*(5), 621-638.
- [92] O. Ehlert, R. Thomann, M. Darbandi, T. Nann: "A Four-Color Colloidal Multiplexing Nanoparticle System", *ACS Nano* **2008**, *2*(1), 120-124.
- [93] S. Heer, K. Kompe, H. U. Gudel, M. Haase: "Highly efficient multicolour upconversion emission in transparent colloids of lanthanide-doped NaYF₄ nanocrystals", *Advanced Materials* **2004**, *16*(23-24), 2102-+.
- [94] J. C. Boyer, L. A. Cuccia, J. A. Capobianco: "Synthesis of Colloidal Upconverting NaYF₄: Er³⁺/Yb³⁺ and Tm³⁺/Yb³⁺ Monodisperse Nanocrystals", *Nano Lett.* **2007**, *7*(3), 847-852.
- [95] M. Darbandi, W. Hoheisel, T. Nann: "Silica coated, water dispersible and photoluminescent Y (V,P)O₄:Eu³⁺,Bi³⁺ nanophosphors", *Nanotechnology* **2006**, *17*(16), 4168-4173.
- [96] T. Shen, R. Weissleder, M. Papisov, A. Bogdanov, T. J. Brady: "Monocrystalline iron oxide nanocompounds (MION): Physicochemical properties", *Mag. Res. Med.* **1993**, *29*(5), 599-604.
- [97] D. Vollath, D. V. Szabo, R. D. Taylor, J. O. Willis, K. E. Sickafus: "Synthesis and properties of nanocrystalline superparamagnetic γ -Fe₂O₃", *Nanostructured Materials* **1995**, *6*, 941-944.
- [98] M. Klotz, A. Ayrat, C. Guizard, C. Menager, V. Cabuil: "Silica Coating on Colloidal Maghemite Particles", *Journal of Colloid and Interface Science* **1999**, *220*, 357-361.
- [99] L. Babes, B. Denizot, G. Tanguy, J. J. L. Jeune, P. Jallet: "Synthesis of Iron Oxide Nanoparticles Used as MRI Contrast Agents: A Parametric Study", *Journal of Colloid and Interface Science* **1999**, *212*, 474-482.
- [100] D. K. Kim, Y. Zhang, W. Voit, K. V. Rao, M. Muhammed: "Synthesis and characterization of surfactant-coated superparamagnetic monodispersed iron oxide nanoparticles", *Journal of Magnetism and Magnetic Materials* **2001**, *225*, 30-36.
- [101] D. K. Kim, Y. Zhang, W. Voit, K. V. Rao, J. Kehr, B. Bjelke, M. Muhammed: "Superparamagnetic Iron Oxide Nanoparticles for Biomedical Applications", *Scripta Materialia* **2001**, *44*, 1713-1717.
- [102] Y. Ni, X. Ge, Z. Zhang, Q. Ye: "Fabrication and Characterization of the Plate-Shaped γ -Fe₂O₃ Nanocrystals", *Chemistry of Materials* **2002**, *14*, 1048-1052.
- [103] Z. L. Liu, Y. J. Liu, K. L. Yao, Z. H. Ding, J. Tao, X. Wang: "Synthesis and Magnetic Properties of Fe₃O₄ Nanoparticles", *Journal of Materials Synthesis and Processing* **2002**, *10*(2), 83-87.
- [104] V. F. Puentes, K. M. Krishnan, A. P. Alivisatos: "Colloidal Nanocrystal Shape and Size Control: The Case of Cobalt", *Science* **2001**, *291*(16 March), 2115-2117.
- [105] V. F. Puentes, K. Krishnan, A. P. Alivisatos: "Synthesis of Colloidal Cobalt Nanoparticles with Controlled Size and Shapes", *Topics in Catalysis* **2002**, *19*(2), 145-148.
- [106] L. T. Lu, L. D. Tung, I. Robinson, D. Ung, B. Tan, J. Long, A. I. Cooper, D. G. Fernig, N. T. K. Thanh: "Size and shape control for water-soluble magnetic cobalt nanoparticles using polymer ligands", *Journal of Materials Chemistry* **2008**, *18*(21), 2453-2458.
- [107] K. Butter, A.P.Philipse, G.J.Vroege: "Synthesis and properties of iron ferrofluids", *Journal of Magnetism and Magnetic Materials* **2002**, *252*, 1-3.
- [108] J. Wagner, T. Autenrieth, R. Hempelmann: "Core shell particles consisting of cobalt ferrite and silica as model ferrofluids [CoFe₂O₄-SiO₂ core shell particles]", *Journal of Magnetism and Magnetic Materials* **2002**, *252*, 4-6.

- [109] P. D. Cozzoli, E. Snoeck, M. A. Garcia, C. Giannini, A. Guagliardi, A. Cervellino, F. Gozzo, A. Hernando, K. Achterhold, N. Ciobanu, F. G. Parak, R. Cingolani, L. Manna: "Colloidal synthesis and characterization of tetrapod-shaped magnetic nanocrystals", *Nano Lett* **2006**, 6(9), 1966-1972.
- [110] T. Hyeon: "Chemical synthesis of magnetic nanoparticles", *Chem. Commun.* **2003**, 8, 927-934.
- [111] X. M. Lin, A. C. S. Samia: "Synthesis, assembly and physical properties of magnetic nanoparticles", *Journal of Magnetism and Magnetic Materials* **2006**, 305(1), 100-109.
- [112] N. R. Jana: "Gram-Scale Synthesis of Soluble, Near-Monodisperse Gold Nanorods and Other Anisotropic Nanoparticles", *Small* **2005**, 1(8-9), 875-882.
- [113] X. Peng, L. Manna, W. Yang, J. Wickham, E. Scher, A. Kadavanich, A. P. Alivisatos: "Shape control of CdSe nanocrystals", *Nature* **2000**, 404, 59-61.
- [114] L. Manna, D. J. Milliron, A. Meisel, E. C. Scher, A. P. Alivisatos: "Controlled growth of tetrapod-branched inorganic nanocrystals", *Nature Materials* **2003**, 2(june 2003), 382-385.
- [115] D. Tari, M. De_Giorgi, F. Della_Sala, L. Carbone, Roman Krahne, L. Manna, R. Cingolani, S. Kudera, W. J. Parak: "Optical properties of tetrapod-shaped CdTe nanocrystals", *Applied Physics Letters* **2005**, 87, 224101.
- [116] A. G. Kanaras, C. Sonnichsen, H. T. Liu, A. P. Alivisatos: "Controlled synthesis of hyperbranched inorganic nanocrystals with rich three-dimensional structures", *Nano Letters* **2005**, 5(11), 2164-2167.
- [117] D. J. Milliron, S. M. Hughes, Y. Cui, L. Manna, J. Li, L.-W. Wang, A. P. Alivisatos: "Colloidal nanocrystal heterostructures with linear and branched topology", *Nature* **2004**, 430, 190-195.
- [118] L. R. Hirsch, A. M. Gobin, A. R. Lowery, F. Tam, R. A. Drezek, N. J. Halas, J. L. West: "Metal nanoshells", *Annals Of Biomedical Engineering* **2006**, 34(1), 15-22.
- [119] S. J. Son, X. Bai, S. Lee: "Inorganic hollow nanoparticles and nanotubes in nanomedicine. Part 2: Imaging, diagnostic, and therapeutic applications", *Drug Discovery Today* **2007**, 12(15-16), 657-663.
- [120] N. Pinna, K. Weiss, J. Urban, M.-P. Pileni: "Triangular CdS Nanocrystals: Structural and Optical Studies", *Advanced Materials* **2001**, 13(4), 261-264.
- [121] T. S. Ahmadi, Z. L. Wang, T. C. Green, A. Henglein, M. A. El-Sayed: "Shape-Controlled Synthesis of Colloidal Platinum Nanoparticles", *Science* **1996**, 272, 1924-1926.
- [122] S. H. Choi, E. G. Kim, T. Hyeon: "One-Pot Synthesis of Copper-Indium Sulfide Nanocrystal Heterostructures with Acorn, Bottle, and Larva Shapes", *journal of the american chemical society* **2006**, 128(8), 2520-2521.
- [123] Z. A. Peng, X. Peng: "Mechanisms of the Shape Evolution of CdSe Nanocrystals", *Journal of the American Chemical Society* **2001**, 123(7), 1389-1395.
- [124] C. Burda, X. Chen, R. Narayanan, M. A. El-Sayed: "Chemistry and Properties of Nanocrystals of Different Shapes", *Chem. Rev.* **2005**, 105(4), 1025-1102.
- [125] J. Perez-Juste, I. Pastoriza-Santos, L. M. Liz-Marzan, P. Mulvaney: "Gold nanorods: Synthesis, characterization and applications", *Coordination Chemistry Reviews* **2005**, 249, 1870-1901.
- [126] Y. Yin, A. P. Alivisatos: "Colloidal nanocrystal synthesis and the organic-inorganic interface", *Nature* **2005**, 437(7059), 664.
- [127] S. Kumar, T. Nann: "Shape control of II-VI semiconductor nanomaterials", *Small* **2006**, 2(3), 316-329.
- [128] S. Kudera, L. Carbone, L. Manna, W. J. Parak, in *Semiconductor Nanocrystal Quantum Dots* (Ed.: A. L. Rogach), Springer, Wien, **2008**, pp. 1-34.
- [129] A. R. Tao, S. Habas, P. Yang: "Shape Control of Colloidal Metal Nanocrystals", *Small* **2008**, 4(3), 310-325.
- [130] T. Mokari, E. Rothenberg, I. Popov, R. Costi, U. Banin: "Selective Growth of Metal Tips onto Semiconductor Quantum Rods and Tetrapods", *Science* **2004**, 304, 1787-1790.
- [131] T. Mokari, C. G. Sztrum, A. Salant, E. Rabani, U. Banin: "Formation of asymmetric one-sided metal-tipped semiconductor nanocrystal dots and rods", *Nature Materials* **2005**, 4(11), 855-863.
- [132] S. Kudera, L. Carbone, M. F. Casula, R. Cingolani, A. Falqui, E. Snoeck, W. J. Parak, L. Manna: "Selective growth of PbSe on one or both tips of colloidal semiconductor nanorods", *Nanoletters* **2005**, 5(3), 445-449.
- [133] H. Yu, M. Chen, P. M. Rice, S. X. Wang, R. L. White, S. Sun: "Dumbbell-like Bifunctional Au-Fe₃O₄ Nanoparticles", *Nanoletters* **2005**, 5(2), 379-382.
- [134] T. Pellegrino, A. Fiore, E. Carlino, C. Giannini, P. D. Cozzoli, G. Ciccarella, M. Respaud, L. Palmirotta, R. Cingolani, L. Manna: "Heterodimers based on CoPt₃-Au nanocrystals with tunable domain size", *Journal Of The American Chemical Society* **2006**, 128(20), 6690-6698.
- [135] L. Zhang, Y. H. Dou, H. C. Gu: "Synthesis of Ag-Fe₃O₄ heterodimeric nanoparticles", *Journal Of Colloid And Interface Science* **2006**, 297(2), 660-664.
- [136] H. Gu, R. Zheng, X. X. Zhang, B. Xu: "Facile One-Pot Synthesis of Bifunctional Heterodimers of Nanoparticles: A Conjugate of Quantum Dot and Magnetic Nanoparticles", *Journal of the American Chemical Society* **2004**, 126(18), 5664-5665.
- [137] H. Kim, M. Achermann, L. P. Balet, J. A. Hollingsworth, V. I. Klimov: "Synthesis and characterization of Co/CdSe core/shell nanocomposites: Bifunctional magnetic-optical nanocrystals", *Journal Of The American Chemical Society* **2005**, 127(2), 544-546.
- [138] E. E. Carpenter, A. Kumbhar, J. A. Wiemann, H. Srikanth, J. Wiggins, W. Zhou, C. J. O'Connor: "Synthesis and magnetic properties of gold-iron-gold nanocomposites", *Materials Science and Engineering A* **2000**, 286, 81-86.

- [139] A. Quarta, R. Di Corato, L. Manna, A. Ragusa, T. Pellegrino: "Fluorescent-magnetic hybrid nanostructures: Preparation, properties, and applications in biology", *Ieee Transactions On Nanobioscience* **2007**, *6*, 298-308.
- [140] M. Zanella, A. Falqui, S. Kudera, L. Manna, M. F. Casula, W. J. Parak: "Growth of colloidal nanoparticles of group II-VI and IV-VI semiconductors on top of magnetic iron-platinum nanocrystals", *Journal of Materials Chemistry* **2008**, *18*, 4311-4317.
- [141] C. S. Weisbecker, M. V. Merritt, G. M. Whitesides: "Molecular Self-Assembly of Aliphatic Thiols on Gold Colloids", *Langmuir* **1996**, *12*, 3763-3772.
- [142] S. Y. Lin, Y. T. Tsai, C. C. Chen, C. M. Lin, C. h. Chen: "Two-Step Functionalization of Neutral and Positively Charged Thiols onto Citrate-Stabilized Au Nanoparticles", *J. Phys. Chem. B* **2004**, *108*(7), 2134-2139.
- [143] J. C. Love, L. A. Estroff, J. K. Kriebel, R. G. Nuzzo, G. M. Whitesides: "Self-assembled monolayers of thiolates on metals as a form of nanotechnology", *Chemical Reviews* **2005**, *105*(4), 1103-1169.
- [144] H. Döllefeld, K. Hoppe, J. Kolny, K. Schilling, H. Weller, A. Eychmüller: "Investigations on the stability of thiol stabilized semiconductor nanoparticles", *Physical Chemistry Chemical Physics* **2002**, *4*(19), 4747-4753.
- [145] X. Ji, D. Copenhaver, C. Sichmeller, X. Peng: "Ligand Bonding and Dynamics on Colloidal Nanocrystals at Room Temperature: The Case of Alkylamines on CdSe Nanocrystals", *J. Am. Chem. Soc.* **2008**, *130*(17), 5726-5735.
- [146] S. J. Clarke, C. A. Hollmann, Z. Zhang, D. Suffern, S. E. Bradforth, N. Dimitrijevic, W. G. Minarik, J. L. Nadeau: "Photophysics of dopamine-modified quantumdots and effects on biological systems", *Nature Materials* **2006**, *5*, 409-417.
- [147] J. Aldana, Y. A. Wang, X. Peng: "Photochemical instability of CdSe nanocrystals coated by hydrophilic thiols", *Journal of the American Chemical Society* **2001**, *123*(36), 8844-8850.
- [148] J. Aldana, N. Lavelle, Y. Wang, X. Peng: "Size-Dependent Dissociation pH of Thiolate Ligands from Cadmium Chalcogenide Nanocrystals", *Journal of the American Chemical Society* **2005**, *127*(8), 2496-2504.
- [149] T. Laaksonen, P. Ahonen, C. Johans, K. Kontturi: "Stability and Electrostatics of Mercaptoundecanoic Acid-Capped Gold Nanoparticles with Varying Counterion Size", *ChemPhysChem* **2006**, *7*(10), 2143-2149.
- [150] K. Kimura, S. Takashima, H. Ohshima: "Molecular Approach to the Surface Potential Estimate of Thiolate-Modified Gold Nanoparticles", *Journal of Physical Chemistry B* **2002**, *106*(29), 7260-7266.
- [151] V. S. Stenkamp, P. McGuiggan, J. C. Berg: "Restabilization of Electrosterically Stabilized Colloids in High Salt Media", *Langmuir* **2001**, *17*(3), 637-651.
- [152] G. Fritz, V. Schadler, N. Willenbacher, N. J. Wagner: "Electrosteric Stabilization of Colloidal Dispersions", *Langmuir* **2002**, *18*(16), 6381-6390.
- [153] Y. A. Wang, J. J. Li, H. Chen, X. Peng: "Stabilization of Inorganic Nanocrystals by Organic Dendrons", *Journal of the American Chemical Society* **2002**, *124*(10), 2293-2298.
- [154] C. J. Ackerson, P. D. Jadzinsky, R. D. Kornberg: "Thiolate Ligands for Synthesis of Water-Soluble Gold Clusters", *J. Am. Chem. Soc.* **2005**, *127*(18), 6550-6551.
- [155] M. J. Hostetler, A. C. Templeton, R. W. Murray: "Dynamics of Place-Exchange Reactions on Monolayer-Protected Gold Cluster Molecules", *Langmuir* **1999**, *15*(11), 3782-3789.
- [156] K. Aslan, V. H. Pérez-Luna: "Surface Modification of Colloidal Gold by Chemisorption of Alkanethiols in the Presence of a Nonionic Surfactant", *Langmuir* **2002**, *18*(16), 6059-6065.
- [157] K. S. Mayya, V. Patil, M. Sastry: "On the Stability of Carboxylic Acid Derivatized Gold Colloidal Particles: The Role of Colloidal Solution pH Studied by Optical Absorption Spectroscopy", *Langmuir* **1997**, *13*(15), 3944-3947.
- [158] Y. Zhao, W. Perez-Segarra, Q. Shi, A. Wei: "Dithiocarbamate Assembly on Gold", *J. Am. Chem. Soc.* **2005**, *127*(20), 7328-7329.
- [159] A. P. Alivisatos: "Perspectives on the Physical Chemistry of Semiconductor Nanocrystals", *Journal of Physical Chemistry A* **1996**, *100*(31), 13226-13239.
- [160] I. Moreels, J. C. Martins, Z. Hens: "Solution NMR techniques for investigating colloidal nanocrystal ligands: A case study on trioctylphosphine oxide at InP quantum dots", *Sensors and Actuators B: Chemical* **2007**, *126*(1), 283.
- [161] J. E. Bowen-Katari, V. L. Colvin, A. P. Alivisatos: "X-ray Photoelectron Spectroscopy of CdSe Nanocrystals with Applications to Studies of the Nanocrystal Surface", *J. Phys. Chem.* **1994**, *98*, 4109-4117.
- [162] F. Dubois, B. Mahler, B. Dubertret, E. Doris, C. Mioskowski: "A Versatile Strategy for Quantum Dot Ligand Exchange", *J. Am. Chem. Soc.* **2007**, *129*(3), 482-483.
- [163] S. F. Wuister, C. D. Donega, A. Meijerink: "Influence of thiol capping on the exciton luminescence and decay kinetics of CdTe and CdSe quantum", *Journal of Physical Chemistry B* **2004**, *108*(45), 17393-17397.
- [164] C. Bullen, P. Mulvaney: "The Effects of Chemisorption on the Luminescence of CdSe Quantum Dots", *Langmuir* **2006**, *22*(7), 3007-3013.
- [165] G. Kalyuzhny, R. W. Murray: "Ligand Effects on Optical Properties of CdSe Nanocrystals", *J. Phys. Chem. B* **2005**, *109*, 7012-7021.
- [166] M. Kim, Y. Chen, Y. Liu, X. Peng: "Super-Stable, High-Quality Fe₃O₄ Dendron-Nanocrystals Dispersible in Both Organic and Aqueous Solutions", *Advanced Materials* **2005**, *17*(11), 1429-1432.
- [167] P. Nativo, I. A. Prior, M. Brust: "Uptake and Intracellular Fate of Surface-Modified Gold Nanoparticles", *ACS Nano* **2008**, 1639-1644.
- [168] X. Gao, W. C. W. Chan, S. Nie: "Quantum-dot nanocrystals for ultrasensitive biological labeling and multicolor optical encoding", *Journal of Biomedical Optics* **2002**, *7*(4), 532-537.

- [169] T. Niidome, M. Yamagata, Y. Okamoto, Y. Akiyama, H. Takahashi, T. Kawano, Y. Katayama, Y. Niidome: "PEG-modified gold nanorods with a stealth character for in vivo applications", *Journal Of Controlled Release* **2006**, *114*(3), 343-347.
- [170] S. Pierrat, I. Zins, A. Breivogel, C. Sonnichsen: "Self-assembly of small gold colloids with functionalized gold nanorods", *Nano Letters* **2007**, *7*(2), 259-263.
- [171] R. Levy, Z. X. Wang, L. Duchesne, R. C. Doty, A. I. Cooper, M. Brust, D. G. Fernig: "A Generic Approach to Monofunctionalized Protein-Like Gold Nanoparticles Based on Immobilized Metal Ion Affinity Chromatography", *ChemBioChem* **2006**, *7*(4), 592-594.
- [172] H. Hirai, H. Aizawa, H. Shiozaki: "Preparation of Nonaqueous Dispersion of Colloidal Silver by Phase Transfer", *Chem. Lett.* **1992**, *21*(8), 1527-1530.
- [173] S. Kim, M. G. Bawendi: "Oligomeric Ligands for Luminescent and Stable Nanocrystal Quantum Dots", *Journal of the American Chemical Society* **2003**, *125*, 14652-14653.
- [174] D. I. Gittins, F. Caruso: "Biological and Physical Applications of Water-Based Metal Nanoparticles Synthesised in Organic Solution", *ChemPhysChem* **2002**, *3*(1), 110-113.
- [175] H. Mattoussi, J. M. Mauro, E. R. Goldman, G. P. Anderson, V. C. Sundar, F. V. Mikulec, M. G. Bawendi: "Self-Assembly of CeSe-ZnS Quantum Dot Bioconjugates Using an Engineered Recombinant Protein", *J. Am. Chem. Soc.* **2000**, *122*, 12142-12150.
- [176] W. R. Algar, U. J. Krull: "Luminescence and Stability of Aqueous Thioalkyl Acid Capped CdSe/ZnS Quantum Dots Correlated to Ligand Ionization", *ChemPhysChem* **2007**, *8*(4), 561-568.
- [177] H. T. Uyeda, I. L. Medintz, J. K. Jaiswal, S. M. Simon, H. Mattoussi: "Synthesis of Compact Multidentate Ligands to Prepare Stable Hydrophilic Quantum Dot Fluorophores", *Journal of the American Chemical Society* **2005**, *127*(11), 3870-3878.
- [178] W. Liu, M. Howarth, A. B. Greytak, Y. Zheng, D. G. Nocera, A. Y. Ting, M. G. Bawendi: "Compact Biocompatible Quantum Dots Functionalized for Cellular Imaging", *J. Am. Chem. Soc.* **2008**, *130*(4), 1274-1284.
- [179] A. Kumar, H. Joshi, R. Pasricha, A. B. Mandale, M. Sastry: "Phase transfer of silver nanoparticles from aqueous to organic solutions using fatty amine molecules", *Journal of Colloid and Interface Science* **2003**, *264*(2), 396-401.
- [180] R. Balasubramanian, J. Xu, B. Kim, B. Sadtler, A. Wei: "Extraction and dispersion of large gold nanoparticles in nonpolar solvents", *Journal of Dispersion Science and Technology* **2001**, *22*(5), 485-489.
- [181] T. K. Misra, T.-S. Chen, C.-Y. Liu: "Phase transfer of gold nanoparticles from aqueous to organic solution containing resorcinarene", *Journal of Colloid and Interface Science* **2006**, *297*(2), 584.
- [182] J. Yang, T. C. Deivaraj, H.-P. Too, J. Y. Lee: "An Alternative Phase-Transfer Method of Preparing Alkylamine-Stabilized Platinum Nanoparticles", *Journal of Physical Chemistry B* **2004**, *108*(7), 2181-2185.
- [183] A. Kumar, A. B. Mandale, M. Sastry: "Phase Transfer of Aqueous CdS Nanoparticles by Coordination with Octadecanethiol Molecules Present in Nonpolar Organic Solvents", *Langmuir* **2000**, *16*(24), 9299-9302.
- [184] J. Simard, C. Briggs, A. K. Boal, V. M. Rotello: "Formation and pH-controlled assembly of amphiphilic gold nanoparticles", *Chemical Communications* **2000**(19), 1943-1944.
- [185] N. Gaponik, D. V. Talapin, A. L. Rogach, A. Eychmüller, H. Weller: "Efficient Phase Transfer of Luminescent Thiol-Capped Nanocrystals: From Water to Nonpolar Organic Solvents", *Nanoletters* **2002**, *2*(8), 803-806.
- [186] K. V. Sarathy, G. U. Kulkarni, C. N. R. Rao: "A novel method of preparing thiol-derivatised nanoparticles of gold, platinum and silver forming superstructures", *Chemical Communications* **1997**, *6/1997*, 537-538.
- [187] K. V. Sarathy, G. Raina, R. T. Yadav, G. U. Kulkarni, C. N. R. Rao: "Thiol-Derivatized Nanocrystalline Arrays of Gold, Silver, and Platinum", *Journal of Physical Chemistry B* **1997**, *101*(48), 9876-9880.
- [188] S.-Y. Zhao, S.-H. Chen, S.-Y. Wang, D.-G. Li, H.-Y. Ma: "Preparation, Phase Transfer, and Self-Assembled Monolayers of Cubic Pt Nanoparticles", *Langmuir* **2002**, *18*(8), 3315-3318.
- [189] T. Bala, A. Swami, B. Prasad, M. Sastry: "Phase transfer of oleic acid capped NicoreAgshell nanoparticles assisted by the flexibility of oleic acid on the surface of silver", *Journal of Colloid and Interface Science* **2005**, *283*(2), 422-431.
- [190] L. M. Liz-Marzán, I. Lado-Touriño: "Reduction and Stabilization of Silver Nanoparticles in Ethanol by Nonionic Surfactants", *Langmuir* **1996**, *12*, 3585-3589.
- [191] T. Nann: "Phase-transfer of CdSe@ZnS quantum dots using amphiphilic hyperbranched polyethylenimine", *Chem. Commun.* **2005**, *2005*(13), 1735-1736.
- [192] W. Lin, K. Fritz, G. Guerin, G. R. Bardajee, S. Hinds, V. Sukhovatkin, E. H. Sargent, G. D. Scholes, M. A. Winnik: "Highly Luminescent Lead Sulfide Nanocrystals in Organic Solvents and Water through Ligand Exchange with Poly(acrylic acid)", *Langmuir* **2008**.
- [193] T. Zhang, J. Ge, Y. Hu, Y. Yin: "A General Approach for Transferring Hydrophobic Nanocrystals into Water", *Nano Lett.* **2007**, *7*(10), 3203-3207.
- [194] H. W. Duan, S. M. Nie: "Cell-penetrating quantum dots based on multivalent and endosome-disrupting surface coatings", *Journal Of The American Chemical Society* **2007**, *129*(11), 3333-3338.
- [195] J. M. McMahon, S. R. Emory: "Phase transfer of large gold nanoparticles to organic solvents with increased stability", *Langmuir* **2007**, *23*(3), 1414-1418.
- [196] N. Lala, S. P. Lalbegi, S. D. Adyanthaya, M. Sastry: "Phase Transfer of Aqueous Gold Colloidal Particles Capped with Inclusion Complexes of Cyclodextrin and Alkanethiol Molecules into Chloroform", *Langmuir* **2001**, *17*, 3766-3768.

- [197] Y. Wang, J. F. Wong, X. Teng, X. Z. Lin, H. Yang: "“Pulling” Nanoparticles into Water: Phase Transfer of Oleic Acid Stabilized Monodisperse Nanoparticles into Aqueous Solutions of α -Cyclodextrin", *nanoletters* **2003**, 3(11), 1555-1559.
- [198] E. R. Zubarev, J. Xu, A. Sayyad, J. D. Gibson: "Amphiphilic Gold Nanoparticles with V-Shaped Arms", *J. Am. Chem. Soc.* **2006**, 128(15), 4958-4959.
- [199] K. S. Mayya, F. Caruso: "Phase Transfer of Surface-Modified Gold Nanoparticles by Hydrophobization with Alkylamines", *Langmuir* **2003**, 19(17), 6987-6993.
- [200] J. Liu, J. Alvarez, W. Ong, E. Román, A. E. Kaifer: "Phase Transfer of Hydrophilic, Cyclodextrin-Modified Gold Nanoparticles to Chloroform Solutions", *Journal of the American Chemical Society* **2001**, 123(45), 11148-11154.
- [201] D. I. Gittins, F. Caruso: "Spontaneous Phase Transfer of Nanoparticulate Metals from Organic to Aqueous Media", *Angew. Chem. Int. Ed.* **2001**, 40(16), 3001-3004.
- [202] L. Shen, P. E. Laibinis, T. A. Hatton: "Bilayer Surfactant Stabilized Magnetic Fluids: Synthesis and Interactions at Interfaces", *Langmuir* **1999**, 15, 447-453.
- [203] A. Wooding, M. Kilner, D. B. Lambrick: "Studies of the Double Surfactant Layer Stabilization of Water-Based Magnetic Fluids", *Journal of Colloid and Interface Science* **1991**, 144(1), 236-242.
- [204] H. Yao, O. Momozawa, T. Hamatani, K. Kimura: "Phase Transfer of Gold Nanoparticles across a Water/Oil Interface by Stoichiometric Ion-Pair Formation on Particle Surfaces", *Bulletin of the Chemical Society of Japan* **2000**, 73(12), 2675-2678.
- [205] Y. Tian, J. H. Fendler: "Langmuir-Blodgett film formation from fluorescence-activated, surface-capped, size-selected CdS nanoparticles spread on water surfaces", *Chem. Mater.* **1996**, 8(4), 969-974.
- [206] H. Zhang, Z. Cui, Y. Wong, K. Zhang, X. J. C. Lu, B. Yang, M. Gao: "From Water-Soluble CdTe Nanocrystals to Fluorescent Nanocrystal-Polymer Transparent Composites Using Polymerizable Surfactants", *Advanced Materials* **2003**, 15(10), 777-780.
- [207] A. Swami, A. Kumar, M. Sastry: "Formation of Water-Dispersible Gold Nanoparticles Using a Technique Based on Surface-Bound Interdigitated Bilayers", *Langmuir* **2003**, 19, 1168-1172.
- [208] B. Dubertret, P. Skourides, D. J. Norris, V. Noireaux, A. H. Brivanlou, A. Libchaber: "In Vivo Imaging of Quantum Dots Encapsulated in Phospholipid Micelles", *Science* **2002**, 298(29 November), 1759-1762.
- [209] O. Carion, B. Mahler, T. Pons, B. Dubertret: "Synthesis, encapsulation, purification and coupling of single quantum dots in phospholipid micelles for their use in cellular and in vivo imaging", *Nature Protocols* **2007**, 2(10), 2383-2390.
- [210] M. Stroh, J. P. Zimmer, D. G. Duda, T. S. Levchenko, K. S. Cohen, E. B. Brown, D. T. Scadden, V. P. Torchilin, M. G. Bawendi, D. Fukumura, R. K. Jain: "Quantum dots spectrally distinguish multiple species within the tumor milieu in vivo", *Nature Medicine* **2005**, 11(6), 678-682.
- [211] C. Srinivasan, J. Lee, F. Papadimitrakopoulos, L. K. Silbart, M. Zhao, D. J. Burgess: "Labeling and Intracellular Tracking of Functionally Active Plasmid DNA with Semiconductor Quantum Dots", *Mol Ther* **2006**, 14(2), 192.
- [212] G. Gopalakrishnan, C. Danelon, P. Izewska, M. Prummer, P.-Y. Bolinger, I. Geissbühler, D. Demurtas, J. Dubochet, H. Vogel: "Multifunctional Lipid/Quantum Dot Hybrid Nanocontainers for Controlled Targeting of Live Cells¹³", *Angewandte Chemie International Edition* **2006**, 45(33), 5478-5483.
- [213] W. J. M. Mulder, R. Koole, R. J. Brandwijk, G. Storm, P. T. K. Chin, G. J. Strijkers, C. D. Donega, K. Nicolay, A. W. Griffioen: "Quantum dots with a paramagnetic coating as a bimodal molecular imaging probe", *Nano Letters* **2006**, 6(1), 1-6.
- [214] W. J. M. Mulder, G. J. Strijkers, G. A. F. van Tilborg, A. W. Griffioen, K. Nicolay: "Lipid-based nanoparticles for contrast-enhanced MRI and molecular imaging", *NMR in Biomedicine* **2006**, 19(1), 142-164.
- [215] K. T. Wang, I. Iliopoulos, R. Audebert: "Viscometric behaviour of hydrophobically modified poly(sodium acrylate)", *Polymer Bulletin* **1988**, 20, 577-582.
- [216] M. X. Wu, H. Liu, J. Liu, K. N. Haley, J. A. Treadway, J. P. Larson, N. Ge, F. Peale, M. P. Bruchez: "Immunofluorescent labeling of cancer marker Her2 and other cellular targets with semiconductor quantum dots", *Nature Biotechnology* **2003**, 21, 41-46.
- [217] M. A. Petruska, A. P. Bartko, V. I. Klimov: "An Amphiphilic Approach to Nanocrystal Quantum Dot-Titania Nanocomposites", *J. Am. Chem. Soc.* **2004**, 126(3), 714-715.
- [218] C. Luccardini, C. Tribet, F. Vial, V. Marchi-Artzner, M. Dahan: "Size, Charge, and Interactions with Giant Lipid Vesicles of Quantum Dots Coated with an Amphiphilic Macromolecule", *Langmuir* **2006**, 22(5), 2304 - 2310.
- [219] R. E. Anderson, W. C. W. Chan: "Systematic Investigation of Preparing Biocompatible, Single, and Small ZnS-Capped CdSe Quantum Dots with Amphiphilic Polymers", *ACS Nano* **2008**, 2(7), 1341-1352.
- [220] P. T. Snee, R. C. Somers, G. Nair, J. P. Zimmer, M. G. Bawendi, D. G. Nocera: "A ratiometric CdSe/ZnS nanocrystal pH sensor", *Journal Of The American Chemical Society* **2006**, 128(41), 13320-13321.
- [221] B. A. Kairdolf, M. C. Mancini, A. M. Smith, S. Nie: "Minimizing Nonspecific Cellular Binding of Quantum Dots with Hydroxyl-Derivatized Surface Coatings", *Anal. Chem.* **2008**, 80(8), 3029-3034.
- [222] B. A. Kairdolf, A. M. Smith, S. Nie: "One-Pot Synthesis, Encapsulation, and Solubilization of Size-Tuned Quantum Dots with Amphiphilic Multidentate Ligands", *J. Am. Chem. Soc.* **2008**, 130(39), 12866 - 11286.

- [223] T. Pellegrino, L. Manna, S. Kudera, T. Liedl, D. Koktysh, A. L. Rogach, S. Keller, J. Rädler, G. Natile, W. J. Parak: "Hydrophobic nanocrystals coated with an amphiphilic polymer shell: a general route to water soluble nanocrystals", *Nanoletters* **2004**, 4(4), 703-707.
- [224] R. Di Corato, A. Quarta, P. Piacenza, A. Ragusa, A. Figuerola, R. Buonsanti, R. Cingolani, L. Manna, T. Pellegrino: "Water solubilization of hydrophobic nanocrystals by means of poly(maleic anhydride-alt-1-octadecene)", *Journal Of Materials Chemistry* **2008**, 18(17), 1991-1996.
- [225] L. Qi, X. Gao: "Quantum Dot-Amphipol Nanocomplex for Intracellular Delivery and Real-Time Imaging of siRNA", *ACS Nano* **2008**, 2(7), 1403-1410.
- [226] M. V. Yezhelyev, L. Qi, R. M. Regan, S. Nie, X. Gao: "Proton-Sponge Coated Quantum Dots for siRNA Delivery and Intracellular Imaging", *J. Am. Chem. Soc.* **2008**, 130(28), 9006-9012.
- [227] W. W. Yu, E. Chang, C. M. Sayes, R. Drezek, V. L. Colvin: "Aqueous dispersion of monodisperse magnetic iron oxide nanocrystals through phase transfer", *Nanotechnology* **2006**, 17(17), 4483-4487.
- [228] W. W. Yu, E. Chang, J. C. Falkner, J. Zhang, A. M. Al-Somali, C. M. Sayes, J. Johns, R. Drezek, V. L. Colvin: "Forming Biocompatible and Nonaggregated Nanocrystals in Water Using Amphiphilic Polymers", *J. Am. Chem. Soc.* **2007**, 129(10), 2871-2879.
- [229] L. Guo, S. Yang, C. Yang, P. Yu, J. Wang, W. Ge, G. K. L. Wong: "Highly monodisperse polymer-capped ZnO nanoparticles: Preparation and optical properties", *Applied Physics Letters* **2000**, 76(20), 2901-2903.
- [230] A. Sukhanova, J. Devy, L. Venteo, H. Kaplan, M. Artemyev, V. Oleinikov, D. Klinov, M. Pluot, J. H. M. Cohen, I. Nabieva: "Biocompatible fluorescent nanocrystals for immunolabeling of membrane proteins and cells", *Analytical Biochemistry* **2004**, 324, 60-67.
- [231] S. Kim, S. Kim, J. Tracy, A. Jasanoff, M. Bawendi: "Phosphine oxide polymer for water-soluble nanoparticles", *Journal of the American Chemical Society* **2005**, 127(13), 4556-4557.
- [232] I. Potapova, R. Mruk, C. Hübner, R. Zentel, T. Basche, A. Mews: "CdSe/ZnS nanocrystals with dye-functionalized polymer ligands containing many anchor groups", *Angewandte Chemie International Edition* **2005**(44), 2-5.
- [233] I. Potapova, R. Mruk, S. Prehl, R. Zentel, T. Basché, A. Mews: "Semiconductor Nanocrystals with Multifunctional Polymer Ligands", *Journal of the American Chemical Society* **2003**, 125(2), 320-321.
- [234] M. Wang, T. E. Dykstra, X. Lou, M. R. Salvador, G. D. Scholes, M. A. Winnik: "Colloidal CdSe Nanocrystals Passivated by a Dye-Labeled Multidentate Polymer: Quantitative Analysis by Size-Exclusion Chromatography", *Angew. Chem. Int. Ed.* **2006**, 45, 2221-2224.
- [235] A. M. Smith, S. Nie: "Minimizing the Hydrodynamic Size of Quantum Dots with Multifunctional Multidentate Polymer Ligands", *J. Am. Chem. Soc.* **2008**, 130(34), 11278-11279.
- [236] T. K. Mandal, M. S. Fleming, D. R. Walt: "Preparation of Polymer Coated Gold Nanoparticles by Surface-Confined Living Radical Polymerization at Ambient Temperature", *Nanoletters* **2002**, 2(1), 3-7.
- [237] W. Jiang, S. Mardiyani, H. Fischer, W. C. W. Chan: "Design and Characterization of Lysine Cross-Linked Mercapto-Acid Biocompatible Quantum Dots", *Chemistry of Materials* **2006**, 18(4), 872-878.
- [238] Y. Zheng, Z. Yang, Y. Li, J. Y. Ying: "From Glutathione Capping to a Crosslinked, Phytochelatin-Like Coating of Quantum Dots", *Advanced Materials* **2008**, 20(18), 3410-3415.
- [239] K. J. Watson, J. Zhu, S. T. Nguyen, C. A. Mirkin: "Hybrid Nanoparticles with Block Copolymer Shell Structures", *Journal of the American Chemical Society* **1999**, 121(2), 462-463.
- [240] M. Möller, J. P. Spatz, A. Roescher: "Gold nanoparticles in micellar poly(styrene)-b-poly(ethylene oxide) films - size and interparticle distance control in monoparticulate films", *Advanced Materials* **1996**, 8(4), 337-340.
- [241] M. Rutnakornpituk, M. S. Thompson, L. A. Harris, K. E. Farmer, A. R. Esker, J. S. Riffle, J. Conolly, T. G. S. Pierre: "Formation of cobalt nanoparticle dispersions in the presence of polysiloxane block copolymers", *Polymer* **2002**, 43, 2337-2348.
- [242] J. P. Stevenson, M. Rutnakornpituk, M. Vadala, A. R. Esker, S. W. Charles, S. Wells, J. P. Dailey, J. S. Riffle: "Magnetic cobalt dispersions in poly(dimethylsiloxane) fluids", *Journal of Magnetism and Magnetic Materials* **2001**, 225, 47-58.
- [243] J. F. Berret, A. Sehgal, M. Morvan, O. Sandre, A. Vacher, M. Airiau: "Stable oxide nanoparticle clusters obtained by complexation", *J Colloid Interface Sci* **2006**, 303(1), 315-318.
- [244] B.-S. Kim, J.-M. Qiu, J.-P. Wang, T. A. Taton: "Magnetomicelles: Composite Nanostructures from Magnetic Nanoparticles and Cross-Linked Amphiphilic Block Copolymers", *Nanoletters* **2005**, 5, 1987-1991.
- [245] Z. Cheng, S. Liu, H. Gao, W. Tremel, N. Ding, R. Liu, P. W. Beines, W. Knoll: "A Facile Approach for Transferring Hydrophobic Magnetic Nanoparticles into Water-Soluble Particles", *Macromolecular Chemistry and Physics* **2008**, 209(11), 1145-1151.
- [246] Y. J. Kang, T. A. Taton: "Controlling shell thickness in core-shell gold nanoparticles via surface-templated adsorption of block copolymer surfactants", *Macromolecules* **2005**, 38(14), 6115-6121.
- [247] L. E. Euliss, S. G. Grancharov, S. O'Brien, T. J. Deming, G. D. Stucky, C. B. Murray, G. A. Held: "Cooperative Assembly of Magnetic Nanoparticles and Block Copolypeptides in Aqueous Media", *Nano Letters* **2003**, 3(11), 1489-1493.
- [248] B.-S. Kim, T. A. Taton: "Multicomponent nanoparticles via self-assembly with cross-linked block copolymer surfactants", *Langmuir* **2007**, 23(4), 2198-2202.
- [249] R. B. Grubbs: "Roles of Polymer Ligands in Nanoparticle Stabilization", *Polymer Reviews* **2007**, 47(2), 197 - 215.

- [250] P. Mulvaney, L. M. Liz-Marzán, M. Giersig, T. Ung: "Silica encapsulation of quantum dots and metal clusters", *Journal of Materials Chemistry* **2000**, *10*(6), 1259-1270.
- [251] C. Graf, D. L. J. Vossen, A. Imhof, A. v. Blaaderen: "A General Method To Coat Colloidal Particles with Silica", *Langmuir* **2003**, *19*(17), 6693-6700.
- [252] N. R. Jana, C. Earhart, J. Y. Ying: "Synthesis of Water-Soluble and Functionalized Nanoparticles by Silica Coating", *Chem. Mater.* **2007**, *19*(21), 5074-5082.
- [253] Y. Han, J. Jiang, S. S. Lee, J. Y. Ying: "Reverse Microemulsion-Mediated Synthesis of Silica-Coated Gold and Silver Nanoparticles", *Langmuir* **2008**, *24*(11), 5842-5848.
- [254] L. M. Liz-Marzán, M. Giersig, P. Mulvaney: "Synthesis of Nanosized Gold-Silica Core-Shell Particles", *Langmuir* **1996**, *12*(18), 4329-4335.
- [255] P. A. Buining, B. M. Humbel, A. P. Philipse, A. J. Verkleij: "Preparation of Functional Silane-Stabilized Gold Colloids in the (Sub)nanometer Size Range", *Langmuir* **1997**, *13*(15), 3921-3926.
- [256] V. V. Hardikar, E. Matijevic: "Coating of Nanosize Silver Particles with Silica", *Journal of Colloid and Interface Science* **2000**, *221*(1), 133-136.
- [257] D. Gerion, F. Pinaud, S. C. Williams, W. J. Parak, D. Zanchet, S. Weiss, A. P. Alivisatos: "Synthesis and Properties of Biocompatible Water-Soluble Silica-Coated CdSe/ZnS Semiconductor Quantum Dots", *Journal of Physical Chemistry B* **2001**, *105*(37), 8861-8871.
- [258] T. Nann, P. Mulvaney: "Single Quantum Dots in Spherical Silica Particles", *Angewandte Chemie International Edition* **2004**, *43*(40), 5393-5396.
- [259] M. Darbandi, R. Thomann, T. Nann: "Single Quantum Dots in Silica Spheres by Microemulsion Synthesis", *Chem. Mater.* **2005**, *17*(23), 5720-5725.
- [260] M. Ohmori, E. Matijevic: "Preparation and Properties of Uniform Coated Inorganic Colloidal Particles 8. Silica on Iron", *Journal of Colloid and Interface Science* **1993**, *160*(2), 288-292.
- [261] Y. Kobayashi, M. Horie, M. Konno, B. Rodriguez-Gonzalez, L. M. Liz-Marzan: "Preparation and Properties of Silica-Coated Cobalt Nanoparticles", *J. Phys. Chem. B* **2003**, *107*, 7420-7425.
- [262] A. Hoshino, K. Fujioka, T. Oku, M. Suga, Y. F. Sasaki, T. Ohta, M. Yasuhara, K. Suzuki, K. Yamamoto: "Physicochemical Properties and Cellular Toxicity of Nanocrystal Quantum Dots Depend on Their Surface Modification", *Nano Letters* **2004**, *4*(11), 2163-2169.
- [263] K. Susumu, H. T. Uyeda, I. L. Medintz, T. Pons, J. B. Delehanty, H. Mattoussi: "Enhancing the Stability and Biological Functionalities of Quantum Dots via Compact Multifunctional Ligands", *J. Am. Chem. Soc.* **2007**, *129*(45), 13987-13996.
- [264] M. Howarth, W. H. Liu, S. Puthenveetil, Y. Zheng, L. F. Marshall, M. M. Schmidt, K. D. Wittrup, M. G. Bawendi, A. Y. Ting: "Monovalent, reduced-size quantum dots for imaging receptors on living cells", *Nature Methods* **2008**, *5*(5), 397-399.
- [265] S. F. Wuister, I. Swart, F. V. Driel, S. G. Hickey, C. d. M. Donega: "High Luminescent Water-Soluble CdTe Quantum Dots", *Nano Lett.* **2003**, *3*, 503-507.
- [266] M. E. Akerman, W. C. W. Chan, P. Laakkonen, S. N. Bhatia, E. Ruoslahti: "Nanocrystal targeting in vivo", *Proceeding of the National Academy of Science of the United States of America* **2002**, *99*(20), 12617-12621.
- [267] C. Wilhelm, C. Bilottey, J. Roger, J. N. Pons, J.-C. Bacri, F. Gazeau: "Intracellular uptake of anionic superparamagnetic nanoparticles as a function of their surface coating", *Biomaterials* **2003**, *24*, 1001-1011.
- [268] N. Fauconnier, J. N. Pons, J. Roger, A. Bee: "Thiolation of Maghemite Nanoparticles by Dimercaptosuccinic Acid", *Journal of Colloid and Interface Science* **1997**, *194*(2), 427-433.
- [269] G. T. Hermanson, *Bioconjugate Techniques*, 2nd ed., Academic Press, San Diego, **2008**.
- [270] S. J. Kuhn, S. K. Finch, D. E. Hallahan, T. D. Giorgio: "Facile production of multivalent enzyme-nanoparticle conjugates", *Journal of Magnetism and Magnetic Materials* **2007**, *311*(1), 68.
- [271] E. Y. Sun, L. Josephson, K. A. Kelly, R. Weissleder: "Development of Nanoparticle Libraries for Biosensing", *Bioconjugate Chemistry* **2006**, *17*(1), 109-113.
- [272] E. A. Schellenberger, F. Reynolds, R. Weissleder, L. Josephson: "Surface-Functionalized Nanoparticle Library Yields Probes for Apoptotic Cells", *ChemBioChem* **2004**, *5*, 275-279.
- [273] Y. C. Li, Y. S. Lin, P. J. Tsai, C. T. Chen, W. Y. Chen, Y. C. Chen: "Nitritotriacetic Acid-Coated Magnetic Nanoparticles as Affinity Probes for Enrichment of Histidine-Tagged Proteins and Phosphorylated Peptides", *Anal. Chem.* **2007**, *79*(19), 7519-7525.
- [274] M. Meldal, C. W. Tornøe: "Cu-Catalyzed Azide-Alkyne Cycloaddition", *Chem. Rev.* **2008**, *108*(8), 2952-3015.
- [275] W. H. Binder, R. Sachsenhofer: "'Click' Chemistry in Polymer and Material Science: An Update", *Macromolecular Rapid Communications* **2008**, *29*(12-13), 952-981.
- [276] D. A. Fleming, C. J. Thode, M. E. Williams: "Triazole Cycloaddition as a General Route for Functionalization of Au Nanoparticles", *Chem. Mater.* **2006**, *18*(9), 2327-2334.
- [277] W. H. Binder, L. Petraru, R. Sachsenhofer, R. Zirbs: "Synthesis of Surface-Modified Nanoparticles via Cycloaddition-Reactions", *Monatshefte für Chemie / Chemical Monthly* **2006**, *137*(7), 835.
- [278] E. Y. Sun, L. Josephson, R. Weissleder: "'Clickable' Nanoparticles for Targeted Imaging", *Molecular Imaging* **2006**, *5*(2), 122-128.

- [279] J. L. Brennan, N. S. Hatzakis, T. R. Tshikhudo, N. Dirvianskyte, V. Razumas, S. Patkar, J. Vind, A. Svendsen, R. J. M. Nolte, A. E. Rowan, M. Brust: "Bionanoconjugation via click chemistry: The creation of functional hybrids of lipases and gold nanoparticles", *Bioconjugate Chemistry* **2006**, *17*(6), 1373-1375.
- [280] L. Polito, D. Monti, E. Caneva, E. Delnevo, G. Russo, D. Prosperi: "One-step bioengineering of magnetic nanoparticles via a surface diazo transfer/azide-alkyne click reaction sequence", *Chem Commun (Camb)* **2008**(5), 621-623.
- [281] R. K. O'Reilly, M. J. Joralemon, K. L. Wooley, C. J. Hawker: "Functionalization of Micelles and Shell Cross-linked Nanoparticles Using Click Chemistry", *Chem. Mater.* **2005**, *17*(24), 5976-5988.
- [282] R. Voggu, P. Suguna, S. Chandrasekaran, C. N. R. Rao: "Assembling covalently linked nanocrystals and nanotubes through click chemistry", *Chemical Physics Letters* **2007**, *443*(1-3), 118.
- [283] H. C. Kolb, M. G. Finn, K. B. Sharpless: "Click Chemistry: Diverse Chemical Function from a Few Good Reactions", *Angewandte Chemie International Edition* **2001**, *40*(11), 2004-2021.
- [284] V. V. Rostovtsev, L. G. Green, V. V. Fokin, K. B. Sharpless: "A Stepwise Huisgen Cycloaddition Process: Copper(I)-Catalyzed Regioselective "Ligation" of Azides and Terminal Alkynes", *Angewandte Chemie International Edition* **2002**, *41*(14), 2596-2599.
- [285] T. Schiestel, H. Brunner, G. E. M. Tovar: "Controlled Surface Functionalization of Silica Nanospheres by Covalent Conjugation Reactions and Preparation of High Density Streptavidin Nanoparticles", *Journal of Nanoscience and Nanotechnology* **2004**, *4*(5), 504-511.
- [286] K. M. Sung, D. W. Mosley, B. R. Peelle, S. G. Zhang, J. M. Jacobson: "Synthesis of monofunctionalized gold nanoparticles by Fmoc solid-phase reactions", *Journal of the American Chemical Society* **2004**, *126*(16), 5064-5065.
- [287] A. W. Shaffer, JG; Huo, G: "Comparison Study of the Solution Phase versus Solid Phase Place Exchange Reactions in the Controlled Functionalization of Gold Nanoparticles", *Langmuir* **2004**, *20*, 8343 - 8351.
- [288] J. G. Worden, A. W. Shaffer, Q. Huo: "Controlled functionalization of gold nanoparticles through a solid phase synthesis approach", *ChemComm* **2004**, *2004*, 518-519.
- [289] X. Liu, J. G. Worden, Q. Dai, J. Zou, J. Wang, Q. Huo: "Monofunctional Gold Nanoparticles Prepared via a Noncovalent-Interaction-Based Solid-Phase Modification Approach", *Small* **2006**, *2*(10), 1126-1129.
- [290] J. H. Zou, Q. Dai, J. H. Wang, X. Liu, Q. Huo: "Solid phase monofunctionalization of gold nanoparticles using ionic exchange resin as polymer support", *Journal of Nanoscience and Nanotechnology* **2007**, *7*(7), 2382-2388.
- [291] D. Safer, L. Bolinger, J. S. Leigh: "Undecagold clusters for site-specific labeling of biological macromolecules: simplified preparation and model applications", *Journal of Inorganic Biochemistry* **1986**, *26*(2), 77.
- [292] D. Zanchet, C. M. Micheel, W. J. Parak, D. Gerion, A. P. Alivisatos: "Electrophoretic isolation of discrete Au nanocrystal/DNA conjugates", *Nanoletters* **2001**, *1*(1), 32-35.
- [293] F. A. Aldaye, H. F. Sleiman: "Dynamic DNA Templates for Discrete Gold Nanoparticle Assemblies: Control of Geometry, Modularity, Write/Erase and Structural Switching", *J. Am. Chem. Soc.* **2007**, *129*(14), 4130-4131.
- [294] D. Zanchet, C. M. Micheel, W. J. Parak, D. Gerion, S. C. Williams, A. P. Alivisatos: "Electrophoretic and Structural Studies of DNA-Directed Au Nanoparticle Groupings", *Journal of Physical Chemistry B* **2002**, *106*(45), 11758-11763.
- [295] F. A. Aldaye, H. F. Sleiman: "Sequential Self-Assembly of a DNA Hexagon as a Template for the Organization of Gold Nanoparticles", *Angew. Chem. Int. Ed.* **2006**, *45*, 2204-2209.
- [296] S. A. Claridge, H. W. Liang, S. R. Basu, J. M. J. Frechet, A. P. Alivisatos: "Isolation of Discrete Nanoparticle-DNA Conjugates for Plasmonic Applications", *Nano Lett.* **2008**, *8*(4), 1202-1206.
- [297] T. Pons, H. T. Uyeda, I. L. Medintz, H. Mattoussi: "Hydrodynamic dimensions, electrophoretic mobility, and stability of hydrophilic quantum dots", *Journal Of Physical Chemistry B* **2006**, *110*(41), 20308-20316.
- [298] G. A. DeVries, M. Brunnbauer, Y. Hu, A. M. Jackson, B. Long, B. T. Neltner, O. Uzun, B. H. Wunsch, F. Stellacci: "Divalent Metal Nanoparticles", *Science* **2007**, *315*(5810), 358-361.
- [299] K. Nakata, Y. Hu, O. Uzun, O. Bakr, F. Stellacci: "Chains of Superparamagnetic Nanoparticles", *Advanced Materials* **2008**, doi:10.1002/adma.200800022.
- [300] C. Krüger, S. Agarwal, A. Greiner: "Stoichiometric Functionalization of Gold Nanoparticles in Solution through a Free Radical Polymerization Approach", *J. Am. Chem. Soc.* **2008**, *130*(9), 2710-2711.
- [301] H. M. Zareie, C. Boyer, V. Bulmus, E. Nateghi, T. P. Davis: "Temperature-Responsive Self-Assembled Monolayers of Oligo(ethylene glycol): Control of Biomolecular Recognition", *ACS Nano* **2008**, *2*(4), 757-765.
- [302] F. M. Veronese: "Peptide and protein PEGylation: a review of problems and solutions", *Biomaterials* **2001**, *22*, 405 - 417.
- [303] R. Gref, M. Lück, P. Quellec, M. Marchand, E. Dellacherie, S. Harnisch, T. Blunk, R. H. Müller: "'Stealth' corona-core nanoparticles surface modified by polyethylene glycol (PEG): influences of the corona (PEG chain length and surface density) and of the core composition on phagocytic uptake and plasma protein adsorption", *Colloids and Surfaces B* **2000**, *18*(3-4), 301-313.
- [304] B. Ballou, B. C. Lagerholm, L. A. Ernst, M. P. Bruchez, A. S. Waggoner: "Noninvasive Imaging of Quantum Dots in Mice", *Bioconjugate Chemistry* **2004**, *15*(1), 79-86.

- [305] Y. L. Liu, M. K. Shipton, J. Ryan, E. D. Kaufman, S. Franzen, D. L. Feldheim: "Synthesis, stability, and cellular internalization of gold nanoparticles containing mixed peptide-poly(ethylene glycol) monolayers", *Analytical Chemistry* **2007**, 79(6), 2221-2229.
- [306] L. van Vlerken, T. Vyas, M. Amiji: "Poly(ethylene glycol)-modified Nanocarriers for Tumor-targeted and Intracellular Delivery", *Pharmaceutical Research* **2007**, 24(8), 1405.
- [307] M. J. B. Roberts, M.D.; Harris, J.M.: "Chemistry for peptide and protein PEGylation", *Advanced Drug Delivery Reviews* **2002**, 54, 459 - 476.
- [308] X. Gao, Y. Cui, R. M. Levenson, L. W. K. Chung, S. Nie: "In vivo cancer targeting and imaging with semiconductor quantum dots", *Nature Biotechnology* **2004**, 22(8), 969-976.
- [309] L. R. Hirsch, R. J. Stafford, J. A. Bankson, S. R. Sershen, B. Rivera, R. E. Price, J. D. Hazle, N. J. Halas, J. L. West: "Nanoshell-mediated near-infrared thermal therapy of tumors under magnetic resonance guidance", *Proceedings of the National Academy of Science of the United States of America* **2003**, 100(23), 13549-13554.
- [310] A. Jayagopal, P. K. Russ, F. R. Haselton: "Surface Engineering of Quantum Dots for In Vivo Vascular Imaging", *Bioconjugate Chem.* **2007**, 18(5), 1424-1433.
- [311] M. D. Butterworth, L. Illum, S. S. Davis: "Preparation of ultrafine silica- and PEG-coated magnetite particles", *Colloids and Surfaces A: Physicochemical and Engineering Aspects* **2001**, 179, 93-102.
- [312] J. C. Zillies, K. Ziorek, G. Winter, C. Coester: "Method for Quantifying the PEGylation of Gelatin Nanoparticle Drug Carrier Systems Using Asymmetrical Flow Field-Flow Fractionation and Refractive Index Detection", *Anal. Chem.* **2007**, 79(12), 4574-4580.
- [313] L. Qi, A. Sehgal, J.-C. Castaing, J.-P. Chapel, J. Fresnais, J.-F. Berret, F. Cousin: "Redispersible Hybrid Nanopowders: Cerium Oxide Nanoparticle Complexes with Phosphonated-PEG Oligomers", *ACS Nano* **2008**, 2(5), 879-888.
- [314] H. Skaff, T. Emrick: "The use of 4-substituted pyridines to afford amphiphilic, pegylated cadmium selenide nanoparticles", *Chemical Communications* **2003**, 2003(1), 52-53.
- [315] C. J. Fee, J. M. V. Alstine: "Prediction of the Viscosity Radius and the Size Exclusion Chromatography Behavior of PEGylated Proteins", *Bioconjugate Chemistry* **2004**, 15(6), 1304-1313.
- [316] C. J. Fee: "Size comparison between proteins PEGylated with branched and linear poly(ethylene glycol) molecules", *Biotechnology and Bioengineering* **2007**, 98(4), 725-731.
- [317] N. Green: "Avidin", *Adv. Protein Chem.* **1975**, 29, 85-133.
- [318] M. Wilchek, E. A. Bayer: "Avidin Biotin Technology 10 Years On - Has It Lived Up to Its Expectations", *Trends in Biochemical Sciences* **1989**, 14(October), 408-412.
- [319] M. Wilchek, E. A. Bayer: "The Avidin-Biotin Complex in Bioanalytical Applications", *Analytical Biochemistry* **1988**, 171, 1-32.
- [320] M. Wilchek, E. A. Bayer, (eds): "Avidin-Biotin Technology", *Methods in Enzymology* **1990**, 184, 3-746.
- [321] S.-C. Wu, S.-L. Wong: "Engineering Soluble Monomeric Streptavidin with Reversible Biotin Binding Capability", *J. Biol. Chem.* **2005**, 280(24), 23225-23231.
- [322] M. Howarth, A. Y. Ting: "Imaging proteins in live mammalian cells with biotin ligase and monovalent streptavidin", *Nat. Protocols* **2008**, 3(3), 534.
- [323] J. F. Hainfeld, W. Liu, C. M. R. Halsey, P. Freimuth, R. D. Powell: "Ni-NTA-Gold Clusters Target His-Tagged Proteins", *Journal of Structural Biology* **1999**, 127(2), 185.
- [324] S. K. Kufer, H. Dietz, C. Albrecht, K. Blank, A. Kardinal, M. Rief, H. E. Gaub: "Covalent immobilization of recombinant fusion proteins with hAGT for single molecule force spectroscopy", *European Biophysics Journal With Biophysics Letters* **2005**, 35(1), 72-78.
- [325] S. Lata, A. Reichel, R. Brock, R. Tampe, J. Piehler: "High-Affinity Adaptors for Switchable Recognition of Histidine-Tagged Proteins", *J. Am. Chem. Soc.* **2005**, 127(29), 10205-10215.
- [326] R. P. Brinas, M. Hu, L. Qian, E. S. Lyman, J. F. Hainfeld: "Gold Nanoparticle Size Controlled by Polymeric Au(I) Thiolate Precursor Size", *J. Am. Chem. Soc.* **2008**, 130(3), 975-982.
- [327] J. Kim, H.-Y. Park, J. Kim, J. Ryu, D. Y. Kwon, R. Grailhe, R. Song: "Ni-nitrilotriacetic acid-modified quantum dots as a site-specific labeling agent of histidine-tagged proteins in live cells", *Chemical Communications* **2008**(16), 1910-1912.
- [328] M. Gupta, A. Caniard, A. Touceda-Varela, D. J. Campopiano, J. C. Mareque-Rivas: "Nitrilotriacetic Acid-Derivatized Quantum Dots for Simple Purification and Site-Selective Fluorescent Labeling of Active Proteins in a Single Step", *Bioconjugate Chem.* **2008**, doi:10.1021/bc800273j.
- [329] K. E. Sapsford, T. Pons, I. L. Medintz, S. Higashiya, F. M. Brunel, P. E. Dawson, H. Mattoussi: "Kinetics of metal-affinity driven self-assembly between proteins or peptides and CdSe-ZnS quantum dots", *Journal Of Physical Chemistry C* **2007**, 111(31), 11528-11538.
- [330] T. Pons, I. L. Medintz, X. Wang, D. S. English, H. Mattoussi: "Solution-phase single quantum dot fluorescence resonance energy transfer", *Journal Of The American Chemical Society* **2006**, 128(47), 15324-15331.
- [331] K. Aslan, C. C. Luhrs, V. H. Pérez-Luna: "Controlled and Reversible Aggregation of Biotinylated Gold Nanoparticles with Streptavidin", *Journal of Physical Chemistry B* **2004**, 108, 15631-15639.
- [332] F. Pinaud, D. King, H.-P. Moore, S. Weiss: "Bioactivation and Cell Targeting of Semiconductor CdSe/ZnS Nanocrystals with Phytochelatin-Related Peptides", *Journal of the American Chemical Society* **2004**, 126(19), 6115-6123.

- [333] E. R. Goldman, E. D. Balighian, H. Mattoussi, M. K. Kuno, J. M. Mauro, P. T. Tran, G. P. Anderson: "Avidin: A Natural Bridge for Quantum Dot-Antibody Conjugates", *Journal of the American Chemical Society* **2002**, *124*(22), 6378-6382.
- [334] Z. Lin, X. Su, Y. Wan, H. Zhang, Y. Mu, B. Yang, Q. Jin: "Labeled avidin bound to water soluble nanocrystals by electrostatic interactions", *Russian Chemical Bulletin, International Edition* **2004**, *53*(12), 2690-2694.
- [335] J. K. Herr, J. E. Smith, C. D. Medley, D. Shangguan, W. Tan: "Aptamer-Conjugated Nanoparticles for Selective Collection and Detection of Cancer Cells", *Anal. Chem.* **2006**, *78*(9), 2918-2924.
- [336] F. Meiser, C. Cortez, F. Caruso: "Biofunctionalization of Fluorescent Rare-Earth-Doped Lanthanum Phosphate Colloidal Nanoparticles", *Angew. Chem. Int. Ed.* **2004**, *43*, 5954-5957.
- [337] C. A. Mirkin, R. L. Letsinger, R. C. Mucic, J. J. Storhoff: "A DNA-Based Method For Rationally Assembling Nanoparticles Into Macroscopic Materials", *Nature* **1996**, *382*, 607-609.
- [338] L. M. Demers, C. A. Mirkin, R. C. Mucic, I. Robert A. Reynolds, R. L. Letsinger, R. Elghanian, G. Viswanadham: "A Fluorescence-Based Method for Determining the Surface Coverage and Hybridization Efficiency of Thiol-Capped Oligonucleotides Bound to Gold Thin Films and Nanoparticles", *Analytical Chemistry* **2000**, *72*(22), 5535-5541.
- [339] L. He, M. D. Musick, S. R. Nicewarner, F. G. Salinas, S. J. Benkovic, M. J. Natan, C. D. Keating: "Colloidal Au-Enhanced Surface Plasmon Resonance for Ultrasensitive Detection of DNA Hybridization", *Journal of the American Chemical Society* **2000**, *122*(38), 9071-9077.
- [340] R. Jin, G. Wu, Z. Li, C. A. Mirkin, G. C. Schatz: "What Controls the Melting Properties of DNA-Linked Gold Nanoparticle Assemblies?" *Journal of the American Chemical Society* **2003**, *125*(6), 1643-1654.
- [341] R. L. Letsinger, R. Elghanian, G. Viswanadham, C. A. Mirkin: "Use of a Steroid Cyclic Disulfide Anchor in Constructing Gold Nanoparticle-Oligonucleotide Conjugates", *Bioconj. Chem.* **2000**, *11*, 289-291.
- [342] Z. Li, R. Jin, C. A. Mirkin, R. L. Letsinger: "Multiple thiol-anchor capped DNA-gold nanoparticle conjugates", *Nucleic Acids Research* **2002**, *30*(7), 1558-1562.
- [343] E. Dujardin, L.-B. Hsin, C. R. C. Wang, S. Mann: "DNA-driven self-assembly of gold nanorods", *Chem. Comm.* **2001**(14), 1264-1265.
- [344] D. G. Thompson, A. Enright, K. Faulds, W. E. Smith, D. Graham: "Ultrasensitive DNA Detection Using Oligonucleotide-Silver Nanoparticle Conjugates", *Anal. Chem.* **2008**, *80*(8), 2805-2810.
- [345] G. P. Mitchell, C. A. Mirkin, R. L. Letsinger: "Programmed Assembly of DNA Functionalized Quantum Dots", *Journal of the American Chemical Society* **1999**, *121*(35), 8122-8123.
- [346] R. Gill, I. Willner, I. Shweky, U. Banin: "Fluorescence resonance energy transfer in CdSe/ZnS-DNA conjugates: Probing hybridization and DNA cleavage", *Journal Of Physical Chemistry B* **2005**, *109*(49), 23715-23719.
- [347] S. J. Hurst, A. K. R. Lytton-Jean, C. A. Mirkin: "Maximizing DNA Loading on a Range of Gold Nanoparticle Sizes", *Anal. Chem.* **2006**, *78*(24), 8313-8318.
- [348] S. R. N. Peña, S. Raina, G. P. Goodrich, N. V. Fedoroff, C. D. Keating: "Hybridization and Enzymatic Extension of Au Nanoparticle-Bound Oligonucleotides", *Journal of the American Chemical Society* **2002**, *124*(25), 7314-7323.
- [349] A. B. Steel, R. L. Levicky, T. M. Herne, M. J. Tarlov: "Immobilization of Nucleic Acids at Solid Surfaces: Effect of Oligonucleotide Length on Layer Assembly", *Biophysical Journal* **2000**, *79*(2), 975-981.
- [350] W. J. Parak, T. Pellegrino, C. M. Micheel, D. Gerion, S. C. Williams, A. P. Alivisatos: "Conformation of oligonucleotides attached to gold nanocrystals probed by gel electrophoresis", *Nanoletters* **2003**, *3*(1), 33-36.
- [351] Y. Lu, J. Liu: "Functional DNA nanotechnology: emerging applications of DNazymes and aptamers", *Current Opinion in Biotechnology* **2006**, *17*(6), 580.
- [352] D. H. Bunka, P. G. Stockley: "Aptamers come of age - at last", *Nat Rev Microbiol* **2006**, *4*(8), 588-596.
- [353] T. Mairal, V. Cengiz Özalp, P. Lozano Sánchez, M. Mir, I. Katakis, C. O'Sullivan: "Aptamers: molecular tools for analytical applications", *Analytical and Bioanalytical Chemistry* **2008**, *390*(4), 989.
- [354] W. Zhao, W. Chiuman, J. C. F. Lam, S. A. McManus, W. Chen, Y. Cui, R. Pelton, M. A. Brook, Y. Li: "DNA Aptamer Folding on Gold Nanoparticles: From Colloid Chemistry to Biosensors", *J. Am. Chem. Soc.* **2008**, *130*(11), 3610 - 3618.
- [355] J. Liu, J. H. Lee, Y. Lu: "Quantum dot encoding of aptamer-linked nanostructures for one-pot simultaneous detection of multiple analytes", *Anal Chem* **2007**, *79*(11), 4120-4125.
- [356] V. Bagalkot, L. Zhang, E. Levy-Nissenbaum, S. Jon, P. W. Kantoff, R. Langer, O. C. Farokhzad: "Quantum dot-aptamer conjugates for synchronous cancer imaging, therapy, and sensing of drug delivery based on bi-fluorescence resonance energy transfer", *Nano Lett* **2007**, *7*(10), 3065-3070.
- [357] N. R. Jana, J. Y. Ying: "Synthesis of Functionalized Au Nanoparticles for Protein Detection", *Advanced Materials* **2008**, *20*(3), 430-434.
- [358] M. Levy, S. F. Cater, A. D. Ellington: "Quantum-dot aptamer beacons for the detection of proteins", *ChemBiochem* **2005**, *6*(12), 2163-2166.
- [359] C. M. McIntosh, I. Edward A. Esposito, A. K. Boal, J. M. Simard, C. T. Martin, V. M. Rotello: "Inhibition of DNA Transcription Using Cationic Mixed Monolayer Protected Gold Clusters", *Journal of the American Chemical Society* **2001**, *123*(31), 7626-7629.
- [360] K. K. Sandhu, C. M. McIntosh, J. M. Simard, S. W. Smith, V. M. Rotello: "Gold Nanoparticle-Mediated Transfection of Mammalian Cells", *Bioconjugate Chemistry* **2002**, *13*(1), 3-6.

- [361] G. Wang, R. W. Murray: "Controlled Assembly of Monolayer-Protected Gold Clusters by Dissolved DNA", *NanoLetters* **2004**, 4(1), 95-101.
- [362] J. J. Storhoff, R. Elghanian, C. A. Mirkin, R. L. Letsinger: "Sequence-Dependent Stability of DNA-Modified Gold Nanoparticles", *Langmuir* **2002**, 18(17), 6666-6670.
- [363] A. P. Alivisatos, K. P. Johnsson, X. Peng, T. E. Wilson, C. J. Loweth, M. P. B. Jr., P. G. Schultz: "Organization of 'nanocrystal molecules' using DNA", *Nature* **1996**, 382(15 August), 609-611.
- [364] S. Pathak, S.-K. Choi, N. Arnheim, M. E. Thompson: "Hydroxylated Quantum Dots as Luminescent Probes for in Situ Hybridization", *Journal of the American Chemical Society* **2001**, 123(17), 4103-4104.
- [365] C. M. Niemeyer, W. Bürger, J. Peplies: "Covalent DNA-Streptavidin Conjugates as Building Blocks for Novel Biometallic Nanostructures", *Angew. Chem. Int. Ed.* **1998**, 37(16), 2265-2268.
- [366] R. Levy, N. T. K. Thanh, R. C. Doty, I. Hussain, R. J. Nichols, D. J. Schiffrin, M. Brust, D. G. Fernig: "Rational and Combinatorial Design of Peptide Capping Ligands for Gold Nanoparticles", *J. Am. Chem. Soc.* **2004**, 126(32), 10076-10084.
- [367] Z. Wang, R. Lévy, D. G. Fernig, M. Brust: "The Peptide Route to Multifunctional Gold Nanoparticles", *Bioconjugate Chemistry* **2005**, 16(3), 497-500.
- [368] I. L. Medintz, A. R. Clapp, F. M. Brunel, T. Tiefenbrunn, H. T. Uyeda, E. L. Chang, J. R. Deschamps, P. E. Dawson, H. Mattoussi: "Proteolytic activity monitored by fluorescence resonance energy transfer through quantum-dot peptide conjugates", *Nature Materials* **2006**, 5, 581-589.
- [369] E. Garanger, E. Aikawa, F. Reynolds, R. Weissleder, L. Josephson: "Simplified syntheses of complex multifunctional nanomaterials", *Chemical Communications* **2008**, DOI: 10.1039/b809537j, -.
- [370] J. M. de la Fuente, C. C. Berry: "Tat peptide as an efficient molecule to translocate gold nanoparticles into the cell nucleus", *Bioconjugate Chemistry* **2005**, 16(5), 1176-1180.
- [371] W. Cai, D.-W. Shin, K. Chen, O. Gheysens, Q. Cao, S. X. Wang, S. S. Gambhir, X. Chen: "Peptide-Labeled Near-Infrared Quantum Dots for Imaging Tumor Vasculature in Living Subjects", *Nano Letters* **2006**, 6(4), 669-676.
- [372] L. Josephson, C.-H. Tung, A. Moore, R. Weissleder: "High-Efficiency Intracellular Magnetic Labeling with Novel Superparamagnetic-Tat Peptide Conjugates", *Bioconjugate Chemistry* **1999**, 10(2), 186-191.
- [373] M. Zhao, M. F. Kircher, L. Josephson, R. Weissleder: "Differential Conjugation of Tat Peptide to Superparamagnetic Nanoparticles and Its Effect on Cellular Uptake", *Bioconjugate Chemistry* **2002**, 13(4), 840-844.
- [374] F. Chen, D. Gerion: "Fluorescent CdSe/ZnS Nanocrystal-Peptide Conjugates for Long-term, Nontoxic Imaging and Nuclear Targeting in Living Cells", *Nanoletters* **2004**, 4(10), 1827-1832.
- [375] B. C. Lagerholm, M. Wang, L. A. Ernst, D. H. Ly, H. Liu, M. P. Bruchez, A. S. Waggoner: "Multicolor Coding of Cells with Cationic Peptide Coated Quantum Dots", *Nanoletters* **2004**, 4(10), 2019-2022.
- [376] T. Q. Vu, R. Maddipati, T. A. Blute, B. J. Nehilla, L. Nusblat, T. A. Desai: "Peptide-Conjugated Quantum Dots Activate Neuronal Receptors and Initiate Downstream Signaling of Neurite Growth", *Nanoletters* **2005**, 5(4), 603-607.
- [377] Y.-P. Kim, Y.-H. Oh, E. Oh, S. Ko, M.-K. Han, H.-S. Kim: "Energy Transfer-Based Multiplexed Assay of Proteases by Using Gold Nanoparticle and Quantum Dot Conjugates on a Surface", *Anal. Chem.* **2008**, 80(12), 4634-4641.
- [378] T. Pons, I. L. Medintz, K. E. Sapsford, S. Higashiyama, A. F. Grimes, D. S. English, H. Mattoussi: "On the quenching of semiconductor quantum dot photoluminescence by proximal gold nanoparticles", *Nano Letters* **2007**, 7(10), 3157-3164.
- [379] A. Gole, C. Dash, V. Ramakrishnan, S. R. Sainkar, A. B. Mandale, M. Rao, M. Sastry: "Pepsin-Gold Colloid Conjugates: Preparation, Characterization, and Enzymatic Activity", *Langmuir* **2001**, 17(5), 1674-1679.
- [380] Z. Lin, S. Cui, H. Zhang, Q. Chen, B. Yang, X. Su, J. Zhang, Q. Jin: "Studies on quantum dots synthesized in aqueous solution for biological labeling via electrostatic interaction", *Analytical Biochemistry* **2003**, 319, 239-243.
- [381] S. Bucak, D. A. Jones, P. E. Laibinis, T. A. Hatton: "Protein Separations Using Colloidal Magnetic Nanoparticles", *Biotechnol. Prog.* **2003**, 19, 477-484.
- [382] W. P. Faulk, G. M. Taylor: "An immunocolloid method for the electron microscope", *Immunochemistry* **1971**, 8(11), 1081.
- [383] C. A. J. Putman, B. G. d. Grooth, P. K. Hansma, N. F. v. Hulst, J. Greve: "Immunogold labels: cell-surface markers in atomic force microscopy", *Ultramicroscopy* **1993**, 48, 177-182.
- [384] R. Hermann, P. Walther, M. Müller: "Immunogold labeling in scanning electron microscopy", *Histochemistry and Cell Biology* **1996**, 106(1), 31-39.
- [385] J. Roth: "The silver anniversary of gold: 25 years of the colloidal gold marker system for immunocytochemistry and histochemistry", *Histochemistry and Cell Biology* **1996**, 106(1), 1-8.
- [386] J. Ni, R. J. Lipert, G. B. Dawson, M. D. Porter: "Immunoassay Readout Method Using Extrinsic Raman Labels Adsorbed on Immunogold Colloids", *Anal. Chem.* **1999**, 71(21), 4903-4908.
- [387] K. Hanaki, A. Momo, T. Oku, A. Komoto, S. Maenosono, Y. Yamaguchi, K. Yamamoto: "Semiconductor quantum dot/albumin complex is a long-life and highly photostable endosome marker", *Biochemical and Biophysical Research Communications* **2003**, 302(3), 496-501.
- [388] W. C. W. Chan, S. Nie: "Quantum Dot Bioconjugates for Ultrasensitive Nonisotopic Detection", *Science* **1998**, 281, 2016-2018.

- [389] J. A. Kloepper, R. E. Mielke, M. S. Wong, K. H. Neilson, G. Stucky, J. L. Nadeau: "Quantum Dots as Strain- and Metabolism-Specific Microbiological Labels", *Applied and Environmental Microbiology* **2003**, *69*(7), 4205-4213.
- [390] K. T. Yong, J. Qian, I. Roy, H. H. Lee, E. J. Bergey, K. M. Trampusch, S. He, M. T. Swihart, A. Maitra, P. N. Prasad: "Quantum Rod Bioconjugates as Targeted Probes for Confocal and Two-Photon Fluorescence Imaging of Cancer Cells", *Nano Lett.* **2007**, *7*(3), 761-765.
- [391] D. Casanova, D. Giaume, M. Moreau, J. L. Martin, T. Gacoin, J. P. Boilot, A. Alexandrou: "Counting the number of proteins coupled to single nanoparticles", *J Am Chem Soc* **2007**, *129*(42), 12592-12593.
- [392] A. K. Oyelere, P. C. Chen, X. Huang, I. H. El-Sayed, M. A. El-Sayed: "Peptide-Conjugated Gold Nanorods for Nuclear Targeting", *Bioconjugate Chem.* **2007**, *18*(5), 1490-1497.
- [393] S. Courty, C. Luccardini, Y. Bellaiche, G. Cappello, M. Dahan: "Tracking individual kinesin motors in living cells using single quantum-dot imaging", *Nano Letters* **2006**, *6*(7), 1491-1495.
- [394] D. S. Lidke, P. Nagy, R. Heintzmann, D. J. Arndt-Jovin, J. N. Post, H. E. Grecco, E. A. Jares-Erijman, T. M. Jovin: "Quantum dot ligands provide new insights into erbB/HER receptor-mediated signal transduction", *Nature Biotechnology* **2004**, *22*, 198-203.
- [395] A. M. Dennis, G. Bao: "Quantum Dot-Fluorescent Protein Pairs as Novel Fluorescence Resonance Energy Transfer Probes", *Nano Lett.* **2008**, *8*(5), 1439-1445.
- [396] A. V. Sukhanova, Lydie. Devy, Jerome. Artemyev, Mikhail. Oleinikov, Vladimir. Pluot, Michel. Nabiev, Igor.: "Highly Stable Fluorescent Nanocrystals as a Novel Class of Labels for Immunohistochemical Analysis of Paraffin-Embedded Tissue Sections", *Laboratory Investigation* **2002**, *82*(9), 1259-1261.
- [397] D. Wang, J. He, N. Rosenzweig, Z. Rosenzweig: "Superparamagnetic Fe₂O₃ Beads-CdSe/ZnS Quantum Dots Core-Shell Nanocomposite Particles for Cell Separation", *Nanoletters* **2004**, *4*(3), 409-413.
- [398] A. Wolcott, D. Gerion, M. Visconte, J. Sun, A. Schwartzberg, S. W. Chen, J. Z. Zhang: "Silica-Coated CdTe Quantum Dots Functionalized with Thiols for Bioconjugation to IgG Proteins", *Journal of Physical Chemistry B* **2006**, *110*(11), 5779-5789.
- [399] M. Dahan, S. Levi, C. Luccardini, P. Rostaing, B. Riveau, A. Triller: "Diffusion Dynamics of Glycine Receptors Revealed by Single-Quantum Dot Tracking", *Science* **2003**, *302*(5644), 442-445.
- [400] Y. Xing, Q. Chaudry, C. Shen, K. Y. Kong, H. E. Zhou, L. W. Chung, J. A. Petros, R. M. O'Regan, M. V. Yezhelyev, J. W. Simons, M. D. Wang, S. Nie: "Bioconjugated quantum dots for multiplexed and quantitative immunohistochemistry", *Nat. Protocols* **2007**, *2*(5), 1152.
- [401] J. M. Perez, L. Josephson, R. Weissleder: "Use of Magnetic Nanoparticles as Nanosensors to Probe for Molecular Interactions", *ChemBioChem* **2004**, *5*, 261-264.
- [402] L. Josephson, J. M. Perez, R. Weissleder: "Magnetic Nanosensors for the Detection of Oligonucleotide Sequences", *Angewandte Chemie International Edition* **2001**, *40*(17), 3204-3206.
- [403] J. M. Perez, F. J. Simeone, Y. Saeki, L. Josephson, R. Weissleder: "Viral-Induced Self-Assembly of Magnetic Nanoparticles Allows the Detection of Viral Particles in Biological Media", *Journal of the American Chemical Society* **2003**, *125*(34), 10192-10193.
- [404] H. Liao, J. H. Hafner: "Gold Nanorod Bioconjugates", *Chemistry of Materials* **2005**, *17*, 4636-4641.
- [405] S. J. Clarke, C. A. Hollmann, F. A. Aldaye, J. L. Nadeau: "Effect of Ligand Density on the Spectral, Physical, and Biological Characteristics of CdSe/ZnS Quantum Dots", *Bioconjugate Chem.* **2008**, *19*(2), 562-568.
- [406] S. J. Rosenthal, I. Tomlinson, E. M. Adkins, S. Schroeter, S. Adams, L. Swafford, J. McBride, Y. Wang, L. J. DeFelice, R. D. Blakely: "Targeting Cell Surface Receptors with Ligand-Conjugated Nanocrystals", *Journal of the American Chemical Society* **2002**, *124*(17), 4586-4594.
- [407] J. M. de la Fuente, M. Fandel, C. C. Berry, M. Riehle, L. Cronin, G. Aitchison, A. S. Curtis: "Quantum dots protected with tiopronin: a new fluorescence system for cell-biology studies", *ChemBiochem* **2005**, *6*(6), 989-991.
- [408] C. M. Niemeyer: "Nanoparticles, Proteins, and Nucleic Acids: Biotechnology Meets Materials Science", *Angew. Chem. Int. Ed.* **2001**, *40*, 4128-4158.
- [409] X. Gao, L. Yang, J. A. Petros, F. F. Marshall, J. W. Simons, S. Nie: "In vivo molecular and cellular imaging with quantum dots", *Curr Opin Biotechnol* **2005**, *16*(1), 63-72.
- [410] J. E. Ghadiali, M. M. Stevens: "Enzyme-Responsive Nanoparticle Systems", *Advanced Materials* **2008**, DOI: 10.1002/adma.200703158, 1-5.
- [411] A. C. Templeton, D. E. Cliffel, R. W. Murray: "Redox and Fluorophore Functionalization of Water-Soluble, Tiopronin-Protected Gold Clusters", *J. Am. Chem. Soc.* **1999**, *121*(30), 7081-7089.
- [412] T. T. Nikiforov, J. M. Beechem: "Development of homogeneous binding assays based on fluorescence resonance energy transfer between quantum dots and Alexa Fluor fluorophores", *Analytical Biochemistry* **2006**, *357*(1), 68.
- [413] A. M. Funston, J. J. Jasieniak, P. Mulvaney: "Complete Quenching of CdSe Nanocrystal Photoluminescence by Single Dye Molecules", *Advanced Materials* **2008**, DOI: 10.1002/adma.200703186, NA.
- [414] M. L. Schipper, Z. Cheng, S.-W. Lee, L. A. Bentolila, G. Iyer, J. Rao, X. Chen, A. M. Wu, S. Weiss, S. S. Gambhir: "microPET-Based Biodistribution of Quantum Dots in Living Mice", *J Nucl Med* **2007**, *48*(9), 1511-1518.
- [415] M. Shokeen, N. M. Fettig, R. Rossin: "Synthesis, in vitro and in vivo evaluation of radiolabeled nanoparticles", *Quarterly Journal Of Nuclear Medicine And Molecular Imaging* **2008**, *52*(3), 267-277.
- [416] R. Bakalova, Z. Zhelev, I. Aoki, I. Kanno: "Designing quantum-dot probes", *Nature Photonics* **2007**, *1*(9), 487-489.

- [417] J. Kim, H. S. Kim, N. Lee, T. Kim, H. Kim, T. Y. I. C. Song, W. K. Moon, T. Hyeon: "Multifunctional Uniform Nanoparticles Composed of a Magnetite Nanocrystal Core and a Mesoporous Silica Shell for Magnetic Resonance and Fluorescence Imaging and for Drug Delivery", *Angewandte Chemie International Edition* **2008**, *47*, 1-5.
- [418] F. Bertorelle, C. Wilhelm, J. Roger, F. Gazeau, C. Menager, V. Cabuil: "Fluorescence-modified superparamagnetic nanoparticles: Intracellular uptake and use in cellular imaging", *Langmuir* **2006**, *22*(12), 5385-5391.
- [419] M. Liong, J. Lu, M. Kovochich, T. Xia, S. G. Ruehm, A. E. Nel, F. Tamanoi, J. I. Zink: "Multifunctional Inorganic Nanoparticles for Imaging, Targeting, and Drug Delivery", *ACS Nano* **2008**, *2*(5), 889-896.
- [420] H.-Y. Xie, C. Zuo, Y. Liu, Z.-L. Zhang, D.-W. Pang, X.-L. Li, J.-P. Gong, C. Dickinson, W. Zhou: "Cell-Targeting Multifunctional Nanospheres with both Fluorescence and Magnetism", *Small* **2005**, *1*(5), 506-509.
- [421] G. B. Sukhorukov, A. L. Rogach, M. Garstka, S. Springer, W. J. Parak, A. Muñoz-Javier, Oliver Kreft, A. G. Skirtach, A. S. Susha, Y. Ramaye, R. Palankar, M. Winterhalter: "Multifunctionalized Polymer Microcapsules: Novel Tools for Biological and Pharmacological Applications", *SMALL* **2007**, *3*(6), 944-955.
- [422] M. Kuno, J. K. Lee, B. O. Dabbousi, F. V. Mikulec, M. G. Bawendi: "The band edge luminescence of surface modified CdSe nanocrystallites: Probing the luminescing state", *Journal of Chemical Physics* **1997**, *106*(23), 9869-9882.
- [423] M. J. Hostetler, J. J. Stokes, R. W. Murray: "Infrared Spectroscopy of Three-Dimensional Self-Assembled Monolayers: N-Alkanethiolate Monolayers on Gold Cluster Compounds", *Langmuir* **1996**, *12*(15), 3604-3612.
- [424] D. R. Whitcomb, B. J. Stwertka, S. Chen, P. J. Cowdery-Corvan: "SERS characterization of metallic silver nanoparticle self-assembly within thin films", *Journal of Raman Spectroscopy* **2008**, *39*(3), 421-426.
- [425] A. Scheffer, C. Engelhard, M. Sperling, W. Buscher: "ICP-MS as a new tool for the determination of gold nanoparticles in bioanalytical applications", *Analytical And Bioanalytical Chemistry* **2008**, *390*(1), 249-252.
- [426] A. Helfrich, W. Bruchert, J. Bettmer: "Size characterisation of Au nanoparticles by ICP-MS coupling techniques", *Journal Of Analytical Atomic Spectrometry* **2006**, *21*(4), 431-434.
- [427] T. Liedl, S. Keller, F. C. Simmel, J. O. Rädler, W. J. Parak: "Fluorescent Nanocrystals as Colloidal Probes in Complex Fluids Measured by Fluorescence Correlation Spectroscopy", *Small* **2005**, *1*(10), 997-1003.
- [428] S. Doose, J. M. Tsay, F. Pinaud, S. Weiss: "Comparison of Photophysical and Colloidal Properties of Biocompatible Semiconductor Nanocrystals Using Fluorescence Correlation Spectroscopy", *Anal. Chem.* **2005**, *77*, 2235-2242.
- [429] P. Zhang, L. Li, C. Dong, H. Qian, J. Ren: "Sizes of water-soluble luminescent quantum dots measured by fluorescence correlation spectroscopy", *Analytica Chimica Acta* **2005**, *546*, 46-51.
- [430] S. Dühr, D. Braun: "Why molecules move along a temperature gradient", *PNAS* **2006**, *103*(52), 19678-19682.
- [431] C. S. Xu, H. Cang, D. Montiel, H. Yang: "Rapid and Quantitative Sizing of Nanoparticles Using Three-Dimensional Single-Particle Tracking", *J. Phys. Chem. C* **2007**, *111*(1), 32-35.
- [432] G. A. Lessard, P. M. Goodwin, J. H. Werner: "Three-dimensional tracking of individual quantum dots", *Applied Physics Letters* **2007**, *91*(22), 224106.
- [433] K. McHale, A. J. Berglund, H. Mabuchi: "Quantum Dot Photon Statistics Measured by Three-Dimensional Particle Tracking", *Nano Lett.* **2007**, *7*(11), 3535-3539.
- [434] M. Calabretta, J. A. Jamison, J. C. Falkner, Y. P. Liu, B. D. Yuhas, K. S. Matthews, V. L. Colvin: "Analytical ultracentrifugation for characterizing nanocrystals and their bioconjugates", *Nano Letters* **2005**, *5*(5), 963-967.
- [435] J. A. Jamison, K. M. Krueger, C. T. Yavuz, J. T. Mayo, D. LeCrone, J. J. Redden, V. L. Colvin: "Size-Dependent Sedimentation Properties of Nanocrystals", *ACS Nano* **2008**, *2*(2), 311-319.
- [436] J. F. Berret, O. Sandre, A. Mauger: "Size distribution of superparamagnetic particles determined by magnetic sedimentation", *Langmuir* **2007**, *23*(6), 2993-2999.
- [437] Z. Grubisic, P. Rempp, H. Benoit: "A Universal Calibration For Gel Permeation Chromatography", *Journal Of Polymer Science Part B-Polymer Letters* **1967**, *5*(9PB), 753-759.
- [438] L. Hagel, in *Protein Purification. Principles, High Resolution Methods and Applications*, 2 ed. (Eds.: J.-C. Janson, L. Ryden), John Wiley & Sons, New York, **1998**, pp. 79-143.
- [439] M. L. Steigerwald, A. P. Alivisatos, J. M. Gibson, T. D. Harris, R. Kortan, A. J. Muller, A. M. Thayer, T. M. Duncan, D. C. Douglass, L. E. Brus: "Surface derivatization and isolation of semiconductor cluster molecules", *Journal of the American Chemical Society* **1988**, *110*, 3046-3050.
- [440] J. P. Wilcoxon, J. E. Martin, P. Provencio: "Size Distributions of Gold Nanoclusters Studied by Liquid Chromatography", *Langmuir* **2000**, *16*(25), 9912-9920.
- [441] A. M. Al-Somali, K. M. Krueger, J. C. Falkner, V. L. Colvin: "Recycling Size Exclusion Chromatography for the Analysis and Separation of Nanocrystalline Gold", *Analytical Chemistry* **2004**, *76*(19), 5903-5910.
- [442] K. M. Krueger, A. M. Al-Somali, J. C. Falkner, V. L. Colvin: "Characterization of Nanocrystalline CdSe by Size Exclusion Chromatography", *Analytical Chemistry* **2005**, *77*(11), 3511-3515.
- [443] T. Siebrands, M. Giersig, P. Mulvaney, C.-H. Fischer: "Steric Exclusion Chromatography of Nanometer-Sized Gold Particles", *Langmuir* **1993**, *9*(9), 2297-2300.
- [444] C.-H. Fischer, M. Giersig, T. Siebrands: "Analysis of colloidal particles V. Size-exclusion chromatography of colloidal semiconductor particles", *Journal of Chromatography A* **1994**, *670*(1-2), 89-97.
- [445] G.-T. Wei, F.-K. Liu, C. R. C. Wang: "Shape Separation of Nanometer Gold Particles by Size-Exclusion Chromatography", *Analytical Chemistry* **1999**, *71*(11), 2085-2091.

- [446] G.-T. Wei, F.-K. Liu: "Separation of nanometer gold particles by size exclusion chromatography", *Journal of Chromatography A* **1999**, *836*, 253–260.
- [447] Á. V. Delgado, F. J. Arroyo, in *Interfacial electrokinetics and electrophoresis* (Eds.: Á. V. Delgado, F. J. Arroyo), Dekker, New York, **2002**, pp. 1-54.
- [448] S. Park, K. Hamad-Schifferli: "Evaluation of Hydrodynamic Size and Zeta-Potential of Surface-Modified Au Nanoparticle-DNA Conjugates via Ferguson Analysis", *J. Phys. Chem. C* **2008**, *112*(20), 7611-7616.
- [449] A. C. Templeton, D. E. Cliffler, R. W. Murray: "Redox and Fluorophore Functionalization of Water-Soluble, Tiopronin-Protected Gold Clusters", *Journal of the American Chemical Society* **1999**, *121*(30), 7081-7089.
- [450] A. Morneau, V. Pillai, S. Nigam, F. M. Winnik, R. F. Ziolo: "Analysis of ferrofluids by capillary electrophoresis", *Colloids and Surfaces A* **1999**, *154*, 295-301.
- [451] F.-K. Liu, Y.-Y. Lin, C.-H. Wu: "Highly efficient approach for characterizing nanometer-sized gold particles by capillary electrophoresis", *Analytica Chimica Acta* **2005**, *528*(2), 249-254.
- [452] X. Song, L. Li, H. Qian, N. Fang, J. Ren: "Highly efficient size separation of CdTe quantum dots by capillary gel electrophoresis using polymer solution as sieving medium", *Electrophoresis* **2006**, *27*, 1341-1346.
- [453] W. Bücking, T. Nann: "Electrophoretic Analysis of Gold Nanoparticles: Size-dependent Electrophoretic Mobility of Nanoparticles", *IEE proceedings - Nanobiotechnology* **2006**, *153*(3), 47-53.
- [454] S. Philip: "Agarose gels: Properties and use for electrophoresis", *Electrophoresis* **1983**, *4*(6), 375-382.
- [455] G. A. Griess, E. T. Moreno, R. A. Easom, P. Serwer: "The Sieving of Spheres During Agarose Gel Electrophoresis: Quantitation and Modeling", *Biopolymers* **1989**, *28*(8), 1475-1484.
- [456] M. Hanauer, S. Pierrat, I. Zins, A. Lotz, C. Sonnichsen: "Separation of Nanoparticles by Gel Electrophoresis According to Size and Shape", *Nano Letters* **2007**, *7*(9), 2881-2885.
- [457] H. Ohshima: "Electrokinetics of soft particles", *Colloid & Polymer Science* **2007**, *285*(13), 1411.
- [458] R. J. Hill, D. A. Saville: "'Exact' solutions of the full electrokinetic model for soft spherical colloids: Electrophoretic mobility", *Colloids and Surfaces A: Physicochemical and Engineering Aspects* **2005**, *267*(1-3), 31.
- [459] P. A. Sandström, Björn: "Electrophoretic Properties of DNA-Modified Colloidal Gold Nanoparticles", *Langmuir* **2004**, *20*(10), 4182-4186.
- [460] S. Park, K. A. Brown, K. Hamad-Schifferli: "Changes in Oligonucleotide Conformation on Nanoparticle Surfaces by Modification with Mercaptohexanol", *Nanoletters* **2004**, *4*(10), 1925-1929.
- [461] X. Xu, K. K. Caswell, E. Tucker, S. Kabisatpathy, K. L. Brodhacker, W. A. Scrivens: "Size and shape separation of gold nanoparticles with preparative gel electrophoresis", *Journal of Chromatography A* **2007**, *1167*(1), 35.
- [462] M. M. Alvarez, J. T. Houry, T. G. Schaaff, M. N. Shafiqullin, I. Vezmar, R. L. Whetten: "Optical Absorption Spectra of Nanocrystal Gold Molecules", *J. Phys. Chem. B* **1997**, *101*(19), 3706-3712.
- [463] W. Haiss, N. T. K. Thanh, J. Aveyard, D. G. Fernig: "Determination of Size and Concentration of Gold Nanoparticles from UV-Vis Spectra", *Anal. Chem.* **2007**, *79*(11), 4215-4221.
- [464] S. Underwood, P. Mulvaney: "Effect of the Solution Refractive Index on the Color of Gold Colloids", *Langmuir* **1994**, *10*(10), 3427-3430.
- [465] V. Myroshnychenko, J. Rodriguez-Fernandez, I. Pastoriza-Santos, A. M. Funston, C. Novo, P. Mulvaney, L. M. Liz-Marzan, F. J. G. d. Abajo: "Modelling the optical response of gold nanoparticles", *Chemical Society Reviews* **2008**, *37*(9), 1792-1805.
- [466] W. W. Yu, L. Qu, W. Guo, X. Peng: "Experimental Determination of the Extinction Coefficient of CdTe, CdSe, and CdS Nanocrystals", *Chemistry of Materials* **2003**, *15*(14), 2854-2860.
- [467] Y. Ebinstein, E. Nahum, U. Banin: "Tapping Mode Atomic Force Microscopy for Nanoparticle Sizing: Tip-Sample Interaction Effects", *Nanoletters* **2002**, *2*(9), 945-950.
- [468] T. Liu, J. a. Tang, H. Zhao, Y. Deng, L. Jiang: "Particle Size Effect of the DNA Sensor Amplified with Gold Nanoparticles", *Langmuir* **2002**, *18*(14), 5624-5626.
- [469] B. J. Nehilla, T. Q. Vu, T. A. Desai: "Stoichiometry-dependent formation of quantum dot-antibody bioconjugates: A complementary atomic force microscopy and agarose gel electrophoresis study", *Journal of Physical Chemistry B* **2005**, *109*(44), 20724-20730.
- [470] Y. Ebinstein, T. Mokari, U. Banin: "Fluorescence quantum yield of CdSe/ZnS nanocrystals investigated by correlated atomic-force and single-particle fluorescence microscopy", *Applied Physics Letters* **2002**, *80*(21), 4033.
- [471] H. Mattoussi, A. W. Cumming, C. B. Murray, M. G. Bawendi, R. Ober: "Characterization of CdSe nanocrystallite dispersions by small angle x-ray scattering", *J. Chem. Phys.* **1996**, *105*(22), 9890-9896.
- [472] L. Broussous, C. V. Santilli, S. H. Pulcinelli, A. F. Craievich: "SAXS Study of Formation and Growth of Tin Oxide Nanoparticles in the Presence of Complexing Ligands", *The Journal of Physical Chemistry B* **2002**, *106*(11), 2855-2860.
- [473] H. Borchert, E. V. Shevchenko, A. Robert, I. Mekis, A. Kornowski, G. Grübel, H. Weller: "Determination of Nanocrystal Sizes: A Comparison of TEM, SAXS, and XRD Studies of Highly Monodisperse CoPt₃ Particles", *Langmuir* **2005**, *21*(5), 1931-1936.
- [474] M. Zackrisson, A. Stradner, P. Schurtenberger, J. Bergenholtz: "Small-Angle Neutron Scattering on a Core-Shell Colloidal System: A Contrast-Variation Study", *Langmuir* **2005**, *21*, 10835-10845.
- [475] S. K. Ghosh, T. Pal: "Interparticle Coupling Effect on the Surface Plasmon Resonance of Gold Nanoparticles: From Theory to Applications", *Chem. Rev.* **2007**, *107*(11), 4797-4862.

- [476] S. M. C. Sari, P. J. Debouttiere, R. Lamartine, F. Vocanson, C. Dujardin, G. Ledoux, S. Roux, O. Tillement, P. Perriat: "Grafting of colloidal stable gold nanoparticles with lissamine rhodamine B: an original procedure for counting the number of dye molecules attached to the particles", *Journal of Materials Chemistry* **2004**, *14*(3), 402-407.
- [477] Z. Wang, J. Lee, A. R. Cossins, M. Brust: "Microarray-Based Detection of Protein Binding and Functionality by Gold Nanoparticle Probes", *Anal. Chem.* **2005**, *77*(17), 5770-5774.
- [478] Z. Wang, J. Lee, A. Cossins, M. Brust: "Selective enzymatic cleavage of gold nanoparticle-labelled DNA on a microarray", *IEE Proceedings -- Nanobiotechnology* **2005**, *152*(2), 85.
- [479] G. R. Newman, B. Jasani: "Silver development in microscopy and bioanalysis: past and present", *The Journal of Pathology* **1998**, *186*(2), 119-125.
- [480] M. T. Castañeda, S. A. A. Merkoçi: "Electrochemical Sensing of DNA Using Gold Nanoparticles", *Electroanalysis* **2007**, *19*(7-8), 743-753.
- [481] Y.-F. Huang, Y.-W. Lin, Z.-H. Lin, H.-T. Chang: "Aptamer-modified gold nanoparticles for targeting breast cancer cells through light scattering", *Journal of Nanoparticle Research* **2008**.
- [482] L. Cognet, C. Tardin, D. Boyer, D. Choquet, P. Tamarat, B. Lounis: "Single metallic nanoparticle imaging for protein detection in cells", *PNAS* **2003**, *100*(20), 11350-11355.
- [483] D. L. Chamberland, A. Agarwa, N. Kotov, J. B. Brian Fowlkes, P. L. Carson, X. Wang: "Photoacoustic tomography of joints aided by an Etanercept-conjugated gold nanoparticle contrast agent—an *ex vivo* preliminary rat study", *Nanotechnology* **2008**, 1-7.
- [484] J. Kneipp, H. Kneipp, K. Kneipp: "SERS—a single-molecule and nanoscale tool for bioanalytics", *Chemical Society Reviews* **2008**, *37*(5), 1052-1060.
- [485] W. S. Sutherland, J. J. Laserna, M. J. Angebrannt, J. D. Winefordner: "Surface-Enhanced Raman Analysis Of Sulfa Drugs On Colloidal Silver Dispersion", *Analytical Chemistry* **1990**, *62*(7), 689-693.
- [486] X. Qian, X.-H. Peng, D. O. Ansari, Q. Yin-Goen, G. Z. Chen, D. M. Shin, L. Yang, A. N. Young, M. D. Wang, S. Nie: "In vivo tumor targeting and spectroscopic detection with surface-enhanced Raman nanoparticle tags", *Nat Biotech* **2008**, *26*(1), 83.
- [487] X. M. Qian, S. M. Nie: "Single-molecule and single-nanoparticle SERS: from fundamental mechanisms to biomedical applications", *Chemical Society Reviews* **2008**, *37*(5), 912-920.
- [488] J. F. Hainfeld, D. N. Slatkin, T. M. Focella, H. M. Smilowitz: "Gold nanoparticles: a new X-ray contrast agent", *British Journal Of Radiology* **2006**, *79*(939), 248-253.
- [489] R. E. Gosselin: "The uptake of radiocolloids by macrophages in vitro - a kinetic analysis with radioactive colloidal gold", *The Journal of General Physiology* **1956**, *39*(5), 625-649.
- [490] A. M. Smith, H. Duan, A. M. Mohs, S. Nie: "Bioconjugated quantum dots for in vivo molecular and cellular imaging", *Advanced Drug Delivery Reviews* **2008**, *60*(11), 1226-1240.
- [491] J. K. Jaiswal, H. Mattoussi, J. M. Mauro, S. M. Simon: "Long-term multiple color imaging of live cells using quantum dot bioconjugates", *Nature Biotechnology* **2003**, *21*(January 2003), 47-51.
- [492] H. Tada, H. Higuchi, T. M. Wanatabe, N. Ohuchi: "In vivo real-time tracking of single quantum dots conjugated with monoclonal anti-HER2 antibody in tumors of mice", *Cancer Research* **2007**, *67*(3), 1138-1144.
- [493] R. G. Thorne, C. Nicholson: "In vivo diffusion analysis with quantum dots and dextrans predicts the width of brain extracellular space", *Proc Natl Acad Sci U S A* **2006**, *103*(14), 5567-5572.
- [494] U. Resch-Genger, M. Grabolle, S. Cavaliere-Jaricot, R. Nitschke, T. Nann: "Quantum dots versus organic dyes as fluorescent labels", *Nat Meth* **2008**, *5*(9), 763.
- [495] M. Nakamura, M. Shono, K. Ishimura: "Synthesis, Characterization, and Biological Applications of Multifluorescent Silica Nanoparticles", *Anal. Chem.* **2007**, *79*(17), 6507-6514.
- [496] C. Tortiglione, A. Quarta, A. Tino, L. Manna, R. Cingolani, T. Pellegrino: "Synthesis and Biological Assay of GSH Functionalized Fluorescent Quantum Dots for Staining *Hydra Vulgaris*", *Bioconjugate Chemistry* **2007**, *18*, 829-835.
- [497] Y. T. Lim, S. Kim, A. Nakayama, N. E. Stott, M. G. Bawendi, J. V. Frangioni: "Selection of Quantum Dot Wavelengths for Biomedical Assays and Imaging", *Molecular Imaging* **2003**, *2*(1), 50-64.
- [498] J. H. Rao, A. Dragulescu-Andrasi, H. Q. Yao, H. Q. Yao: "Fluorescence imaging in vivo: recent advances", *Current Opinion in Biotechnology* **2007**, *18*(1), 17-25.
- [499] D. R. Larson, W. R. Zipfel, R. M. Williams, S. W. Clark, M. P. Bruchez, F. W. Wise, W. W. Webb: "Water-soluble quantum dots for multiphoton fluorescence imaging in vivo", *Science* **2003**, *300*, 1434-1436.
- [500] W. C. W. Chan, D. J. Maxwell, X. Gao, R. E. Bailey, M. Han, S. Nie: "Luminescent quantum dots for multiplexed biological detection and imaging", *Current Opinion in Biotechnology* **2002**, *13*(1), 40-46.
- [501] A. Watson, X. Wu, M. Bruchez: "Lighting Up Cells With Quantum Dots, Biotechniques", *Biotechniques* **2003**, *34*(2), 296-303.
- [502] J. K. Jaiswal, S. M. Simon: "Potentials and pitfalls of fluorescent quantum dots for biological imaging", *Trends in Cell Biology* **2004**, *14*(9), 497-504.
- [503] I. L. Medintz, H. T. Uyeda, E. R. Goldman, H. Mattoussi: "Quantum dot bioconjugates for imaging, labelling and sensing", *Nature Materials* **2005**, *4*(6), 435-446.

- [504] P. K. Chattopadhyay, D. A. Price, T. F. Harper, M. R. Betts, J. Yu, E. Gostick, S. P. Perfetto, P. Goepfert, R. A. Koup, S. C. De Rosa, M. P. Bruchez, M. Roederer: "Quantum dot semiconductor nanocrystals for immunophenotyping by polychromatic flow cytometry", *Nat Med* **2006**, *12*(8), 972.
- [505] J. H. Lee, Y. M. Huh, Y. Jun, J. Seo, J. Jang, H. T. Song, S. Kim, E. J. Cho, H. G. Yoon, J. S. Suh, J. Cheon: "Artificially engineered magnetic nanoparticles for ultra-sensitive molecular imaging", *Nature Medicine* **2007**, *13*(1), 95-99.
- [506] C. C. Berry, A. S. G. Curtis: "Functionalisation of magnetic nanoparticles for applications in biomedicine", *Journal of Applied Physics* **2003**, *36*, R198-R206.
- [507] A. H. Lu, E. L. Salabas, F. Schuth: "Magnetic nanoparticles: Synthesis, protection, functionalization, and application", *Angewandte Chemie-International Edition* **2007**, *46*(8), 1222-1244.
- [508] S. Laurent, D. Forge, M. Port, A. Roch, C. Robic, L. Vander Elst, R. N. Muller: "Magnetic Iron Oxide Nanoparticles: Synthesis, Stabilization, Vectorization, Physicochemical Characterizations, and Biological Applications", *Chemical Reviews* **2008**, *108*(6), 2064.
- [509] S. Ueno, M. Sekino: "Biomagnetics and bioimaging for medical applications", *Journal of Magnetism and Magnetic Materials* **2006**, *304*(1), 122.
- [510] R. Elghanian, J. J. Storhoff, R. C. Mucic, R. L. Letsinger, C. A. Mirkin: "Selective Colorimetric Detection of Polynucleotides Based on the Distance-Dependent Optical Properties of Gold Nanoparticles", *Science* **1997**, *277*(August 22), 1078-1081.
- [511] J. J. Storhoff, R. Elghanian, R. C. Mucic, C. A. Mirkin, R. L. Letsinger: "One-Pot Colorimetric Differentiation of Polynucleotides with Single Base Imperfections Using Gold Nanoparticle Probes", *Journal of the American Chemical Society* **1998**, *120*(9), 1959-1964.
- [512] R. A. Reynolds, C. A. Mirkin, R. L. Letsinger: "Homogeneous, Nanoparticle-Based Quantitative Colorimetric Detection of Oligonucleotides", *JACS* **2000**, *122*(15), 3795-3796.
- [513] T. A. Taton, C. A. Mirkin, R. L. Letsinger: "Scanometric DNA Array Detection with Nanoparticle Probes", *Science* **2000**, *289*(8 September), 1757-1760.
- [514] J.-M. Nam, S.-J. Park, C. A. Mirkin: "Bio-Barcodes Based on Oligonucleotide-Modified Nanoparticles", *Journal of the American Chemical Society* **2002**, *124*(15), 3820-3821.
- [515] J. M. Nam, S. I. Stoeva, C. A. Mirkin: "Bio-Bar-Code-Based DNA Detection with PCR-like Sensitivity", *J. Am. Chem. Soc.* **2004**, *126*(19), 5932-5933.
- [516] J.-M. Nam, C. S. Thaxton, C. A. Mirkin: "Nanoparticle-Based Bio-Bar Codes for the Ultrasensitive Detection of Proteins", *Science* **2003**, *301*, 1884-1886.
- [517] N. L. Rosi, C. A. Mirkin: "Nanostructures in biodiagnostics", *Chemical Reviews* **2005**, *105*(4), 1547-1562.
- [518] J. M. Perez, T. O'Loughin, F. J. Simeone, R. Weissleder, L. Josephson: "DNA-Based Magnetic Nanoparticle Assembly Acts as a Magnetic Relaxation Nanoswitch Allowing Screening of DNA-Cleaving Agents", *Journal of the American Chemical Society* **2002**, *124*(12), 2856-2857.
- [519] C. S. K. Yun, G. A.; Vergona, D. E.; Reich, N. O.; Strouse, G. F.: "Enzymatic Manipulation of DNA-Nanomaterial Constructs", *Journal of the American Chemical Society* **2002**, *124*(26), 7644-7645.
- [520] A. G. Kanaras, Z. Wang, A. D. Bates, R. Cosstick, M. Brust: "Towards Multistep Nanostructure Synthesis: Programmed Enzymatic Self-Assembly of DNA/Gold Systems", *Angew. Chem. Int. Edn. Engl.* **2003**, *42*, 191-194.
- [521] A. Laromaine, L. Koh, M. Murugesan, R. V. Ulijn, M. M. Stevens: "Protease-Triggered Dispersion of Nanoparticle Assemblies", *J. Am. Chem. Soc.* **2007**, *129*(14), 4156-4157.
- [522] G. Raschke, S. Kowarik, T. Franzl, C. Sonnichsen, T. A. Klar, J. Feldmann, A. Nichtl, K. Kurzinger: "Biomolecular recognition based on single gold nanoparticle light scattering", *Nano Letters* **2003**, *3*(7), 935-938.
- [523] R. Wilson: "The use of gold nanoparticles in diagnostics and detection", *Chemical Society Reviews* **2008**, *37*(9), 2028-2045.
- [524] I. L. Medintz, A. R. Clapp, H. Mattoussi, E. R. Goldman, B. Fisher, J. M. Mauro: "Self-assembled nanoscale biosensors based on quantum dot FRET donors", *Nature Materials* **2003**, *2*, 630-638.
- [525] M. Suzuki, Y. Husimi, H. Komatsu, K. Suzuki, K. T. Douglas: "Quantum dot FRET biosensors that respond to pH, to proteolytic or nucleolytic cleavage, to DNA synthesis, or to a multiplexing combination", *J Am Chem Soc* **2008**, *130*(17), 5720-5725.
- [526] K. E. Sapsford, T. Pons, I. L. Medintz, H. Mattoussi: "Biosensing with luminescent semiconductor quantum dots", *Sensors* **2006**, *6*(8), 925-953.
- [527] W. Algar, U. Krull: "Quantum dots as donors in fluorescence resonance energy transfer for the bioanalysis of nucleic acids, proteins, and other biological molecules", *Analytical and Bioanalytical Chemistry* **2008**, *391*(5), 1609.
- [528] R. Hiergeist, W. Andrä, N. Buske, R. Hergt, I. Hilger, U. Richter, W. Kaiser: "Application of magnetite ferrofluids for hyperthermia", *Journal of Magnetism and Magnetic Materials* **1999**, *201*, 420-422.
- [529] M. Johannsen, U. Gneveckow, B. Thiesen, K. Taymoorian, C. H. Cho, N. Waldofner, R. Scholz, A. Jordan, S. A. Loening, P. Wust: "Thermotherapy of Prostate Cancer Using Magnetic Nanoparticles: Feasibility, Imaging, and Three-Dimensional Temperature Distribution", *European Urology* **2007**, *52*(6), 1653.
- [530] S. Mornet, S. Vasseur, F. Gasset, E. Duguet: "Magnetic nanoparticle design for medical diagnosis and therapy", *Journal of Materials Chemistry* **2004**, *14*(14), 2161-2175.

- [531] M. R. Choi, K. J. Stanton-Maxey, J. K. Stanley, C. S. Levin, R. Bardhan, D. Akin, S. Badve, J. Sturgis, J. P. Robinson, R. Bashir, N. J. Halas, S. E. Clare: "A cellular Trojan horse for delivery of therapeutic nanoparticles into tumors", *Nano Letters* **2007**, 7(12), 3759-3765.
- [532] T. B. Huff, L. Tong, Y. Zhao, M. N. Hansen, J. X. Cheng, A. Wei: "Hyperthermic effects of gold nanorods on tumor cells", *Nanomedicine* **2007**, 2(1), 125-132.
- [533] V. C. Mosqueira, P. Legrand, J. L. Morgat, M. Vert, E. Mysiakine, R. Gref, J. P. Devissaguet, G. Barratt: "Biodistribution of long-circulating PEG-grafted nanocapsules in mice: effects of PEG chain length and density", *Pharm. Res.* **2001**, 18, 1411-1419.
- [534] C. Sun, J. S. H. Lee, M. Zhang: "Magnetic nanoparticles in MR imaging and drug delivery", *Advanced Drug Delivery Reviews* **2008**, 60(11), 1252.
- [535] C. Xu, S. Sun: "Monodisperse magnetic nanoparticles for biomedical applications", *Polymer International* **2007**, 56(7), 821-826.
- [536] W. Jiang, Y. S. KimBetty, J. T. Rutka, C. W. ChanWarren: "Nanoparticle-mediated cellular response is size-dependent", *Nat Nano* **2008**, 3(3), 145.
- [537] J. Delehanty, H. Mattoussi, I. Medintz: "Delivering quantum dots into cells: strategies, progress and remaining issues", *Analytical and Bioanalytical Chemistry* **2008**, DOI:10.1007/s00216-008-2410-4.
- [538] P. Ghosh, G. Han, M. De, C. K. Kim, V. M. Rotello: "Gold nanoparticles in delivery applications", *Advanced Drug Delivery Reviews* **2008**, 60(11), 1307-1315.
- [539] A. G. Skirtach, A. M. Javier, O. Kreft, K. Köhler, A. P. Alberola, H. Möhwald, W. J. Parak, G. B. Sukhorukov: "Laser-Induced Release of Encapsulated Materials inside Living Cells", *Angew. Chem. Int. Ed.* **2006**, 45, 4612-4617.
- [540] Y. S. Liu, Y. Sun, P. T. Vernier, C. H. Liang, S. Y. C. Chong, M. A. Gundersen: "pH-Sensitive Photoluminescence of CdSe/ZnSe/ZnS Quantum Dots in Human Ovarian Cancer Cells", *J. Phys. Chem. C* **2007**, 111(7), 2872-2878.
- [541] P. K. Stoimenov, R. L. Klinger, G. L. Marchin, K. J. Klabunde: "Metal Oxide Nanoparticles as Bactericidal Agents", *Langmuir* **2002**, 18(17), 6679-6686.
- [542] X. Chen, H. J. Schluesener: "Nanosilver: A nanoproduct in medical application", *Toxicology Letters* **2008**, 176(1), 1.
- [543] H. J. Lee, S. Y. Yeo, S. H. Jeong: "Antibacterial effect of nanosized silver colloidal solution on textile fabrics", *Journal Of Materials Science* **2003**, 38(10), 2199-2204.
- [544] M. De, P. S. Ghosh, V. M. Rotello: "Applications of Nanoparticles in Biology", *Advanced Materials* **2008**, 20, 1-17.
- [545] J. Riu, A. Maroto, F. X. Rius: "Nanosensors in environmental analysis", *Talanta* **2006**, 69(2), 288-301.
- [546] T. Jennings, G. Strouse, in *Bio-Applications Of Nanoparticles*, Vol. 620, **2007**, pp. 34-47.
- [547] C. Z. Hotz: "Applications of quantum dots in biology: an overview", *Methods Mol Biol* **2005**, 303, 1-17.
- [548] X. Michalet, F. F. Pinaud, L. A. Bentolila, J. M. Tsay, S. Doose, J. J. Li, G. Sundaresan, A. M. Wu, S. S. Gambhir, S. Weiss: "Quantum Dots for Live Cells, in Vivo Imaging, and Diagnostics", *Science* **2005**, 307(5709), 538-544.
- [549] W. W. Yu, E. Chang, R. Drezek, V. L. Colvin: "Water-soluble quantum dots for biomedical applications", *Biochemical And Biophysical Research Communications* **2006**, 348(3), 781-786.
- [550] J. M. Klostranec, W. C. W. Chan: "Quantum Dots in Biological and Biomedical Research: Recent Progress and Present Challenges", *Advanced Materials* **2006**, 18(15), 1953-1964.
- [551] C. C. Huang, H. T. Chang: "Selective Gold-Nanoparticle-Based "Turn-On" Fluorescent Sensors for Detection of Mercury(II) in Aqueous Solution", *Anal. Chem.* **2006**, 78(24), 8332-8338.
- [552] C. C. Huang, Z. Yang, K. H. Lee, H. T. Chang: "Synthesis of highly fluorescent gold nanoparticles for sensing Mercury(II)", *Angewandte Chemie-International Edition* **2007**, 46(36), 6824-6828.
- [553] W. J. Jin, M. T. Fernandez-Argüelles, J. M. Costa-Fernandez, R. Pereiro, A. Sanz-Medel: "Photoactivated luminescent CdSe quantum dots as sensitive cyanide probes in aqueous solutions", *Chem. Commun.* **2005**, 2005, 883-885.
- [554] M. T. Fernandez-Argüelles, W. J. Jin, J. M. Costa-Fernandez, R. Pereiro, A. Sanz-Medel: "Surface-modified CdSe quantum dots for the sensitive and selective determination of Cu(II) in aqueous solutions by luminescent measurements", *Analytica Chimica Acta* **2005**, 549, 20-25.
- [555] E. R. Goldman, I. L. Medintz, J. L. Whitley, A. Hayhurst, A. R. Clapp, H. T. Uyeda, J. R. Deschamps, M. E. Lassman, H. Mattoussi: "A Hybrid Quantum Dot-Antibody Fragment Fluorescence Resonance Energy Transfer-Based TNT Sensor", *Journal of the American Chemical Society* **2005**, 127, 6744-6751.
- [556] J. Guasto, P. Huang, K. Breuer: "Statistical particle tracking velocimetry using molecular and quantum dot tracer particles", *Experiments in Fluids* **2006**, 41(6), 869.
- [557] J. Guasto, K. Breuer: "Simultaneous, ensemble-averaged measurement of near-wall temperature and velocity in steady micro-flows using single quantum dot tracking", *Experiments in Fluids* **2008**, 45(1), 157.
- [558] M. Tomasulo, I. Yildiz, S. L. Kaanumalle, F. M. Raymo: "pH-sensitive ligand for luminescent quantum dots", *Langmuir* **2006**, 22(24), 10284-10290.
- [559] A. Y. Nazzal, L. Qu, X. Peng, M. Xiao: "Photoactivated CdSe Nanocrystals as Nanosensors for Gases", *Nano Letters* **2003**, 3(6), 819-822.
- [560] J. Lee, A. O. Govorov, N. A. Kotov: "Nanoparticle Assemblies with Molecular Springs: A Nanoscale Thermometer", *Angewandte Chemie* **2005**, 117(45), 7605-7608.
- [561] D. L. Klein, R. Roth, A. K. L. Lim, A. P. Alivisatos, P. L. McEuen: "A single-electron transistor made from a cadmium selenide nanocrystal", *Nature* **1997**, 389, 699-701.

- [562] A. J. Nozik: "Quantum dot solar cells", *Physica E* **2002**, *14*, 115-120.
- [563] R. Plass, S. Pelet, J. Krueger, M. Grätzel, U. Bach: "Quantum Dot Sensitization of Organic-Inorganic Hybrid Solar Cells", *Journal of Physical Chemistry B* **2002**, *106*(31), 7578-7580.
- [564] W. U. Huynh, J. J. Dittmer, A. P. Alivisatos: "Hybrid Nanorod-Polymer Solar Cells", *Science* **2002**, *295*(29 March), 2425-2427.
- [565] P. Wang, A. Abrusci, H. M. Wong, M. Svensson, M. R. Andersson, N. C. Greenham: "Photoinduced charge transfer and efficient solar energy conversion in a blend of a red polyfluorene copolymer with CdSe nanoparticles", *Nano Lett* **2006**, *6*(8), 1789-1793.
- [566] V. L. Colvin, M. C. Schlamp, A. P. Alivisatos: "Light-emitting diodes made from cadmium selenide nanocrystals and a semiconducting polymer", *Nature* **1994**, *370*, 354-357.
- [567] B. O. Dabbousi, M. G. Bawendi, O. Onotsuka, M. F. Rubner: "Electroluminescence from CdSe quantum-dot/polymer composites", *Appl. Phys. Lett.* **1995**, *66*, 1316.
- [568] M. C. Schlamp, X. Peng, A. P. Alivisatos: "Improved efficiencies in light emitting diodes made with CdSe(CdS) core/shell type nanocrystals and a semiconducting polymer", *Journal of Applied Physics* **1997**, *82*(11), 5837-5842.
- [569] A. Rizzo, Y. Q. Li, S. Kudera, F. Della Sala, M. Zanella, W. J. Parak, R. Cingolani, L. Manna, G. Gigli: "Blue light emitting diodes based on fluorescent CdSe/ZnS nanocrystals", *Applied Physics Letters* **2007**, *90*(5).
- [570] J. Jasieniak, J. Pacifico, R. Signorini, A. Chiasera, M. Ferrari, A. Martucci, P. Mulvaney: "Luminescence and Amplified Stimulated Emission in CdSe-ZnS-Nanocrystal-Doped TiO₂ and ZrO₂ Waveguides", *Advanced Functional Materials* **2007**, *17*(10), 1654-1662.
- [571] U. Bach, D. Lupo, P. Comte, J. E. Moser, F. Weissortel, J. Salbeck, H. Spreitzer, M. Grätzel: "Solid-state dye-sensitized mesoporous TiO₂ solar cells with high photon-to-electron conversion efficiencies", *Nature* **1998**, *395*(6702), 583-585.
- [572] M. Grätzel: "Photoelectrochemical cells", *Nature* **2001**, *414*(14 November), 338-344.
- [573] H. Zou, S. Wu, J. Shen: "Polymer/Silica Nanocomposites: Preparation, Characterization, Properties, and Applications", *Chem. Rev.* **2008**, *108*(9), 3893-3957.
- [574] G. Schottner: "Hybrid Sol-Gel-Derived Polymers: Applications of Multifunctional Materials", *Chem. Mater.* **2001**, *13*(10), 3422-3435.
- [575] M. Han, X. Gao, J. Z. Su, S. Nie: "Quantum-dot-tagged microbeads for multiplexed optical coding of biomolecules", *Nature Biotechnology* **2001**, *19*(July 2001), 631-635.
- [576] W. Sheng, S. Kim, J. Lee, S. W. Kim, K. Jensen, M. G. Bawendi: "In-Situ Encapsulation of Quantum Dots into Polymer Microspheres", *Langmuir* **2006**, *22*(8), 3782-3790.
- [577] S. Fournier-Bidoz, T. L. Jennings, J. M. Klostranec, W. Fung, A. Rhee, D. Li, W. C. W. Chan: "Facile and Rapid One-Step Mass Preparation of Quantum-Dot Barcodes", *Angewandte Chemie International Edition* **2008**, *47*(30), 5577-5581.
- [578] T. Vossmeier, G. Reck, L. Katsikas, E. T. K. Haupt, B. Schulz, H. Weller: "A "Double-Diamond Superlattice" Built Up of Cd₁₇S₄(SCH₂CH₂OH)₂₆ Clusters", *Science* **1995**, *267*, 1476-.
- [579] A. Gole, C. J. Murphy: "Polyelectrolyte-Coated Gold Nanorods: Synthesis, Characterization and Immobilization", *Chemistry of materials* **2005**, *17*(6), 1325-1330.
- [580] M. Gao, J. Sun, E. Dulkeith, N. Gaponik, U. Lemmer, J. Feldmann: "Lateral Patterning of CdTe Nanocrystal Films by the Electric Field Directed Layer-by-Layer Assembly Method", *Langmuir* **2002**, *18*(10), 4098-4102.
- [581] A. Gole, N. R. Jana, S. T. Selvan, J. Y. Ying: "Langmuir-Blodgett Thin Films of Quantum Dots: Synthesis, Surface Modification, and Fluorescence Resonance Energy Transfer (FRET) Studies", *Langmuir* **2008**, *24*(15), 8181-8186.
- [582] Z. Tang, N. A. Kotov: "One-Dimensional Assemblies of Nanoparticles: Preparation, Properties, and Promise", *Advanced Materials* **2005**, *17*(8), 951-962.
- [583] A. Fu, C. M. Micheel, J. Cha, H. Chang, H. Yang, A. P. Alivisatos: "Discrete Nanostructures of Quantum Dots/Au with DNA", *JACS* **2004**, *126*, 10832-10833.
- [584] J. P. Novak, D. L. Feldheim: "Assembly of Phenylacetylene-Bridged Silver and Gold Nanoparticle Arrays", *JACS* **2000**, *122*, 3979-3980.
- [585] R. Shenhar, T. B. Norsten, V. M. Rotello: "Polymer-Mediated Nanoparticle Assembly: Structural Control and Applications", *Advanced Materials* **2005**, *17*(6), 657-669.
- [586] Y. Ofir, B. Samanta, V. M. Rotello: "Polymer and biopolymer mediated self-assembly of gold nanoparticles", *Chemical Society Reviews* **2008**, *37*(9), 1814-1825.
- [587] D. V. Talpin: "LEGO Materials", *ACS Nano* **2008**, *2*(6), 1097-1100.
- [588] R. Narayanan, M. A. El-Sayed: "Some aspects of colloidal nanoparticle stability, catalytic activity, and recycling potential", *Topics In Catalysis* **2008**, *47*(1-2), 15-21.
- [589] C. Kirchner, T. Liedl, S. Kudera, T. Pellegrino, A. M. Javier, H. E. Gaub, S. Stölzle, N. Fertig, W. J. Parak: "Cytotoxicity of Colloidal CdSe and CdSe/ZnS Nanoparticles", *Nanoletters* **2005**, *5*(2), 331-338.
- [590] A. Shiohara, A. Hoshino, K. Hanaki, K. Suzuki, K. Yamamoto: "On the cyto-toxicity caused by quantum dots", *Microbiology and Immunology* **2004**, *48*(9), 669-675.
- [591] A. M. Derfus, W. C. W. Chan, S. N. Bhatia: "Probing the Cytotoxicity of Semiconductor Quantum Dots", *NanoLetters* **2004**, *4*(1), 11-18.

- [592] M. Tsoli, H. Kuhn, W. Brandau, H. Esche, G. Schmid: "Cellular Uptake and Toxicity of Au₅₅ Clusters", *Small* **2005**, 1(8-9), 841-844.
- [593] D. E. Ferrara, D. Weiss, P. H. Carnell, R. P. Vito, D. Vega, X. Gao, S. Nie, W. R. Taylor: "Quantitative 3D fluorescence technique for the analysis of en face preparations of arterial walls using quantum dot nanocrystals and two-photon excitation laser scanning microscopy", *Am J Physiol Regul Integr Comp Physiol* **2006**, 290(1), R114-123.
- [594] H. A. Lee, M. Imran, N. A. Monteiro-Riviere, V. L. Colvin, W. W. Yu, J. E. Riviere: "Biodistribution of Quantum Dot Nanoparticles in Perfused Skin: Evidence of Coating Dependency and Periodicity in Arterial Extraction", *Nano Lett.* **2007**, 7(9), 2865-2870.
- [595] S. Rieger, R. P. Kulkarni, D. Darcy, S. E. Fraser, R. W. Koster: "Quantum dots are powerful multipurpose vital labeling agents in zebrafish embryos", *Dev Dyn* **2005**, 234(3), 670-681.
- [596] N. Y. Morgan, S. English, W. Chen, V. Chernomordik, A. Russo, P. D. Smith, A. Gandjbakhche: "Real time in vivo non-invasive optical imaging using near-infrared fluorescent quantum dots", *Acad Radiol* **2005**, 12(3), 313-323.
- [597] C. Tortiglione, A. Quarta, A. Tino, L. Manna, R. Cingolani, T. Pellegrino: "Synthesis and biological assay of GSH functionalized fluorescent quantum dots for staining *Hydra vulgaris*", *Bioconjugate Chemistry* **2007**, 18(3), 829-835.
- [598] K. Cho, X. Wang, S. Nie, Z. Chen, D. M. Shin: "Therapeutic Nanoparticles for Drug Delivery in Cancer", *Clin Cancer Res* **2008**, 14(5), 1310-1316.
- [599] H. Liao, C. L. Nehl, J. H. Hafner: "Biomedical applications of plasmon resonant metal nanoparticles", *Nanomed* **2006**, 1(2), 201-208.
- [600] H. C. Fischer, L. C. Liu, K. S. Pang, W. C. W. Chan: "Pharmacokinetics of nanoscale quantum dots: In vivo distribution, sequestration, and clearance in the rat", *Advanced Functional Materials* **2006**, 16(10), 1299-1305.
- [601] H. S. Choi, W. Liu, P. Misra, E. Tanaka, J. P. Zimmer, B. Itty Ipe, M. G. Bawendi, J. V. Frangioni: "Renal clearance of quantum dots", *Nat Biotechnol* **2007**, 25(10), 1165-1170.
- [602] R. Weissleder, D. Stark, B. L. Engelstad, B. R. Bacon, C. C. Compton, D. L. White, P. Jacobs, J. Lewis: "Superparamagnetic iron oxide: Pharmacokinetics and toxicity", *American Journal of Roentgenology* **1989**, 152, 167-173.
- [603] E. I. Altinoğlu, T. J. Russin, J. M. Kaiser, B. M. Barth, B. C. Eklund, M. Kester, J. H. Adair: "Near-Infrared Emitting Fluorophore-Doped Calcium Phosphate Nanoparticles for In Vivo Imaging of Human Breast Cancer", *ACS Nano* **2008**.
- [604] K. Tiede, A. B. A. Boxall, S. P. Tear, J. Lewis, H. David, M. Hasselov: "Detection and characterization of engineered nanoparticles in food and the environment", *Food Additives And Contaminants* **2008**, 25(7), 795-821.

8 Appendix [A1] – [A12]

Publications:

[A1] R. A. Sperling, T. Pellegrino, J. K. Li, W. H. Chang, W. J. Parak: "Electrophoretic separation of nanoparticles with a discrete number of functional groups", *Advanced Functional Materials* **2006**, *16*, 943-948.

[A2] C.-A. J. Lin*, R. A. Sperling*, J. K. Li, T.-Y. Yang, P.-Y. Li, M. Zanella, W. H. Chang, W. J. Parak: "Design of an amphiphilic polymer for nanoparticle coating and functionalization", *SMALL* **2008**, *4*, 334-341.

[A3] R. A. Sperling, T. Liedl, S. Duhr, S. Kudera, M. Zanella, C.-A. J. Lin, W. Chang, D. Braun, W. J. Parak: "Size determination of (bio-) conjugated water-soluble colloidal nanoparticles - a comparison of different techniques", *Journal of Physical Chemistry C* **2007**, *111*, 11552 -11559.

[A4] T. Pellegrino*, R. A. Sperling*, A. P. Alivisatos, W. J. Parak: "Geoelectrophoresis of Gold-DNA Nanoconjugates", *Journal of Biomedicine and Biotechnology* **2007**, *2007*, article ID 26796.

[A5] G.-M. Kim, A. Wutzler, H.-J. Radosch, G. H. Michler, P. Simon, R. A. Sperling, W. J. Parak: "One-Dimensional Arrangement of Gold Nanoparticles by Electrospinning", *Chemistry of Materials* **2005**, *17*, 4949-4957.

[A6] M. T. Fernández-Argüelles, A. Yakovlev, R. A. Sperling, C. Luccardini, S. Gaillard, A. S. Medel, J.-M. Mallet, J.-C. Brochon, A. Feltz, M. Oheim, W. J. Parak: "Synthesis and characterization of polymer-coated quantum dots with integrated acceptor dyes as FRET-based nanoprobess", *NanoLetters* **2007**, *7*, 2613-2617.

[A7] U. I. Tromsdorf, N. C. Bigall, M. Kaul, O. T. Bruns, M. S. Nikolic, B. Mollwitz, R. A. Sperling, R. Reimer, H. Hohenberg, W. J. Parak, S. Förster, U. Beisiegel, G. Adam, H. Weller: "Size and Surface Effects on the MRI Relaxivity of Manganese Ferrite Nanoparticle Contrast Agents ", *Nanoletters* **2007**, *7*, 2422-2427.

[A8] A. Pandey, M. K. Roy, A. Pandey, M. Zanella, R. C. Sperling, W. J. Parak, H. C. Verma: "Chloroform- and water-soluble sol-gel derived $\text{Eu}^{+++}/\text{Y}_2\text{O}_3$ (red) and $\text{Tb}^{+++}/\text{Y}_2\text{O}_3$ (green) nanophosphors: synthesis, characterisation and surface modification ", *Nanotechnology* **2007**, *submitted*.

[A9] C.-A. Lin, R. A. Sperling, M. Zanella, W. Chang, J. Li, T.-Y. Yang, J.-L. Shen, H.-I. Yeh, W. Parak: "Synthesis, Characterization and Bio-conjugation of Fluorescent Gold Nanoclusters toward Biological Labeling Applications", *ACS Nano* **2008**, *submitted*.

[A10] J. Stehr, C. Hrelescu, R. A. Sperling, G. Raschke, M. Wunderlich, A. Nichtl, D. Heindl, K. Kürzinger, W. J. Parak, T. A. Klar, J. Feldmann: "Gold Nano-Stoves for Microsecond DNA Melting Analysis", *Nanoletters* **2008**, *8*, 619-623.

[A11] C.-A. J. Lin, T. Liedl, R. A. Sperling, M. T. Fernández-Argüelles, J. M. Costa-Fernández, R. Pereiro, A. Sanz-Medel, W. H. Chang, W. J. Parak: "Bioanalytics and Biolabeling with Semiconductor Nanoparticles (Quantum Dots)", *Journal of Materials Chemistry* **2007**, *17*, 1343-1346.

[A12] R. A. Sperling, P. R. Gil, F. Zhang, M. Zanella, W. J. Parak: "Biological Applications of Gold Nanoparticles", *Chemical Society Reviews* **2008**, *37*(9), 1896 - 1908.

DOI: 10.1002/adfm.200500589

Electrophoretic Separation of Nanoparticles with a Discrete Number of Functional Groups**

By Ralph A. Sperling, Teresa Pellegrino, Jimmy K. Li, Walter H. Chang, and Wolfgang J. Parak*

A concept is describe that facilitates the modification of colloidal nanoparticles of different materials with an exactly known number of variable functional groups. In particular, a procedure for the surface functionalization of nanoparticles with a controlled number of mono- or bifunctional poly(ethylene glycol) (PEG) molecules of suitable chain length is reported. Conjugates of nanoparticles with one, two, and three PEG molecules per nanoparticle could be separated using gel electrophoresis. Molecules with additional functionalities could be conjugated to the free ends of the bifunctional PEG molecules. In this way the PEG molecules act as convenient spacers that allow for the sorting of nanoparticles with a discrete number of functional groups.

1. Introduction

For many experiments, nanoparticle labels with a discrete and controlled number of attached ligands (or even more general, functional groups) would be very desirable. Depending on material, size, and shape, nanoparticles can exhibit different functional properties, such as fluorescence, optical absorption, or magnetic moments, and can thus be detected using different techniques.^[1–6] Ligand molecules attached to the surfaces of such nanoparticles will specifically bind to their corresponding receptors. Such constructs, e.g., gold or semiconductor nanoparticles decorated with oligonucleotides, streptavidin, or antibodies, have been successfully used in life sciences to trace the position of single proteins within the membranes of living cells,^[7–9] and to visualize the structure of artificially created nanoassemblies.^[10,11] In addition, similar constructs have been used in materials science for the assembly of nanoparticles into

well-defined structures. In pioneering work, the groups of Alivisatos and Mirkin have demonstrated that oligonucleotide-decorated gold nanoparticles can be organized in solution through the high specificity of the hybridization between complementary DNA strands attached to the nanoparticles.^[12,13] Whereas these first DNA-mediated assemblies of gold particles were not very well defined in terms of their size and composition, successive work has demonstrated that, based on these principles, precisely defined DNA-mediated groupings of gold nanoparticles can be formed.^[14–17] The grouping of gold nanoparticles has also been achieved using receptor–ligand pairs other than complementary oligonucleotides, such as the biotin–avidin system.^[18]

One key issue for some of the above-mentioned applications is the ability to control the number of ligand molecules bound to each nanoparticle. By exactly controlling the number of binding sites per nanoparticle, unwanted crosslinking effects between the labels or between the structures to be labeled, which eventually can lead to agglomeration, can be avoided. For the controlled assembly of particle groupings, such defined building blocks are a prerequisite. Apart from some exceptions,^[19–21] so far it has not been possible to directly synthesize such particles. Instead, functional groups have been attached to the particles, after which the particles with the desired number of functional groups have been sorted. For this purpose, gel electrophoresis has been demonstrated to be a powerful technique. The idea of this strategy is simple: If the molecules bound to a particle change their overall effective size (or charge) sufficiently, particles containing different numbers of molecules attached per particle can be separated. Such a protocol has been described for single-stranded DNA linked to Au particles.^[22,23] Au particles can be synthesized in aqueous solution with a weakly attached monolayer of ligands (citric acid or phosphines). Therefore, the size distribution of Au particles is excellent (each additional shell would make the size distribution worse) and DNA can be directly attached to the Au surface via –SH groups. Each attached DNA molecule increases

[*] Prof. W. J. Parak, R. A. Sperling, Dr. T. Pellegrino, Dr. J. K. Li
Center for Nanoscience, Ludwig-Maximilians-Universität München
Amalienstr. 54, 80799 Munich (Germany)
E-mail: Wolfgang.Parak@physik.uni-muenchen.de

Dr. J. K. Li, Prof. W. H. Chang
Center for Nano Bioengineering and R&D Center for
Membrane Technology
Chung-Yuan Christian University
No. 200, Chungbei Rd., Chung Li 32023 (Taiwan)

Dr. T. Pellegrino
INFN-NNL, National Nanotechnology Laboratory
Distretto Tecnologico ISUF1 Via Arnesano, 73100 Lecce (Italy)

[**] This work was supported in part by the Deutsche Forschungsgemeinschaft (DFG, Emmy Noether Grant), and the European Union (SA-NANO STREP project). The CdSe/ZnS particles used in this study were prepared by courtesy of Stefan Kudera. The authors are grateful to Dr. Liberato Manna and Prof. Dr. Hermann Gaub for helpful discussions. Supporting Information is available online from Wiley InterScience or from the author.

the overall size of a DNA/Au-particle conjugate significantly. As a result of this increment in size, Au particles with different numbers of DNA molecules attached per particle can be sorted and extracted using gel electrophoresis.^[22] So far this process has been limited to Au particles and thiolated DNA molecules of at least 30 bases in length, because this length was needed in order to produce a sufficient change in electrophoretic mobility.^[24]

In order to extend this strategy to other types of nanoparticles and molecules, three basic requirements have to be fulfilled: i) The size distribution (or charge distribution) of the plain nanoparticles must be sufficiently narrow in order to result in a sharp band in gel electrophoresis, ii) the ligand molecules have to be attached to the surfaces of the nanoparticles with sufficient stability, and iii) the attachment of each molecule must result in a change in conjugate size (or charge) that is large enough to be resolved by the applied separation technique. Nowadays, the first two of the three presuppositions

are state of the art. High-quality inorganic nanoparticles of many materials with excellent size distributions, which have been synthesized in organic solvents, can be transferred to aqueous solution by embedding them in an amphiphilic polymer shell (see Fig. 1a).^[25,26] This process yields nanoparticles with an excellent size distribution (i.e., the size distribution does not get significantly worse because of the polymer shell) that yield narrow bands in gel electrophoresis. On covalently attaching bifunctional short poly(ethylene glycol) (PEG) molecules to this polymer shell, the particles became very stable in electrolytic solution.^[27] This approach results in stable water-soluble nanoparticles of different materials with identical surface chemistry and many functional groups, e.g., $-\text{NH}_2$ on the free ends of PEG molecules. The covalent linkage of (biological) molecules to the surfaces of such particles has been demonstrated by using crosslinker reagents.^[2,28] PEG molecules on the particles' surfaces simplify bioconjugation of the particles. Nanoparticles are typically stabilized in aqueous solution by

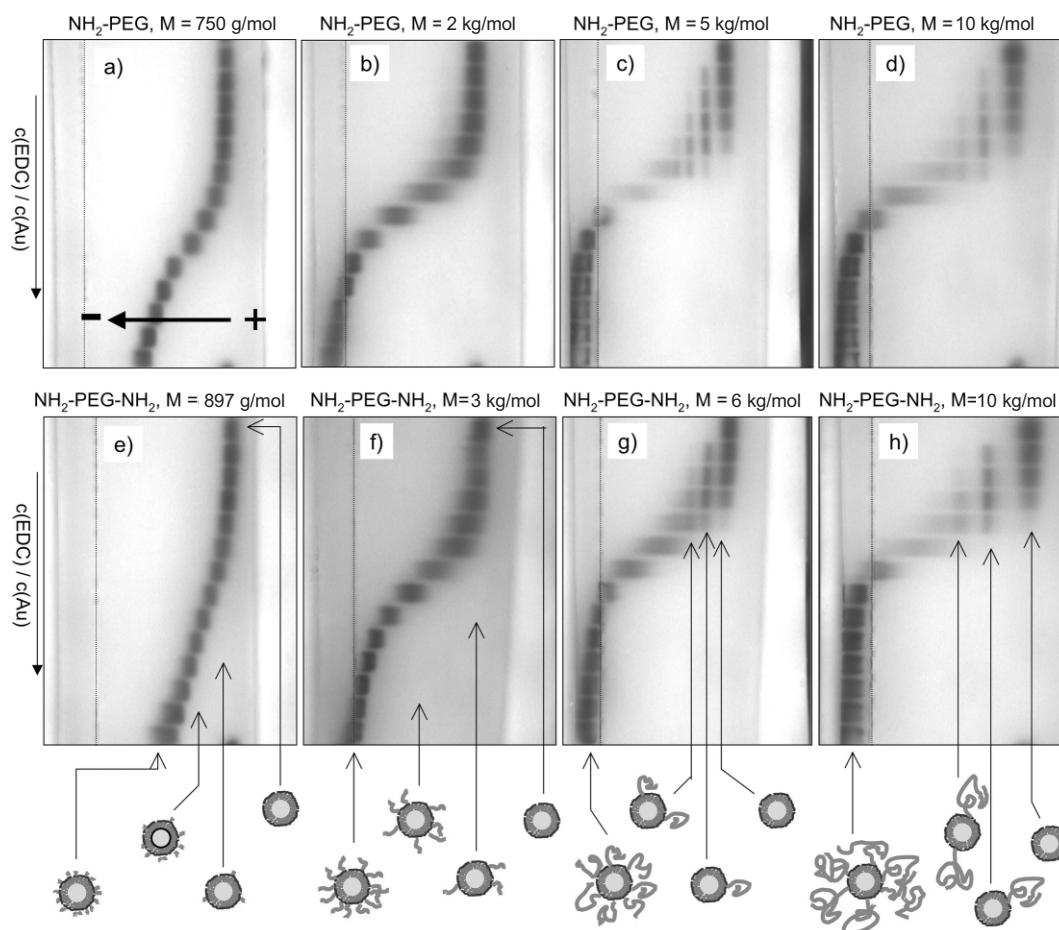


Figure 1. Gel electrophoresis of poly(ethylene glycol) (PEG)/Au conjugates: PEG molecules with one or two $-\text{NH}_2$ groups were covalently attached to polymer-coated 4 nm Au nanocrystals. a) $\text{NH}_2\text{-PEG}$, molecular weight, $M = 750 \text{ g mol}^{-1}$; b) $\text{NH}_2\text{-PEG}$, $M = 2000 \text{ g mol}^{-1}$; c) $\text{NH}_2\text{-PEG}$, $M = 5000 \text{ g mol}^{-1}$; d) $\text{NH}_2\text{-PEG}$, $M = 10000 \text{ g mol}^{-1}$; e) $\text{NH}_2\text{-PEG-NH}_2$, $M = 897 \text{ g mol}^{-1}$; f) $\text{NH}_2\text{-PEG-NH}_2$, $M = 3000 \text{ g mol}^{-1}$; g) $\text{NH}_2\text{-PEG-NH}_2$, $M = 6000 \text{ g mol}^{-1}$; h) $\text{NH}_2\text{-PEG-NH}_2$, $M = 10000 \text{ g mol}^{-1}$. The number of attached PEG molecules per Au particle was adjusted by changing the concentration of 1-ethyl-3-(3-dimethylaminopropyl)carbodiimide hydrochloride ($c(\text{EDC})$), in the following range: $c(\text{EDC})/c(\text{Au particle}) = 0, 31, 63, 125, 250, 500, 1000, 2000, 4000, 8000, 16000, 32000, 64000, 128000$. Gel electrophoresis was performed on 2% agarose gels for 80–90 min; the dashed line marks the positions on the gels where the samples were loaded; the lanes from top to bottom show the samples with decreasing EDC concentration. Because of the increased number of attached PEG molecules with increasing $c(\text{EDC})/c(\text{Au particle})$ ratio, the particles gain size and become more retarded on the gels.

electrostatic repulsion. Since, in addition, many biological molecules are charged, repulsive interactions between the molecule and the particle (for like-charged particles and molecules) or electrostatic adsorption (for oppositely charged particles and molecules) can occur. In order to suppress unwanted repulsive interactions, salt can be added to screen the charge of the particles and molecules. However, this eventually leads to agglomeration of the particles, which do not repel each other with sufficient force anymore. On the other hand, nanoparticles modified with PEG on their surfaces repel each other by steric interaction, and bioconjugation can be performed at high salt concentrations.^[29] In this way, PEG reduces the risk of particle agglomeration and enhances the binding yield.

The third prerequisite is the most complicated to meet. It is not feasible to yield a sufficient change in size (or charge) for separation when only small individual molecules (e.g., biotin or -SH groups) are attached to the nanoparticles. For this reason, it is not practicable to directly isolate nanoparticles with exactly one small molecule (such as biotin) per particle by means of gel electrophoresis (or size-exclusion liquid chromatography), because the shift on the gel would be too small. Therefore, we suggest a two-step process involving a so-called spacer molecule. This spacer molecule must be either big enough in size or sufficiently charged so that attachment of one individual spacer molecule leads to a sufficient change that can be detected by standard separation techniques (for separation by charge or by size, such as gel electrophoresis or size exclusion chromatography). The spacer molecule must have two functional ends. On one end it must be reactive towards the surface of the nanoparticles. The other end (pointing towards solution) is either the desired functional group or must be reactive towards a molecule bearing the functional group. In this work, we demonstrate that PEG with a molecular weight higher than a certain threshold ($\geq 5000 \text{ g mol}^{-1}$) can act as such a spacer molecule.

2. Results

Amino-modified PEG, bearing an amino group on only one end of the PEG chain (in the following called $\text{NH}_2\text{-PEG}$), has been attached to $-\text{COOH}$ groups on the surfaces of polymer-coated Au nanoparticles via standard bioconjugation chemistry using 1-ethyl-3-(3-dimethylaminopropyl)carbodiimide hydrochloride (EDC)^[30] (all experimental methods can be found in detail in the Supporting Information). The more $\text{NH}_2\text{-PEG}$ molecules bound per Au particle, the bigger the resulting conjugate. This can be easily observed using gel electrophoresis: Negatively charged polymer-coated Au particles migrate towards the positive pole; they become more retarded the larger the number of $\text{NH}_2\text{-PEG}$ molecules attached (see Figs. 1a and b, and see also Supporting Information). If $\text{NH}_2\text{-PEG}$ with a molecular weight $\geq 5000 \text{ g mol}^{-1}$ is used, discrete bands can be observed (see Figs. 1c and d). In analogy to DNA/Au-particle conjugates,^[22] we ascribe these bands to Au particles with zero, exactly one, exactly two, etc. $\text{NH}_2\text{-PEG}$ molecules attached per particle. To test this assumption, we performed the same

control experiments as have been used in the case of DNA/Au-particle conjugates,^[22] as will be described below. In order to introduce functional groups as anchor points for further attachment of biological molecules, PEG molecules with two modified ends were used. PEG molecules modified with amino groups at both ends (in the following called $\text{NH}_2\text{-PEG-NH}_2$) were covalently attached to the surfaces of polymer-coated Au nanoparticles using EDC, as described above. An appropriate choice of the relative concentrations prevented interparticle crosslinking. This was confirmed by comparing the migration of Au particles modified under the same conditions with $\text{NH}_2\text{-PEG}$ and $\text{NH}_2\text{-PEG-NH}_2$ using gel electrophoresis (Figs. 1e-h, see also Supporting Information). Particles modified with $\text{NH}_2\text{-PEG-NH}_2$ exhibit free amino groups on their surfaces, so that molecules bearing an *N*-hydroxysuccinimide ester (NHS) functionality can be directly attached via the formation of an amide bond.^[30] We demonstrated this for the case of NHS-PEG-biotin, which resulted in biotin-modified particles.

3. Discussion

In the following, the key experiments are described in more detail.

3.1. Length Dependence

For short $\text{NH}_2\text{-PEG}$ molecules (molecular weight $< 5000 \text{ g mol}^{-1}$) the change in size of a particle due to the addition of one single PEG molecule is too small to be detected with gel electrophoresis. If more PEG is attached per particle, the sizes of the conjugates get continuously bigger and the bands on the gel are more retarded. At one point, the particle surface is saturated with PEG, and the retardation of the particles in the gels remains constant (Fig. 1a). The higher the molecular weight of the PEG, the bigger the maximum retardation of the conjugates (Figs. 1a-d, see also Supporting Information). Because of steric hindrance, the maximum number of PEG molecules that can be attached per particle will decrease with increasing length of the PEG molecule. At molecular weights $\geq 5000 \text{ g mol}^{-1}$, the change upon binding one PEG molecule to the particle surface yields a size change big enough to be detected as a discrete band on the gel (Figs. 1c and d). The higher the molecular weight of the PEG, the bigger the retardation in the gel upon the addition of one single PEG molecule (Figs. 1c and d, see also Supporting Information). We have strong experimental evidence that, similar to DNA/Au-particle conjugates, the main cause of retardation of the bands in the gel upon binding PEG to Au particles is the change in the overall size of the particles: Upon attachment of each $\text{NH}_2\text{-PEG}$ molecule via bond formation between the $-\text{NH}_2$ group of the PEG and a $-\text{COOH}$ group on the particle surface, one negative charge on the particle surface (which originated from the $-\text{COOH}$ group) is lost. This effect does not depend on the length of the PEG molecule. However, since retardation in the

gel was found to increase with the length of the PEG molecules, this retardation cannot be predominantly ascribed to the loss of negative charge, because this effect does not depend on the length of the PEG molecule. In the case of saturation of particles with short-chain PEG (i.e., in the situation when the maximum amount of PEG is attached per particle) the conjugates migrate towards the positive pole, which indicates that, even in the case of saturation, PEG molecules were only attached to a fraction of the $-\text{COOH}$ groups on the particle surfaces. Upon saturation with long-chain PEG, the retardation of the conjugates even leads to a change in the direction of migration (Figs. 1b–d). We speculate that this effect might be associated with the complexation of positively charged ions with the neutral PEG.^[31]

3.2. Introduction of Discrete Functional Groups

$\text{NH}_2\text{-PEG-NH}_2$ molecules of varying molecular weight were attached using EDC to the polymer surfaces of Au particles, as described above for $\text{NH}_2\text{-PEG}$. Gel-electrophoresis experiments demonstrated that Au particles conjugated to $\text{NH}_2\text{-PEG-NH}_2$ and $\text{NH}_2\text{-PEG}$ yield bands with comparable retardation in the gel (Figs. 1e–h, see also Supporting Information). This means that interparticle crosslinking, which would only be possible in the case of $\text{NH}_2\text{-PEG-NH}_2$ if one PEG molecule binds with both NH_2 groups to two different particles, can be neglected. In the case of interparticle crosslinking, the bands for the Au particles conjugated to $\text{NH}_2\text{-PEG-NH}_2$ should be more retarded than for Au particles conjugated to $\text{NH}_2\text{-PEG}$. For both $\text{NH}_2\text{-PEG}$ and $\text{NH}_2\text{-PEG-NH}_2$ with a molecular weight $\geq 5000 \text{ g mol}^{-1}$, discrete bands could be observed under gel electrophoresis (Figs. 1g and h). Since the bands can be ascribed to Au particles with zero, exactly one, exactly two, etc. PEG molecules per Au particle, these conjugates are, in fact, conjugates with a precisely controlled number of reactive groups on their surfaces. Whereas the polymer surfaces of the Au particles comprise only accessible $-\text{COOH}$ groups, each attached $\text{NH}_2\text{-PEG-NH}_2$ bears one free $-\text{NH}_2$ group at its end that points away from the particle. In this way, conjugates with exactly one, two, etc. $-\text{NH}_2$ groups per particle can be obtained.

3.3. Stability of the Conjugates

As mentioned above, the retardation of the conjugates that we ascribe to Au particles with one and two bound PEG molecules increases with the length of the PEG molecule. The formation of non-specifically formed Au-particle clusters, on the other hand, should not depend on the length of the PEG molecule. This fact strongly indicates that the discrete retarded bands cannot be ascribed to non-specifically formed dimers and trimers of Au particles. As a further control, we extracted the particles within the discrete bands from the gel and performed electrophoresis on the purified and re-concentrated sample again in a second gel (Fig. 2, see also Supporting Infor-

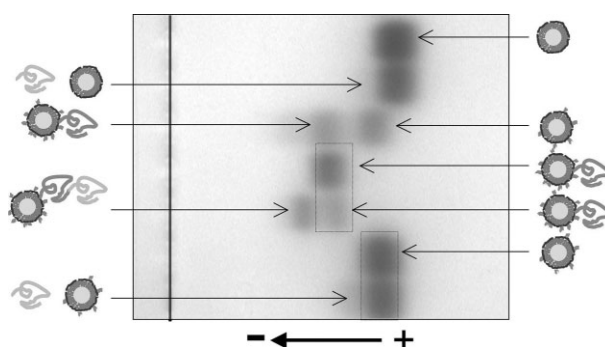


Figure 2. Polymer-coated Au nanoparticles were reacted with a 1:20 mixture of $\text{NH}_2\text{-PEG-NH}_2$ ($M=10\,000 \text{ g mol}^{-1}$) and $\text{NH}_2\text{-PEG}$ ($M=750 \text{ g mol}^{-1}$) and EDC. After the extraction and purification of particles with exactly 0 and 1 $\text{NH}_2\text{-PEG-NH}_2$ molecules, the particles were reacted with biotin-PEG-NHS ($M=5000 \text{ g mol}^{-1}$) to demonstrate the reactivity of a single free $-\text{NH}_2$ group and its conversion to biotin. Lane 1 (top lane): polymer-coated Au particles; lane 2: polymer-coated Au particles with biotin-PEG-NHS; lane 3: Au particles with covalently attached short $\text{NH}_2\text{-PEG}$ and long $\text{NH}_2\text{-PEG-NH}_2$ molecules; lane 4: extracted second band (from lane 3) with exactly one free amino group; lane 5: particles with exactly one free amino group (from lane 4), reacted with biotin-PEG-NHS; lane 6: extracted first band (from lane 3) with no free amino group; lane 7 (bottom lane): particles from lane 6 with biotin-PEG-NHS. The samples were run for 60 min at 100 V on a 2% agarose gel. The slight retardation of the first bands (without attached $\text{NH}_2\text{-PEG-NH}_2$) in lanes 3, 6 and 7 in comparison to the plain polymer-coated particles is due to some attached short $\text{NH}_2\text{-PEG}$ molecules, while the appearance of discrete bands indicates the attachment of a defined number of long $\text{NH}_2\text{-PEG-NH}_2$ molecules.

mation). Most of the extracted conjugates were found to migrate with the same speed as the original ones. Only a very weak band in the gel was found at the position of Au particles without PEG. This indicates that the conjugates are stable upon extraction from the gel, purification, and re-concentration, and that the PEG is removed from the particles for only a minor fraction of the conjugates.

3.4. Reactivity of the Discrete Functional Groups

As described above, conjugates of Au particles with exactly one, two, etc. $-\text{NH}_2$ groups per particle were synthesized. Using standard bioconjugation chemistry, it should be possible to convert the $-\text{NH}_2$ groups to other functional groups or to attach biomolecules. This possibility has been demonstrated for biotin using NHS-modified biotin as the biomolecule. Every biotin bearing an NHS group should be reactive towards the discrete $-\text{NH}_2$ groups of the conjugates. NHS-PEG-biotin (5000 g mol^{-1}) was added to Au particles with zero or exactly one $-\text{NH}_2$ group per particle. As can be seen in Figure 2, addition of NHS-PEG-biotin to Au particles with no NH_2 group did not result in any shift in the gel and, thus, it can be deduced that non-specific adsorption of PEG onto the particles does not play a major role (Fig. 2, lanes 2 and 7). In the case of Au particles with exactly one NH_2 group per particle, the addition of NHS-PEG-biotin resulted in the formation of a second, more-retarded band in the gel (Fig. 2, lane 5, see also Support-

ing Information). This indicates that part of the Au particles have reacted with the PEG, which in turn increased the size of the conjugates and, thus, reduced the mobility in the gel. This second band now corresponds to Au particles with exactly one biotin group per particle. However, in addition to the second retarded band, a band remains that has the same mobility as the original particles with one NH_2 -PEG molecule per particle. This means that the yield of the conversion of the $-\text{NH}_2$ group to biotin is not optimum. It must be pointed out that this relates to a fundamental problem. Particles with a precisely controlled number of functional groups have been synthesized, but it is not known how many of these functional groups are accessible for reactions. In the case of DNA, it is known that DNA molecules can wrap around particles in a non-specific way.^[24,32] In a similar manner, it seems very plausible that some of the PEG molecules have adopted a configuration that hinders the access of potential reaction partners to the reactive groups on their ends.

4. Conclusions

In previous work, it was demonstrated that by embedding particles in a polymer shell particles of different materials (such as fluorescent or magnetic ones) that have identical surfaces can be synthesized.^[26] For this reason, the concept of the attachment of individual molecules per particle is not restricted to one type of particle, but should be applicable to particles of most materials. To demonstrate this generalization, polymer-coated fluorescent CdSe/ZnS nanoparticles have been conjugated with individual NH_2 -PEG molecules using the same protocols that have been applied for Au nanoparticles. As can be seen in Figure 3 (see also Supporting Information), conjugates of PEG with Au and CdSe/ZnS particles show the same behavior upon gel electrophoresis, which demonstrates that the conjugation reaction does not depend on the properties of the inorganic nanoparticle inside the polymer shell. As a next step, we tried to demonstrate that this concept should work also for different functional groups, X. By conjugating polymer-coated Au particles with NH_2 -PEG-X molecules for which the PEG was of sufficient length (molecular weight of the PEG $\geq 5000 \text{ g mol}^{-1}$) and running the conjugates on a gel, discrete bands corresponding to particles with exactly zero, one, two, etc. functional groups per particle could be obtained. This has been demonstrated for the case of $\text{X}=\text{NH}_2$ and for the case without X (see Figs. 1g and h, and Figs. 1c and d, respectively). Alternatively, by conjugating polymer-coated Au particles with NH_2 -PEG- NH_2 molecules made from PEG of sufficient length (molecular weight of the PEG $\geq 5000 \text{ g mol}^{-1}$), running the conjugates in a gel, and extracting the discrete bands from the gel, conjugates corresponding to particles with exactly zero, one, two, etc. $-\text{NH}_2$ groups per particle were obtained. In a subsequent step, the discrete $-\text{NH}_2$ groups could be converted to functional groups by reacting them with NHS-X . We have demonstrated this for the case of $\text{X}=\text{PEG-biotin}$ (see Fig. 2).

The trick of the concept described here for the synthesis of particles with a controlled number of functional groups per

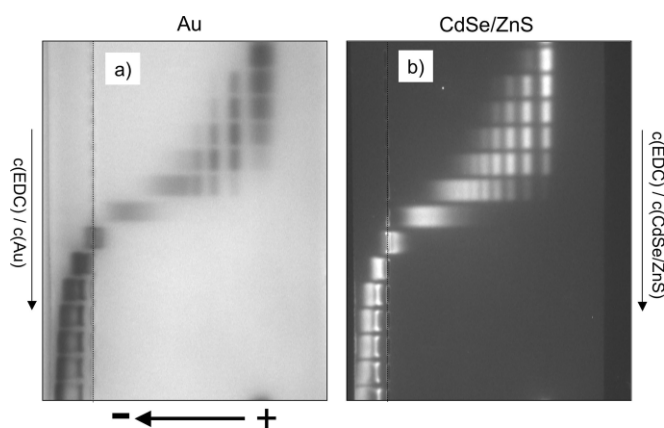


Figure 3. Gel electrophoresis of PEG/Au and PEG/CdSe/ZnS conjugates. Amino-modified PEG molecules (NH_2 -PEG, $M=5000 \text{ g mol}^{-1}$) were added to a) polymer-coated Au nanoparticles (diameter ca. 4 nm, identical to Fig. 1c) and b) CdSe/ZnS nanoparticles (diameter of the CdSe/ZnS core/shell particles: ca. 7 nm) and the number of attached PEG molecules per particle was adjusted by using different concentrations of EDC: $c(\text{EDC})/c(\text{Au-particle})$ and $c(\text{EDC})/c(\text{CdSe/ZnS-particle})=0, 31, 63, 125, 250, 500, 1000, 2000, 4000, 8000, 16\,000, 32\,000, 64\,000, 128\,000$. The lanes in the gel correspond to samples with decreasing EDC concentrations from top to bottom. By comparing Figures 3a and b, it can be seen that the position of the bands on the gel does not depend on the nature of the inorganic nanoparticle material that is embedded in the polymer shell.

particle is the division of “separation” and “functionalization”. Either the spacer molecule (as shown here for PEG of sufficient length) is first modified on one of its ends with the desired functional group X, then attached via its other end to the nanoparticle, and the different conjugates are sorted, e.g., by electrophoresis, or, the spacer molecule is first attached on one side to the nanoparticle, the different conjugates are sorted, e.g., by electrophoresis, and the free end of the spacer is afterwards converted to the desired functional group. By successive application of the sorting process it should also be possible to synthesize heterofunctional particles with a controlled number of two different functional groups.

The next consequent step will be the formation of precisely controlled particle groupings of mixed species, e.g., the formation of dimers comprising a fluorescent CdSe/ZnS particle with exactly one functional group, X, and a magnetic CoPt_3 particle with exactly one functional group, Y, which is reactive towards X. As already mentioned above, this step is not straightforward because, first, the accessibility of the functional groups on the particles' surfaces has to be improved. We believe that the concept described here is an important step towards the construction of advanced building blocks on the nanoscale.

5. Experimental

Colloidal nanocrystals were synthesized, coated with polymer [26], and purified by high-performance liquid chromatography (Agilent 1100 with a self-packed internal diameter $16 \text{ mm} \times 70 \text{ cm}$ Sephacryl S-300 HR column, the mobile phase was 150 mM NaCl in $50 \text{ mM sodium borate pH 9.0}$).

For all experiments, stock solutions of 6.0 μM polymer-coated nanoparticles (NPs) in 50 mM sodium borate buffer (pH 9.0) were prepared. The same buffer was used to dissolve the methoxy-PEG-amine (NH_2 -PEG) and diamine-PEG (NH_2 -PEG- NH_2) reagents, and EDC (1-ethyl-3-(3-dimethylaminopropyl)carbodiimide hydrochloride, Sigma Aldrich).

For the coupling experiments shown in Figures 1 and 3, equal amounts of the 6 μM nanoparticle solution and the 3 mM PEG solution were mixed and split into 20 μL samples. To these, 10 μL of an EDC solution of appropriate concentration was added to achieve ratios of EDC molecules to particles, $c(\text{EDC})/c(\text{NP})$, of 128 000, 64 000, 32 000, ... 31. The ratio of PEG molecules to particles was kept constant for all samples at $c(\text{PEG})/c(\text{NP})=500$. The large excess of PEG molecules was chosen to prevent interparticle crosslinking in the case of NH_2 -PEG- NH_2 . The samples were mixed with a pipette and allowed to react for at least 90 min.

Prior to gel electrophoresis, about 6 μL of gel-loading buffer containing Orange G and 30 % glycerol was added to each sample. 2 % agarose gels were prepared with 0.5 \times TBE buffer and run for 60–90 min at 10 V cm^{-1} .

For the preparation of a larger amount of nanoparticles with a few functional groups, a 20:1 mixture of 3 mM methoxy-PEG-amine (molecular weight, $M=750 \text{ g mol}^{-1}$, Sigma Aldrich) and 3 mM diamine-PEG ($M=10000 \text{ g mol}^{-1}$, Rapp Polymere) was prepared in 50 mM sodium borate buffer (pH 9.0).

1 mL of this mixture was added to 1 mL of polymer-coated 4 nm Au nanoparticles and reacted with 1 mL of an EDC solution to yield $c(\text{EDC})/c(\text{NP})=1000$. After reaction the sample was concentrated and run on a 2 % agarose gel for 90 min in order to separate nanoparticles with a defined number of functional groups. The mixture of a long monoamine-PEG and a short diamine-PEG was chosen to increase the stability of the particles during the several concentration and purification steps. Because of the attachment of short NH_2 -PEG molecules, all reacted particles showed a slight retardation compared to the plain polymer-coated particles, while the discrete bands were caused by a significant shift resulting from the attachment of long NH_2 -PEG- NH_2 .

The bands consisting of nanoparticles with exactly 0, 1, or 2 attached diamine molecules (and thus exactly 0, 1, or 2 free amino groups) were cut out and immersed separately in 0.5 \times TBE buffer over night. The buffer containing the extracted nanoparticles was replaced, and on the next day the separately pooled samples were concentrated by ultrafiltration. The buffer was replaced by 50 mM sodium borate buffer of pH 9 on a NAP25 gel column and the concentration was adjusted to 6 μM .

In order to investigate the reactivity of the free functional amino groups, 10 μL of the extracted particles with one free amino group (from band 1) were reacted with 10 μL of 6 mM solution of biotin-PEG-NHS ($M=5000 \text{ g mol}^{-1}$, Nektar) in 50 mM sodium borate buffer (pH 9.0). As control experiments, the same experiment was carried out with particles from band 0 and with plain polymer-coated particles. The gel with the corresponding samples is shown in Figure 2.

Received: September 1, 2005

Final version: December 12, 2005

Published online: April 12, 2006

- [1] X. Gao, W. C. W. Chan, S. Nie, *J. Biomed. Opt.* **2002**, *7*, 532.
 [2] X. Michalet, F. F. Pinaud, L. A. Bentolila, J. M. Tsay, S. Doose, J. J. Li, G. Sundaresan, A. M. Wu, S. S. Gambhir, S. Weiss, *Science* **2005**, *307*, 538.

- [3] J. K. Jaiswal, S. M. Simon, *Trends Cell Biol.* **2004**, *14*, 497.
 [4] J. Roth, *Histochem. Cell Biol.* **1996**, *106*, 1.
 [5] J. J. Storhoff, R. Elghanian, R. C. Mucic, C. A. Mirkin, R. L. Letsinger, *J. Am. Chem. Soc.* **1998**, *120*, 1959.
 [6] Q. A. Pankhurst, J. Connolly, S. K. Jones, J. Dobson, *J. Phys. D* **2003**, *36*, R167.
 [7] M. Dahan, S. Levi, C. Luccardini, P. Rostaing, B. Riveau, A. Triller, *Science* **2003**, *302*, 442.
 [8] F. Pinaud, D. King, H.-P. Moore, S. Weiss, *J. Am. Chem. Soc.* **2004**, *126*, 6115.
 [9] L. Cognet, C. Tardin, D. Boyer, D. Choquet, P. Tamarat, B. Lounis, *Proc. Natl. Acad. Sci. USA* **2003**, *100*, 11 350.
 [10] S. Xiao, F. Liu, A. E. Rosen, J. F. Hainfeld, N. C. Seeman, K. Musier-Forsyth, R. A. Kiel, *J. Nanopart. Res.* **2002**, *4*, 313.
 [11] S. Beyer, P. Nickels, F. C. Simmel, *Nano Lett.* **2005**, *5*, 719.
 [12] C. A. Mirkin, R. L. Letsinger, R. C. Mucic, J. J. Storhoff, *Nature* **1996**, *382*, 607.
 [13] A. P. Alivisatos, K. P. Johnsson, X. Peng, T. E. Wilson, C. J. Loweth, M. P. Bruchez, P. G. Schultz, *Nature* **1996**, *382*, 609.
 [14] C. J. Loweth, W. B. Caldwell, X. G. Peng, A. P. Alivisatos, P. G. Schultz, *Angew. Chem. Int. Ed.* **1999**, *38*, 1808.
 [15] D. Zanchet, C. M. Micheel, W. J. Parak, D. Gerion, S. C. Williams, A. P. Alivisatos, *J. Phys. Chem. B* **2002**, *106*, 11 758.
 [16] A. Fu, C. M. Micheel, J. Cha, H. Chang, H. Yang, A. P. Alivisatos, *J. Am. Chem. Soc.* **2004**, *126*, 10 832.
 [17] S. A. Claridge, S. L. Goh, J. M. J. Fréchet, S. C. Williams, C. M. Micheel, A. P. Alivisatos, *Chem. Mater.* **2005**, *17*, 1628.
 [18] K. K. Caswell, J. N. Wilson, U. H. F. Bunz, C. J. Murphy, *J. Am. Chem. Soc.* **2003**, *125*, 13 914.
 [19] J. G. Worden, A. W. Shaffer, Q. Huo, *Chem. Commun.* **2004**, 518.
 [20] K. M. Sung, D. W. Mosley, B. R. Peelle, S. G. Zhang, J. M. Jacobson, *J. Am. Chem. Soc.* **2004**, *126*, 5064.
 [21] A. W. Shaffer, J. G. Huo, *Langmuir* **2004**, *20*, 8343.
 [22] D. Zanchet, C. M. Micheel, W. J. Parak, D. Gerion, A. P. Alivisatos, *Nano Lett.* **2001**, *1*, 32.
 [23] S. D. Jhaveri, E. E. Foos, D. A. Lowy, E. L. Chang, A. W. Snow, M. G. Ancona, *Nano Lett.* **2004**, *4*, 737.
 [24] W. J. Parak, T. Pellegrino, C. M. Micheel, D. Gerion, S. C. Williams, A. P. Alivisatos, *Nano Lett.* **2003**, *3*, 33.
 [25] M. X. Wu, H. Liu, J. Liu, K. N. Haley, J. A. Treadway, J. P. Larson, N. Ge, F. Peale, M. P. Bruchez, *Nat. Biotechnol.* **2003**, *21*, 452.
 [26] T. Pellegrino, L. Manna, S. Kudera, T. Liedl, D. Koktysh, A. L. Rogach, S. Keller, J. Rädler, G. Natile, W. J. Parak, *Nano Lett.* **2004**, *4*, 703.
 [27] B. Ballou, B. C. Lagerholm, L. A. Ernst, M. P. Bruchez, A. S. Waggoner, *Bioconjugate Chem.* **2004**, *15*, 79.
 [28] W. J. Parak, T. Pellegrino, C. Plank, *Nanotechnology* **2005**, *16*, R5.
 [29] W. J. Parak, D. Gerion, D. Zanchet, A. S. Woerz, T. Pellegrino, C. Micheel, S. C. Williams, M. Seitz, R. E. Bruehl, Z. Bryant, C. Bustamante, C. R. Bertozzi, A. P. Alivisatos, *Chem. Mater.* **2002**, *14*, 2113.
 [30] G. T. Hermanson, *Bioconjugate Techniques*, Academic Press, San Diego, CA **1996**.
 [31] R. Sartori, L. Sepulveda, F. Quina, E. Lissi, E. Abuin, *Macromolecules* **1990**, *23*, 3878.
 [32] S. Park, K. A. Brown, K. Hamad-Schifferli, *Nano Lett.* **2004**, *4*, 1925.

DOI: 10.1002/sml.200700654

Design of an Amphiphilic Polymer for Nanoparticle Coating and Functionalization***Cheng-An J. Lin, Ralph A. Sperling, Jimmy K. Li, Ting-Ya Yang, Pei-Yun Li, Marco Zanella, Walter H. Chang, and Wolfgang J. Parak**

Inorganic colloidal nanoparticles, such as quantum dots or Au nanoparticles, have been extensively investigated for two decades in physics as well as in chemistry. Applications in a variety of fields such as optics, electronics, and biology are envisaged and important proof of concept studies have been reported. In particular, with regard to biologically motivated applications, colloidal stability is a key requirement. Apart from nanoparticles stabilized with small ligand molecules,^[1–5] lipids,^[6–8] and surface silanization,^[9–13] amphiphilic polymers have been also used by several groups to disperse originally hydrophobic nanoparticles in aqueous solution.^[14–24] This class of amphiphilic particle coatings not only enables the phase transfer of the nanoparticles from or

organic solvents to aqueous solution, but also serves as a versatile platform for chemical modification and bioconjugation of the particles because biological molecules can be covalently linked to the polymer surface.^[14,23,25] Because the stability of the amphiphilic coating around the nanoparticle solely depends on the hydrophobic interaction, this procedure is very general and does, for example, not depend on the material of the inorganic nanoparticle core, as it is the case for ligand exchange protocols. Because of the numerous contact points mediated by hydrophobic interaction, the attachment of the polymer to the particle surface is highly stable and can be improved further by crosslinking of the polymer shell.^[5,15,19] Nowadays quantum dots coated with amphiphilic polymers and with various biological molecules attached to their surface are commercially available (e.g., Invitrogen).

The amphiphilic polymers that have been used so far for coating hydrophobic inorganic nanoparticles consist of hydrophobic side chains for the linkage to the nanoparticle surface and a hydrophilic backbone that provides water solubility through charged groups (in general COO^-) and also acts as an anchor for the attachment of biological molecules with bioconjugate chemistry. In this report, we introduce an amphiphilic polymer which involves a third kind of building block: functional organic molecules. The functional organic molecules are linked to the hydrophobic side chains in a similar way as the hydrophilic backbone and provide additional functionality in the particle surface (Figure 1).

The amphiphilic polymer described here is based on a poly(maleic anhydride) backbone. Reaction of a fraction of the anhydride rings with alkylamines leads to the formation of the hydrophobic side chains that are needed for intercalation with the hydrophobic surfactant layer on the nanoparticle surface. Another fraction of the anhydride rings is used to link functional organic molecules to the backbone. Like the alkylamines, organic molecules bearing amino groups can be directly linked to the anhydride rings by reaction of the anhydride with the amino group.^[26] In this way alkyl amines and organic molecules with amino terminations can be linked to the polymer backbone in a one pot reaction. The resulting amphiphilic polymer is then wrapped around hydrophobic capped nanoparticles and the organic solvent is replaced by aqueous solution according to our previously published procedure.^[15] By linking some of the remaining anhydride rings with diamine linkers, the polymer molecules around each nanoparticle are interconnected and, thus, the shell is crosslinked. Upon phase transfer to aqueous solution, the remaining anhydride rings open to yield negatively charged carboxyl groups, which provide electrostatic repulsion resulting in a stable dispersion of the nanoparticles. Apart from negatively charged carboxyl groups, the polymer surface of the nanoparticles also contains embedded functional organic molecules.

The strategy reported here has several advantageous features: 1) The maleic anhydride moieties react spontaneously with high yield with both amino modified hydrophobic side chains (such as alkylamines) and functional organic molecules with amino terminal groups. 2) No additional reagents are needed for the coupling. In comparison,

[*] R. A. Sperling,* M. Zanella, Prof. W. J. Parak
Fachbereich Physik, Philipps Universität Marburg
Renthof 7, 35037 Marburg (Germany)
E mail: Wolfgang.Parak@physik.uni-marburg.de

C. A. J. Lin,* R. A. Sperling,* P. Y. Li, M. Zanella, Prof. W. J. Parak
Center for NanoScience
Ludwig Maximilians Universität München
Munich (Germany)

C. A. J. Lin,* T. Y. Yang, W. H. Chang
Department of Biomedical Engineering
Chung Yuan Christian University
Taiwan (ROC)

C. A. J. Lin,* J. K. Li,# W. H. Chang
R&D Center for Membrane Technology
Center for Nano Bioengineering
Chung Yuan Christian University
Taiwan (ROC)

[†] These authors contributed equally to this work.

[#] Present address: Institute of Biotechnology, National Cheng Kung University, Taiwan (ROC)

[**] The authors are grateful to the DAAD NSC sandwich program for facilitating this project. The German and Taiwanese partners were funded by the German research foundation (DFG Emmy Noether fellowship) and the European Union (SA Nano grant), and by the National Nanotechnology Program (NSC) and the Center of Excellence (MOE) of Taiwan, respectively. Marco Zanella acknowledges a fellowship from the ITKD graduate school at the Center for Nanoscience in Munich. We are very grateful to Prof. Dr. Warren Chan for many important ideas and valuable technical discussions. We are also grateful to Maria Teresa Fernandez and to Dr. Feng Zhang for experimental support and technical discussions at different stages of the project and to Dr. Maria Casula for help in the synthesis of iron oxide nanoparticles.



Supporting Information is available on the WWW under <http://www.smalljournal.com> or from the author.

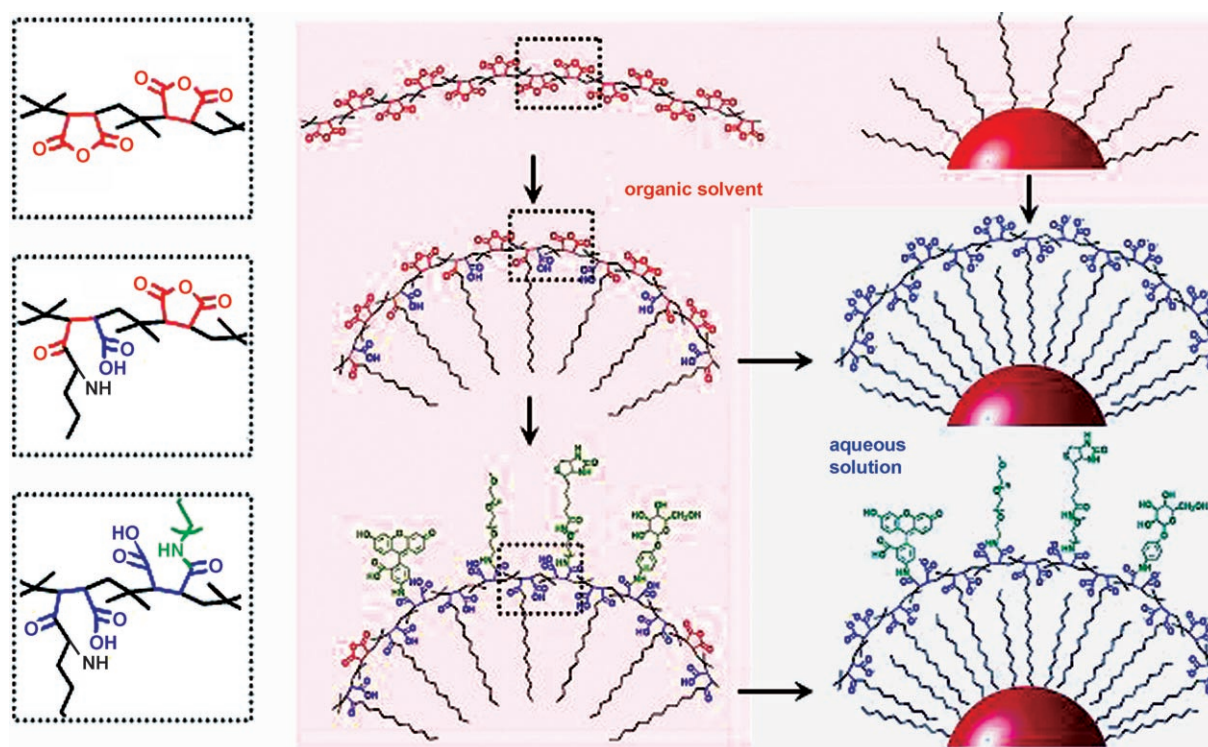


Figure 1. Scheme of the synthesis of the amphiphilic polymer and the coating of nanoparticles. In the center column the synthesis of the amphiphilic polymer is shown. To the polymer backbone, poly(isobutylene *alt* maleic anhydride) (top line), alkylamine chains are linked by the direct amidation between maleic anhydride and the amino ligand (middle line). In an additional step, functional groups (drawn in green) with an amino terminal group are also linked to the polymer (bottom line). In the left column the amide linkage between the amino ligands and the anhydride rings is shown in detail. Nanoparticles with hydrophobic capping (right column, top line) are coated with the amphiphilic polymer by hydrophobic interaction between the alkyl chains of the polymer and the surfactant molecules on the nanoparticles (middle line). This works in the same way for polymers with (bottom) and without (middle) embedded functional molecules. Water solubility is provided by opening the anhydride rings (drawn in red) for carboxylic groups (drawn in blue) which introduces negative charge to the particle surface and leads to electrostatic repulsion between the particles.

crosslinkers such as EDC (1 ethyl 3 (3 dimethylamino propyl) carbodiimide) have to be used in traditional approaches for adding functionality to the particle surface.^[25] 3) While EDC mediated coupling of functional molecules to the polymer shell involves a post modification of already polymer coated nanoparticles in aqueous solution, the present protocol is based on coupling functional molecules in organic solvent to the polymer before the actual embedding of the particles in the polymer shell. In this way, functional molecules which are not soluble in aqueous solution, can be introduced to the particle surface as the coupling is performed in organic solvents. 4) By variation of the amount and type of the hydrophobic side chains, as well as of the functional organic molecules within the amphiphilic polymer, tailored nanoparticle surfaces can be obtained with one universal method.

The commercially available backbone, poly(isobutylene *alt* maleic anhydride), is an alternating copolymer consisting of maleic anhydride rings connected by butylene residues (Figure 1). Hereafter, one anhydride ring with butylene is referred to as a monomer unit. Maleic anhydride moieties react spontaneously with amines, resulting in an amide bond and one free carboxylic group. As a first step, alkylamines are added to the backbone in hot tetrahydrofuran (THF),

resulting in a transparent polymer solution when more than 50% of the maleic anhydride monomers are reacted with an alkylamine. Usually, 75% of the maleic anhydride monomers of the backbone were modified with dodecylamine, leaving 25% of the anhydride rings intact. Part of the remaining anhydride rings were used in a second step for linking additional functional molecules (Figure 1) to the polymer. In practice, a large variety of different functional molecules can be used, as long as they have an amino terminal and are soluble in an organic solvent that is miscible with THF or chloroform. In this study, four different types of functional molecules were chosen to demonstrate the concept: methoxy PEG amine, biotin PEG amine, aminophenyl galactopyranoside, and fluorescein amine. All reactions were carried out as one pot syntheses in water free solvents (THF or CHCl_3) to prevent hydrolysis of the anhydride groups. Because of the quantitative reaction of the amines with the maleic anhydride monomers, the resulting amphiphilic polymer could be used directly, without purification from byproducts or unreacted species.

The resulting amphiphilic polymer showed excellent performance for the phase transfer of hydrophobic nanoparticles to aqueous solution. The coating process was independent of the core material, as demonstrated for Au,^[27] CdSe/

ZnS,^[28] and Fe₃O₄^[29] nanoparticles (Figure 2). Hydrophobic purified nanoparticles dissolved in chloroform were first mixed with appropriate amounts of the amphiphilic poly

on the particle surface.^[6,22,33] Furthermore PEGylated surfaces offer reduced nonspecific interaction with biological molecules and cells.^[34,35] The more PEG that is attached to

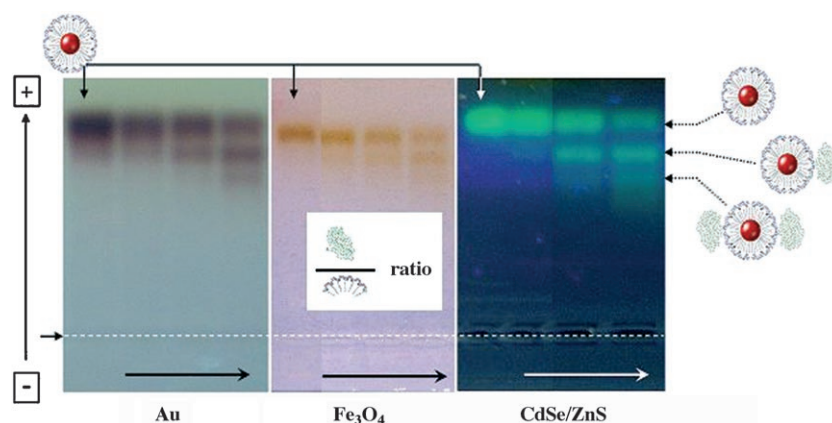


Figure 2. PEG molecules with amino terminal groups ($M_w = 5000 \text{ g mol}^{-1}$) were incorporated by amidation into the amphiphilic polymer so that 0%, 0.25%, 0.5%, and 1% of the anhydride rings are reacted with the PEG. Gold, iron oxide, and semiconductor nanoparticles were coated with these polymers and the resulting water soluble particles were run on agarose gels. The arrows on the left indicate the wells where the particles were loaded onto the gel and where they migrated to in the applied electric field. For each material the conjugates with 0 (left lane), 0.25%, 0.5%, and 1% PEG (right lane) were run on one gel. The horizontal arrow on the bottom indicates the direction in which the PEG/polymer ratio is increased. The first lane (0 PEG) serves as a control and corresponds to particles with no PEG in the polymer shell. For increasing PEG/polymer ratios, discrete bands become visible on the gel that correspond to particles with exactly one or exactly two PEG molecules bound per particle.

mer, whereby the number of added polymer molecules scaled linearly with the particle surface area. The organic solvents were evaporated and the nanoparticles became water soluble in alkaline buffer as a result of the repulsion of the negatively charged carboxyl groups on the particle surface (the carboxyl groups originate from maleic anhydride groups through hydrolyzation or linkage to amino modified molecules, see Figure 1). Empty polymer micelles (i.e. polymer without a nanoparticle inside) were subsequently removed by size exclusion chromatography (SEC), gel electrophoresis, or ultrafiltration.^[30,31] Like our previously published reports, the resulting polymer coated nanoparticles of various materials were found to be stable for months in aqueous solution (as assessed by gel electrophoresis, SEC, and fluorescence correlation spectroscopy^[15,25,30,32]) and single PEG molecules could be attached using EDC chemistry in a postmodification step according to a previous protocol.^[25] All experiments are described in detail in the Supporting Information (SI). The results demonstrate that hydrophobic nanoparticles embedded in a shell of amphiphilic polymers with incorporated functional groups show the same colloidal properties as the previously published nanoparticles that have no functional groups in their shells.

PEG was chosen as the first example of a functional organic molecule to be incorporated in the amphiphilic polymer. PEG is known to increase the colloidal stability of nanoparticles in a salt containing solution due to steric repulsion of the hydrated, and therefore bulky, PEG chains

the polymer shell, the bigger the size of the resulting particle.^[30] The attachment of amino modified PEG (Molecular weight, $M_w \geq 5000 \text{ g mol}^{-1}$) with EDC chemistry in a postmodification step using particles that are already polymer coated has been proven to yield big enough changes in the particle size for them to be resolved as individual band upon gel electrophoresis.^[25] Here we demonstrate that PEG can also be directly incorporated into the polymer before the actual polymer coating procedure and that discrete bands of nanoparticles with a different number of PEG molecules bound per particle can be resolved with gel electrophoresis (Figure 2). The more the PEG was incorporated in the polymer, the bigger the poly

mer coated nanoparticles became and the more retarded their bands were during gel electrophoresis. Retardation during gel electrophoresis is a clear indication of the presence of PEG molecules on the particle surface. A discrete band resulting from particles with a controllable number of PEG molecules were obtained for Au nanoparticles, quantum dots (CdSe/ZnS), and magnetic iron oxide nanoparticles (Fe₃O₄). This indicates the universality of the approach, which does not depend on the material of the inorganic nanoparticle. A similar study has been recently reported by the Colvin group.^[23] PEG molecules on the nanoparticle surface offer the possibility to reduce nonspecific interaction in biological environments, but also allow for preparing particles with a discrete number of free functional groups pointing towards solution.

The streptavidin biotin system has extensively been used to assemble particles on the nanometer scale^[36,37] and streptavidin (SA) modified nanoparticles are commercially available, for example, quantum dots and magnetic nanoparticles. In these cases either biotin or SA was attached to the surface of nanoparticles in a postmodification of particles that were already soluble in aqueous solution. In the following we demonstrate that our approach allows us to directly embed biotin into the amphiphilic polymer before the actual polymer coating procedure. For this purpose PEG of different molecular weights ($M_w = 720 \text{ g mol}^{-1}$ and $M_w = 5000 \text{ g mol}^{-1}$) that has an amino group on one end and a biotin group on the other was reacted with the polymer as described above. Because the amino groups reacted with

the anhydride rings on the polymer backbone, the biotinylated ends of the PEG pointed away from the polymer backbone. Gold particles coated with the biotin PEG modified polymer were retarded in gel electrophoresis experiments compared to particles coated with the plain polymer, which proves the binding of the biotin PEG to the particle surface. In the case of biotin PEG molecules of sufficient molecular weight ($M_w \geq 5000 \text{ g mol}^{-1}$), nanoparticles with a discrete number of attached biotin molecules could be isolated by gel electrophoresis.

Though gel electrophoresis clearly proved the existence of biotin PEG in the polymer shell these experiments did not reveal whether biotin was accessible on the particle surface and had therefore preserved its functionality. Biotin is a small biomolecule that specifically binds with high affinity to the natural protein avidin or derivatives such as streptavidin or neutravidin. Because these proteins have four binding sites for biotin, the addition of avidin leads to crosslinking of biotinylated multivalent nanoparticles. In order to exclude uncontrolled binding of SA (additional experiments with avidin and neutravidin are shown in the Supporting Information) to multivalent particles, we used gold particles with no (Au 0), exactly one (Au 1 bio), and exactly two biotin molecules (Au 2 bio) per particle. For each of these particles, a series was prepared in which the Au concentration was kept constant and different amounts of SA were added. The Au SA mixtures of each series were then analyzed with gel electrophoresis. An example in which SA was added to Au 1 bio particles is shown in Figure 3, whereby the SA Au 1 bio ratio was increased from the left to the right. Au 1 bio with almost no added SA showed the same electrophoretic mobility as Au 1 biotin conjugates. Upon addition of more and more SA per Au 1 bio, first a retarded band and then a doublet of two shifted bands appeared. By increasing the SA Au 1 bio ratio the intensities within the doublet shift from the less retarded to the more retarded band. The shifts were not visible in the case of SA Au 0 mixtures (see SI). This demonstrates that the shifts in the band of SA Au 1 bio mixtures are caused by specific binding of SA to the biotin protruding from the polymer shell

around the Au nanoparticle. Under these experimental conditions nonspecific adhesion of SA to the surface of Au nanoparticles can be neglected. When SA was added to Au 2 bio, bigger shifts on the gel were observed. In the case of (divalent) Au 2 bio, networks of crosslinked particles can be formed as each Au particle has two binding sites, whereas the biggest possible conjugate in mixtures of SA and (monovalent) Au 1 bio would be one SA molecule with four Au particles attached (as a result of the four binding sites of SA for biotin). An additional proof for the attachment of SA to biotin containing Au was performed with fluorescence labeled FITC SA. No fluorescence could be observed in the unshifted bands of the Au particles, whereas fluorescence could be observed in all shifted bands that were associated to SA Au conjugates. Though we demonstrated specific attachment of SA to mono and divalent biotinylated Au nanoparticles, we could not unequivocally identify the structure of the conjugates. Transmission electron microscopy (TEM) analysis of the conjugates that had been extracted from the gel showed groupings of Au particles, but in our opinion the data lacked the statistical significance needed to associate the bands to one particular grouping. It also has to be pointed out that the actual shift of the conjugates on the

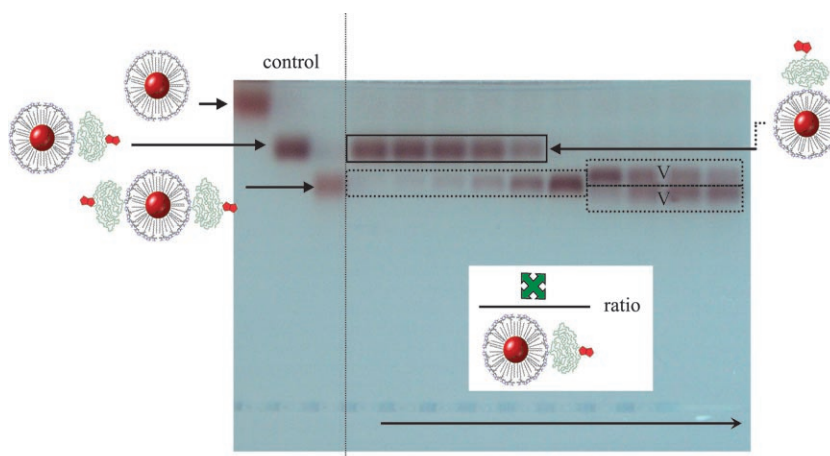


Figure 3. Au particles with no (Au 0), exactly one (Au 1 bio), and exactly two (Au 2 bio) biotin PEG molecules per particle were run with 1% agarose gel electrophoresis (the samples were loaded in the wells on the bottom of the gel and the particles migrated towards the positive pole that had been arranged close to the top of the gel). The biotin terminal at the free end of the PEG is drawn in red. These three control samples are shown on the three left lanes of the gel. The other lanes correspond to samples to which streptavidin (SA, drawn in green) was added, in different molar ratios, to Au particles with exactly one biotin functionality per particle. The lanes from the left to the right correspond to samples in which the SA Au particle ratio has been increased (by a factor of 2 between two adjacent lines, max. 46 SA/Au NP on the right), while the number of Au nanoparticles was kept constant for all samples. Upon binding of SA to the biotinylated Au particles three different positions of retarded bands can be observed. Though the gel data do not allow for a detailed analysis of the structures of the conjugates, the three bands are in agreement with the following hypothesis: In the condition of a large excess of SA to Au 1 bio (right side on the gel), each SA molecule can be coordinated to at most one Au 1 bio particle (when neglecting nonspecific adhesion). Because of the excess of SA, no Au 1 bio without SA is expected and on the gel there are only retarded bands present (double bands at right of gel). Within the retarded band on the right side of the gel the intensity of the more retarded band gets lower upon decreasing the SA/Au 1 bio ratio. As more Au 1 bio per SA is present for lower SA/Au 1 bio ratios each SA molecule might now be coordinated to two Au particles. On further lowering of the SA Au 1 bio ratio, at one point there will be less SA molecules than Au 1 biotin particles. This means that each SA molecule can bind up to four Au 1 bio particles, whereas the unbound Au 1 bio particles that remain will appear at the nonretarded position.

gel is caused by a complex interplay of changes in charge and size. As the scope of this study is the modification of particles with functional groups (such as biotin), we did not focus on pursuing the defined assemblies of SA biotin mediated particle groupings further. Most importantly, we could demonstrate that the biotin molecules, which are incorporated in the polymer shell, are still reactive and specifically bind to SA molecules. The universality of this approach was again shown by performing similar experiment with different types of particles such as Au nanoparticles and colloidal quantum dots. Nanoparticles with biotin on their surface could be used as building blocks for common reactions based on SA biotin linkages, as for example, for the bioconjugation of biotinylated nanoparticles with biotinylated proteins or other biomolecules through SA.

As another model for a small biomolecule, an amine containing sugar derivative (4 aminophenyl β D galactopyranoside) was directly bound to the polymer using the standard synthetic process shown above. After the coating and phase transfer to aqueous buffers, the galactose polymer coated nanoparticles could be detected by the reversible aggregation of the particles after the addition of lectin that binds specifically to galactose moieties.^[38–40] By the addition of an excess of free galactose, these molecules compete against the binding of lectin with the galactose attached to the nanoparticles, resulting in the dissolution of nanoparticle aggregates (Figure 4). Nanoparticle aggregation was experimentally determined using UV vis absorption spectroscopy. Whereas freely dispersed gold nanoparticles formed a clear red translucent solution and did not show absorption at longer wavelengths, aggregated nanoparticles ultimately resulted in dark red precipitate and showed significant absorption at longer wavelengths due to light scattering.^[41,42] When aggregates had been formed upon addition of lectin to galactose modified nanoparticles, the aggregates could be dissolved again by the addition of an excess of free galactose molecules, as the bond formation of galactose and lectin is reversible. Addition of an

excess of a different sugar, such as glucose, on the other hand, did not dissolve the lectin mediated aggregates of galactose modified nanoparticles because glucose cannot displace galactose bound to lectin. Nanoparticles without galactose in their polymer shell did not show any signs of aggregation on addition of lectins. This demonstrates the incorporation of galactose in the polymer shell and the preservation of the specific binding capability of galactose to lectin. Nanoparticles with sugar molecules present on their surface have, for example, been used for specific recognition by cells.^[43,44]

Fluorescein amine was incorporated into the amphiphilic polymer as an example of organic fluorophores. Au particles coated with unmodified polymer did not exhibit any fluorescence. Dye modified polymer without nanoparticles was transferred to aqueous solution in order to form empty micelles. After purification from unbound dye molecules by ultrafiltration (100 kDa M_w cut off), the polymer micelles showed strong green fluorescence (Figure 5). Au particles

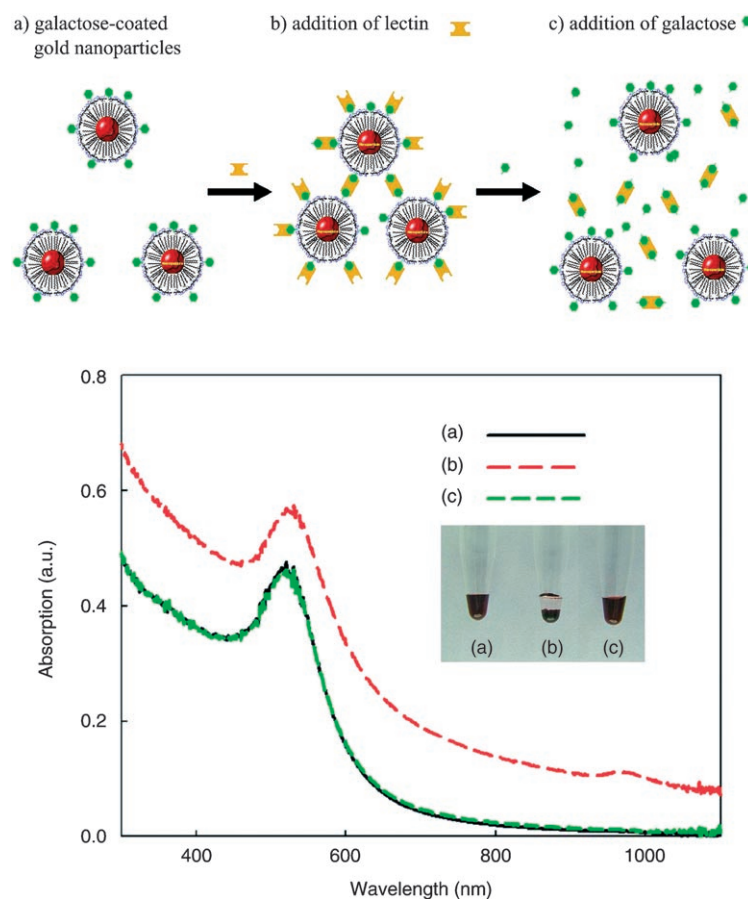


Figure 4. Au nanoparticles have been transferred to aqueous solution by embedding them in an amphiphilic polymer shell. The polymer that was used had 4% anhydride rings that were used to link galactose. These particles form a red translucent solution and have the regular UV vis absorption spectrum of colloidal gold (sample a). Addition of lectin starts crosslinking the particles. This results in aggregates and ultimately to a dark red precipitate and thus to absorption at longer wavelengths due to light scattering (sample b). Further addition of free excess galactose displaces the bonds between the galactose incorporated in the polymer shell and the lectin and thus the aggregates dissolve again. This results in the original red translucent solution and the normal UV vis spectrum of colloidal gold with no absorption at longer wavelengths (sample c). The aggregated nanoparticles (sample b) were redispersed by mixing with a pipette before measuring the spectrum.

coated with the dye modified polymer were purified from empty micelles by gel electrophoresis or SEC. While the UV vis absorption spectrum of the Au particles coated with the dye modified polymer is dominated by the absorption of the Au particles, the characteristic peak of fluorescein was found in the emission spectrum (Figure 5).

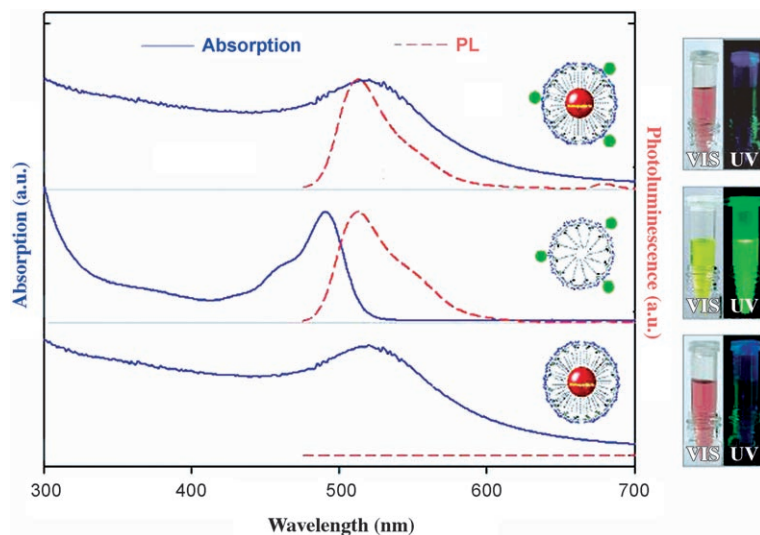


Figure 5. Au particles have been transferred to aqueous solution by an amphiphilic polymer coating in which 1% of the anhydride rings were used to link fluoresceinamine. The normalized absorption and photoluminescence (PL) spectra as well as images of the solution with a digital camera under daylight and upon UV excitation are shown in the top row. The UV vis absorption spectrum is dominated by the absorption of the Au, which can be seen also in the red color of the translucent solution. Upon UV excitation, weak fluorescence can be observed. If the same polymer coating procedure is applied without the addition of Au particles empty polymer micelles are obtained (middle row). As there is no Au present, the absorption originates from the fluorescein (yellow solution) and there is green fluorescence. As a control Au particles were transferred to aqueous solution with a polymer that did not contain fluorescein (bottom row). The absorption of this solution is again dominated by the Au particles, but there is no fluorescence observed.

However, for fluorescein containing polymer shells with embedded Au particles, the fluorescence was strongly quenched (by around two orders of magnitude). This phenomenon indicates close proximity of dye to the Au surface. Quenching of fluorophores close to Au surfaces has been investigated in detail by several groups.^[45–47] There are two potential applications for inorganic colloidal nanoparticles with a fluorescent dye directly immobilized in their surface coating. First, nanoparticles that do not quench dyes (as it might be the case for magnetic insulators) could be directly fluorescently labeled and visualized with fluorescence microscopy. Second, colloidal quantum dots as donors with acceptor dyes in the polymer shell could be used as fluorescence resonance energy transfer (FRET) based sensors^[31,48–51] because of the close proximity between acceptor and donor.

In this report, a general approach for synthesizing an amphiphilic polymer is described that can be used for the coating of hydrophobic nanoparticles in order to transfer them to aqueous solution. The amphiphilic polymer is based on a poly(maleic anhydride) backbone that is modified with hydrophobic side chains and functional organic molecules.

The amphiphilic polymer was used successfully to transfer inorganic colloidal nanoparticles of different materials (Au, CdSe/ZnS, Fe₃O₄) to aqueous solution. As the initial nanoparticles were capped with different hydrophobic surfactant molecules (e.g. trioctylphosphine oxide (TOPO), trioctylphosphine, dodecanethiol), this demonstrates the universality of the approach, in which the attachment of the polymer to the inorganic nanoparticles is only mediated by the hydrophobic interaction and does not depend on the particular surface chemistry of the inorganic nanoparticles. The polymer coated particles were found to have good colloidal stability, which was assessed by gel electrophoresis. In accordance with previous reports (bio) molecules such as PEG could be attached with EDC chemistry to the particle surface in a postmodification step. Most importantly, the polymer could be directly modified, before the coating process, with functional amine containing (bio) molecules without the need of crosslinker reagents or subsequent purification. This prefunctionalization, that is, the attachment of functional molecules in the polymer before the actual polymer coating, introduces new flexibility.

Also (small) functional molecules, which are not soluble in aqueous solution, can be introduced to the particle surface, as the linkage of the functional molecules to the polymer is performed in organic solvent. As the linkage is performed before the actual coating of the particles with the polymer, the reaction can be performed at higher concentration and, therefore, eventual colloidal instabilities during a postmodification step under high salt condition can be circumvented. We have demonstrated, in particular, the linkage of PEG, biotin, galactose, and fluorescein to the polymer. The functionality of the molecules incorporated in the polymer shell around the particles was retained. However, depending on their hydrophobicity, part of the molecules might be inside the polymer shell and thus not accessible on the particle surface. In summary, we introduced one additional degree of control to colloidal nanoparticles. Apart from the functional inorganic core that can be fluorescent (CdSe/ZnS), magnetic (Fe₃O₄) or heatable (Au), additional functionality can be incorporated in the polymer shell around the particles, which can reduce nonspecific adhesion (PEG), introduce specific binding sites (biotin, galactose), or introduce fluorescence (fluorescein). We believe that

ability. Also (small) functional molecules, which are not soluble in aqueous solution, can be introduced to the particle surface, as the linkage of the functional molecules to the polymer is performed in organic solvent. As the linkage is performed before the actual coating of the particles with the polymer, the reaction can be performed at higher concentration and, therefore, eventual colloidal instabilities during a postmodification step under high salt condition can be circumvented. We have demonstrated, in particular, the linkage of PEG, biotin, galactose, and fluorescein to the polymer. The functionality of the molecules incorporated in the polymer shell around the particles was retained. However, depending on their hydrophobicity, part of the molecules might be inside the polymer shell and thus not accessible on the particle surface. In summary, we introduced one additional degree of control to colloidal nanoparticles. Apart from the functional inorganic core that can be fluorescent (CdSe/ZnS), magnetic (Fe₃O₄) or heatable (Au), additional functionality can be incorporated in the polymer shell around the particles, which can reduce nonspecific adhesion (PEG), introduce specific binding sites (biotin, galactose), or introduce fluorescence (fluorescein). We believe that

such design of particle coatings might bring new impact to bridge hydrophobic nanomaterials with biological and medical applications.

Experimental Section

Polymer synthesis: All reactions were carried out at room temperature and all organic solvents were purchased in anhydrous quality, unless stated otherwise. Polymer(isobutylene-*alt*-maleic anhydride) ($M_w \approx 6000 \text{ g mol}^{-1}$, Aldrich; corresponding to roughly 39 monomer units per polymer chain) was vigorously mixed with dodecylamine (Sigma) in THF solution (100 mL), whereby the amount of added dodecylamine was sufficient to react with 75% of the anhydride rings. The cloudy solution became transparent upon heating for several hours (60 °C). After evaporation of the solvent, the resulting polymer was redissolved in anhydrous chloroform. For the functionalization of the polymer, appropriate amounts of either methoxy-PEG-amine (M_w 5000 g mol^{-1} from Rapp Polymere or M_w 750 g mol^{-1} from Fluka) dissolved in chloroform, biotin-PEG-amine (M_w 5000 g mol^{-1} from Rapp Polymere (Germany) or M_w 720 g mol^{-1} from Sigma) dissolved in chloroform/THF, amino-phenyl β -D-galactopyranoside (Sigma) dissolved in THF, or fluorescein-amine (Aldrich) dissolved in THF were slowly dropped into the diluted polymer solution and reacted overnight under stirring. The amount of added molecules was calculated in such ways that between 0.25% and 4% of the anhydride rings of the polymer backbone were reacted. After evaporation of the organic solvent (chloroform with or without THF) under reduced pressure, the polymer was re-dissolved in chloroform.

Polymer coating: A polymer solution in chloroform and a solution of hydrophobically capped nanoparticles in chloroform were mixed for 30 min at room temperature. The amount of polymer was calculated so that 100 monomers units per nm^2 of nanoparticle surface were used. After evaporating all the solvent under reduced pressure, a solid thin film formed that was then dissolved in alkaline sodium borate buffer (SBB) solution (pH 12). After this phase transfer of the nanoparticles from chloroform to aqueous solution, the buffer was exchanged for one of moderate pH (SBB, pH 9) by two rounds of dilution and reconcentration through a centrifuge filter. The residual polymer was removed by size exclusion chromatography (Agilent 1100 HPLC system with a Sephacryl S-300 HR column, the mobile phase was 150 mM NaCl in 50 mM sodium borate, pH 9.0) and gel electrophoresis.

Experiments with functional polymer: The following molecules were used for selective binding to the functionalized nanoparticle surface: streptavidin (Sigma S4762), streptavidin-FITC (Sigma S3762), lectin RCA₁₂₀ (Sigma L7886), galactose (Sigma–Aldrich, G0625), glucose (Sigma–Aldrich, G5767).

A more detailed description of materials and methods is available in the Supporting Information.

Keywords:

biomolecules • coatings • colloids • conjugation • quantum dots

- [1] M. Gao, S. Kirstein, H. Möhwald, A. L. Rogach, A. Kornowski, A. Eychmüller, H. Weller, *J. Phys. Chem. B* **1998**, *102*, 8360.
- [2] W. C. W. Chan, S. Nie, *Science* **1998**, *281*, 2016.
- [3] F. Pinaud, D. King, H. P. Moore, S. Weiss, *J. Am. Chem. Soc.* **2004**, *126*, 6115.
- [4] A. G. Kanaras, F. S. Kamounah, K. Schaumburg, C. J. Kiely, M. Brust, *Chem. Commun.* **2002**, 2294.
- [5] W. Jiang, S. Mardiyani, H. Fischer, W. C. W. Chan, *Chem. Mater.* **2006**, *18*, 872.
- [6] B. Dubertret, P. Skourides, D. J. Norris, V. Noireaux, A. H. Brivanlou, A. Libchaber, *Science* **2002**, *298*, 1759.
- [7] H. Fan, E. W. Leve, C. Scullin, J. Gabaldon, D. Tallant, S. Bunge, T. Boyle, M. C. Wilson, C. J. Brinker, *Nano Lett.* **2005**, *5*, 645.
- [8] W. J. M. Mulder, R. Koole, R. J. Brandwijk, G. Storm, P. T. K. Chin, G. J. Strijkers, C. D. Donega, K. Nicolay, A. W. Griffioen, *Nano Lett.* **2006**, *6*, 1.
- [9] L. M. Liz Marzán, M. Giersig, P. Mulvaney, *Chemical Commun.* **1996**, *6*, 731.
- [10] M. J. Bruchez, M. Moronne, P. Gin, S. Weiss, A. P. Alivisatos, *Science* **1998**, *281*, 2013.
- [11] D. Gerion, F. Pinaud, S. C. Williams, W. J. Parak, D. Zanchet, S. Weiss, A. P. Alivisatos, *J. Phys. Chem. B* **2001**, *105*, 8861.
- [12] S. T. Selvan, T. T. Tan, J. Y. Ying, *Adv. Mater.* **2005**, *17*, 1620.
- [13] Z. Zhelev, H. Ohba, R. Bakalova, *J. Am. Chem. Soc.* **2006**, *128*, 6324.
- [14] M. X. Wu, H. Liu, J. Liu, K. N. Haley, J. A. Treadway, J. P. Larson, N. Ge, F. Peale, M. P. Bruchez, *Nat. Biotechnol.* **2003**, *21*, 41.
- [15] T. Pellegrino, L. Manna, S. Kudera, T. Liedl, D. Koktysh, A. L. Rogach, S. Keller, J. Rädler, G. Natile, W. J. Parak, *Nano Lett.* **2004**, *4*, 703.
- [16] X. Gao, Y. Cui, R. M. Levenson, L. W. K. Chung, S. Nie, *Nat. Biotechnol.* **2004**, *22*, 969.
- [17] T. Nann, *Chem. Commun.* **2005**, 1735.
- [18] S. Kim, S. Kim, J. Tracy, A. Jasanoff, M. Bawendi, *J. Am. Chem. Soc.* **2005**, *127*, 4556.
- [19] Y. J. Kang, T. A. Taton, *Angew. Chem., Int. Ed.* **2005**, *44*, 409.
- [20] C. Luccardini, C. Tribet, F. Vial, V. Marchi Artzner, M. Dahan, *Langmuir* **2006**, *22*, 2304.
- [21] W. W. Yu, E. Chang, C. M. Sayes, R. Drezek, V. L. Colvin, *Nano technology* **2006**, *17*, 4483.
- [22] M. S. Nikolic, M. Krack, V. Aleksandrovic, A. Kornowski, S. Forster, H. Weller, *Angew. Chem., Int. Ed.* **2006**, *45*, 6577.
- [23] W. W. Yu, E. Chang, J. C. Falkner, J. Zhang, A. M. Al Somali, C. M. Sayes, J. Johns, R. Drezek, V. L. Colvin, *J. Am. Chem. Soc.* **2007**, *129*, 2871.
- [24] H. W. Duan, S. M. Nie, *J. Am. Chem. Soc.* **2007**, *129*, 3333.
- [25] R. A. Sperling, T. Pellegrino, J. K. Li, W. H. Chang, W. J. Parak, *Adv. Funct. Mater.* **2006**, *16*, 943.
- [26] G. H. Hu, J. T. Lindt, *Polym. Bull.* **1992**, *29*, 357.
- [27] M. Brust, M. Walker, D. Bethell, D. J. Schiffrin, R. Whyman, *J. Chem. Soc., Chem. Commun.* **1994**, 1994, 801.
- [28] B. O. Dabbousi, J. Rodriguez Viejo, F. V. Mikulec, J. R. Heine, H. Mattoussi, R. Ober, K. F. Jensen, M. G. Bawendi, *J. Phys. Chem. B* **1997**, *101*, 9463.
- [29] M. F. Casula, Y. W. Jun, D. J. Zaziski, E. M. Chan, A. Corrias, A. P. Alivisatos, *J. Am. Chem. Soc.* **2006**, *128*, 1675.
- [30] R. A. Sperling, T. Liedl, S. Dühr, S. Kudera, M. Zanella, C. A. J. Lin, W. Chang, D. Braun, W. J. Parak, *J. Phys. Chem. C* **2007**, *111*, 11552.
- [31] M. T. Fernández Argüelles, A. Yakovlev, R. A. Sperling, C. Luccardini, S. Gaillard, A. S. Medel, J. M. Mallet, J. C. Brochon, A. Feltz, M. Oheim, W. J. Parak, *Nano Lett.* **2007**, *7*, 2613–2617.
- [32] T. Liedl, S. Keller, F. C. Simmel, J. O. Rädler, W. J. Parak, *Small* **2005**, *1*, 997.
- [33] W. J. Parak, D. Gerion, D. Zanchet, A. S. Woerz, T. Pellegrino, C. Micheel, S. C. Williams, M. Seitz, R. E. Bruehl, Z. Bryant, C. Bus

- tamante, C. R. Bertozzi, A. P. Alivisatos, *Chem. Mater.* **2002**, *14*, 2113.
- [34] B. Ballou, B. C. Lagerholm, L. A. Ernst, M. P. Bruchez, A. S. Waggoner, *Bioconjugate Chem.* **2004**, *15*, 79.
- [35] E. L. Bentzen, I. D. Tomlinson, J. Mason, P. Gresch, M. R. Warne, D. Wright, E. Sanders Bush, R. Blakely, S. J. Rosenthal, *Bioconjugate Chem.* **2005**, *16*, 1488.
- [36] K. K. Caswell, J. N. Wilson, U. H. F. Bunz, C. J. Murphy, *J. Am. Chem. Soc.* **2003**, *125*, 13914.
- [37] A. Salant, E. Amitay Sadvovsky, U. Banin, *J. Am. Chem. Soc.* **2006**, *128*, 10006.
- [38] H. Otsuka, Y. Akiyama, Y. Nagasaki, K. Kataoka, *J. Am. Chem. Soc.* **2001**, *123*, 8226.
- [39] H. Otsuka, Y. Nagasaki, K. Kataoka, *Adv. Drug Delivery Rev.* **2003**, *55*, 403.
- [40] S. R. Popielarski, S. H. Pun, M. E. Davis, *Bioconjugate Chem.* **2005**, *16*, 1063.
- [41] C. A. Mirkin, R. L. Letsinger, R. C. Mucic, J. J. Storhoff, *Nature* **1996**, *382*, 607.
- [42] T. A. Taton, R. C. Mucic, C. A. Mirkin, R. L. Letsinger, *J. Am. Chem. Soc.* **2000**, *122*, 6305.
- [43] J. Rojo, V. Diaz, J. M. d. l. Fuente, I. Segura, A. G. Barrientos, H. H. Riese, A. Bernad, S. Penades, *ChemBioChem* **2004**, *5*, 291.
- [44] C. C. Lin, Y. C. Yeh, C. Y. Yang, C. L. Chen, G. F. Chen, C. C. Chen, Y. C. Wu, *J. Am. Chem. Soc.* **2002**, *124*, 3508.
- [45] B. Dubertret, M. Calame, A. J. Libchaber, *Nat. Biotechnol.* **2001**, *19*, 365.
- [46] E. Dulkeith, A. C. Morteani, T. Niedereichholz, T. A. Klar, J. Feldmann, S. A. Levi, F. C. J. M. van Veggel, D. N. Reinhoudt, M. Möller, D. I. Gittins, *Phys. Rev. Lett.* **2002**, *89*, 203002.
- [47] E. Dulkeith, M. Ringler, T. A. Klar, J. Feldmann, A. M. Javier, W. J. Parak, *Nano Lett.* **2005**, *5*, 585.
- [48] P. T. Tran, G. P. Anderson, J. M. Mauro, H. Mattoussi, *Phys. Status Solidi B* **2002**, *229*, 427.
- [49] I. L. Mednitz, A. R. Clapp, H. Mattoussi, E. R. Goldman, B. Fisher, J. M. Mauro, *Nat. Mater.* **2003**, *2*, 630.
- [50] I. L. Mednitz, H. T. Uyeda, E. R. Goldman, H. Mattoussi, *Nat. Mater.* **2005**, *4*, 635.
- [51] L. F. Shi, V. De Paoli, N. Rosenzweig, Z. Rosenzweig, *J. Am. Chem. Soc.* **2006**, *128*, 10378.

Received: August 7, 2007

Published online on February 13, 2008

Size Determination of (Bio)conjugated Water-Soluble Colloidal Nanoparticles: A Comparison of Different Techniques

R. A. Sperling,[†] T. Liedl,[†] S. Duhr,[†] S. Kudera,[†] M. Zanella,[†] C.-A. J. Lin,^{†,‡} W. H. Chang,[‡] D. Braun,[†] and W. J. Parak^{*,†}

Center for Nanoscience, Ludwig Maximilians Universität, München, Germany, and Center for Nano Bioengineering and R&D Center for Membrane Technology, Chung Yuan Christian University, Taiwan, R.O.C.

Received: February 5, 2007; In Final Form: April 21, 2007

The size of inorganic colloidal nanoparticles coated with organic layers of different thickness has been measured with different techniques, including transmission electron microscopy, gel electrophoresis, size exclusion chromatography, fluorescence correlation spectroscopy, and thermophoresis. The results are critically compared, and the advantages and disadvantages of the respective methods are discussed.

Introduction

In the past decades, improved synthesis techniques have influenced significantly research and applications of inorganic colloidal nanoparticles. This is mainly due to advances in the control of particle growth. Nowadays, samples with very narrow size distribution and controlled shape can be grown.^{1–3} Colloidal stability is provided by a layer of organic molecules around the inorganic particle core. This layer can be either hydrophobic or hydrophilic, and the respective particles are soluble in organic solvents or aqueous solution. Naturally, this layer contributes to the overall diameter of the particles. Whereas the colloidal stability of particles in organic solvents is usually achieved by a monolayer of hydrophobic molecules,⁴ thicker (hydrophilic) layers are often used to stabilize particles in aqueous solution, which in turn results in significantly increased particle diameters.^{5,6} The effective diameter of the particles increases further when additional (biological) molecules are bound to the particle surface in order to provide functionality. In particular, for biological applications, it is important to know the effective diameter of the particles, as bigger particles, for example, might not be able to enter pores of a certain size. However, due to the composite nature of the particles—a “hard” inorganic core and a “soft” organic shell with attached biological molecules—this is not a trivial task. The problem is that some techniques are more sensitive for the inorganic part, and others may eventually influence the conformation and thus the size of the organic part.

The size of the first generation of colloidal semiconductor nanoparticles was investigated extensively several years ago by the group of Henglein and Weller.^{7–9} These particles were directly synthesized in water, and the organic shell around the inorganic cores comprised just a monolayer of mercaptocarbonic acid molecules. In this study, we want to investigate the size of more complex nanoparticles that first have been synthesized in organic solvents, then have been transferred to aqueous solution by embedding them in a hydrophilic polymer shell,^{10–13} and finally have been modified by the conjugation of polyethylene glycol (PEG) molecules with different molecular weight.¹⁴ These

particles represent the general case where the samples differ in the thickness of a (soft) organic shell, while the (hard) inorganic particle core is the same.

For this work, nanoparticle size was characterized by the following methods: transmission electron microscopy (TEM),^{15–17} gel electrophoresis,^{9,18–24} size exclusion chromatography (SEC),^{7,8,21,25–35} fluorescence correlation spectroscopy (FCS),^{11,36–44} and thermophoresis.^{45–47} These and other relevant methods not used in this study are described in more detail in the Supporting Information (SI).

Materials and Methods

Particle Synthesis. CdSe/ZnS core/shell nanoparticles were synthesized in organic solvent according to standard protocols^{48,49} and transferred to aqueous solution by embedding them in a shell of an amphiphilic polymer.¹¹ All protocols are reported in detail in the Supporting Information (SI §I.1–§I.5). The first exciton peak in the absorption spectrum of the CdSe cores was at 610 nm (corresponding to a diameter of the inorganic core of 4.7 nm⁵⁰) and, after overcoating with the ZnS shell, at 614nm (see Table 1). PEG molecules of different molecular weight, which were modified with an amino group on one end, were attached at different coverages by standard EDC chemistry to the polymer shell around the nanoparticles¹⁴ (SI §I.6). Sketches of the resulting particles are drawn in Tables 1–3. For particles whose surfaces were saturated with PEG, unbound excess PEG molecules were removed in five subsequent purification steps with centrifuge filters. Mixtures of particles with a discrete number of PEG molecules attached per particle were first run on 1% agarose gels in order to separate particles with zero, one, two, and three PEG molecules attached per particle. After extraction of the particles from the gel, they were purified on a desalting column. As additional samples, Au nanoparticles^{16,51} with the same modifications as those described for the CdSe/ZnS particles were also used. Detailed protocols have been published previously.^{11,14} We also measured the diameter of commercially available quantum dots with and without streptavidin modification (Table 4).

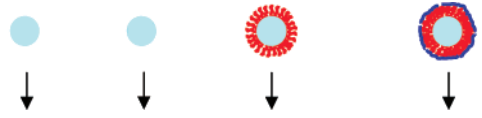
Transmission Electron Microscopy. TEM images of CdSe/ZnS particles dissolved in chloroform and water were recorded before and after embedding them in a shell of amphiphilic

* Corresponding author. E-mail: Wolfgang.Parak@physik.uni-muenchen.de.

[†] Ludwig Maximilians Universität.

[‡] Chung Yuan Christian University.

TABLE 1: The Inorganic Hard Core Diameter $\langle d \rangle$ and the Effective Diameters $\langle d_{\text{eff}} \rangle$ of CdSe, CdSe/ZnS, and Au Particles (Drawn in Gray) Determined with Optical Methods and by TEM Images



particle type	$\langle d \rangle_{\text{abs}}$ [nm] ^a	$\langle d \rangle_{\text{TEM}}$ [nm] ^b	$\langle d_{\text{eff}} \rangle_{\text{TEM}}$ [nm] before polymer coating	$\langle d_{\text{eff}} \rangle_{\text{TEM}}$ [nm] after polymer coating ^c
CdSe	5.1	4.7	6.0	
CdSe/ZnS	5.3	5.3	6.4	9.6
Au		4.6	5.6	9.0

^a For the CdSe particles, the diameter was derived from absorption spectra.⁵⁰ ^b By analyzing the spacing between the particles in the TEM images, the effective diameters $\langle d_{\text{eff}} \rangle$, which comprise the inorganic particles plus the organic layers (drawn in red and blue) attached to their surfaces, were determined before and after coating the particles with an amphiphilic polymer. Before the polymer coating, the particle is just surrounded by the hydrophobic surfactant layer (drawn in red). After the polymer coating, an amphiphilic polymer (with hydrophobic tails drawn in red and a hydrophilic backbone drawn in blue) is also wrapped around the particles.^{11,14} ^c These values have to be considered as an approximation (see SI §II.2).

polymer. Drops of the particle solution were placed on TEM grids, and images were recorded after evaporation of the solvent. The distribution of the inorganic particle diameters and the distances between the centers of adjacent particles were derived from the images by an image analysis program (SI §II.1).

Gel Electrophoresis. CdSe/ZnS and Au particles saturated with PEG molecules of different length were run on agarose gels (1–2%, 1–2 h, 100 V). As a control, phosphine-stabilized 10 nm Au particles were also run on the same gel.^{19,20} After running the particles on the gel, the bands of the CdSe/ZnS and Au particles were identified by their fluorescence and red color, respectively (see Figure 1) (SI §III). The mobilities of the different particles were determined from their position on the gel relative to the position where they had been loaded to the gel.^{19,20} For CdSe/ZnS and Au particles with a discrete number of PEG molecules attached per particle, a low amount of PEG molecules of different length was reacted to the polymer-coated CdSe/ZnS and Au particles, and the reaction mixtures were run on agarose gels. After running the gel, discrete bands corresponding to CdSe/ZnS and Au particles with no, exactly one, exactly two, and exactly three PEG molecules bound per particle were observed as individual bands on the gel (see Figure 1).^{19,20} The bands were extracted from the gel, and the obtained CdSe/ZnS– and Au–PEG conjugates with a different number of PEG molecules attached per particle were purified on a desalting column before using them for the SEC, FCS, and thermophoresis experiments. From gel electrophoresis, the mobilities m of all conjugates were then transformed in corresponding effective diameters d_{eff} by using a mobility–diameter calibration curve created with phosphine-stabilized Au nanoparticles²⁰ (SI §III):

$$d_{\text{eff},1\%}(m) = -85.0 \cdot \ln[(m/m_{10\text{nm},1\%})/1.05] + 6 \text{ [nm]}$$

$$d_{\text{eff},2\%}(m) = -37.7 \cdot \ln[(m/m_{10\text{nm},2\%})/1.12] + 6 \text{ [nm]} \quad (\text{Formula 1})$$

Here, $m/m_{10\text{nm},y}$ refers to the electrophoretic mobility of the conjugates (m) in relation to the mobility of 10 nm phosphine-stabilized Au particles ($m_{10\text{nm},y}$) that have been run on a gel with the same agarose concentration y ($y = 1\%$ or 2%).^{19,20}

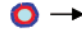

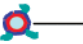



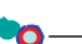






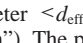
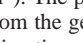




Size Exclusion Chromatography. CdSe/ZnS and Au particles saturated with PEG molecules of different molecular weight were run on different high-performance liquid chromatography (HPLC) size exclusion columns, and the elution volume v_e (i.e., the total volume of the mobile phase when the particles come out of the column) of the particles was measured (similarly, elution times t_e , i.e., the time after which the particle fraction is eluted from the column, could have been measured) (see Figure 2) (SI §IV). In order to normalize the data to one universal curve, the elution volumes v_e were transformed into partition coefficients K_{SEC} .^{52,53} The partition coefficient corresponds to the fraction of accessible pore volume for sample particles and can obtain values $0 \leq K_{\text{SEC}} \leq 1$. Very small particles or molecules can occupy the total pore volume (as they are small enough to fully penetrate the pores of the gel), and $K_{\text{SEC}} = 1$. Very large particles are totally excluded from the pore volume, and $K_{\text{SEC}} = 0$. In this way, the K_{SEC} value is a measure of the size of the particles: the smaller and larger the particles are, the closer their K_{SEC} values come to 1 and 0, respectively. In contrast to elution volumes or elution times, the K_{SEC} values are normalized quantities and thus do not depend in first order on experimental parameters such as sample volume, flow rate, or column geometry (SI §IV):

$$\begin{aligned} K_{\text{SEC}}(\text{particle}) &= [(t_e(\text{particle}) - t_e(\text{biggest particle})) / \\ &\quad (t_e(\text{smallest particle}) - t_e(\text{biggest particle}))] \\ &= [(v_e(\text{particle}) - v_e(\text{biggest particle})) / \\ &\quad (v_e(\text{smallest particle}) - v_e(\text{biggest particle}))] \\ &= [(v_e(\text{particle}) - v_0) / (v_1 - v_0)] \quad (\text{Formula 2}) \end{aligned}$$

The elution volume of the very small particles is referred to as the total liquid volume v_1 , and the elution volume of the very large particles is referred to as dead or void volume v_0 . In order to experimentally obtain v_1 and v_0 , acetone (a very small particle) and λ -DNA (a very big particle) were run, and their elution volumes ($= v_1$ and v_0) were measured. For generating a calibration curve that relates partition coefficients K_{SEC} to effective diameters d_{eff} , protein standards were run through the columns, and their elution volumes were determined from the elution peak maxima and converted into partition coefficients. The size d_{eff} of each protein standard was estimated as 2 times the hydrodynamic radius of the protein.⁵³ By plotting the partition coefficients of different proteins versus their effective diameter and extrapolating these data, a calibration curve $d_{\text{eff}}(K_{\text{SEC}})$ was obtained (see Figure 2). By using this calibration curve, the partition coefficients derived for the CdSe/ZnS–PEG and Au–PEG conjugates could be converted into effective diameters. As for the gel electrophoresis experiments, the effective diameters are obtained by a comparison with standard samples of known diameter. In the case of the gel electrophoresis experiments, phosphine-stabilized Au nanoparticles were used. These particles could not be used for the SEC measurements, as they got stuck in the columns. Therefore a series of globular proteins had to be used as standard samples for the SEC measurements.





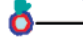

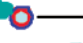





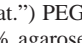
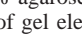

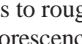
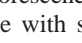
Fluorescence Correlation Spectroscopy. Samples of CdSe/ZnS–PEG conjugates were mounted on an Axiovert200 confocal microscope with a 40 \times water immersion objective (C-Apochromat, NA = 1.2) and a ConfoCor2 FCS module (whole setup: Zeiss, Germany). Fluorescence was excited with the 488 nm line of an Ar ion laser. The focal volume was calibrated with Alexa488 (diffusion coefficient $D = 316 \mu\text{m}^2\text{s}^{-1}$, Molecular Probes). The nanocrystals were diluted to a concentration

TABLE 2: Effective Diameters d_{eff} [nm] of CdSe/ZnS-PEG Conjugates

PEG/ polymer- coated CdSe/ZnS particle ^a	$M(\text{PEG})$ [g/mol]	$\langle d_{\text{eff}} \rangle_{\text{TEM}}$ [nm]	$\langle d_{\text{eff}} \rangle_{\text{gel},1\%}$ [nm]	$\langle d_{\text{eff}} \rangle_{\text{gel},2\%}$ [nm]	$\langle d_{\text{eff}} \rangle_{\text{SEC}}$ [nm]	$\langle d_{\text{eff}} \rangle_{\text{FCS}}$ [nm]	$\langle d_{\text{eff}} \rangle_{\text{Therm}}$ [nm]
	0	-	9.6 ^b	14.5	-	-	20.5
	0 5000	-	-	14.5	14.5	-	20.1
	1 5000	-	24.5	19.3	-	-	22.8
	2 5000	-	34.2	24.1	-	-	24.4
	3 5000	-	43.6	28.5	-	-	25.8
	4 5000	-	51.9 ^c	32.8	-	-	-
	0 10000	-	-	14.5	-	-	25.0
	1 10000	-	29.4	-	-	-	25.8
	2 10000	-	43.5	-	-	-	26.6
	3 10000	-	56.5 ^c	-	-	-	-
	0 20000	-	-	14.5	-	-	22.2
	1 20000	-	39.6	-	-	-	26.3
	2 20000	-	62.7 ^c	-	-	-	30.2
	0	-	-	14.5	12.6	19.4	12.2
	sat. 750	-	-	46.1 ^c	14.6	25.4	22.0
	sat. 2000	-	-	180.2 ^c	18.3	25.6	23.6
	sat. 5000	-	-	neg. ^c	23.9	27.6	25.0
	sat. 10000	-	-	neg. ^c	26.2	30.2	30.0
	sat. 20000	-	-	neg. ^c	34.8	34.2	40.0

^a PEG molecules (drawn in green) of different molecular weight M_w have been attached to the surface of polymer-coated CdSe/ZnS particles, as already sketched in Table 1.¹⁴ Either zero, one, two, three, or as many as possible (“sat.”) PEG molecules were attached per particle, and the effective particle diameter $\langle d_{\text{eff}} \rangle$ was measured with TEM, gel electrophoresis (“gel”, 1% and 2% agarose concentration), FCS, SEC, and thermophoresis (“Therm”). The particles with single PEGs attached per particle (first 13 samples) had been separated with gel electrophoresis with subsequent extraction from the gel and purification before their diameters were measured with SEC, FCS, and thermophoresis. ^b This value has to be considered as approximation. ^c These values are not realistic (as they are either too big or negative) due to limitations of the applied technique (see SI §II.2).

TABLE 3: Effective Diameters d_{eff} [nm] of Au-PEG Conjugates

PEG/ polymer- coated Au particle ^a	$M(\text{PEG})$ [g/mol]	$\langle d_{\text{eff}} \rangle_{\text{TEM}}$ [nm]	$\langle d_{\text{eff}} \rangle_{\text{gel},1\%}$ [nm]	$\langle d_{\text{eff}} \rangle_{\text{gel},2\%}$ [nm]	$\langle d_{\text{eff}} \rangle_{\text{SEC}}$ [nm]
	0	-	8.6	12.7	12.5
	0 5000	-	-	12.7	12.5
	1 5000	-	26.3	18.4	-
	2 5000	-	38.2 ^b	24.5	-
	3 5000	-	-	29.9	-
	0 10000	-	-	13.4	12.5
	1 10000	-	44.5 ^b	21.6	-
	2 10000	-	70.7 ^b	29.3	-
	0 20000	-	-	14.4	12.5
	1 20000	-	52.5 ^b	27.7	-
	2 20000	-	83.5 ^b	40.2	-
	0	-	-	-	12.5
	sat. 750	-	-	-	49.7 ^b
	sat. 2000	-	-	-	140.1 ^b
	sat. 5000	-	-	-	neg. ^b
	sat. 10000	-	-	-	neg. ^b
	sat. 20000	-	-	-	neg. ^b

^a PEG molecules of different molecular weight M_w have been attached to the surface of polymer-coated Au particles.¹⁴ Either zero, one, two, three, or as many as possible (“sat.”) PEG molecules were attached per particle, and the effective particle diameter $\langle d_{\text{eff}} \rangle$ was measured with gel electrophoresis (“gel”, 1% and 2% agarose concentration) and SEC. ^b These values cannot be taken into account (as they are too big or negative) and demonstrate the limitations of gel electrophoresis for size measurements (see SI §II.2).

of ~ 10 nm, which corresponds to roughly one particle per focal volume. Time traces of the fluorescence intensity were recorded with an avalanche photodiode with single-photon sensitivity. From the fluorescence intensity traces, autocorrelation functions

were calculated (see Figure 3) (SI §V). By fitting the experimentally obtained autocorrelation functions with model functions for freely diffusing particles, the diffusion coefficients of the particles were obtained as fit parameters.^{37–39,54} The diffusion

TABLE 4: Effective Diameters d_{eff} of Commercially Available Quantum Dots^{a,b}

sample	$\langle d_{\text{eff}} \rangle_{\text{gel,2\%}}$ [nm]	$\langle d_{\text{eff}} \rangle_{\text{SEC}}$ [nm]	$\langle d_{\text{eff}} \rangle_{\text{Therm}}$ [nm]	$\langle d_{\text{eff}} \rangle_{\text{mean-value}}$ [nm]
QD655 carboxyl	16.6	11.8	14.0	14.1 ± 2.4^d
QD655 SA	133.0 ^c	20.5	25.6	23.1 ± 1.6

^a Quantum Dot Corporation, 655 nm emission, polymer shell with carboxyl groups and with additional streptavidin (SA) modification (Qdot655 ITK carboxyl, #2132-1, and Qdot655 streptavidin conjugate, #1012-01). ^b The values were obtained with gel electrophoresis (2% agarose gels), SEC (column with Sephadex S-400), and thermophoresis. ^c This value cannot be taken into account due to charge effects (see SI §II.2). ^d This value is in the same range as the diameter obtained from Pons et al²⁴ for particles with slightly smaller cores.

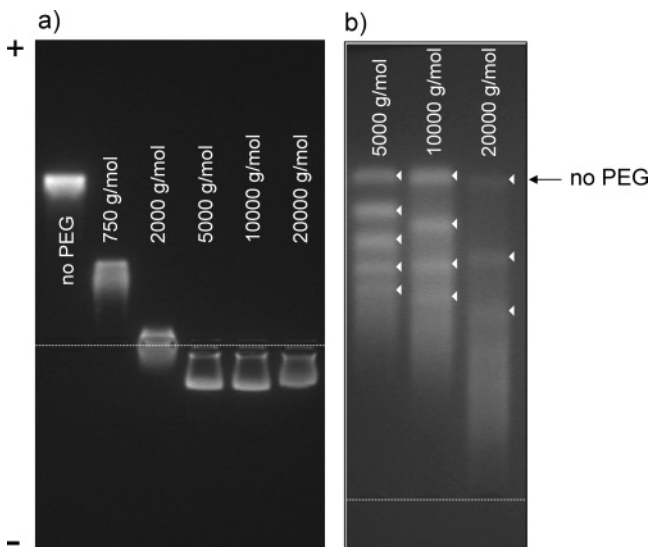


Figure 1. Gel electrophoresis for polymer-coated CdSe/ZnS nanoparticles. The “+” and “-” symbols indicate the direction of the applied electric field, and the dashed line marks the position where the samples have been loaded into the wells of the gel. (a) 2% agarose gel with particles with no PEG and particles whose surface has been saturated with PEG of 750, 2000, 5000, 10000, and 20000 Da molecular weight. (b) 1% agarose gel of particles to whose surface only a few PEG molecules of different molecular weight have been bound. The particles with no, one, two, and so forth PEG molecules attached per particle yield discrete bands on the gel.

coefficients were then converted into effective diameters by using the Stokes–Einstein relation. In contrast to the gel electrophoresis and HPLC measurements, the effective diameters obtained with FCS measurements are absolute values and do not depend on a direct comparison with standard samples of known diameter. However, the setup has to be calibrated with a dye of known diffusion constant for all measurements. Since the Au–PEG conjugates do not fluoresce, they could not be analyzed with FCS.

Thermophoresis. Strong local temperature gradients were used to manipulate concentration patterns in solution, all optically. Figure 4a shows the typical time course of an experiment. A solution of nanoparticles was continuously monitored by fluorescence microscopy, and the local fluorescence was used as measure for the particle concentration. An infrared laser was then used to introduce an inhomogeneous radial symmetric concentration pattern by inducing thermophoretic motion. After a few seconds, when the concentration in the center of the heat spot had decreased to at least 90% of the initial condition, the heating source was turned off. The temperature relaxed nearly instantaneously and was followed by the much slower flattening of the concentration profile by

diffusion. These time-resolved concentration profile data were compared with data obtained in a one-dimensional (1D) radial simulation over time (Figure 4b). By comparison of the experimental and simulated data, the mean diffusion coefficient of the fluorescent particles in solution was obtained, and from this the hydrodynamic diameter of the particles was derived using the Stokes–Einstein relation (SI §VI). In contrast to the gel electrophoresis and HPLC measurements the effective diameters obtained with thermophoresis measurements do not depend on a comparison with standard samples of known diameter, but are absolute values. Since the Au–PEG conjugates do not fluoresce, they could not be analyzed with thermophoresis.

PEG Radius. The increase in size of particles with a PEG shell should correspond to the dimensions of the PEG molecules. The effective diameters of free PEG molecules can be calculated from Formula 3, which was obtained by SEC,⁵⁵ whereby r_h is the hydrodynamic radius, and M_w is the molecular weight of the PEG:

$$d_{\text{eff,PEG}} = 2r_h = 0.03824 M_w^{0.559} \quad (\text{Formula 3})$$

Results and Discussion

Transmission Electron Microscopy. The results for the TEM analysis on particles without PEG modification are summarized in Table 1. However, these values have to be considered as very rough estimates with only limited reliability (SI §II.2). First of all, measurements had to be performed on dried samples. While, in solution, the hydrophobic surfactant chains repel each other, on a TEM grid, the particles can come so close to each other that the surfactant chains intercalate. More severe, the size distribution after the polymer coating, that is, the size-distribution of the entire system inorganic core plus organic shell, is by far not as good as that of the original particle solution, and the particles therefore do not assemble anymore nicely into two-dimensional lattices. Therefore, the particle-to-particle distance curves are smeared out, and the derived effective particle diameters have to be interpreted with care. As the particles have to be measured in the dried state, the effective diameters as determined by TEM do not contain any interaction with the solvent (as, for example, a cloud of counterions). Therefore, the values obtained for the effective diameter for CdSe/ZnS as well as Au particles with TEM are significantly smaller than the effective diameters determined with methods in which the particles are dispersed in their solvents (see first lines of Tables 2 and 3).

Gel Electrophoresis. In Figure 1, examples for particles separated by gel electrophoresis are shown. As with SEC, not only can the particle diameter be estimated, but the particles can also be sorted and fractionated by size in small preparative scale. In comparison to SEC, the size resolution of gel electrophoresis is significantly better, as particles with zero, one, two, and so forth PEG molecules can be clearly separated by gel electrophoresis, but not with the columns used for SEC. However, there are severe limitations for the determination of effective diameters. The particles need to possess a very high colloidal stability in the electrolytic solution, which is needed to drive the current, otherwise they agglomerate and get stuck on the gel. The biggest problem, however, is obtaining an appropriate calibration curve that relates electrophoretic mobility to effective size. As electrophoretic mobility depends on both size and charge, any calibration curve for size can only be valid for objects of similar charge. Furthermore, the physical properties such as stiffness and flexibility of the particles used to obtain

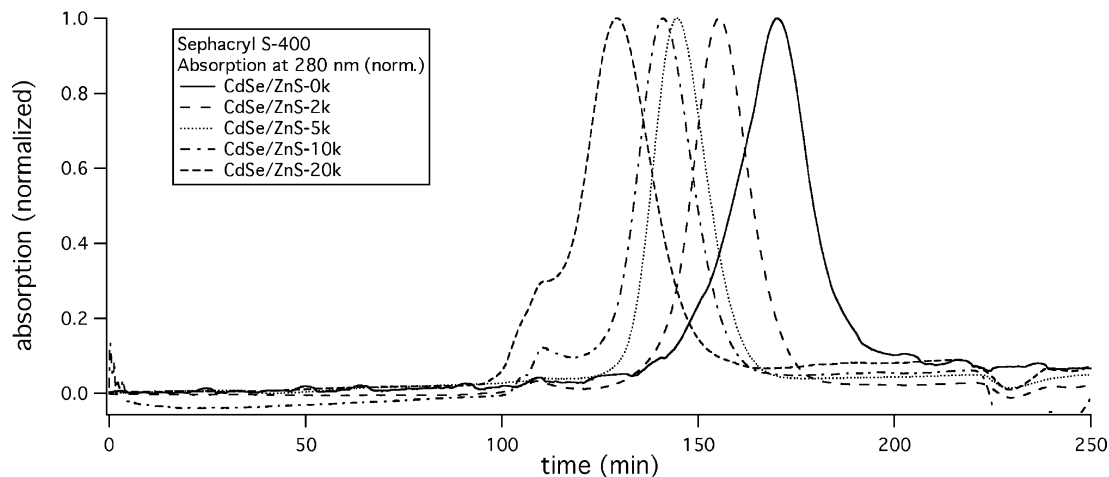


Figure 2. Size exclusion chromatograph (SEC) with a Sphacryl S-400 filled column of CdSe/ZnS nanoparticles whose surface is saturated with PEG molecules of different molecular weight (no PEG, 2 kDa, 5 kDa, 10 kDa, 20 kDa). Plotted is the absorption of the eluted solution versus the elution time. The bigger the particles are, due to the attachment of PEG of higher molecular weight, the earlier they are eluted from the column.

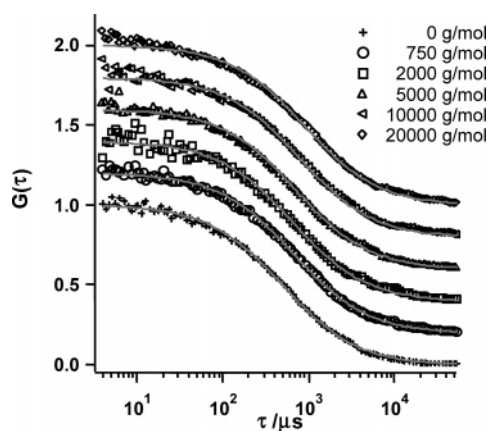


Figure 3. Autocorrelation functions $G(\tau)$ obtained from the FCS data for polymer-coated CdSe/ZnS particles whose surface is saturated with PEG molecules of different molecular weight (750 g/mol, 2 kg/mol, 5 kg/mol, 10 kg/mol, 20 kg/mol). The curves for the respective particles are shifted along the y -axis for the purpose of better visualization. The particles with no PEG attached are referred to as particles with PEG of molecular weight 0 (bottom graph). The experimental data were fitted with an analytical function (shown as gray lines), which yielded the effective diffusion coefficient as one fit parameter (see SI §V).

the calibration curve must be similar to those of the particles that are to be investigated. Basically, two different types of particles could be used in order to obtain calibration curves: biological macromolecules or colloidal nanoparticles. We have tried oligonucleotides^{19,20} as well as proteins for calibration, but both yielded very different mobility values compared to the ones obtained for colloidal nanoparticles. As linear flexible molecules, oligonucleotides can move in a different way through the pores of a gel compared to rigid inorganic colloidal nanoparticles. On the other hand, the surface charge density of oligonucleotides is, in first order, constant, therefore oligonucleotides are sorted by size and not by charge. In contrast to average oligonucleotides, proteins possess a secondary and tertiary structure and can be thought of in crude approximation as elastic spherical particles. However, proteins can have different surface charge densities comprising the full spectra from negative to neutral to positive. Because it is hard to find a set of proteins with different sizes but with the same charge density as the particles that are to be investigated, proteins are also not suited as standard particles for obtaining a calibration curve that relates electrophoretic mobilities to size. Therefore we have chosen inorganic colloidal nanoparticles of different size but with identical

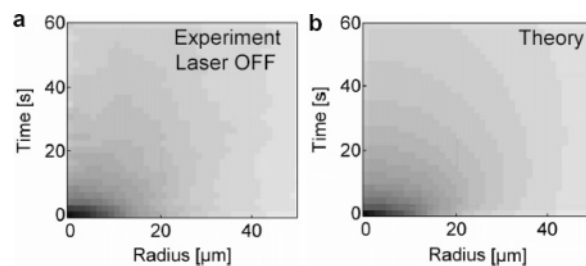


Figure 4. Thermophoresis and back-diffusion of nanometer-sized particles in solution. Thermodiffusion is used to form a concentration gradient in solution by heating a micrometer-sized spot. (a) (experiment) The graph shows the development of radial concentration averages over time after the heating laser is switched off (black: low concentration; gray: high concentration). As can be seen from the plot, the concentration inhomogeneity relaxes within 60 s. The data shown correspond to a particle size of approximately 30 nm in diameter. (b) (theory) The diffusion constant D is obtained by performing 1D finite element simulations with D as a free parameter, until the theory in b matches the experiment in a.

negatively charged surface coatings (bis(*p*-sulfonatophenyl)-phenylphosphine dihydrate) as size standards. There are known problems for these standards as well. First, there is an inherent uncertainty in the standard, as the effective hydrodynamic diameter is not known and is assumed to be the hard core Au particle diameter plus 2 times the length of the phosphine molecules, without taking into account the cloud of counterions.²⁰ However, comparison with the literature data obtained from dynamic light scattering shows that they are in good agreement with the assumed values. Second, attached macromolecules (such as DNA²⁰) form a soft shell around the hard inorganic core, which can be compressed by the gel. This can be seen in the data of Tables 2 and 3: the effective diameters derived from 1% agarose gels are always larger than the ones from 2% agarose gels, as the soft shell is compressed more on gels of higher percentage. This difference in data obtained with gels of different percentages has already been observed with DNA-modified sulfonate-stabilized Au particles.²⁰ Even in this case where there is only a minor influence of charge on the electrophoretic mobilities, the diameters obtained with gels of different percentages differed significantly, whereby the differences were most significant for long DNA strands and particles with a lot of attached DNA (= thick soft shells). In this study, PEG molecules were used for particle modification. As has already been reported,¹⁴ attachment of sufficient amounts of PEG to negatively charged polymer-coated particles can reverse

the polarity of the particles to a positive net charge, so that they migrate toward the negative electrode during gel electrophoresis (see Figure 1). This effect might be due to positive ions adsorbed to the PEG.⁵⁶ At any rate, this charge effect makes the determination of effective diameters of PEGylated particles with gel electrophoresis almost impossible. Due to the charge effect, the derived diameters are too large, and, for particles saturated with long PEG, no diameter can be derived due to the change in polarity (see Tables 2 and 3). The more PEG is attached per particle and the higher the molecular weight of the PEG, the more unreliable the results become. Although, in our experience, gel electrophoresis is the most sensitive of the here-described methods to resolve changes in size (e.g., the attachment of a single molecule), reliable absolute numbers of effective diameters can be only derived under very restricted conditions when the charge density of the sample to be investigated is highly similar to that of the particles used as size standards.

Size Exclusion Chromatography. Analogous to gel electrophoresis, SEC is not only an analytical method, but particles of different diameter can be fractionated on a preparative scale. Here, sorting by size is also achieved by a porous matrix, but, in contrast to gel electrophoresis where particles are driven by an electric current and small particles run faster, in SEC smaller particles are retarded because they can access a larger pore volume of the column packing. For all the columns used in this study, the resolution by size was lower for SEC compared to gel electrophoresis, since, with SEC, particles with zero, one, two, three, and so forth PEG molecules bound per particle could never be separated, while this was easily achieved with gel electrophoresis. Size measurements with both methods rely on appropriate size standards. In SEC, charge effects, that is, electrostatic interaction of charged particles with charges in the gel, are typically reduced by a mobile phase with a high salt concentration that screens residual charges of the column material. Unfortunately, this rules out the use of the sulfonate-stabilized Au particles that were used for gel electrophoresis as size standards, as these particles tend to agglomerate at high salt concentrations and get stuck in the columns. We therefore used globular proteins as size standards, as we could exclude charge effects as in the case of gel electrophoresis. Good estimates for effective hydrodynamic diameters exist for many proteins. On the other hand, the size range of available proteins is limited. We were unable to find spherically shaped (globular) proteins with a diameter as large as the largest of our PEG-modified nanoparticles (ca. 40 nm). The derived effective diameters for PEGylated nanoparticles from the extrapolated calibration curve are therefore more reliable the smaller the particles are (see Tables 2 and 3 and Figure 2).

Fluorescence Correlation Spectroscopy. Unlike gel electrophoresis or SEC, FCS is a purely analytical method and does not allow for separation and subsequent collection of fractions of particles with different diameters. The effective diameters derived from the FCS measurements (see Table 2 and Figure 3) are consistent with our previous findings^{11,41} and also consistent within themselves. The more and the longer PEG is added to the particles, the bigger the measured effective diameters are. Since FCS is based on single-particle experiments, each effective diameter reported in Table 2 corresponds to the mean value of the diameters of hundreds of particles from each sample. Within one sample series (i.e., different PEGs have been attached to the same batch of polymer-coated particles and the measurements were performed directly after each other with exactly the same FCS setup conditions), even the attachment

of single PEG molecules could be resolved, that is, the resolution limit is better than that for the increase in diameters for particles upon attachment of zero, one, two, and three PEGs per particle (see Table 2). However, the absolute values of effective diameters that have been recorded on the same type of particles but under different experimental conditions (i.e., when the particles were extracted from different gels before the measurements, when the FCS setup was recalibrated, etc.) vary significantly. As an example, we take the mean diameters for plain polymer-coated particles (i.e., zero PEGs per particle) from the different series from Table 2. The mean effective diameter and standard deviation of the five different samples ($\langle d_{\text{eff,FCS}} \rangle = \langle 20.5 \text{ nm}, 20.1 \text{ nm}, 25.0 \text{ nm}, 22.2 \text{ nm}, 19.4 \text{ nm} \rangle$) is $22.0 \pm 2.8 \text{ nm}$. The standard deviation has to be seen as an error bar for absolute measurements. The error bar is in the same range as the increase in the particle diameter upon the attachment of individual PEG molecules per particle. We therefore conclude that, although relative changes in the effective particle diameter upon the attachment of molecules within the same batch of particles and under the same setup conditions can be resolved with good precision, there is a significant error of about 3 nm in the determination of absolute effective diameters. There are two main sources for systematic errors in deriving absolute effective diameters: (i) Although FCS does not need a size standard, the focal volume has to be calibrated for each set of measurements with a dye molecule of known diffusion constant and thus known hydrodynamic diameter. Each error of the calibration is propagated to the results of the following measurements. (ii) In contrast to organic fluorophores, colloidal quantum dots exhibit no exponential triplet state decay but rather blinking behavior on all time-scales, which influences the recorded fluorescence intensity time traces. To our knowledge, so far, no analytical expression has been derived to account for this fact.^{11,41,42}

Thermophoresis. The values obtained by thermophoresis increase as expected with the molecular weight of the covalently coupled PEG molecules. The method measures the mean diffusion coefficients of the whole ensemble. Species without or with less surface modification would, in principle, lead to a higher overall diffusion coefficient and smaller radius, respectively. The sizes obtained for nanoparticles saturated with PEG molecules are listed in Table 2, and a typical experiment is shown in Figure 4. In contrast to gel electrophoresis and SEC, no calibration curve of size standards is needed to obtain the effective diameters. Although thermophoresis, like FCS, is based on obtaining effective diameters by measuring the diffusion of the dispersed particles, the values obtained with both methods differ significantly (see Table 2). The standard deviation in the measurements between similar samples is in the same range as that with FCS (polymer-coated CdSe/ZnS with no PEG: $\langle d_{\text{eff,Therm}} \rangle = \langle 8.2 \text{ nm}, 12.2 \text{ nm} \rangle = 10.2 \pm 2.8 \text{ nm}$; see last column of Table 2; the deviations within one method are attributed to variations in the sample, e.g., due to differences in the gel extraction procedure). The difference in the effective diameter of about a factor of 2 ($\langle d_{\text{eff,Therm}} \rangle \approx 10 \text{ nm}$; $\langle d_{\text{eff,FCS}} \rangle \approx 22 \text{ nm}$) for plain polymer-coated nanoparticles as determined with thermophoresis and FCS can therefore not be explained by the resolution limit due to sample variations ($\approx 3 \text{ nm}$) of both methods. Although we cannot explain the origin of this discrepancy, we speculate that it might arise from the different particle concentrations used for the measurements. Whereas FCS is a single-molecule-based method and thus requires extremely diluted particle solutions, thermophoresis is an ensemble-based method, and typically more

TABLE 5: Polymer-Coated Au and CdSe/ZnSe Nanoparticles Coated with Saturated Layers of PEG Molecules of Different Molecular Weight M_w^a

M_w (PEG) [g/mol]	$\langle d_{\text{eff}} \rangle_{\text{SEC}}$ [nm] Au core	$\langle d_{\text{eff}} \rangle_{\text{SEC}}$ [nm] CdSe/ZnS core	$\langle d_{\text{eff}} \rangle_{\text{FCS}}$ [nm] CdSe/ZnS core	$\langle d_{\text{eff}} \rangle_{\text{Therm}}$ [nm] CdSe/ZnS core	$1/2\Delta d_{\text{eff,SEC}}$ [nm] Au core	$1/2\Delta d_{\text{eff,SEC}}$ [nm] CdSe/ZnS core	$1/2\Delta d_{\text{eff,FCS}}$ [nm] CdSe/ZnS core	$1/2\Delta d_{\text{eff,Therm}}$ [nm] Au core	$1/2\langle \Delta d_{\text{eff}} \rangle$ [nm]	$d_{\text{eff,PEG}}$ [nm]
0	11.1	12.6	19.4	12.2						
750	12.5	14.6	25.4	22.0	0.7	1.0	3.0	4.9	2.4 ± 2.0	1.5
2000	16.5	18.3	25.6	23.6	2.7	2.9	3.1	5.7	3.6 ± 1.4	2.7
5000	21.0	23.9	27.6	25.0	5.0	5.7	4.1	6.4	5.3 ± 1.0	4.5
10000	28.8	26.2	30.2	30.0	8.9	6.8	5.4	8.9	7.5 ± 1.7	6.6
20000	34.8	34.8	34.2	40.0	11.9	11.1	7.4	13.9	11.1 ± 2.7	9.7

^a The first line hereby corresponds to plain polymer-coated nanoparticles without PEG modification. In columns 2–5, the mean effective diameters $\langle d_{\text{eff}} \rangle$ of the particles as determined with different methods are listed. These values originate from the data in Tables 2 and 3. The thickness of the PEG layers of different molecular weight around polymer-coated particles are derived as half of the difference of the total diameters of the PEG-coated and the plain polymer-coated particles: $1/2\Delta d_{\text{eff}}(M_w(\text{PEG}) = X) = (\langle d_{\text{eff}}(M_w(\text{PEG}) = X) \rangle - \langle d_{\text{eff}}(M_w(\text{PEG}) = 0) \rangle)/2$. These values are listed in columns 6–9. In column 10, the mean thickness of the PEG layers (as the average value of the different methods) $1/2\Delta d_{\text{eff}}$ is given. The last column shows the diameters of free PEG molecules as calculated with Formula 3.⁵⁵

concentrated particle solutions are used in order to obtain signals with sufficient intensity. Particle–particle interaction plays a different role under both conditions. Also the statistical effect of a certain amount of aggregated particles is different. We estimate the relative concentration of aggregates to contribute less than linearly to the diffusion coefficient measured by thermophoresis, since larger particles are depleted more strongly and the back diffusion is slower. Thus, the measured signal stems mostly from single-particle diffusion. The role of particle interactions will be analyzed in future experiments under optimized conditions with particle concentrations of less than 10 nM. This would allow direct comparison with FCS experiments. The values obtained with SEC in ensemble measurements of relatively concentrated particle solutions for plain polymer-coated particles correspond more to the values obtained with thermophoresis than those obtained with FCS, which also gives some indication about the importance of the particle concentration used for the measurements.

Thickness of Organic Coating Layers. In the following, we focus on the polymer-coated particles according to our own procedure (Tables 2 and 3). The mean value of all our different methods for the effective diameters of polymer-coated CdSe/ZnS is $\langle d_{\text{eff,gel}}, (d_{\text{eff,FCS}}), d_{\text{eff,SEC}}, d_{\text{eff,Therm}} \rangle = \langle 14.4, 12.6, (19.5), 12.2 \rangle = 13.1 \pm 1.2$ nm (14.7 ± 3.4 nm with the value obtained with FCS), and, for Au nanoparticles, it is $\langle d_{\text{eff,gel}}, d_{\text{eff,SEC}}, d_{\text{eff,Therm}} \rangle = \langle 12.5, 11.6 \rangle = 12.0 \pm 0.6$ nm. The hard core diameter as determined by TEM is 5.3 nm for CdSe/ZnS and 4.6 nm for the Au nanoparticles. This leads to an effective thickness of the organic shell of $(13.1 - 5.3)$ nm/2 = 3.9 nm in the case of CdSe/ZnS and $(12.0 - 4.6)$ nm/2 = 3.7 nm in the case of Au. Besides the values obtained with FCS, the values derived with the other techniques correspond well, and we conclude that, after polymer coating, the effective thickness of the organic layer around the inorganic particle core is around 3.5–4.0 nm. Whereas this value for the plain polymer-coated particles seems quite reliable, the uncertainties in absolute size determination get higher the larger the molecules attached to the polymer shell are. The addition of a saturated layer of 20 kDa PEG molecules to the polymer surface increases the thickness of the organic layer by $\langle \Delta d_{\text{eff,gel}}, \Delta d_{\text{eff,FCS}}, \Delta d_{\text{eff,SEC}} \rangle / 2 = \langle (34.8 - 12.6), (34.2 - 19.4), (40.0 - 12.2) \rangle$ nm/2 = 10.8 ± 3.3 nm in the case of the CdSe/ZnS particles.

In Table 5, the thickness of the saturated layer of the PEG molecules bound to the particle surface is compared with the effective diameter of free PEG molecules as determined by Formula 3, whereby the thickness of the PEG layer was calculated as half of the difference in diameter of the PEG-

coated and plain polymer-coated particles. All obtained values for the PEG molecules bound to the nanoparticles are slightly larger than those of free PEG molecules. This finding can be explained by a more stretched configuration of the random coil of the PEG molecules when they are attached by one end to the densely occupied surface of a saturated nanoparticle, compared to the presumably more symmetric configuration of PEG molecules in free solution. In any case, the agreement demonstrates that relative increments in particle size can be determined with much higher accuracy than absolute diameters.

Conclusions

The total particle diameter can be estimated by the core diameter plus 2 times the thickness of the organic layer, which is, for simple coatings, the length of the surfactant molecule. While this eventually works well for short molecules when the length of these molecules is small compared to the particle, it becomes more complicated for longer and more complex molecules or even complex polymer (multi)layers. Here the size depends strongly on assumptions about the steric configuration of the molecules on the curved nanoparticle surface. Furthermore, the effective hydrodynamic diameter also depends on hydration: interaction of the particles with the solvent results in larger effective sizes,⁵⁷ even in the most simple case where the stabilizer molecules form a monolayer around the inorganic core. Although several studies exist in which the effective diameters of particles have been measured, most of these studies are either based on only one method or only one type of particle surface.^{24,58,59} A more detailed discussion can be found in the Supporting Information.

The more molecules are attached and thus the bigger the particles become, the more unreliable size measurements are. First, the hybrid nature of the particles with a rigid inner inorganic core and a soft organic shell becomes more pronounced, which eventually leads to problems for the methods in which the measurements take place in a matrix that can compress the particles. Especially, a random coil of a linear polymer such as PEG can be easily deformed depending on the technique used for the size determination. Second, for the methods using calibration with size standards, there is the problem of a lack of appropriate size standards of sufficient size. Third, the charge composition can also change (in particular, if positively charged molecules are attached), which leads to the failure of gel electrophoresis but might also affect the other methods.

Thus, depending on the actual particle nature but also on the intended application, the adequate method for measurement has

to be chosen with great care. For instance, when particles are designed to enter into pores, the diameter determined by gel electrophoresis or SEC might be better suited than the one determined by free diffusion.

Different methods to measure effective sizes of colloidal nanoparticles are based on different physical principles, resulting in deviations of the resulting particle diameters between the different methods. This finding is not surprising and points to a general problem and uncertainty: although within one measurement effective diameters can be determined in a consistent way with relatively small errors, bigger discrepancies arise between values obtained with different methods. This implies that the comparison with control samples (e.g., before and after a certain conjugation step) remains indispensable and that all derived absolute numbers for nanoparticle diameters have to be considered with care.

Acknowledgment. The authors would like to thank Andrea Rauh for help with the analysis of the TEM images and Dr. Fritz Simmel and Prof. Dr. Joachim Rädler for helpful discussion. The authors are grateful to Prof. Dr. Joachim Rädler for providing the FCS setup and expertise of his institute. Quantum dots with organic and streptavidin coating were a gift from Quantum Dots Corp. The project was funded by the Deutsche Forschungsgemeinschaft (DFG Emmy Noether Grant) and the European Union (STREP NanoInteract grant). M.Z. is grateful for a fellowship from the International Doctorate Program Nano-Bio-Technology at the Center for Nanoscience.

Supporting Information Available: Details of particle synthesis, TEM analysis, gel electrophoresis, SEC, FCS, and thermophoresis experiments, and a comparison of the different methods. This material is available free of charge via the Internet at <http://pubs.acs.org>.

References and Notes

- (1) Scher, E. C.; Manna, L.; Alivisatos, A. P. *Philos. Trans. R. Soc. London, Ser. A* **2002**, *361*, 241.
- (2) Kumar, S.; Nann, T. *Small* **2006**, *2*, 316.
- (3) Kudera, S.; Carbone, L.; Zanella, M.; Cingolani, R.; Parak, W. J.; Manna, L. *Phys. Status Solidi C* **2006**, *203*, 1329.
- (4) Templeton, A. C.; Wuelfing, W. P.; Murray, R. W. *Acc. Chem. Res.* **2000**, *33*, 27.
- (5) Michalet, X.; Pinaud, F. F.; Bentolila, L. A.; Tsay, J. M.; Doose, S.; Li, J. J.; Sundaresan, G.; Wu, A. M.; Gambhir, S. S.; Weiss, S. *Science* **2005**, *307*, 538.
- (6) Pellegrino, T.; Kudera, S.; Liedl, T.; Javier, A. M.; Manna, L.; Parak, W. J. *Small* **2005**, *1*, 48.
- (7) Fischer, C.-H.; Lilie, J.; Weller, H.; Katsikas, L.; Henglein, A. *Ber. Bunsen-Ges. Phys. Chem.* **1989**, *93*, 61.
- (8) Fischer, C.-H.; Weller, H.; Katsikas, L.; Henglein, A. *Langmuir* **1989**, *5*, 429.
- (9) Eychmüller, A.; Katsikas, L.; Weller, H. *Langmuir* **1990**, *6*, 1605.
- (10) Wu, M. X.; Liu, H.; Liu, J.; Haley, K. N.; Treadway, J. A.; Larson, J. P.; Ge, N.; Peale, F.; Bruchez, M. P. *Nat. Biotechnol.* **2003**, *21*, 41.
- (11) Pellegrino, T.; Manna, L.; Kudera, S.; Liedl, T.; Koktysh, D.; Rogach, A. L.; Keller, S.; Rädler, J.; Natile, G.; Parak, W. J. *Nano Lett.* **2004**, *4*, 703.
- (12) Luccardini, C.; Tribet, C.; Vial, F.; Marchi-Artzner, V.; Dahan, M. *Langmuir* **2006**, *22*, 2304.
- (13) Nann, T. *Chem. Commun.* **2005**, *2005*, 1735.
- (14) Sperling, R. A.; Pellegrino, T.; Li, J. K.; Chang, W. H.; Parak, W. J. *Adv. Funct. Mater.* **2006**, *16*, 943.
- (15) Zanchet, D.; Moreno, M. S.; Ugarte, D. *Phys. Rev. Lett.* **1999**, *82*, 5277.
- (16) Fink, J.; Kiely, C. J.; Bethell, D.; Schiffrin, D. J. *Chem. Mater.* **1998**, *10*, 922.

- (17) Yonezawa, T.; Onoue, S.-y.; Kimizuka, N. *Langmuir* **2001**, *17*, 2291.
- (18) Zanchet, D.; Micheel, C. M.; Parak, W. J.; Gerion, D.; Alivisatos, A. P. *Nano Lett.* **2001**, *1*, 32.
- (19) Parak, W. J.; Pellegrino, T.; Micheel, C. M.; Gerion, D.; Williams, S. C.; Alivisatos, A. P. *Nano Lett.* **2003**, *3*, 33.
- (20) Pellegrino, T.; Sperling, R. A.; Alivisatos, A. P.; Parak, W. J. *J. Biomed. Biotechnol.*, submitted for publication, 2007.
- (21) Pinaud, F.; King, D.; Moore, H.-P.; Weiss, S. *J. Am. Chem. Soc.* **2004**, *126*, 6115.
- (22) Song, X.; Li, L.; Qian, H.; Fang, N.; Ren, J. *Electrophoresis* **2006**, *27*, 1341.
- (23) Nehilla, B. J.; Vu, T. Q.; Desai, T. A. *J. Phys. Chem. B* **2005**, *109*, 20724.
- (24) Pons, T.; Uyeda, H. T.; Medintz, I. L.; Mattoussi, H. *J. Phys. Chem. B* **2006**, *110*, 20308.
- (25) Wilcoxon, J. P.; Provencio, P. P. *J. Phys. Chem. B* **2005**, *109*, 13461.
- (26) Siebrands, T.; Giersig, M.; Mulvaney, P.; Fischer, C.-H. *Langmuir* **1993**, *9*, 2297.
- (27) Fischer, C.-H.; Giersig, M.; Siebrands, T. *J. Chromatogr., A* **1994**, *670*, 89.
- (28) Fischer, C.-H.; Kenndler, E. *J. Chromatogr., A* **1997**, *773*, 179.
- (29) Wei, G.-T.; Liu, F.-K. *J. Chromatogr., A* **1999**, *836*, 253.
- (30) Wei, G.-T.; Liu, F.-K.; Wang, C. R. C. *Anal. Chem.* **1999**, *71*, 2085.
- (31) Jimenez, V. L.; Leopold, M. C.; Mazzitelli, C.; Jorgenson, J. W.; Murray, R. W. *Anal. Chem.* **2003**, *75*, 199.
- (32) Al-Somali, A. M.; Krueger, K. M.; Falkner, J. C.; Colvin, V. L. *Anal. Chem.* **2004**, *76*, 5903.
- (33) Krueger, K. M.; Al-Somali, A. M.; Falkner, J. C.; Colvin, V. L. *Anal. Chem.* **2005**, *77*, 3511.
- (34) Kuga, S. *J. Chromatogr., A* **1981**, *206*, 449.
- (35) Holtzhauer, M.; Rudolph, M. *J. Chromatogr., A* **1992**, *605*, 193.
- (36) Magde, D.; Elson, E.; Webb, W. W. *Phys. Rev. Lett.* **1972**, *29*, 705.
- (37) Eigen, M.; Rigler, R. *Proc. Natl. Acad. Sci. U.S.A.* **1994**, *91*, 5740.
- (38) Schwille, P.; Bieschke, J.; Oehlenschläger, F. *Biophys. Chem.* **1997**, *66*, 211.
- (39) Krichevsky, O.; Bonnet, G. *Rep. Prog. Phys.* **2002**, *65*, 251.
- (40) Zhang, P.; Li, L.; Dong, C.; Qian, H.; Ren, J. *Anal. Chim. Acta* **2005**, *546*, 46.
- (41) Liedl, T.; Keller, S.; Simmel, F. C.; Rädler, J. O.; Parak, W. J. *Small* **2005**, *1*, 997.
- (42) Doose, S.; Tsay, J. M.; Pinaud, F.; Weiss, S. *Anal. Chem.* **2005**, *77*, 2235.
- (43) Dong, C.; Bi, R.; Qian, H.; Li, L.; Ren, J. *Small* **2006**, *2*, 534.
- (44) Jin, T.; Fujii, F.; Yamada, E.; Nodasaka, Y.; Kinjo, M. *J. Am. Chem. Soc.* **2006**, *128*, 9288.
- (45) Duhr, S.; Arduini, S.; Braun, D. *Eur. Phys. J. E* **2004**, *15*, 277.
- (46) Duhr, S.; Braun, D. *Phys. Rev. Lett.* **2006**, *96*, 168301.
- (47) Duhr, S.; Braun, D. *Proc. Natl. Acad. Sci. U.S.A.* **2006**, *103*, 19678.
- (48) Reiss, P.; Bleuse, J.; Pron, A. *Nano Lett.* **2002**, *2*, 781.
- (49) Dabbousi, B. O.; Rodriguez-Viejo, J.; Mikulec, F. V.; Heine, J. R.; Mattoussi, H.; Ober, R.; Jensen, K. F.; Bawendi, M. G. *J. Phys. Chem. B* **1997**, *101*, 9463.
- (50) Yu, W. W.; Qu, L.; Guo, W.; Peng, X. *Chem. Mater.* **2003**, *15*, 2854.
- (51) Brust, M.; Walker, M.; Bethell, D.; Schiffrin, D. J.; Whyman, R. *J. Chem. Soc., Chem. Commun.* **1994**, 801.
- (52) Mori, S.; Barth, H. G. *Size Exclusion Chromatography*; Springer: New York, 1999.
- (53) Hagel, L. Gel Filtration. In *Protein Purification. Principles, High Resolution Methods and Applications*, 2nd ed.; Janson, J.-C., Ryden, L., Eds.; John Wiley & Sons: New York, 1998.
- (54) Amediek, A.; Hausteiner, E.; Scherfeld, D.; Schwille, P. *Single Mol.* **2002**, *3*, 201.
- (55) Fee, C. J.; Alstine, J. M. V. *Bioconjugate Chem.* **2004**, *15*, 1304.
- (56) Sartori, R.; Sepulveda, L.; Quina, F.; Lissi, E.; Abuin, E. *Macromolecules* **1990**, *23*, 3878.
- (57) Xu, X.; Rosi, N. L.; Wang, Y.; Huo, F.; Mirkin, C. A. *J. Am. Chem. Soc.* **2006**, *128*, 9286.
- (58) Smith, A. M.; Duan, H.; Rhyner, M. N.; Ruan, G.; Nie, S. *Phys. Chem. Chem. Phys.* **2006**, *8*, 3895.
- (59) Yu, W. W.; Chang, E.; Falkner, J. C.; Zhang, J.; Al-Somali, A. M.; Sayes, C. M.; Johns, J.; Drezek, R.; Colvin, V. L. *J. Am. Chem. Soc.* **2007**, *129*, 2871.

Research Article

Gel Electrophoresis of Gold-DNA Nanoconjugates

T. Pellegrino,^{1,2,3} R. A. Sperling,^{1,4} A. P. Alivisatos,² and W. J. Parak^{1,2,4}

¹Center for Nanoscience, Ludwig Maximilians University Munich, 80799 München, Germany

²Department of Chemistry and Lawrence Berkeley National Lab, University of California, Berkeley, CA 94720, USA

³National Nanotechnology Laboratory, INFN, 73100 Lecce, Italy

⁴Fachbereich Physik, Philipps Universität Marburg, 35037 Marburg, Germany

Correspondence should be addressed to W. J. Parak, Wolfgang.parak@physik.uni-marburg.de

Received 20 July 2007; Accepted 13 December 2007

Recommended by Marek Osinski

Gold-DNA conjugates were investigated in detail by a comprehensive gel electrophoresis study based on 1200 gels. A controlled number of single-stranded DNA of different length was attached specifically via thiol-Au bonds to phosphine-stabilized colloidal gold nanoparticles. Alternatively, the surface of the gold particles was saturated with single stranded DNA of different length either specifically via thiol-Au bonds or by nonspecific adsorption. From the experimentally determined electrophoretic mobilities, estimates for the effective diameters of the gold-DNA conjugates were derived by applying two different data treatment approaches. The first method is based on making a calibration curve for the relation between effective diameters and mobilities with gold nanoparticles of known diameter. The second method is based on Ferguson analysis which uses gold nanoparticles of known diameter as reference database. Our study shows that effective diameters derived from gel electrophoresis measurements are affected with a high error bar as the determined values strongly depend on the method of evaluation, though relative changes in size upon binding of molecules can be detected with high precision. Furthermore, in this study, the specific attachment of DNA via gold-thiol bonds to Au nanoparticles is compared to nonspecific adsorption of DNA. Also, the maximum number of DNA molecules that can be bound per particle was determined.

Copyright © 2007 T. Pellegrino et al. This is an open access article distributed under the Creative Commons Attribution License, which permits unrestricted use, distribution, and reproduction in any medium, provided the original work is properly cited.

1. INTRODUCTION

DNA-functionalized gold nanoparticles are an interesting system with applications ranging from biological sensors to the construction of self-assembled materials. Experiments are based on attaching single-stranded DNA molecules via thiol-gold bonds to the surface of Au nanoparticles and a subsequent self-assembly process of these conjugates by making use of base pairing of complementary DNA molecules [1–5]. For example, by employing Au-DNA conjugates, several groups have developed schemes to detect target DNA sequences [6] and to assemble nanoparticles into macroscopic materials [7, 8]. DNA-functionalized Au nanoparticles are the building blocks for the above-mentioned experiments. Therefore, it is of great interest to investigate the properties of these conjugates in detail.

Due to the high affinity of thiol groups to gold surfaces, thiol-modified DNA molecules can be directly bound to the

surface of citrate- or phosphine-stabilized Au nanoparticles [9, 10]. Although commonly a random number of DNA molecules are attached per Au nanoparticle [1], also particles with an exactly defined number of one, two, or three attached DNA molecules per nanoparticles can be obtained [11–15]. Certainly, several parameters have significant influence on the properties of Au-DNA conjugates, such as coverage of the Au surface with DNA, configuration of the attached DNA molecules, and hybridization efficiency of DNA attached to Au surfaces. These parameters are strongly connected. The degree of DNA coverage will influence the DNA conformation, which, in turn, will affect the hybridization efficiency. Also, nonspecific adsorption has to be considered.

A body of experiments investigating these parameters has been reported for DNA attached to flat Au surfaces using different techniques such as atomic force microscopy (AFM) [16–18], surface plasmon resonance (SPR) spectroscopy [19–21], radioisotopic techniques [22, 23], ellipsometry [23], and X-ray photoelectron spectroscopy (XPS) [23]. These experiments allow for a detailed picture of DNA bound to planar gold surfaces and the results have clarified

T. Pellegrino and R. Sperling contributed equally to the work.

the binding mechanism, the surface coverage, the hybridization efficiency, and the role of nonspecific adsorption, all in dependence of the length of the DNA.

Since the effect of surface curvature has to be taken into account [24], the results obtained for planar Au surfaces may be transferred to spherical Au nanoparticles only under certain restrictions. The surface coverage of Au nanoparticles with DNA has been investigated using the displacement of fluorescence-labeled DNA molecules with mercaptoethanol [25] and by gel electrophoresis [26]. Also, the conformation of bound DNA [27, 28], hybridization [29], and the role of nonspecific adsorption [26, 28, 30] have been investigated for Au nanoparticles.

In this report, we present a detailed study of electrophoretic mobility of Au-DNA conjugates. With this study, we want to determine the possibilities and limitations of this technique. Besides our own previous work [27, 31], also other groups [28, 32, 33] have recently reported about the possibility to extract effective diameters for bioconjugated colloidal nanoparticles from electrophoretic mobilities. The aim of this study is, in particular, to investigate the limitations of this analysis.

2. MATERIALS AND METHODS

2.1. Sample preparation

Citrate-coated gold nanoparticles of 5, 10, and 20 nm diameter were purchased from BBI/TED Pella (Redding, Calif, USA). In order to improve their stability in buffer solution, the adsorbed citrate molecules were replaced by a phosphine (bis(p-sulfonatophenyl)phenylphosphine dehydrate, dipotassium salt) [11]. The concentration of the Au nanoparticles was determined by UV/vis spectroscopy by using the molecular extinction coefficient of their absorption at the plasmon peak. Thiol- and Cy5-modified and unmodified single-stranded DNA were purchased from IDT (Coralville, Iowa, USA) or Metabion (München, Germany). All sequences can be found in the Supplementary Material (available online at doi: 10.1155/2007/26796). The concentration of the DNA was determined by UV/vis spectroscopy by using the molecular extinctions coefficient of their absorption at 260 nm. The thiol-modified and plain DNA were added to the phosphine-coated Au nanoparticles at pH = 7.3, $c(\text{NaCl}) = 50 \text{ mM}$, and samples were incubated for some hours up to several days [11, 27]. Generally, in such experiments, DNA is always added in large excess, thus that the number of attached molecules is related but not fully controlled by the stoichiometry of DNA:Au-NP because of the rather low binding yield.

2.2. Gel electrophoresis experiments

The resulting Au-DNA conjugates were loaded on 0.5%–6% agarose gels (agarose: Gibco BRL, number 15510-027; $0.5 \times \text{TBE}$ buffer, pH 9) and run for one hour at 100 V [11, 27]. (Since 6% gels can be inhomogeneous due to their high viscosity, the data obtained with these gels have to be interpreted with care.) As reference, always unconjugated Au nanoparti-

cles of the same diameter were run on the same gel. In addition, gels with unconjugated Au nanoparticles of different diameter and free DNA of different length were run. The bands of the plain and DNA-conjugated Au nanoparticles were directly visible by the red color of the Au colloid and the free DNA was visualized by an attached fluorescence label (fluorescein, Cy3, or Cy5). The bands of the gels were photographed using a digital camera system (Eagle Eye III, Stratagene). The mobility of each sample was determined by measuring the position of each band referring to the start position where the samples had been loaded. This resulted in a comprehensive set of data which relates the mobility of Au-DNA conjugates to the diameter of the Au particles, where the relation between the amount and the length of the attached DNA, nonspecific versus specific attachment via thiol-gold bonds, and the gel percentage was studied.

2.3. Calculation of the effective diameter of the Au-DNA conjugates

Since mobility is not an illustrative quantity, we have attempted to convert the mobilities of Au-DNA conjugates in effective diameters. The evaluation of the gels in which plain Au-nanoparticles of known diameter were run yielded a calibration curve in which the mobility is plotted versus the diameter. By using this calibration curve, the mobility of the Au-DNA conjugates could be directly converted into effective diameters [27]. Alternatively, the mobility of Au-DNA conjugates at different agarose concentrations was used to obtain Ferguson plots [34] and fits of the Ferguson plots yielded the retardation coefficients [28]. First, Ferguson plots were made for plain Au-nanoparticles of known diameter and a calibration curve in which the retardation coefficients were plotted versus the particle diameter was obtained [28]. By using this calibration curve, the effective diameters of Au-DNA conjugates could be derived from the retardation coefficients derived from the Ferguson plots of the Au-DNA conjugates [28].

2.4. Determination of the maximum number of attached DNA molecules per particle

We have also quantified the maximum number of DNA molecules that can be attached per gold nanoparticle for particles with 5 nm and 10 nm diameter and single-stranded DNA with 8 and 43 bases. For this purpose, single-stranded DNA that had been modified with a thiol group on the 3' and a Cy5 dye on the 5' end has been attached via formation of thiol-Au bonds to the surface of Au particles. DNA was added in different DNA to Au ratios and the conjugates were run on an agarose gel. The more DNA bound per Au nanoparticle, the more the band of this conjugate was retarded on the gel [27]. At a certain amount of added DNA, the retardation of the band of the conjugates did not further increase, which indicates that the Au surface is fully saturated with DNA [27]. The bands were extracted from the gel by cutting out the agarose piece that contained the band and immersing it into $0.5 \times \text{TBE}$ buffer solution. After two days, the Au-DNA conjugates had diffused out of the gel into the buffer. The

extraction procedure ensures that all DNA is really attached to the Au particles, since free DNA migrates in a much faster band. UV/vis spectra were recorded of the extracted Au-DNA conjugates. For each of the conjugates, the DNA concentration was determined by the Cy5 absorption and the Au concentration was determined by the absorption at the plasmon peak and from both concentrations the number of attached DNA molecules per particles was derived. As we quantified the number of attached Cy5 molecules only with absorption and not with fluorescence measurements, the effect that the fluorescence of Cy5 close to Au surfaces is quenched [35] did not interfere with our analysis.

All methods and additional experiments can be found in detail in the supplementary material.

3. RESULTS AND DISCUSSION

3.1. *The attachment of DNA to particles increases the effective diameter and thus lowers the electrophoretic mobility*

The attachment of DNA to Au nanoparticles can be clearly observed by gel electrophoresis [9, 11, 13, 26–28, 36–38]. The mobility of particles on the gel depends on two factors: size and charge. The bigger the size, the slower and the higher the charge, the faster particles will migrate. In the case of negatively charged Au particles (e.g., with citrate or phosphine molecules adsorbed to the particles), the attachment of negatively charged DNA molecules causes in first place an increase of size that can be seen as a retardation of the band of the gel [27]. If the change in charge dominated, then the mobility of the Au particles should be increased (addition of negative charge) or drastically decreased (addition of positive charge) up to change in the direction of migration. Although this effect has been observed for different systems [31, 39], it has not been observed for the Au-DNA conjugates used in this study. Upon attachment of DNA, the mobility of the resulting conjugates was always moderately decreased. Therefore, in agreement with previous reports, we assume throughout this manuscript that attachment of DNA to Au nanoparticles in first order increases the effective diameter of the conjugates which can be directly seen in the retardation of the band of the conjugates in gel electrophoresis experiments [9, 11, 26–28, 36–38].

3.2. *Generation of a calibration curve that relates electrophoretic mobilities to effective diameters*

One aim of this study was to obtain calibration curves in which measured electrophoretic mobilities m can be related to effective diameters d_{eff} . By running phosphine-stabilized Au particles of known diameter (the overall diameter of phosphine-coated Au NP was assumed as the core diameter plus two times 0.5 nm for the thickness of the phosphine layer and the smallest nanoparticle size used for calibration was 6 nm) on gels, by measuring their mobility, by fitting the data empirically with an exponential function, and by using the inverse of the fit function, we obtained a function in which the effective diameter of Au particles and Au-

TABLE 1: Experimentally obtained parameters for deriving effective diameters from electrophoretic mobilities for different gel percentages γ . The data have been derived by fitting an experimentally obtained dataset of electrophoretic mobilities of Au nanoparticles of known diameter and represent the mean values and standard deviations.

γ	A_γ	T_γ (nm)
0.5%	1.017 ± 0.015	189 ± 19
1%	1.049 ± 0.012	85.0 ± 3.7
2%	1.120 ± 0.024	37.7 ± 1.9
3%	1.236 ± 0.025	18.8 ± 0.8
4%	1.476 ± 0.061	10.3 ± 0.9
5%	1.759 ± 0.079	7.16 ± 0.66
6%	2.073 ± 0.083	5.77 ± 0.49

DNA conjugates can be directly calculated from their electrophoretic mobility:

$$d_{\text{eff}}(m) = -T_\gamma * \ln((m/m_{10\text{nm},\gamma})/A_\gamma) + 6 \text{ nm}. \quad (1)$$

The parameters for $\gamma = 0.5\%$, 1%, 2%, 3%, 4%, 5%, and 6% agarose gels are enlisted in Table 1. In order to enhance the accuracy by making relative instead of absolute measurements, we always normalized the mobilities m to the mobilities $m_{10\text{nm},\gamma}$ of plain phosphine-stabilized Au particles of 10 nm core diameter on the same gel. Therefore, although the primary data of all electrophoresis measurements are electrophoretic mobilities, we are discussing the experimental results in terms of effective diameters. The diameters have been obtained with the above-described formula from the mobility data.

Since obviously the effective diameter of Au-DNA conjugates is a fixed physical property, it should not depend on the form of measurement and analysis. We, therefore, compared the effective diameters derived from 1%, 2%, 3% gels via the respective mobility-diameter calibration curves and from Ferguson plots [34]. For the Ferguson plots, the mobility data from all gel percentages are required.

3.3. *Evaluation of the accuracy of effective diameters obtained from electrophoretic mobilities via mobility-diameter calibration curves*

The determined effective diameters for Au-DNA conjugates for Au particles saturated with DNA and for Au particles with only few DNA strands attached per particle are plotted in Figures 1 and 2 for DNA of different length. In all cases, regardless the length of the DNA, whether DNA was attached by specific thiol-gold linkage or by nonspecific adsorption, or whether only a few or a many as possible DNA molecules were bound per Au nanoparticles, the effective diameters derived with the mobility-diameter calibration curves are different for different gel percentages. Though most of the times the effective diameters derived from gels with higher percentage were found to be larger than the ones obtained from gels with lower percentage, also the opposite effect was observed within the experimental error bars (see, e.g., Figure 2). The

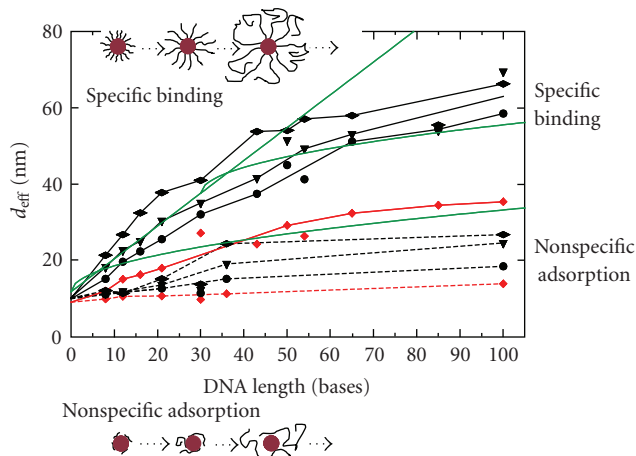


FIGURE 1: Effective diameter d_{eff} of Au-DNA conjugates for Au surfaces saturated with DNA. The surface of 10 nm phosphine-stabilized Au nanoparticles was saturated with single-stranded DNA of different lengths and the conjugates were run on 1%, 2%, and 3% gels. From the measured mobilities, the effective diameters of the conjugates were determined. The effective diameters obtained from 1%, 2%, and 3% gels are plotted in black with diamond, triangle, and circle symbols, the effective diameters obtained from Ferguson analysis are plotted in red. The effective diameters of conjugates in which the DNA was linked to the Au particles via specific thiol-gold bonds are connected with straight lines, the effective diameters of conjugates in which the DNA is nonspecifically adsorbed to the Au particles are connected with dotted lines. The green lines correspond to rudimentary theoretical models of the effective diameters of DNA molecules attached via thiol-gold to Au particles [27]. For fully stretched DNA (bottom curve), $d_{\text{eff,linear}}(N) = 10 \text{ nm} + 2 \cdot (0.92 \text{ nm} + N \cdot 0.43 \text{ nm})$, for randomly coiled DNA (top curve) $d_{\text{eff,coil}}(N) = 10 \text{ nm} + 2 \cdot (0.92 \text{ nm} + 2 \cdot [3^{-1} \cdot N \cdot 0.43 \text{ nm} \cdot 2 \text{ nm}]^{1/2})$, and for DNA partly stretched and partly coiled DNA (middle curve) $d_{\text{eff,mixed}}(N) = 10 \text{ nm} + 2 \cdot (0.92 \text{ nm} + 30 \cdot 0.43 \text{ nm} + 2 \cdot [3^{-1} \cdot (N - 30) \cdot 0.43 \text{ nm} \cdot 2 \text{ nm}]^{1/2})$ was used [27]. We assumed 0.92 nm for the length of the thiol-hydrocarbon (C_6) spacer at the reactive end of the DNA, 0.43 nm per base for the contour length and 2 nm for the persistence length [42, 43]. N corresponds to the number of bases.

effective diameters derived from Ferguson plots were always smaller than the ones derived from the mobility-diameter calibration curves. This clearly demonstrates a severe limitation of deriving effective diameters from electrophoretic mobilities. If always the effective diameters derived from the gel of higher percentage were smaller than the one derived from gels with lower percentage, one could have argued that the soft DNA shell around the rigid Au cores would be squeezed or compressed more while migrating through the gel of higher agarose concentration, which would lead to smaller effective diameters. However, since no clear correlation between the gel concentration and the derived effective diameters was observed, we have to consider the difference between the effective diameters that have been obtained from gels of different concentrations as error bars. The bigger the Au particles become due to attachment of DNA, the bigger the error in deriving their effective diameter from electrophoretic mobilities becomes. For example, according to Figure 1, the effective diameters of 10 nm Au particles saturated with 100

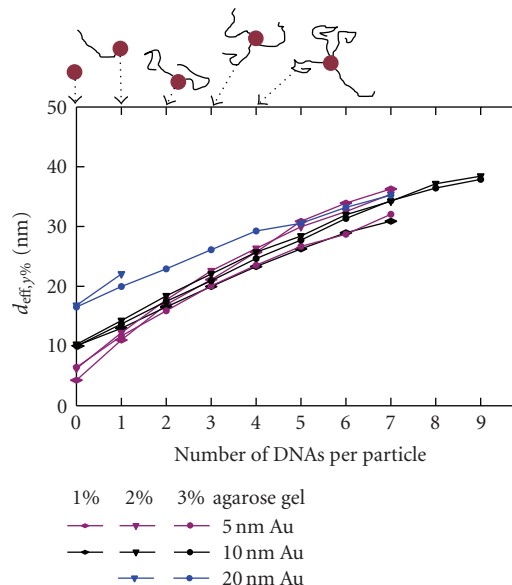


FIGURE 2: Effective diameter of Au-DNA conjugates with a discrete number of DNA molecules attached per Au nanoparticle. 10 nm Au particles were incubated with thiol-modified single-stranded DNA of 43 and 100 bases length and run on 1%, 2%, and 3% agarose gels. On the gels, particles with exactly 0, 1, 3, 4, ... DNA molecules attached per Au particle could be identified as discrete bands. From the mobilities of the bands on the gels, the effective diameters d_{eff} were derived by using a calibration curve that relates mobilities and diameters. The effective diameters corresponding to effective diameters derived from 1%, 2%, and 3% gels are plotted in black with diamond, triangle, and circle symbols, respectively. From the mobility data of the gels of different percentage effective diameters were also obtained by the Ferguson method and are plotted in red. The upper and lower sets of curves belong to the Au-DNA conjugates with 100 bases and 43 bases DNA, respectively.

bases DNA that is specifically linked via thiol-Au bonds are 66.3 nm, 69.5 nm, and 58.5 nm as determined from 1%, 2%, and 3% gels. We believe that from these data we can assume that the effective diameter of these conjugates is around 60 nm with an error bar of around 10 nm. From these and additional similar data (not shown), we conclude that deriving absolute effective diameters from electrophoretic mobilities via mobility-diameter calibration curves is possible only under certain restrictions. It is not sufficient to extract the data just from gels of one percentage. Only by using gels of different percentage an average value for the effective diameter and an estimate about the error can be obtained. Part of this limitation might be due to our principal assumption that in the case of phosphine-stabilized Au particles conjugated with DNA, the electrophoretic mobility is in first order only determined by the size of the conjugates. Charge effects may hamper obtaining more precise data for effective diameters. For other systems in which charge effects certainly will play a more important role [39], it might be even impossible to derive effective diameters from electrophoretic mobilities with the here-reported mobility-diameter calibration curves. It also has to be pointed out that the possible application of

the here-reported calibration curves is limited to relatively rigid objects similar in nature to Au nanoparticles. As these objects were used in first order to obtain the experimental data on which the calibration functions are based, the calibration functions certainly will not describe the diameters of soft objects, such as DNA, very well. A likely explanation for the deviation in the effective diameters obtained for the DNA-Au conjugates with the calibration functions for the gels of different percentage can be seen in the fact that the calibration functions are directly only applicable for Au particle-like rigid objects. Attaching soft objects as DNA to the Au particle surface changes their electrophoretic behavior so that the calibration curves can be only applied in a restricted way.

3.4. Evaluation of the accuracy of effective diameters obtained from Ferguson plots

We have also evaluated the possibility to obtain effective diameters of Au-DNA conjugates via Ferguson plots, as had already suggested by the group of Hamad-Schifferli [28]. From Figures 1 and 2, it is evident that the effective diameters obtained from Ferguson plots are always significantly smaller than the ones obtained from mobility-diameter calibration curves. It has to be pointed out that both evaluation methods are based on the same set of experimentally obtained mobilities. In a classical Ferguson plot, for example for free DNA, the logarithm of the mobilities is linear to the gel percentage. However, in the case of Au and Au-DNA conjugates, this linearity holds no longer true, in particular for gels of higher percentage [36]. We, therefore, had to restrict our analysis to gels from 1% to 3% although in some cases data for 4% to 6% had also been available. Additional experiments can be found in the supplementary material. Though theories for nonlinear, convex Ferguson plots exist [40, 41], we did not try to apply them here. Due to the significant deviation from the data obtained with the Ferguson plots to the data obtained with mobility-diameter calibration curves and due to the above-mentioned limitations, we conclude that the linear Ferguson analysis is less suited to obtain absolute effective diameters. However, relative increases in size due to binding of molecules can be observed with sufficient resolution with Ferguson analysis.

3.5. Specific thiol-Au bond-mediated attachment of DNA versus nonspecific DNA adsorption

Our data clearly indicate that there is also nonspecific adsorption of DNA to the surface of Au particles in case the particles are exposed to many DNA molecules, see Figure 1. It is important to point out that in Figure 1, the data of Au particles that have been exposed to as much DNA as possible and that are, therefore, saturated with DNA are described. This is different from the case in which the Au particles are exposed to only to a few strands of DNA as in Figure 2, where no nonspecific adsorption could be observed, as already reported by Zanchet et al. [11]. Nonspecific adsorption of DNA to Au particles is significantly lower compared to specific thiol-Au bond-mediated attachment and thus can only be observed in

case of exposure of the particles to very high DNA concentrations.

Although the absolute numbers derived for effective diameters for Au-DNA conjugates are afflicted with significant error bars as described above, these data nevertheless contain valuable information about the binding of DNA to Au particles. Any attachment of DNA leads to an increase in the effective diameter, dependent on the nature of attachment, the amount of bound DNA, and the length of each DNA molecule, see Figure 1. With very simple models, we can assume that DNA attached to the surface of Au particles can adopt two basic types of conformation [27]. In the first case, the confirmation of DNA is not effected by the presence of the Au particles and it will form a random coil. In the second case, DNA has to compete for the binding places at the gold surface and thus, in order to bind as many DNA molecules per area as possible, the DNA has to be stretched. Actually, a combination of both models will best describe the reality. In Figure 1, the effective diameters for the different models (randomly coiled DNA, fully stretched DNA, and DNA that is stretched for the first 30 bases and randomly coiled for the rest of the bases) are plotted versus the DNA length for Au particles that are saturated with DNA. Clearly, thiol-gold-bond specific attachment can be distinguished from nonspecific adsorption of DNA. Similar observations have been reported also before by Sandström et al. [26, 37]. First, the increase in the effective diameter tells that also DNA without thiol modification can be adsorbed to the surface of phosphine-stabilized Au nanoparticles. Second, a comparison with the effective diameters of the theoretical models clearly proves that nonspecifically adsorbed DNA does not exist in a stretched configuration perpendicular to the Au surface. The data rather indicate that even when the particle surface is saturated with nonspecifically attached DNA, only parts of the DNA molecules will be randomly coiled, as the experimentally obtained effective diameters are smaller than the diameter of conjugates in which the adsorbed DNA is randomly coiled. From this, one can conclude that due to nonspecific Au-DNA interaction, the adsorbed DNA is at least partly wrapped around the surface of the Au particles, which is in agreement with other studies [44]. In case of Au surfaces saturated with thiol-modified DNA, the effective diameters are significantly bigger compared to nonspecifically adsorbed DNA, see Figure 1. By comparison with basic models, we conclude in agreement to our previous study that specifically bound DNA adopts a stretched configuration so that as many DNA molecules as possible can bind to the Au surface. Due to the spherical geometry, DNA longer than around 30 bases only needs to be stretched due to this space limitation within around the first 30 bases, whereas the parts of the DNA molecules further away from the Au particle are not affected by space limitation and thus can be randomly coiled. These results again show the possibilities and limitations of the here-described method. Though it is complicated to derive accurate absolute effective diameters of Au-DNA conjugates, the binding of DNA molecules can be clearly seen as an increase in the effective diameters and a comparison with theoretical models can give indications about the conformation of the attached DNA. These

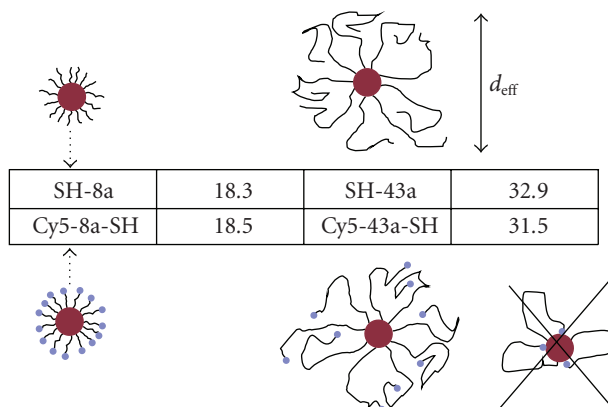


FIGURE 3: 10 nm diameter Au particles have been saturated with thiol-modified single-stranded DNA of 8 and 43 bases lengths and were run on 2% agarose gels. From the resulting mobilities, effective diameters were derived via a mobility-diameter calibration curve (for 2% agarose gels). In the table, the effective diameters of particles are given in nm. In the upper row, the data for DNA modified at one end with an-SH group are shown. In the bottom row, the data for DNA modified at one end with an-SH and at the other end with a -Cy5 organic fluorophore are shown. The results are within the error bars identical for DNA with and without Cy5, which indicates that the Cy5 at the free end does not interfere with the binding process of the DNA to the Au particle surface.

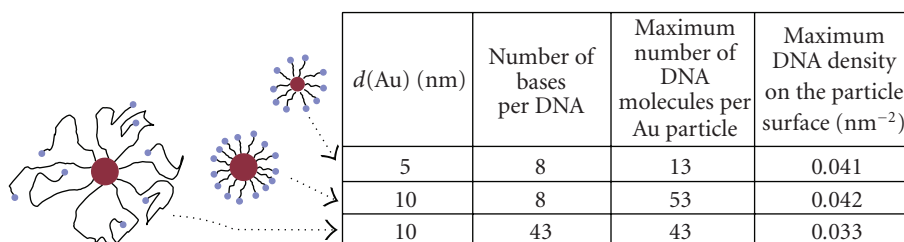


FIGURE 4: Maximum number of thiol-modified single-stranded DNA molecules that can be bound to the surface of phosphine-stabilized Au particles. Au particles of different core-diameter ($d = 5$ nm, 10 nm) and thiol modified single-stranded DNA of different length (8 and 43 bases) have been used. The maximum possible number of DNA molecules per Au particle and the maximum surface density (in DNA per particle surface) are given.

types of binding assays via gel electrophoresis are an attractive complementary method compared to other techniques, such as light scattering [45]. Presumably a combination of gel electrophoresis, light scattering, and zeta potential measurements of identical samples would give the most accurate analysis about Au-DNA conjugates. It remains to note that although electrophoresis of free DNA is well studied both experimentally and theoretically, the case of Au-DNA conjugates is more complex because several properties (total charge, charge density, and elasticity) are not constant but depend all at the same time on the binding of DNA to the Au nanoparticles. A theoretical model for gel electrophoresis of such conjugates would be helpful for data analysis.

3.6. Effect of organic fluorophores linked to DNA on the binding of DNA to Au particles

When organic fluorophores are attached to Au-DNA conjugates at the free end of the DNA, which is pointing towards solution, then energy transfer between the fluorophore and the Au nanoparticle can be observed [35]. This effect can be,

for example, employed for DNA sensors [46]. Since energy transfer depends on the distance between the organic fluorophore and the Au surface [35, 47], certainly the configuration of the bound fluorophore-modified DNA is important for this process. In case of nonspecific adsorption of the fluorophore to the Au surface, the distance between the fluorophore and the Au would be much smaller than for the case in which the DNA is linked with its thiol-modified end, see Figure 3. In this study, we have shown that the attachment of Cy5 to the free end of thiol-modified DNA does not change the effective diameter in the case of Au particles saturated with DNA, see Figure 3. These results demonstrate that the direct adsorption of Cy5 to the Au surface is much less probable than the formation of thiol-Au bonds and that, therefore, the dye points towards the solution.

3.7. Determination of the maximum number of DNA molecules that can be bound per one Au particle

The number of bound DNA molecules per Au particle has already been determined with several methods [25, 26, 48].

In comparison to methods in which the number of DNA molecules is quantified by the fluorescence of attached fluorophores, the counting of DNA via absorption measurements (as reported in this study) is not affected by photobleaching and quenching effects. Extracting the Au-DNA conjugates from the gel also helps that no unbound excess DNA is present in the solution, as it still might be possible in the case of purification with filter membranes. The results of this study are summarized in Figure 4 and are in the same range as the results obtained by other groups [25, 26, 48] though our determined DNA densities are rather lower than the ones determined by other groups. This might be due to the fact that the phosphine stabilization is harder to be displaced by DNA than citrate stabilization and in particular due to the fact that our incubation was performed at lower NaCl concentrations [48]. In our measurements, we could not find any effect of the different curvature between 5 nm and 10 nm gold particles on the density of attached DNA molecules. This can be understood as the surface curvature difference between both types of particles is not very high and DNA attachment to both types of particles was done under the same buffer conditions. Recently, Qin and Yung have instead demonstrated that the most relevant parameter for the maximum number of attached DNA molecules per particle is the salt concentration under which the attachment was performed [48]. High salt concentrations reduce electrostatic repulsion and thus allow for higher DNA surface densities.

3.8. Attachment of an exactly known number of DNA molecules per Au particle

As already reported in earlier publications, gel electrophoresis allows for a separation of Au-DNA conjugates with 0, 1, 2, ... DNA molecules attached per particle [9, 11]. In Figures 2 and 5, the effective diameters of such conjugates as determined from their electrophoretic mobilities are presented. The dependence of DNA length and Au core diameter on the effective diameter is as expected. The longer the DNA, the more the effective diameter of Au-DNA conjugates upon which attachment of another DNA molecule to one gold particle is increased (see Figure 2). The more long DNA strands are attached per individual gold particle, the fewer the effective diameter of the Au-DNA conjugated depends on the initial diameter of the Au core (see Figure 5). Although no simple model for Au-DNA conjugates is available that could predict the exact mobility in gel electrophoresis, the bands of particles with a defined number of DNA strands can be identified with their structure by relative (qualitative) comparison and control experiments that include hybridization. So far, we are not aware of another separation technique (such as HPLC) that can resolve Au particles with an individual number of attached DNA molecules as it is possible with gel electrophoresis. The concept of separating conjugates of particles with a discrete number of attached molecules by gel electrophoresis could be also generalized and used besides for Au-DNA conjugates for other systems [49]. Because of their defined composition, we think that such conjugates of particles with a defined number of linked molecules are very

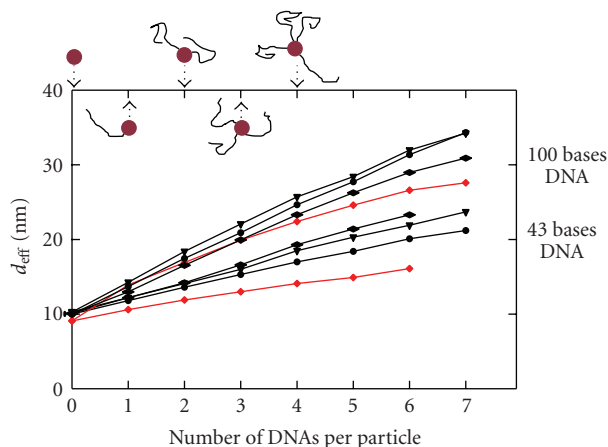


FIGURE 5: Effective diameters d_{eff} of Au-DNA conjugates with a discrete number of DNA molecules per particle for Au particles of different diameter. Single-stranded DNA (100 bases) had been specifically attached via thiol-gold bonds to the surface of 5 nm, 10 nm, and 20 nm Au particles. The conjugates were run on 1%, 2%, and 3% agarose gels and their effective diameters d_{eff} were derived from the measured electrophoretic mobilities. Here, the effective diameters for Au particles with a discrete number of attached DNA molecules (100 bases) per particle are shown. Data for 5 nm, 10 nm, and 20 nm particles are plotted in violet, black, and blue, respectively. Data derived from 1%, 2%, and 3% gels are plotted with diamond, triangle, and circle symbols.

interesting model systems and several applications have been already demonstrated [50, 51].

4. CONCLUSIONS

In this manuscript, the analysis of Au-DNA conjugates by gel electrophoresis is discussed. Whereas the principal effects are already known by our previous studies and reported by other groups, the aim of this work was the detailed analysis about the possibilities and limitations of this technique. For this purpose, an extensive study with 1200 gels was performed. From these data, we can conclude that the determination of absolute effective diameters from electrophoretic mobilities has severe limitations. In order to get an estimate about the accuracy of the data gels of different percentages have to be compared. The deviation between these data sets is an indicator for the error bars in the derived effective diameters. We believe that this strategy leads to more reliable values for effective diameters than Ferguson analysis. Pointing out these limitations is important as several studies exist in which this method has been applied without investigating its limitations first [27, 28, 32]. Though the extraction of absolute values for effective diameters from the mobility data has very limited accuracy, the attachment of molecules to particles can on the other hand be detected with high sensitivity as an increase in the effective diameters. In this way, even the attachment of single molecules can be resolved, which to our knowledge has not been demonstrated yet with an alternative separation technique such as HPLC. Besides such binding assays, also

indications about the conformation of the DNA molecules that are bound to the particles can be derived from the obtained effective diameters. In this way, we believe that gel electrophoresis is a very powerful method to investigate the attachment of DNA molecules to Au nanoparticles though it has also clear limitations. Whereas specific and nonspecific attachment of DNA can be detected with high sensitivity, the quantitative determination of effective hydrodynamic diameters is not possible in a straightforward way.

ACKNOWLEDGMENTS

The authors are grateful to Dr. Eric Dulkeith for helpful comments. This work was supported in part by the German Research Foundation (DFG, Emmy Noether program), the European Union (STREP program NANO-SA), the Center for Nanoscience (CeNS), and the U.S. Department of Energy (Contract no. DE-AC02-05CH11231).

REFERENCES

- [1] W. Fritzsche and T. A. Taton, "Metal nanoparticles as labels for heterogeneous, chip-based DNA detection," *Nanotechnology*, vol. 14, no. 12, pp. R63–R73, 2003.
- [2] C. A. Mirkin, "Programming the assembly of two- and three-dimensional architectures with DNA and nanoscale inorganic building blocks," *Inorganic Chemistry*, vol. 39, no. 11, pp. 2258–2272, 2000.
- [3] E. Dujardin and S. Mann, "Bio-inspired materials chemistry," *Advanced Materials*, vol. 14, no. 11, pp. 775–788, 2002.
- [4] Z. Wang, R. Lévy, D. G. Fernig, and M. Brust, "The peptide route to multifunctional gold nanoparticles," *Bioconjugate Chemistry*, vol. 16, no. 3, pp. 497–500, 2005.
- [5] A. G. Kanaras, Z. Wang, A. D. Bates, R. Cosstick, and M. Brust, "Towards multistep nanostructure synthesis: programmed enzymatic self-assembly of DNA/gold systems," *Angewandte Chemie International Edition*, vol. 42, no. 2, pp. 191–194, 2003.
- [6] R. Elghanian, J. J. Storhoff, R. C. Mucic, R. L. Letsinger, and C. A. Mirkin, "Selective colorimetric detection of polynucleotides based on the distance-dependent optical properties of gold nanoparticles," *Science*, vol. 277, no. 5329, pp. 1078–1081, 1997.
- [7] C. A. Mirkin, R. L. Letsinger, R. C. Mucic, and J. J. Storhoff, "A DNA-based method for rationally assembling nanoparticles into macroscopic materials," *Nature*, vol. 382, no. 6592, pp. 607–609, 1996.
- [8] A. Paul Alivisatos, K. P. Johnsson, X. Peng, et al., "Organization of 'nanocrystal molecules' using DNA," *Nature*, vol. 382, no. 6592, pp. 609–611, 1996.
- [9] C. J. Loweth, W. Brett Caldwell, X. G. Peng, A. Paul Alivisatos, and P. G. Schultz, "DNA-based assembly of gold nanocrystals," *Angewandte Chemie International Edition*, vol. 38, no. 12, pp. 1808–1812, 1999.
- [10] R. L. Letsinger, R. Elghanian, G. Viswanadham, and C. A. Mirkin, "Use of a steroid cyclic disulfide anchor in constructing gold nanoparticle-oligonucleotide conjugates," *Bioconjugate Chemistry*, vol. 11, no. 2, pp. 289–291, 2000.
- [11] D. Zanchet, C. M. Micheel, W. J. Parak, D. Gerion, and A. Paul Alivisatos, "Electrophoretic isolation of discrete Au nanocrystal/DNA conjugates," *Nano Letters*, vol. 1, no. 1, pp. 32–35, 2001.
- [12] K.-M. Sung, D. W. Mosley, B. R. Peelle, S. Zhang, and J. M. Jacobson, "Synthesis of monofunctionalized gold nanoparticles by Fmoc solid-phase reactions," *Journal of the American Chemical Society*, vol. 126, no. 16, pp. 5064–5065, 2004.
- [13] S. D. Jhaveri, E. E. Foos, D. A. Lowy, E. L. Chang, A. W. Snow, and M. G. Ancona, "Isolation and characterization of trioxethylene-encapsulated gold nanoclusters functionalized with a single DNA strand," *Nano Letters*, vol. 4, no. 4, pp. 737–740, 2004.
- [14] C. J. Ackerson, M. T. Sykes, and R. D. Kornberg, "Defined DNA/nanoparticle conjugates," *Proceedings of the National Academy of Sciences of the United States of America*, vol. 102, no. 38, pp. 13383–13385, 2005.
- [15] W. J. Qin and L. Y. L. Yung, "Nanoparticle-DNA conjugates bearing a specific number of short DNA strands by enzymatic manipulation of nanoparticle-bound DNA," *Langmuir*, vol. 21, no. 24, pp. 11330–11334, 2005.
- [16] N. Mourougou-Candoni, C. Naud, and F. Thibaudau, "Adsorption of thiolated oligonucleotides on gold surfaces: an atomic force microscopy study," *Langmuir*, vol. 19, no. 3, pp. 682–686, 2003.
- [17] E. Huang, M. Satjapipat, S. Han, and F. Zhou, "Surface structure and coverage of an oligonucleotide probe tethered onto a gold substrate and its hybridization efficiency for a polynucleotide target," *Langmuir*, vol. 17, no. 4, pp. 1215–1224, 2001.
- [18] E. Huang, F. Zhou, and L. Deng, "Studies of surface coverage and orientation of DNA molecules immobilized onto preformed alkanethiol self-assembled monolayers," *Langmuir*, vol. 16, no. 7, pp. 3272–3280, 2000.
- [19] A. W. Peterson, R. J. Heaton, and R. M. Georgiadis, "The effect of surface probe density on DNA hybridization," *Nucleic Acids Research*, vol. 29, no. 24, pp. 5163–5168, 2001.
- [20] A. W. Peterson, L. K. Wolf, and R. M. Georgiadis, "Hybridization of mismatched or partially matched DNA at surfaces," *Journal of the American Chemical Society*, vol. 124, no. 49, pp. 14601–14607, 2002.
- [21] K. A. Peterlinz, R. M. Georgiadis, T. M. Herne, and M. J. Tarlov, "Observation of hybridization and dehybridization of thiol-tethered DNA using two-color surface plasmon resonance spectroscopy," *Journal of the American Chemical Society*, vol. 119, no. 14, pp. 3401–3402, 1997.
- [22] A. B. Steel, R. L. Levicky, T. M. Herne, and M. J. Tarlov, "Immobilization of nucleic acids at solid surfaces: effect of oligonucleotide length on layer assembly," *Biophysical Journal*, vol. 79, no. 2, pp. 975–981, 2000.
- [23] T. M. Herne and M. J. Tarlov, "Characterization of DNA probes immobilized on gold surfaces," *Journal of the American Chemical Society*, vol. 119, no. 38, pp. 8916–8920, 1997.
- [24] D. V. Leff, L. Brandt, and J. R. Heath, "Synthesis and characterization of hydrophobic, organically-soluble gold nanocrystals functionalized with primary amines," *Langmuir*, vol. 12, no. 20, pp. 4723–4730, 1996.
- [25] L. M. Demers, C. A. Mirkin, R. C. Mucic, et al., "A fluorescence-based method for determining the surface coverage and hybridization efficiency of thiol-capped oligonucleotides bound to gold thin films and nanoparticles," *Analytical Chemistry*, vol. 72, no. 22, pp. 5535–5541, 2000.
- [26] P. Sandström, M. Boncheva, and B. Åkerman, "Nonspecific and thiol-specific binding of DNA to gold nanoparticles," *Langmuir*, vol. 19, no. 18, pp. 7537–7543, 2003.
- [27] W. J. Parak, T. Pellegrino, C. M. Micheel, D. Gerion, S. C. Williams, and A. Paul Alivisatos, "Conformation of oligonucleotides attached to gold nanocrystals probed by gel electrophoresis," *Nano Letters*, vol. 3, no. 1, pp. 33–36, 2003.

- [28] S. Park, K. A. Brown, and K. Hamad-Schifferli, "Changes in oligonucleotide conformation on nanoparticle surfaces by modification with mercaptohexanol," *Nano Letters*, vol. 4, no. 10, pp. 1925–1929, 2004.
- [29] K. Hamad-Schifferli, J. J. Schwartz, A. T. Santos, S. Zhang, and J. M. Jacobson, "Remote electronic control of DNA hybridization through inductive coupling to an attached metal nanocrystal antenna," *Nature*, vol. 415, no. 6868, pp. 152–155, 2002.
- [30] J. J. Storhoff, R. Elghanian, C. A. Mirkin, and R. L. Letsinger, "Sequence-dependent stability of DNA-modified gold nanoparticles," *Langmuir*, vol. 18, no. 17, pp. 6666–6670, 2002.
- [31] R. A. Sperling, T. Liedl, S. Duhr, et al., "Size determination of (Bio)conjugated water-soluble colloidal nanoparticles: a comparison of different techniques," *Journal of Physical Chemistry C*, vol. 111, no. 31, pp. 11552–11559, 2007.
- [32] T. Pons, H. Tetsuo Uyeda, I. L. Medintz, and H. Mattoussi, "Hydrodynamic dimensions, electrophoretic mobility, and stability of hydrophilic quantum dots," *Journal of Physical Chemistry B*, vol. 110, no. 41, pp. 20308–20316, 2006.
- [33] M. Hanauer, S. Pierrat, I. Zins, A. Lotz, and C. Sönnichsen, "Separation of nanoparticles by gel electrophoresis according to size and shape," *Nano Letters*, vol. 7, no. 9, pp. 2881–2885, 2007.
- [34] K. A. Ferguson, "Starch-gel electrophoresis—application to the classification of pituitary proteins and polypeptides," *Metabolism*, vol. 13, pp. 985–1002, 1964.
- [35] E. Dulkeith, M. Ringler, T. A. Klar, J. Feldmann, A. Muñoz Javier, and W. J. Parak, "Gold nanoparticles quench fluorescence by phase induced radiative rate suppression," *Nano Letters*, vol. 5, no. 4, pp. 585–589, 2005.
- [36] D. Zanchet, C. M. Micheel, W. J. Parak, D. Gerion, S. C. Williams, and A. Paul Alivisatos, "Electrophoretic and structural studies of DNA-directed Au nanoparticle groupings," *Journal of Physical Chemistry B*, vol. 106, no. 45, pp. 11758–11763, 2002.
- [37] P. Sandström and B. Åkerman, "Electrophoretic properties of DNA-modified colloidal gold nanoparticles," *Langmuir*, vol. 20, no. 10, pp. 4182–4186, 2004.
- [38] M.-E. Aubin, D. G. Morales, and K. Hamad-Schifferli, "Labeling ribonuclease S with a 3 nm Au nanoparticle by two-step assembly," *Nano Letters*, vol. 5, no. 3, pp. 519–522, 2005.
- [39] W. J. Parak, D. Gerion, D. Zanchet, et al., "Conjugation of DNA to silanized colloidal semiconductor nanocrystalline quantum dots," *Chemistry of Materials*, vol. 14, no. 5, pp. 2113–2119, 2002.
- [40] D. Tietz and A. Chrambach, "Analysis of convex ferguson plots in agarose gel electrophoresis by empirical computer modeling," *Electrophoresis*, vol. 7, pp. 241–250, 1986.
- [41] D. Tietz and A. Chrambach, "Concave ferguson plots of DNA fragments and convex ferguson plots of bacteriophages: evaluation of molecular and fiber properties, using desktop computers," *Electrophoresis*, vol. 13, no. 1, pp. 286–294, 1992.
- [42] B. Tinland, A. Pluen, J. Sturm, and G. Weill, "Persistence length of single-stranded DNA," *Macromolecules*, vol. 30, no. 19, pp. 5763–5765, 1997.
- [43] C. Rivetti, M. Guthold, and C. Bustamante, "Scanning force microscopy of DNA deposited onto mica: equilibration versus kinetic trapping studied by statistical polymer chain analysis," *Journal of Molecular Biology*, vol. 264, no. 5, pp. 919–932, 1996.
- [44] G. Han, C. T. Martin, and V. M. Rotello, "Stability of gold nanoparticle-bound DNA toward biological, physical, and chemical agents," *Chemical Biology & Drug Design*, vol. 67, no. 1, pp. 78–82, 2006.
- [45] M. Cárdenas, J. Barauskas, K. Schillén, J. L. Brennan, M. Brust, and T. Nylander, "Thiol-specific and nonspecific interactions between DNA and gold nanoparticles," *Langmuir*, vol. 22, no. 7, pp. 3294–3299, 2006.
- [46] C. K. Kim, R. R. Kalluru, J. P. Singh, et al., "Gold-nanoparticle-based miniaturized laser-induced fluorescence probe for specific DNA hybridization detection: studies on size-dependent optical properties," *Nanotechnology*, vol. 17, no. 13, pp. 3085–3093, 2006.
- [47] E. Dulkeith, A. C. Morteani, T. Niedereichholz, et al., "Fluorescence quenching of dye molecules near gold nanoparticles: radiative and nonradiative effects," *Physical Review Letters*, vol. 89, no. 20, Article ID 203002, 4 pages, 2002.
- [48] W. J. Qin and L. Y. L. Yung, "Efficient manipulation of nanoparticle-bound DNA via restriction endonuclease," *Bio-macromolecules*, vol. 7, no. 11, pp. 3047–3051, 2006.
- [49] R. A. Sperling, T. Pellegrino, J. K. Li, W. H. Chang, and W. J. Parak, "Electrophoretic separation of nanoparticles with a discrete number of functional groups," *Advanced Functional Materials*, vol. 16, no. 7, pp. 943–948, 2006.
- [50] J. Sharma, R. Chhabra, Y. Liu, Y. Ke, and H. Yan, "DNA-templated self-assembly of two-dimensional and periodical gold nanoparticle arrays," *Angewandte Chemie International Edition*, vol. 45, no. 5, pp. 730–735, 2006.
- [51] J. Zheng, P. E. Constantinou, C. Micheel, A. Paul Alivisatos, R. A. Kiehl, and N. C. Seeman, "Two-dimensional nanoparticle arrays show the organizational power of robust DNA motifs," *Nano Letters*, vol. 6, no. 7, pp. 1502–1504, 2006.

One-Dimensional Arrangement of Gold Nanoparticles by Electrospinning

Gyeong-Man Kim,^{*,†} Andre Wutzler,[†] Hans-Joachim Radusch,[†] Goerg H. Michler,[†]
Paul Simon,[‡] Ralph A. Sperling,[§] and Wolfgang J. Parak[§]

Department of Materials Science, Martin-Luther University, Halle-Wittenberg, D-06099 Halle/S, Germany,
Center of Nanoscience, Ludwig-Maximilians University Munich, Schellingstrasse 4,
D-80799 Munich, Germany, and Max Plank Institute for Chemical Physics of Solids,
Nöthnitzer Strasse 40, D-01187 Dresden, Germany

Received April 18, 2005. Revised Manuscript Received July 12, 2005

The electrospinning technique was used successfully to fabricate one-dimensional arrays of Au nanoparticles within nanofibers in which the intrinsic nature of the semicrystalline polymer poly(ethylene oxide) (PEO) was employed as a template for the controlled nanoscale organization of nanoparticles. Differential scanning calorimetry (DSC), Fourier transform infrared spectroscopy, UV–visible spectroscopy, scanning electron microscopy, atomic force microscopy, and transmission electron microscopy (TEM) were performed to characterize the resulting electrospun fibers in comparison with pure PEO and PEO/Au nanocomposite before electrospinning. By choosing chloroform as the solvent in this work the observed electrospun fibers were about 400–650 nm in diameter and revealed a well-defined Gaussian distribution. Thermal analysis showed that the dodecanethiol-capped Au nanoparticles preferentially act as heterogeneous nucleating agents for PEO crystallization. Conformational changes occurred by incorporating Au nanoparticles as well as electrospinning. The most common helical structure of PEO was transformed into a trans zigzag planar structure due to the high extensional flow caused by electrospinning. As a striking result, fairly long and one-dimensional chainlike structures consisting of Au nanoparticles within the electrospun fibers were observed by TEM. The present findings demonstrate that the electrospinning process provides not only a fundamental understanding of the conformational changes upon process conditions, but also a straightforward and cost-effective technique to fabricate one-dimensional arrays of nanoparticles for future nanodevices with unique properties in various applications, such as biological sensors, single-electron transistors, photonic materials, etc.

1. Introduction

Metal nanoparticles,¹ which represent particularly attractive building blocks of individual atoms, hold promise for use as advanced materials with new electronic,² magnetic,³ optical,⁴ thermal,⁵ and catalytic properties.⁶ Compared with bulk materials, these unique properties mainly arise from the quantum-confinement effects and their enormous large specific surface areas. These nanoparticles provide a starting point for fabricating future nanodevices with unique elec-

tronic, optoelectronic, electrochemical, and electromechanical properties. Because the physical properties of these nanodevices are dominated by the formation of size-controlled nanoparticles, interparticle distances and their spatially ordered assemblies (superlattices) in predefined geometries, such as linear, two- and three-dimensional superstructures, have become the focus of intense research in recent years.⁷ Among this line, two-dimensional (2D) and three-dimensional (3D) superlattices have been prepared by self-assembly,⁸ the Langmuir–Blodgett method,⁹ or electrophoretic deposition,¹⁰ and their optical and electron transport properties have been intensely investigated. In contrast, one-dimensional (1D) arrays of nanoparticles still remain a great

* To whom correspondence should be addressed E-mail: gyeong-man.kim@iw.uni-halle.de

[†] Martin-Luther University Halle-Wittenberg

[‡] Max Plank Institute for Chemical Physics of Solids

[§] Ludwig-Maximilians University Munich

- (1) Pileni, M. P. *Metal Nanoparticles-Synthesis, Characterization, and Applications*; Feldheim, D. L., Colby, A. F., Jr., Eds.; Marcel Dekker: New York, 2002; Chapter 9. (b) Simon, U. *Metal clusters in Chemistry*; Braunstein, P., Oro, L. A., Raithby, P. R., Eds.; Wiley-VCH: Weinheim, 1999. (c) Schmid, G.; Bäuml, M.; Geerkens, M.; Heim, I.; Osemann, C.; Sawitowski, T. *Chem. Soc. Rev.* **1999**, *28*, 179. (d) Whetten, R. L.; Shafiqullin, M. N.; Khoury, J. T.; Schaaff, T. G.; Vezmar, I.; Alvarez, M. M.; Wilkinson, A. *Acc. Chem. Res.* **1999**, *32*, 397.
- (2) Kastner, M. A. *Phys. Today* **1993**, *46* (1), 24.
- (3) (a) Sufi, R.; Kofinas, P. *J. Magn. Magn. Mater.* **2005**, *288*, 219. (b) Awschalom, D. D. *Science* **1996**, *271*, 937.
- (4) (a) Alivisatos, A. P. *Science* **1996**, *271*, 933. (b) Brus, L. *Appl. Phys. A* **1991**, *53*, 465.
- (5) Negishi, N.; Takeuchi, K. *Thin Solid Films* **2001**, *392*, 249.
- (6) Lewis, L. N. *Chem. Rev.* **1993**, *258*, 414.

(7) Wang, Z. L. *Adv. Mater.* **1998**, *10*, 13.

(8) (a) Lu, N.; Chen, X.; Molenda, D.; Naber, A.; Fuchs, H.; Talapin, D. V.; Weller, H.; Müller, J.; Lupton, J. M.; Feldmann, J.; Rogach, A.; Chi, L. *Nano Lett.* **2004**, *4*, 885. (b) Lopes, W. A.; Jaeger, H. M. *Nature* **2001**, *414*, 735.

(9) (a) Kim, F.; Kwan, J.; Akana, J.; Yang, P. *J. Am. Chem. Soc.* **2001**, *123*, 4360. (b) Martin, J. E.; Wilcoxon, J. P.; Odinek, J.; Provencio, P. *J. Phys. Chem. B* **2000**, *104*, 9475.

(10) (a) Li, Q.; Newberg, J. T.; Walter, E. C.; Hemminer, J. C.; Penner, R. M. *Nano Lett.* **2004**, *4*, 277. (b) Walter, E. C.; Zach, M. P.; Favier, F.; Murray, B.; Inazu, K.; Hemminger, J. C.; Penner, R. M. *Chemphyschem* **2003**, *4*, 131. (c) Limmer, S. J.; Seraji, S.; Tammy Y. W.; Chou, P.; Nguyen, C.; Cao, G. *Adv. Funct. Mater.* **2002**, *12*, 59. (d) Teranishi, T.; Hosoe, M.; Tanaka, T.; Miyake, M. *J. Phys. Chem. B* **1999**, *103*, 3818.

challenge in nanotechnology¹¹ because it is quite difficult to organize metal nanoparticles in low symmetry. Successful realization of these structures in the future may provide a new tool to integrate these 1D nanostructures into functional devices and circuitry. Several approaches have been proposed to construct such structures by means of appropriate templates, such as DNA strands,¹² bacteria and viruses,¹³ other linear polymers,¹⁴ or lithographically patterned substrates.¹⁵

In the present work we demonstrate an alternative new approach based on the electrospinning (ES) technique for fabricating 1D arrangements of metal nanoparticle arrays within submicrometer polymer fibers. Recently, electrostatic fiber spinning, or “electrospinning”, has received a growing attention because polymer fibers prepared by this technique achieve fiber diameters in the submicrometer range straightforwardly and cost-effectively.¹⁶ To form such fibers using ES a polymer solution is forced through a capillary, forming a drop of polymer solution at the tip of capillary. Then a high voltage is applied between the tip and a grounded collection target. When the electric field strength overcomes the surface tension of the droplet, a polymer solution jet is initiated and accelerated toward the collection target. As the jet travels through the air, the solvent evaporates and a nonwoven polymeric fabric is formed on the target. This approach becomes particularly powerful when the ease and control offered by the nanofibers is combined with the electronic, magnetic, or photonic properties of inorganic components. To date, it has been well established that the ES process allows easily incorporating particles of materials, such as layered silicates,¹⁷ carbon nanotubes,¹⁸ and many others,¹⁹ into the nanofibers.

The objectives of this research are 2-fold: One is to develop a single-step processing route for the production of

synthetic fibers comprising a 1D arrangement of well-controlled metal nanoparticles. The other is to study the effect of electrospinning on the conformational changes of the resulting fibers with and without metal nanoparticles, which can provide fundamental insights into the nature of the electrospinning process. To achieve these objectives we employ semicrystalline polymer poly(ethylene oxide) (PEO) and its composites incorporated with gold nanoparticles. The choice of PEO is not only motivated by its wide variety of applications,²⁰ such as biomaterials including scaffolds,²¹ drug delivery,²² tissue engineering, wound healing,²³ and conductive fibers²⁴ for electrolytes in polymer batteries, but also by control of the dispersion of nanoparticles assisted by its intrinsic crystallinity that will contribute to fiber stability as well as responsibility for controlled dispersion of nanoparticles. Furthermore, the amphiphilic nature of PEO (soluble both in water and nonpolar solvents) and the strong dependence of local conformations on the used solvents make PEO an excellent model polymer for gaining a fundamental understanding of the conformational changes upon process conditions. The capability and feasibility of this technique demonstrates a promising alternative approach for the fabrication of polymer nanostructured composite fibers by controlling a set of experimental parameters.

2. Experimental Section

2.1. Materials. *Synthesis of Dodecanethiol-Capped Gold Nanoparticles.* Colloidal Au nanoparticles were synthesized according to standard protocols.²⁵ Briefly, 300 mg of hydrogen tetrachloroaurate (HAuCl₄·3H₂O) dissolved in distilled water was added to 80 mL of a 50 μM tetraoctylammonium bromide ([CH₃(CH₂)₇]₄-NBr) solution dissolved in toluene. Transfer of the metal salt to the toluene phase was clearly observed within a few seconds. An aqueous solution of 334 mg of sodium borohydride (NaBH₄) was added to the mixture while stirring, which immediately caused the reduction reaction. After 1 h the two phases were separated, and the toluene phase was washed with 0.01 M HCl, 0.01 M NaOH, and three times distilled H₂O. Afterward, a surfactant exchange procedure was carried out. A 10 mL amount of 1-dodecanethiol was added to the Au nanoparticles in toluene. The solution was heated to 65 °C and stirred for 2 h. During this process the mercapto groups of the dodecanethiol (CH₃(CH₂)₁₁SH) molecules bind to the surface of the Au nanocrystals, displacing the Br ions. Upon completion of the reaction, the final dodecanethiol-capped Au nanoparticles were precipitated twice with methanol and redissolved

- (11) (a) Vidini, O.; Reuter, T.; Torma, V.; Meyer-Zaika, W.; Schmid, G. *J. Mater. Chem.* **2001**, *11*, 3188. (b) Thurn-Albrecht, T.; Schotter, J.; Kästle, G. A.; Emley, N.; Shibauch, T.; Krusin-Elbaum, L.; Guarini, K.; Black, C. T.; Tuominen, M. T.; Russell, T. P. *Science* **2000**, *290*, 2126.
- (12) (a) Warner, M. G.; Hutchison, J. E. *Nature* **2003**, *2*, 272. (b) Mirkin, C. A. *Inorg. Mater.* **2000**, *39*, 2258. (c) Braun, E.; Eichen, Y.; Sivan, U.; Ben-Yoseph, G. *Nature* **1998**, *391*, 775. (c) Mirkin, C. A.; Letsinger, R. L.; Mucic, R. C.; Storhoff, J. J. *Nature* **1996**, *382*, 607.
- (13) Hall, S. R.; Shenton, W.; Engelhardt, H.; Mann, S. *Chem. Phys. Chem.* **2001**, *3*, 184.
- (14) Wyrna, D.; Beyer, N.; Schmid, G. *Nano Lett.* **2002**, *2*, 419.
- (15) (a) Cui, Y.; Björk, M. T.; Liddle, J. A.; Sönnichsen, C.; Boussert, B.; Alivisatos, A. P. *Nano Lett.* **2004**, *4*, 1093. (b) Tsirlin, T.; Zhu, J.; Somorjai, G. A. *Top. Catal.* **2002**, *19*, 165.
- (16) (a) Li, D.; Xia, Y. *Adv. Mater.* **2004**, *16*, 1151. (b) Sun, Z.; Zussman, E.; Yarin, A. L.; Wendorff, J. H.; Greiner, A. *Adv. Mater.* **2003**, *15*, 1929. (c) Shin, Y. M.; Hohman, M. M.; Brenner, M. P.; Rutledge, G. C. *Polymer* **2001**, *42*, 9955. (d) Deitzel, J. M.; Kleinmeyer, J.; Harris, D.; Beck, T. N. C. *Polymer* **2001**, *42*, 261. (e) Bognitzki, M.; Hou, H.; Ishaque, M.; Frese, T.; Hellwig, M.; Schwarte, C.; Schaper, A.; Wendorff, J. H.; Greiner, A. *Adv. Mater.* **2000**, *12*, 637. (f) Reneker, D. H.; Yarin, A. L.; Fong, H.; Koombhonges, S. *J. Appl. Phys.* **2000**, *87*, 4531. (g) Reneker, D. H.; Chun, I. *Nanotechnology* **1996**, *7*, 216. (h) Baumgarten, P. K. *J. Colloid Interface Sci.* **1971**, *36*, 71.
- (17) (a) Fong, H.; Liu, W.; Wang, C.-S.; Vaia, R. A. *Polymer* **2002**, *43*, 775. (b) Kim, G.-M.; Lach, R.; Michler, G. H.; Chang, C. H. *Macromol. Rapid Commun.* **2005**, *26*, 728.
- (18) (a) Dror, Y.; Salalha, W.; Khalfin, R. L.; Cohen, Y.; Yarin, A. L.; Zussman, E. *Langmuir* **2003**, *19*, 7012. (b) Salalha, W.; Dror, Y.; Khalfin, R. L.; Cohen, Y.; Yarin, A. L.; Zussman, E. *Langmuir* **2004**, *20*, 9852. (c) Kim, G.-M.; Michler, G. H.; Pötschke, P. *Polymer*, **2005**, *46*, 7346.
- (19) Wang, M.; Singh, H.; Hatton, T. A.; Rutledge, G. C. *Polymer* **2004**, *45*, 5505.
- (20) Christie, A. M.; Lilley, S. J.; Staunton, E.; Yuri, G.; Andreev, Y. G.; Bruce, P. G. *Nature* **2005**, *433*, 50.
- (21) Duan, B.; Dong, C.; Yuan, X.; Yao, K. *J. Biomater. Sci., Polym. Ed.* **2004**, *15*, 797.
- (22) (a) Zeng, J.; Xu, X.; Chen, X.; Liang, Q.; Bian, X.; Yang, L.; Jing, X. *J. Controlled Release* **2003**, *92*, 227. (b) Kenaway, E. R.; Bowling, G. L.; Wnek, G. E. *J. Controlled Release* **2002**, *81*, 57.
- (23) Hirano, S.; Zhang, M.; Nakagawa, M.; Miyata, T. *Biomaterials* **2000**, *21*, 997.
- (24) (a) Qin, X. Y.; Wan, Y. Q.; He, J. H.; Zhang, J.; Yu, J. Y.; Wang, S. Y. *Polymer* **2004**, *45*, 6409. (b) MacDiarmid, A. G.; Ones, W. E.; Norris, I. D., Jr.; Gao, J.; Johnson, A. T.; Pinto, N. *J. Synth. Met.* **2001**, *119*, 27.
- (25) (a) Gittins, D. I.; Caruso, F. *Angew. Chem., Int. Ed.* **2001**, *40*, 3001. (b) Templeton, A. C.; Wuelfing, W. P.; Murray, R. W. *Acc. Chem. Res.* **2000**, *33*, 27. (c) Kiely, C. J.; Fink, J.; Zheng, J. G.; Brust, M.; Bethell, D.; Schiffrin, D. J. *Adv. Mater.* **2000**, *12*, 640. (d) Fink, J.; Kiely, C. J.; Bethell, D.; Schiffrin, D. J. *Chem. Mater.* **1998**, *10*, 922. (e) Leff, D. V.; O'Hara, P. C.; Heath, J. R.; Gelbart, W. M. *J. Phys. Chem.* **1995**, *99*, 7036–7041.

in chloroform (CHCl_3) to prepare the PEO nanocomposites and electrospinning of them. The overall concentration of the resulting Au nanoparticle solution was 20 μM .

PEO and PEO/Au Nanocomposites. The semicrystalline polymer poly(ethylene oxide) (PEO, $M_w = 600\,000$ g/mol) was purchased from Aldrich Chemical Co. Inc. and used as received without further purification. PEO/Au composite films were prepared by a solution-cast technique using chloroform as the solvent at room temperature. First, PEO powder was dissolved in chloroform to make a 2 wt % solution and then mixed with a 1 wt % solution of dodecanethiol-capped Au dissolved in chloroform. The mixture was vigorously stirred with a magnetic stir bar for at least 24 h at room temperature and casted onto glass dishes, and subsequently the solvent was evaporated slowly in air at room temperature for 2 days. To ensure complete solvent removal, the final nanocomposites (NCs) were annealed at 55 °C for 12 h in a vacuum oven at 0.5 Torr.

2.2. Methods. Electrospinning Process. To obtain electrospinnable solutions, pure PEO and its NCs were dissolved in chloroform to prepare a 2 wt % solution. The solution was vigorously stirred with a magnetic stir bar for at least 24 h at room temperature, which was followed by sonication for 30 min to ensure a homogeneous solution. ES was carried out under ambient temperature in a vertical spinning configuration using a 1 mm i.d. flat-end needle with a 5 cm working distance. The applied voltages were in the range from 3 to 20 kV, driven by a high-voltage power supply (Knürr-Heizinger PNC, Germany). The electrospun fibers were collected either on Cu grids or slide glasses. The samples were annealed at 55 °C for 12 h and cooled to room temperature under vacuum (0.5 Torr).

Investigation of Fiber Morphology: Electron Microscopy and Atomic Force Microscopy (AFM). To characterize the size of the Au nanoparticles and their spatial dispersion within the electrospun fibers, the PEO fibers were directly electrospun on Cu grids covered with an ultrathin carbon layer and investigated by conventional transmission electron microscopy (TEM) (JEOL 200CX operated at 200 kV) as well as by high-resolution TEM (Philips CM200 FEG\ST Lorentz electron microscope with a field emission gun and at an acceleration voltage of 200 kV). For the analysis of the diameter of the electrospun fibers and their distribution the electrospun fibers collected on the slide glasses were investigated by field emission gun-environmental scanning electron microscopy (FEG-ESEM, Philips ESEM XL 30 FEG). To study the morphology of the PEO crystals upon the electrospinning process, AFM (Digital Instrument, NanoScope IIIa) with commercially available Si_3N_4 cantilevers was employed. The tapping mode of AFM was selected to obtain both height and phase images. The scanner was calibrated with a standard grid in both lateral size and height.

Differential Scanning Calorimetry (DSC). DSC measurements were conducted to measure the melting and crystallization behavior with a Mettler-Toledo DSC 820 under a nitrogen atmosphere. The samples were sealed in aluminum pans and heated and cooled in the temperature range 25–100 °C in the DSC instrument with a rate of 10 °C/min. The weight of each sample was approximately 0.5 mg. The DSC temperature and heat flow values were calibrated with indium as the standard. The degree of crystallinity, X_c , was calculated from the endothermic area by the following equation

$$X_c = \Delta H_{\text{fus}} / \Delta H_{\text{fus}}^0$$

where ΔH_{fus}^0 , the heat of fusion of 100% crystalline PEO ($M_w = 600\,000$ g/mol), was taken as 190 J/g from the literature²⁶ and ΔH_{fus} is the heat of fusion for the sample obtained from the endothermic area of the melting trace.

Optical Measurements. An FTIR spectrometer (FTIR Spectrometer S2000, Perkin-Elmer) equipped with a fixed 100 μm diameter aperture and a mercury–cadmium–telluride (MCT) detector was used to analyze the absorbance in the wavenumber range of 400–4000 cm^{-1} with a resolution of 2 cm^{-1} , monitoring the conformational changes caused by introduction of Au nanoparticles into PEO and the electrospinning process. To obtain a spectrum of pure amorphous PEO, PEO powder (about 1 mg) was melted on the surface of a diamond single attenuated total reflectance (ATR) cell (Golden Gate) at 100 °C. To characterize the PEO molecular orientation within electrospun fibers with and without Au nanoparticles, polarized FTIR measurements using a Zn–Se wire grid infrared polarizer were performed on two or three selected areas in a single electrospun fiber. At each area the parallel and perpendicular spectra relative to the fiber axis were recorded. UV–visible absorption spectra of colloidal Au nanoparticles using a 1 cm quartz cuvette were measured on a Perkin-Elmer Lambda 3B spectrophotometer.

3. Results and Discussion

3.1. Fiber Morphology. Figure 1 shows FEM–SEM micrographs of the electrospun fibers from pure PEO and PEO/Au NC and their diameter distribution. In both cases the fibers, which were electrospun under the optimized ES conditions used (5 cm working distance, 2 wt % solution in chloroform), are uniform without any evidence of “beads on a string” morphology. This observation is consistent with the results by R. Jaeger et al.²⁷ Pure PEO fibers exhibit a smooth surface, whereas the PEO/Au nanocomposite fibers are rather rough. The diameter of the electrospun fibers in both cases resembles a Gaussian distribution. The average diameter lies at 500 nm in pure PEO fibers and shifts to 550 nm in the PEO/Au nanocomposite fibers with broader distribution.

The dispersion of Au nanoparticles within the electrospun fibers was examined by TEM. A striking feature observed on all electrospun fibers containing Au nanoparticles is the formation of extended and closely packed linear nanoparticle chains along the fiber direction, as shown in Figure 2. Within the electrospun fibers of PEO/Au nanocomposite fairly long, closely spaced nanoparticles and a high degree of linearity were observed. All of the linear assemblies observed by TEM display an extended chainlike “necklace” structure. The length of these assemblies appears to be nearly several hundreds micrometers, which is not surprising because ES can straightforwardly produce long continuous fibers up to millimeters in length.

Hereby, the intrinsic semicrystalline feature of PEO may play a crucial role to direct the particular arrangements of nanoparticles during the electrospinning process. In addition, gold nanoparticles were organized with an almost regular spacing due to the dodecanethiol molecules on the particle surface (Figure 3a). Figure 3b shows a HR-TEM micrograph of an individual gold nanoparticle and its fast Fourier transform (FFT) image (inset). The average particle size was about 4 nm in diameter. The HR-TEM image clearly shows crystal lattice fringes of 0.24 nm, corresponding to the (111)

(26) (a) Booth, C.; Devoy, C. J.; Gee, G. *Polymer* **1971**, *12*, 327. (b) Marco, C.; Fatou, J. G.; Gomez, M. A.; Tanaka, H.; Tonelli, A. E. *Macromolecules* **1990**, *23*, 2183.

(27) Jaeger, R.; Bergshoef, M.; Batle, C. M.; Schönherr, H.; Vancso, G. J. *Macromol. Symp.* **1998**, *127*, 141.

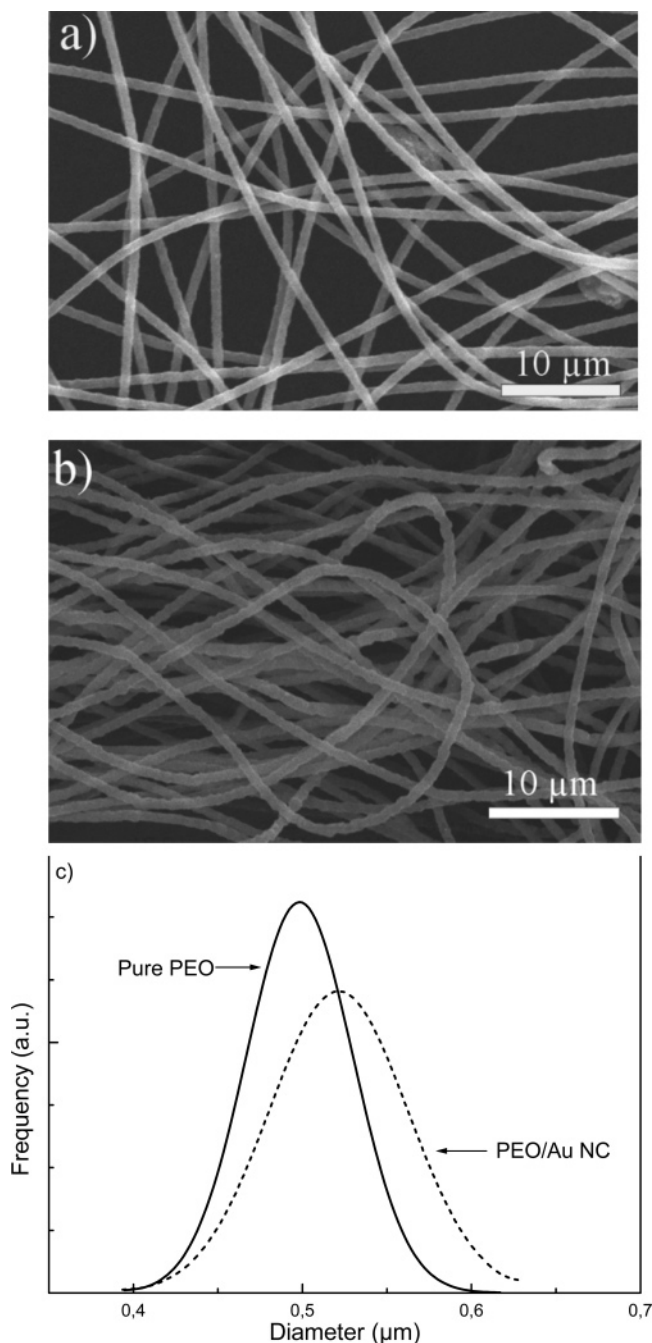


Figure 1. SEM micrographs: (a) electrospun PEO fibers, (b) electrospun PEO/Au NC fibers, and (c) their diameter distributions.

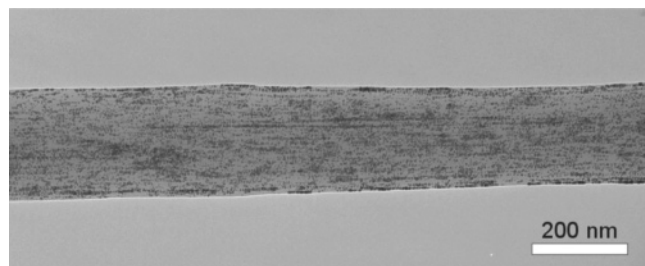


Figure 2. TEM micrograph of 1D chainlike arrays of Au nanoparticles.

lattice planes of fcc.²⁸ It is also noticed here that other areas in the electrospun fibers provide evidence that some chains

(28) Andres, R. P.; Bielefeld, J. D.; Henderson, J. I.; Janes, D. B.; Kolagunta, V. R.; Kubiak, C. P.; Mahoney, W.; Osifchin, R. G. *Science* **1996**, *273*, 1690.

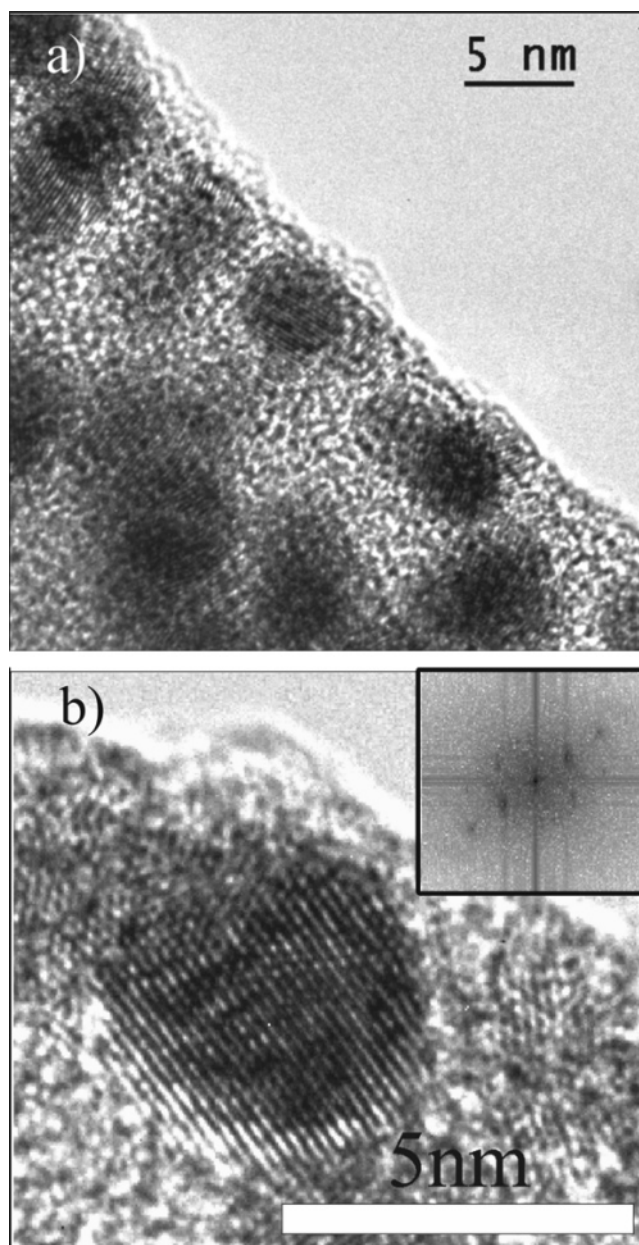


Figure 3. HR-TEM images: (a) close-up image from an area near the surface of the fibers and (b) image of an individual Au nanoparticle and its FFT image shown as inset.

are assembled into 3D bundles, which may be caused by overlapping of the 1D chains of Au nanoparticles.

The UV-vis absorption spectrum shows an absorption band with a peak maximum at 518 nm which arises from surface plasmon absorption of Au nanoparticles (Figure 4) with an assumed optical extinction coefficient of $8.7 \times 10^6 \text{ M}^{-1} \text{ cm}^{-1}$. The electrospun fibers, both with and without Au nanoparticles, revealed a well-defined birefringence in a polarized optical microscope (data not shown here). This indicates that the PEO molecules may be aligned along the fiber axis due to the elongational flow during electrospinning. Figure 5 shows AFM surface images of electrospun fibers exhibiting a perpendicular arrangement of PEO lamellae to the fiber axis, where a and b are taken from pure PEO and PEO/Au nanocomposite, respectively. As expected for

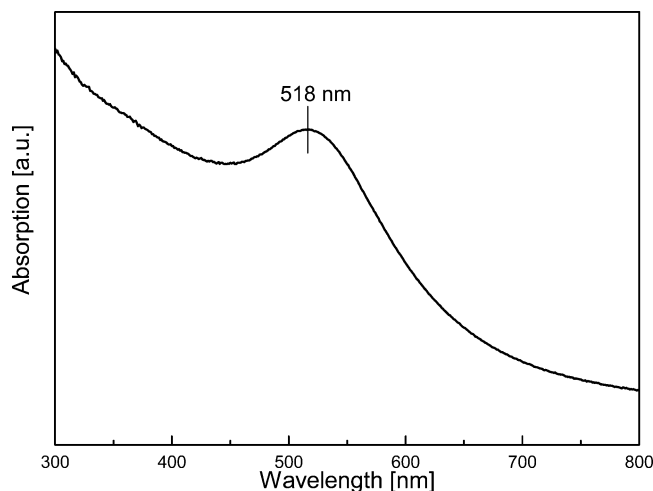


Figure 4. UV-vis spectrum of dodecanethiol-capped Au nanoparticle.

molecule chains aligned parallel to the fiber direction, the resulting lamellae should be perpendicular to the fiber axis, i.e., a so-called shish-kebab structure.^{18a} Figure 5 clearly confirms this argument. AFM shows that the lamellae in the PEO electrospun fibers are thicker and less perpendicularly organized compared to those of the PEO/Au nanocomposite fibers. The lamellar thickness and their long period are 25 and 36 nm in pure PEO electrospun fibers, whereas they are 18 and 30 nm in PEO/Au nanocomposite fibers. These results are consistent with those from DSC and FTIR measurements as will be discussed later. Such a parallel arrangement of nanoparticles with respect to a host polymer with distinct chainlike nanowires should be useful to fabricate future nanodevices.

3.2. Differential Scanning Calorimetry (DSC). To investigate the thermal behavior, such as melting, crystallization, and formation of a crystalline structure, we performed DSC measurements. The most interesting feature in the DSC traces in this study is that all samples show a single endo- and exothermal peak (Figure 6). The endothermic peaks during the heating stage, which are centered at 63–66 °C, are shown in Figure 6a. This is attributed to the melting of the crystalline PEO phase.²⁹ From the enthalpy associated with the melting endotherm the crystallinity of samples studied was calculated using the value 190 J/g as the enthalpy of fusion of 100% crystalline PEO ($M_w = 600\,000$ g/mol) from the literature.²³

As reported in Table 1, after incorporation of Au nanoparticles as well as after the electrospinning procedure the melting temperature shifts moderately to higher values compared with pure PEO. However, the melting enthalpy—degree of crystallinity—increases drastically after incorporation of Au nanoparticles; the most significant change occurs in electrospun fibers of PEO/Au NC. These results indicate that there are some interactions between PEO and Au nanoparticles. Furthermore, the electrospinning procedure favors increasing both the melting temperature and crystallinity. From these results it is concluded that the nanoparticles preferentially serve as heterogeneous nucleation sites for PEO

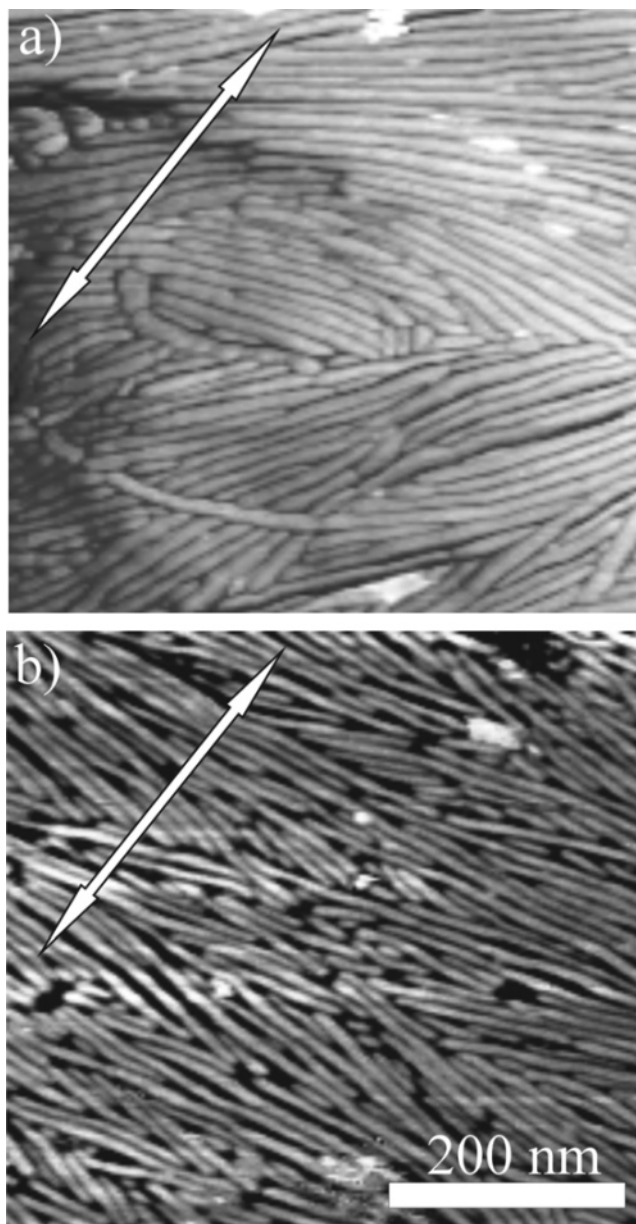


Figure 5. AFM images showing the surface morphology: (a) electrospun PEO fibers and (b) electrospun PEO/Au NC fibers (the arrow indicates the fiber direction).

crystallization. In addition, the electrospinning procedure causes breakage of the long chains of the crystalline complex into small parts. As a consequence, the lamellae in PEO/Au NC fibers appear to be thinner compared to pure PEO fibers (see Figure 5). Figure 6b shows the exotherms upon cooling the melt. Although the exothermic peak of pure PEO is unaffected by the presence of Au nanoparticle in the PEO matrix, it is significantly shifted to higher temperatures upon electrospinning, corresponding to promoted rapid crystallization. This may be caused by confined crystallization through the dimensional reduction of the material during the electrospinning process.

It is interesting to note from the DSC diagrams that the crystallization and melting peak in both systems containing Au nanoparticles appear sharper and narrower before and after electrospinning compared to those without Au nanoparticles. This result may be at least in part attributed to the higher thermal conductivity of Au nano-

(29) Buckley, C. P.; Kovacs, A. J. *Structure of Crystalline Polymers*; Hall, I. H., Ed.; Elsevier Applied Science: London, 1984.

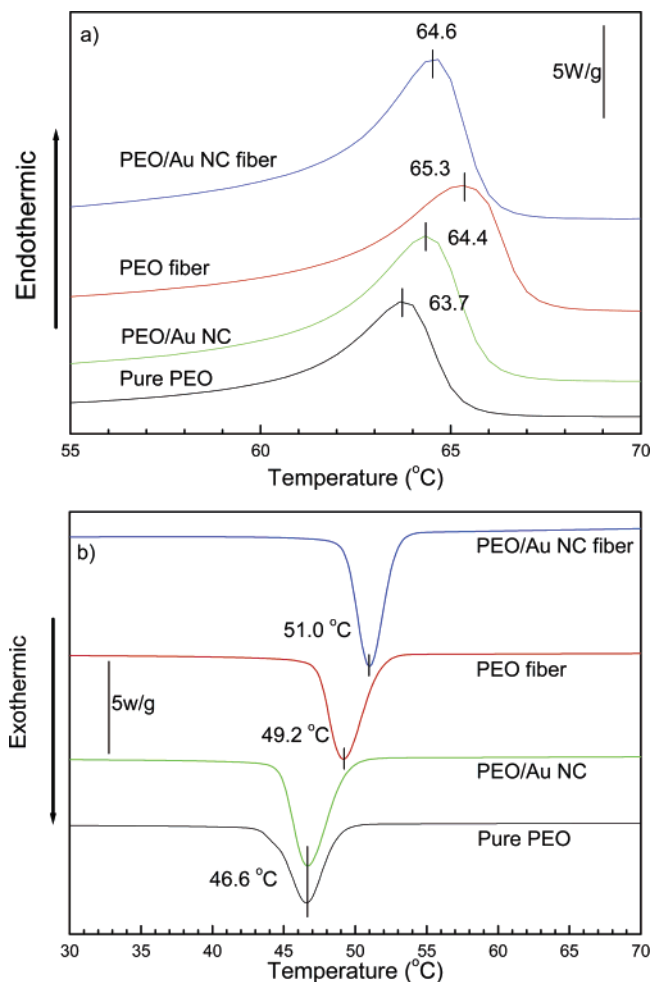


Figure 6. DSC diagrams for pure PEO, PEO/Au NC, electrospun PEO fibers, and electrospun PEO/Au NC fibers: (a) endothermic and (b) exothermic traces.

Table 1: Melting and Crystallization Temperatures, Melting Enthalpies, and Calculated Crystallinities

	T_m (°C)	T_c (°C)	ΔH_m (J/g)	crystallinity (%)
pure PEO	63.7	46.5	83.22	44
PEO/Au NC	64.4	46.5	113.57	60
PEO fiber	65.3	49	110.51	58
PEO/Au NC fiber	64.6	51	117.33	62

particles compared to that of PEO as heat will be more diversely distributed in the samples containing the Au nanoparticles. Thus, Au nanoparticles provide a high degree of supercooling during the crystallization processes while electrospinning, which leads to rapid formation of heterogeneous crystallization nuclei. Consequently, narrow crystallization and melting peak are associated with a narrow crystallite size distribution in the PEO/Au NC electrospun fibers compared to PEO fibers and in the PEO/Au nanocomposite compared to pure PEO. These results are also consistent with AFM results.

3.3. FTIR. Although DSC is informative for the thermal behavior, it does not give any information about the nature of the conformational changes upon introduction of Au nanoparticles and the electrospinning procedure. To characterize the conformational changes we conducted FTIR measurements. Figure 7a shows a FTIR spectrum (600–4000 cm^{-1}) from dodecanethiol-capped Au nanoparticles. The band positions and their assignments are listed in Table 2.³⁰

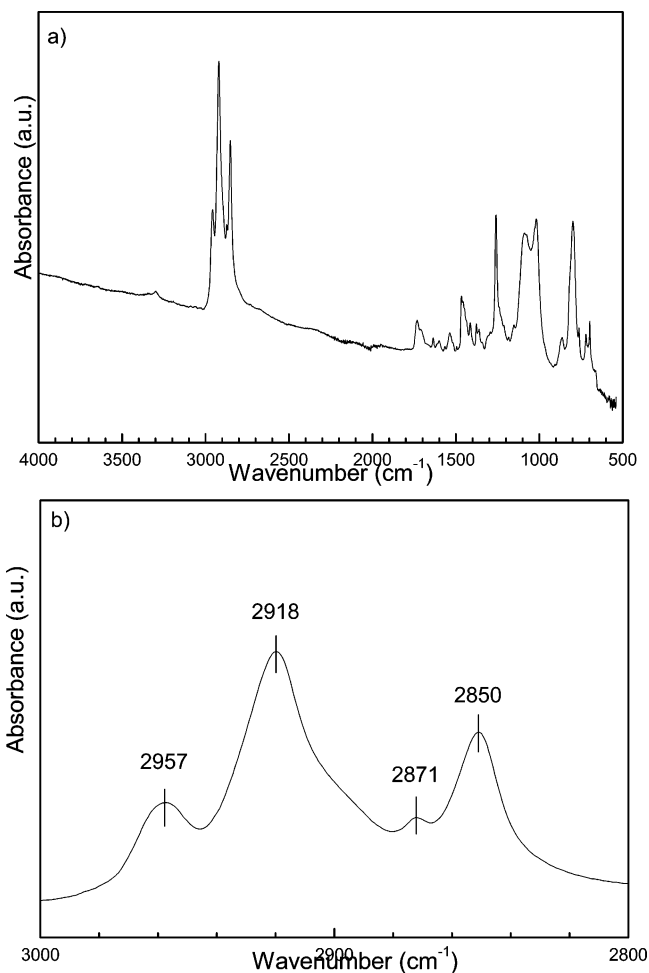


Figure 7. FTIR spectrum for dodecanethiol-capped Au nanoparticles: (a) whole range studied and (b) close-up spectrum from 2800 to 3000 cm^{-1} .

Table 2: FTIR Data for Dodecanethiol-Capped Au Nanoparticles and Their Assignments

absorbance peak (cm^{-1})	assignment
2957	CH_3 asymmetric stretching
2918	CH_2 asymmetric stretching
2871	CH_3 symmetric stretching
2850	CH_2 symmetric stretching
1466	CH_2 scissoring
1413	CH_2 scissoring adjacent to the Au-S bond
1377	CH_3 symmetric bending ⁴⁰

The very weak SH stretching vibration mode is usually observed at 2560 cm^{-1} .³¹ However, this is not visible for dodecanethiol-capped Au nanoparticles, indicating that bonding of the dodecanethiol ligands to the Au surface takes place via Au–S bonds. As a consequence, a new band appearing at 1413 cm^{-1} can be assigned to a scissoring vibration mode of the CH_2 group adjacent to the Au–S bond. These results are consistent with those reported by others.³² The bands at 1466 and 1377 cm^{-1} arise from the asymmetric and sym-

(30) (a) Manna, A.; Imae, T.; Yogo, T.; Aoi, K.; Okazaki, M. *J. Colloid Interface Sci.* **2002**, *256*, 297. (b) Porter, M. D.; Bright, T. B.; Allara, D. L.; Chidsey, C. E. D. *A. Am. Chem. Soc.* **1987**, *109*, 3559.

(31) (a) Laibinis, P. E.; Whitesides, G. M.; Allara, D. L.; Tao, Y.-T.; Parikh, A. N.; Nuzzo, R. G. *J. Am. Chem. Soc.* **1991**, *113*, 7152. (b) Hayashi, M.; Shiro, Y.; Murata, H. *Bull. Chem. Soc. Jpn.* **1966**, *39*, 112.

(32) (a) Hasan, M.; Bethell, D.; Brust, M. *J. Am. Chem. Soc.* **2002**, *124*, 1132. (b) Hostetler, J. M.; Stokes, J. J.; Murray, R. W. *Langmuir* **1996**, *12*, 3604. (c) Smith, E. L.; Porter, M. D. *J. Phys. Chem.* **1993**, *97*, 8032.

metric bending vibration of the methyl group (CH_3), respectively. They can be attributed to the assignments caused by the capping effect. Common vibrational features due to the presence of thiols are represented in the range $2800\text{--}3000\text{ cm}^{-1}$ (Figure 7b). The fact that in the spectrum of nanoparticles the CH_2 asymmetric and symmetric stretching bands are observed at 2918 and 2850 cm^{-1} suggests that the alkyl chains of dodecanethiol are extended with a trans zigzag conformation onto the gold particle surface.³³ The higher wavenumbers of CH_3 stretching modes are observed at 2957 and 2855 cm^{-1} . This indicates that the thiol molecules are not leached out after washing of the particles during the synthesis of Au nanoparticles.

PEO ($[-(\text{CH}_2)_2\text{O}-]_n$) is a semicrystalline polymer whose the crystal structure is well known from X-ray scattering, neutron diffraction, and IR absorption, usually in a monoclinic phase.³⁴ The polymer chains consist of seven $\text{O}-\text{CH}_2-\text{CH}_2$ repeat units, which have an extended structure of 19.3 \AA length over two turns of the helix, i.e., $7/2$ helical conformation. Internal rotations around the $\text{O}-\text{CH}_2$, CH_2-CH_2 , and CH_2-O bonds yield the trans (T), gauche (G), and trans (T) form, respectively, and the resulting helical conformation, TGT. This helical conformation is thermodynamically stable and therefore most commonly observed.³² It has been well established that PEO is preferentially transformed into a planar zigzag conformation (TTT) under tension³⁵ or when water is added, exhibiting a triclinic crystal structure with an identical chain length of 7.12 \AA .^{31,35,36}

To characterize the conformational change in the PEO matrix upon incorporation of Au nanoparticles and electrospinning, FTIR measurements were first performed on the pure PEO. Figure 8 illustrates the vibrational bands of pure PEO from powder and its melt at $120\text{ }^\circ\text{C}$.

The absorption peaks, their assignments, and the type of dominant conformations are summarized in Table 2. The vibrational bands of the crystalline PEO are observed as follows:^{31–37} The bands at 1467 and 1455 cm^{-1} correspond to CH_2 bending, the bands at 1411 and 1341 cm^{-1} to a CH_2 wagging motion, the band 1358 cm^{-1} to the mixed motion of CH_2 wagging and CC stretching, the 1278 , 1240 , and 1235 cm^{-1} bands to CH_2 twisting, the band at 1144 cm^{-1} to the mixed motion of CC and COC stretching, the 1093 cm^{-1} band to COC stretching, the band at 1060 cm^{-1} to the mixed motion of CH_2 rocking and COC stretching, the bands at 961 and 947 cm^{-1} to CH_2 rocking, and the 842 cm^{-1} band to CH_2 bending. For comparison, the FTIR spectrum of purely amorphous PEO was obtained from the molten state of PEO. The doublet bands at 1341 , 1358 , 943 , and 964 cm^{-1}

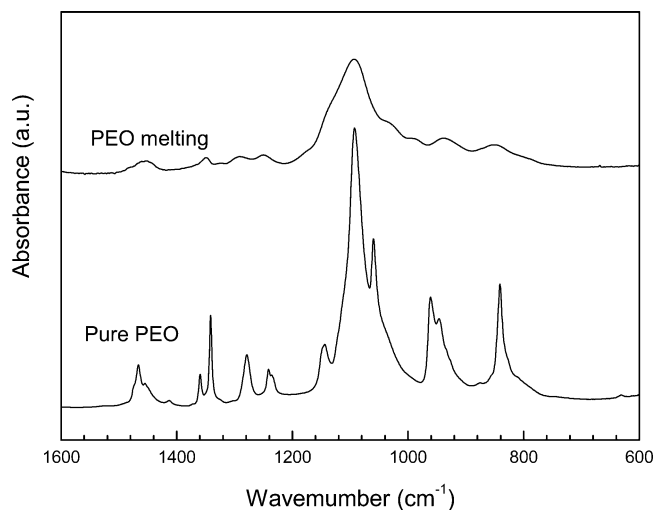


Figure 8. FTIR spectra taken from PEO powder (crystalline) and its melt (amorphous).

which were visible for the crystalline PEO phase disappear completely in the molten state and turn into singlets at 1457 , 1350 , 1292 , 1250 , 939 , and 850 cm^{-1} . These singlet bands are attributed to the vibrational modes of conformationally irregular PEO chains (purely amorphous).^{31a} In the spectrum of amorphous PEO we do not find any indication of either helical or trans planar zigzag conformations, as will be discussed later.

The FTIR spectra of all different samples investigated here are shown in Figure 9. Except for variations in the intensity of these bands, all peaks remain at the same location, i.e., no significant shifts are visible. In addition, the spectra obtained at room temperature do not contain any vibrational bands of amorphous PEO. These results strongly suggest that all materials at room temperature are in the semicrystalline state. It is most interesting to note here that FTIR spectra recorded in the present work indicate a coexistence of at least two different molecular chain conformations. The most characteristic bands of the thermodynamically stable helical structure are located at 1358 , 1278 , 1235 , 1060 , 947 , and 842 cm^{-1} and those of the trans planar conformation at 1341 , 1240 , and 961 cm^{-1} . For simplicity, here we denote the helical and trans planar structures as H and T, respectively. It can be clearly seen in Figure 9 that the band at 1060 cm^{-1} , which is attributed to the H structure of PEO, almost disappears in the electrospun fibers of both systems with and without Au nanoparticles. This indicates that the high extensional force caused by the electrospinning process causes the PEO chains to be preferentially more aligned in the fiber direction, thus forming the T rather than the H conformation. This is consistent with the results observed from PEO under simple tension.

To obtain a deeper insight of the H and T population, we selectively considered the ratio between 1358 and 1341 cm^{-1} (arrows a and b of Figure 9), respectively.³⁸ Other strong lines more or less correspond to the two conformational modifications and, therefore, are not taken into account here. As listed in Table 4, the T/H absorbance ratio (i.e., $A_{1341}/$

(33) (a) Nuzzo, R. G.; Dubios, L. H.; Allara, D. L. *J. Am. Chem. Soc.* **1990**, *112*, 558. (b) Proter, M. D.; Bright, T. B.; Allara, D. L.; Chidsey, C. E. D. *J. Am. Chem. Soc.* **1987**, *109*, 3559.

(34) (a) Dissanayake, M. A. K. L.; Frech, R. *Macromolecules* **1995**, *28*, 5312. (b) Shimomura, M.; Tanabe, Y.; Watanabe, Y.; Kobayashi, M. *Polymer* **1990**, *31*, 1411. (c) Takahashi, Y.; Tadokoro, H. *Macromolecules* **1973**, *6*, 672. (d) Tadokoro, H.; Chatani, Y.; Yoshihara, T.; Tahara, S.; Murahashi, S. *Makromol. Chem.* **1964**, *73*, 109.

(35) (a) Tai, K.; Tadokoro, H. *Macromolecules* **1974**, *7*, 507. (b) Takahashi, Y.; Sumita, I.; Tadokoro, H. *J. Polym. Sci., Polym. Phys. Ed.* **1973**, *11*, 2113.

(36) Rao, G. R.; Castiglioni, C.; Gussoni, M.; Zerbi, G.; Martuscelli, E. *Polymer* **1986**, *26*, 811.

(37) (a) Marenttite, J. M.; Brown, G. R. *Polymer* **1998**, *39*, 1405.

(38) Shieh, Y.-T.; Liu, K.-H. *J. Polym. Sci., Part B Polym. Phys.* **2004**, *42*, 2479.

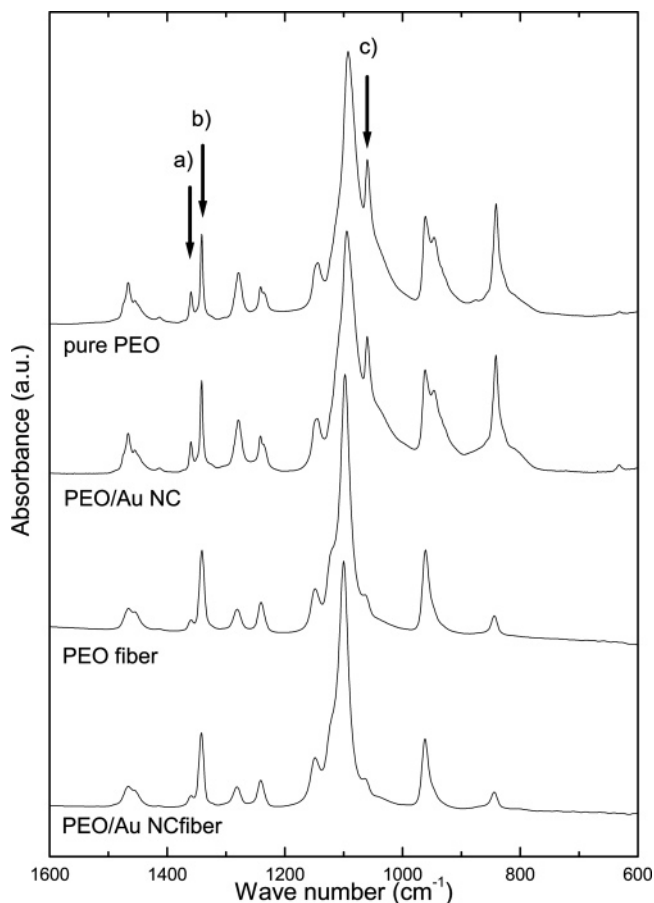


Figure 9. FTIR spectra for pure PEO, PEO/Au NC, electrospun PEO fibers, and PEO/Au NC fibers.

Table 3: FTIR Absorption Peaks for Amorphous (a) and Crystalline (x) PEO, Their Assignments, and Corresponding Dominant Conformational Types

absorption peak from a. PEO (cm ⁻¹)	absorption peak from x PEO (cm ⁻¹)	assignment	type of dominant conformation ^a
1457	1467	CH ₂ bending	
	1455	CH ₂ bending	
	1411	CH ₂ wagging	
	1358	CH ₂ wagging and CC stretching	H
1350	1341	CH ₂ wagging	T
1292	1278	CH ₂ twisting	H
1250	1240	CH ₂ twisting	T
	1235	CH ₂ twisting	H
	1144	CC stretching and COC stretching	
	1093	COC stretching	
	1060	CH ₂ rocking and COC stretching	H
	961	CH ₂ rocking	T
939	947	CH ₂ rocking	H
850	842	CH ₂ bending	H

^a H and T are denoted by the helical and trans planar structure.

A_{1358}) increases after incorporation of Au nanoparticles and electrospinning, indicating an increase in the T population. The degree of the H-to-T conformational transformation of PEO upon incorporation of Au nanoparticles and electro-

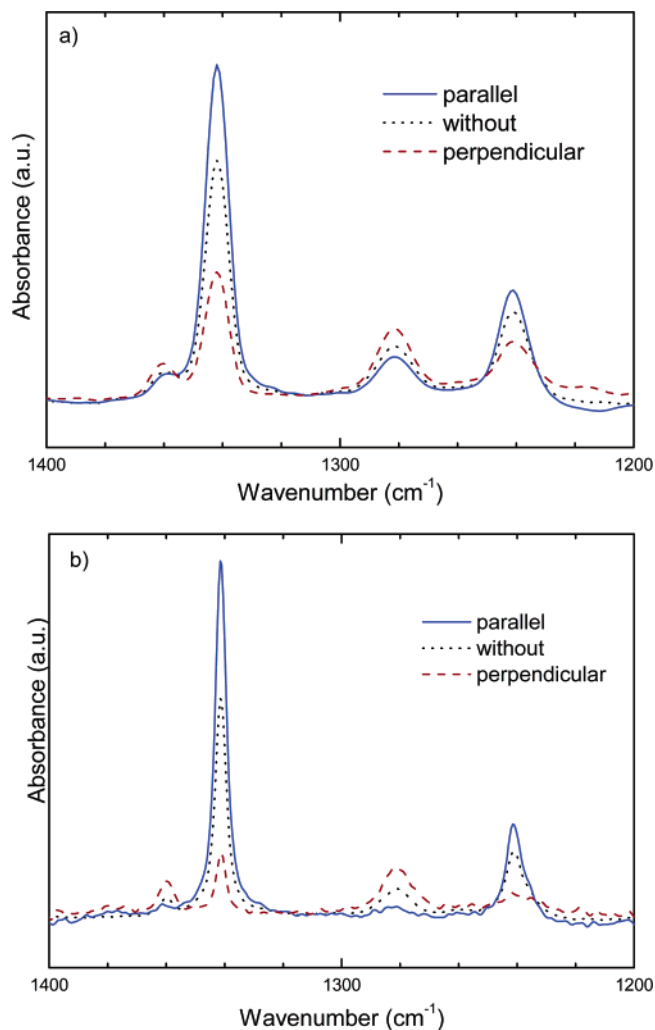


Figure 10. Polarized FTIR spectra for electrospun PEO fibers and PEO/Au NC fibers compared with spectra recorded without polarizing filter.

Table 4: Absorbance Peaks for Trans and Helix Conformation, Relative Population Ratios, and Fractions of the H-to-T Transformation

	T (A_{1341})	H (A_{1358})	T/H ratio	HT%
PEO	1429	1140	1.25	
PEO/Au NC	932	620	1.50	20
PEO fiber	696	508	1.37	10
PEO/Au NC fiber	1800	542	3.32	166

spinning can be calculated as follows

$$HT(\%) = \left[\frac{(A_{1358}/A_{1341})_{\text{PEO/Au-NC-fiber-and-PEO-fiber}}}{(A_{1358}/A_{1341})_{\text{PEO}}} - 1 \right] \times 100\%$$

As mentioned above, whereas an H band at 1060 cm⁻¹ disappears after electrospinning of PEO (see arrow c in Figure 9), it can be clearly seen from Table 4 that the absolute T/H ratio of PEO/Au nanocomposite shifts to a higher value than that of electrospun PEO fibers without Au nanoparticles (twice in HT%). This means that Au nanoparticles preferentially induce the H-to-T conformational transformation, even more than electrospinning by itself. At the molecular level this may be associated with the fact that the dodecanethiol-capped Au nanoparticles interact with a sizable fraction of helical PEO chains, forcing them to become planar, thus favoring the conformational formation of T PEO.

Due to the combination of Au nanoparticles with electrospinning, the electrospun PEO/Au fibers show the highest HT% of 170, which indicates that almost all PEO molecules in these fibers are in the trans state.³⁹

To characterize the degree of molecular orientation of PEO within the electrospun fibers upon incorporation of Au nanoparticles, polarized FTIR measurements were performed. The results are shown in Figure 10, where the most characteristic T band at 1341 cm⁻¹ was taken into consideration. Analysis was carried out by calculating the dichroic ratio, R , as the degree of molecule orientation, defined as follows

$$R = \frac{A_{1341\parallel}}{A_{1341\perp}}$$

where the subscripts \parallel and \perp denote parallel and perpendicular orientation relative to the fiber axis, respectively. The observed R values are 2.60 and 5.69 for the electrospun pure PEO fibers (Figure 10a) and PEO/Au NC fibers (Figure 10b), respectively. This indicates that the PEO molecules are more oriented parallel to the fiber axis in PEO/Au NC fibers than in pure PEO fibers, as expected according to the AFM results discussed before. As result, Au nanoparticles effectively facilitate the molecules aligning in the extensional flow direction during the electrospinning process.

(39) Bedrov, D.; Smith, G. D. *J. Chem. Phys.* **2003**, *118*, 6656.

(40) Known as the umbrella mode, which is essentially limited to the motion of the methyl group and therefore is relatively insensitive to the conformation of the rest of the chain. Hostetler, M. J.; Stokes, J. J.; Murray, R. W. *Langmuir* **1999**, *12*, 3604–3612.

4. Conclusions

In the present work the electrospinning process was successfully used to fabricate polymer nanofibers containing one-dimensional arrays of Au nanoparticles. The intrinsic nature of semicrystalline PEO was used as a template to arrange the Au nanoparticles within the fibers during electrospinning. TEM revealed that Au nanoparticles form quite long and one-dimensionally arranged chainlike arrays within the electrospun fibers. Thermal analysis and FTIR measurements showed that Au nanoparticles preferentially serve as nucleating sites during PEO crystallization and favor transforming the PEO molecular conformation from a helix to trans planar zigzag structure. The conformational transformation was dominantly affected by the presence of Au nanoparticles rather than by electrospinning itself. By means of combination of Au nanoparticles and electrospinning, the PEO molecules were preferentially aligned along the fiber axis, resulting in a perpendicularly arranged lamellar morphology, the so-called shish-kebab structure. Finally, the hybrid electrospinning shown in the present work provides great potential as a convenient and simple technique for the fabrication of one-dimensional arrays of metal nanoparticles suitable for processing into quantum-confined superstructures, in particular, future nanodevices. Their electrical and optical properties are currently under investigation.

Acknowledgment. The authors thank Dr. R. Adikari and Mr. M. Rosenthal for AFM investigation.

CM0508120

Synthesis and Characterization of Polymer-Coated Quantum Dots with Integrated Acceptor Dyes as FRET-Based Nanoprobes

María Teresa Fernández-Argüelles,^{†,‡,§} Aleksey Yakovlev,^{†,||} Ralph A. Sperling,[‡] Camilla Luccardini,[⊥] Stéphane Gaillard,⁺ Alfredo Sanz Medel,[§] Jean-Maurice Mallet,⁺ Jean-Claude Brochon,[#] Anne Feltz,^{*,||} Martin Oheim,^{*,⊥} and Wolfgang J. Parak^{*,‡}

Center for Nanoscience, Ludwig-Maximilians Universität Munich, Amalienstrasse 54, Munich, D-80799 München, Germany, Fakultät Physik, Philipps Universität Marburg, Renthof 7, 35037 Marburg, Germany, Analytical Spectrometry Research Group, Department of Physical and Analytical Chemistry, University of Oviedo, c/Julián Clavería, 8, Oviedo, ES-33006 Spain, ENS-CNRS UMR 8544, Laboratoire de Neurobiologie, Département de Biologie, Ecole Normale Supérieure, 46 rue d'Ulm, Paris, F-75005 France, INSERM S603, Paris, F-75006 France, University Paris Descartes, Laboratory of Neurophysiology and New Microscopies, 45 rue des Saints Pères, Paris, F-75006 France, ENS-CNRS UMR 8642, Glycoscience, Département de Chimie, 24 rue Lhomond, Paris, F-75231 France, and Laboratoire de Biotechnologies et Pharmacologie génétique Appliquée (LBPA) ENS-CNRS UMR 8113, Ecole Normale Supérieure de Cachan, 61 avenue du Président Wilson, Cachan, F-94235 France

Received April 24, 2007; Revised Manuscript Received July 10, 2007

ABSTRACT

A fluorescence resonance energy transfer pair consisting of a colloidal quantum dot donor and multiple organic fluorophores as acceptors is reported and the photophysics of the system is characterized. Most nanoparticle-based biosensors reported so far use the detection of specific changes of the donor/acceptor distance under the influence of analyte binding. Our nanoparticle design on the other hand leads to sensors that detect spectral changes of the acceptor (under the influence of analyte binding) at fixed donor/acceptor distance by the introduction of the acceptor into the polymer coating. This approach allows for short acceptor–donor separation and thus for high-energy transfer efficiencies. Advantageously, the binding properties of the hydrophilic polymer coating further allows for addition of poly(ethylene glycol) shells for improved colloidal stability.

Fluorescence resonant energy transfer (FRET)-based semiconductor nanocrystal (NC) sensors have emerged over the past years as promising nanoscale sensors for analyte

detection.^{1–5} Apart from their larger absorption cross sections and higher photostability when compared with organic fluorophores, the interest in NCs as FRET donors particularly stems from the reduced spectral cross-talk between donor and acceptor signals. The possibility of an efficient blue-shifted donor excitation at wavelengths remote from acceptor, direct excitation minimizes cross-excitation, and the size-tunable donor emission allows for optimal spectral overlap with acceptor absorption. At the same time, the narrow symmetric donor spectrum alleviates the common problem of donor red tailing into acceptor emission wavelengths. With only few exceptions,⁶ the NC typically has been used as a central donor and scaffold for the attachment of multiple

* Corresponding authors: Anne Feltz, anne.feltz@ens.fr; Martin Oheim, martin.oheim@univ-paris5.fr; Wolfgang Parak, wolfgang.parak@physik.uni-marburg.de.

† These authors contributed equally.

‡ Center for Nanoscience, Ludwig-Maximilians Universität Munich and Fakultät Physik, Philipps Universität Marburg.

§ Analytical Spectrometry Research Group, Department of Physical and Analytical Chemistry, University of Oviedo.

|| ENS-CNRS UMR 8544, Laboratoire de Neurobiologie, Département de Biologie, Ecole Normale Supérieure.

⊥ INSERM S603 and University Paris Descartes.

+ ENS-CNRS UMR 8642, Glycoscience, Département de Chimie.

Laboratoire de Biotechnologies et Pharmacologie génétique Appliquée (LBPA), ENS-CNRS UMR 8113, Ecole Normale Supérieure de Cachan.

organic fluorophores or quenchers. In many of these nanosensors, the acceptors are coupled via receptor–ligand interaction, by linking the receptor to the NC and the ligand to the organic acceptor/quencher. The presence of an analyte engenders a change of the donor/acceptor distance that is measured as a change in the FRET efficiency, either in intensity measurements as donor quenching or sensitized acceptor fluorescence or as a decrease in the donor lifetime. Several strategies for analyte-mediated distance changes have been demonstrated: (1) The analyte acts as a competitive ligand for receptor binding by displacing the original fluorescent ligand.^{7,8} (2) The analyte specifically cleaves the linkage between the NC donor and the acceptor.^{9,10} (3) The analyte mediates the binding of the acceptor to the donor.^{11,12} (4) The analyte changes the conformation of the linkage between the donor and the acceptor.¹³ These sensor geometries have in common that the FRET contrast is based on (reversibly or irreversibly) displacing the acceptor from the NC donor.

In an alternative sensor configuration, the acceptor is statically bound on the NC surface and analyte binding/unbinding rather changes the overlap integral between donor emission and acceptor excitation and thus modifies the FRET efficiency.¹⁴ Thus, rather than changing the donor/acceptor distance, the acceptor fluorophore conveys its indicator function to the FRET pair. Finally, one can imagine a slightly modified configuration in which the donor constantly transfers energy to the acceptor, the fluorescence emission of which is changed through a modulation of its quantum efficiency upon ligand binding.

For such static systems to provide sufficient signal and stability, the acceptor should be linked as close to the donor as possible, and the linkage should be stable. Furthermore, sufficient colloidal stability is desirable, which goes hand in hand with stable linkage. Unfortunately there is a tradeoff between both demands. When the acceptor is directly linked to the surfactant-stabilized NC surface through partial ligand exchange, then the acceptor will be as close as possible to the particle surface. Yet, surfactant-stabilized NCs have only limited long-term stability in aqueous solution and tend to aggregate, as eventually the ligands and hence also the acceptor will unbind from the donor.¹⁵ Alternatively, embedding the NC donor in a more complex shell, such as encapsulation between zipper proteins,¹⁶ in a cross-linked ligand shell,¹⁷ in a glass shell,¹⁸ in micelles,¹⁹ or in a polymer coat,^{20–24} and the subsequent functionalization with poly(ethylene glycol) (PEG)^{25,26} permit a good colloidal stability but increases the effective diameter of the nanoparticle^{24,27–30} and hence donor/acceptor separation distance. While the polymer shell adds on the order of 3–4 nm to the particle radius,³⁰ additional coating with PEG adds another few nanometers.³⁰ The resulting donor/acceptor distances are hence much larger than typical Förster radii, which are on the order of a nanometer so that colloidally stable (PEG-coated) NC-based biosensors typically have lower FRET efficiencies and signal.

In this study, we introduce a FRET geometry in which the acceptor is directly incorporated into the encapsulation

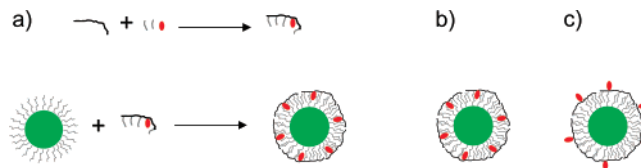


Figure 1. (a) An amphiphilic polymer is synthesized by reacting hydrophobic hydrocarbon chains (dark gray) and an organic dye (red) to a polar polymer backbone (light gray). Quantum dots (inorganic CdSe/ZnS core/shell drawn in green capped with trioctylphosphine oxide and similar surfactants drawn in dark gray) are coated with the amphiphilic polymer by intercalation of the hydrophobic side chains of the polymer with the hydrophobic surfactant molecules on the quantum dot surface and the resultant polymer-coated quantum dot is hydrophilic due to the polar polymer backbone.²¹ The following dye/quantum dot configurations were used in this study: (b) polymer-coated quantum dots with dye incorporated in the polymer; (c) polymer-coated quantum dots with dye linked to the polymer shell with a postmodification process.

shell used to provide colloidal stability to the NC donor. In this way, the linkage of the acceptor to the NC donor is very stable, the whole assembly has excellent colloidal stability, and the donor/acceptor distance is potentially reduced. We here compare the performance of this system to assemblies reported so far, in which the acceptor has been linked in a postmodification to the outside of a polymer shell around the NC donor.

An amphiphilic polymer is synthesized by linking amino-functionalized hydrophobic hydrocarbon chains (dodecylamine) to a polar backbone (poly(isobutylene-*alt*-maleic anhydride), $M_w = 6$ kDa) under reaction of the amino group of the hydrocarbon chain with the anhydride rings of the polymer backbone (reaction in anhydrous tetrahydrofuran; the quantity of dodecylamine is calculated in a way that 75% of the anhydride rings react with one dodecylamine molecule each; for a detailed protocol see Supporting Information).^{20,31,32} The acceptor fluorophore (amino-modified ATTO590) was incorporated into the amphiphilic polymer by reaction of the amino group of the dye with the anhydride rings of the polymer backbone (reaction in anhydrous chloroform; the quantity of dye is calculated in a way that 1% (or alternatively 2%, 4%, or 8%) of the anhydride rings react with one dye molecule each, see Figure 1a. CdSe/ZnS quantum dots (Qdot 545 ITK organic quantum dots, Invitrogen, # Q21791MP) were then coated with the dye (ATTO590)-modified amphiphilic polymer according to a previously published protocol (see Figure 1a,b).²¹ The particles are colloidally stabilized in aqueous solution by negatively charged carboxyl groups originating from opened anhydride rings. Assuming a Förster-type r^{-6} interaction between Qdot 545 ITK and ATTO590, we estimate from their overlap integral a Förster radius of 6.4 nm. As a control, we coated under the same conditions Qdots 545 ITK with amphiphilic polymer devoid of ATTO dye. In one set of experiments, we linked to these particles ATTO dye in a postmodification procedure with EDC chemistry (linkage of the amino group of the amino-modified ATTO590 with the carboxyl groups of the polymer, mediated by *N*-(3-dimethylaminopropyl)-*N'*-ethylcarbodiimide hydrochloride, see Figure 1c). We note that the polymer-coating procedure



Figure 2. Quantum dots were coated with an amphiphilic polymer without (2) and with (3) incorporated ATTO590 dye. As control, empty polymer micelles with incorporated dye (1) are used. The three samples were loaded on a 1% agarose gel (arrow), and a voltage of 100 V was applied for around 1 h. During this time the negatively charged particles migrated toward the plus pole. Fast (F) and slow (S) migrating bands were observed by illumination the gel with a hand-held UV lamp. The empty polymer micelles (lane 1) can be seen as “fast” band by the red fluorescence of the ATTO dye incorporated in the polymer. The polymer coated quantum dots (without dye in the polymer, lane 2) can be seen as “slow” band by the green fluorescence of the quantum dots. Presumably, the polymer-coating procedure also produces empty micelles, which are not fluorescent and are not detected in our assay. The sample with the polymer coated quantum dots with dye incorporated in the polymer (lane 3) yields one “slow” band with orange fluorescent and one “fast” band with red fluorescence. The fast band (which migrated at the same speed as the control sample (1) with the empty polymer micelles) can be attributed to empty polymer micelles, which had been formed during the polymer coating process, and they can be observed due to the fluorescence of the ATTO dye incorporated in the polymer. The slow band (which migrated at the same speed as the polymer-coated quantum dots (2)) can be attributed to polymer coated quantum dots with dye incorporated in the polymer. The emission from these nanoparticles appears orange, as part of the energy absorbed by the quantum dots is transferred via FRET to the dye in the polymer, and for this reason an overlap of the quantum dot and dye fluorescence is observed.

results in some empty polymer micelles³² in addition to polymer-coated particles. In contrast to earlier reports for a similar system³³ size-exclusion chromatography failed to separate excess polymer (in the form of micelles) from the polymer-coated NCs. However, gel electrophoresis¹⁸ reliably separated the polymer micelles (see Figure 2). We used for all spectroscopic measurements NCs that were purified from excess micelles by gel electrophoresis.

To characterize the efficiency of energy transfer from the NC donor to the ATTO590 acceptor, we measured both spectrally resolved intensities (Figure 3a) and fluorescence decays, using a time-correlated single photon counting (TCSPC) approach³⁴ (Figure 3b). Lifetime measurements allow the FRET measurement independent of the donor concentration, by calculating $E = 1 - \langle \tau_{DA} \rangle / \langle \tau_D \rangle$, where τ_{DA} and τ_D are the donor lifetimes in the presence and absence of the acceptor, respectively, and $\langle \rangle$ denotes the weighted average over all lifetime components, see Figure 3b and Supporting Information for details.

The measured absorption spectra of the QD545/ATTO590 conjugates were dominated by the acceptor absorption. In the 550–600 nm range, the contribution of the NC to the total absorption was barely detected so that we could not determine the donor/acceptor ratio from absorbance measure-

ments (see Supporting Information for details). With NCs and ATTO molecules having an absorbance of 156 000 vs 22 000 $M^{-1} \text{ cm}^{-1}$ at 450 nm, respectively, and $\sim 15\%$ noise, we can estimate that at least 47 ATTO590 molecules are required to obscure the NC absorption. This number is plausible in view of the number of dye molecules that have been added during the polymer coating (≤ 56 ATTO molecules per quantum dot in the case that only 1% of these anhydride sites were occupied with dye). Thus, for the case of the polymer with the least attached ATTO molecules (1% of the sites), each NC donor is decorated with about 50 ATTO dye acceptors.

In as much as we could determine the ATTO590 dye concentration but not the exact stoichiometry (donor/acceptor ratio) for the QD545/ATTO590 conjugates, we first normalized all measured fluorescence emission spectra to the (total) number of ATTO590 molecules, in the NC polymer coat or free in solution. To estimate the total number of ATTO590 molecules, we first directly excited the ATTO590 acceptor at 590 nm (where little interference from donor fluorescence is expected). Each of the emission spectra of the donor/acceptor conjugates, recorded at 450 nm excitation (where direct excitation of ATTO590 is low) was normalized by division through the peak fluorescence measured at 590 nm excitation (Figure 3). This first normalization scales the curves to an equal quantity of acceptors. Next, to account for fluctuations in the excitation power we further scaled the normalized emission spectra of the ATTO dye in the absence of the QD545, excited at 450 nm to a peak emission of 1.

Figure 3a displays these doubly normalized fluorescence emission spectra for the different QD545/ATTO590 dye assemblies, measured in 1 cm cuvettes. The red curve corresponds to empty micelles devoid of NCs but with ATTO dye embedded in the polymer. The spectral emission of the ATTO dye did not change by embedding it into the amphiphilic polymer, as the micelle spectrum matches that of the normalized spectrum of free ATTO590 dye (data shown in Supporting Information). The orange trace represents QD545 nanoparticles with ATTO590 dye incorporated in the polymer shell. Two emission peaks are readily apparent. The emission peak in the green/yellow (545 nm) corresponds to the NC donor, the one in the red (622 nm) to the ATTO590 acceptor. Part of the energy absorbed by the NCs is directly emitted (fluorescence emission of the quantum dots in the green/yellow) and another part is transferred by FRET to the ATTO dye, from where it also can be emitted (fluorescence emission of the ATTO dye in the red). The emission intensity of the ATTO dye bound to the NC is more than five times larger than the direct excitation of free ATTO dye molecules, indicating sensitized acceptor fluorescence due to FRET. Time-resolved measurements corroborated this interpretation. Using femtosecond-pulsed-laser excitation at 450 nm, we measured the fluorescence decay of the emission of the NCs, Figure 3b. Weighted average decay times of bare polymer coated NCs without the ATTO dye (green curve) were around 10 ns. FRET offered an alternative pathway for donor relaxation, reducing

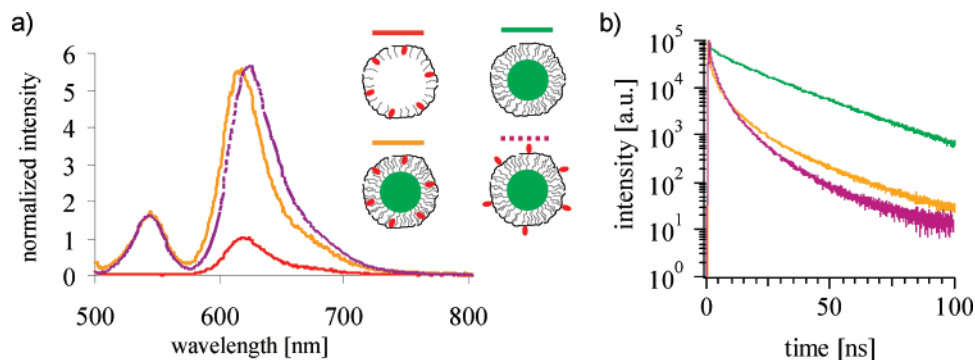


Figure 3. Spectroscopic characterization of different samples. (a) Normalized fluorescence intensity upon excitation at 450 nm. The spectra were normalized in a way that they all refer to solutions with the same amount of ATTO dye molecules and that the emission intensity of free ATTO dye is 1. (b) Normalized fluorescence decays. The pulse rate of a frequency-doubled Ti:sapphire laser was reduced to 4 MHz to accommodate the long NC decay times. Traces are normalized to 10^5 counts at peak. The noise under these conditions was on the order of 10^0 .

its lifetime to about 2 ns in the presence of ATTO dye embedded in the polymer shell (orange trace).

In addition to NCs containing ~ 50 ATTO molecules per donor (1%), we also prepared conjugates with an amphiphilic polymer layer in which 4% and 8% of the anhydride rings had been reacted with amino-modified ATTO dye. Increasing the amount of dye embedded in the polymer during synthesis decreased the measured average donor lifetime from 2.5 ns (1%) to 2.1 (4%) and 1.7 ns (8%). The corresponding FRET efficiencies are estimated as 0.75, 0.79, and 0.84, respectively. This observation is in line with the measured normalized emission spectra for these conjugates (orange line on Figure 3a). With the peak emission of the acceptor normalized as above, the peak at donor emission is getting increasingly smaller when increasing the ATTO concentration from 1% to 8%.

When the ATTO dye is linked via EDC chemistry to the polymer shell of the NCs (see Figure 1b for a schematic representation), the normalized intensity as well as the photoluminescence decay time (dotted purple traces in parts a and b of Figure 3, respectively) were comparable to those obtained with ATTO dye within the polymer shell (straight orange line). However, the fluorescence emission peak was ~ 10 nm red-shifted compared to the pure ATTO590 dye or the other tested geometries, probably due to a change in the local microenvironment of the dye. As before, we equally varied the donor/acceptor ratio by increasing their concentration ratio during synthesis. Again, the FRET efficiencies systematically increased when increasing the acceptor concentration. There is no significant difference in FRET efficiency and hence donor/acceptor distance between including the ATTO during synthesis or adding it afterward to the polymer shell. FRET efficiencies ranged between 0.77 and 0.84 and were thus not markedly different from the conjugates in which the acceptor was directly included into the polymer coat. Thus, the sketches in Figure 1 are probably too idealized. Nevertheless, there are several distinctive advantages of embedding the dye into the polymer shell rather than adding it afterward to the polymer shell. First, acceptor binding was very efficient, as basically all used ATTO molecules were incorporated into the polymer shell.

Second, in contrast to postmodification in aqueous solution, which requires a water-soluble dye, also hydrophobic dyes can be readily incorporated into the polymer shell, as the actual synthesis of the amphiphilic polymer is performed in organic solvent. Third, problems with colloidal stability are equally circumvented when adding the dye directly into the polymer shell, as no condition with high salt concentration as needed for EDC chemistry is required. Thus, from a practical standpoint, the inclusion of the acceptor facilitates shipping the conjugates to the end user and permits a long shelf life, without concerns about the sensor stability.

In conclusion, our experiments indicate that embedding the acceptor dye directly in the amphiphilic polymer used to make the donor nanoparticle water soluble leads to a novel and advantageous geometry that can be used for FRET-based nanosensors, for which the acceptor needs to be statically fixed to the donor.¹⁴ This assembly is known to provide an excellent colloidal stability^{21,26} and it allows for all post-modification steps that have been already demonstrated for polymer-coated particles. In particular, the polymer-coated NCs (with the dye incorporated into the polymer shell) could be further colloidally stabilized with an additional PEG shell and also be modified with a precisely controlled number of functional groups.²⁶ This makes them promising candidates for the investigation of cellular traffic on a single particle level.^{35,36}

Acknowledgment. This project was funded by the GIP-ANR PNANO consortium ‘NanoFRET’ (J.-M.M., A.F., M.O., W.J.P.), and, in part, by the European Union (W.J.P., SA-Nano) and the German Research Foundation (W.J.P., Emmy Noether fellowship). Maria Teresa Fernández-Argüelles acknowledges a grant (BP04-040) from the Consejería de Educación y Ciencia of the Principado de Asturias. The authors are grateful to Cheng-An J. Lin for developing the here used polymer coating procedure.³²

Supporting Information Available: Descriptions of synthesis of the amphiphilic polymer, polymer coating of quantum dots, sample purification with gel electrophoresis, normalization procedure for the evaluation of fluorescence

spectra, evaluation of the fluorescence spectra, and time resolved measurements. This material is available free of charge via the Internet at <http://pubs.acs.org>.

References

- (1) Medintz, I. L.; Uyeda, H. T.; Goldman, E. R.; Mattoussi, H. *Nat. Mater.* **2005**, *4* (6), 635–446.
- (2) Clapp, A. R.; Medintz, I. L.; Mattoussi, H. *ChemPhysChem* **2006**, *7*, 47–57.
- (3) Dubertret, B. *Nat. Mater.* **2005**, *4*, 797–798.
- (4) Medintz, I. L.; Deschamps, J. R. *Curr. Opin. Biotechnol.* **2006**, *17* (1), 17–27.
- (5) Lin, C.-A. J.; Liedl, T.; Sperling, R. A.; Fernández-Argüelles, M. T.; Costa-Fernández, J. M.; Pereiro, R.; Sanz-Medel, A.; Chang, W. H.; Parak, W. J. *J. Mater. Chem.* **2007**, *17* (14), 1343–1346.
- (6) So, M.-K.; Xu, C.; Loening, A. M.; Gambhir, S. V.; Rao, J. *Nat. Biotechnol.* **2006**, *24* (3), 339–343.
- (7) Medintz, I. L.; Clapp, A. R.; Mattoussi, H.; Goldman, E. R.; Fisher, B.; Mauro, J. M. *Nat. Mater.* **2003**, *2*, 630–638.
- (8) Goldman, E. R.; Medintz, I. L.; Whitley, J. L.; Hayhurst, A.; Clapp, A. R.; Uyeda, H. T.; Deschamps, J. R.; Lassman, M. E.; Mattoussi, H. *J. Am. Chem. Soc.* **2005**, *127*, 6744–6751.
- (9) Gill, R.; Willner, I.; Shweky, I.; Banin, U. *J. Phys. Chem. B* **2005**, *109* (49), 23715–23719.
- (10) Medintz, I. L.; Clapp, A. R.; Brunel, F. M.; Tiefenbrunn, T.; Uyeda, H. T.; Chang, E. L.; Deschamps, J. R.; Dawson, P. E.; Mattoussi, H. *Nat. Mater.* **2006**, *5*, 581–589.
- (11) Zhang, C.-Y.; Yeh, H.-C.; Kuroki, M. T.; Wang, T.-H. *Nat. Mater.* **2005**, *4*, 826–831.
- (12) Patolsky, F.; Gill, R.; Weizmann, Y.; Mokari, T.; Banin, U.; Willner, I. *J. Am. Chem. Soc.* **2003**, *125* (46), 13918–13919.
- (13) Medintz, I. L.; Clapp, A. R.; Melinger, J. S.; Deschamps, J. R.; Mattoussi, H. *Adv. Mater.* **2005**, *17*, 2450–2455.
- (14) Snee, P. T.; Somers, R. C.; Nair, G.; Zimmer, J. P.; Bawendi, M. G.; Nocera, D. G. *J. Am. Chem. Soc.* **2006**, *128* (41), 13320–13321.
- (15) Boldt, K.; Bruns, O. T.; Gaponik, N.; Eychmüller, A. *J. Phys. Chem. B* **2006**, *110* (5), 1959–1963.
- (16) Mattoussi, H.; Mauro, J. M.; Goldman, E. R.; Green, T. M.; Anderson, G. P.; Sundar, V. C.; Bawendi, M. G. *Phys. Status Solidi B* **2001**, *224* (1), 277–283.
- (17) Jiang, W.; Mardiyani, S.; Fischer, H.; Chan, W. C. W. *Chem. Mater.* **2006**, *18* (4), 872–878.
- (18) Parak, W. J.; Gerion, D.; Zanchet, D.; Woerz, A. S.; Pellegrino, T.; Micheel, C.; Williams, S. C.; Seitz, M.; Bruehl, R. E.; Bryant, Z.; Bustamante, C.; Bertozzi, C. R.; Alivisatos, A. P. *Chem. Mater.* **2002**, *14* (5), 2113–2119.
- (19) Dubertret, B.; Skourides, P.; Norris, D. J.; Noireaux, V.; Brivanlou, A. H.; Libchaber, A. *Science* **2002**, *298* (29 November), 1759–1762.
- (20) Wu, M. X.; Liu, H.; Liu, J.; Haley, K. N.; Treadway, J. A.; Larson, J. P.; Ge, N.; Peale, F.; Bruchez, M. P. *Nat. Biotechnol.* **2003**, *21*, 41–46.
- (21) Pellegrino, T.; Manna, L.; Kudera, S.; Liedl, T.; Koktysh, D.; Rogach, A. L.; Keller, S.; Rädler, J.; Natile, G.; Parak, W. J. *Nano Lett.* **2004**, *4* (4), 703–707.
- (22) Petruska, M. A.; Bartko, A. P.; Klimov, V. I. *J. Am. Chem. Soc.* **2004**, *126* (3), 714–715.
- (23) Yu, W. W.; Chang, E.; Sayes, C. M.; Drezek, R.; Colvin, V. L. *Nanotechnology* **2006**, *17* (17), 4483–4487.
- (24) Luccardini, C.; Tribet, C.; Vial, F.; Marchi-Artzner, V.; Dahan, M. *Langmuir* **2006**, *22* (5), 2304–2310.
- (25) Ballou, B.; Lagerholm, B. C.; Ernst, L. A.; Bruchez, M. P.; Waggoner, A. S. *Bioconjugate Chem.* **2004**, *15* (1), 79–86.
- (26) Sperling, R. A.; Pellegrino, T.; Li, J. K.; Chang, W. H.; Parak, W. J. *Adv. Funct. Mater.* **2006**, *16*, 943–948.
- (27) Liedl, T.; Keller, S.; Simmel, F. C.; Rädler, J. O.; Parak, W. J. *Small* **2005**, *1* (10), 997–1003.
- (28) Pons, T.; Uyeda, H. T.; Medintz, I. L.; Mattoussi, H. *J. Phys. Chem. B* **2006**, *110* (41), 20308–20316.
- (29) Smith, A. M.; Duan, H.; Rhyner, M. N.; Ruan, G.; Nie, S. *Phys. Chem. Chem. Phys.* **2006**, *8*, 3895–3903.
- (30) Sperling, R. A.; Liedl, T.; Duhr, S.; Kudera, S.; Zanella, M.; Lin, C.-A. J.; Chang, W.; Braun, D.; Parak, W. J. *J. Phys. Chem. C* **2007**, *111*, 11552–11559.
- (31) Wang, K. T.; Iliopoulos, I.; Audebert, R. *Polym. Bull.* **1988**, *20*, 577–582.
- (32) Lin, C.-A. J.; Sperling, R. A.; Li, J. K.; Yang, T.-Y.; Li, P.-Y.; Zanella, M.; Chang, W. H.; Parak, W. J. Submitted to *Small*.
- (33) Wang, M.; Dykstra, T. E.; Lou, X.; Salvador, M. R.; Scholes, G. D.; Winnik, M. A. *Angew. Chem., Int. Ed.* **2006**, *45*, 2221–2224.
- (34) Brochon, J. C., Maximum-Entropy Method Of Data-Analysis In Time-Resolved Spectroscopy. In *Numerical Computer Methods, Part B*; Academic Press: San Diego, CA, 1994; Vol. 240, pp 262–311.
- (35) Lidke, D. S.; Nagy, P.; Heintzmann, R.; Arndt-Jovin, D. J.; Post, J. N.; Grecco, H. E.; Jares-Erijman, E. A.; Jovin, T. M. *Nat. Biotechnol.* **2004**, *22*, 198–203.
- (36) Dahan, M.; Levi, S.; Luccardini, C.; Rostaing, P.; Riveau, B.; Triller, A. *Science* **2003**, *302* (5644), 442–445.

NL070971D

Size and Surface Effects on the MRI Relaxivity of Manganese Ferrite Nanoparticle Contrast Agents

Ulrich I. Tromsdorf,^{†,#} Nadja C. Bigall,^{†,#} Michael G. Kaul,[‡] Oliver T. Bruns,[§] Marija S. Nikolic,[†] Birgit Mollwitz,[§] Ralph A. Sperling,^{||} Rudolph Reimer,[⊥] Heinz Hohenberg,[⊥] Wolfgang J. Parak,^{||} Stephan Förster,[†] Ulrike Beisiegel,[§] Gerhard Adam,[‡] and Horst Weller^{*,†}

Institute of Physical Chemistry, University of Hamburg, Grindelallee 117, 20146 Hamburg, Germany, Department of Diagnostic and Interventional Radiology, University Medical Center Hamburg-Eppendorf, Martinistrasse 52, 20246 Hamburg, Germany, Department of Biochemistry and Molecular Biology II: Molecular Cell Biology, University Medical Center Hamburg-Eppendorf, Martinistrasse 52, 20246 Hamburg, Germany, Ludwig-Maximilians-University, Center of NanoScience, Amalienstrasse 54, 80799 Munich, Germany, and Department of Electron Microscopy and Micro Technology, Heinrich-Pette Institute, Martinistrasse 52, 20251 Hamburg, Germany

Received May 11, 2007; Revised Manuscript Received July 2, 2007

ABSTRACT

Superparamagnetic MnFe_2O_4 nanocrystals of different sizes were synthesized in high-boiling ether solvent and transferred into water using three different approaches. First, we applied a ligand exchange in order to form a water soluble polymer shell. Second, the particles were embedded into an amphiphilic polymer shell. Third, the nanoparticles were embedded into large micelles formed by lipids. Although all approaches lead to effective negative contrast enhancement, we observed significant differences concerning the magnitude of this effect. The transverse relaxivity, in particular r_2^* , is greatly higher for the micellar system compared to the polymer-coated particles using same-sized nanoparticles. We also observed an increase in transverse relaxivities with increasing particle size for the polymer-coated nanocrystals. The results are qualitatively compared with theoretical models describing the dependence of relaxivity on the size of magnetic spheres.

Magnetic nanoparticles became more and more important for applications in biotechnology and biomedicine¹ as well as technical ones like magnetic data storage² over the past few years. Examples are magnetothermal therapy^{3,4} or in vivo imaging.^{5–7} Here we present the synthesis and potential use of superparamagnetic manganese ferrite nanocrystals (MnFe_2O_4) as contrast agents in magnetic resonance imaging (MRI).⁸ Whereas enormous progress has been achieved in the technological development of MRI, including sophisticated pulse sequences for image generation, the development of chemical contrast agents still has a great potential for improvement. In particular, T_2 contrast agents under clinical

use consist of very polydisperse and aggregated iron oxide nanoparticles. Recent investigations impressively show that the contrast enhancement of nanoparticles is strongly determined by their size, surface properties, and the degree of aggregation.^{9–11} The aim of this work is to clearly distinguish between these effects by using monodisperse samples of 3–18 nm MnFe_2O_4 particles and to subject these samples to various methods of surface functionalization and compartmentalization in lipid micelles. We will also distinguish between the impact of these effects in the various pulse sequence modes for the detection of both the transverse relaxation (T_2 process) and the effective transverse relaxation (T_2^* process).

The MRI signal that is detected after the excitation of magnetic moments by a radio frequency (rf) pulse is determined by the examined object and the imaging sequence. The imaging sequence is weighting the impact of the net magnetization of hydrogen atoms and the relaxation mechanisms. The first mechanism describes the relaxation

* Corresponding author. E-mail: weller@chemie.uni-hamburg.de.

[†] Institute of Physical Chemistry, University of Hamburg.

[‡] Department of Diagnostic and Interventional Radiology, University Medical Center Hamburg-Eppendorf.

[§] Department of Biochemistry and Molecular Biology II: Molecular Cell Biology, University Medical Center Hamburg-Eppendorf.

^{||} Ludwig-Maximilians-University, Center of NanoScience.

[⊥] Department of Electron Microscopy and Micro Technology, Heinrich-Pette Institute.

[#] These authors contributed equally to this work.

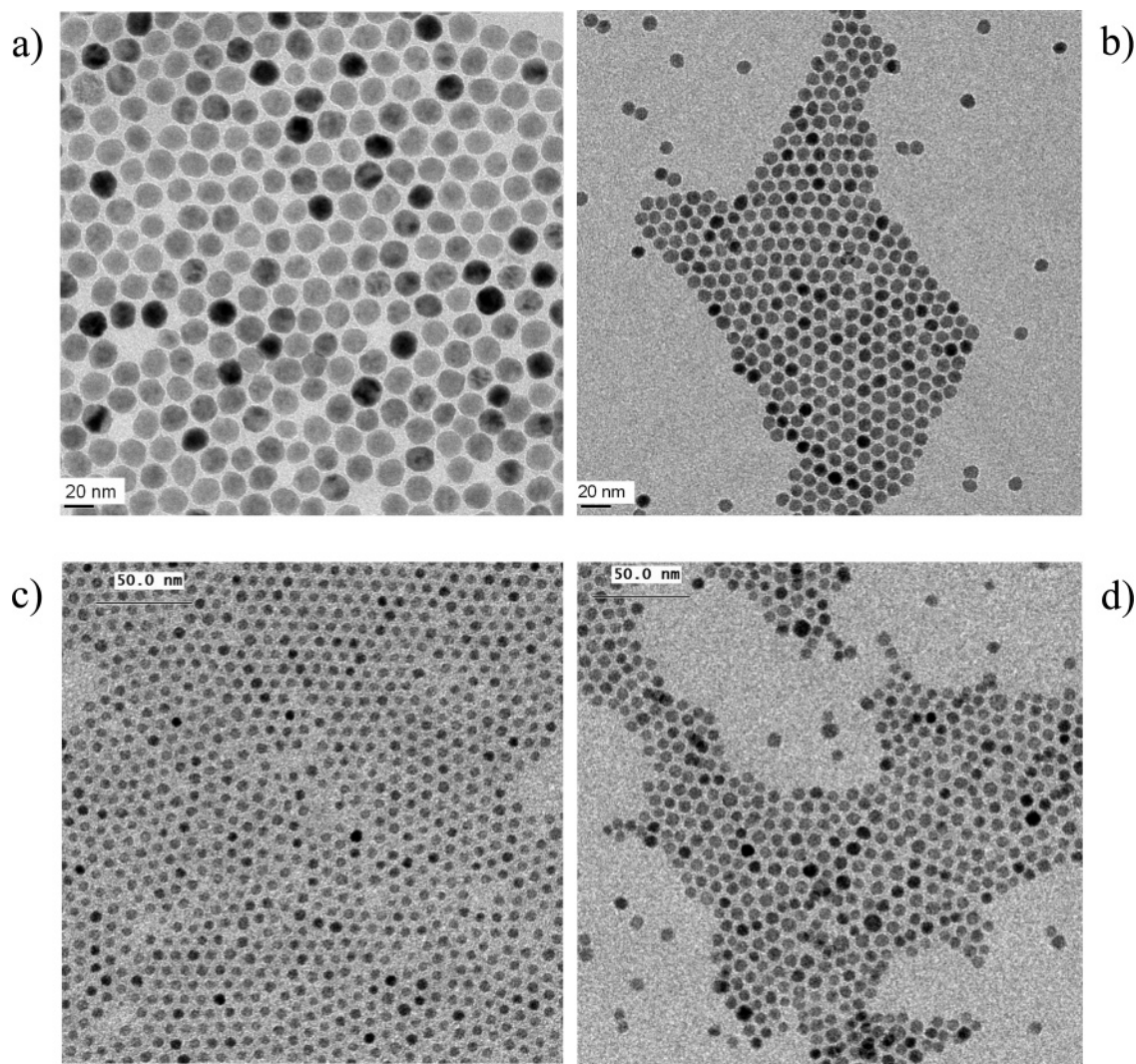


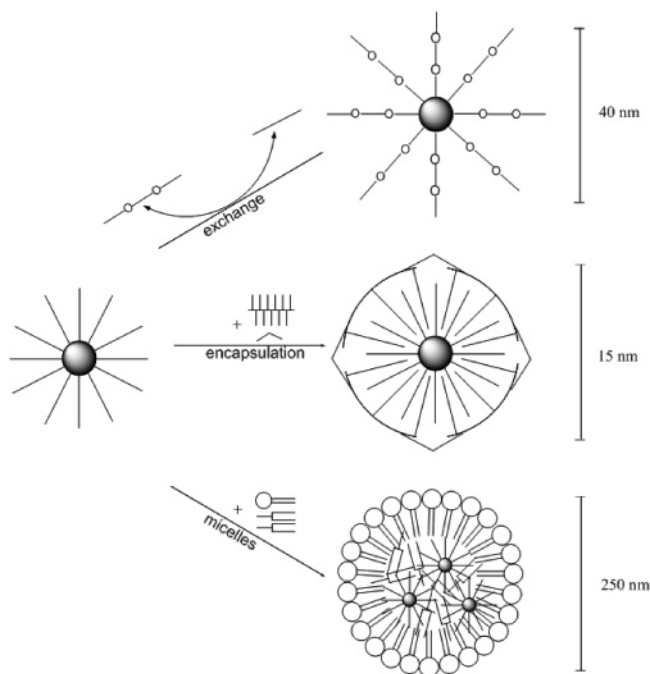
Figure 1. TEM image of 18 nm (a) and 9 nm (b) monodisperse samples (less than 10% standard deviation) of MnFe_2O_4 nanocrystals as well as fractions of 6 nm (c) and 7.5 nm (d) manganese-doped iron oxide nanoparticles (standard deviation about 10%).

to the equilibrium occupancy of α and β spins and is referred to as longitudinal or spin–lattice relaxation. This process is characterized by the time constant T_1 . The second mechanism characterizes the dephasing of coherent spins that are generated during the rf pulse and is referred to as transverse or spin–spin relaxation with the time constant T_2 . Furthermore, the effective transverse relaxation time T_2^* describes the relaxation increase due to additional inhomogeneities in the magnetic field. These inhomogeneities can be caused by the nonperfect homogeneous magnetic field itself or by susceptibility effects implied by tissue interfaces with different magnetization or by para- and ferromagnetic materials. Therefore, T_2^* can be significantly smaller than T_2 . Whereas the T_1 relaxation leads to an increase in signal intensity and thus causing positive contrast, the T_2 and T_2^* processes result in signal loss and negative contrast with conventional imaging techniques. Because superparamagnetic nanoparticles greatly shorten T_2 and T_2^* due to their large magnetic moment they commonly act as negative contrast agents. This effect is quantified in the concentration-independent transverse relaxivities r_2 and r_2^* , that is, the ability of the contrast agent to shorten T_2 and T_2^* , respectively, per millimolar

concentration of paramagnetic ions. MnFe_2O_4 nanoparticles have recently been demonstrated to act as powerful negative contrast agents¹¹ and were even stronger than magnetite.

To synthesize the nanoparticles, we used the high-temperature organometallic synthesis reported by Kang et al., which yields highly crystalline and monodisperse nanocrystals with no tendency to agglomerate.^{12a} This method is based on thermal decomposition of $\text{Fe}(\text{CO})_5$ and $\text{Mn}_2(\text{CO})_{10}$, resulting in the formation of FeMn alloy nanoparticles followed by oxidation with trimethylamine-*N*-oxide. The synthesis yielded nearly monodisperse nanoparticles (less than 10% standard deviation), which were characterized by transmission electron microscopy (TEM) (Figure 1) and X-ray diffraction (XRD) (Supporting Information Figure S1). EDX measurements indicated that the ratio of iron and manganese was almost 2:1. By varying the ratio of initial precursor to oleic acid, particles between 3 and 18 nm could be synthesized. Moreover, we used a hot injection method based on a modification of ref 12b. The high-temperature reaction of iron(III)acetylacetonate and manganese(II)acetylacetonate with 1,2-hexadecanediol in the presence of oleic acid and oleyl amine yielded polydisperse samples that could

Scheme 1. Schematic Illustration of the Phase Transfer Approaches: Ligand Exchange of Oleic Acid against Water Soluble Polymer (above), Coating of Individual Nanoparticles with Amphiphilic Polymer and Embedding into Lipid Micelles (below)



be easily separated into size fractions of 4.5, 6, and 7.5 nm (standard deviation approximately 10%), respectively (Figure 1). Moreover, the ratio of manganese to iron decreased from 0.32 for the 4.5 nm particles to 0.12 for 7.5 nm particles.

Because of the synthesis conditions, the particles are hydrophobic and thus not soluble in aqueous media. To transfer the nanoparticles into water, we used different approaches. In the first one, we applied a ligand exchange of oleic acid against a water-soluble copolymer obtained by coupling poly(ethylene glycol) to a small branched poly(ethylene imine), PEG-PEI, which has already been employed for CdSe/CdS nanocrystals¹³ and will be referred to as “exchange” here. This copolymer ligand consists of a branched PEI moiety with a molecular weight of 400 g/mol and two PEG chains attached to it with molecular weight of 5000 g/mol. We used three different sizes (3, 9, and 18 nm) of nanoparticles in order to investigate size-dependent effects on contrast enhancement. In another approach, the above-mentioned hydrophobic manganese-doped iron oxide nanoparticles were encapsulated within an amphiphilic polymer shell according to Pellegrino et al.,¹⁴ which consists of poly(maleic anhydride-*alt*-1-tetradecene) and is crosslinked by bis(6-aminohexyl)amine. For simplification, we will call it “encapsulation”. Finally, we employed an embedding of the nanoparticles into lipid micelles without a ligand exchange. Several block copolymer micelles loaded with iron oxide nanoparticles have recently been demonstrated to act as excellent negative contrast enhancers.^{6,15} The different processes are pictured in Scheme 1. The PEG-PEI block copolymer employed for the ligand exchange possesses multiple amino groups that can bind to the particle surface.

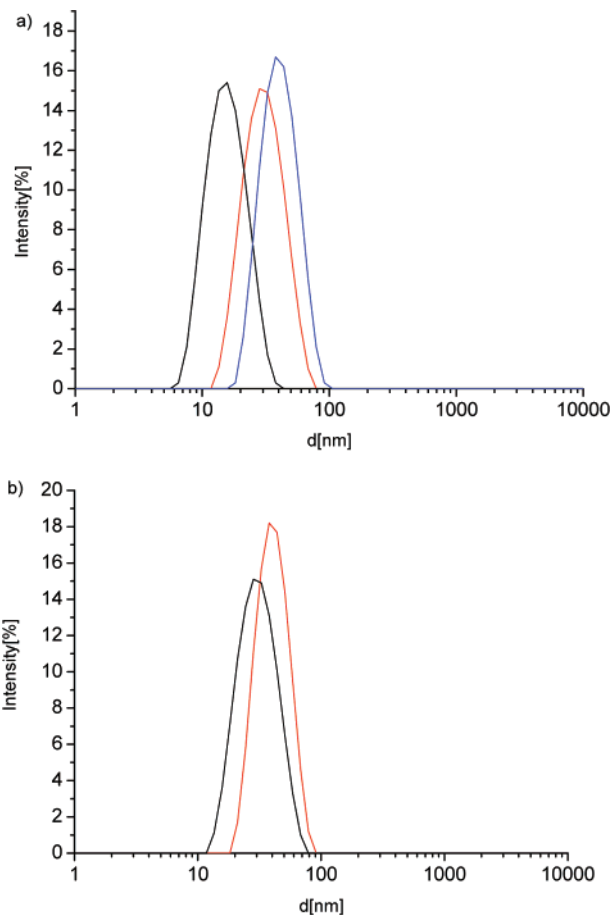


Figure 2. (a) Hydrodynamic diameter of the 9 nm nanoparticles (core size) before (black curve) ligand exchange in chloroform and after ligand exchange with PEG-PEI copolymer in water (red curve) and chloroform (blue curve). (b) Hydrodynamic diameter of PEG-PEI coated particles with 9 nm (black curve) and 18 nm (red curve) core size in water.

To compare the results of ligand exchange to the other approaches, it is essential to know whether the particles are individually dispersed or whether they tend to aggregate. Therefore, we performed dynamic light scattering experiments, the results of which are depicted in Figure 2.

First, it can be noticed from Figure 2a that the hydrodynamic diameter increases after ligand exchange from 15 to 30 nm and 40 nm in water and chloroform, respectively, due to the larger polymer shell. It is further observable that the size distribution of nanoparticles that are covered with PEG-PEI copolymer is not significantly broadened after ligand exchange, indicating that the particles do not tend to form larger agglomerates but exist as individually dispersed particles with a narrow size distribution in both water and chloroform. In addition, Figure 2b shows that the difference in hydrodynamic diameter between nanoparticles with core size of 9 and 18 nm is about 10 nm, demonstrating approximately the same thickness of the polymer shell for particles with different core sizes. Individually dispersed particles were also present after encapsulating the hydrophobic particles in an amphiphilic copolymer shell. This was confirmed by gel electrophoresis and size exclusion chromatography. A TEM image of the as prepared nanoparticles

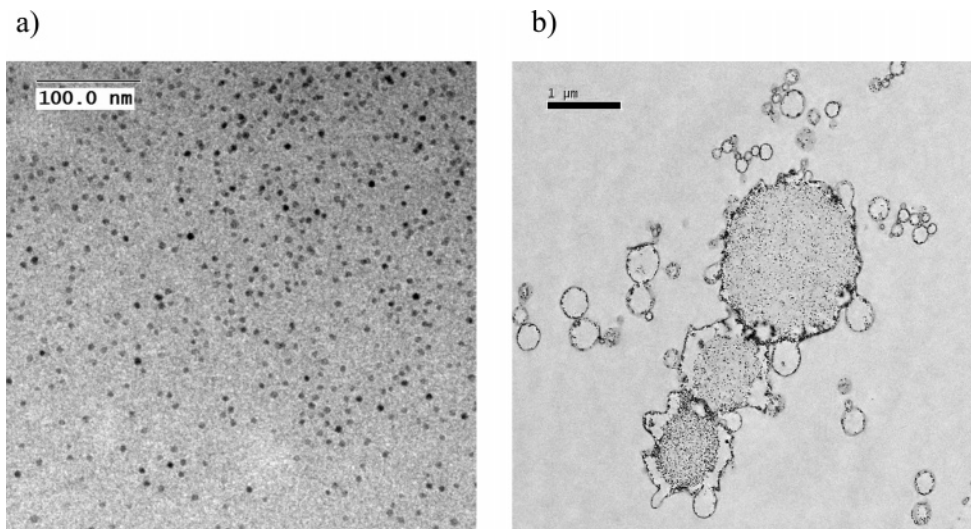


Figure 3. TEM images of manganese-doped iron oxide nanoparticles coated with amphiphilic polymer shell confirming that particles are still well separated after phase transfer (a) and lipid micelles loaded with nanoparticles showing a random distribution within lipid phase and that the particles do not agglomerate within the micelles (b).

is shown in Figure 3a. It is observable that the particles are still well separated after the phase transfer.

The third approach of embedding the particles into lipid micelles differs substantially from the other processes because the particles are concentrated to the small volume in the micellar core. TEM images (Figure 3b) demonstrated the nanoparticles to be randomly distributed inside the micelles. Dynamic light scattering measurements indicated that the micelles are about 250 nm in diameter with a broad size distribution.

To check whether the different postpreparative treatments have a significant influence on the magnetization behavior of the nanocrystals, we measured the magnetic mass susceptibility of 9 nm MnFe_2O_4 particles before and after ligand exchange as well as after embedding them into lipid micelles. We found values of $1.5 \times 10^{-4} \text{ m}^3/\text{kg Fe}$ for both as prepared and after ligand exchange and $1.0 \times 10^{-4} \text{ m}^3/\text{kg}$ for the micelle sample, respectively. The deviation is rather small and probably within the experimental error of the magnetic measurements and iron analytics.

MRI measurements were carried out on a clinical 3 T magnetic resonance scanner at room temperature, using three different sizes of MnFe_2O_4 nanoparticles (3, 9, and 18 nm) with a shell of PEG–PEI copolymer. Furthermore, MRI measurements were accomplished on the 4.5, 6.0, and 7.5 nm manganese-doped iron oxide particles that were transferred into water using Pellegrino's approach, thus forming a comparable system as the particles are individually dispersed in both cases. In contrast, several sizes of MnFe_2O_4 and manganese-doped iron oxide nanoparticles were embedded into lipid micelles. As a reference, we measured Resovist (Schering), a commercially used contrast agent, consisting of iron oxide. For further discussion, we will focus on transverse relaxation process. For a T_2^* map, reconstructed from T_2^* -weighted data from a multiecho gradient echo sequence showing a concentration series of MnFe_2O_4 nanoparticles beside a concentration series of Resovist, see Supporting Information Figure S2.

From the experimental values, r_2 and r_2^* were determined as exemplarily shown in Figure 4a. Here the reciprocal relaxation times, $1/T_2^* = R_2^*$, defined as the relaxation rates, are plotted versus the concentration of paramagnetic ions. The slopes of these curves yield the concentration independent relaxivities, r_2 and r_2^* , respectively, which will be used in the further discussion. These values are plotted in Figure 4b as a function of particle size. All results are also summarized in Table S1 (Supporting Information).

First, it can be noticed from Figure 4b that, in the case of polymer-coated samples, the transverse relaxivities (r_2 and r_2^*) increase with increasing particle size for the polymer exchanged and encapsulated particle systems. Figure 4a demonstrates this fact, as the slope of the straight line is higher for larger particles. Furthermore, we observed only small differences between r_2 and r_2^* . In the case of encapsulated particles, one has to take into account that the ratio of iron and manganese increased with increasing particle size for the manganese-doped iron oxides. An effect of changing composition is thus superimposing the size dependence for these particles.

On the other hand, r_2 and r_2^* of the particle-loaded micelles were higher than those of the corresponding polymer-coated samples. We also observed significant differences between r_2 and r_2^* up to 1 order of magnitude (Figure 4b). The strong decrease in r_2^* with increasing particle size is in contrast to the expected behavior. A possible explanation could involve different degrees of particle loading within the micelles. In a control experiment, we investigated different loadings with pure Fe_3O_4 of 6 nm size in order to eliminate size and composition effects. As can be seen from Figure 4c, r_2 and r_2^* differ significantly if the loading ratio is changed from 0.025 to 0.05 mg Fe_3O_4 per 1 mg lipid. Thus, the very high r_2^* relaxivities for the micelles are probably due to the relatively high particle density within the micelles, which may cause an increased interparticle interaction inside the hydrophobic cores. Such strong particle interactions might be induced by the static

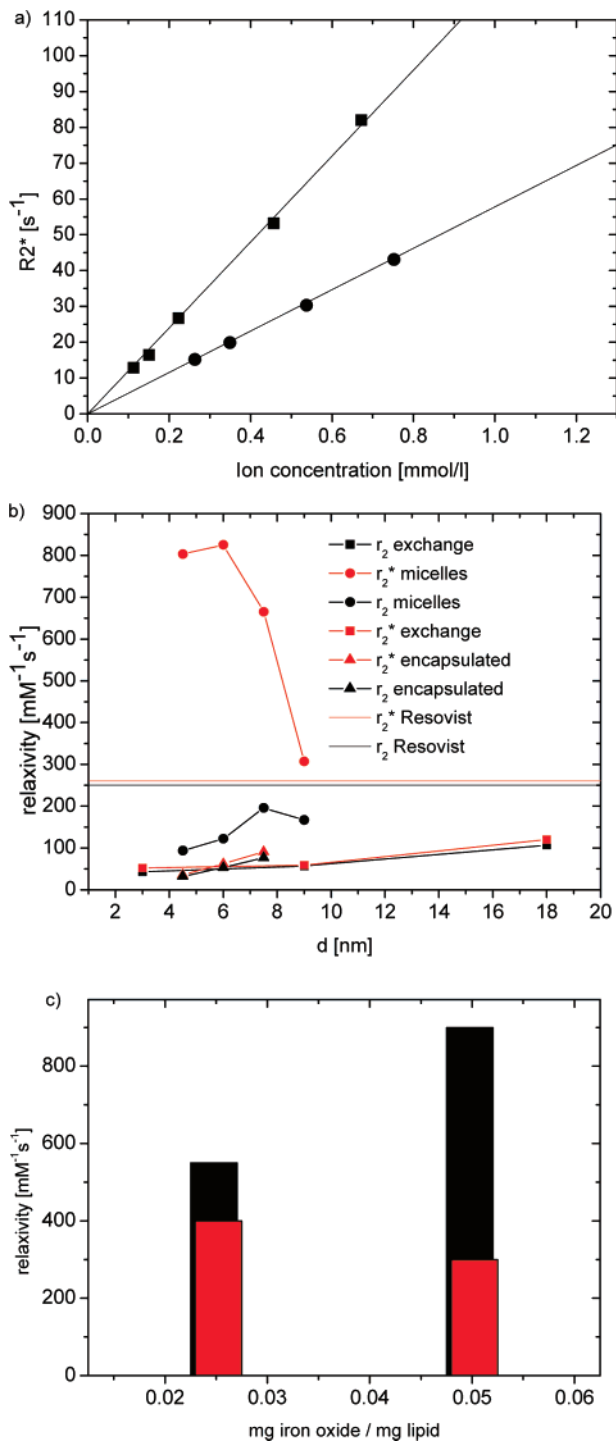


Figure 4. Relaxation rates R_2^* for 9 nm (circles) and 18 nm (squares) MnFe₂O₄ nanocrystals with respect to a concentration series (a). r_2 (red spots) and r_2^* (black spots) for PEG-PEI coated particles (squares), encapsulated particles (triangles) and nanoparticle loaded micelles (circles) (b). Whereas r_2 and r_2^* are almost equal in case of homogeneously dispersed particles, r_2^* is greatly higher than r_2 for the micelles. r_2 (red bar) and r_2^* (black bar) for micelles loaded with different amounts of iron oxide nanoparticles (6 nm) indicating that r_2^* increases with increasing loading whereas r_2 slightly decreases (c).

magnetic field of the tomograph. Indeed, we found that even small permanent magnets induce an aggregation of particles in solution. Thus, compartmentalization of nanoparticles in

the lipid core of the micelles strongly favors a spatially confined aggregation and thereby produces strong field gradients in the environment.

For the contrast enhancement of magnetic spheres, different regimes are predicted.^{16,17} The first one, which is called “motional averaging regime” (MAR) or “motional narrowing regime” describes the transverse relaxation for relatively small particles that are homogeneously dispersed in solution. This theory implies that water diffusion between particles occurs on a much faster time scale than the resonance frequency shift and predicts identical values for R_2 and R_2^* . In this regime, the transverse relaxivity increases with increasing particle size. For larger particles, this theory breaks down. In this case, the relaxation rates are given by the “static dephasing regime” (SDR) theory. The SDR, first introduced by Yablonskiy and Haacke,¹⁸ implies that a large magnetic perturber produces strong dipolar fields in its surroundings, the result of which is the fact that, in contrast to the MAR, diffusion has a minimal influence on nuclear magnetic resonance signal decay. The SDR places an absolute limit in the transverse relaxation rate: increasing the perturber size will not result in higher relaxation rates. Thus, a plateau is reached. However, R_2 is always lower than R_2^* , reflecting the fact that the use of refocusing pulses in spin-echo sequences leads to a decrease in signal decay (“echo-limiting”), particularly for large magnetic spheres and short echo times. Recently, these regimes have been experimentally demonstrated to exist for an induced clustering process in solution¹⁹ as well as for cells loaded with iron oxides.²⁰

The transverse relaxivity for the polymer-coated particles increases with increasing size, thus showing typical behavior of particles in the MAR. r_2 and r_2^* should be equal, a condition that is basically fulfilled because the phase loss is mainly caused by diffusion effects in this regime and is thus irreversible with respect to a refocusing pulse. Similar results were obtained for the encapsulated manganese-doped iron oxide nanoparticles. On the other hand, the transverse relaxivities of the micelles are likely to be describable by the “echo-limiting” due to the big differences between r_2 and r_2^* . Thus, the ceiling for r_2^* given by the SDR should be achieved for the considered systems. For micelles loaded with a higher amount of magnetic nanoparticles, larger r_2^* values are observed. This effect is also predicted by SDR theory, as the value of R_2^* is proportional to the magnetization of the sphere, i.e., R_2^* increases with increasing local magnetic dose (LMD)¹⁸ and thus by particle aggregation. In addition, r_2^* is remarkably high, indicating that these micelles could act as powerful negative contrast agents. In this size range, refocusing pulses could be effective and, as a result, r_2 is significantly lower than r_2^* . On the other hand, for a further increase in size of the superparamagnetic core of polymer-coated particles, the increase in r_2 and r_2^* should be violated at some point due to the decreasing influence of diffusion and thus reaching the SDR condition. Furthermore, the dephasing proton spins of the lipid molecules contribute also to the signal reduction due to the high viscosity of these molecules. This effect has been demonstrated in an experi-

ment where the iron oxide nanoparticles were dispersed in pure olive oil. Large relaxivities were observed in this case. Therefore, the SDR condition is expected to be reached at even smaller perturber sizes within the micelles due to the lower diffusion velocities. Future work will deal with a comprehensive investigation of these effects.

In conclusion, we comparatively investigated the capability of highly crystalline and monodisperse MnFe_2O_4 nanoparticles to enhance negative contrast in MRI with respect to appropriate matrices. For these purposes, we applied a ligand exchange with poly(ethylene glycol)-*b*-poly(ethylene imine) copolymer, a coating of hydrophobic nanoparticles with amphiphilic polymer as well as an embedding of nanoparticles into large lipid micelles. We found that, individually, homogeneously dispersed nanoparticles satisfy MAR theory because transverse relaxivities, r_2 and r_2^* , increase with increasing core size. On the other hand, if these particles are embedded into lipid micelles, they greatly enhance contrast in T_2^* -weighted images, which is in agreement with the static dephasing regime theory. Reasonable explanations for this behavior are the controlled particle aggregation as well as a very low influence of diffusion effects of lipid molecules inside the micelles and water molecules in their surroundings. Further investigations in terms of bioapplicability are currently underway.

Acknowledgment. We thank The Free and Hanseatic City of Hamburg for funding the Molecular Imaging North (MOIN) project. We furthermore thank Rosemarie Kongi, Barbara Holstermann, and Sylvia Bartholdi-Nawrath for excellent technical assistance. Oliver Bruns is supported by a fellowship from the Studienstiftung des Deutschen Volkes.

Supporting Information Available: Detailed experimental procedures and additional data on magnetic and structural characterization. This material is available free of charge via the Internet at <http://pubs.acs.org>.

References

- (1) Bomati-Miguel, O.; Morales, M. P.; Tartaj, P.; Ruiz-Cabello, J.; Bonville, P.; Santos, M.; Zhao, X.; Veintemillas-Verdagner, S. *Biomaterials* **2005**, *26*, 5695.
- (2) Huber, D. L. *Small* **2005**, *1*, 482–501.
- (3) Jordan, A.; Scholz, R.; Wust, P.; Fahling, H.; Felix, R. *J. Magn. Magn. Mater.* **1999**, *201*, 413–419.
- (4) Gonzales, M.; Krishnan, K. M. *J. Magn. Magn. Mater.* **2005**, *293*, 265–270.
- (5) Jun, Y. W.; Huh, Y. M.; Choi, J. S.; Lee, H. J.; Song, H. T.; Kim, S.; Yoon, S.; Kim, K. S.; Shin, J. S.; Suh, J. S.; Cheon, J. *J. Am. Chem. Soc.* **2005**, *127*, 5732–5733.
- (6) Nasongkla, N.; Bey, E.; Ren, J.; Ai, H.; Khemtong, C.; Guthi, J. S.; Chin, S.-F.; Sherry, A. D.; Boothman, D. A.; Gao, J. *Nano Lett.* **2006**, *6*, 2427–2430.
- (7) Huh, Y.-M.; Jun, Y.-W.; Song, H.-T.; Kim, S.; Choi, J.-S.; Lee, J.-H.; Yoon, S.; Kim, K.-S.; Shin, J.-S.; Suh, J.-S.; Cheon, J. *J. Am. Chem. Soc.* **2005**, *127*, 12387.
- (8) Taupitz, M.; Schmitz, S.; Hamm, B. *RoeFo, Fortschr. Geb. Roentgenstr. Nuklearmed.* **2003**, *175*, 752.
- (9) Perez, J. M.; Josephson, L.; O'Loughlin, T.; Högemann, D.; Weissleder, R. *Nat. Biotechnol.* **2002**, *20*, 816–820.
- (10) Berret, J. F.; Schonbeck, N.; Gazeau, F.; El Kharrat, D.; Sandre, O.; Vacher, A.; Airiau, M. *J. Am. Chem. Soc.* **2006**, *128*, 1755.
- (11) Lee, J.-H.; Huh, Y.-M.; Jun, Y.-w.; Seo, J.-w.; Jang, J.-t.; Song, H.-T.; Kim, S.; Cho, E.-J.; Yoon, H.-G.; Suh, J.-S.; Cheon, J. *Nat. Med.* **2007**, *13*, 95–99.
- (12) (a) Kang, E.; Park, J.; Hwang, Y.; Kang, M.; Park, J.; Hyeon, T. *J. Phys. Chem. B* **2004**, *108*, 13932–13935. (b) Sun, S.; Zeng, H.; Robinson, D. B.; Raoux, S.; Rice, P. M.; Wang, S. X.; Li, G. *J. Am. Chem. Soc.* **2004**, *126*, 273–279.
- (13) Nikolic, M. S.; Krack, M.; Aleksandrovic, V.; Kornowski, A.; Förster, S.; Weller, H. *Angew. Chem., Int. Ed.* **2006**, *45*, 6577–6580.
- (14) Pellegrino, T.; Manna, L.; Kudera, S.; Liedl, T.; Koktysh, D.; Rogach, A. L.; Keller, S.; Rädler, J.; Natile, G.; Parak, W. J. *Nano Lett.* **2004**, *4*, 703–707.
- (15) Ai, H.; Flask, C.; Weinberg, B.; Xintao, S.; Pagel, M. D.; Farrell, D.; Duerk, J.; Gao, J. *Adv. Mater.* **2005**, *17*, 1949–1952.
- (16) Gillis, P.; Moiny, F.; Brooks, R. A. *Magn. Reson. Med.* **2002**, *47*, 257–263.
- (17) Brooks, R. A.; Moiny, F.; Gillis, P. *Magn. Reson. Med.* **2001**, *45*, 1014–1020.
- (18) Yablonskiy, D. A.; Haacke, E. M. *Magn. Reson. Med.* **1994**, *32*, 749–763.
- (19) Roch, A.; Gossuin, Y.; Muller, R. N.; Gillis, P. *J. Magn. Magn. Mater.* **2005**, *293*, 532.
- (20) Bowen, C. V.; Zhang, X.; Saab, G.; Gareau, P. J.; Rutt, B. K. *Magn. Reson. Med.* **2002**, *48*, 52–61.

NL071099B

Chloroform- and water-soluble sol-gel derived $\text{Eu}^{+++}/\text{Y}_2\text{O}_3$ (red) and $\text{Tb}^{+++}/\text{Y}_2\text{O}_3$ (green) nanophosphors: synthesis, characterization and surface modification

Ashutosh Pandey^{1*}, M. K. Roy², Anjana Pandey³, Marco Zanella⁴, Ralph A. Sperling⁴, W. J. Parak⁴, A. B. Samaddar¹ and H. C. Verma²

¹Department of Chemistry; MNNIT Allahabad, INDIA

²Department of Physics; IIT Kanpur, INDIA

³Nanotechnology and Molecular Biology Laboratory, Center of Biotechnology, University of Allahabad, INDIA

⁴Center for Nanoscience, Ludwig Maximilians Universität München, GERMANY and Fachbereich Physik, Philipps Universität Marburg, GERMANY

* Corresponding Author: apandey70@yahoo.com

Abstract:

Eu^{+++} and Tb^{+++} ions have been incorporated into nano-dimensional yttrium oxide host matrices in both 0.02:1.0 and 0.2:1.0 (dopant ion:host matrix) molar ratios via a sol-gel process using $\text{Y}_5\text{O}(\text{OPr}^i)_{13}$ as precursor ($\text{OPr}^i = \text{iso-propoxy}$). The as-synthesised white powders have been annealed at different temperatures ranging from 400 °C to 800 °C for 5 hours. Photoluminescence (PL) spectroscopy and X-ray diffraction (XRD) have been used as tools for documenting the characteristics of these powders. For Eu^{+++} doped powders a comparison of the $\text{Eu}^{+++} \ ^5\text{D}_0 \rightarrow \ ^7\text{F}_1$ and $\ ^5\text{D}_0 \rightarrow \ ^7\text{F}_2$ peak intensities in the emission spectra reveals that the dopant ions are occupying unsymmetrical sites in the host yttrium oxide in all the samples. For Tb^{+++} doped powders the characteristic terbium $\ ^5\text{D}_3 \rightarrow \ ^7\text{F}_n$ and $\ ^5\text{D} \rightarrow \ ^7\text{F}_n$ ($n=2-6$) transitions were visible only in the samples that had been annealed above 500 °C. All the samples for 0.2 M doped Eu^{+++} and Tb^{+++} were suspended in chloroform by fragmenting the powder with and without sonification under the presence of trioctylphosphine oxide (TOPO), or a mixture of oleic acid and dioctyl ether, to give clear colorless (for Eu^{+++}) and light green translucent (for Tb^{+++}) solutions of the dispersed particles which respectively give red and green luminescence upon UV excitation. In addition, suspension in water has been achieved by fragmenting the powder in the presence of dichloroacetic acid. TEM investigation of the soluble particles shows single dispersed particles along with some agglomerates. The changes in the luminescence due to fragmentation of the particle powder and due the influence of the surfactant of the suspended colloidal particles are discussed.

Keywords: Nanophosphors, luminescent solutions, colloidal nanoparticles, particle suspension, photoluminescence spectroscopy, sol-gel process

1. Introduction

Rare-earth ion doped nanocrystalline metal oxides are a class of luminescent materials (also called upconverting phosphors) which has been proved to be excellent for applications such as in FEDs (field emission displays) and sensors [1,2]. Under UV irradiation a variety of colors is available in these systems. For example, Eu^{+++} doped Y_2O_3 is a red phosphor while Tb^{+++} and Tm^{+++} incorporated in Y_2O_3 are green and blue phosphors, respectively [2]. The “caged atoms” in the host matrix retain their own atomic levels within the band gap of the host material. This combination of host and impurity energy levels leads to a large excitation cross-section resulting in high phosphorescence. It is anticipated that, due to their high quantum efficiency they might serve as improved luminescent markers [3] for bio-molecule detection in comparison to the reported non oxide semiconductor quantum dots [4,5]. This has been further substantiated by the fact that the LD_{50} values for rare earth oxides are about 1000mg/kg [6], while for example for selenium oxide (which is present even in many quantum dots that do not contain the far more toxic cadmium) it is only about 1mg/kg. Therefore, it is recommendable to explore the suitability of aforementioned nanophosphors for bioconjugation. However, one of the key issues for biological applications is that these probes have to be suspended in water while retaining their characteristic colors along with high stability. The group of Caruso has first suspended rare earth doped fluorescent lanthanum phosphate nanoparticles in water by surface modification with aminohexanoic acid [7] and subsequently the particles have successfully been conjugated with biological molecules. Recently, nonaggregated green emitting nanophosphors [8] of a size range of 50-200nm have been incorporated and imaged in the worm *Caenorhabditis elegans* and have further been examined by SEM. Several methods are known for the synthesis of these doped nanocrystallites [9-26], whereby among them the Sol-Gel process has especially attractive features. We have recently reported the synthesis and characterization of $\text{Eu}^{+++}/\text{Y}_2\text{O}_3$ nanophosphors by using the sol-gel method in which the dopant ion : host matrix ratio was kept as 0.001 : 1.0 [26]. Although the europium emission spectra is clearly visible at such a low concentration, the powders and their transparent suspensions (surfactant coated) in organic solvents showed very faint red luminescence when examined by naked eye under UV irradiation. Furthermore, in order to use these materials for any water-based application first the particle-powder would have to be dispersed into single hydrophilic colloiddally stable particles. In sol-gel hydrolytic systems, the particles are characterized by hydroxylated surfaces that lead to strong interparticle interaction, and therefore a suitable stabilization is needed during the sol processing stage. Otherwise, very large and unstable particles would be readily formed. The situation becomes even more complex if a dopant ion like Eu^{+++} (for which the red phosphorescence gets significantly quenched by the -OH groups) [27] is required within the framework of sol-gel derived metal oxide nanoparticle powders, which also generally have water or alcohol molecules trapped inside. Therefore, these nanoparticle powders have to be annealed to high temperatures (i.e. up to 500 °C) to completely remove these volatile molecules [26]. However, high temperatures at the same time often lead to sintering, resulting in wide particle size distributions within the interconnected particle powder. Due to this it becomes rather difficult to prepare stable suspensions consisting of doped monodisperse particles and so

far we are aware of only few reports in this direction [7, 9, 28, 29]. Very recently also microwave assisted synthesis of doped nanocrystals has been reported [25].

The aim of this study was to generate and characterize stable suspensions for both red and green nanophosphors which should exhibit bright luminescence. In this connection, we hereby report the synthesis and spectral characterization of solid nanophosphors with dopant ion : Y_2O_3 molar ratios of 0.02 : 1 and 0.2 : 1, which exhibit bright red (Eu^{+++}) and green (Tb^{+++}) luminescence by visual examination in UV light. These powders were then suspended as well in organic solvents as in aqueous solution. For dispersion in organic solvents the powders were fragmented to nanoparticles under the presence of both, Trioctyl phosphine oxide (TOPO) and oleic acid / dioctyl ether, to give clear and stable suspensions in chloroform. These particle suspensions show the characteristic bright color (under UV irradiation) and emission spectra of the dopant ions. Transmission electron micrograph (TEM) studies show single particles along with agglomerates. In a further step these hydrophobically capped particles might be modified with an amphiphilic polymer in order to transfer them into aqueous solution [5]. In an alternative route the powders were also suspended in water by fragmenting them under the presence of dichloroacetic acid, whereby also their characteristic luminescence was retained.

2. Experimental details

2.1. General: Proton and ^{13}C NMR spectra were recorded with a GEOL –300 MHz spectrometer at B.H.U. Varanasi, India. X-ray diffraction pattern were recorded on a Seifert powder diffractometer using $Cu-K_{\alpha}$ X-rays. Photoluminescence (PL) spectra of the solid powders were recorded on an ocean optics system with range of 200nm to 1800nm by using an excitation wavelength of 440 nm. TEM images of nanostructures were taken on a transmission electron microscope (JEOL JEM-1011). The solution PL spectra were recorded on a Fluoromax-3 (JOBIN YVON HORIBA) spectrometer at the excitation wavelength 255nm. For performing sonication a BANDELIN sonicator (Sonorex Super RK 103H) was used. The solvents were dried and purified by standard procedures. Water was double distilled and deionized before being used.

2.2. Synthesis of $Y_5O(OPr^i)_{13}$ precursor: $Y_5O(OPr^i)_{13}$ was used as precursor in the sol-gel process for making the yttrium oxide particles. The manipulations pertaining to synthesis of $Y_5O(OPr^i)_{13}$ precursor were performed under dry argon atmosphere using Schlenk techniques as reported [26]. For this, yttrium chips (Aldrich) were refluxed with isopropanol in toluene in the presence of $Hg(OAc)_2$ catalyst (all Qualigens) to give a turbid solution which was filtered while hot. Upon cooling the hot solution the precursor was obtained in 73% yield. It was characterized by elemental analysis (Found (%) C 38.15, H 7.70; Calculated C 38.12, H 7.12) and NMR spectroscopy $\{^1H$ NMR in ppm, 1.29 (doublet), 4.30 (septet) $\}$ in dry $CDCl_3$ and was in accordance with reported values.

2.3. Synthesis of Eu^{+++} and Tb^{+++} doped Y_2O_3 powders: 8.0 g of $Y_5O(OPr^i)_{13}$ was dissolved in 30 ml toluene to give a clear solution which was kept in a bath at $-70^{\circ}C$. A mixture of 0.278 g $Eu(NO_3)_3 \cdot 5H_2O$ (for 0.02M doping), 0.582 g water and 30 ml.

isopropanol was added to it dropwise under stirring. For 0.2 M doping 2.78 g $\text{Eu}(\text{NO}_3)_3 \cdot 5\text{H}_2\text{O}$ was utilized. After the addition was complete the mixture was allowed to warm to room temperature resulting in a white gel. The gel was left for two days and then was dried in an oven at 100°C to give a white powder. It was subjected to heat treatment and samples treated with 400°C , 500°C , 600°C , 700°C and 800°C were made. Upon heating to different temperatures both (0.02M and 0.2M doped) of the europium doped materials did not show any discernable change in white color of the starting powder. A similar procedure was applied for Tb^{+++} doped powders for which 0.283 g of $\text{Tb}(\text{NO}_3)_3 \cdot 5\text{H}_2\text{O}$ was used for 0.02 M doping and 2.83 g for 0.2 M doping. In both cases the resulting gel was left for two days and was then warmed in an oven at 100°C to give a white powder. 0.02 M Tb^{+++} doped Y_2O_3 powders also did not undergo any color change upon heat treatments in the range of 400°C to 800°C . In contrast to the 0.2 M Eu^{+++} doped the 0.2M Tb^{+++} doped Y_2O_3 powders exhibited different colors after annealing at different temperatures. The samples heated to 400°C and 500°C have dusky orange and gray sand colors while the powders heated to 600°C , 700°C and 800°C exhibit light magenta ash appearance.

2.4. Dissolution of 0.2M Eu^{+++} / Tb^{+++} : 1M Y_2O_3 powders in chloroform or toluene under the presence of trioctylphosphine oxide (TOPO): The following general procedure was applied for preparing suspensions of all types of annealed powders. 100 mg of the particle powder were added to 5ml of chloroform in a vial and stirred for 30 minutes. To this suspension 1.0 g of TOPO (Sigma-Aldrich 98 %) was added and stirring was continued for two hours (stirring for higher duration led to no further changes). The so obtained suspension was centrifuged at 1500 rpm for 5 minutes and a white residue (64.5 mg) was set aside and the supernatant was collected in another vial. To purify the particles in this solution methanol was added until turbidity appeared and the mixture was centrifuged at 2000 rpm for 5 minutes. The particle-containing precipitate was collected and re- dissolved in chloroform (2ml) giving a clear solution, whereas the supernatant was discarded. The so obtained solution was centrifuged at 3000 rpm for 5 minutes to give a small amount of residue which was discarded and the supernatant solution was collected and used for further experiments (PL and TEM). Toluene may also be used in place of chloroform. However, in toluene the phosphorescence of the particles in UV light was more quenched than in chloroform.

2.5. Dissolution of 0.2M Eu^{+++} / Tb^{+++} : 1M Y_2O_3 powders in chloroform/toluene by oleic acid/dioctyl ether: The following general procedure was applied for preparing suspensions of all types of annealed powders. 100 mg of the powder was transferred in a three neck flask fitted with condenser and stirred in 5ml chloroform for 30 minutes. Then the chloroform was removed under low vacuum. 500 mg oleic acid and 3 ml dioctyl ether were injected separately under stirring and the mixture was heated to 200°C for 2 hours while stirring, which resulted in a clear solution. The solution was cooled to 50°C and 50 ml methanol was quickly added to give a turbid solution. This solution was centrifuged at 2000 rpm for 5 minutes and the supernatant was discarded. The particle containing precipitate was dissolved in 2 ml chloroform to give a clear solution. For removal of aggregated particles the solution was centrifuged at 3000 rpm for 5 minutes to give a very small residue at the bottom of the vial. The precipitate containing agglomerated was

discarded and the particle containing supernatant was used for all further experiments (PL and TEM).

2.6. Dissolution of 0.2M Eu⁺⁺⁺ / Tb⁺⁺⁺ : 1M Y₂O₃ powders in water by dichloroacetic acid: The following general procedure was applied for preparing suspensions of all types of annealed powders. 100 mg of the particle powder were added to 5ml of water in a vial and stirred for 30 minutes. To this suspension 200mg of dichloroacetic acid (Sigma-Aldrich, 98 %) was added dropwise and within the next 20 minutes a turbid solution was obtained. This solution was centrifuged at 1500 rpm for 5 minutes and the residue with the undissolved particle powder was discarded. To the clear supernatant with suspended particles 60 ml isopropanol was added and the mixture was stirred for 30 minutes resulting in a turbid solution. The solution was centrifuged at 2000 rpm for 5 minutes and the supernatant was discarded. To the residue which contained the particles 5 ml water was added together with a drop of dichloroacetic acid to get a clear solution which was used for all further experiments (PL and TEM).

3. Results and Discussion

The sol-gel derived and 100 °C warmed europium and terbium doped (both in 0.02M and 0.2M concentrations) Y₂O₃ white powders were annealed to 400 °C, 500 °C, 600 °C, 700 °C and 800 °C for five hours to prepare in total twenty samples ((Eu / Tb) x (0.02M / 0.02M) x (400, 500, 600, 700, 800°C) = 2 x 2 x 5 = 20). All europium doped powders showed bright red and the terbium doped samples bright green luminescence under UV light excitation. We have very recently published the XRD patterns of 0.001M Eu⁺⁺⁺ : 1M Y₂O₃ particle powders obtained via the sol-gel method which were heated in a range of 400 °C to 800 °C [26]. In the present work we found similar X-ray diffractograms for the powders that had been heat-treated in the range from 400°C to 800 °C as well for europium as for terbium doping for both concentrations. The average sizes of the crystalline domains in the particle powder calculated from XRD with respect to the annealing temperature were 17 nm (400 °C), 24nm (500 °C), 42 nm (700 °C) and 45nm (800 °C).

The distribution of the Eu⁺⁺⁺ ions within the host yttrium oxide matrix has been worked out by examination of the photoluminescence (PL) spectra, which are shown in Figure 1 for the 0.2M Eu⁺⁺⁺ : 1M Y₂O₃ particle powders (for spectra of 0.02M Eu⁺⁺⁺ : 1M Y₂O₃ powders see the Supporting Information). The most intense emission in the photoluminescence spectrum of Eu⁺⁺⁺ is observed at about 580-595 nm (⁵D₀→⁷F₁), 610-625 nm (⁵D₀→⁷F₂), and 675-690 nm (⁵D₀→⁷F₄) [27]. In general the sharp emission lines point towards the occupation of europium ions in those crystallographic sites which are situated in the interior of the nanocrystal. It is well known that the intensity ratio of the ⁵D₀→⁷F₂ and ⁵D₀→⁷F₁ transitions is a good indicator of the symmetry of the environment around the rare earth ion. This feature is apparent (see the Supporting Information) in our 0.02M samples annealed at 400 °C and 500 °C, where the ⁵D₀→⁷F₂ transitions are much more intense than the ⁵D₀→⁷F₁ emissions. It is important to point out here that for 0.001M Eu⁺⁺⁺ : 1MY₂O₃ powders annealed (up to 700 °C) under similar conditions the

$^5D_0 \rightarrow ^7F_1$ transitions were found to be very intense and it was concluded that the dopant ions are occupying only the symmetrical sites in the interior of the particles [26]. However, in the data obtained in the present study we find that with higher concentrations the europium ions are more accommodated in unsymmetrical environments at the surface of the nanoparticles. This is not surprising because in particle powders with nanocrystalline domains it is highly probable that the atoms in the grain boundary region may get displaced from their lattice positions to new, non lattice equilibrium positions. The distribution of atoms in these non lattice positions may be fully disordered or have short range order. The PL spectrum of the 0.02M Eu^{+++} : 1M Y_2O_3 particle powder which has been heated to 400 $^{\circ}C$ shows a broad $^5D_0 \rightarrow ^7F_2$ emission (612nm) with a shoulder centered at 625nm. The $^5D_0 \rightarrow ^7F_4$ transition which is found around 697 nm is most intense in the spectrum of the powder heated to 600 $^{\circ}C$, while it is completely absent in the 500 $^{\circ}C$ annealed sample (see Supporting Information).

The PL spectra of all the 0.2M Eu^{+++} : 1M Y_2O_3 (Figure 1a) particle powders prominently show the $^5D_0 \rightarrow ^7F_2$ transition and are in many ways similar to spectra reported before [14,17,27], except for the absence of the peak at 697 nm corresponding to the $^5D_0 \rightarrow ^7F_4$ emission. The $^5D_0 \rightarrow ^7F_4$ emission seems to be weakly present in the spectrum of the 0.2M doped Eu^{+++} / 1M Y_2O_3 particle powder that had been heated to 400 $^{\circ}C$. The PL spectrum of the 0.2M Eu^{+++} : 1M Y_2O_3 particle powder that had been heated to 800 $^{\circ}C$ turns out to be completely different to the corresponding spectra of the 0.001 M [26] and 0.02 M doped particle powders (see Supporting Information). It clearly shows the $^5D_0 \rightarrow ^7F_2$ peak (Figure 1a) accompanied with a tiny $^5D_0 \rightarrow ^7F_1$ transition indicating the presence of Eu^{+++} ions in unsymmetrical sites. Therefore, it seems that for fairly high (i.e. 0.2 M) doping concentration enough europium ions are still present in unsymmetrical environments and/or at the surface of the nanocrystalline domains, even at 800 $^{\circ}C$, to show their characteristic spectrum.

A TEM image of untreated 0.2 M Eu^{+++} : 1M Y_2O_3 particle powder is shown in Figure 1a which exhibits tremendous agglomeration of the particles. Therefore in the next step the particle powders were fractionated with the aim to obtain colloidal particles suspended in solution. Since these oxide particle powders are in first place insoluble as well in organic solvents as in aqueous medium, dispersion had to be provided by an appropriated surfactant on the particle surface. For suspending the particle powders in organic solvents such as chloroform and toluene we tested several pathways which included heating and stirring the particle powder under the presence of oleic acid in dioctyl ether, and stirring the particle powder in chloroform or toluene under the presence of trioctyl phosphine (TOP), trioctyl phosphine oxide (TOPO), aminohexanoic acid, octylamine, or decylamine. We found that treatment of the particle powders with trioctyl phosphine oxide (TOPO) and oleic acid in dioctyl ether to give best suspension of the particles in toluene and chloroform. Dispersion in TOPO was found to be the most promising method as it could be performed at ambient temperature and did not require heating as was the case with oleic acid in dioctyl ether. TOPO and oleic acid molecules presumably stick with their polar headgroups to the oxide particle surface so that their hydrophobic tails point towards the solvent and thus provide repulsion and thus colloidal stability of the particles in organic solvents. The TOPO coated particles were found to yield clear

suspensions in both chloroform and toluene. However, in toluene the red luminescence of the phosphors under UV irradiation was quenched significantly, whereas in chloroform very bright phosphorescence was observed. Therefore, all further spectroscopic analysis of hydrophobic particles was performed in chloroform.

Figure 1b shows the PL spectra of TOPO coated 0.2M Eu^{+++} : 1M Y_2O_3 particles (of particle powders that had been annealed to 400 °C - 800 °C) suspended in CHCl_3 . For all suspensions, in the PL spectrum the intensity ratio of the $^5\text{D}_0 \rightarrow ^7\text{F}_2$ and $^5\text{D}_0 \rightarrow ^7\text{F}_1$ transitions clearly confirms the occupation of unsymmetrical sites by the dopant ions within the Y_2O_3 matrix as also seen in the corresponding solid particles powders (cf. Figure 1a). This confirms that fragmentation of the solid particle powders to colloidal TOPO capped particles suspended in chloroform retains the basic photoluminescence properties of europium doped particles. However, unlike the spectra of the corresponding solid particle powder (Figure 1a) for the colloidal particles made out of the powder and that had been annealed at 400 °C the $^5\text{D}_0 \rightarrow ^7\text{F}_4$ peak is absent in solution (Figure 1b).

A TEM image of TOPO coated 0.2 M Eu^{+++} : 1M Y_2O_3 particles made out of a particle powder that had been annealed to 400 °C is shown in Figure 1b. Although the particles are relatively well dispersed and have a fair size distribution, some aggregates can also be seen that comprise several small particles. The average diameter of the particles seen in the TEM is clearly bigger than the average diameter of 17nm obtained with XRD for the crystalline domains for the particle powder. This suggests that the fragmentation procedure of the particle powder to colloidal particles under the presence of TOPO is not sufficient to break up all agglomerates present in the particle powder to primary single particles. However, in comparison to the uncoated powders (Figure 1a) significant fragmentation has taken place. We also performed sonification of the particle powder in the TOPO / chloroform mixture during the fragmentation process to further reduce the average size of the particles. However, we were never able to completely remove the particle aggregates. TEM examination of TOPO coated particles suspended in chloroform that had been made out of particle powders annealed at 500 °C -800 °C also clearly revealed larger agglomerates together with separated single particles (see Supporting Information). Similar observations were also found with other surfactants in the present work. Although for all these particles sonification helped to reduce the size of the aggregates no discernable change in the solution PL spectra was observed for all the three surfactants.

We also employed oleic acid in presence of dioctyl ether to disperse suspend particles in chloroform. The PL spectra of these transparent suspensions are shown in Figure 1c, whereby the characteristic europium peaks similar to the ones shown in Figure 1b are visible. Furthermore, the TEM images of particles obtained from the particle powder which had been heated to 400 °C heated powders are similar to the ones obtained for TOPO coated particles. This indicates that both TOPO and oleic acid / dioctyl ether are working similarly in regard to the fragmentation capability whereby the TOPO coating has the advantage that it can be performed at ambient temperature.

Alternatively the surface of the nanophosphor particle powders was etched with dichloroacetic acid to suspend them in aqueous solution. This fragmentation was significantly faster than the one reported above in chloroform under the presence of TOPO or oleic acid / dioctyl ether. Although water is reported to significantly quench the europium emission [27] we found that the clear aqueous suspensions of the particles showed red phosphorescence under UV light excitation. The chloroacetic acids might act similar to aminohexanoic acid [7] where chlorine atoms with lone pair are directed towards the surface of the nanoparticles while the hydrophilic carboxylic groups are pointing outside. The PL spectra for aqueous suspensions of particles from powders which before had been annealed at 400^oC - 800^oC is shown in Figure 1d. Similar to the above discussion the characteristic peaks of Eu⁺⁺⁺ are clearly visible. As can be seen from the corresponding TEM image in Figure 1d the fragmentation of the particle powders with di-chloroacetic acid results in many particle aggregates. Compared to suspension in chloroform (Figures 1b and 1c) particles suspended in water showed more and larger aggregates. This also can be seen in the scattering at low wavelengths for the PL spectra of the particle solutions (Figure 1d).

Doping of yttrium oxide with Tb⁺⁺⁺ ions leads to green phosphors. Terbium related spectra are characterized by a series of ⁵D₃ → ⁷F_n transitions wherein for n = 0, 1, 2, 3, 4, 5, and 6 the corresponding peaks are observed at 486nm, 481nm, 470nm, 456nm, 436nm, 414nm and 381nm. Besides these, ⁵D₄ → ⁷F₅ (~ 544 nm), ⁵D₄ → ⁷F₄ (~ 585 nm), and ⁵D₄ → ⁷F₃ (~ 620 nm) transitions are also characteristic of terbium ions. In general, the preparation conditions including the nature of the host metal oxide matrix, concentration of terbium ions, thermal synthesis conditions and the conditioning regime are factors that influence photoluminescence characteristics of Tb⁺⁺⁺ incorporated Y₂O₃ phosphor [20,21,22]. Furthermore, distinct differences in the optical behavior of the bulk and nanoparticles for the same material have also been observed. For example, the excitation spectra of the nanophosphors were systematically found to be blue-shifted relative to bulk spectra [20]. Tb⁺⁺⁺ transitions for a 0.02 M doping concentration within the Y₂O₃ matrix for particle powders heated at different temperatures ranging from 400 ^oC to 800 ^oC are given in the Supporting Information. Evidently, in all the samples the ⁵D₃ → ⁷F_n transitions with n = 2 to 6 overlap which results in a very broad spectrum in the corresponding region which indicates simultaneous emission from sites with different crystal field splitting [28]. However, the particle powders annealed at 700 ^oC, and 800 ^oC clearly show the ⁵D₃ → ⁷F₀ (486nm), ⁵D₃ → ⁷F₁ (481nm) and ⁵D₄ → ⁷F₆ (490nm) peaks which are characteristic of doped terbium ions. In comparison, the spectra of 0.2 M Tb⁺⁺⁺ : 1M Y₂O₃ powders (Figure 2a) are more intense but unlike for the 0.02M doped samples (700 ^oC, and 800 ^oC heated) the ⁵D₃ → ⁷F_{0,1} and ⁵D₄ → ⁷F₆ transitions are merged to give a broad feature in the spectra.

As with the 0.2M Eu⁺⁺⁺ : 1M Y₂O₃ red phosphors we also fragmented the 0.2M Tb⁺⁺⁺ : 1M Y₂O₃ green phosphor particle powders, as due to sintering they are in highly agglomerated state (Figure 2b). Suspension in chloroform under the presence of TOPO yielded transparent light green solutions. Under UV excitation these solutions were found to give green luminescence. The PL spectra of the suspensions of TOPO coated green phosphors are shown in Figure 2b. Notably in all spectra a prominent peak is visible at around 348 nm which may be attributed to the ⁵D₃ → ⁷F₆ transition. Generally for particle

powders in solid state this peak is found at 381nm [20], but it appears that in the presence of surfactant (in solution) it has shifted. However, the visibility of the $^5D_3 \rightarrow ^7F_5$ (414 nm) and $^5D_3 \rightarrow ^7F_4$ (436nm) transitions in 700 °C and 800 °C annealed samples confirms the presence of terbium ions in the host oxide matrix [20, 21]. The TEM image (Figure 2b) of a grid made by placing a drop of the particle suspension in chloroform (derive from the particle powder that had been heated to 400 °C) is almost similar to the corresponding europium doped sample (Figure 1b). The presence of a small fraction of aggregates further confirms the above discussed limitation of TOPO with regard to fragmentation capability in the given set of experimental conditions.

0.2M Tb⁺⁺⁺ doped 1M Y₂O₃ particle powders were also fragmented in chloroform by coating with oleic acid/dioctyl ether. They were also found to be luminescent at UV light excitation. Their solution PL spectra are shown in Figure 2c. Evidently here also a peak is present around 348 nm, which as mentioned above, may be due to the $^5D_3 \rightarrow ^7F_6$ transition. This is also accompanied with some other aforementioned transitions. TEM pictures (Figure 2c) of the corresponding particles coated with oleic acid/dioctyl ether were again found to be fairly similar to the corresponding red phosphors as shown in Figure 1c. Also for Tb⁺⁺⁺ doping dispersed particles together with some aggregates were found to be present.

Finally, the PL spectra of aqueous suspensions of dichloroacetic acid capped 0.2M Tb⁺⁺⁺ / 1M Y₂O₃ particles were recorded (Figure 2d). Each had a peak at 348 nm, which may be assigned to the $^5D_3 \rightarrow ^7F_6$ transition, along with the other usual peaks as shown in Figures 2b and 2c. Similar to the corresponding red phosphors agglomeration of the particles can be seen in the scattering in the PL spectra. Furthermore, as the red phosphors, fragmentation in aqueous solution results in a higher number and also in bigger particle aggregates than fragmentation in chloroform, as is evident from the TEM images.

Therefore, in the present investigation we find that both, TOPO and oleic acid/di-octyl ether are capable of fragmenting and suspending the sol-gel derived and annealed doped yttrium oxide particles in organic solvents, whereas chloroacetic acids can suspend them in water yielding transparent suspensions that are stable for months at ambient temperature. In terms of the particle size distributions the performance of both TOPO and oleic acid/di-octyl ether is about similar. The advantage of using TOPO is that it does not require high temperature reaction conditions. In comparison, although di-chloroacetic acid could not provide single primary particles, it leads to well conserved PL characteristics of the dopant ions which are known to be quenched in the presence of hydroxyl groups.

4. Conclusions

The sol-gel process is an efficient way to dope rare earth ions into nano dimensional yttrium oxide. For Eu⁺⁺⁺ doping with 0.02 M and 0.2 M doping concentration the europium ions are preferentially residing in unsymmetrical sites in the Y₂O₃ matrix for particle powders annealed in the range of 400 °C to 800 °C which are red phosphors. For

Tb⁺⁺⁺ doping with 0.02 M and 0.2 M doping concentration the terbium ions are also incorporated into the Y₂O₃ matrix and the particle powders annealed in the range of 400 °C to 800 °C are green phosphors. The phosphor particle powders have been fragmented and suspended in chloroform by coating their surface with either TOPO or oleic acid/dioctyl ether. These colloidal suspensions retain the characteristic PL spectra of the particle powders and exhibit luminescence upon UV excitation. TEM pictures reveal the presence of dispersed particles along with particle aggregates. In presence of dichloroacetic acid the particle powders can also be suspended in water. Again, their PL properties are conserved, though water is known to significantly quench Eu⁺⁺⁺ spectra. However, in contrast to colloidal particles suspended in chloroform the particles suspended in aqueous medium exhibit many aggregates.

Acknowledgements

Anjana Pandey, Ashutosh Pandey and Wolfgang J Parak are thankful to DST New Delhi and DAAD Germany for funding support. The German partner also acknowledges funding from the European Union (STREP SA-Nano) and the Deutsche Forschungsgemeinschaft (Emmy Noether grant).

References

- [1] R. N. Bhargava, D. Gallagher and T. Walker, Doped nanocrystals of semiconductors - a new class of luminescent materials, *J. Luminescence* 60 (1994) 275-280.
- [2] J Hao, S A Studenikin and M Cocivera, Blue, green and red cathodoluminescence of Y_2O_3 phosphor films prepared by spray pyrolysis, *J. Luminescence* 93 (2001) 313-319.
- [3] M Darbandi, W Hoheisel and T Nann, Silica coated, water dispersible and photoluminescent $Y(V,P)O_4:Eu^{3+},Bi^{3+}$ nanophosphors, *Nanotechnology* 17 (2006) 4168-4173.
- [4] W. J Parak., T. Pellegrino and C. Planck, Labelling of cells with quantum dots *Nanotechnology*, 16 (2005) R9-R25
- [5] T. Pellegrino, L.Manna, S.Kudera, T. Liedl, D.Koktysh, A. L.Rogach., S.Keller, J Rädler., G. Natile and W. J. Parak., Hydrophobic nanocrystals coated with an amphiphilic polymer shell: A general Route to water soluble nanocrystals, *Nanoletters* 4 (2004) 703-707.
- [6] R J Palmer, J L Butenhoff and J B Stevens, Cytotoxicity of the rare earth metals cerium, lanthanum, and neodymium in vitro: Comparisons with cadmium in a pulmonary macrophage primary culture system, *Environ. Res.* 43 (1987). 142-156.
- [7] F Meiser, C Cortez and F Caruso, Biofunctionalization of Fluorescent Rare-Earth-Doped Lanthanum Phosphate Colloidal Nanoparticles, *Angew. Chem. Int. Ed* 43 (2004). 5954-5957.
- [8] F L Shuang, R Riehn, W S Ryu, N Khanarian, C K Tung, D Tank, and R H Austin, In vivo and scanning electron microscopy imaging of upconverting nanophosphors in *caenorhabditis elegans* *Nano letters* 6 (2006) 169-174.
- [9] Wet-Chemical Synthesis of Doped Colloidal Nanomaterials: Particles and Fibers of $LaPO_4:Eu$, $LaPO_4:Ce$, and $LaPO_4:Ce,Tb$, H Meyssamy, R Riwotzki, A Kornowski, S Nauseef and M Haase, *Adv. Mater* 11(1999). 840-844.
- [10] F Wang, F Xianping M Wang and Y Zhang, Multicolour $PEI/NaGdF_4:Ce^{3+},Ln^{3+}$ nanocrystals by single-wavelength excitation, *Nanotechnology* 17(5) (2006) 1527-1532.
- [11] M Danek, K F Jensen, C B Murray and MG Bawendi, Synthesis of Luminescent Thin-Film $CdSe/ZnSe$ Quantum Dot Composites Using $CdSe$ Quantum Dots Passivated with an Overlay of $ZnSe$, *Chem Mater* 8 (1996) 173-180.
- [12] E T Goldbert, B Kulkarni, R N Bhargava, J Taylor and M Libera, Size dependent efficiency in Tb doped Y_2O_3 nanocrystalline phosphor, *J. Luminescence* 72-74 (1997), 190-192.
- [13] B M Tissue, Synthesis and Luminescence of Lanthanide Ions in Nanoscale Insulating Hosts, *Chem Mater* 10 (1998) 2837-2845.
- [14] J A Nelson, E L Brant and M J Wagner, Nanocrystalline $Y_2O_3:Eu$ Phosphors Prepared by Alkalide Reduction, *Chem Mater* 15 (2003) 688-693.
- [15] K Devlin, O Kelly, Z R Tang, C McDonagh and J F McGilp, A structural study of the sol-gel process by optical fluorescence and decay time spectroscopy *J. Noncrystalline solids* 135 (1991) 8-14.

- [16] P K Sharma, MH Jilavi, R Nass and H Schmidt , Tailoring the particle size from μm → nm scale by using a surface modifier and their size effect on the fluorescence properties of europium doped yttria, *J Lumin.* 82 (1999).187-193.
- [17] T Hirai, T Hirano and I Komasaawa , Preparation of Y_2O_3 Eu^{3+} phosphor fine particles using an emulsion liquid membrane system , *J. Mater. Chem.* 10 (2000) 2306-2310.
- [18] X Lingling, B Wei, Z Zhang, L Zhe, G Hong and Y Zhang, Synthesis and luminescence of europium doped yttria nanophosphors via a sucrose-templated combustion method, *Nanotechnology* 17 (2006) 4327-4331.
- [19] O L Hersh and N Herbert, Concentration dependence curves of cathodoluminescence of $\text{Y}_2\text{O}_2\text{S}:\text{Tb}$ *Applied Physics Letters* 28 (1976) 727-729.
- [20] L G Jacobsohn, B L Bennett, R E Muenchausen, J F Smith, DW Cooke, Optical structural characterization of nanostructured $\text{Y}_2\text{O}_3:\text{Tb}$, *Proceedings of SPIE on Nanophotonic Materials III*, Edited by Gaburro, Zeno; Cabrini, Stefano, 6321 (2006) 63210-63213.
- [21] N Hiromitsu and M Toshiyuki, Correlation between Y_2O_3 concentration and photoluminescence excitation spectra of Tb^{3+} impurity in Y_2O_3 -stabilized ZrO_2 , *Journal of Applied Physics* 97 (2005) 023503-023506.
- [22] J Weiyi, W Yanyun, F Fernandez, X Wang, S Huang and W M Yen, Photoluminescence of $\text{Ce}^{3+}, \text{Tb}^{3+}:\text{Y}_2\text{O}_3$ nanoclusters embedded in SiO_2 sol-gel glasses, *Materials Science and Engineering C* 16 (1-2) (2001) 55-58.
- [23] M A F Gonzalez, G Ledoux, S Roux, K Lebbou, P Perriat and O Tillement, Preparing nanometer scaled Tb-doped Y_2O_3 luminescent powders by the polyol method, *Journal of Solid State Chemistry*, 178(4) (2005) 989-997.
- [24] L . Mursean, E J Popovici, A Hristea, E Indrea and M Vasilescu, Spectral investigation on terbium activated yttrium oxysulphide phosphors, *SPIE ROMOPTO Seventh Conference on Optics*, 775 (2003) 5581-5584.
- [25] G. Buhler and C. Feldmann, Microwave-Assisted Synthesis of Luminescent $\text{LaPO}_4:\text{Ce}, \text{Tb}$ Nanocrystals in Ionic Liquids, *Angew. Chem. Int. Ed.* 45 (2006) 4864–4867
- [26] A Pandey, A Pandey, M K Roy and H C Verma, Sol–gel synthesis and characterization of $\text{Eu}^{+++}/\text{Y}_2\text{O}_3$ nanophosphors by an alkoxide precursor, *Mat. Chem. Phy* 96 (2006). 466-470.
- [27] F Paraspour, D F Kelley and R S Williams, Spectroscopy of Eu^{3+} -Doped PtS_2 Nanoclusters, *J. Phys. Chem B* 102 (1998) 7971-7977.
- [28] K K mpe, O Lehmann and M Haase, Spectroscopic Distinction of Surface and Volume Ions in Cerium(III)- and Terbium(III)-Containing Core and Core/Shell Nanoparticles, *Chem Mater* 18 (2006) 4442-4446.
- [29] K K mpe, H Borchert, J Storz, A Lobo, S Adams, T M ller and M Haase, Green-Emitting $\text{CePO}_4:\text{Tb}/\text{LaPO}_4$ Core-Shell Nanoparticles with 70 % Photoluminescence Quantum Yield *Angew. Chem. Int. Ed.* 42 (2003) 5513-5516.

Figures

Figure 1: a) Photoluminescence spectra of 0.2 M europium doped Y_2O_3 particle powders that had been annealed at temperatures ranging from 400 °C to 800 °C at 440 nm excitation wavelength and a corresponding TEM image of the particle powder (for the particles annealed at 400 °C). b) Photoluminescence spectra of solutions with TOPO coated colloidal 0.2M Eu^{+++} / Y_2O_3 nanoparticles in $CHCl_3$ at 250 nm excitation wavelength. Before transferring the particles from the powder to solution they had been annealed in the powder state at temperatures ranging from 400 °C to 800 °C. The TEM image corresponds to TOPO coated particles from the particle powder that had been annealed at 400 °C. c) Photoluminescence spectra of solutions with oleic acid/di-octyl ether coated colloidal 0.2M Eu^{+++} / Y_2O_3 nanoparticles in $CHCl_3$ at 250 nm excitation wavelength. Before transferring the particles from the powder to solution they had been annealed in the powder state at temperatures ranging from 400 °C to 800 °C. The TEM image corresponds to oleic acid/di-octyl ether coated particles from the particle powder that had been annealed at 400 °C. d) Photoluminescence spectra of solutions with di-chloro acetic acid coated colloidal 0.2M Eu^{+++} / Y_2O_3 nanoparticles in H_2O at 250 nm excitation wavelength. Before transferring the particles from the powder to solution they had been annealed in the powder state at temperatures ranging from 400 °C to 800 °C. The TEM image corresponds to di-chloro acetic acid coated particles from the particle powder that had been annealed at 400 °C.

Figure 2: a) Photoluminescence spectra of 0.2 M terbium doped Y_2O_3 particle powders that had been annealed at temperatures ranging from 400 °C to 800 °C at 440 nm excitation wavelength and a corresponding TEM image of the particle powder (for the particles annealed at 400 °C). b) Photoluminescence spectra of solutions with TOPO coated colloidal 0.2M Tb^{+++} / Y_2O_3 nanoparticles in $CHCl_3$ at 250 nm excitation wavelength. Before transferring the particles from the powder to solution they had been annealed in the powder state at temperatures ranging from 400 °C to 800 °C. The TEM image corresponds to TOPO coated particles from the particle powder that had been annealed at 400 °C. c) Photoluminescence spectra of solutions with oleic acid/di-octyl ether coated colloidal 0.2M Tb^{+++} / Y_2O_3 nanoparticles in $CHCl_3$ at 250 nm excitation wavelength. Before transferring the particles from the powder to solution they had been annealed in the powder state at temperatures ranging from 400 °C to 800 °C. The TEM image corresponds to oleic acid/di-octyl ether coated particles from the particle powder that had been annealed at 400 °C. d) Photoluminescence spectra of solutions with di-chloro acetic acid coated colloidal 0.2M Tb^{+++} / Y_2O_3 nanoparticles in H_2O at 250 nm excitation wavelength. Before transferring the particles from the powder to solution they had been annealed in the powder state at temperatures ranging from 400 °C to 800 °C. The TEM image corresponds to di-chloro acetic acid coated particles from the particle powder that had been annealed at 400 °C.

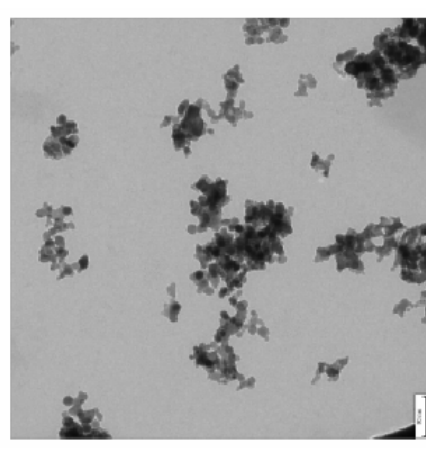
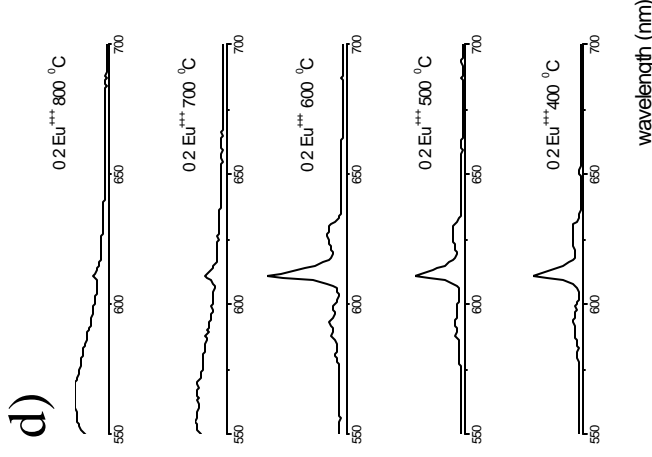
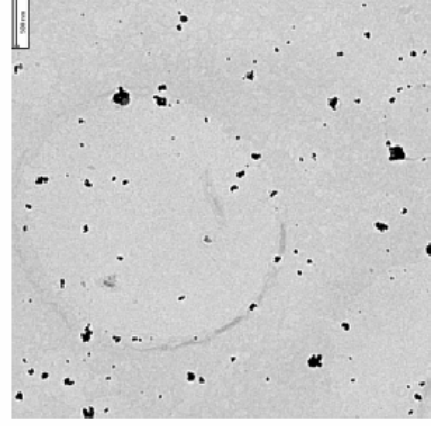
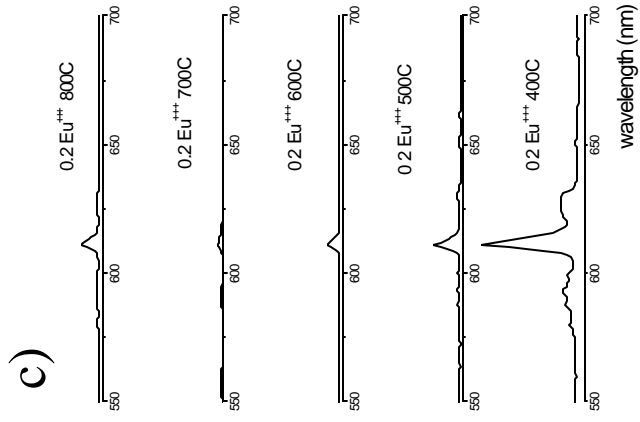
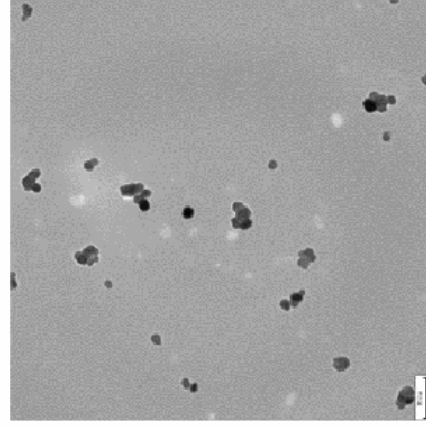
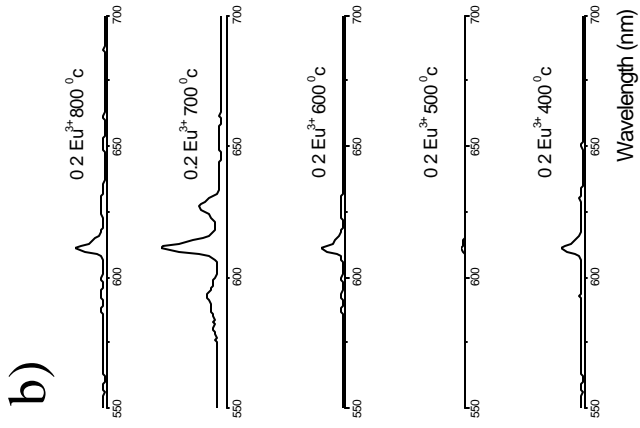
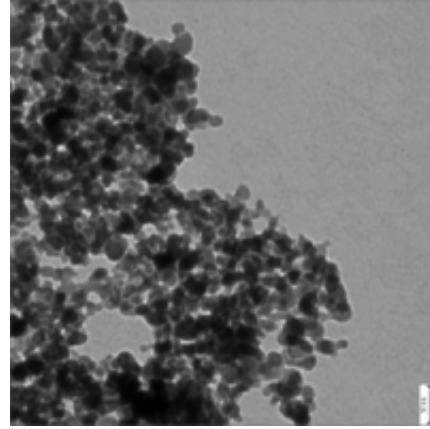
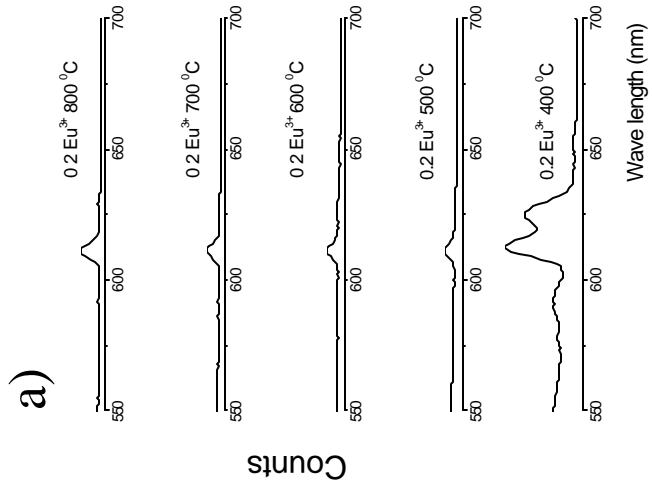


Figure 1

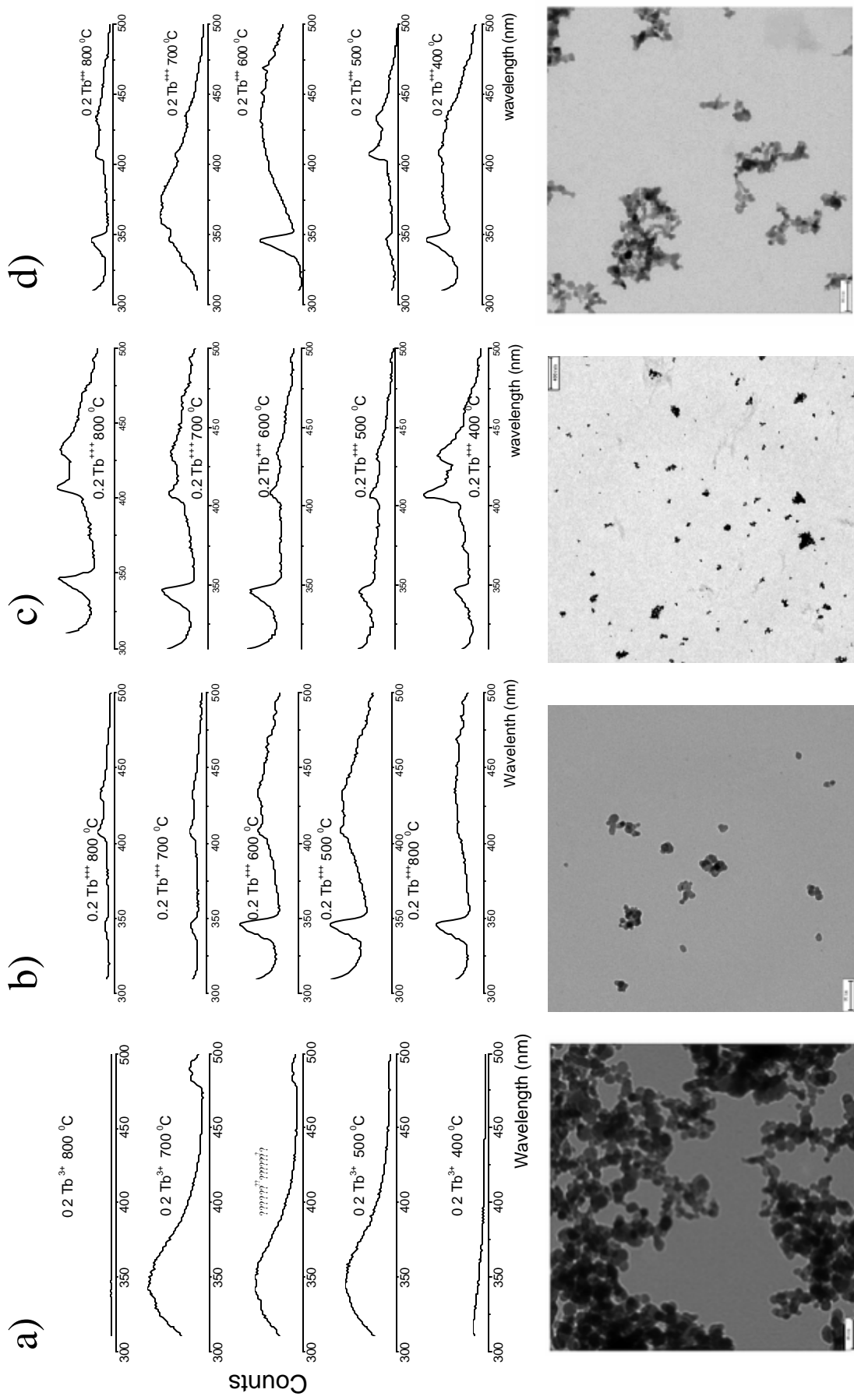


Figure 2

Synthesis, Characterization and Bio-conjugation of Fluorescent Gold Nanoclusters toward Biological Labeling Applications

Cheng-An J. Lin^{1,5}, Ting-Ya Yang^{1,5}, Chih-Hsien Lee^{1,5}, Sherry H. Huang^{1,5}, Ralph A. Sperling², Marco Zanella², Jimmy K. Li^{1,5#}, Ji-Lin Shen³, Hsueh-Hsiao Wang³, Hung-I Yeh³, Wolfgang J. Parak^{2}, Walter H. Chang^{1,5*}*

¹ Department of Biomedical Engineering, Chung Yuan Christian University, Chung-Li 32023, Taiwan (R.O.C.)

² Fachbereich Physik, Philipps Universität Marburg, Renthof 7, 35037 Marburg (Germany)

³ Department of Physics, Chung Yuan Christian University, Chung-Li 32023, Taiwan (R.O.C.)

⁴ Cardiac Medicine, Mackay Memorial Hospital, Taipei, Taiwan (R.O.C.)

⁵ R&D Center for Membrane Technology, Center for Nano Bioengineering, Chung Yuan Christian University, Chung-Li 32023, Taiwan (R.O.C.)

Present address: Harvard–MIT Health Sciences and Technology, Brigham and Women's Hospital, Harvard Medical School, Cambridge, MA, 02139

* Corresponding author: Prof. Walter H. Chang, email: whchang@cycu.edu.tw; Prof. Dr. Wolfgang Parak, email: Wolfgang.Parak@physik.uni-marburg.de

Abstract

Synthesis of ultrasmall water-soluble fluorescent gold nanoclusters is reported. The clusters have a decent quantum yield, high colloidal stability, and can be readily conjugated with biological molecules. Specific staining of cells and nonspecific uptake by living cells is demonstrated.

Introduction

Noble metal nanoclusters (NCs) such as Au and Ag with sizes below 2 nm have gained great attention in the last decade. Focus of interest ranges from fundamental properties such as photoluminescence¹⁻⁸, optical chirality⁹⁻¹², ferromagnetism¹³, redox-like and quantized double layer charging behavior¹⁴⁻¹⁷ to potential applications such as single molecule optoelectronics^{18, 19}, sensing²⁰ and bioassay^{21, 22}. This is based on the particular size-dependent properties of the clusters. They can be considered as intermediates between atomic and nanoparticle (> 2 nm) behavior²³. Gold nanoparticles (NPs) show a size-dependent plasmon absorption band when their conduction electrons are confined to

dimensions smaller than the electron mean free path-length (ca. 20 nm)²⁴. However, Au nanoparticles smaller than 2 nm (which we term Au nanoclusters) no longer possess plasmon resonance and Mie's theory no longer can be applied²⁵⁻²⁷. In fact small metal NCs have sizes comparable to the Fermi wavelength of electrons (ca. 0.7 nm), which results in molecule-like properties including size-dependent fluorescence^{20, 23, 28} and discrete size-dependent electronic states^{14, 29-31}. So far there are only few studies about the fluorescence of metal NCs^{32, 33 34}, though photoluminescence (PL) of noble metals is a known phenomenon. First reports are based on bulk metals³⁵, but soon quasi size dependence was discovered by the fact that the PL is enhanced on roughened surfaces³⁶ (i.e. at conditions with reduced radius of curvature).

The fluorescent properties of Au NCs make them potential labels for biologically motivated experiments³⁷. Compared to commonly used CdSe/ZnS semiconductor NPs (so-called quantum dots), which possess size-dependent fluorescence in case the particle size is smaller than the exciton Bohr radius (about 4-5 nm for CdSe)³⁸, Au NCs do not contain toxic heavy metals³⁹. Though depending on their size also Au NCs can have cytotoxic effects, for example by binding to DNA⁴⁰, they are a potential alternative to quantum dots as fluorescence labels. In this work we describe an easy synthesis for water-soluble fluorescent Au NCs and compare their performance in terms of colloidal and photophysical properties to the one of colloidal CdSe/ZnS NPs. The focus hereby is set on a detailed characterization of practically important parameters rather than on understanding the underlying mechanisms.

Synthesis

Synthesis of Au NCs was based on precursor-induced Au NP etching. First 6-nm diameter gold NPs stabilized with didodecyldimethylammonium bromide (AuNP@DDAB) were synthesized in toluene via an established single-phase reaction⁴¹ (experimental details can be found in the Supporting Information). Remaining residual reducing agent was removed by purification. The resulting red translucent NP solution showed the typical plasmon absorption peak at 520 nm and transmission electron microscopy (TEM) analysis revealed a mean particle diameter of the inorganic Au core of 5.55 ± 0.68 nm. Subsequent further dropwise addition of gold precursor solution (AuCl₃ or HAuCl₄ in DDAB-toluene solution) caused a gradual loss of plasmon absorption until the solution turned colorless transparent (see Figure 1). TEM analysis of the transparent solution discovered the presence of small NCs with homogeneous size distribution (mean diameter 3.17 ± 0.35 nm as determined with TEM). This suggests that continuous addition of precursor started to etch the original nanoparticles of around 6 nm diameter (AuNP@DDAB) into smaller nanoclusters of around 3 nm diameter (AuNC@DDAB)^{20 42} (for a set of time-dependent absorption spectra

see the Supporting Information). As no change in solvent was involved in the etching procedure the Au NCs at this step still were dispersed in toluene. However, because for intended biological applications water-soluble Au NCs are required, a phase transfer to aqueous solution was carried out. For this purpose ligand exchange with reduced lipoic acid (DHLA, dihydrolipoic acid) was performed, a capping ligand which as already been successfully used for phase transfer⁴³. Lipoic acid was freshly reduced by tetrabutylammonium borohydride (TBAB) with a molar ratio of lipoic acid to of TBAB = 4:1 and added to the AuNC@DDAB particles dispersed in toluene. This lead to dark-brown particle agglomerates in the resulting mixture. Particles were precipitated by centrifugation, the toluene based supernatant was discarded and the remaining particle precipitate could be dispersed in alkaline aqueous solution (pH 9) or methanol (basified by a small amount of alkaline buffer). Further purification was achieved by two runs of ultracentrifugation (110,000 rpm) for removing excess DHLA and the particle solution was concentrated with a centrifuge filter of 30 kDa MWCO (molecular weight cut-off), leading to a colloiddally stable transparent solution of NCs without plasmon peak. Successful transfer from toluene to alkaline buffer solution suggests that the added DHLA had replaced the DDAB surfactants driven by the formation of gold-thiol bonds. TEM images showed that the resulting AuNC@DHLA particles were well-dispersed and had an average core diameter of 1.56 ± 0.3 nm. This demonstrates that the diameter of the Au NCs was further decreased during the ligand exchange procedure.

Photophysical characterization

Most important, after phase transfer to aqueous solution the NCs exhibited a pronounced red photoluminescence. Exposure of the AuNC@DHLA particle solution to UV light (365 nm) led to an increase in photoluminescence (photobrightening). Photoluminescence (PL) and photoluminescence excitation (PLE) spectra of the cluster solution are shown in Figure 2. The non-shifted emission peak via changing the excitation wavelength gives strong evidence that the observed emission is a real luminescence from the relaxed states rather than scattering effects. Using Rhodamine 6G ($Q=0.95$ in ethanol) as the reference, the quantum yield (Q) of AuNC@DHLA was determined to be $3.45 \pm 0.41\%$ in methanol and $1.83 \pm 0.32\%$ in water (pH 9). This is eight orders of magnitude higher with respect to the quantum yield reported for bulk gold ($Q=10^{-10}$)³⁵, approximately 1~2 orders of magnitude higher than the quantum yield of Au NCs derived with other synthesis routes ($Q=10^{-3} - 10^{-6}$)^{1, 2, 5, 30, 44, 45} and comparable to the quantum yield recently reported by Huang et al. for similar Au NCs²⁰. Though the quantum yield of the AuNC@DHLA nanoclusters is still one order of magnitude lower than that of most organic fluorophores and quantum dots it is already in the range which is needed for applications in optical devices and biosensors.

Impurities are always problematic for working with colloidal particles, as they can co-exist in the solution so that the optical properties detected from this solution comprise both, the particles and the impurities. As will be explained in the following sections we were able to separate particles from potential impurities such as excess ligands or precursors by size exclusion chromatography and gel electrophoresis and presence of the NCs in the purified solutions was verified with TEM. In this way it was assured that the photoluminescence originates from the NCs.

Photoluminescence of Au NCs has been reported before and several models have been proposed to explain this photoluminescence mechanism. Though this study does not contribute in understanding the origin and mechanism of photoluminescence of Au NCs there is work by other groups in this direction. A theoretical study explains photoluminescence of nanosized noble metals by electronic transitions between occupied d bands and states above the Fermi level (usually the sp bands)²⁹. Whetten et al. attribute photoluminescence in the red / near-infrared (NIR) of Au NCs comprising 28 Au atoms capped with glutathione to the recombination between the ground state and two distinctively different excited states, i.e. an intraband and interband transition⁵. Murray et al. associated the photoluminescence to interband transitions between the filled 5d¹⁰ band and the 6(sp)¹ conduction band² or to participation of localized core surface states⁴⁶. Other possible mechanisms have been suggested such as ligand-to-metal charge transfer (LMCT) which is mainly affected by the types of ligands²⁰, and ligand-to-metal-metal charge transfer (LMMCT) which is commonly referred to as aurophilic interaction⁴⁷.

In an additional experiment photostability of different water-soluble fluorophores was compared (for data see the Supporting Information). The fluorescent gold nanoclusters (AuNC@DHLA) as synthesized here exhibited less photobleaching than organic fluorophores (fluorescein, rhodamine 6G). However, AuNC@DHLA was more prone to photobleaching than semiconductor quantum dots (CdSe/ZnS), which show an excellent photostability.

Colloidal characterization

In order to purify the NCs from eventual residual impurities size exclusion chromatography and gel electrophoresis was applied. These methods fractionate the initial particle solution and only the desired fraction containing the particles is extracted from the elution profile. As both methods are sensitive to size (gel electrophoresis is in addition

sensitive to charge) also estimates of size of the NCs can be extracted from the time resolved elution profiles⁴⁸. The hydrodynamic diameter d_{eff} of AuNC@DHLA nanoclusters was determined with size exclusion chromatography to be $1.3 \text{ nm} < d_{\text{eff}} < 3.4 \text{ nm}$ using 1 - 3 kDa polyethylene glycol (PEG) molecules as size standard⁴⁸ (Figure 3a). Similarly the hydrodynamic diameter of AuNC@DHLA was determined with gel electrophoresis to be smaller than 5 nm (Figure 3b), using bis(p-sulfonatophenyl)phenylphosphine capped Au NPs of different size as standard. Hereby similar negative charge on the reference Au NPs and the Au NCs reported in this study was assumed⁴⁸. These data suggest very small effective particle diameters in colloidal solution well below 5 nm. The size increment compared to the TEM results which refer to the diameter of only the inorganic Au core is attributed to the thickness of the organic capping of the particle surface with DHLA and adsorbed counter ions. Due to their small size the AuNC@DHLA particles also showed excellent colloidal stability in buffer solution such as 150 mM NaCl.

(Bio-) conjugation

Polyethylene glycol (PEG, 5 kDa) was chosen as the first example of a molecule to conjugate to the surface of AuNC@DHLA. PEG-coated particles are known for excellent biocompatibility, reduced nonspecific interaction with biological molecules and cells^{49, 50}, and increased colloidal stability in a salt-containing solution due to steric repulsion⁵¹⁻⁵³. In previous studies^{54, 55} we have described that the more PEG molecules are attached to nanoparticles, the slower the PEGylated nanoparticles run with gel electrophoresis due to increased size of the conjugates. Attachment of single amino-terminated PEG molecules (methoxy-PEG-NH₂, $M_w \geq 5000 \text{ g/mol}$) to nanoparticles using EDC chemistry can yield to distinctly shifted bands upon gel electrophoresis⁵⁴. Here we demonstrate that PEG-NH₂ can also be covalently attach to fluorescent AuNC@DHLA particles via EDC, which forms an amine-reactive *O*-acylisourea intermediate with carboxyl groups and thus mediates amide formation with primary amines. The results shown in Figure 4 indicate that EDC-mediated attachment of PEG-NH₂ retards the band of the conjugates on the gel. At least one discrete retarded band exists which we ascribe to Au NCs with exactly one PEG attached per particle in analogy to previous interpretations⁵⁵. As the Au NCs are very small attachment of more PEG leads to complete retardation on the gel and conjugates with higher stoichiometry could not be resolved. PEGylation extraordinarily improved the stability of AuNC@DHLA in salt-containing buffer (1M NaCl) as well as in acidic buffer (pH < 7). Similarly also biotin-PEG-amine could be attached to AuNC@DHLA following the same conjugation chemistry. In this case the end of the PEG containing the biotin moiety points towards solution and the first discrete band can be ascribed to Au NCs with exactly one biotin functionality per NC. In a control experiment biotinylation of AuNC@DHLA was proven by

cutting the biotinylated Au NCs from gel, incubating them with streptavidin and observation of the resulting increase in diameter due to biotin-streptavidin bond formation with gel electrophoresis (for date see the Supporting Information). PEGylation of AuNC@DHLA did not lead to reduction in photoluminescence intensity.

Avidin, a glycoprotein was chosen as second example for direct conjugation to AuNC@DHLA, as avidin-biotin technology has been widely used in biomedical research. Avidin molecules contain NH₂ groups and therefore can be conjugated to fluorescent AuNC@DHLA by EDC chemistry. Again attachment of avidin led to a reduction in mobility of the conjugates due to its high molecular weight of approximately 66 kDa (see Supporting Information for data). Similar results were obtained for streptavidin. In both cases conjugation of AuNC@DHLA did not lead to a reduction in particle photoluminescence.

Specific labeling of fixed cells

Biotin, a vitamin essential for the metabolism, is widely distributed in the body. Significant amounts of endogenous biotin have been detected in rat kidney, liver and brain⁵⁶. Probing the intracellular distribution of endogenous biotin within liver cells with streptavidin-conjugated AuNC@DHLA was therefore used as example for confirming the functionality of streptavidin-conjugation. Human hepatoma cells (HepG₂) were fixed with 2% paraformaldehyde and stained with streptavidin-conjugated AuNC@DHLA. Unconjugated, PEG-conjugated, and BSA-conjugated AuNC@DHLA was used as negative control and FITC-avidin as positive control (Figure 5). Bovine serum albumine (BSA) served hereby as control for a protein which does not specifically bind to biotin. However, some red fluorescence can be observed in the labeling of the cells incubated with unconjugated and with BSA-conjugated Au NCs. In both cases this has to be referred to as nonspecific background. Conjugation of the Au NCs with PEG reduced nonspecific binding as expected, which can be seen in the very low red fluorescence intensity. Streptavidin-conjugated Au NCs on the other hand stained the biotin containing cells with high intensity. These results are in agreement with the positive control in which streptavidin-coated FITC was used, which is a common way to label the endogenous biotin⁵⁶. The consensus of *in situ* observation within liver cells showed that the streptavidin-conjugated AuNC@DHLA can specifically label endogeneous biotin.

Nonspecific uptake by living cells

In addition preliminary data indicate that fluorescent AuNC@DHLA without any modification did not cause any acute toxicity. Au NCs were nonspecifically incorporated by

cells, as it is known also for colloidal quantum dots⁵⁷. Uptake of unconjugated AuNC@DHLA was observed in living endothelial cells after around 5 hours incubation (Figure 6). Hereby the uptake efficiency depended significantly on the culture medium, as incorporation was stronger in serum-free than in serum-supplemented medium.

Conclusions

In this report we describe the synthesis of water-soluble fluorescent gold nanoclusters capped with dihydrolipoic acid (DHLA). The resulting AuNC@DHLA particles have a quantum yield of around 1- 3 %, reduced photobleaching compared to organic fluorophores, and very good colloidal stability. AuNC@DHLA can be conjugated with EDC chemistry to biologically relevant molecules such PEG, BSA, avidin, and streptavidin. Uptake of AuNC@DHLA by cells did not cause acute toxicity. By their small hydrodynamic diameter (< 5 nm) and inert nature fluorescent Au NCs might become an interesting alternative to colloidal quantum dots, in particular for applications in which the size and biocompatibility of the label is critical. The weakest point so far remains the relatively low quantum yield. Based on the current report as well as on previous breakthrough findings^{5, 8, 14, 23, 34, 58} we believe that fluorescent gold nanoclusters have a great potential for applications to biomedical research to offer.

Acknowledgment

This project was supported by the National Science Council (NSC 96-2320-B-033; NSC 97-2627-B-033), the Ministry of Education from Taiwan and in part by the Deutsche Forschungsgesellschaft (DFG, grant PA794/4-1) and the Bundesministerium für Bildung und Forschung (BMBF, grant 13N9192).

References

1. Bigioni, T. P.; Whetten, R. L.; Dag, O. *Journal of Physical Chemistry B* **2000**, 104, (30), 6983-6986.
2. Huang, T.; Murray, R. W. *Journal of Physical Chemistry B* **2001**, 105, (50), 12498-12502.
3. Peyser, L. A.; Vinson, A. E.; Bartko, A. P.; Dickson, R. M. *Science* **2001**, 291, (5501), 103-106.
4. Zheng, J.; Dickson, R. M. *Journal of the American Chemical Society* **2002**, 124, (47), 13982-13983.

5. Link, S.; Beeby, A.; FitzGerald, S.; El-Sayed, M. A.; Schaaff, T. G.; Whetten, R. L. *Journal of Physical Chemistry B* **2002**, 106, (13), 3410-3415.
6. Yang, Y.; Chen, S. *Nano Letters* **2003**, 3, (1), 75-79.
7. Zheng, J.; Petty, J. T.; Dickson, R. M. *Journal of the American Chemical Society* **2003**, 125, (26), 7780-7781.
8. Negishi, Y.; Takasugi, Y.; Sato, S.; Yao, H.; Kimura, K.; Tsukuda, T. *Journal of the American Chemical Society* **2004**, 126, (21), 6518-6519.
9. Schaaff, T. G.; Whetten, R. L. *Journal of Physical Chemistry B* **2000**, 104, (12), 2630-2641.
10. Garzon, I. L.; Reyes-Nava, J. A.; Rodriguez-Hernandez, J. I.; Sigal, I.; Beltran, M. R.; Michaelian, K. *Physical Review B* **2002**, 66, (7), 073403.
11. Gautier, C.; Burgi, T. *Journal of the American Chemical Society* **2008**, ASAP.
12. Roman-Velazquez, C. E.; Noguez, C.; Garzon, I. L. *Journal of Physical Chemistry B* **2003**, 107, (44), 12035-12038.
13. Crespo, P.; Litran, R.; Rojas, T. C.; Multigner, M.; de la Fuente, J. M.; Sanchez-Lopez, J. C.; Garcia, M. A.; Hernando, A.; Penades, S.; Fernandez, A. *Physical Review Letters* **2004**, 93, (8), 087204.
14. Chen, S.; Ingram, R. S.; Hostetler, M. J.; Pietron, J. J.; Murray, R. W.; Schaaff, T. G.; Khoury, J. T.; Alvarez, M. M.; Whetten, R. L. *Science* **1998**, 280, (5372), 2098-101.
15. Hicks, J. F.; Templeton, A. C.; Chen, S. W.; Sheran, K. M.; Jasti, R.; Murray, R. W.; Debord, J.; Schaaf, T. G.; Whetten, R. L. *Analytical Chemistry* **1999**, 71, (17), 3703-3711.
16. Hicks, J. F.; Miles, D. T.; Murray, R. W. *Journal of the American Chemical Society* **2002**, 124, (44), 13322-13328.
17. Quinn, B. M.; Liljeroth, P.; Ruiz, V.; Laaksonen, T.; Kontturi, K. *Journal of the American Chemical Society* **2003**, 125, (22), 6644-6645.
18. Lee, T. H.; Gonzalez, J. I.; Zheng, J.; Dickson, R. M. *Accounts of Chemical Research* **2005**, 38, (7), 534-541.
19. Vosch, T.; Antoku, Y.; Hsiang, J. C.; Richards, C. I.; Gonzalez, J. I.; Dickson, R. M. *Proceedings of the National Academy of Sciences of the United States of America* **2007**, 104, (31), 12616-12621.
20. Huang, C. C.; Yang, Z.; Lee, K. H.; Chang, H. T. *Angewandte Chemie-International Edition* **2007**, 46, (36), 6824-6828.
21. Triulzi, R. C.; Micic, M.; Giordani, S.; Serry, M.; Chiou, W. A.; Leblanc, R. M. *Chemical Communications* **2006**, (48), 5068-5070.
22. Huang, C. C.; Chiang, C. K.; Lin, Z. H.; Lee, K. H.; Chang, H. T. *Analytical Chemistry* **2008**, 80, (5), 1497-1504.
23. Zheng, J.; Zhang, C. W.; Dickson, R. M. *Physical Review Letters* **2004**, 93, (7), 077402.

24. Link, S.; El-Sayed, M. A. *Annu Rev Phys Chem* **2003**, 54, 331-66.
25. Alvarez, M. M.; Houry, J. T.; Schaaff, T. G.; Shafigullin, M. N.; Vezmar, I.; Whetten, R. L. *Journal of Physical Chemistry B* **1997**, 101, (19), 3706-3712.
26. Schaaff, T. G.; Shafigullin, M. N.; Houry, J. T.; Vezmar, I.; Whetten, R. L.; Cullen, W. G.; First, P. N.; GutierrezWing, C.; Ascensio, J.; JoseYacaman, M. J. *Journal of Physical Chemistry B* **1997**, 101, (40), 7885-7891.
27. Hostetler, M. J.; Wingate, J. E.; Zhong, C. J.; Harris, J. E.; Vachet, R. W.; Clark, M. R.; Londono, J. D.; Green, S. J.; Stokes, J. J.; Wignall, G. D.; Glish, G. L.; Porter, M. D.; Evans, N. D.; Murray, R. W. *Langmuir* **1998**, 14, (1), 17-30.
28. Schaeffer, N.; Tan, B.; Dickinson, C.; Rosseinsky, M. J.; Laromaine, A.; McComb, D. W.; Stevens, M. M.; Wang, Y.; Petit, L.; Barentin, C.; Spiller, D. G.; Cooper, A. I.; Lévy, R. *Chemical Communications* **2008**, (34), 3986 - 3988.
29. Apell, P.; Monreal, R.; Lundqvist, S. *Physica Scripta* **1988**, 38, 174-179.
30. Lee, D.; Donkers, R. L.; Wang, G. L.; Harper, A. S.; Murray, R. W. *Journal of the American Chemical Society* **2004**, 126, (19), 6193-6199.
31. Lin, Z. Y.; Kanters, R. P. F.; Mingos, D. M. P. *Inorganic Chemistry* **1991**, 30, (1), 91-95.
32. Fedrigo, S.; Harbich, W.; Buttet, J. *Journal of Chemical Physics* **1993**, 99, (8), 5712-5717.
33. Konig, L.; Rabin, I.; Schulze, W.; Ertl, G. *Science* **1996**, 274, (5291), 1353-1355.
34. Wilcoxon, J. P.; Martin, J. E.; Parsapour, F.; Wiedenman, B.; Kelley, D. F. *Journal of Chemical Physics* **1998**, 108, (21), 9137-9143.
35. Mooradian, A. *Physical Review Letters* **1969**, 22, 185-187.
36. Boyd, G. T.; Yu, Z. H.; Shen, Y. R. *Physical Review B* **1986**, 33, (12), 7923-7936.
37. Sperling, R. A.; Gil, P. R.; Zhang, F.; Zanella, M.; Parak, W. J. *Chemical Society Reviews* **2008**, 37, 1896 -1908.
38. Alivisatos, A. P. *Science* **1996**, 271, (16 February), 933-937.
39. Kirchner, C.; Liedl, T.; Kudera, S.; Pellegrino, T.; Javier, A. M.; Gaub, H. E.; Stolzle, S.; Fertig, N.; Parak, W. J. *Nano Letters* **2005**, 5, (2), 331-338.
40. Pan, Y.; Neuss, S.; Leifert, A.; Fischler, M.; Wen, F.; Simon, U.; Schmid, G.; Brandau, W.; Jahnen-Dechent, W. *Small* **2007**, 3, (11), 1941-1949.
41. Jana, N. R.; Peng, X. G. *Journal of the American Chemical Society* **2003**, 125, (47), 14280-14281.
42. Kruger, D.; Fuchs, H.; Rousseau, R.; Marx, D.; Parrinello, M. *Journal of Chemical Physics* **2001**, 115, (10), 4776-4786.
43. Mattoussi, H.; Mauro, J.; Goldman, E.; Anderson, G.; Sundar, V.; Mikulec, F.; Bawendi, M. *Journal of the American Chemical Society* **2000**, 122, (49), 12142-12150.
44. Negishi, Y.; Tsukuda, T. *Chemical Physics Letters* **2004**, 383, (1-2), 161-165.
45. Negishi, Y.; Nobusada, K.; Tsukuda, T. *Journal of the American Chemical Society* **2005**,

- 127, (14), 5261-5270.
46. Wang, G. L.; Huang, T.; Murray, R. W.; Menard, L.; Nuzzo, R. G. *Journal of the American Chemical Society* **2005**, 127, (3), 812-813.
 47. Cha, S. H.; Kim, J. U.; Kim, K. H.; Lee, J. C. *Chemistry of Materials* **2007**, 19, (25), 6297-6303.
 48. Sperling, R. A.; Liedl, T.; Duhr, S.; Kudera, S.; Zanella, M.; Lin, C.-A. J.; Chang, W. H.; Braun, D.; Parak, W. J. *Journal of Physical Chemistry C* **2007**, 111, (31), 11552-11559.
 49. Ballou, B.; Lagerholm, B. C.; Ernst, L. A.; Bruchez, M. P.; Waggoner, A. S. *Bioconjugate Chemistry* **2004**, 15, (1), 79-86.
 50. Bentzen, E. L.; Tomlinson, I. D.; Mason, J.; Gresch, P.; Warnement, M. R.; Wright, D.; Sanders-Bush, E.; Blakely, R.; Rosenthal, S. J. *Bioconjugate Chemistry* **2005**, 16, (6), 1488-1494.
 51. Dubertret, B.; Skourides, P.; Norris, D. J.; Noireaux, V.; Brivanlou, A. H.; Libchaber, A. *Science* **2002**, 298, (29 November), 1759-1762.
 52. Parak, W. J.; Gerion, D.; Zanchet, D.; Woerz, A. S.; Pellegrino, T.; Micheel, C.; Williams, S. C.; Seitz, M.; Bruehl, R. E.; Bryant, Z.; Bustamante, C.; Bertozzi, C. R.; Alivisatos, A. P. *Chemistry of Materials* **2002**, 14, (5), 2113-2119.
 53. Nikolic, M. S.; Krack, M.; Aleksandrovic, V.; Kornowski, A.; Forster, S.; Weller, H. *Angewandte Chemie-International Edition* **2006**, 45, (39), 6577-6580.
 54. Sperling, R. A.; Pellegrino, T.; Li, J. K.; Chang, W. H.; Parak, W. J. *Advanced Functional Materials* **2006**, 16, (7), 943-948.
 55. Lin, C. A. J.; Sperling, R. A.; Li, J. K.; Yang, T. Y.; Li, P. Y.; Zanella, M.; Chang, W. H.; Parak, W. G. J. *Small* **2008**, 4, (3), 334-341.
 56. Wang, H.; Pevsner, J. *Cell Tissue Research* **1999**, 296, 511-516.
 57. Parak, W.; Boudreau, R.; Le Gros, M.; Gerion, D.; Zanchet, D.; Micheel, C.; Williams, S.; Alivisatos, A.; Larabell, C. *Advanced Materials* **2002**, 14, (12), 882-885.
 58. Jadzinsky, P. D.; Calero, G.; Ackerson, C. J.; Bushnell, D. A.; Kornberg, R. D. *Science* **2007**, 318, (5849), 430-433.

Figures

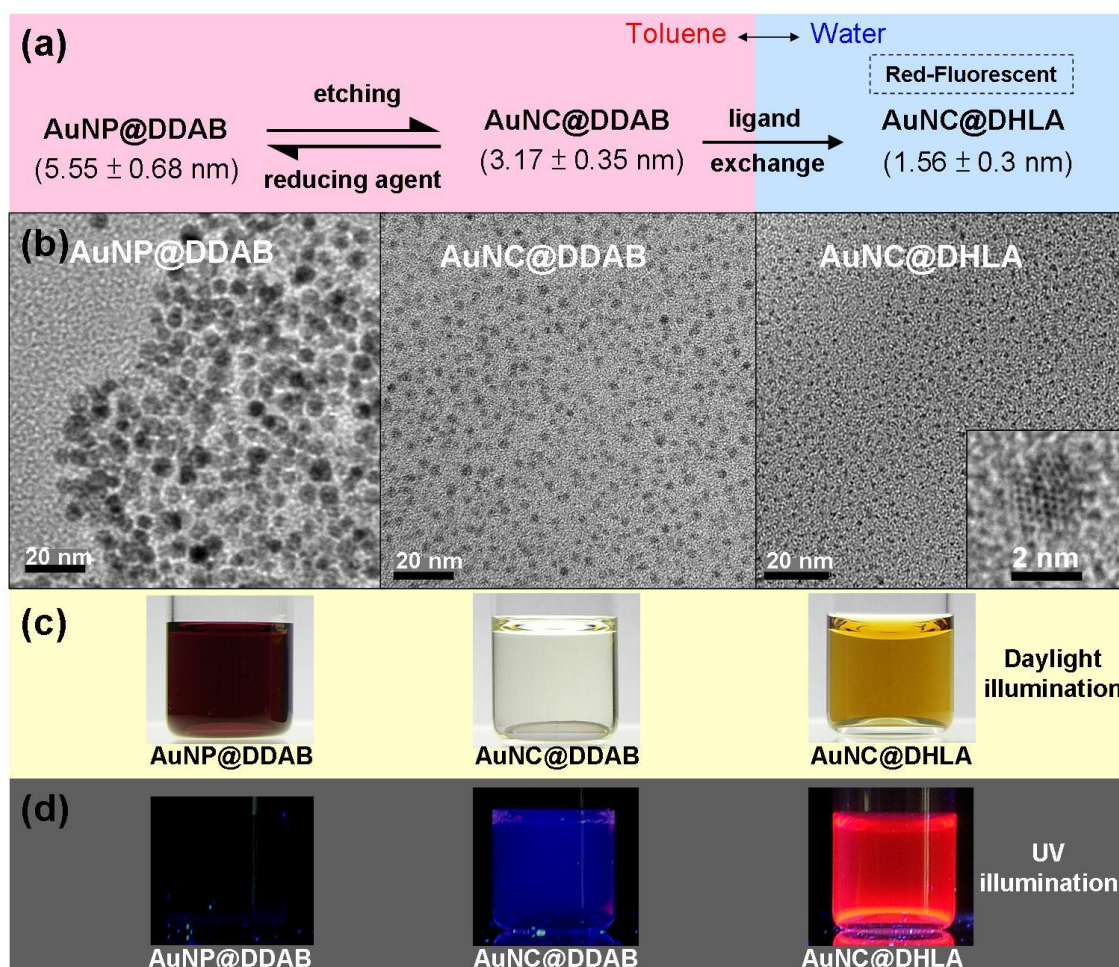


Figure 1. a) General strategy to fabricate water-soluble fluorescent Au nanoclusters. DDAB-stabilized gold nanoparticles (AuNP@DDAB) are etched by the addition of Au precursors (HAuCl_4 or AuCl_3) to smaller nanoclusters (AuNC@DDAB). By the addition of reducing agent (TBAB) the Au NCs grow again reversibly into bigger Au NPs. The hydrophobic AuNC@DDAB become water soluble upon ligand exchange with dihydrolipoic acid (AuNC@DHLA); b) TEM images of AuNP@DDAB, AuNC@DDAB, and AuNC@DHLA. 100 particles were randomly selected for measuring the size distribution, resulting in 5.55 ± 0.68 nm, 3.17 ± 0.35 nm, and 1.56 ± 0.3 nm in diameter respectively. c) Pictures of particle solutions under daylight. Contrary to AuNP@DDAB solution which features the red color of surface plasmon absorption, AuNC@DDAB and AuNC@DHLA display a colorless and brown translucent solution without plasmon absorption, respectively. d) Pictures of the same particle solutions under UV excitation. The AuNC@DHLA solution show red photoluminescence.

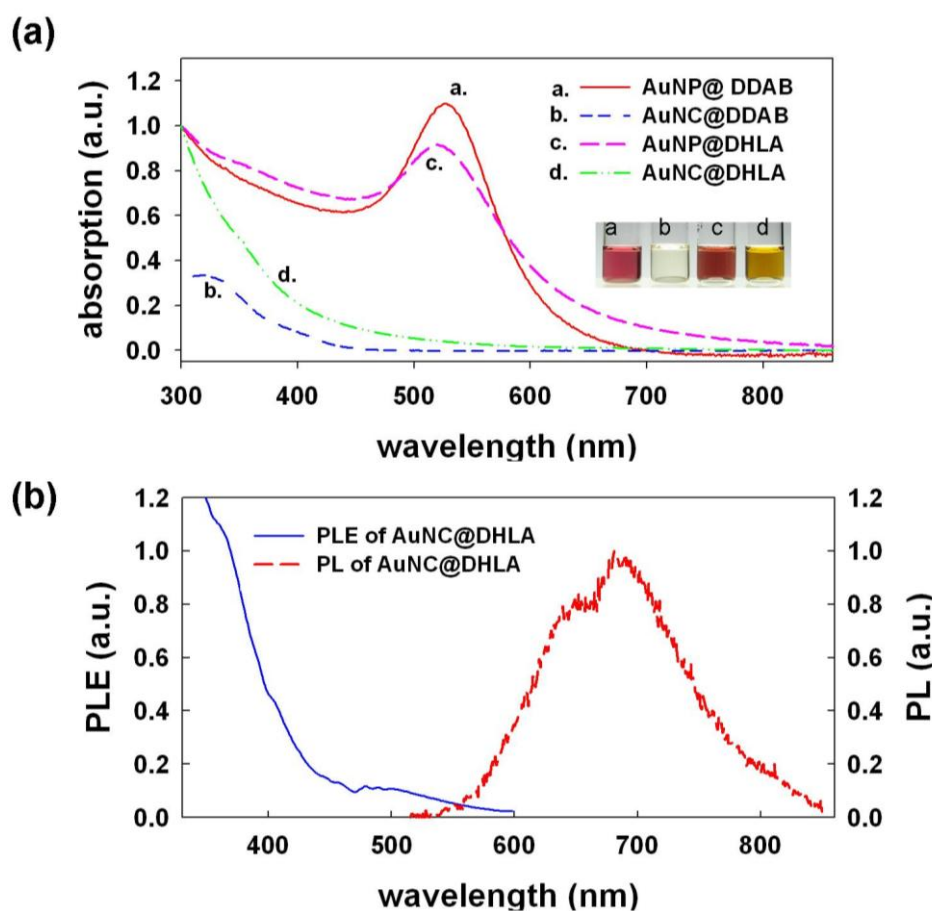


Figure 2. a) UV/vis absorption spectra of the as-prepared gold nanoparticles (AuNP@DDAB), after etching (AuNC@DDAB) and after ligand exchange (AuNC@DHHLA). The AuNP@DHHLA sample was obtained by ligand exchange from the original AuNP@DDAB sample without etching step. Au samples with DDAB capping were dissolved in toluene, sample with DHHLA capping in aqueous solution. b) Photoluminescence (PL, dashed) and photoluminescence excitation spectra (PLE, solid) of AuNC@DHHLA particles. For the PL spectrum excitation at 490 nm was used. For the PLE spectrum a fixed emission at 650 nm was used.

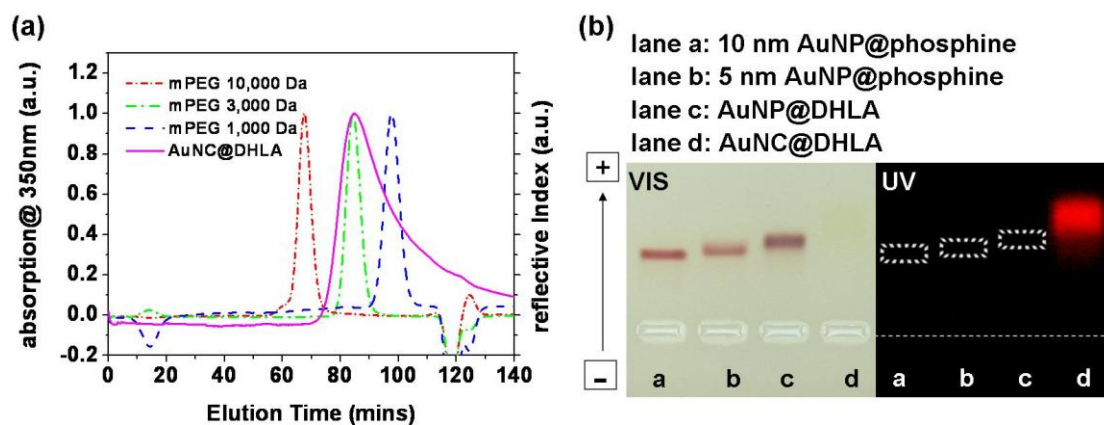


Figure 3. a) Elution profile of size exclusion chromatography (Sephacryl S-200 gel) AuNC@DHLA particles versus PEG standards (1,000, 3000, 10,000 g/mol) as recorded via absorption or refractive index measurements. The PEG standards correspond to theoretically estimated diameters of 6.6, 3.4 and 1.8 nm. b) Electrophoretic mobility of Au particles in 2% agarose gels (7.5V/cm electric field, 20 min running time) Phosphine stabilized Au NPs of 10 nm and 5 nm core diameter were run in lanes a and b as control. In lanes c and d AuNP@DHLA and AuNC@DHLA solutions are run. The AuNP@DHLA corresponds to AuNP@DDAB after ligand exchange. Images were recorded at daylight (left) and under UV excitation (right).

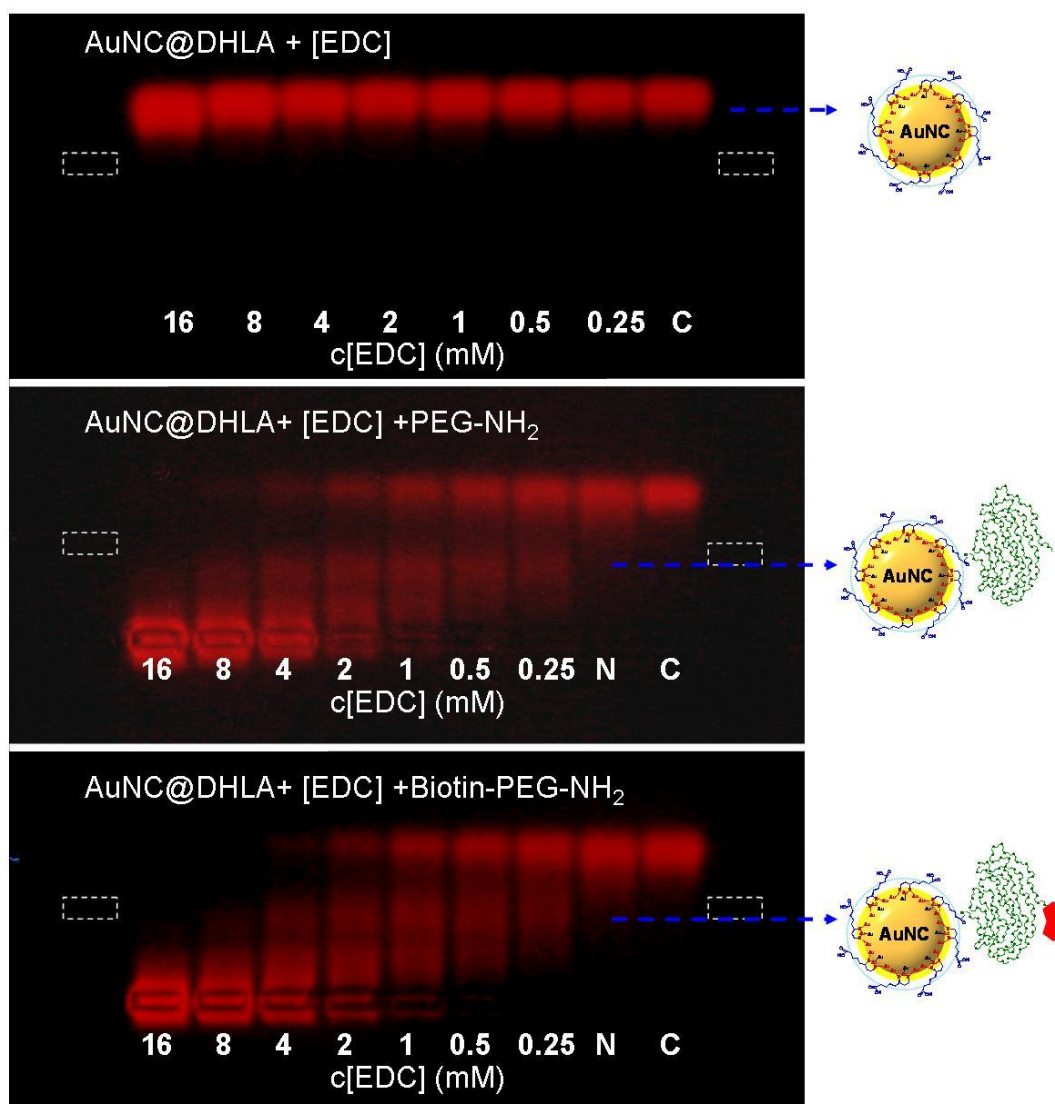


Figure 4. PEGylation and biotinylation of fluorescent Au nanoclusters (AuNC@DHHLA) as probed with gel electrophoresis. The COOH groups present on the surface of AuNC@DHHLA due to the DHHLA capping allow for covalent linkage of NH₂-modified PEG molecules via EDC activation. a) Addition of EDC only to AuNC@DHHLA serves as negative control without major effect in mobility. b) Addition of EDC under the presence of PEG-NH₂ retards the particle bands. c) Addition of EDC under the presence of biotin-PEG-NH₂ retards the particle bands. The biotin-group points towards solution. In both cases retardation is caused by linkage of PEG to the Au particles and the corresponding increment in size. The more the PEG is attached to AuNC@DHHLA the larger the conjugates and thus the retardation become. We ascribe the first discrete band to Au particles with exactly one PEG linked per particle. The negative control (lane “N”) represent AuNC@DHHLA with PEG in the absence of EDC, and lane “C” is a control with AuNC@DHHLA only.

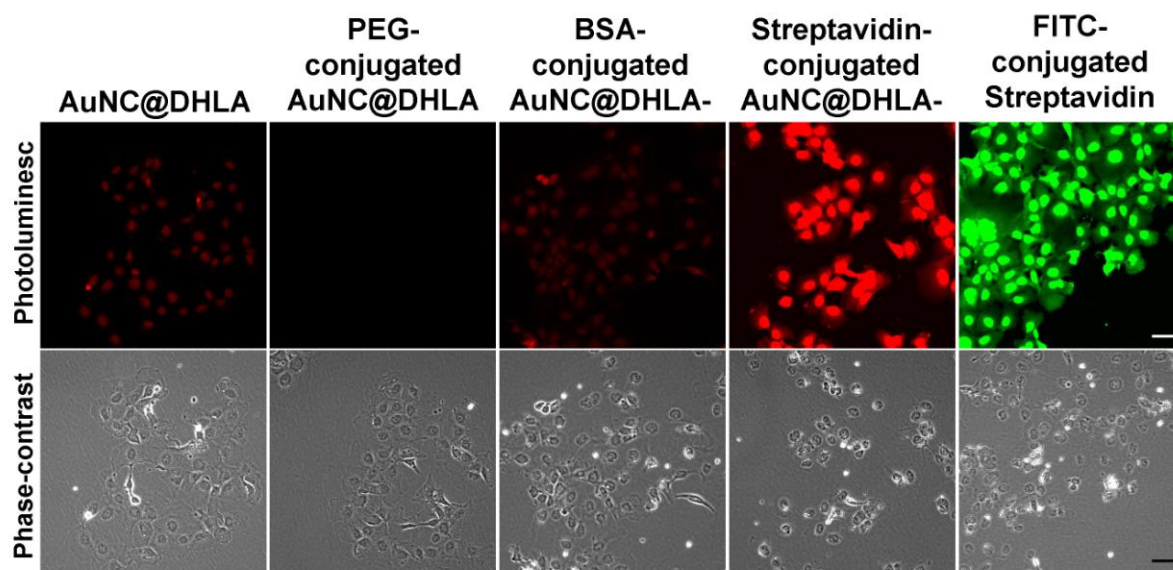


Figure 5. Labeling of endogenous biotin within human hepatoma cells (HepG₂) with fluorescent Au NCs conjugated to streptavidin (streptavidin-conjugated AuNC@DHLA). Three negative controls were used: unconjugated AuNC@DHLA, PEG-conjugated AuNC@DHLA, and BSA-conjugated AuNC@DHLA. Streptavidin-conjugated FITC served as positive control. All images were recorded with a 20x objective (PLAN NEOFLUAR) with a Zeiss confocal microscope. The fluorescence images were recorded with the following filter sets: AuNC@DHLA: LP 585 em/ 488 ex, FITC: LP 530/ 488 ex. The scale bars indicate 50 μ m.

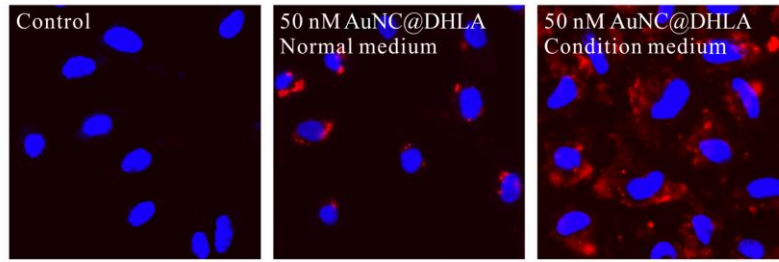


Figure 6. Nonspecific uptake of unconjugated fluorescent Au nanoclusters (AuNC@DHLA) by human aortic endothelial cells. Cell nuclei were stained in with (Hochest 33258) to yield blue fluorescence. The red fluorescence corresponds to the Au NCs. a) control without Au NCs. b) serum-supplemented cell medium with 50 nM AuNC@DHLA added. c) serum-free cell medium with 50 nM AuNC@DHLA added for 5 hours.

Gold NanoStoves for Microsecond DNA Melting Analysis

Joachim Stehr,[†] Calin Hrelescu,[†] Ralph A. Sperling,^{‡,||} Gunnar Raschke,[†]
Michael Wunderlich,[§] Alfons Nichtl,[§] Dieter Heindl,[§] Konrad Kurzinger,[§]
Wolfgang J. Parak,^{‡,||} Thomas A. Klar,^{*,†,⊥} and Jochen Feldmann^{*,†}

*Photonics and Optoelectronics Group, Physics Department, CeNS,
Ludwig-Maximilians-Universität München, Amalienstrasse 54, 80799 Munich,
Germany, and Roche Diagnostics GmbH, Nonnenwald 2, 82372 Penzberg, Germany*

Received November 20, 2007; Revised Manuscript Received January 8, 2008

ABSTRACT

In traditional DNA melting assays, the temperature of the DNA-containing solution is slowly ramped up. In contrast, we use 300 ns laser pulses to rapidly heat DNA bound gold nanoparticle aggregates. We show that double-stranded DNA melts on a microsecond time scale that leads to a disintegration of the gold nanoparticle aggregates on a millisecond time scale. A perfectly matching and a point-mutated DNA sequence can be clearly distinguished in less than one millisecond even in a 1:1 mixture of both targets.

Compared to the current standard of blood cultures, fast DNA analysis can speed up the search of pathogens causing severe illnesses such as sepsis. Numerous pathogens can cause sepsis, and the death toll could be drastically reduced if the specific pathogen could be identified more quickly than it is usually done today using blood cultures.^{1,2} Determining the pathogen's DNA is potentially faster than blood cultures,³ but it requires a rapid DNA assay with the potential for mutant identification and multiplexing. Most current DNA assays are based on thermal dehybridization or melting of the DNA duplex helix.^{4–8} This is because the melting temperature of DNA is determined by its base sequence.⁴ Usually, melting analysis of DNA is realized by slowly increasing the temperature of the DNA-containing solution.^{5,6} The heating element, the container, and the solution have to be heated to finally warm up the DNA, and the whole system must be in thermal equilibrium throughout the measurement. This severely limits the speed of the temperature ramp. Currently, typical time scales for a melting analysis range from several minutes up to 1 h. A faster detection of the DNA melting point is highly desirable especially for high throughput DNA analysis where process time is critical.

Gold nanoparticles (AuNPs) can act as very efficient light absorbers in the visible due to the particle plasmon resonance. When irradiated by short laser pulses, AuNPs convert the

absorbed light energy into thermal energy within ~ 1 ps.^{9,10} Within the subsequent ~ 100 ps, a single hot nanoparticle thermally equilibrates with its surrounding.^{10,11} Large amounts of optical energy absorbed by AuNPs have been used for destructive applications like denaturation of proteins,^{12,13} destruction of cell membranes,¹⁴ thermal ablative therapy for cancer,¹⁵ and selective cell damage.¹⁶ If high-energy laser pulses of 10^6 kW/mm² are applied to DNA-functionalized AuNPs, the thiol bond between the DNA and the particle can break.¹⁷

In contrast to these destructive applications of AuNP-mediated optical heating, we apply AuNPs as nanoscopic stoves for gentle, controlled, and reversible heating. This allows us for the first time to use AuNPs for optically induced DNA melting and to establish a DNA assay. We use DNA bound AuNP aggregates as light absorbers to locally convert optical energy from 300 ns laser pulses into thermal energy. This thermal energy is used to melt double-stranded DNA (dsDNA) on a microsecond time scale. Subsequently, the aggregates disintegrate on a millisecond time scale. Both, the perfectly matching and the single base pair (bp) mismatched DNA can be clearly distinguished even in a 1:1 mixture of both targets. The millisecond observation window provides the fastest time frame for a DNA melting analysis to date with a potential for multiplexing and mutant identification.

The temperature gradient outside a single hot AuNP is very steep^{16,18} so that a single AuNP efficiently heats a thin shell of water of approximately 5 nm thickness only. Therefore, DNA of a typical length of 10 nm would be heated very inhomogeneously and inefficiently if attached to a single AuNP. However, when AuNPs are arranged in big aggregates interconnected with DNA,^{19,20} the heat is accumulated

* To whom correspondence should be addressed.

[†] Photonics and Optoelectronics Group, Physics Department, and CeNS, Ludwig-Maximilians-Universität München.

[‡] CeNS, Ludwig-Maximilians-Universität München.

[§] Roche Diagnostics GmbH.

^{||} Present address: Fachbereich Physik, Philipps Universität Marburg, Renthof 7, 35037 Marburg, Germany.

[⊥] Present address: Institute of Physics, Technical University of Ilmenau, 98684 Ilmenau, Germany.

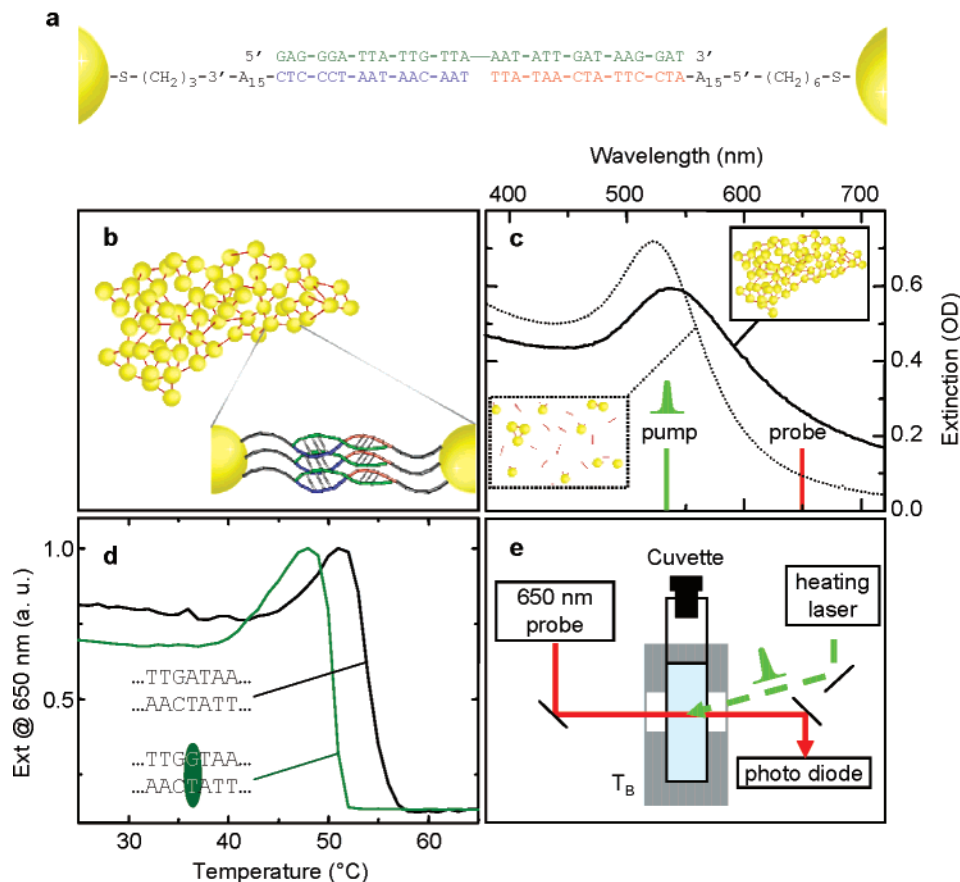


Figure 1. Gold nanostoves as DNA melting assay. (a) The sequences for a perfect matching target and AuNP-linked detection sequences. (b) After the addition of the target to the functionalized AuNPs, multiple interparticle connections form resulting in stable DNA–AuNP networks. (c) Extinction spectrum of DNA bound gold nanoparticle aggregates at 25 °C (solid line) and of dispersed particles at 60 °C (dotted line). The aggregate spectrum shows a red shift of the plasmon resonance peak and broadening of the resonance with respect to the spectrum of dissolved AuNPs. The green line indicates the wavelength of the pump laser for heating and the red line shows the probe laser wavelength. (d) Extinction of the DNA–AuNP hybrid system at 650 nm. The melting temperature of the dsDNA is 54.0 °C for the perfect matching target and 50.5 °C for a target with one bp mismatch. (e) Experimental setup: The pulsed pump-laser (green) heats the gold-aggregates. The resulting change in the sample's extinction is detected with a fast photodiode detecting the transmitted light of a 650 nm cw diode laser.

between the AuNPs and distributed homogeneously over the whole aggregate. Consequently, the linking DNA in between the AuNPs is heated homogeneously.

Apart from acting as nanostoves, AuNPs can also act as spectroscopic reporters of DNA melting. The plasmonic properties of AuNPs are very sensitive to the nanoparticles' surrounding.²¹ Therefore, AuNPs perform well for optical biosensing.^{22–24} The change of the optical properties is particularly strong for coupled particle plasmon oscillations.²⁵ The plasmon resonance of aggregated AuNPs is broadened and red-shifted as compared to dispersed AuNPs.²⁵ The aggregates act as indicators for the hybridization state of the DNA because a spectral shift and broadening of the particle plasmon resonance can easily be observed in the extinction spectra.^{7,19} Classical melting curves of AuNP aggregates are obtained by slowly increasing the temperature and monitoring the extinction. Different phenotypes of DNA will then melt at different temperatures and can therefore be distinguished.⁷

In our work, AuNPs with a diameter of 10 nm (BBI) are functionalized with two different types of single-stranded (ss) DNA (Figure 1a). Both types of ssDNA consist of a thiolated A₁₅ sequence and 15 further bases as a detection sequence.

These two detection sequences of 15 bases each are complementary to the 30 bases of the target ssDNA. To functionalize the AuNPs, 150 mg 4,4'-(phenylphosphini-dene)-bis(benzenesulfonic acid) dipotassium salt hydrate was added to 200 mL gold nanoparticle solution. The mixture was allowed to stand for several days to replace the original ligands on the gold surface with phosphine. The solution was then concentrated to $\sim 1 \mu\text{M}$ by ultrafiltration and incubated for several days with thiolated DNA (purchased from Metabion, 3' and 5' thiol modification) in a DNA/gold nanoparticle ratio of $\sim 200/1$. After removing the unbound DNA by repeated washing with PBS buffer, the AuNPs with 3' and 5' thiolated DNA were mixed in a ratio 1/1 in PBS buffer with 300 mM NaCl. After addition of the 30 base target in a molar ratio of ~ 30 targets per gold nanoparticle, the solution was heated to 65 °C for several minutes and subsequently was allowed to stand at 10 °C for typically 3 h. This led to hybridization and a formation of aggregates due to interlinking of the AuNPs in a tail-to-tail configuration,²⁶ as shown in Figure 1b. AuNP-DNA-networks are formed with multiple interparticle linkages⁶ due to several binding sites per particle.²⁷

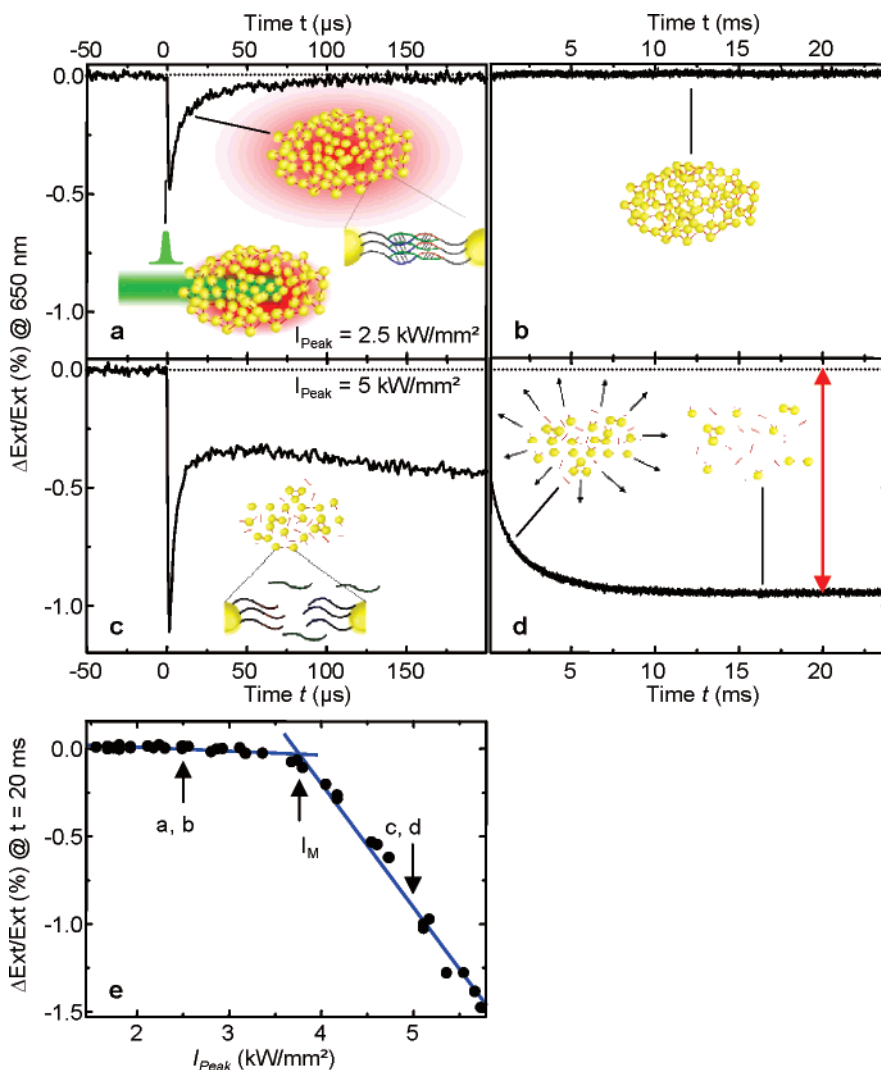


Figure 2. Testing for optically induced DNA melting. (a) Relative change in the extinction $\Delta\text{Ext}/\text{Ext}$ after a low-power laser pulse has been applied ($I_{\text{Peak}} = 2.5 \text{ kW/mm}^2$). The bath temperature is set to $25 \text{ }^\circ\text{C}$, which is far below the melting temperature of the DNA. The pump laser heats the aggregates for 300 ns. The extinction shows an initial sharp decrease but fully recovers on a microsecond time scale, indicating that the aggregates cool down on a microsecond time scale without dissociation (inset). (b) After aggregate cooling, there is no long-lived change in extinction, because the laser power was not sufficient to induce enough heat for DNA melting. (c) At $I_{\text{Peak}} = 5 \text{ kW/mm}^2$, the initially decreased $\Delta\text{Ext}/\text{Ext}$ signal is larger than in Figure 2a because the induced temperature is higher. The reached temperature is now sufficient to melt the DNA in the aggregates. This changes the aggregate structure (inset) and consequently the extinction stays on a decreased level after the cooling period ($t > 25 \mu\text{s}$). (d) The extinction decreases further on a millisecond time scale as the unlinked nanoparticles now diffuse apart (left inset). The red arrow indicates the amplitude of the long-lived decrease in extinction as a result of DNA melting and consequent aggregate dissociation (right inset). (e) The amplitude of the $\Delta\text{Ext}/\text{Ext}$ signal at 20 ms as a function of the applied laser intensity shows a clear thresholdlike behavior. The blue lines are linear fits in the melting and nonmelting regime for an exact determination of the melting threshold I_M (crossing point). Data in panels a–d are averaged over 20 single shot measurements to reduce noise.

The extinction spectrum of aggregates (Figure 1c, solid line) shows a plasmon resonance that is red-shifted and broadened compared to the plasmon resonance of dispersed AuNPs (Figure 1c, dotted line). The optical extinction at 650 nm is a good indicator for DNA melting and the successive dissociation of the aggregates. This is shown in Figure 1d, where a steep decrease in the extinction can be observed when the samples are heated and the aggregates dissolve because of DNA melting (see also ref 7). The exact values for the melting temperature are deduced from the derivatives of the melting curves in Figure 1d. As can be observed in Figure 1d, aggregates formed with a target DNA comprising a single bp mismatch (green line) show a decreased

melting temperature as compared to aggregates formed with a perfect matching target (black line). Instead of performing a time-consuming temperature ramp as shown in Figure 1d, we use single laser pulses from a Nd:YLF solid-state laser of 300 ns duration, a wavelength of 527 nm, and a repetition rate of 0.5 Hz to optically heat the aggregates (Figure 1e). A 650 nm continuous wave probe laser beam is spatially overlapped with the heating laser pulses in a 2 mm thick cuvette (Figure 1e). The intensity of the transmitted probe light is detected with a fast photodiode (Thorlabs DET110) connected to a 1 GHz oscilloscope (LeCroy Waverunner LT584). The temporal resolution of the setup is 20 ns. The bath temperature T_B of the solution in the

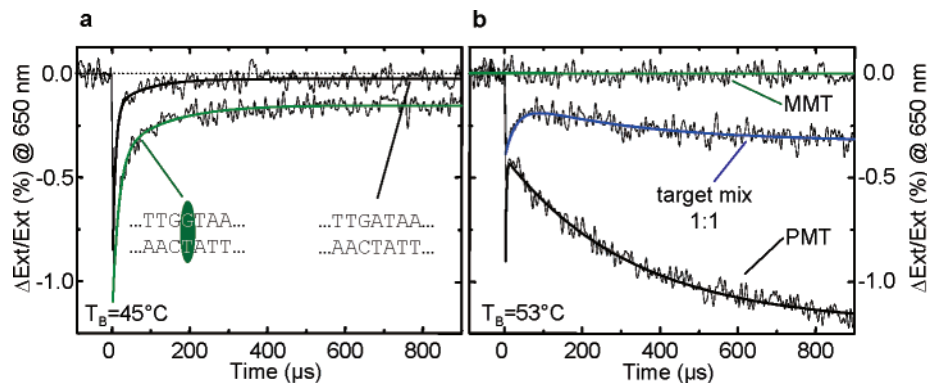


Figure 3. Mutant identification on a microsecond time scale. (a) Transient extinction after one single laser pulse. Double exponential fits are added as a guide to the eye. Perfect matching target DNA (black line) and mismatched target DNA (green line) can be distinguished with one single laser pulse. The long-lived decrease in extinction is only present with the mismatched target DNA. The applied laser power density is 2.9 kW/mm². The bath temperature T_B is 45 °C, close to the melting temperature of the targets. (b) The same measurement at $T_B = 53$ °C. The applied power density is 3.8 kW/mm². The aggregates containing only mismatched target (green line) are completely dissociated at $T_B = 53$ °C and show no response to the heating laser. The perfect matching target (black line) melts with a clear long-lived change in the extinction. A mixture of both targets (blue line) shows a long-lived $\Delta\text{Ext}/\text{Ext}$ signal as well but with a smaller amplitude compared to the perfect matching target. All three cases can be distinguished in the microsecond time range with one single laser pulse.

cuvette can be preset by a temperature-controlled cuvette holder.

Figure 2a shows a transient of the relative change of extinction $\Delta\text{Ext}/\text{Ext}$ of aggregates at $T_B = 25$ °C. The applied laser pulse has a peak power density I_{Peak} of 2.5 kW/mm². During the laser pulse, a sharp decrease in the extinction is observed. This can be due to a thermally induced change of the dielectric permittivity in the AuNPs,¹⁰ the water, and/or the DNA. Another reason could be heat-induced inflation of the aggregates and a temporary increase of the interparticle distance. Probably, the sharp decrease in the extinction is due to a mixture of these effects, and a detailed investigation is beyond the scope of this letter. Importantly, the $\Delta\text{Ext}/\text{Ext}$ signal fully recovers with a time constant of ~ 4 μs and remains recovered also on a millisecond time scale (Figure 2b). The time constant for recovery coincides with calculated cooling times for aggregates with a diameter of a few micrometers,^{18,28} which is a realistic size for DNA bound nanoparticle aggregates.⁷ T_B is virtually not affected even in the laser spot, otherwise a cooling time in the order of seconds would be expected,¹⁸ which is in contrast to our observations. We can conclude that after a laser pulse with $I_{\text{Peak}} = 2.5$ kW/mm², the AuNP aggregates remain intact and no melting of DNA has occurred.

The situation changes dramatically, when I_{Peak} is doubled (Figure 2c,d) to 5 kW/mm². Doubling the power density in the laser pulses roughly doubles the amplitude of the sharp decrease in the extinction during the pulse (Figure 2c). Indeed, calculations show a linear dependence of the induced temperature increase on the applied laser power.¹⁸ The 4 μs time scale of the subsequent cooling of the aggregate is unchanged compared to the previous experiment using only $I_{\text{Peak}} = 2.5$ kW/mm². However, the $\Delta\text{Ext}/\text{Ext}$ signal does not recover to zero in contrast to the previous experiment with a lower applied I_{Peak} (Figure 2a). In fact, the absolute value of the $\Delta\text{Ext}/\text{Ext}$ signal increases again on a millisecond time scale with a time constant of 1.5 ms (Figure 2d). It saturates

on a ms time scale and stays as a persistent signal for seconds until the extinction recovers due to the diffusion of fresh, undissolved AuNP aggregates into the focus (not shown). These observations can be explained in the following way: The heat that stays within the aggregate for a few microseconds is sufficient to melt the dsDNA (Figure 2c, inset). The linkages between the AuNPs are loosened and the NPs subsequently diffuse apart on a ms time scale (insets in Figure 2d).

In Figure 2e, the relative change of the extinction at time $t = 20$ ms after the heating pulse (see red arrow in Figure 2d) is plotted against the applied power density of the heating laser pulses. A clear thresholdlike behavior is observed. A $\Delta\text{Ext}/\text{Ext}$ signal cannot be observed below a threshold power density $I_M = 3.8$ kW/mm², where the optically induced thermal energy is not sufficient to melt the dsDNA. Above the melting threshold I_M , the relative extinction decreases linearly with the applied laser power. This thresholdlike behavior can be explained by the sharp melting curve in Figure 1d. At a given T_B , a certain amount of optothermal heating is required to kick the temperature of the aggregates over the melting barrier. However, in contrast to a temperature-ramped melting assay, our optothermal assay provokes controlled DNA melting on a much faster time scale.

In the following, the influence of a mismatch in the target DNA will be analyzed. We compare aggregates linked by a perfect matching target (PMT) and aggregates linked by a single base pair mismatched target (MMT) (sequence given in the inset in Figure 3a). T_B was set to 45 °C, which is slightly below the melting temperature of the MMT-aggregates. The transient extinction after a single laser pulse is shown in Figure 3a. In contrast to Figure 2a–d, there is no averaging over several events. A biexponential fit to the single shot raw data is added to the graph in Figure 3 as a guide to the eye (black line). The applied laser power density for this experiment was chosen to be just below the melting threshold $I_M = 3.1$ kW/mm² of the PMT-aggregates.

Therefore, no long-lived change in extinction was observed for this target. The result changes if the MMT-aggregates are optically heated under exactly the same conditions. A long-lived decrease in extinction now indicates DNA melting (green line). The MMT can clearly be distinguished from the PMT within an observation window of only 1 ms.

Up to now, we have shown that we can distinguish two solutions containing a perfect matching target and a mismatched target, respectively. However, it is a prerequisite for a multiplexing DNA assay to discriminate different DNA targets that are present in one and the same solution. To test the AuNP-nanostove-assay also for this requirement, we prepared a mixed solution (MIX) with a 1:1 mixture of the targets PMT and MMT. T_B was preset to 53 °C (Figure 3b). The pure MMT-aggregates were completely dissolved at this temperature (Figure 1d). Consequently, the transient extinction for the pure MMT-sample showed no response to the laser pulse (Figure 3b, green line). In the PMT-containing samples, the AuNPs were still aggregated at 53 °C. The transient extinction of the pure PMT-aggregates clearly showed a long-lived decrease in the extinction (black line). In the case of the MIX-sample (blue line), the extinction transient can be clearly distinguished from both transients of the PMT and the MMT samples. At 53 °C, the MIX-solution obviously is a composite of dissolved AuNPs and PMT-bound aggregates. MMT-, PMT-, and MIX-solutions can clearly be discriminated with only one single laser pulse and an observation time below one millisecond.

Our results demonstrate the high potential of the gold-nanostove-assay for rapid high-throughput DNA analysis with an option for multiplexing. The read-out time of the assay is less than a millisecond after the 300 nanosecond laser pulse has been applied. The aggregates of nanoparticles serve as both converters of optothermal energy to heat the DNA and as a spectral reporter of DNA melting that allows for the discrimination of different targets even when they are mixed in one and the same solution. Therefore, classification of DNA is possible on a microsecond time scale without time-consuming temperature ramps. The concept of pulsed laser heating of gold nanostoves has great potential to improve the speed of pathogen detection. It is substantially less time-consuming compared to the current standard of blood cultures or DNA melting assays that require a full temperature ramp to determine the concrete pathogen and possible antibiotic resistance. The sooner patients can be treated with specific antibiotics instead of broad-band antibiotics, the less probable is the breeding of hospital-acquired strains with multiple resistance. Apart from high-

speed pathogen DNA identification, the gold nanostove DNA assay may also be beneficial for phenotyping or for high throughput assays.

Acknowledgment. We thank Werner Stadler and Anna Helfrich for excellent technical assistance. This work has been supported by the Deutsche Forschungsgemeinschaft (DFG) through the SFB 486, by the Gottfried-Wilhelm-Leibniz Program, and via the “Nanosystems Initiative Munich (NIM)”, and by the Bavarian Science Foundation.

References

- (1) Ibrahim, E. H.; Sherman, G.; Ward, S.; Fraser, V. J.; Kollef, M. H. *Chest* **2000**, *118*, 146.
- (2) Kost, G. J.; et al. *Point of Care* **2003**, *2*, 163.
- (3) Klaschik, S.; et al. *J. Clin. Microbiol.* **2004**, *42*, 512.
- (4) Rice, S. A.; Doty, P. *J. Am. Chem. Soc.* **1957**, *79*, 3937.
- (5) Tyagi, S.; Kramer, F. R. *Nat. Biotechnol.* **1996**, *14*, 303.
- (6) Elghanian, R.; Storhoff, J. J.; Mucic, R. C.; Letsinger, R. L.; Mirkin, C. A. *Science* **1997**, *277*, 1078.
- (7) Storhoff, J. J.; Elghanian, R.; Mucic, R. C.; Mirkin, C. A.; Letsinger, R. L. *J. Am. Chem. Soc.* **1998**, *120*, 1959.
- (8) Hamad-Schifferli, K.; Schwartz, J. J.; Santos, A. T.; Zhang, S.; Jacobson, J. M. *Nature* **2002**, *415*, 152.
- (9) Ahmadi, T. S.; Logunov, S. L.; El-Sayed, M. A. *J. Phys. Chem.* **1996**, *100*, 8053.
- (10) Perner M.; et al. *Phys. Rev. Lett.* **1997**, *78*, 2192.
- (11) Hu, M.; Hartland, G. V. *J. Phys. Chem. B* **2002**, *106*, 7029.
- (12) Hüttmann, G.; Birngruber, R. *IEEE J. Sel. Top. Quantum Electron.* **1999**, *5*, 954.
- (13) Radt, B. Inaktivierung von Proteinen und Zellen durch Laserbestrahlung von Mikropartikeln. dissertation.de, Verlag im Internet GmbH, Berlin, 2003.
- (14) Yao, C.; et al. *J. Biomed. Opt.* **2005**, *10*, 064012.
- (15) Hirsch, L.R.; et al. *Proc. Natl. Acad. Sci. U.S.A.* **2003**, *100*, 13549.
- (16) Pitsillides, C. M.; Joe, E. K.; Wei, X.; Anderson, R. R.; Lin, C. P. *Biophys. J.* **2003**, *84*, 4023.
- (17) Jain, P. K.; Qian, W.; El-Sayed, M. A. *J. Am. Chem. Soc.* **2006**, *128*, 2426.
- (18) Govorov, A. O.; et al. *Nanoscale Res. Lett.* **2006**, *1*, 84.
- (19) Mirkin, C. A.; Letsinger, R. L.; Mucic, R. C.; Storhoff, J. J. *Nature* **1996**, *382*, 607.
- (20) Alivisatos, A. P.; et al. *Nature* **1996**, *382*, 609.
- (21) Kreibig, U.; Vollmer, M. *Optical Properties of Metal Clusters*; Springer: Berlin, 1995.
- (22) Englebienne, P. *Analyst* **1998**, *123*, 1599.
- (23) Raschke, G.; et al. *Nano Lett.* **2003**, *3*, 935.
- (24) Klar, T. A. *Nanophotonics with Surface Plasmons*; Shalaev, V. M., Kawata, S., Eds.; Elsevier: Amsterdam, 2007; Chapter 8.
- (25) Quinten, M.; Kreibig, U. *Surf. Sci.* **1986**, *172*, 557.
- (26) Jin, R.; Wu, G.; Li, Z.; Mirkin, C. A.; Schatz, G. C. *J. Am. Chem. Soc.* **2003**, *125*, 1643.
- (27) Zanchet, D.; Micheel, C. M.; Parak, W. J.; Gerion, D.; Alivisatos, A. P. *Nano Lett.* **2001**, *1*, 32.
- (28) Keblinski, P.; Cahill, D. G.; Bodapati, A.; Sullivan, C. R.; Taton, T. A. *J. Appl. Phys.* **2006**, *100*, 054305.

NL073028I

Bioanalytics and biolabeling with semiconductor nanoparticles (quantum dots)

Cheng-An J. Lin,^{ab} Tim Liedl,^a Ralph A. Sperling,^a María T. Fernández-Argüelles,^{ac} Jose M. Costa-Fernández,^c Rosario Pereiro,^c Alfredo Sanz-Medel,^c Walter H. Chang^b and Wolfgang J. Parak^{*a}

DOI: 10.1039/b618902d

In this mini-review recent applications of quantum dots in bioanalytics and biolabeling are discussed. The state-of-the-art of the field is summarized, some selected applications are highlighted, and future directions are suggested.

Colloidal semiconductor nanoparticles—alternative fluorescence dyes

Colloidal quantum dots (QDs) are fluorescent dyes, which in contrast to organic fluorophores are based on inorganic semiconductor nanoparticles. When these particles are photo excited, electron hole pairs are generated and upon their recombination fluorescence light is emitted. Due to their small size quantum effects play an important role, which finally results in size dependent wavelengths of fluorescence. The smaller the particles, the more blue shifted their fluorescence.¹ In this way all colors in the visible and infrared can be obtained by synthesizing nanoparticles of different size. In contrast to organic fluorophores, QDs have some unique photophysical properties. They have a continuous absorption spectrum for wavelengths shorter than the wavelength of fluorescence emission.² Their emission spectra are quite narrow and symmetric, and do not show any red tail. In this way many different colors can be excited with just one wavelength of excitation and can be spectrally well resolved. The fluorescence lifetime is a few ns and thus is significantly higher than that of organic fluorophores. Also their photobleaching is reduced. The general advantages of these

properties towards applications with a biological background have been discussed in several recent reviews.^{3–8}

Nowadays the synthesis of quantum dots in organic solvents is well established, so that control of the size, shape, and even composition is possible.⁹ The most frequently used system is cadmium selenide particles with a zinc sulfide shell.¹⁰ Historically the first particle syntheses were performed in aqueous solution and thus the resultant particles were automatically water soluble.¹¹ Nowadays particles are often also synthesized in organic solvents, as such synthesis routes allow for advanced shape and composition control.^{12,13} These hydrophobic particles can be routinely transferred into aqueous solution with several methods including ligand exchange, surface silanization, embedding in a polymer shell, incorporation in micelles (detailed references can be found in some recent reviews^{14–17}), and they are also commercially available from several vendors. A number of reports has been published in which biological molecules have been attached to the surface of such water soluble quantum dots (detailed references can be found in several reviews^{18–20}), even with such control that an exactly known number of molecules can be attached per particle.²¹ However, so far no general conjugation scheme which would allow the use of the same strategy for controlled conjugation of different species of biological molecules to different particles is available. We believe that improved general conjugation optimized for quantum dots is still a technical hurdle which has to be solved before biologists will routinely use quantum dots for their applications.

Analyte detection in aqueous solution

QDs can be used in different ways to detect analytes. As active sensor elements the fluorescence properties of the QDs are changed upon reaction with the analyte. Fundamental studies have revealed that chemical or physical interactions between a given chemical species (the analyte) with the particle surface can result in changes in the QDs' surface charges and thus affect significantly their photoluminescence emission.²² Binding of analytes to the nanoparticle surface can create surface state traps, which results in quenching of the luminescence of the QDs.²³ Specific fluorescence quenching has been used for example to measure cationic concentrations, such as Zn²⁺ or Cu²⁺,^{22,24} or toxic anions such as CN⁻,²⁵ see Fig. 1a. On the other hand, by passivation of surface state traps (by “filling” them or moving them energetically closer to the band edges) binding of analytes can also cause enhancement of the luminescence of the QDs. Specific fluorescence enhancement of QDs has been demonstrated for the optical sensing of trace levels of ionic species such as Ag⁺.²⁶ Such reported methods are very simple, easy to develop and some of them have shown very high sensitivity. Unfortunately they appear to be restricted to sense just a few reactive small molecules or ions that are able to interact directly with the QDs' surface. Moreover, the reactions are usually not highly specific, and they also depend strongly on the surface properties of the QDs (including their coating). Slight variations in the QDs' surface properties from synthesis to synthesis complicate

^aCenter for NanoScience, Ludwig Maximilians Universität München, Munich, Germany.

E-mail: Wolfgang.Parak@physik.uni-muenchen.de

^bDepartment of Biomedical Engineering and R&D Center for Membrane Technology, Chung Yuan Christian University, Taiwan, R.O.C.

^cDepartment of Physical and Analytical Chemistry, University of Oviedo, Oviedo, Spain

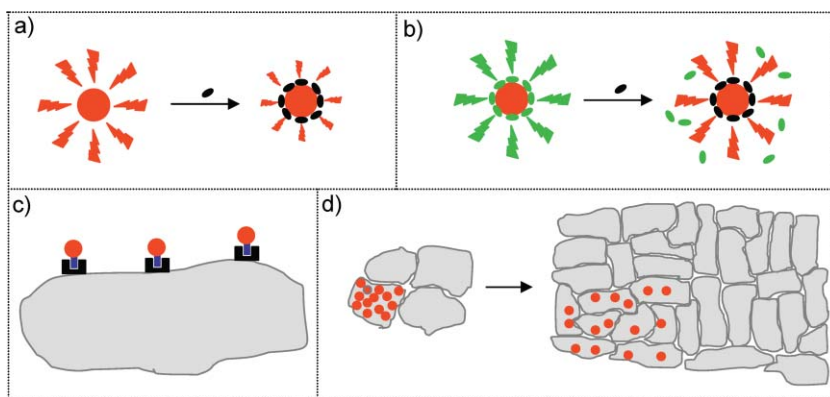


Fig. 1 a) Analyte detection by quenching of the quantum dot fluorescence (red) upon binding of the analyte (black) to the quantum dot surface. b) By binding an appropriate organic fluorophore (green) as acceptor to the surface of the donor quantum dot fluorescence energy transfer (FRET) occurs. FRET is stopped upon displacement of the acceptor dye from the quantum dots surface by the analyte. c) Specific cellular receptors (black) can be labeled with quantum dots that have been modified with appropriate ligand molecules. d) If a cell (grey) within a cell colony is labeled with quantum dots this cells passes the quantum dots to all its daughter cells and the “fate” of this cell can be observed.

absolute fluorescence measurements. We therefore predict limited use of QDs in industrial applications as active element in sensors of the above described type.

QDs can also be used as passive labels in sensor applications. Conjugation of selective receptor molecules (*e.g.* antibodies) to the surface of QDs has been used for the development of QD based fluorescent probes. This approach has allowed for example the design of simple multiplexed immunoassays. Capture antibodies are immobilized on a substrate to which the analyte is added. In a second step QD labeled antibodies are used to visualize and quantify the bound analyte.²⁷ By using QDs of different size and thus color several different analytes can be labeled in parallel. In pioneer work four toxins were simultaneously detected.²⁸ In our opinion in the field of analyte detection QDs will have the biggest impact in fluorescence resonance energy transfer (FRET) based assays.²⁹ QDs have great potential to be used as energy transfer donors for organic fluorophores as acceptor. The capability of choosing the QDs’ emission wavelengths by synthesizing particles of the appropriate diameter allows for efficient energy transfer with a wide number of conventional organic dyes due to the perfect overlap of their emission spectrum with the absorption spectrum of the acceptor dye. Since QDs can be excited at any wavelength shorter than their fluorescence they can be excited at

wavelengths far away from the excitation of the acceptor dye. Furthermore, the QD emission spectrum is narrower and more symmetric than the emission of conventional organic fluorophores, which makes it much easier to distinguish the emission of the donor from that of the acceptor. However, it should be mentioned that one drawback is the relatively large size of QDs, which hinders the needed closeness of the acceptor to the donor for FRET to occur efficiently. Nevertheless, several studies have already confirmed that QDs are excellent donors in FRET based assays. In competitive FRET assay the surface of the QDs is modified with a recognition site for the analyte. By blocking the recognition site with an acceptor dye that binds to it the fluorescence of the QDs is quenched by FRET, see Fig. 1b. Present analyte molecules now can displace the acceptor dye from the recognition site which can be detected by an increase in the QD fluorescence^{30,31} In this way sensors to detect sugars³¹ and explosives^{30,31} have been realized. For the detection of enzymes alternative assays have been developed. An acceptor dye is attached to the QD surface *via* a linker molecule and due to the resulting FRET the QD fluorescence is quenched. Enzymes that are able to cut the linker molecule cause a release of the acceptor from the QD surface and thus an increase of QD fluorescence.³² This assay enabled the detection of proteolytic

enzymes.³² Whereas in the so far mentioned sensors addition of analyte results in reduction of FRET the opposite scheme is also possible. A sensor for single stranded DNA comprises QDs and acceptor dye molecules that are both attached to single stranded DNA molecules that are complementary to different parts of the target DNA. When target DNA (the analyte to be detected) is present it hybridizes with one end of the DNA attached to the QDs and with the other end of the DNA attached to the acceptor dyes. In this way the QD donors and dye acceptors are linked together and due to FRET fluorescence emission of the dye can be detected upon QD excitation.^{33,34} Similarly, the enzyme telomerase can be detected when it links acceptor dye labeled nucleotides to a short primer DNA that is bound to the surface of QDs by onset of acceptor dye emission upon QD excitation due to FRET.³⁵ Certainly even more efficient FRET assays will be available in the future by optimizing the bioconjugation scheme and thus the closest possible distance between QD donor and dye acceptor. Recently QDs have also been used as acceptors for bioluminescent donors.³⁶

Cellular labeling

QDs also can be used for labeling biological cells. In the following, several types of such applications are described and discussed. 1) In conventional staining experiments QDs are bound to antibodies specific to target structures in cells,³⁷ see Fig. 1c. Here the QDs simply substitute organic fluorophores as fluorescence marker of the antibody. Compared to organic fluorophores they offer the following advantages. For multi color staining potentially more structures can be labeled simultaneously due to their narrow emission spectra and it is possible to excite all colors of fluorescence with one single excitation wavelength. Due to the reduced photo bleaching it is also easier to obtain 3 dimensional (stacked) images. Another advantage is the enhanced fluorescence decay time. By making time gated images the background can be reduced.³⁸ However, in this type of application QDs have to be seen only as an alternative fluorescence dye. With the

same idea QD labeled DNA has been used as a marker for fluorescence *in situ* hybridization (FISH).^{39–41} 2) Instead of labeling whole cellular structures also individual molecules can be fluorescence labeled with QDs. In this way it was possible to trace the movement of individual membrane proteins.^{42,43} We think that QDs will have huge potential for such tracking studies. First, single QDs can be brighter than single organic fluorophores and therefore it is relatively easy to observe single QDs. Second, the reduced photobleaching is essential for any tracking application over extended periods of time. Already first tracking experiments have been reported that would not be possible with conventional organic fluorophores. 3) QDs can be used to trace cells in cell cultures. When cells are exposed to a solution of QDs they start to ingest them.⁴⁴ When cells of different types have been incubated with QDs of different color before seeding them in a co culture, the type of each cell can be identified afterwards by its color of fluorescence.^{17,45} Also the fate of particular cells within cell or tissue cultures can be followed by fluorescence labeling them with QDs, see Fig. 1d. For these applications the following properties of QDs play an important role: because of their reduced photobleaching and the fact that upon cell division they are passed to both daughter cells, the fluorescence labels can be observed over extended periods of time. Since fluorescence labeling is possible simply by incubating the cells with the QDs, we predict a significant impact of QDs for tracing studies of cells. 4) QDs have also been used for labeling of tissues in animals and there is hope to use them as contrast agents in human beings.^{36,46–51} For example, lymph nodes have been fluorescence labeled with QDs before surgery.⁵² Compared to standard procedures this method offers the possibility to see the target structure before making an incision into the skin and that during the actual cutting process it is easy to identify all remaining parts of the target structure. Since skin absorbs light it is a general problem to observe fluorescence deep inside tissues. Here the QDs offer clear advantages. First, QDs can be synthesized that emit in the infrared at wavelengths that are only moderately absorbed by tissue.

Second, QDs can also be excited by 2 photon excitation and thus infrared light can be used to excite them.⁵³ Although already significant progress has been achieved in this type of application we claim that the final breakthrough will still take time until the biocompatibility issues of the QDs are resolved.

Open challenges

Although QDs are nowadays already used in several “real” applications, some general problems still have to be overcome in the future. The process of “blinking”, *i.e.* when luminescence switches on and off, is so far still not completely understood. Blinking limits quantitative single QD based sensor applications. So far most QDs are based on Cd containing materials. Although appropriated coverage of these particles with additional shells can seal the Cd containing core, these particles are potentially cytotoxic.^{54,55} We predict that in the future other QDs that do not contain cadmium and therefore are more biocompatible will be made available, such as for example doped zinc selenide particles.⁵⁶ The other general problem is specificity. Although major effort has been invested in the surface modification of QDs effects such as nonspecific adsorption still cannot be ruled out. Thus, there is still room for further development in all these directions.

Conclusion

QDs have finally taken the step from pure demonstration experiments to real applications. We claim that QDs will never replace organic fluorophores as such, but they will be the dominant fluorescence dyes in certain types of applications. Certainly, QDs will have a severe impact in particular in single molecule tracing studies, in FRET based immunoassays, and in tracking the fate of cells in tissues.

Acknowledgements

Chen An Lin acknowledges funding from the DAAD NSC Sandwich program. Maria Teresa Fernández Argüelles acknowledges a grant (BP04 040) from the Consejería de Educación y Ciencia of the Principado de Asturias. The project

was funded by the Deutsche Forschungsgemeinschaft (DFG, Emmy Noether Grant), the Fonds der Chemischen Industrie and the European Union (STREP NanoInteract grant).

References

- 1 W. J. Parak, L. Manna, F. C. Simmel, D. Gerion and P. Alivisatos, in *Nano particles From Theory to Application*, ed. G. Schmid, Wiley VCH, Weinheim, 2004, pp. 4–49.
- 2 C. B. Murray, C. R. Kagan and M. G. Bawendi, *Annu. Rev. Mater. Sci.*, 2000, **30**, 545–610.
- 3 I. L. Medintz, H. T. Uyeda, E. R. Goldman and H. Mattoussi, *Nat. Mater.*, 2005, **4**, 635–646.
- 4 X. Michalet, F. F. Pinaud, L. A. Bentolila, J. M. Tsay, S. Doose, J. J. Li, G. Sundaresan, A. M. Wu, S. S. Gambhir and S. Weiss, *Science*, 2005, **307**, 538–544.
- 5 A. Alivisatos, W. Gu and C. Larabell, *Annu. Rev. Biomed. Eng.*, 2005, **7**, 55–76.
- 6 M. P. Bruchez, *Curr. Opin. Chem. Biol.*, 2005, **9**, 533–537.
- 7 F. Pinaud, X. Michalet, L. A. Bentolila, J. M. Tsay, S. Doose, J. J. Li, G. Iyer and S. Weiss, *Biomaterials*, 2006, **27**, 1679–1687.
- 8 A. M. Smith, S. Dave, S. M. Nie, L. True and X. H. Gao, *Expert Rev. Mol. Diagn.*, 2006, **6**, 231–244.
- 9 P. D. Cozzoli, T. Pellegrino and L. Manna, *Chem. Soc. Rev.*, 2006, **35**, 1195–1208.
- 10 B. O. Dabbousi, J. Rodriguez Viejo, F. V. Mikulec, J. R. Heine, H. Mattoussi, R. Ober, K. F. Jensen and M. G. Bawendi, *J. Phys. Chem. B*, 1997, **101**, 9463–9475.
- 11 M. Gao, S. Kirstein, H. Mohwald, A. L. Rogach, A. Kornowski, A. Eychmuller and H. Weller, *J. Phys. Chem. B*, 1998, **102**, 8360–8363.
- 12 S. Kumar and T. Nann, *Small*, 2006, **2**, 316–329.
- 13 S. Kudera, L. Carbone, M. Zanella, R. Cingolani, W. J. Parak and L. Manna, *Phys. Status Solidi C*, 2006, **203**, 1329–1336.
- 14 A. M. Smith, H. Duan, M. N. Rhyner, G. Ruan and S. Nie, *Phys. Chem. Chem. Phys.*, 2006, **8**, 3895–3903.
- 15 A. M. Smith, G. Ruan, M. N. Rhyner and S. Nie, *Ann. Biomed. Eng.*, 2006, **34**, 3–14.
- 16 J. M. Klostranec and W. C. W. Chan, *Adv. Mater.*, 2006, **18**, 1953–1964.
- 17 T. Pellegrino, S. Kudera, T. Liedl, A. M. Javier, L. Manna and W. J. Parak, *Small*, 2005, **1**, 48–63.
- 18 A. J. Sutherland, *Curr. Opin. Solid State Mater. Sci.*, 2002, **6**, 365–370.
- 19 W. C. W. Chan, D. J. Maxwell, X. Gao, R. E. Bailey, M. Han and S. Nie, *Curr. Opin. Biotechnol.*, 2002, **13**, 40–46.
- 20 W. J. Parak, T. Pellegrino and C. Plank, *Nanotechnology*, 2005, **16**, R5–R25.
- 21 R. A. Sperling, T. Pellegrino, J. K. Li, W. H. Chang and W. J. Parak, *Adv. Funct. Mater.*, 2006, **16**, 943–948.
- 22 Y. R. Chen, *Anal. Chem.*, 2002, **74**, 5132–5138.

- 23 A. S. Susha, A. Munoz Javier, W. J. Parak and A. L. Rogach, *Colloids Surf., A*, 2006, **281**, 40–43.
- 24 M. T. Fernandez Arguelles, W. J. Jin, J. M. Costa Fernandez, R. Pereiro and A. Sanz Medel, *Anal. Chim. Acta*, 2005, **549**, 20–25.
- 25 W. J. Jin, M. T. Fernandez Arguelles, J. M. Costa Fernandez, R. Pereiro and A. Sanz Medel, *Chem. Commun.*, 2005, 883–885.
- 26 J. L. Chen and C. Q. Zhu, *Anal. Chim. Acta*, 2005, **546**, 147–153.
- 27 B. Sun, W. Xie, G. Yi, D. Chen, Y. Zhou and J. Cheng, *J. Immunol. Methods*, 2001, **249**, 85–89.
- 28 E. R. Goldman, A. R. Clapp, G. P. Anderson, H. T. Uyeda, J. M. Mauro, I. L. Medintz and H. Mattoussi, *Anal. Chem.*, 2004, **76**, 684–688.
- 29 A. R. Clapp, I. L. Medintz and H. Mattoussi, *ChemPhysChem*, 2006, **7**, 47–57.
- 30 E. R. Goldman, I. L. Medintz, J. L. Whitley, A. Hayhurst, A. R. Clapp, H. T. Uyeda, J. R. Deschamps, M. E. Lassman and H. Mattoussi, *J. Am. Chem. Soc.*, 2005, **127**, 6744–6751.
- 31 I. L. Medintz, A. R. Clapp, H. Mattoussi, E. R. Goldman, B. Fisher and J. M. Mauro, *Nat. Mater.*, 2003, **2**, 630–638.
- 32 I. L. Medintz, A. R. Clapp, F. M. Brunel, T. Tiefenbrunn, H. T. Uyeda, E. L. Chang, J. R. Deschamps, P. E. Dawson and H. Mattoussi, *Nat. Mater.*, 2006, **5**, 581–589.
- 33 C. Y. Zhang, H. C. Yeh, M. T. Kuroki and T. H. Wang, *Nat. Mater.*, 2005, **4**, 826–831.
- 34 B. Dubertret, *Nat. Mater.*, 2005, **4**, 797–798.
- 35 F. Patolsky, R. Gill, Y. Weizmann, T. Mokari, U. Banin and I. Willner, *J. Am. Chem. Soc.*, 2003, **125**, 13918–13919.
- 36 M. K. So, C. Xu, A. M. Loening, S. V. Gambhir and J. Rao, *Nat. Biotechnol.*, 2006, **24**, 339–343.
- 37 M. X. Wu, H. Liu, J. Liu, K. N. Haley, J. A. Treadway, J. P. Larson, N. Ge, F. Peale and M. P. Bruchez, *Nat. Biotechnol.*, 2003, **21**, 41–46.
- 38 M. Dahan, T. Laurence, F. Pinaud, D. S. Chemla, A. P. Alivisatos, M. Sauer and S. Weiss, *Opt. Lett.*, 2001, **26**, 825–827.
- 39 S. Pathak, S. K. Choi, N. Arnheim and M. E. Thompson, *J. Am. Chem. Soc.*, 2001, **123**, 4103–4104.
- 40 P. M. Chan, T. Yuen, F. Ruf, J. Gonzalez Maeso and S. C. Sealson, *Nucleic Acids Res.*, 2005, **33**, E161.
- 41 S. M. Wu, X. Zhao, Z. L. Zhang, H. Y. Xie, Z. Q. Tian, J. Peng, Z. X. Lu, D. W. Pang and Z. X. Xie, *ChemPhysChem*, 2006, **7**, 1062–1067.
- 42 M. Dahan, S. Levi, C. Luccardini, P. Rostaing, B. Riveau and A. Triller, *Science*, 2003, **302**, 442–445.
- 43 D. S. Lidke, P. Nagy, R. Heintzmann, D. J. Arndt Jovin, J. N. Post, H. E. Grecco, E. A. Jares Erijman and T. M. Jovin, *Nat. Biotechnol.*, 2004, **22**, 198–203.
- 44 W. J. Parak, R. Boudreau, M. L. Gros, D. Gerion, D. Zanchet, C. M. Micheel, S. C. Williams, A. P. Alivisatos and C. A. Larabell, *Adv. Mater.*, 2002, **14**, 882–885.
- 45 L. C. Mattheakis, J. M. Dias, Y. J. Choi, J. Gong, M. P. Bruchez, J. Liu and E. Wang, *Anal. Biochem.*, 2004, **327**, 200–208.
- 46 E. B. Voura, J. K. Jaiswal, H. Mattoussi and S. M. Simon, *Nat. Med.*, 2004, **10**, 993–998.
- 47 B. Ballou, B. C. Lagerholm, L. A. Ernst, M. P. Bruchez and A. S. Waggoner, *Bioconjugate Chem.*, 2004, **15**, 79–86.
- 48 X. Gao, Y. Cui, R. M. Levenson, L. W. K. Chung and S. Nie, *Nat. Biotechnol.*, 2004, **22**, 969–976.
- 49 W. Jiang, E. Papa, H. Fischer, S. Mardiyani and W. C. W. Chan, *Trends Biotechnol.*, 2004, **22**, 607–609.
- 50 W. Cai, D. W. Shin, K. Chen, O. Gheysens, Q. Cao, S. X. Wang, S. S. Gambhir and X. Chen, *Nano Lett.*, 2006, **6**, 669–676.
- 51 S. Santra, H. Yang, J. T. Stanley, P. H. Holloway, B. M. Moundgil, G. Walter and R. A. Mericle, *Chem. Commun.*, 2005, 3144–3146.
- 52 S. Kim, Y. T. Lim, E. G. Soltész, A. M. D. Grand, J. Lee, A. Nakayama, J. A. Parker, T. Mihaljevic, R. G. Laurence, D. M. Dor, L. H. Cohn, M. G. Bawendi and J. V. Frangioni, *Nat. Biotechnol.*, 2004, **22**, 93–97.
- 53 D. R. Larson, W. R. Zipfel, R. M. Williams, S. W. Clark, M. P. Bruchez, F. W. Wise and W. W. Webb, *Science*, 2003, **300**, 1434–1436.
- 54 A. M. Derfus, W. C. W. Chan and S. N. Bhatia, *Nano Lett.*, 2004, **4**, 11–18.
- 55 C. Kirchner, T. Liedl, S. Kudera, T. Pellegrino, A. M. Javier, H. E. Gaub, S. Stolze, N. Fertig and W. J. Parak, *Nano Lett.*, 2005, **5**, 331–338.
- 56 N. Pradhan, D. Goorskey, J. Thessing and X. G. Peng, *J. Am. Chem. Soc.*, 2005, **127**, 17586–17587.

Biological applications of gold nanoparticles†

Ralph A. Sperling, Pilar Rivera Gil, Feng Zhang, Marco Zanella and Wolfgang J. Parak*

Received 24th April 2008

First published as an Advance Article on the web 17th July 2008

DOI: 10.1039/b712170a

This *critical review* gives a short overview of the widespread use of gold nanoparticles in biology. We have identified four classes of applications in which gold nanoparticles have been used so far: labelling, delivering, heating, and sensing. For each of these applications the underlying mechanisms and concepts, the specific features of the gold nanoparticles needed for this application, as well as several examples are described (142 references).

1. Introduction

Colloidal gold nanoparticles have been used technologically since ancient times due to their optical properties, in particular for staining glass. Systematic investigations on gold colloids go back to the days of Faraday, though in their use for biological applications the breakthrough happened only in the last decade.¹ This goes hand in hand with the advent of (bio) nanotechnology, which nowadays allows for controlled synthesis and functionalization of materials on the nanometre scale and thus provides a toolbox that did not exist before. It is legitimate to ask whether the increasing use of gold nanoparticles in biology is just an effect of the “nano hype”, or whether colloidal gold offers particular properties which go beyond the performance of previously used materials or even allow for unprecedented techniques. The purpose of this review is to outline the conceptual properties of colloidal gold nanoparticles and to outline

Fachbereich Physik, Philipps Universität Marburg, Renthof 7, 35037 Marburg, Germany. E mail: wolfgang.parak@physik.uni-marburg.de
† Part of a thematic issue covering the topic of gold: chemistry, materials and catalysis.

the motivation for their use in different areas of biologically related research. We have classified the uses of gold nanoparticles into four concepts of applications: labelling, delivering, heating, and sensing.

2. Some aspects of the synthesis and properties of gold nanoparticles

2.1 Synthesis and phase transfer

The synthesis of gold nanoparticles with diameters ranging from a few to several hundreds of nanometres is well established in aqueous solution as well as in organic solvents. In typical syntheses, gold salts such as AuCl₃ are reduced by the addition of a reducing agent which leads to the nucleation of Au ions to nanoparticles. In addition, a stabilizing agent is also required which is either adsorbed or chemically bound to the surface of the Au nanoparticles. This stabilizing agent (often also called a surfactant) is typically charged, so that the equally charged nanoparticles repel each other so that they are colloidally stable. For the most common synthesis route in



Wolfgang Parak

Wolfgang Parak studied general physics at the Technische Universität München (Germany) and finished with a diploma thesis about cell semiconductor hybrids at the Institute for Biophysics (chair: Prof. Dr Erich Sackmann) in the group of Prof. Dr Hermann Gaub. He continued this research as a PhD student at the Institute of Applied Physics at the Ludwig Maximilians Universität München (Germany) (chair: Prof. Dr Hermann Gaub). After obtaining his PhD he started working on colloidal nanoparticles as a postdoctoral fellow at the Department of Chemistry at the University of California

at Berkeley (California, USA) in the Institute of Prof. Dr Paul Alivisatos. In 2002 he received an Emmy Noether fellowship from the German Research Foundation (DFG) and continued working on biological applications of colloidal nanoparticles as Assistant Professor at the Center for Nanoscience at the Ludwig Maximilians Universität München (Germany), hosted by the institute of Prof. Dr Hermann Gaub. In 2005 he had a temporary position as Associate Professor for Physical Chemistry at the Department of Chemistry and Pharmacy at the Ludwig Maximilians Universität München (Germany).

In 2007 he was appointed Full Professor with a chair in Experimental Physics at the Philipps Universität of Marburg (Germany). His group focuses on the investigation of new nano and micro systems and their applications in a wide variety of fields such as medicine, biology and electronic devices. The research activities are structured in three branches: synthesis of colloidal nanoparticles, surface chemistry and bioconjugation of colloidal nanoparticles, and application of colloidal nanoparticles in life science.

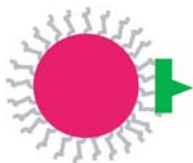


Fig. 1 Schematic of a ligand conjugated gold nanoparticle. The gold core (red) is surrounded by stabilizer molecules (grey) which provide colloidal stability. Ligands (green) can be either linked to the shell of stabilizer molecules (as shown here) or directly attached to the gold surface by replacing part of the stabilizer molecules.

aqueous solution, citric acid serves first to reduce the gold salt and thus to trigger nucleation, and secondly by adsorption to the particles it provides colloidal stability to the particles by its negative charges.^{2,3} Similar synthesis routes can also be performed in organic solvents,^{4,5} though in this case the reducing agent is different from the stabilizing agent. For particles dispersed in organic solvent frequently surfactants based on hydrophobic alkane chains are bound to the particle surface in order to provide colloidal stability. A sketch of the geometry of Au nanoparticles is given in Fig. 1. Besides growing of gold particles of spherical shape other geometries such as rod shaped particles or hollow shells can also be synthesized.^{6,7}

2.2 Surface modification and bioconjugation

Colloidal gold nanoparticles are surrounded by a shell of stabilizing molecules. With one of their ends these molecules are either adsorbed or chemically linked to the gold surface, while the other end points towards the solution and provides colloidal stability. After synthesis of the particles the stabilizer molecules can be replaced by other stabilizer molecules in a ligand exchange reaction. As thiol moieties bind with high affinity to gold surfaces, most frequently thiol modified ligands are used which bind to the surface of the Au particles (which are by several groups also called “monolayer protected clusters”) by formation of Au–sulfur bonds.⁸ Ligand exchange is motivated by several aspects. Ligand exchange allows, for example, the transfer of Au particles from an aqueous to an organic phase (and *vice versa*) by exchanging hydrophilic surfactants with hydrophobic surfactants (and *vice versa*).⁹ In this way, by choosing the surfactant molecules, it is possible to adjust the surface properties of the particles.

For applications in aqueous solution typically thiol based surfactants with carboxylic groups at the other end pointing towards the solution are used. These molecules provide colloidal stability due to their negative charges; in addition they can also be used as anchor points for the further attachment of biological molecules. Often poly(ethylene glycol) (PEG) is used as a ligand as PEG reduces nonspecific adsorption of molecules to the particle surface and it provides colloidal stability because particles with PEG brushes on their surface repel each other for steric reasons.¹⁰ Other surface coating techniques such as embedding particles in a silica shell have been used by several groups.¹¹

Biological molecules can be attached to the particles in several ways. If the biological molecules have a functional group which can bind to the gold surface (like thiols or specific peptide sequences), the biological molecules can replace some of the original stabilizer molecules when they are added

directly to the particle solution. In this way molecules like oligonucleotides, peptides or PEG can be readily linked to Au particles and subsequent sorting techniques even allow particles with an exactly defined number of attached molecules per particle to be obtained.^{12,13} Alternatively, biological molecules can also be attached to the shell of stabilizer molecules around the Au particles by bioconjugate chemistry. The most common protocol is the linkage of amino groups on the biological molecules with carboxy groups at the free ends of stabilizer molecules by using EDC (1 ethyl 3 (3 dimethylaminopropyl) carbodiimide HCl),^{14,15} With related strategies almost all kinds of biological molecules can be attached to the particle surface. Though such protocols are relatively well established, bioconjugation of Au nanoparticles still is not trivial and characterization of synthesized conjugates is necessary, in particular to rule out aggregation effects or unspecific binding during the conjugation reaction. In particular, in many conjugation protocols the number of attached molecules per gold nanoparticle is only a rather rough estimate, as no standard method for determining the surface coverage of particles modified with molecules has yet been established.^{16,17}

2.3 Cytotoxicity

Although gold nanoparticles are composed of an inert material, biocompatibility issues have to be considered. Cells exposed to gold nanoparticles will incorporate the particles (similar to nanoparticles of other materials) and the particles are stored inside the cells in perinuclear compartments, vesicular structures close to the cell nucleus.^{18,19} Due to particle internalization cells or tissues in contact with gold nanoparticles will be exposed to the particles for extended periods of time. Concerning cytotoxic effects²⁰ one has to distinguish between effects related to the nature of the material (here: gold) and effects common to nanoparticles of even inert materials. Also for inert particles such as gold, inflammatory effects in tissues caused by particles have been demonstrated. However, in cell culture experiments Au nanoparticles are regarded as biocompatible, and acute cytotoxicity has not been observed so far.²¹ In particular, no release of toxic ions as in the case of cadmium based nanoparticles²² has been reported. On the other hand, there are few examples of toxic effects related to the nature of Au, which might depend on the cell line,^{19,23} on surface chemistry,²⁴ and on the nanoparticle size.²⁵ Actin fibres inside the cell, for example, can be affected by the presence of nanoparticles,²⁶ and very small Au clusters have been demonstrated to fit into the grooves of DNA molecules and thus cause cytotoxic effects.^{25,27} A more detailed discussion can be found in another article in this issue.²⁸

3. Gold nanoparticles for labelling and visualizing

Traditionally, Au nanoparticles have been primarily used for labelling applications. In this regard, the particles are directed and enriched at the region of interest and they provide contrast for the observation and visualization of this region. The particles are used here as “passive” reporters; there is no change of particle properties required for the read out as is the case for active sensor applications (see section 6). Gold nanoparticles are

a very attractive contrast agent as they can be visualized with a large variety of different techniques. The most prominent detection techniques are based on the interaction between gold nanoparticles and light.²⁹ Gold particles strongly absorb and scatter visible light. Upon light absorption the light energy excites the free electrons in the Au particles to a collective oscillation, the so called surface plasmon.³⁰ In particular, close to the plasmon resonance frequency the absorption cross section is very high. The excited electron gas relaxes thermally by transferring the energy to the gold lattice; finally the light absorption leads to heating of the gold particles.

Interaction with light can be used for the visualization of particles in several ways. Gold particles larger than around 20 nm can be directly imaged with optical microscopy in phase contrast or differential interference contrast (DIC) mode.³¹ In dark field microscopy only light scattered from gold particles is detected with an optical microscope³² whereby particles larger than 20–30 nm can be imaged. As the colour of the light scattered by gold particles depends on their sizes and shapes, gold particles can be used for labelling with different colours.^{30,33} For small particles the scattering cross section decreases rapidly whereas the absorption cross section decreases less.

Absorbed light ultimately leads to heating of the particles and upon heat transport subsequently to heating of the particle environment. This can be observed in two ways. Photothermal imaging records density fluctuations (*i.e.* local variations of the refractive index) of the liquid environment around the particles by DIC microscopy.^{34,35} Photoacoustic imaging, on the other hand, makes use of the fact that the liquids expand due to heat. A local heat pulse due to light absorption leads to expansion of the liquid surrounding the gold particles and thus to the creation of a sound wave which can be detected by a microphone.^{36,37} Both photothermal and photoacoustic imaging make use of the large light absorption cross section of gold nanoparticles. Small gold particles have recently also been reported to emit fluorescence upon photo excitation and thus can be visualized with fluorescence microscopy.^{38,39} All of the above mentioned methods involving photoexcitation (phase contrast/interference contrast microscopy, dark field microscopy, photothermal imaging, photoacoustic imaging, and fluorescence microscopy) provide sufficient sensitivity to allow for detection at the single particle level.

Besides the interaction with visible light, the interaction with both electron waves and X rays can also be used for visualization of Au nanoparticles. Due to their high atomic weight Au nanoparticles provide high contrast in transmission electron microscopy (TEM).⁴⁰ Au particles also scatter X rays efficiently and thus provide contrast in X ray imaging,⁴¹ see also section 3.3. Finally, Au nanoparticles can also be radioactively labelled by neutron activation⁴² and can be detected in this way by gamma radiation.

3.1 Immunostaining

Immunostaining is one of the traditional uses of Au nanoparticles in biology before the advent of “nanobiotechnology”. The idea of immunostaining is the labelling of specific molecules or compartments of cells (see Fig. 2a) by antibodies. Without labelling, the molecules or cell compartments of interest cannot be visualized because of a lack of contrast with the other structures or

molecules of the cell. For immunostaining, cells are typically fixed and permeabilized and Au nanoparticles are added that are conjugated with antibodies specific against the molecules of interest. Guided by molecular recognition, the antibody modified Au particles will bind to the molecule (antigen) or target regions containing the antigen. As the cells are fixed and permeabilized, targets outside as well as inside cells can be labelled with gold particles in this way. The Au particles then provide excellent contrast for TEM imaging with high lateral resolution⁴³ and larger structures can also be imaged with optical microscopy.⁴⁴ Compared to fluorescence labelling, Au particles are more stable as they do not suffer from photobleaching which is a major limitation for fluorescence based methods, and in the case of TEM imaging better lateral resolution with high contrast can also be obtained. In immunostaining, molecules/structures are labelled with an excess of Au nanoparticles so that virtually all entities are labelled (possibly with several markers) in order to provide high contrast. In this case the local density of Au particles at the sites where the labelled molecules/structures are present is quite high. Therefore the resolution limit of the optical microscope (of a few hundreds of nm) does not allow for optically resolving individual molecules labelled by antibody conjugated Au nanoparticles (of a few tens of nm in diameter), as the distance between adjacent Au nanoparticles is smaller than the optical resolution limit. However, due to better lateral resolution in electron microscopy, individual receptors can be resolved by visualizing the bound Au nanoparticles with TEM.

Immunostaining is also possible without fixing and permeabilizing cells, but in this case only structures/domains on the surface of the cell can be labelled. For immunostaining of the outer cell surface photoacoustic imaging can also be used besides the imaging techniques mentioned above. Photoacoustic imaging provides an additional feature in contrasting. When Au nanoparticles come close together (*i.e.* form small aggregates) the frequency of the plasmon resonance shifts to higher wavelengths. When freely dispersed colloidal Au nanoparticles are optically illuminated at wavelengths well above their plasmon resonance, the light is not absorbed and thus there will not be any photoacoustic signal. Small aggregates of Au nanoparticles, on the other hand, can absorb light at wavelengths above the plasmon resonance of freely dispersed, single Au particles. If, therefore, light with a wavelength above the plasmon resonance of freely dispersed Au particles is used for excitation there will be a photoacoustic signal for aggregates of Au nanoparticles, but not for single dispersed Au nanoparticles. If Au nanoparticles modified with antibodies against membrane receptors are used they will bind to the regions of the outer cell surface where the receptors are present. As several Au nanoparticles will bind to such regions there is a local “aggregation” of Au nanoparticles present which can provide a photoacoustic signal, whereas Au nanoparticles which are still in solution or which are randomly distributed on the cell surface due to nonspecific adsorption will not exhibit any photoacoustic signal.³⁶

3.2 Single particle tracking

The molecules/structures on the outer cell surface can be labelled with Au nanoparticles which are conjugated with specific antibodies against these molecules/structures. In

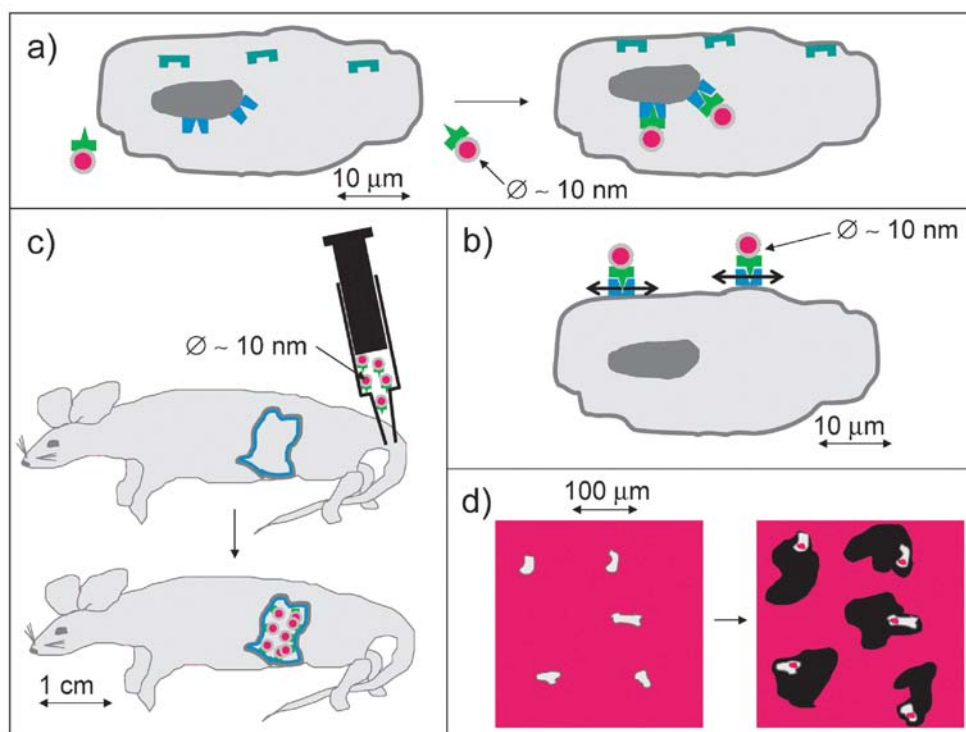


Fig. 2 Labelling with gold nanoparticles. Gold nanoparticles (core in red, stabilizing shell in grey) are conjugated with ligands (green) which bind to specific receptors (blue) but not to other structures (as the receptors shown in dark green). (a) Immunostaining: Gold nanoparticles conjugated with ligands against the structures to be labelled are added to fixed and permeabilized cells (shown in grey). Guided by molecular recognition they bind to the designated structures which are in this way stained with gold particles. In the image the particles are conjugated with ligands that bind to receptors on the surface of the nucleus, but not to other receptors, for example present at the inner cell membrane. (b) Single particle tracking: Gold particles conjugated with ligands specific for membrane bound molecules are added to living cells. In this way individual membrane bound molecules are labelled with gold particles and their diffusion within the cell membrane can be traced *via* observation of the gold particles. (c) X ray contrasting: Gold particles conjugated with ligands that permit specific uptake in target organs are injected into the bloodstream of animals. The organ can then be visualized by X ray tomography due to the locally enriched gold particles. (d) Phagokinetic tracks: a surface is covered with a layer of gold nanoparticles. When cells (shown in grey) are cultured on top of the surface they will ingest the underlying nanoparticles. Upon cellular migration along the surface the cells incorporate all nanoparticles along their pathway leaving behind an area free of nanoparticles, which is a blueprint of their migration pathway. Images are not drawn to scale and important length scales are indicated in the images.

contrast to immunostaining, for single particle tracking only a few antibody conjugated Au nanoparticles are added, so that after binding to the cell the particle labels present on the cell surface are very diluted. As in this case the average distance between adjacent Au nanoparticles is larger than the optical resolution limit, individual Au nanoparticles can be optically resolved. For imaging the movement of molecules/structures, living cells without fixation and permeabilization have to be used, which limits the labelling of molecules/structures to the outer cell surface and the visualization to optical techniques (phase/interference contrast microscopy, dark field microscopy, photothermal imaging, fluorescence imaging, or in combination with acoustics: photoacoustic imaging).

Most frequently, membrane bound receptor molecules are investigated by single particle tracking. By time resolved imaging of the receptors which are labelled with Au nanoparticles, their trajectories and thus their diffusion within the cell membrane can be observed (see Fig. 2b).⁴⁵ Movement of Au nanoparticles larger than around 40 nm can be traced directly with phase contrast or differential interference contrast microscopy.⁴⁶ For gold particles larger than around 20–30 nm the light scattered by individual Au nanoparticles can be recorded

with dark field microscopy.⁴⁷ Movement of receptors labelled with even smaller Au nanoparticles (down to 5 nm) has been visualized with photothermal imaging.^{48,49} Also other labels are used for the tracking of single receptors on cell surfaces and each of the methods has certain intrinsic advantages and disadvantages. The larger the particle label is, the easier (with regard to the required set up) it can be optically imaged. The principle is the same for 40 nm Au nanoparticles as for latex and silica beads, whereby the beads can be impregnated with organic fluorophores and thus can be imaged with fluorescence microscopy.⁵⁰

One could argue that gold nanoparticles can be more easily conjugated with antibodies than latex/silica beads (due to the thiol gold chemistry), though surely the fluorescence of beads provides a better signal to noise ratio. At any rate, attachment of particles larger than around 40 nm to receptors might severely change the diffusion properties of the receptor molecules. For this reason the real challenge of single particle tracking is to use an as small (and as stable) label as possible. Organic fluorophores exist that are smaller than colloidal particles; however, they suffer from photobleaching and therefore their fluorescence can be traced only for limited periods of

time. Alternatively, colloidal fluorescent semiconductor nanoparticles (so called quantum dots) can be used for single particle tracking of membrane molecules.⁵¹ Though they are slightly larger than small organic fluorophores they suffer much less from photobleaching and thus allow for extended observation periods. Colloidally stable quantum dots are typically larger than 10 nm in diameter, as sophisticated coatings are needed to ensure colloidal stability. On the other hand, movement of gold particles down to 5 nm diameter can be imaged with photothermal microscopy^{48,49} and as no fluorescence detection method is used, there is no limitation in observation time by photobleaching. For this reason photothermal microscopy of small Au nanoparticles is particularly advantageous when long periods of observation are required.

3.3 Contrast agents for X-rays

Whereas immunostaining and single particle tracking are used for visualizing structures within single cells, the same concept can also be applied for providing contrast *in vivo* to whole organs in animals and potentially in humans. Again the Au particles are conjugated with antibodies or ligands which bind as specifically as possible to the organ of interest in the animal. When particles are administered to the blood circulation a part of them will eventually bind *via* receptor ligand interaction at the designated organ. The particles bound to the organ provide contrast for imaging and resolving the structure of the organ (see Fig. 2c). However, the big general problem of contrasting organs with colloidal nanoparticles is their short circulation time in the bloodstream, so that only a fraction of the particles has a chance to bind to the designated organ whereas a significant part is cleared from the bloodstream by the liver and kidneys. On the other hand, colloidal nanoparticles can provide better contrast compared to organic molecules. Gold nanoparticles can, for example, be imaged with high signal to noise ratio with X ray computer tomography^{41,52} and therefore only short exposure times are required, which helps to reduce radiation damage to surrounding tissues. X rays penetrate skin and therefore organs deep inside the body can be imaged or addressed for therapy.⁵³ Furthermore, X ray tomography set ups are readily available in many hospitals. Here again, Au nanoparticles have to compete with fluorescent semiconductor nanoparticles (quantum dots).^{54,55} In order to reduce the X ray exposure of patients certainly fluorescence detection would be preferable compared to imaging with X rays. On the other hand, light is absorbed by tissues even partly in the infrared (IR), so that fluorescence contrasting of organs deep inside the body is complicated. Furthermore colloidal gold nanoparticles are likely to cause less cytotoxic damage than the generation of colloidal quantum dots presently used.

3.4 Phagokinetic tracks

Albrecht Bühler has introduced an innovative way of imaging the movement of cells adhering to a substrate.^{56–58} For this purpose the surface of the substrate is coated with a layer of colloidal gold nanoparticles (see Fig. 2d). Cells adhering to the substrate incorporate the Au particles. In this way cells migrating along the substrate leave behind a trail called a

“phagokinetic track” in the nanoparticle layer. By imaging the particle layer with optical transmission microscopy or TEM a blueprint of the migration pathway of the cells is obtained. Compared to time lapse tracing of the migration of cells which requires online video microscopy of individual cells, phagokinetic tracks do not need to be recorded online. Many trails can be recorded in parallel on the same substrate and the trails can be imaged *ex situ*, as they consist of areas in the nanoparticle layer that are permanently free of nanoparticles. Although recently the same technique has also been introduced with both fluorescent quantum dots⁵⁹ and fluorescent latex beads, still gold is the predominantly used label for recording phagokinetic tracks.

4. Gold nanoparticles as a vehicle for delivery

Gold nanoparticles have been used for a long time for delivery of molecules into cells. For this purpose the molecules are adsorbed on the surface of the Au particles and the whole conjugate is introduced into the cells. Introduction into cells can either be forced as in the case of gene guns or achieved naturally by particle ingestion. Inside cells the molecules will eventually detach themselves from the Au particles.

4.1 Gene guns

The idea of gene guns is using Au particles as massive nano bullets for ballistic introduction of DNA into cells (see Fig. 3a).⁶⁰ DNA is adsorbed onto the surface of gold particles which are then shot into the cells. The ballistic acceleration of the gene loaded micro- or nanoparticles is realized by different means like macroscopic bullets, gas pressure or electric discharges⁶¹ and some types of guns are commercially available. Traditionally, gene guns have been used for the introduction of plasmid DNA into plant cells,^{62,63} which results in expression of the corresponding proteins inside the cells. In this case ballistic introduction with massive particles is advantageous as it allows for traversing the rigid cell walls which surround the membranes of plant cells. However, gene guns are also used for delivery of DNA into animal cells, which do not possess cell walls.⁶⁴

4.2 Uptake by cells

Cells naturally ingest colloidal nanoparticles¹⁸ whereby particle incorporation can be specific (*via* receptor ligand interaction) or nonspecific. The goal is again to transfer molecules which are adsorbed on the surface of the Au particles into the cells (see Fig. 3b). For specific uptake ligands specific to receptors on the cell membrane, such as transferrin which binds to membrane bound transferrin receptors,^{65–67} are conjugated to the surface of the gold particles. As specific uptake is more effective than nonspecific uptake, in this way ligand modified Au particles are predominantly incorporated by cells which possess receptors for these ligands, but not by other cells. In this way, it is for example possible to direct particles specifically to cancer cells by conjugating them with ligands specific to receptors which are overexpressed on the surface of cancer cells but that are less present on healthy cells.⁶⁸ After incorporation nanoparticles are stored in endosomal/lysosomal vesicular structures inside

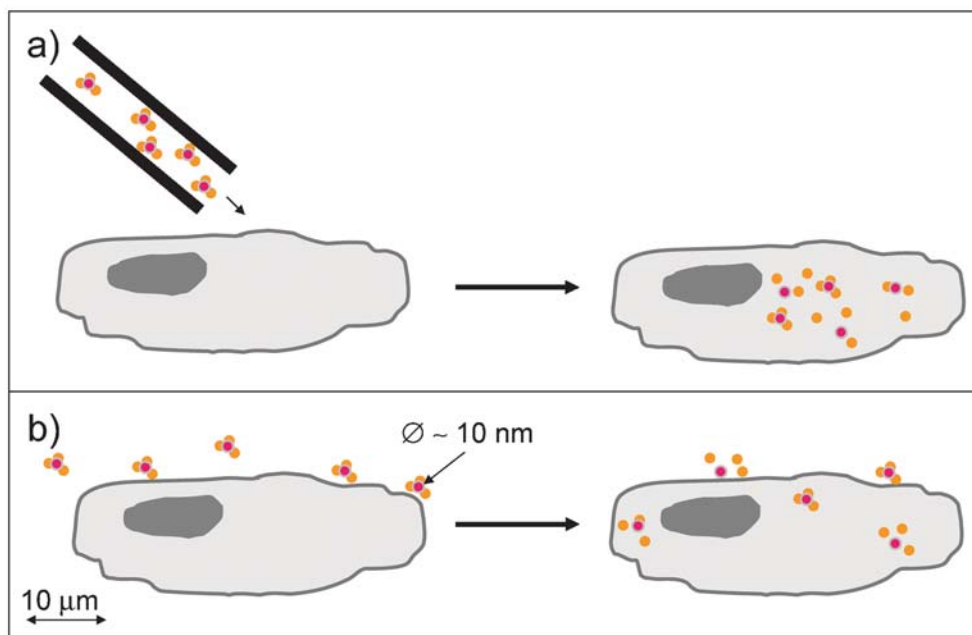


Fig. 3 Delivering with gold nanoparticles. Molecules (shown in orange) which are to be delivered inside cells are adsorbed on the surface of gold nanoparticles (core in red, stabilizing shell in grey). Once inside the cell these molecules will eventually detach themselves from the surface of the nanoparticles. (a) Gene guns: The nanoparticles are shot as a ballistic projectile into the cells using a so called gene gun system. (b) Nanoparticle uptake by cells: The nanoparticles are either specifically or nonspecifically incorporated by cells. After ingestion the particles are stored in vesicular compartments inside the cells.

cells.⁶⁹ In order to release the particles from the vesicular structures to the cytosol their surface can be coated with membrane disruptive peptides or the particles can be modified with peptides which allow for direct transfer across the cell membrane.^{70–73} In this way it is possible to deliver molecules which are adsorbed on the surface of the Au particles upon particle incorporation inside the cells.^{74,75}

Particle uptake mediated delivery of molecules into cells is used mainly for two applications. First, in gene therapy DNA is introduced into cells, which subsequently causes the expression of the corresponding proteins.^{76–78} Second, in drug targeting anti cancer drugs are delivered specifically to cancer tissue.^{68,79} Particle mediated drug delivery by adsorbing molecules onto colloidal particles and transferring them into cells allows for delivery of molecules inside cells which would not have been ingested into the cells by themselves. This is based on the fact that colloidal nanoparticles are taken up by cells. Besides being loaded with the molecules to be delivered, particles can also be conjugated with ligands through which specific uptake by target cells can be facilitated. For such delivery applications no special property of gold particles is exploited, other than that they are small, colloiddally stable, relatively easy to conjugate with ligands *via* thiol gold bonds, and that they are inert and thus relatively biocompatible. Delivery applications using gold nanoparticles have been reviewed recently,⁸⁰ some similar strategies can in principle also be realized with colloidal silica, iron oxide, and organic polymer nanoparticles. Nevertheless, there are a few studies that already make use of the optical properties of Au nanoparticles for detection (which the other types of particles do not offer), after they have been ingested by cells.^{81,82}

5. Gold nanoparticles as a heat source

When gold particles absorb light the free electrons in the gold particles are excited. Excitation at the plasmon resonance frequency causes a collective oscillation of the free electrons. Upon interaction between the electrons and the crystal lattice of the gold particles, the electrons relax and the thermal energy is transferred to the lattice. Subsequently the heat from the gold particles is dissipated into the surrounding environment.⁸³ Besides its combination with imaging techniques (see above in section 3), controlled heating of gold particles can be used in several ways for manipulating the surrounding tissues.⁸⁴

5.1 Hyperthermia

Cells are very sensitive to small increases in temperature. Even temperature rises of a few degrees can lead to cell death. For human beings temperatures above 37 °C lead to fever and temperatures above 42 °C are lethal. This fact can be harnessed for anti cancer therapy in a concept called hyperthermia. The idea is to direct colloidal nanoparticles to the cancerous tissue. This can be done by conjugating the particle surface with ligands that are specific to receptors overexpressed on cancer cells. The particles are then locally enriched in the cancerous tissue (either adherent to the cell membranes or inside the cells after internalization). If the particles can be heated by external stimuli then the temperature of cells close to the particles is raised and in this way cells in the vicinity of the particles can be selectively killed.⁸⁵ As mentioned above, Au particles can be heated by absorption of light, whereby the absorbed light energy is converted into

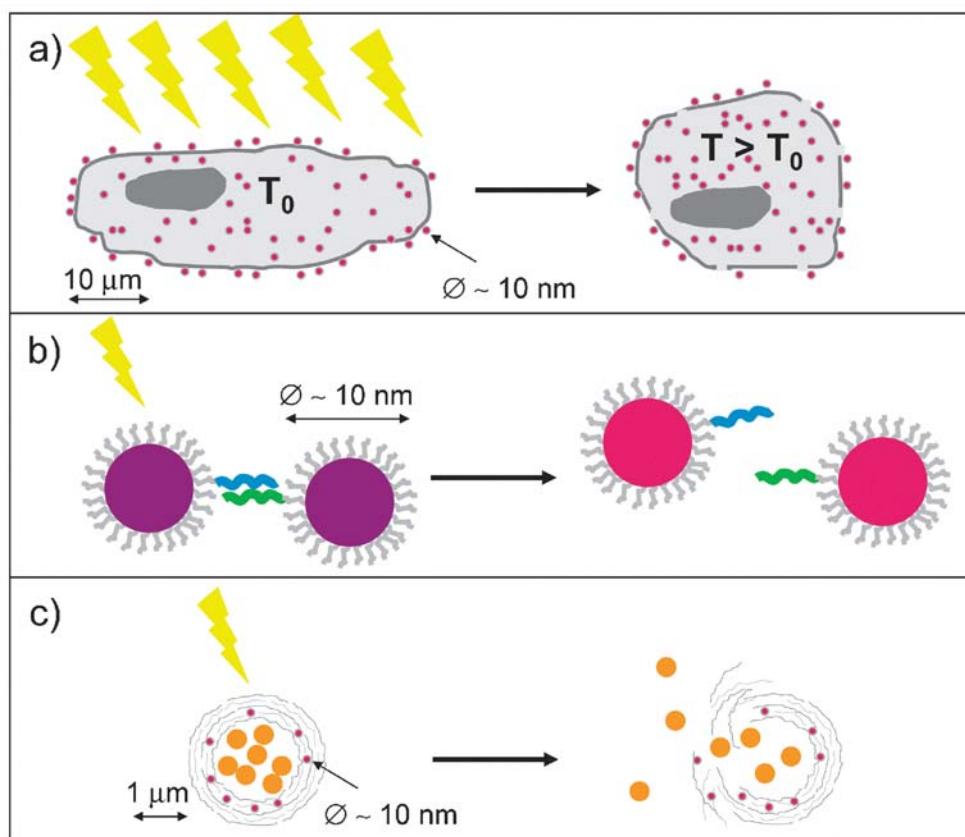


Fig. 4 Heating with gold nanoparticles. Gold particles (core in red, stabilizing shell in grey) are heated upon absorption of light (shown as yellow rays) and mediate the heat to their local environment. (a) Hyperthermia: The temperature inside cells (drawn in grey) is raised by illumination of gold particles. A temperature increase of only a few degrees is sufficient to kill cells. (b) Breaking of bonds: When gold nanoparticles (core in red, stabilizing shell in grey) are conjugated with ligands (shown in green) that are specific to receptors (shown in blue) which are bound to other gold particles, these two kinds of gold particles will be linked to assemblies mediated by receptor ligand binding. As the distance between the particles in such aggregates is small, their plasmon resonance is shifted to higher wavelengths and the particle solution appears violet/blue. Upon illumination the gold particles get hot and the bonds of the receptor ligand pairs melt. Therefore the assemblies are dissolved, the average distance between the particles is increased and the particle solution appears red. (c) Light controlled opening of individual polymer capsules (drawn in grey) by local heating, mediated by Au nanoparticles. Gold nanoparticles are embedded in the walls of polyelectrolyte capsules. The capsule cavity is loaded with cargo molecules (drawn in orange). Upon illumination with light the heat created by the nanoparticles causes local ruptures in the capsule walls and thus release of the cargo.

thermal energy. Thus the idea is to enrich cancerous tissues with gold nanoparticles and to illuminate the tissue. Due to the heat mediated by the gold particles to the surrounding tissue, cancerous tissues can be destroyed locally (see Fig. 4a)^{86–88} without exposing the entire organism to elevated temperatures.

Besides the general problem of local particle enrichment in the target tissue there is also a problem of principle involved. Tissue absorbs light in the visible region, and even infrared (IR) light can only penetrate relatively thin tissue. For this reason gold nanoparticles are needed which absorb light in the IR rather than in the visible range, such as gold rods or hollow structures.^{89,90} Nevertheless hyperthermia by photo induced heating of gold nanoparticles will work best for tissue close to the skin. For tissues deep inside the body heating with magnetic particles is favourable. Upon irradiating magnetic particles with radiofrequency (RF) fields, heat is generated by repetitive cycling of the magnetic hysteresis loop.^{91,92} Compared with the optical excitation of Au nanoparticles at

wavelengths of *ca.* 500–1000 nm, the excitation of magnetic nanoparticles works at lower frequencies (RF). As those are absorbed much less by normal tissue and thus penetrate deeper, particles inside the body can also be heated. On the other hand it is much more complicated to focus microwaves or radiofrequency waves than visible light and therefore photo induced heating of gold particles is favourable for local heating of only small parts of tissue.

5.2 Optically triggered opening of bonds

Photo induced heating of gold nanoparticles can also be used for the opening of chemical bonds (see Fig. 4b). The binding of complementary oligonucleotides (hybridization) to double stranded DNA, for example, is temperature dependent. Upon heating, double stranded DNA melts into two single strands. If DNA is linked to the surface of gold nanoparticles then local melting can be triggered by illuminating and thus heating the Au particles.^{93,94} As light can be easily focused to a micrometre spot size a high degree of spatial control is possible

which allows for very local heating. Similar concepts have also been used for the disassembly of protein aggregates by local heating.⁹⁵

5.3 Opening of containers

Finally, photo induced heating of gold nanoparticles can also be used for remotely controlled release of cargo molecules from containers (see Fig. 4c). This concept is based on embedding cargo molecules in containers, such as polymer capsules, whereby the walls of the containers are functionalized with gold nanoparticles. Upon optical excitation the gold nanoparticles are heated which causes local ruptures in the container walls and thus release of the cargo from the inside of the container.^{96,97} Light induced opening of polymer capsules can be performed on a single capsule level and it has already been demonstrated that upon photo induced heating cargo molecules can be released from capsules inside living cells.⁹⁸ Moreover, cell membranes themselves can be perforated with the help of nanoparticles.⁹⁹

6. Gold nanoparticles as sensors

Besides using gold nanoparticles as (passive) labels they can also be used for (active) sensor applications. Their aim in a sensor is to specifically register the presence of analyte molecules and to provide a read out that indicates the concentration of the analyte. When an optical read out is used, the presence of analyte can, for example, be indicated by changes in the optical properties of gold nanoparticles. Due to their small size, gold particle based sensors could have an important impact in diagnostics.⁸²

6.1 Surface plasmons

The plasmon resonance frequency is a very reliable intrinsic feature present in gold nanoparticles (with wavelengths around 510–530 nm for Au nanoparticles of around 40–40 nm diameter) that can be used for sensing.¹⁰⁰ The binding of molecules to the particle surface can change the plasmon resonance frequency directly,¹⁰¹ which is observable by their scattered light in dark field microscopy, in particular on the single particle level. On the other hand the plasmon resonance frequency is dramatically changed when the average distance between Au particles is reduced so that they form small aggregates.¹⁰² This effect of plasmon coupling can be used for colorimetric detection of analytes (see Fig. 5a). The method was pioneered by Mirkin and coworkers and is nowadays maybe the most well known example of a gold based sensor.^{103–105} The original assay was developed for the detection of DNA. Gold nanoparticles are conjugated with oligonucleotides that are complementary to the target sequence which is to be detected. Without the presence of the target sequence the gold particles are freely dispersed and the colloidal solution appears red. In the presence of the target sequence the gold particles bind to the target by hybridization of complementary strands of DNA. As each gold nanoparticle is bearing several oligonucleotides, hybridization results in the formation of small aggregates of Au particles, which will lead to a change in the plasmon resonance and the colloidal solution appears a violet/blue colour. When the sample is

heated, even single sequence mismatches result in a different melting temperature of the aggregates which causes colour change. Several DNA assays have been derived from this concept and nowadays the method is established in a way that quantitative detection of DNA sequences of very low concentrations is possible.¹⁰⁶

The same concept can also be applied for analytes other than DNA. Gold particles can, for example, be connected by DNA in such a way that the average inter particle distance is large enough to prevent changes in the plasmon resonance frequency. By using *e.g.* DNA sequences that change their conformation upon specific binding (such as DNA, RNA or peptide based sequences are called aptamers) of metals¹⁰⁷ or proteins,^{108,109} the inter particle distance is reduced and thus the colour of the gold colloids changes from red to violet/blue. Also enzyme activity can be monitored with such colorimetric assays, for example by the enzymatic biotinylation of nanoparticles and subsequent formation of aggregates with streptavidin modified nanoparticles.¹¹⁰ In the presence of an enzyme inhibitor, the first nanoparticles are not modified and no aggregation occurs.

Besides the detection of analytes, such colour changes can also be used to measure lengths. The concept of such “rulers on the nanometre scale” is again based on colour changes of gold particles if the gold particles are in close proximity. Different sites of a macromolecule can be linked to gold particles. By observing the colour of the gold particles the distance between these sites can be measured and in this way for example conformation changes in molecules can be observed.¹¹¹

6.2 Fluorescence quenching

The fluorescence of many fluorophores is quenched when they are in close proximity to gold surfaces.^{112–114} This effect can be used for several sensor strategies (see Fig. 5b). The first one is based on competitive displacement. For quantitative detection of a certain analyte, gold particles are conjugated with ligands that specifically bind to this analyte. Then the binding sites of the ligands are blocked by saturating them with analyte molecules (or molecules of similar structure that bind to the ligand), whereby these molecules are modified with fluorophores. As the fluorophores are in this way closely linked to the Au particles their fluorescence is quenched. After washing, these gold particles with blocked ligands are now added to the solution in which the concentration of the analyte should be detected. If no analyte is present there will be no fluorescence, as the fluorophores are quenched by the gold particles. Analyte molecules present in solution on the other hand will compete with the fluorophore labelled analytes previously bound to the Au particles for the binding sites of the ligands on the Au surface.¹⁶ In a continuous dynamic equilibrium analyte molecules in solution will displace analyte molecules bound to the ligands present on the particle surface. For reasons of simple statistics, the higher the concentration of analyte molecules in solution is, the fewer fluorophore labelled prebound molecules will remain on the particle surface in equilibrium. This means that the higher the concentration of analyte molecules is, the more fluorophore labelled molecules

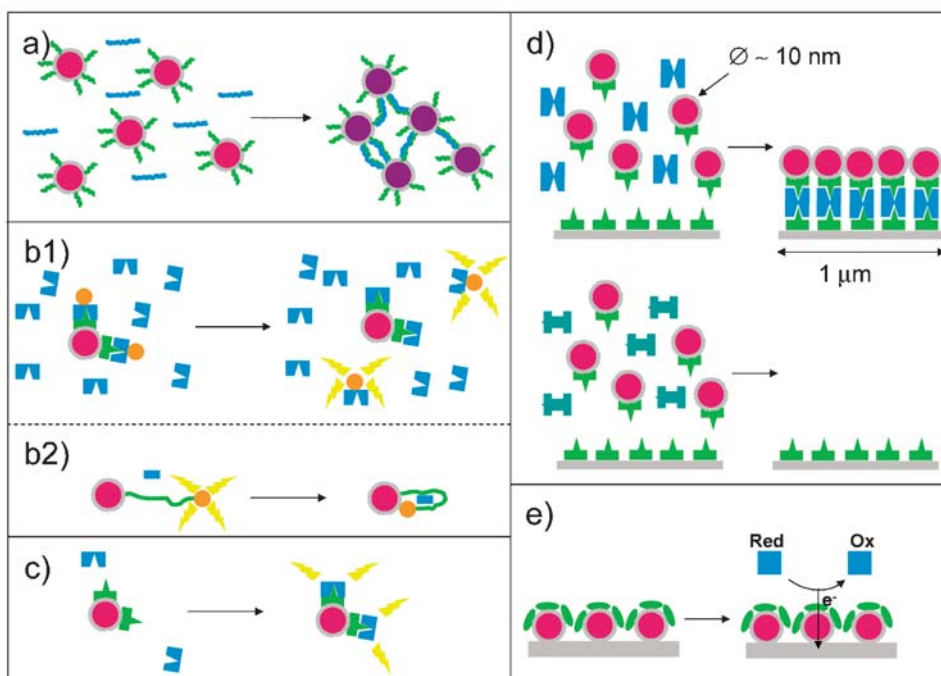


Fig. 5 Sensing with gold nanoparticles. For the specific detection of analytes (shown in blue) gold nanoparticles (core in red, ligand shell in grey) are conjugated with ligands (shown in green) that selectively bind to the analyte. (a) Colorimetric assays: Binding of the analyte to the ligands links several particles together to form small aggregates and the red colour of the colloidal gold solution shifts to purple/blue. (b) Quenching of fluorophores: (b1) Gold nanoparticles are conjugated with ligands that specifically bind to the analyte to be detected. The ligands on the nanoparticle surface are then saturated with molecules that bind to the ligands (shown in blue) and that have a fluorophore (drawn in orange) attached. As the fluorophores are in close proximity to the surface of the Au particles their fluorescence is quenched. The presence of analyte molecules competitively displaces part of the molecules with the fluorophores from the nanoparticle surface. As these fluorophores are no longer in contact with Au particles their fluorescence (symbolized as yellow rays) can be detected. (b2) Fluorophores (drawn in orange) are attached *via* linker molecules (drawn in green) to the surface of Au nanoparticles. Due to the length of the linker the distance between the fluorophore and the gold particles is big enough so that no quenching of the fluorophore occurs. Presence of the analyte (drawn in blue) changes the conformation of the linker molecules and as the fluorophores are now in close proximity to the Au surface their fluorescence is quenched. (c) Surface enhanced Raman scattering: Gold nanoparticles are conjugated to ligand molecules which specifically bind to the analyte to be detected. The analyte (drawn in blue) in solution provides only a weak Raman signal. Upon binding of the analyte to the ligands present on the Au surface the analyte comes into close proximity to the gold particles and the Raman signal is dramatically enhanced (as symbolized by the yellow rays). (d) Gold stains: Ligands specific to the analyte to be detected are immobilized on a surface and conjugated to Au nanoparticles. Presence of the analyte (drawn in blue) causes the binding of the particles to the surface. Other molecules (drawn in dark green) do not cause binding of the particles to the surface and thus a washing step removes all gold particles. The presence of the analyte is then quantified by the number of Au particles bound to the surface. (e) Redox reactions: Redox enzymes (drawn in green) are conjugated to the surface of Au nanoparticles (core in red, ligand shell in grey) which are immobilized on top of an electrode (drawn in grey). The enzymes oxidize their present substrates (drawn in blue) from the reduced form to the oxidized one. The released electrons are transferred *via* the gold nanoparticles to the electrode, which can be measured as current.

will be released from the Au particle surface into solution and as there is no quenching in solution the higher the resulting fluorescence signal will be. A variation of this concept involves using Au nanoparticles as quenchers for quantum dots which are replaced by the analyte. When the Au nanoparticles are released, the fluorescence of the quantum dots increases.¹¹⁵

A second detection scheme works slightly differently. In this case a molecule is needed which changes its conformation upon binding of the analyte. This molecule is used as a spacer to link fluorophores to gold nanoparticles. Without the presence of the analyte the spacer molecule is extended and there is no quenching of the fluorescence of the fluorophore. Analyte molecules on the other hand will bind to the spacer which then changes its conformation in such a way that the attached fluorophore will be brought into close proximity to the Au surface, which results in quenching of the fluorescence. The

higher the concentration of analyte in solution, the lower the recorded fluorescence signal will be. The same principle can be used in the opposite way when binding of the analyte stretches the spacer attached to the particles, and the quenched fluorescence increases after binding.^{116–118} Due to dynamic binding and unbinding of the analytes to the ligand (spacer) molecules present on the Au surface, both of the above introduced sensor concepts are reversible. In contrast to fluorescence quenching by metal nanoparticles, it remains to note that there are also recent findings of metal *enhanced* fluorescence and ideas about the exploitation of this effect for future applications.¹¹⁹

6.3 Surface-enhanced Raman scattering

Due to their characteristic spectra, many (macro) molecules can be detected by Raman scattering.¹²⁰ In Raman scattering the incident light is scattered with a low probability on

vibrational and rotational states of the molecule. The scattering process is inelastic, and thus the scattered light can have a lower (Stokes, by depositing energy into the molecule) or higher energy (anti Stokes, by gaining energy from the molecule) than the incident light. The energy shift is characteristic for the chemical structure where the scattering occurred and complex molecules have therefore a characteristic Raman spectrum that allows for detection and identification. While the scattering efficiency might depend on the wavelength of the incident light, the energy shift remains the same. Typically Raman signals are quite weak and therefore a sufficient analyte concentration is needed in order to provide enough signal. Raman scattering is dramatically enhanced if the molecules are close to a gold surface with very high curvature, as for example small gold nanoparticles. This effect is called surface enhanced Raman scattering (SERS).^{121–123} Due to the plasmon resonance of metal nanoparticles there is a strong enhancement of the electric field in close proximity to the particles, compared to the field strength of the incident light. This results in a much higher scatter probability and thus in a gain of several orders of magnitude of the Raman scattered light intensity that is detected. SERS can be used for the detection of analytes (see Fig. 5c). Again the surface of Au nanoparticles is modified with ligands that can specifically bind the analyte. Upon binding to the Au particle the Raman signal of the analyte is dramatically enhanced and allows for its detection.^{124,125} Recent developments include Au nanoparticles modified with Raman active reporter molecules for the detection of DNA¹²⁶ or proteins,^{127,128} and two photon excitation.¹²⁹

6.4 Gold stains

Instead of using fluorophores or absorbing dyes as read out for ELISA like assays (enzyme linked immunosorbent assays) gold nanoparticles can also be used. The aim of such assays is the specific qualitative or quantitative detection of analytes, which is conceptually related to immunostaining (see section 3.1). For this purpose the analyte is immobilized on a surface, either by simple adsorption or specific binding *e.g.* by a capture antibody. Instead of enzyme labelled antibodies, analyte specific antibodies are conjugated to the surface of gold nanoparticles. The presence of analyte in the assay thus results in binding of gold particles to the surface (Fig. 5d).^{130,131} The concentration of analyte molecules can be quantified by the optical absorption of the gold spot which is a function of the analyte concentration. Sensitivity can be increased by involving secondary antibodies and silver enhancement, where the gold nanoparticles catalyze the reduction of silver and are thus grown larger by a silver coating.¹³² Similar assays using gold stains as read out can also be applied for receptor ligand systems without involving antibodies, such as the detection of target DNA sequences with complementary DNA.^{133,134} In a similar way antibody conjugated gold nanoparticles can be used for the detection of proteins or DNA after blotting the molecules from a gel onto a membrane.¹³⁵ For many years, gold nanoparticles conjugated with a variety of antibodies (“immunogold”) have been commercially available, and they are also used to enhance the contrast in electron microscopy

(section 3.1). Alternatively, conjugated Au nanoparticles can be used to detect antigens (*e.g.* proteins¹³⁶ or DNA¹³⁷) present on an electronic chip. The binding of the nanoparticles is read out by voltammetry, and again the Au nanoparticles can be enhanced by silver deposition in order to amplify the signal.

6.5 Electron transfer

Finally, gold nanoparticles can also be used for the transfer of electrons in redox reactions.¹³⁸ The idea of such assays is to detect analytes which are substrates to redox enzymes. The enzyme can specifically oxidize (or reduce) the analyte molecules (Fig. 5e). The flow of electrons released (or required) in this redox reaction can be measured as electrical current. For this purpose the enzyme is conjugated to the surface of the gold particles.¹³⁹ The enzyme particle conjugates are then immobilized on the surface of an electrode (gold) which is connected to an amplifier for current detection, *e.g.* by cyclic voltammetry. Alternatively, the gold nanoparticles can be first immobilized on the electrode and then modified with enzymes.¹⁴⁰ In principle the enzyme could be directly immobilized on the flat gold electrode of the chip. However, the introduction of Au nanoparticles has several advantages. First an electrode covered with a layer of nanoparticles has a much higher surface roughness and thus larger surface area, which leads to higher currents. Second, because of the small curvature of small gold particles the contact of the Au particle with the enzyme can be more “intimate”, *i.e.* located in close proximity to the reactive centre, which can facilitate the electron transport.^{141,142}

7. Outlook

Colloidal Au nanoparticles possess a lot of interesting properties that make them useful for biological applications. Though similar applications can also be performed with colloidal nanoparticles of different materials, such as quantum dots, there are several features unique to gold particles. So far there is no indication of Au particle corrosion, and Au particles are inert, which makes them relatively biocompatible. Gold nanoparticles can be easily synthesized, they are colloiddally stable, and they can be conjugated with biological molecules in a straightforward way. Due to their optical properties, in particular the surface plasmon resonance, they can be visualized with different methods and sensors based on changes of the plasmon resonance have been demonstrated. For this reason gold particles are now also used for different applications besides the “classic” examples of gene guns and immunostaining. Though in our opinion gold nanoparticles will never play a “dominant” role in biology we predict that they will be routinely used within several standard *in vitro* assays and kits and that there is still plenty of room for new research. In particular, we believe that the shift in plasmon resonance upon binding of molecules or changing the inter particle distance will lead to a number of sensor assays for the detection of analytes which will become commercially available.

Acknowledgements

This work has been supported by the German Research Foundation (DFG, SPP Bio Nano Responses, PA 794/4 1).

References

- 1 T. Jennings and G. Strouse, in *Bio Applications of Nanoparticles*, Springer Science+Business Media, New York, 2007, vol. 620, pp. 34 47.
- 2 J. Turkevich, P. C. Stevenson and J. Hillier, *Discuss. Faraday Soc.*, 1951, 55 75.
- 3 J. Kimling, M. Maier, B. Okenve, V. Kotaidis, H. Ballot and A. Plech, *J. Phys. Chem. B*, 2006, **110**, 15700 15707.
- 4 M. Brust, M. Walker, D. Bethell, D. J. Schiffrin and R. Whyman, *J. Chem. Soc., Chem. Commun.*, 1994, 801 802.
- 5 N. R. Jana and X. Peng, *J. Am. Chem. Soc.*, 2003, **125**, 14280 14281.
- 6 C. Sonnichsen and A. P. Alivisatos, *Nano Lett.*, 2005, **5**, 301 304.
- 7 J. Perez Juste, I. Pastoriza Santos, L. M. Liz Marzan and P. Mulvaney, *Coord. Chem. Rev.*, 2005, **249**, 1870 1901.
- 8 A. C. Templeton, W. P. Wuelfing and R. W. Murray, *Acc. Chem. Res.*, 2000, **33**, 27 36.
- 9 T. Pellegrino, S. Kudera, T. Liedl, A. M. Javier, L. Manna and W. J. Parak, *Small*, 2005, **1**, 48 63.
- 10 A. G. Kanaras, F. S. Kamounah, K. Schaumburg, C. J. Kiely and M. Brust, *Chem. Commun.*, 2002, 2294 2295.
- 11 L. M. Liz Marzán, M. Giersig and P. Mulvaney, *Langmuir*, 1996, **12**, 4329 4335.
- 12 D. Zanchet, C. M. Micheel, W. J. Parak, D. Gerion and A. P. Alivisatos, *Nano Lett.*, 2001, **1**, 32 35.
- 13 R. Levy, Z. X. Wang, L. Duchesne, R. C. Doty, A. I. Cooper, M. Brust and D. G. Fernig, *ChemBioChem*, 2006, **7**, 592 594.
- 14 G. T. Hermanson, *Bioconjugate Techniques*, Academic Press, San Diego, 1996.
- 15 R. A. Sperling, T. Pellegrino, J. K. Li, W. H. Chang and W. J. Parak, *Adv. Funct. Mater.*, 2006, **16**, 943 948.
- 16 L. M. Demers, C. A. Mirkin, R. C. Mucic, A. Robert, I. Reynolds, R. L. Letsinger, R. Elghanian and G. Viswanadham, *Anal. Chem.*, 2000, **72**, 5535 5541.
- 17 T. Pellegrino, R. A. Sperling, A. P. Alivisatos and W. J. Parak, *J. Biomed. Biotechnol.*, 2007, **2007**, 26796, DOI: 10.1155/2007/26796.
- 18 B. D. Chithrani, A. A. Ghazan and C. W. Chan, *Nano Lett.*, 2006, **6**, 662 668.
- 19 H. K. Patra, S. Banerjee, U. Chaudhuri, P. Lahiri and A. K. Dasgupta, *Nanomedicine*, 2007, **3**, 111 119.
- 20 M. A. Albrecht, C. W. Evans and C. L. Raston, *Green Chem.*, 2006, **8**, 417 432.
- 21 E. E. Connor, J. Mwamuka, A. Gole, C. J. Murphy and M. D. Wyatt, *Small*, 2005, **1**, 325 327.
- 22 C. Kirchner, T. Liedl, S. Kudera, T. Pellegrino, A. M. Javier, H. E. Gaub, S. Stolze, N. Fertig and W. J. Parak, *Nano Lett.*, 2005, **5**, 331 338.
- 23 R. Shukla, V. Bansal, M. Chaudhary, A. Basu, R. R. Bhonde and M. Sastry, *Langmuir*, 2005, **21**, 10644 10654.
- 24 C. M. Goodman, C. D. McCusker, T. Yilmaz and V. M. Rotello, *Bioconjugate Chem.*, 2004, **15**, 897 900.
- 25 Y. Pan, S. Neuss, A. Leifert, M. Fischler, F. Wen, U. Simon, G. Schmid, W. Brandau and W. Jahn Dechent, *Small*, 2007, **3**, 1941 1949.
- 26 N. Pernodet, X. H. Fang, Y. Sun, A. Bakhtina, A. Ramakrishnan, J. Sokolov, A. Ulman and M. Rafailovich, *Small*, 2006, **2**, 766 773.
- 27 M. Tsoli, H. Kuhn, W. Brandau, H. Esche and G. Schmid, *Small*, 2005, **1**, 841 844.
- 28 G. Schmid, *Chem. Soc. Rev.*, 2008, **37**(9), DOI: 10.1039/b713631p.
- 29 X. H. Huang, P. K. Jain, I. H. El Sayed and M. A. El Sayed, *Nanomedicine*, 2007, **2**, 681 693.
- 30 C. Sonnichsen, T. Franzl, T. Wilk, G. von Plessen and J. Feldmann, *New J. Phys.*, 2002, **4**.
- 31 A. G. Tkachenko, H. Xie, Y. Liu, D. Coleman, J. Ryan, W. R. Glomm, M. K. Shipton, S. Franzen and D. L. Feldheim, *Bioconjugate Chem.*, 2004, **15**, 482 490.
- 32 G. R. Souza, D. R. Christianson, F. I. Staquicini, M. G. Ozawa, E. Y. Snyder, R. L. Sidman, J. H. Miller, W. Arap and R. Pasqualini, *Proc. Natl. Acad. Sci. U. S. A.*, 2006, **103**, 1215 1220.
- 33 R. Jin, Y. Cao, C. A. Mirkin, K. L. Kelly, G. C. Schatz and J. G. Zheng, *Science*, 2001, **294**, 1901 1903.
- 34 D. Boyer, P. Tamarat, A. Maali, B. Lounis and M. Orrit, *Science*, 2002, **297**, 1160 1163.
- 35 S. Berciaud, L. Cognet, G. A. Blab and B. Lounis, *Phys. Rev. Lett.*, 2004, 93.
- 36 S. Mallidi, T. Larson, J. Aaron, K. Sokolov and S. Emelianov, *Opt. Express*, 2007, **15**, 6583 6588.
- 37 K. Kim, S. W. Huang, S. Ashkenazi, M. O'Donnell, A. Agarwal, N. A. Kotov, M. F. Denny and M. J. Kaplan, *Appl. Phys. Lett.*, 2007, 90.
- 38 J. P. Wilcoxon, J. E. Martin, F. Parsapour, B. Wiedenman and D. F. Kelley, *J. Chem. Phys.*, 1998, **108**, 9137 9143.
- 39 G. L. Wang, T. Huang, R. W. Murray, L. Menard and R. G. Nuzzo, *J. Am. Chem. Soc.*, 2005, **127**, 812 813.
- 40 J. Roth, *Histochem. Cell Biol.*, 1996, **106**, 1 8.
- 41 J. F. Hainfeld, D. N. Slatkin, T. M. Focella and H. M. Smilowitz, *Br. J. Radiol.*, 2006, **79**, 248 253.
- 42 R. E. Gosselin, *J. Gen. Physiol.*, 1956, **39**, 625 649.
- 43 W. P. Faulk and G. M. Taylor, *Immunochemistry*, 1971, **8**, 1081.
- 44 J. D. Mey, A. M. Lambert, A. S. Bajer, M. Moeremans and M. D. Brabander, *Proc. Natl. Acad. Sci. U. S. A.*, 1982, **79**, 1898 1902.
- 45 A. Kusumi, C. Nakada, K. Ritchie, K. Murase, K. Suzuki, H. Murakoshi, R. S. Kasai, J. Kondo and T. Fujiwara, *Annu. Rev. Biophys. Biomol. Struct.*, 2005, **34**, 351 378.
- 46 D. P. Felsenfeld, D. Choquet and M. P. Sheetz, *Nature*, 1996, **383**, 438 440.
- 47 H. Cang, C. M. Wong, C. S. Xu, A. H. Rizvi and H. Yang, *Appl. Phys. Lett.*, 2006, 88.
- 48 D. Lasne, G. A. Blab, S. Berciaud, M. Heine, L. Groc, D. Choquet, L. Cognet and B. Lounis, *Biophys. J.*, 2006, **91**, 4598 4604.
- 49 L. Cognet, C. Tardin, D. Boyer, D. Choquet, P. Tamarat and B. Lounis, *Proc. Natl. Acad. Sci. U. S. A.*, 2003, **100**, 11350 11355.
- 50 Y. L. Wang, J. D. Silverman and L. G. Cao, *J. Cell Biol.*, 1994, **127**, 963 971.
- 51 M. Dahan, S. Levi, C. Luccardini, P. Rostaing, B. Riveau and A. Triller, *Science*, 2003, **302**, 442 445.
- 52 D. Kim, S. Park, J. H. Lee, Y. Y. Jeong and S. Jon, *J. Am. Chem. Soc.*, 2007, **129**, 7661 7665.
- 53 J. F. Hainfeld, D. N. Slatkin and H. M. Smilowitz, *Phys. Med. Biol.*, 2004, N309 N315.
- 54 B. Ballou, B. C. Lagerholm, L. A. Ernst, M. P. Bruchez and A. S. Waggoner, *Bioconjugate Chem.*, 2004, **15**, 79 86.
- 55 S. Kim, Y. T. Lim, E. G. Soltész, A. M. D. Grand, J. Lee, A. Nakayama, J. A. Parker, T. Mihaljevic, R. G. Laurence, D. M. Dor, L. H. Cohn, M. G. Bawendi and J. V. Frangioni, *Nat. Biotechnol.*, 2004, **22**, 93 97.
- 56 G. Albrecht Buehler, *Cell*, 1977, **11**, 395 404.
- 57 G. Albrecht Buehler, *Cell*, 1977, **12**, 333 339.
- 58 G. Albrecht Buehler, *J. Cell Biol.*, 1979, **80**, 53 60.
- 59 T. Pellegrino, W. J. Parak, R. Boudreau, M. LeGros, D. Gerion, A. P. Alivisatos and C. Larabell, *Differentiation*, 2003, **71**, 542 548.
- 60 D. R. Chen, C. H. Wendt and D. Y. H. Pui, *J. Nanopart. Res.*, 2000, **2**, 133 139.
- 61 N. Yang, J. Burkholder, B. Roberts, B. Martinell and D. McCabe, *Proc. Natl. Acad. Sci. U. S. A.*, 1990, **87**, 9568 9572.
- 62 U. W. Hilber, M. Bodmer, F. D. Smith and W. Koller, *Curr. Genet.*, 1994, **25**, 124 127.
- 63 L. M. Yepes, V. Mittak, S. Z. Pang, C. Gonsalves, J. L. Slightom and D. Gonsalves, *Plant Cell Rep.*, 1995, **14**, 694 698.
- 64 S. Kuriyama, A. Mito, H. Tsujinoue, T. Nakatani, H. Yoshiji, T. Tsujimoto, M. Yamazaki and T. Fukui, *Gene Ther.*, 2000, **7**, 1132 1136.
- 65 E. Wagner, D. Curiel and M. Cotten, *Adv. Drug Delivery Rev.*, 1994, **14**, 113 135.
- 66 P. H. Yang, X. Sun, J. F. Chiu, H. Sun and Q. Y. He, *Bioconjugate Chem.*, 2005, **16**, 494 496.

- 67 V. Dixit, J. Van den Bossche, D. M. Sherman, D. H. Thompson and R. P. Andres, *Bioconjugate Chem.*, 2006, **17**, 603 609.
- 68 P. K. Jain, I. H. El Sayed and M. A. El Sayed, *Nano Today*, 2007, **2**, 18 29.
- 69 B. D. Chithrani and W. C. W. Chan, *Nano Lett.*, 2007, **7**, 1542 1550.
- 70 J. M. de la Fuente and C. C. Berry, *Bioconjugate Chem.*, 2005, **16**, 1176 1180.
- 71 M. Lewin, N. Carlesso, C. H. Tung, X. W. Tang, D. Corry, D. T. Scadden and R. Weissleder, *Nat. Biotechnol.*, 2000, **18**, 410 414.
- 72 A. M. Koch, F. Reynolds, H. R. Merkle, R. Weissleder and L. Josephson, *ChemBioChem*, 2005, **6**, 337 345.
- 73 C. L. Murriel and S. F. Dowdy, *Expert Opin. Drug Delivery*, 2006, **3**, 739 746.
- 74 Z. P. Xu, Q. H. Zeng, G. Q. Lu and A. B. Yu, *Chem. Eng. Sci.*, 2006, **61**, 1027 1040.
- 75 G. Han, C. C. You, B. j. Kim, R. S. Turingan, N. S. Forbes, C. T. Martin and V. M. Rotello, *Angew. Chem., Int. Ed.*, 2006, **45**, 3165 3169.
- 76 A. K. Salem, P. C. Searson and K. W. Leong, *Nat. Mater.*, 2003, **2**, 668 671.
- 77 M. M. O. Sullivan, J. J. Green and T. M. Przybycien, *Gene Ther.*, 2003, **10**, 1882 1890.
- 78 N. L. Rosi, D. A. Giljohann, C. S. Thaxton, A. K. R. Lytton Jean, M. S. Han and C. A. Mirkin, *Science*, 2006, **312**, 1027 1030.
- 79 J. Rojo, V. Diaz, J. M. de la Fuente, I. Segura, A. G. Barrientos, H. H. Riese, A. Bernad and S. Penades, *ChemBioChem*, 2004, **5**, 291 297.
- 80 P. Ghosh, G. Han, M. De, C. K. Kim and V. M. Rotello, *Adv. Drug Delivery Rev.*, 2008, **60**, 1307 1315.
- 81 K. Sokolov, J. Aaron, D. Nida, A. Gillenwater, M. Follen, C. MacAulay, K. A. Storthz, B. Korgel, M. Descour, R. Pasqualini, W. Arap, W. Lam and R. Richards Kortum, *Technol. Cancer Res. Treat.*, 2003, **2**, 491 504.
- 82 S. Kumar, N. Harrison, R. Richards Kortum and K. Sokolov, *Nano Lett.*, 2007, **7**, 1338 1343.
- 83 A. O. Govorov, W. Zhang, T. Skeini, H. Richardson, J. Lee and N. A. Kotov, *Nanoscale Res. Lett.*, 2006, **1**, 84 90.
- 84 D. Pissuwan, S. M. Valenzuela and M. B. Cortie, *Trends Biotechnol.*, 2006, **24**, 62 67.
- 85 M. R. Choi, K. J. Stanton Maxey, J. K. Stanley, C. S. Levin, R. Bardhan, D. Akin, S. Badve, J. Sturgis, J. P. Robinson, R. Bashir, N. J. Halas and S. E. Clare, *Nano Lett.*, 2007, **7**, 3759 3765.
- 86 T. B. Huff, L. Tong, Y. Zhao, M. N. Hansen, J. X. Cheng and A. Wei, *Nanomedicine*, 2007, **2**, 125 132.
- 87 X. H. Huang, P. K. Jain, I. H. El Sayed and M. A. El Sayed, *Photochem. Photobiol.*, 2006, **82**, 412 417.
- 88 A. R. Lowery, A. M. Gobin, E. S. Day, N. J. Halas and J. L. West, *Int. J. Nanomed.*, 2006, **1**, 149 154.
- 89 X. Huang, P. Jain, I. El Sayed and M. El Sayed, *Lasers Med. Sci.*, 2008, **23**(3), 217 228.
- 90 J. Chen, D. Wang, J. Xi, L. Au, A. Siekkinen, A. Warsen, Z. Y. Li, H. Zhang, Y. Xia and X. Li, *Nano Lett.*, 2007, **7**, 1318 1322.
- 91 Q. A. Pankhurst, J. Connolly, S. K. Jones and J. Dobson, *J. Phys. D: Appl. Phys.*, 2003, **36**, R167 R181.
- 92 R. Hiergeist, W. Andra, N. Buske, R. Hergt, I. Hilger, U. Richter and W. Kaiser, *J. Magn. Magn. Mater.*, 1999, **201**, 420 422.
- 93 K. Hamad Schifferli, J. J. Schwartz, A. T. Santos, S. Zhang and J. M. Jacobson, *Nature*, 2002, **415**, 152 155.
- 94 J. Stehr, C. Hrelescu, R. A. Sperling, G. Raschke, M. Wunderlich, A. Nichtl, D. Heindl, K. Kurzinger, W. J. Parak, T. A. Klar and J. Feldmann, *Nano Lett.*, 2008, **8**, 619 623.
- 95 M. J. Kogan, N. G. Bastus, R. Amigo, D. Grillo Bosch, E. Arraya, A. Turiel, A. Labarta, E. Giral and V. F. Puntes, *Nano Lett.*, 2006, **6**, 110 115.
- 96 A. S. Angelatos, B. Radt and F. Caruso, *J. Phys. Chem. B*, 2005, **109**, 3071 3076.
- 97 A. G. Skirtach, C. Dejngnat, D. Braun, A. S. Susha, W. J. Parak, H. Mohwald and G. B. Sukhorukov, *Nano Lett.*, 2005, **5**, 1371 1377.
- 98 A. G. Skirtach, A. M. Javier, O. Kreft, K. Kohler, A. P. Alberola, H. Mohwald, W. J. Parak and G. B. Sukhorukov, *Angew. Chem., Int. Ed.*, 2006, **45**, 4612 4617.
- 99 C. M. Pitsillides, E. K. Joe, X. Wei, R. R. Anderson and C. P. Lin, *Biophys. J.*, 2003, **84**, 4023 4032.
- 100 T. A. Klar, in *Nanophotonics with Surface Plasmons*, ed. V. Shalaev and S. Kawata, Elsevier, The Netherlands, 2007, pp. 219 270.
- 101 G. Raschke, S. Kowarik, T. Franzl, C. Sonnichsen, T. A. Klar, J. Feldmann, A. Nichtl and K. Kurzinger, *Nano Lett.*, 2003, **3**, 935 938.
- 102 P. K. Jain, S. Eustis and M. A. El Sayed, *J. Phys. Chem. B*, 2006, **110**, 18243 18253.
- 103 C. A. Mirkin, R. L. Letsinger, R. C. Mucic and J. J. Storhoff, *Nature*, 1996, **382**, 607 609.
- 104 R. Elghamian, J. J. Storhoff, R. C. Mucic, R. L. Letsinger and C. A. Mirkin, *Science*, 1997, **277**, 1078 1081.
- 105 R. Moller and W. Fritzsche, *Curr. Pharm. Biotechnol.*, 2007, **8**, 274 285.
- 106 J. M. Nam, S. I. Stoeva and C. A. Mirkin, *J. Am. Chem. Soc.*, 2004, **126**, 5932 5933.
- 107 J. Liu and Y. Lu, *Chem. Commun.*, 2007, 4872 4874.
- 108 W. Zhao, W. Chiuman, J. C. F. Lam, S. A. McManus, W. Chen, Y. Cui, R. Pelton, M. A. Brook and Y. Li, *J. Am. Chem. Soc.*, 2008, **130**, 3610 3618.
- 109 W. Wang, C. Chen, M. Qian and X. S. Zhao, *Anal. Biochem.*, 2008, **373**, 213.
- 110 Z. Wang, R. Levy, D. G. Fernig and M. Brust, *J. Am. Chem. Soc.*, 2006, **128**, 2214 2215.
- 111 C. Sonnichsen, B. M. Reinhard, J. Liphardt and A. P. Alivisatos, *Nat. Biotechnol.*, 2005, **23**, 741 745.
- 112 J. R. Lakowicz, *Principles of Fluorescence Spectroscopy*, Springer, New York, 3rd edn, 2006.
- 113 E. Dulkeith, A. C. Morteani, T. Niedereichholz, T. A. Klar, J. Feldmann, S. A. Levi, F. C. J. M. van Vegel, D. N. Reinhoudt, M. Moller and D. I. Gittins, *Phys. Rev. Lett.*, 2002, **89**, 203002 1 203002 4.
- 114 E. Dulkeith, M. Ringle, T. A. Klar, J. Feldmann, A. M. Javier and W. J. Parak, *Nano Lett.*, 2005, **5**, 585 589.
- 115 E. Oh, M. Y. Hong, D. Lee, S. H. Nam, H. C. Yoon and H. S. Kim, *J. Am. Chem. Soc.*, 2005, **127**, 3270 3271.
- 116 B. Dubertret, M. Calame and A. J. Libchaber, *Nat. Biotechnol.*, 2001, **19**, 365 370.
- 117 Z. Wang, A. G. Kanaras, A. D. Bates, R. Cosstick and M. Brust, *J. Mater. Chem.*, 2004, **14**, 578 580.
- 118 P. Ray, G. Darbha, A. Ray, J. Walker and W. Hardy, *Plasmonics*, 2007, **2**, 173.
- 119 J. Lakowicz, *Plasmonics*, 2006, **1**, 5.
- 120 H. A. Szymanski, *Raman Spectroscopy*, Plenum Press, New York, 1st edn, 1967.
- 121 M. Fleischmann, P. J. Hendra and A. J. McQuillan, *Chem. Phys. Lett.*, 1974, **26**, 163.
- 122 A. Campion and P. Kambhampati, *Chem. Soc. Rev.*, 1998, **27**, 241 250.
- 123 K. Kneipp, H. Kneipp and J. Kneipp, *Acc. Chem. Res.*, 2006, **39**, 443 450.
- 124 S. Nie and S. R. Emory, *Science*, 1997, **275**, 1102 1106.
- 125 J. T. Krug, G. D. Wang, S. R. Emory and S. Nie, *J. Am. Chem. Soc.*, 1999, **121**, 9208 9214.
- 126 Y. C. Cao, R. Jin and C. A. Mirkin, *Science*, 2002, **297**, 1536 1540.
- 127 J. Ni, R. J. Lipert, G. B. Dawson and M. D. Porter, *Anal. Chem.*, 1999, **71**, 4903 4908.
- 128 X. Qian, X. H. Peng, D. O. Ansari, Q. Yin Goen, G. Z. Chen, D. M. Shin, L. Yang, A. N. Young, M. D. Wang and S. Nie, *Nat. Biotechnol.*, 2008, **26**, 83.
- 129 J. Kneipp, H. Kneipp and K. Kneipp, *Proc. Natl. Acad. Sci. U. S. A.*, 2006, **103**, 17149 17153.
- 130 Z. Wang, J. Lee, A. R. Cossins and M. Brust, *Anal. Chem.*, 2005, **77**, 5770 5774.
- 131 Z. Wang, R. Lévy, D. G. Fernig and M. Brust, *Bioconjugate Chem.*, 2005, **16**, 497 500.
- 132 G. R. Newman and B. Jasani, *J. Pathol.*, 1998, **186**, 119 125.
- 133 G. A. Blab, L. Cognet, S. Berciaud, I. Alexandre, D. Husar, J. Remacle and B. Lounis, *Biophys. J.*, 2006, **90**, L13 L15.
- 134 J. Reichert, A. Csaki, J. M. Kohler and W. Fritzsche, *Anal. Chem.*, 2000, **72**, 6025 6029.
- 135 M. Moeremans, G. Daneels, A. Van Dijck, G. Langanger and J. De Mey, *J. Immunol. Methods*, 1984, **74**, 353.
- 136 W. Joseph, *Electroanalysis*, 2007, **19**, 769 776.

-
- 137 M. T. Castañeda and S. A. A. Merkoçi, *Electroanalysis*, 2007, **19**, 743–753.
- 138 B. Willner, E. Katz and I. Willner, *Curr. Opin. Biotechnol.*, 2006, **17**, 589–596.
- 139 Y. Xiao, F. Patolsky, E. Katz, J. F. Hainfeld and I. Willner, *Science*, 2003, **299**, 1877–1881.
- 140 Y. Xiao, H. X. Ju and H. Y. Chen, *Anal. Chim. Acta*, 1999, **391**, 73.
- 141 A. Yu, Z. Liang, J. Cho and F. Caruso, *Nano Lett.*, 2003, **3**, 1203–1207.
- 142 J. Zhao, R. W. Henkens, J. Stonehuerner, J. P. O'Daly and A. L. Crumbliss, *J. Electroanal. Chem.*, 1992, **327**, 109.

Acknowledgement

Many thanks to Wolfgang Parak, for the project(s), position and in particular the open-minded discussions and his generous attitude in many concerns.

To Hermann Gaub and the people of his lab for hosting our group during our time in Munich.

My special thanks to Teresa Pellegrino for introducing a physicist to wet chemistry while getting started with the project.

Stefan Kudera for his famous CdSe/ZnS 9a quantum dot sample and some TEM pictures, Marco Zanella for some TEM and the unforgettable philosophical discussions about and practical exercises with pizza.

Sabine Faust, S. Thomas and G. Schäfer-Lehnhoff for their kind help with everything related to administration and bureaucracy. Hermann Gump, Andreas Oppermann and Andreas Rentzos for mostly computer-related help, but not only.

Fabienne Quennet and Steffen Klingenhöfer for proof-reading the manuscript.

The other former and present members of the group for everything else, keep it up!

My parents and Estel for mental support and patience.

Wissenschaftlicher Werdegang

- Seit 2007-06 Philipps-Universität Marburg, AG Biophotonik (Prof. W. Parak): Wissenschaftlicher Mitarbeiter, Fortsetzung der Doktorarbeit nach dem Umzug der Arbeitsgruppe.
- 2005-04 – 2007-06 Ludwig-Maximilians-Universität München, Lehrstuhl für Angewandte Physik: Wissenschaftlicher Mitarbeiter, Promotion in der Arbeitsgruppe von Dr. W. Parak.
- 2005-02 Diplom in Physik.
- 2001 – 2005 Ludwig-Maximilians-Universität München: Hauptstudium Physik. Diplomarbeit am Lehrstuhl für Angewandte Physik (Prof. H. Gaub) in der Arbeitsgruppe Dr. W. Parak.
- 2000 – 2001 Université Denis Diderot, Paris, Frankreich: Auslandsjahr als Erasmus-Student.
- 1998 – 2000 Universität Bayreuth: Grundstudium Physik, Vordiplom.
- 1984 – 1997 St.-Ursula-Schule Geisenheim: Gymnasium, Abitur.